The University Of Sheffield.

Electrically Accelerated Leaching of Simulated Cementitious Wasteforms

Andrew John MacArthur

A Thesis submitted in partial fulfilment of the requirements for the degree of Doctor of Philosophy

Department of Materials Science & Engineering

The University of Sheffield

July 2017

Abstract

UK disposal plans for intermediate-level nuclear waste (ILW) foresee its encapsulation in blends of Blast Furnace Slag and Portland cement (BFS:PC), held in steel drums and stored in a Geological Disposal Facility. Following groundwater ingress, wasteform degradation through leaching is possible and radionuclides could escape. Due to the long lifetime of hazardous waste, real-time experiments are infeasible, although it is necessary to gain detailed information about leaching performance of the wasteforms for key radionuclides and their transmutation products. This study aims at better understanding the durability of the wasteform by investigating the interactions of caesium and barium with the cement matrix (3:1 BFS:PC) through an accelerated degradation method: Electrically accelerated leaching. ^{137}Cs, a problematic radionuclide in ILW due to its abundance and mobility, decays into ^{137}Ba over time. This study revealed that when intermixed above ~2.8 wt.%, $CsNO_3$ will precipitate without interacting with the 3:1 BFS:PC matrix. When barium is incorporated as $Ba(NO_3)_2$ and $Ba(OH)_2 \cdot 8H_2O$, barite ($BaSO_4$) forms even at 1 wt.%-equivalent of $CsNO_3$, and ettringite formation decreases. The study also revealed that Ca leaching was accelerated by 19.3±1.9 times when 3:1 BFS:PC is electrically leached at a current density of 25 Am^{-2} for two weeks. This 'Leaching Acceleration Factor' was different for every element studied. Leaching of cations into the anode tank, and vice versa for anions, is actually suppressed compared with static leaching. Electric migration of Ba into pre-cured 3:1 BFS:PC containing Cs resulted in formation of barite in the near-surface region of the cement. This suggests that formation of barite likely takes place following the nuclear decay of ^{137}Cs, which is a desirable result as barite is highly insoluble, becoming strongly immobilised in the cementitious wasteform.

Acknowledgements

There are many people I'd like to thank for their help and support during this PhD over the past few years. My supervisors, Dr. Hajime Kinoshita and Professor John Provis have been invaluable in their guidance, words of advice and suggestions over the course of this very interesting project. My growth as a researcher is thanks to them. Thanks also to Katsufumi Hashimoto, now a Professor at Kyoto University, for the opportunity of a research placement in the Lifetime Engineering Laboratory at Hokkaido University, and your instrumental advice in electrical leaching. Thank you all for taking a chance on a Physicist who wanted to research cement.

Jana, your understanding, love and words of support have given me assurance whilst I worked through many late nights and weekends to complete this Thesis. I could not have done it without you. I would also (of course) like to thank my family and friends in Sheffield. I love you all, and I am proud and grateful to have you in my life. PhDs are difficult, and being able to tell you about my day, and ask for advice when things went wrong, has gotten me through the past few years. This Thesis, and my happiness, is thanks to you all.

Thanks to Dr Oday H. Hussein, whose expert advice and patient training in using all the equipment in the cement lab have made this project possible. I would also like to express my gratitude to Kieran Nash for his assistance in cutting my samples and lending necessary moulds, and to Dr Nik Reeves-McLaren whose knowledge in X-ray diffractometry has helped me greatly. I have been a proud member of the Immobilisation Science Laboratory and the Sheffield Cement Group, and I am grateful to my colleagues for always being there, especially to Adam J Fisher and Brant Walkley for their help with XRF and ICP-OES analysis. The constructive criticism and encouraging advice provided by Dr Ines García-Lodeiro was greatly appreciated in the later stages of this project.

I would like to thank the EPSRC for sponsoring this project through the Nuclear FiRST DTC, and the staff and academics involved from both the University of Manchester and The University of Sheffield. This research was performed in part at the MIDAS Facility, at the University of Sheffield, which was established with support from the Department of Energy and Climate Change.

Key Abbreviations and Cement Chemist Notation

Materials

BFS	Ground Granulated Blast Furnace Slag	
PC	Portland Cement	
w/c	water to cement ratio	
w/b	water to binder ratio	
wt.%	percentage of the total sample's weight that this part constitutes	
C	CaO	Calcium oxide
S	SiO_2	Silicon dioxide
A	Al_2O_3	Aluminium oxide
F	Fe_2O_3	Iron oxide
H	H_2O	Water
$\overline{S}$	SO_3	Sulphate
$\overline{C}$	CO_2	Carbon dioxide

Analytical Techniques

XRF	X-Ray Fluorescence
XRD	X-Ray Diffraction
TG	Thermal Gravimetry
DTG	Differential Thermal Gravimetry
DTA	Differential Thermal Analysis
DSC	Differential Scanning Calorimetry
ICP-OES	Inductively Coupled Plasma – Optical Emission Spectrometry
SEM	Scanning Electron Microscopy
BSE	Back Scattered Electrons
EDX	Energy Dispersive X-ray Spectroscopy
MIP	Mercury Intrusion Porosimetry

Other Terms

ILW	Intermediate Level Radioactive Waste
GDF	Geological Disposal Facility
I	Current (Amps, A)
V	Voltage (Volts, V)
J	Current Density (Am^{-2})

Contents

List of Figures

Figures in Chapter 2: Literature review

Figures in Chapter 3: Materials and Experimental Methods

Figures in Chapter 4: The Incorporation of Cs and Ba in 3:1 BFS:PC

Figures in Chapter 5: Electrical Leaching of 3:1 BFS:PC

Figures in Chapter 6: Simultaneous Electrical Migration of Cs and Ba

Figures in the Appendix

List of Tables

Conference Pulications

2016 "Application of electrical migration: Investigation of increase in barium in simulated wasteforms", **MacArthur A.,** Hashimoto K., Provis J.L., Kinoshita H. Mechanisms and Modelling of Waste/Cement Interactions 2016, Murten, Switzerland.

2015 "Use of Electrical Leaching as an experimental analogy for nuclear decay in ILW", **MacArthur A.**, Kinoshita H., Provis J.L., Hashimoto K., 1st International Conference on Pollutant Toxic Ions and Molecules, Caparica-Almada, Portugal.

2014 "Effect of $CsNO_3$ on 3:1 Blast Furnace Slag:Portland Cement Systems", **MacArthur A.**, Kinoshita H., Provis J.L., Shaw S., 34th Cement and Concrete Science Conference, Sheffield.

2014 "Development of an Electrical Leaching Technique – Evaluation of Leaching from Hardened Cement Body", Hashimoto K., Yokota H., Kinoshita H., Gashier W., **MacArthur, A.**, 34th Cement and Concrete Science Conference, Sheffield.

Chapter 1: Introduction

1.1 Background

The UK has a legacy of long lived nuclear waste resulting from electricity generation by nuclear power plants and the wider nuclear industry (e.g. medical applications and scientific studies) that needs to be contained and isolated from the biosphere for thousands of years due to the long half-lives and high activities of the radionuclides [1]. This PhD project focuses on a type of nuclear waste, Intermediate Level Waste (ILW), which is categorised in the UK as waste that is highly radioactive and so require shielding, but internal heat generation is not a problematic factor unlike High Level Waste (HLW) [2].

^{137}Cs is a problematic radionuclide in ILW due to its abundance, high solubility in water and mobility [3], [4], and decays into ^{137}Ba with a half-life of 30.08 years [5]. The ^{137}Cs in nuclear waste originates from the fission of ^{236}U in nuclear power plants, and can be found in waste categories such as ion-exchange materials, sludges, and pieces of fuel cladding produced during the reprocessing of Oxide Fuel elements at THORP in Sellafield (Thermal Oxide Reprocessing Plant) [1]. During THORP reprocessing, fuel elements are sheared into small lengths, typically sizes of 50-75 mm. These lengths are fed into a dissolver basket, which is placed in a dissolver vessel containing hot nitric acid – typically 7.0M at 100°C [1]. Once the fuel itself has been dissolved out, the basket is removed and contains the fuel cladding and end appendages of the oxide fuel elements, which typically consist of zircaloy or stainless steel. This waste, which can contain ^{137}Cs, is transferred to the Waste Encapsulation Plant (WEP), and 'often includes course fines from the THORP shearing process and has a dilute nitric acid covering liquor.' Bowmer et al., 2007 [1].

ILW is encapsulated in a cement matrix, typically a mixture of blast furnace slag (BFS) and Portland cement (PC) with the exact composition and ratio depending on the ILW

wastestream in question. A 3:1 BFS:PC ratio, typically used for acceptance tests [1], is investigated in this project. It is important to understand the effects on and interactions between the encapsulation matrix and the waste when it is initially mixed, and later when radioactive decay of the waste has occurred. The main hydrate phase in PC is C-S-H, and it has been shown that Cs sorbs from the pore solution onto this phase over time, with a high variability depending on the supplementary cementitious materials (SCMs) used [6]. However, there is little data in the open literature on the interaction between Cs and 3:1 BFS:PC cement systems. When the interaction of Cs with cement is studied, there are two typical compounds examined: CsCl and $CsNO_3$ [7]–[13]. In this project I have chosen to study the interaction between cement and $CsNO_3$. Although CsCl has been studied in the past [12], as explained above, waste containing Cs is typically exposed to nitric acid. Therefore, the presence of $CsNO_3$ in nuclear waste is likely, and it is therefore a suitable molecule to study. Additionally, others working in the field of electrical leaching have used $CsNO_3$ to study the leaching behaviour of Cs [13], [14].

The interaction of Ba with 3:1 BFS:PC also requires investigation, as Ba, despite being a stable decay product can still be chemically harmful [15]. The behaviour of Ba in cement has been studied in the past: for instance, barium sulphate has been observed to precipitate when barium carbonate is added to specific cement phases [16], [17].

The wasteform (the mixture of the waste and the cement matrix) is put into 500 L steel drums, which are then stored for up to 150 years with the eventual aim of placing them in a Geological Disposal Facility (GDF) [18], [19]. Over time, in a GDF groundwater will be able to penetrate the engineered barriers, interact with steel drums, and eventually come into

contact with the wasteform and carry active radionuclides out in a plume. The movement of this groundwater is slow and diffusion of the waste is also a slow process, however the mechanisms and speed of this degradation process need to be investigated and understood for the safety case of a GDF [18], as well as the behaviour of the wasteforms to be able to assure that there will be safe storage and disposal.

The phenomenon of diffusion and its effects on cement is not a new field of investigation, being an important factor in the degradation of large structures such as bridges and dams [20], [21]. It is important to understand how both the cement matrix and the radionuclides encapsulated behave in the long term – studies currently available in the open literature are usually conducted for a few years at the longest. Unfortunately, it is unrealistic to conduct experiments over 100s of years and this is the timescale where the waste will still be hazardous [18]. There is a need, especially with regards to nuclear waste, to investigate accelerated leaching techniques in an attempt to understand how wasteforms placed in a GDF will behave over extended timescales.

Cement consists of a mixture of solid phases which form a porous network that contain a pore solution. Degradation of cement in the natural case when in contact with water or when water passes through the cement body – is actually a joint *diffusion/dissolution* process; ions in the pore solution *diffuse* out into the water, and the pore walls of the cement *dissolve* into the pore solution in order to attain chemical equilibrium. In an experimental context, this process is referred to as leaching. Standard leaching techniques such as semi-static and static leaching aim to replicate these conditions, however they are also typically the most time consuming experiments. In semi-static leaching the leachate is regularly replaced with fresh

leachant, and in static leaching the leachate is not manually altered for the duration of the test. Accelerated leaching tests attempt to predict the behaviour of cement leaching over longer periods of time. One method is by using a leachant that is more aggressive, for instance ammonium nitrate solution [22]. This method largely works to accelerate the leaching by increasing the rate of the dissolution of the solid phases in cement [23]. It accelerates the *dissolution* aspect of leaching.

Another method, and the focus of this research, is electrically accelerated leaching, which accelerates the *diffusion* aspect of leaching. It has been shown that this technique can be used to degrade cement to a similar extent seen in a real material exposed to water for 100 years in a dam [24], yet the details of this technique has not been fully investigated. This PhD project in part is to understand the electrical leaching process. In the electrical leaching technique utilised in this project, a cement sample is placed between two tanks of leachant, typically distilled water, with electrodes in each tank. A direct current is then applied across the cement sample, which enhances the migration of ions, based on their charges in the cement's pore solution. An applied current has been used to study the migration of ions through cement [25], [26], and in this project this technique is applied to investigate how barium will interact with a pre-cured cement sample, as an experimental model for when caesium decays into barium inside the wasteform. Studying the effects of irradiation on cement matrices is not the focus of this work, so in this project, non-radioactive isotopes of Cs were used in the experiments using $CsNO_3$.

1.2 Scope of the Project

The main aims of the project are:

1. To investigate the incorporation of Cs and Ba into 3:1 BFS:PC in the form of a. $CsNO_3$ and b. a mixture of $Ba(NO_3)_2$ and $Ba(OH)_2 \cdot 8H_2O$, to examine firstly, whether they would react with the cement and secondly, their impact on the cement matrix.
2. To investigate electrical leaching and gain further understanding of the technique, to examine its validity and effects on anions and cations other than Ca, as has been studied in the past.
3. To adapt the electrical leaching technique to introduce barium into a pre-cured cement sample initially containing caesium and investigate the interaction with the cement matrix.

1.3 Organisation of the Thesis

Chapter 1: Introduction

This Chapter.

Chapter 2: Literature Review

A literature review was conducted and is shown in this Chapter. The subjects covered include nuclear waste, cement and cement hydration, and leaching techniques with a focus on existing papers on electrical leaching.

Chapter 3: Materials and Experimental Methods

The cement production and experimental techniques are explained, and analytical techniques are introduced together with the information of the raw materials used.

Chapter 4: The Incorporation of Cs and Ba in 3:1 BFS:PC

This Chapter investigates the incorporation of $CsNO_3$ into 3:1 BFS:PC composite cement with varying weight percentages of $CsNO_3$. The incorporation of barium in the form of barium hydroxide ($Ba(OH)_2\,8(H_2O)$) and barium nitrate $Ba(NO_3)_2$ is also studied and discussed.

Chapter 5: Electrical Leaching of 3:1 BFS:PC

The basic nature of electrical leaching and its effects on cement matrices are studied using 3:1 Blast Furnace Slag:Portland Cement (BFS:PC) samples.

Chapter 6: Simultaneous Electrical Migration of Cs and Ba

This Chapter covers the use of electrical migration to introduce Ba as a simulant decay product of ^{137}Cs into simulated cementitious wasteforms that have already been cured, then analysis of the changes this brings to the crystalline phases present and the cement body as a whole is shown.

Chapter 7: Conclusions and Suggestions for Future Work

This Chapter summarises the results obtained in this project, concludes the outcomes and suggests possibilities for future avenues of research.

Appendix

The Appendix contains additional figures and information.

1.4 References

[1] N. J. Bowmer and S. Curwen, "WP1- Details of encapsulation processes at Sellafield." BNFL Commerical, Sellafield, UK, p. 46, 2007.

[2] NDA, "Understanding activities that produce radioactive wastes in the UK," 2015. [Online]. Available: http://ukinventory.nda.gov.uk/wp-content/uploads/sites/2/2014/01/Understanding-activities-that-produce-radioactive-wastes-in-the-UK.pdf. [Accessed: 17-Jun-2017].

[3] C. A. Utton, "The encapsulation of BaCO3 waste in composite cements," University of Sheffield, Sheffield, 2006.

[4] O. Hussein, C. Utton, M. I. Ojovan, and H. Kinoshita, "The effects of BaSO4 loading on OPC cementing system for encapsulation of BaSO4 scale from oil and gas industry," *J. Hazard. Mater.*, vol. 261, no. 1, pp. 11–20, 2013.

[5] National Nuclear Data Centre, "Chart of Nuclides," 2016. [Online]. Available: http://www.nndc.bnl.gov/chart/. [Accessed: 17-Jun-2017].

[6] M. Ochs, I. Pointeau, and E. Giffaut, "Caesium sorption by hydtrated cement as a function of degradation state: Experiments and modelling," *Waste Manag.*, vol. 26, pp. 725–732, 2006.

[7] I. Yanase, J. Konakawa, and H. Kobayashi, "Influence of cesium nitrate and heating rate on densification and microstructure of Cs-deficient pollucite sintered body," *J. Am. Ceram. Soc.*, vol. 188, no. 20365, pp. 184–188, 2006.

[8] J. V. Hanna, L. P. Aldridge, and E. R. Vance, "Cs speciation in cements," in *Materials Research Society*, 2001, vol. 663, pp. 89–101.

[9] J. L. Provis, P. A. Walls, and J. S. J. van Deventer, "Geopolymerisation kinetics. 3. Effects of Cs and Sr salts," *Chem. Eng. Sci.*, vol. 63, pp. 4480–4489, 2008.

[10] E. Revertegat, C. Richet, and P. Gegout, "Effect of pH on the durability of cement pastes," *Cem. Concr. Res.*, vol. 22, no. 2–3, pp. 259–272, 1992.

[11] A. J. Parker, M. J. Joyce, C. Boxall, and A. J. Parker, "Radiometric detection of non-radioactive caesium flux using displaced naturally abundant potassium," *J. Radioanal. Nucl. Chem.*, pp. 769–776, 2016.

[12] F. Frizon, S. Lorente, and C. Auzuech, "Nuclear decontamination of cementitious materials by electrokinetics : An experimental study," *Cem. Concr. Res.*, vol. 35, pp. 2018–2025, 2005.

[13] K. Hashimoto, H. Kinoshita, W. Gashier, A. J. MacArthur, and H. Yokota, "Development of an electrical leaching technique - evaluation of leaching from a hardened cement body," *34th Cement and Concrete Science Conference, Sheffield*. University of Sheffield, 2014.

[14] W. Gashier, T. Miura, K. Hashimoto, R. J. Hand, and H. Kinoshita, "Leaching behaviour of cementitious nuclear wasteforms containing caesium and strontium," *Adv. Appl. Ceram.*, vol. 113, no. 8, pp. 447–452, 2014.

[15] J. Peterson, M. MacDowell, L. Haroun, and F. Monette, "Radiological and chemical fact sheets to support health risk analyses for contaminated areas," 2005. [Online]. Available: https://www.remm.nlm.gov/ANL_ContaminantFactSheets_All_070418.pdf.

[Accessed: 17-Jun-2017].

[16] A. Vollpracht and W. Brameshuber, “Binding and leaching of trace elements in portland cement pastes,” *Cem. Concr. Res.*, vol. 79, no. 1, pp. 76–92, 2016.

[17] C. A. Utton, E. Gallucci, J. Hill, and N. B. Milestone, “Interaction between BaCO3 and OPC/BFS composite cements at 20°C and 60°C,” *Cem. Concr. Res.*, vol. 41, pp. 236–243, 2011.

[18] Department of Energy & Climate Change, “Implementing Geological Disposal,” *White Paper*, 2014. [Online]. Available: https://www.gov.uk/government/uploads/system/uploads/attachment_data/file/332890/GDF_White_Paper_FINAL.pdf. [Accessed: 17-Jun-2017].

[19] OECD and Nuclear Energy Agency, “Cementitious materials in safety cases for geological repositories for radioactive waste: Role evolution and interactions,” 2009. [Online]. Available: https://www.oecd-nea.org/rwm/docs/2012/rwm-r2012-3.pdf. [Accessed: 17-Jun-2017].

[20] B. Lagerblad, “TR-01-27, Leaching performance of concrete based on studies of samples from old concrete constructions,” *TR-01-27*, 2001. [Online]. Available: http://www.skb.com/publication/18731/TR-01-27.pdf. [Accessed: 17-Jun-2017].

[21] T. Ekström, “TVBM-3090, Leaching of concrete,” 2001. [Online]. Available: http://portal.research.lu.se/ws/files/4827018/1766469.pdf. [Accessed: 17-Jul-2017].

[22] C. Carde and R. François, “Effect of the leaching of calcium hydroxide from cement paste on mechanical and physical properties,” *Cem. Concr. Res.*, vol. 27, no. 4, pp. 539–550, 1997.

[23] C. Carde, G. Escadeillas, and R. Francois, “Use of ammonium nitrate solution to simulate and accelerate the leaching of cement pastes due to deionized water,” *Mag. Concr. Res.*, vol. 49, no. 181, pp. 295–301, 1997.

[24] N. Otsuki, H. Minagawa, S. Miyazato, and T. Nishida, “Fundamental study on prediction of concrete deterioration caused by calcium leaching over 100 years,” *Proc. JSCE*, vol. 51, no. 679, 2001.

[25] M. Castellote, C. Andrade, and C. Alonso, “Nondestructive decontamination of mortar and concrete by electro-kinetic methods: application to the extraction of radioactive heavy metals,” *Environ. Sci. Technol.*, vol. 36, pp. 2256–2261, 2002.

[26] M. Castellote, C. Andrade, and C. Alonso, “Characterisation of transport of caesium, strontium, cobalt and iron ions through concrete by steady state migration and natural diffusion tests,” *Adv. Cem. Res.*, vol. 11, no. 4, pp. 161–168, 1999.

Chapter 2: Literature Review

2.1 Introduction

The following review introduces the scientific issues arising from the use of cement for the encapsulation of radioactive nuclear waste. The functioning of nuclear power is shortly summarised and the ensuing waste problems from electricity generation and waste disposal plans in the United Kingdom explained. The specific chemical composition and hydration reactions of Blast Furnace Slag : Portland Cement (BFS:PC) commonly used in nuclear waste disposal are presented, in order to discuss the chemical interaction of caesium (^{137}Cs) and barium (^{137}Ba) with the cement matrix, when they are intermixed during hydration. Previously studied techniques for the acceleration of leaching from cementitious wasteforms are reviewed, with particular attention given to electrical leaching techniques that use an applied current to force migration of ions into and out of hardened cement matrices as an alternative to the intermixing methods.

2.2 An introduction to nuclear fission and fission products

Since its invention, nuclear power has been important for the commercial generation of electricity, because of the large amount of energy it produces. Usable energy from nuclear reactions is gained through a process called fission, where interaction with an incoming neutron causes an atom to spontaneously split and releases energy [1]. The resulting fission products can undergo nuclear decay over time, emitting radiation [2], which poses a significant safety risk and needs to be safely contained for a long period of time [3].

Figure 0.1 shows the nuclear binding energy as a function of the nucleon number, the total number of neutrons and protons in the atom. When the nucleon number is above 62, fission can release energy in accordance with the conservation of mass and energy, shown mathematically in Equation 0.1, adapted from Einstein's equation of mass-energy

equivalence, where m_{fa} is the mass of the atom undergoing fission in kg and m_{fp} is the total mass of the fission products in kg, E is the energy released in Joules and c is the speed of light in a vacuum in ms^{-1} [1]. When the binding energy of the fission products is lower than the original atom, excess energy is released.

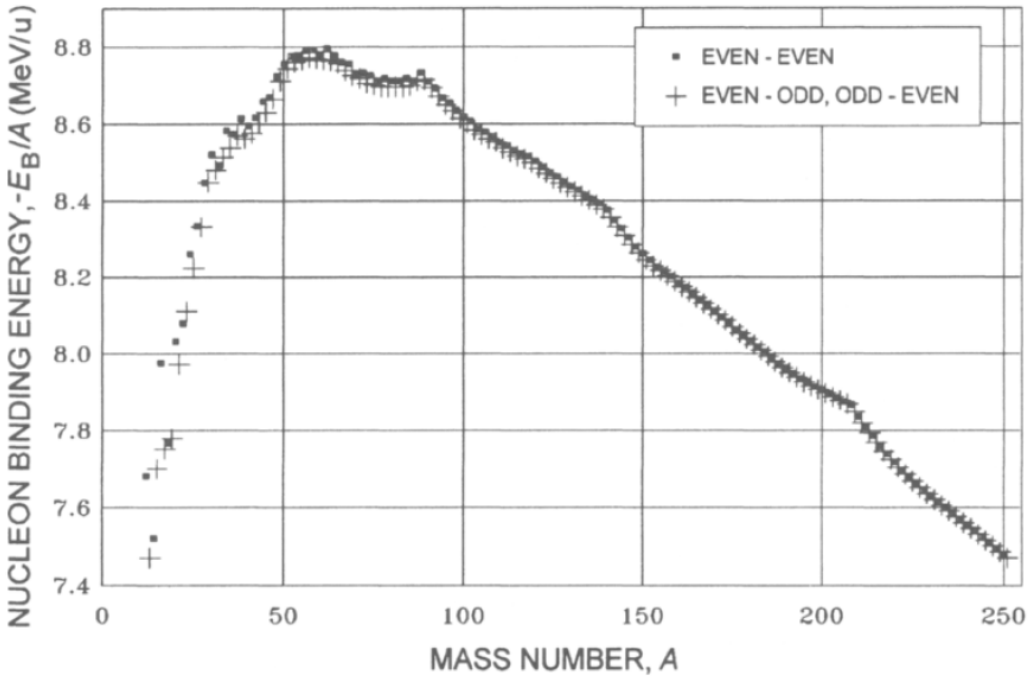

Figure 0.1 Nuclear Binding energy (E_B) per nucleon number(A), plotted against nucleon number for the most stable isobars (source: Choppin, 2002 [2])

$$E = (m_{fa} - m_{fp})c^2$$

Equation 0.1

Uranium 235 is the preferred fuel in nuclear reactors due to the large amount of energy produced when an incoming neutron transforms an atom of U-235 into U-236, which can then fission into various species. When this fission occurs, neutrons are also emitted, which in turn can induce fission in other uranium atoms [1] as illustrated in Figure 0.2. The heat produced from this chain reaction is the main source of energy in nuclear power plants [1], [4], [5].

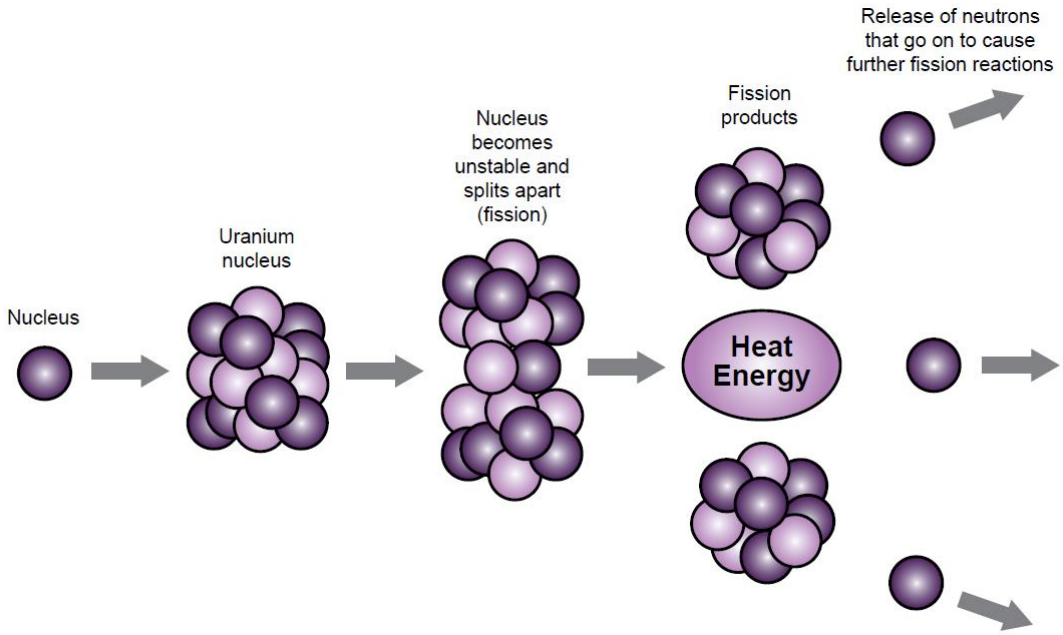

Figure 0.2 Fission of uranium 235 initiated by a free neutron [3]

When processing the spent fuel from the nuclear reactor, for example via the PUREX process [5], fission products are separated and classified as nuclear waste. There are three main classifications of nuclear waste which depend on their activity and potential for heat generation: High Level Waste (HLW) Intermediate Level Waste (ILW) and Low Level Waste (LLW) [6]. This PhD project focuses on ILW, of which there are 529 different waste streams in the UK [7]. ILW is waste that despite little heat production requires a high level of containment due to its contents of long lived isotopes – it has activity that is above the limits of LLW, 4,000 alpha radioactive decays per second per gram of the waste (4,000 Bq/g, Becquerel per gram), or 12,000 Bq/g of beta decay [8]. ILW can be in the form of solids such as the magnesium-aluminium alloy referred to as Magnox, which is used as cladding to surround fuel rods in Magnox reactors, or liquids such as floc slurries [9], [10]. This waste is typically encapsulated in a variety of cement mixes depending on its composition and stored in steel containers [5]. Because of the vast number of waste streams, it is unrealistic to develop a 'one size fits all' wasteform. Instead, it is important to focus on encapsulating problematic radionuclides

(problematic due to their half-life, mobility or activity [11]). Several examples of problematic radionuclides are shown in Table 0.1, all of which undergo Beta decay. Table 2.1 also includes the activity of these radionuclides in the 2D08 Magnox cladding waste stream, which is typical for ILW [7]. There are two different types of Beta decay: Beta minus (β^-), where a neutron in an atom emits an electron and electron antineutrino and becomes a proton, and Beta plus (β^+), where a proton emits a positron and electron neutrino and becomes a neutron [1]. Cs^{137} can undergo β^- decay, and Cs^{129} can decay by β^+ decay, as shown below (Equation 0.2). In nuclear waste, Cs^{137} is more common [7].

Table 0.1 Problematic Radionuclides in ILW and their specific activity in the magnox cladding waste stream "2D08" [7]

Isotope	Half-life (years)	Activity (MBq/g)	2D08 activity MBq/m^3 (01/04/2013) [7]	β Decay Energy (keV)
Cl^{36}	3 x 10^5	1221	12.9	27
Cs^{135}	2.3 x 10^6	4.44	113	67
Cs^{137}	30	3.26 x 10^6	5 x 10^6	190
I^{129}	15.7 x 10^6	6.66	3.65	40.9
Sr^{90}	29	5.18 x 10^6	3.67 x 10^6	200

$$\beta^-: {}^{137}_{55}Cs \rightarrow {}^{137}_{56}Ba + e^- + \bar{V}_e$$

$$\beta^+: {}^{129}_{55}Cs \rightarrow {}^{129}_{54}Xe + e^+ + V_e$$

Equation 0.2 examples of β^- and β^+ decay [1]

2.2.1 Nuclear Waste Disposal

For reasons of safety and regulatory compliance, a solid wasteform that is simple to produce, handle and transport is required [3]; cement is used as a wasteform matrix because it has a high workability, is relatively cheap and shows durability [9]. It also has two important effects in terms of immobilisation: chemically, it has a high internal pH level and acts as a selective binder for species found in radioactive waste, and physically, it can act as a barrier to prevent the waste from escaping.

In the UK, there are two main plans for the ultimate disposal of nuclear wasteforms, which are contained in steel canisters: A Geological Disposal Facility (GDF) and Deep Borehole Disposal (DBD) [11]–[14]. For this thesis, only GDFs are relevant as at this time DBD is being researched to dispose of HLW only [14]. The GDF has a longer history with more research both already conducted and ongoing, and can be used to store both ILW and HLW. Disposal via a GDF would consist of a multi-barrier approach to disposal of the waste, specifically designed depending on the geology of the chosen location [13]. This location will be chosen on a voluntary basis [15]. As the Geological Disposal fact sheet of the Office of the Nuclear Regulator shows [13], the wasteform in a GDF will be contained by three engineered barriers and one natural barrier. The first two barriers are the Wasteform itself, with ILW sealed in a cement composition depending on the source of the waste [3], [7], [16], which is then stored in a steel canister as shown in Figure 0.3. The cement-ILW mixture is then topped off with a capping consisting of Pulverised Fuel Ash (PFA) and PC at PFA:PC = 3:1 with a water to solid ratio of 0.43:1. The water to solid ratios are used to achieve a high fluidity in the cement to assist in the initial pouring into the steel drums [3], [7], [16], [17].The third barrier is planned to be a backfill of cement, possibly one which is called Nirex Reference Vault Backfill (NRVB). The fourth and final barrier will be the natural host geology, the bedrock surrounding the facility itself [13].

Figure 0.3 Photograph of a 500 litre sectioned drum containing immobilised Magnox Swarf (simulated waste) [3]

Figure 0.4 shows a visual representation of the first three barriers held within the host rock. NRVB is a mixture of PC, lime flour, hydrated lime and water with the mass basis ratios PC:LimeFlour:$Ca(OH)_2$:H_2O with 30: 11.333 : 33 : 41 as of 2017 [18], [19]. NRVB has several properties that make it suitable as a backfill, such as high initial viscosity, which would ease the initial pouring around the steel canisters of waste. A key reason its use has been suggested is that it can increase the pH of the incoming groundwater, which helps to limit the solubility of the transition metals and actinides present in the waste.

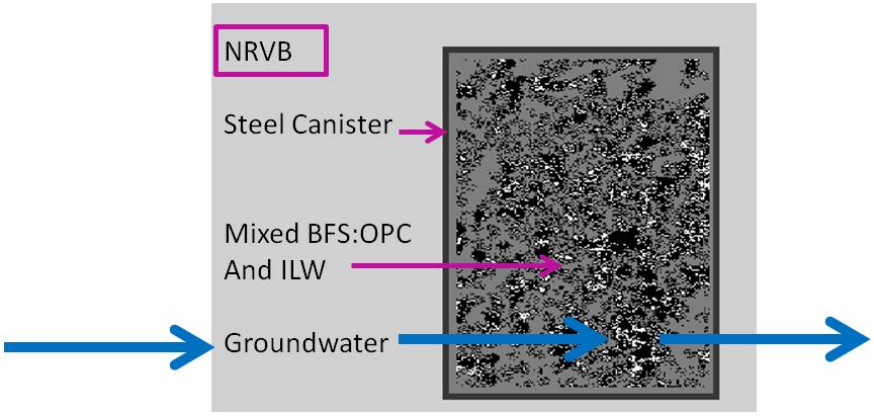

Figure 0.4 Cross-section of NRVB surrounding a canister of ILW

As any GDF is expected to have a lifetime of thousands of years and is or will become lower than the water table, it is possible that groundwater will eventually breach the engineered barriers. If groundwater penetrates the cement, dissolution and subsequent diffusion of the contents of the wasteform could occur and movement of radionuclides still present in the

wasteform is possible given the half-lives of the problematic radionuclides like isotopes of Cs [20]. For obvious safety reasons, it is extremely important to understand fully how Cs behave in and move out of cement matrices. The draining away of a soluble chemical from a substance such as soil or rock due to interaction is referred to as leaching. This thesis focuses on leaching from cementitious materials.

2.3 Hydration of Blast Furnace Slag – Portland Cement Composites

A blend of Blast Furnace Slag (BFS) and Portland Cement (PC) is commonly used for waste encapsulation, with the specific ratio varying depending on the composition of the waste [7], [9], [21]. A blend commonly used for acceptance tests for waste encapsulation in the UK is BFS:PC=3:1 [22], whilst ratio of 3.44:1 is a common formulation used in practice [23]. Some previous studies have also focused on 9:1 ratio [24]. Blends of BFS:PC are commonly used because they have a low redox potential, which reduces the solubility of several nuclides [25]–[27]. Usually, around 1% of sulphide sulphur is dissolved in the glassy slag and becomes available for reactions during hydration, which is understood to induce this low redox potential [9].

2.3.1 Portland Cement

The first record of what was then called PC dates back to 1824, when it was patented by Joseph Aspdin as “an improved method of producing artificial stone [… which he called] Portland cement” [28]. The method of production has vastly improved since then [29], and no longer involves taking limestone “from the roads after it is reduced to a puddle or a powder” [28]. Portland cement is a type of hydraulic material that hardens when put in contact with water, and since 1824 has become one of the highest mass produced material, with 4 x 10^9 tonnes being produced in 2013 [30]. PC is produced in several steps. Raw

materials such as limestone and clay are finely ground and mixed together with a typical weight ratio of 3:1. This mixture, as seen in Table 0.2, is then ground again and put into a rotating kiln, which is heated to a temperature of 1450°C. This is known as the fusion temperature [31], which is high enough to induce a phase transition and sinter the materials into small nodules of clinker with the composition shown in Table 0.3. The weight percentage of the different raw ingredients, as listed in Table 0.2, can vary due to impurities in the limestone and clay used, which in most modern processes is controlled to produce a clinker product with a specific phase composition. PC clinker consists of four main phases: tricalcium silicate (C_3S), dicalcium silicate (C_2S), tricalcium aluminate (C_3A), and tetracalcium aluminoferrite (C_4AF). The most prominent clinker phases are C_3S and C_2S. The clinkers' chemical information are listed in Table 0.3.

Table 0.2 Cement clinker raw ingredients

Source	Name	Amount in %
Limestone	Calcite ($CaCO_3$)	60-70%
Clay	Silica (SiO_2)	20-25%
	Alumina (Al_2O_3)	5-10%
	Ferric Oxide (Fe_2O_3)	2-3%

Table 0.3 Main Clinker phases present in PC

Mineral Name	Abbreviation (Cement chemist notation)	Chemical name	Chemical formula
alite	C_3S	tricalcium silicate	$(CaO)_3 \cdot SiO_2$
belite	C_2S	dicalcium silicate	$(CaO)_2 \cdot SiO_2$
celite	C_3A	tricalcium aluminate	$(CaO)_3 \cdot Al_2O_3$
brownmillerite	C_4AF	tetracalcium aluminoferrite	$(CaO)_4 \cdot Al_2O_3 \cdot Fe_2O_3$

To turn the Portland clinker into PC powder, the clinker is interground with gypsum ($CaSO_4 \cdot 2(H_2O)$). Upon hydration, C_3S develops the early strength of the cement produced, and C_2S contributes to the strength in the later stage due to the slow hydration [32]–[34]. The

reaction of C_3A (and C_4AF to a lesser extent [35]) with water is rapid and needs to be slowed down by the addition of gypsum – the cement would otherwise set too quickly to be usable [32]–[34]. As proposed by Minard et al. [36], the absorption of sulphate ions originating in the gypsum onto reactive dissolution sites reacting to form ettringite is the likely mechanism for this retardation. In suitably sulphated PCs, the most significant hydration reaction of C_3A occurs shortly after the peak in the reaction of C_3S, and the rate of this reaction accelerates 15-18 hours after initial hydration [35].

When the prepared cement powder is mixed with water, the cement cures in two stages. The first, known as setting, is the initial period where the cement paste develops rigidity, transforming from a liquid to a solid, which is typically completed within the first 7 hours of curing. ASTM International states that the maximum acceptable time of setting for all applications should be 375 minutes [37]. It then undergoes hardening as C-S-H (the main binding phase) and other crystalline phases such as portlandite ($Ca(OH)_2$) in the cement develop and interlock, leading to a porous network of phases.

C_3A, C_4AF and gypsum react through hydration to produce the calcium sulphoaluminate phases ettringite $C_3A{\cdot}3CaSO_4{\cdot}32H_2O$ (an AFt phase) and monosulphate $C_3A{\cdot}CaSO_4{\cdot}(11\text{-}19)H_2O$ (an AFm phase – there can be 11-19 water molecules depending on the w/s ratio used [29]). AFt and AFm phases are named using the cement chemist notation – AFt typically has three molecules of $CaSO_4$ (anhydrate) and AFm has one, with ‘t’ and ‘m’ denoting ‘tri’ and ‘mono’ respectively [29]. AFm can form from a conversion of Aft when the ratio of gypsum to C_3A is low, but this reaction can take an extended period of time to complete – at higher ratios the two phases can coexist [29]. Monocarbonate ($C_3A{\cdot}CaCO_3{\cdot}11H_2O$) can form in cements when

$CaCO_3$ originally present in the cement reacts with C_3A, and also when atmospheric CO_2 reacts with the pore solution [34]. Hemicarbonate can form when atmospheric CO_2 reacts with portlandite in the presence of monosulphate. It has been noted that further reaction with calcite can cause the formation of monocarbonate [34]. These reactions mostly occur within the first 24 hours of curing [38].

The heat evolution of the cement can be observed using Isothermal Conduction Calorimetry as well as the electrical conductivity as displayed in Figure 0.5 [39]–[42]. In the first stage of the heat evolution, where water first comes into contact with PC, a rapid reaction occurs causing OH^- and Ca^{2+} ions to be released from the surface of C_3S, and the pH of the paste reaches 12 – this is known as the initial hydrolysis (marked as I in Figure 0.5). There is a high degree of undersaturation, so that the dissolution of the clinker is rapid and the formation of etch pits (holes on the surface of the clinker particles as dissolution occurs) is energetically favourable [35]. This is followed by the induction period marked as II in Figure 0.5, and the ions continue to dissolve until the end of this period where, according to the geochemical theory of Portland cement hydration [35], the mixture reaches a critical supersaturation of portlandite at a ratio of about 1.4 times the saturation concentration of portlandite in the pore solution, and both portlandite and C-S-H begin to form rapidly. This acceleration period (marked as III in Figure 0.5) occurs between 2.5 and 7 hours after initial contact with water [42]. C-S-H develops at the surface of C_3S, and Portlandite starts to crystallise from the solution. After this period, the reactions begin to slow down as hydration continues (IV). This is because a critical degree of undersaturation is being reached where new etch pits can no longer form [35]. The main dissolution mechanism that occurs from this point on is called step retreat [35], where the walls of the etch pits 'retreat' (e.g. the pits get wider) in cohesive

pieces, giving the pits a step like appearance. Eventually the rate of hydration is determined by the diffusion of reactants (e.g. unhydrated material and H_2O) through the C-S-H layer, known as the steady state period (IV). This final period lasts longest, as it continues until all the material has reacted, with even twenty-year-old cement exhibiting changing behaviour over time [43].

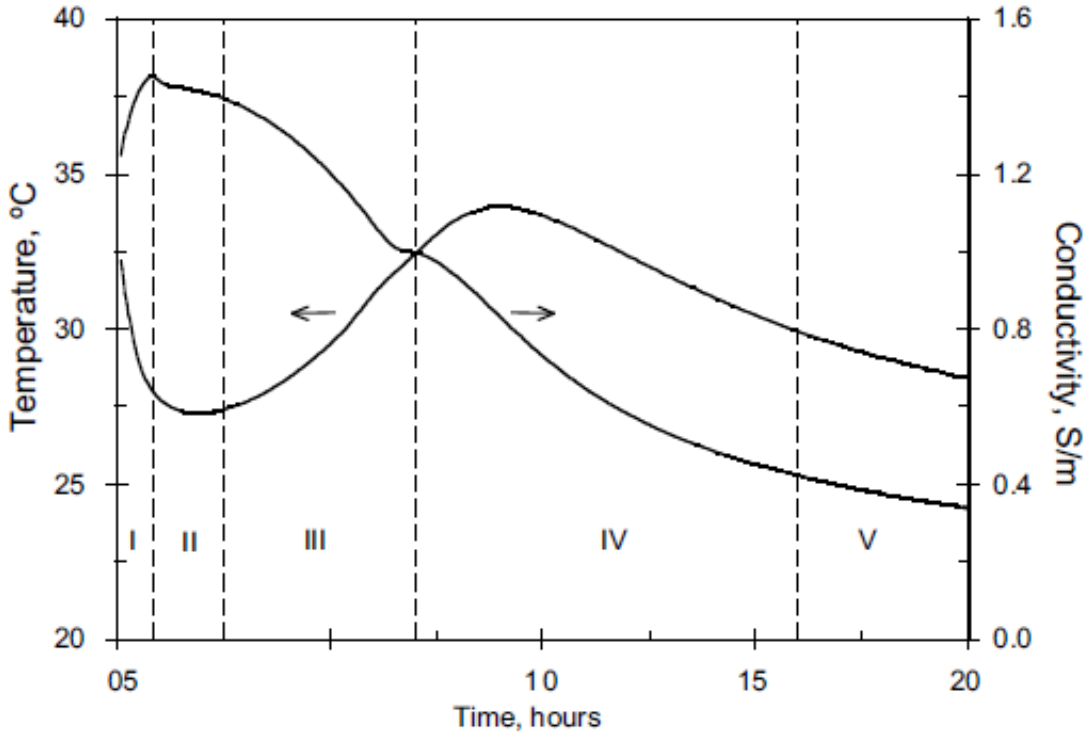

Figure 0.5 Heat evolution and electrical conductivity of PC during the first five stages of hydration[41]

2.3.2 Blast Furnace Slag, and BFS:PC hydration

The hydration of cement is heavily exothermic, especially in the first twenty four hours of curing – the heat produced is typically 200J/g [40]. To change the chemical and structural composition of the cement, Blast Furnace Slag (BFS), a Supplementary Cementitious Material (SCM) is added to PC which reduces the heat of hydration, lowers the amount of CO_2 produced, improves the workability, and ultimately results in a long term increase of the compressive strength of the final product [33], [44], [45]. Blast furnace slag (BFS) is a by-product of the iron making industry. The slag floats to the top of the molten iron with a

temperature of around 1440°C and is then decanted and quenched with jet streams of water to below 800°C [9], [46]. The cooled slag is hydraulic and has a glassy granular structure after quenching, and is then dried and ground into a powder with a similar fineness to PC, so that it can then be mixed with PC and water [47]. Some manufacturers instead interground the BFS with PC to obtain a consistent commercial product. The use of slag to produce glass has also been investigated [48]. The main phases present in BFS can vary depending on the composition of the original ore used in the iron making process, and the fineness can vary from batch to batch from the same vendor which can affect the reactivity [49]. It typically consists of the following constituents: CaO (40%), SiO_2 (35%), Al_2O_3 (12%), MgO (10%), Fe_2O_3 (0.2%) [47], [50]. The overall glass content of the BFS depends on the cooling rate of the slag (i.e. how quickly it is quenched), which along with the chemical composition and the fineness of the particles after grinding affects the reactivity when it is ultimately mixed with cement powder and water [46]. For the purpose of waste encapsulation, as a low heat of hydration is desired, a coarser BFS is used, which helps to lower the reactivity, because it has a lower surface area per unit volume. It is common to observe gehlenite in BFS, which is a mineral in the mellilite group [31], [43], [44], [48].

The main mineral phases observed in BFS:PC composites are shown in Table 0.4. When cement paste is produced using a mixture of PC and BFS, the main phases formed in the cement paste are reported to be C-S-H gel, portlandite, the sulphoaluminate phases AFt and AFm and a hydrotalcite phase rich in magnesium and aluminium [51]. The AFt and AFm phases are usually formed as ettringite and monosulphate. As shown in Equation 0.3, silica phases present in the BFS can react with portlandite to form a C-S-H gel, and it has been shown by Richardson et al. [45] and discussed by Gruyaert [44] that the reaction of portlandite in this

manner actually drives the acceleration of portlandite production and consumption during the initial setting and early curing.

$$3Ca(OH)_2 + 2(SiO_2) = Ca_3Si_2O_7 \cdot 3H_2O$$

Equation 0.3

Table 0.4 Main phases present in BFS:PC [39]

Name/Abbreviation	Chemical formula
gypsum	$CaSO_4 \cdot 2H_2O$
calcite	$CaCO_3$
gehlenite	$Ca_2Al_2SiO_7$
portlandite	Calcium hydroxide, $Ca(OH)_2$
hydrotalcite	$Mg_6Al_2(CO_3) \cdot (O\ H)_{16} \cdot 4(H_2O)$
ettringite, AFt	$Ca_6(Al(OH)_6)_2 \cdot (SO_4)_3 \cdot (H_2O)_{26}$
monosulphate, AFm	$Ca_4Al_2(S\ O_4) \cdot (OH)_{12} \cdot 6(H_2O)$
C-S-H	$Ca_3Si_2O_7 \cdot 3H_2O$*
hydrogarnet	$Ca_3Al_2(OH)_{12}$
monocarbonate	$(Ca_4Al_2(OH)_{12})(OH_{0.4}(CO_3)(H_2O)_3$
hemicarbonate	$(Ca_4Al_2(OH)_{12})(OH_{0.4}(CO_3)_{0.8}(H_2O)_4$
strätlingite	$Ca_2Al_2(SiO_2)(OH)_{10} \cdot 2.5(H_2O)$

* this is just one potential chemical formula, as the stoichiometry of the C-S-H gel phase is not fixed. Especially in slag-rich binders, the Ca/Si ratio can be lowered with the potential for a significant amount of Al substitution to form C-A-S-H gel [11].

The reaction rate of BFS is noted to be slower than PC, with the majority of the slag's reactions taking place after the first day of hydration [52]. According to a recent review of the hydration of PC, the early age strength of the hydrated product in PC:SCM blends is "mainly due to the reaction of [PC] clinker phases" [35]. The reviewers stated that the presence of SCM in the mix (which has a similar effect as BFS, as shown in the review paper) causes "relatively more space [to be] available for the hydrates of the clinker phases to form in" and "the surface of the SCM grains [to] act as sites for the heterogeneous precipitation and growth of hydrates." This enhances the reaction of the clinker components through a filler effect. In another recently published review on the degree of reaction of slag (and fly ash) blended cements [38], several laboratories tested cement samples from the same batch using several 'degree

of reaction' analysis techniques, including selective dissolution by EDTA, consumption of portlandite analysed by mass balance, SEM-image analysis, and especially XRD-PONCKS. The collaboration found that the techniques used to find the degree of hydration had at best a low precision with an absolute uncertainty of ±5%.

2.4 Incorporation of caesium into cement

Cs is a highly soluble/mobile element present in ILW [39], [51]. Whilst there is a degree of knowledge about the leaching of Cs out of cement [17], [53]–[55], the knowledge about its behaviour within the cement matrix is limited and requires further study [11]. In a series of tests lasting up to 40 days where $CsNO_3$ solution was shaken in containers with powders of various PC clinker and hydration phases, Crawford et al. [56] found that there was a small (e.g. not significant) decrease in Cs concentration observed. From this observation they concluded that 'the surfaces of the principle hydration products [in PC] have no sites suitable for sorption of large positive ions' Crawford et al., 1984 [56].

This however, was not a complete picture. Later research showed that Cs simply has a low sorption rate in cement, as Ochs reported in 2006 that in a PC matrix, Cs will mainly remain in the pore solution and sorb onto the C-S-H gel over time with a high variability depending on the composition and SCMs used. Ochs et al. had tested the powdered CEM I to CEM IV in a similar setup to Crawford et al, but their experiments were significantly longer, lasting for 9 months. Ochs et al. stated that Cs competes for sorption sites on the C-S-H structure with other alkali cations present in the pore solution [57]. However, there is little data in the literature on BFS:PC cement systems. The different phases present in cement have different binding capacities, and so the composition is important for a cement matrix – the retention of Cs for instance has been found to increase with increasing $CaO:Al_2O_3$ [26].

Hanna et al. showed that Cs remains in solution regardless of whether BFS is included in the cement matrix, suggesting there is little interaction of the Cs with BFS and its hydration products [58]. Gashier et al. used a 9:1 BFS:PC cement to incorporate 3 wt.% of elemental caesium using $CsNO_3$ with respect to the total weight e.g. "The amount of [$CsNO_3$ was] calculated to provide 3 wt.% of elemental Cs […] with respect to the total weight of the mix (OPC+BFS+water+nitrates)" [17]. They found that formation of portlandite and hydrotalcite seemed to be suppressed by the introduction of $CsNO_3$ into the system, and also observed a precipitation of $CsNO_3$.

2.5 Incorporation of barium into cement

According to Evans [26], barium is able to replace calcium in cement hydrate phases, whilst Vollpracht showed that it precipitates as barium sulphate when added to cement as barium carbonate [59]. Some research has also examined the incorporation of barite ($BaSO_4$) into cements for radiation protection [60]–[62], where the main objective is to identify cement compositions with suitable structural properties. The incorporation of barite has also been investigated, which, depending on its origins, can be classified as a LLW [51]. The formation of gypsum, thaumasite and ettringite in cements can be enhanced in the presence of sulphate-rich soils, which can induce cracking in the cement due to volume expansion [63]. This sulphate attack can be prevented by the addition of witherite (barium carbonate, $BaCO_3$) [64] with synthetic ettringite being observed to decompose in its presence during the first 24 hours of exposure [65] according to Equation 0.4 – this reaction has been observed from room temperature up to 40°C. Carmona-Quiroga and Blanco looked at the effects of using witherite as a gypsum substitute in white cements (cements with a little to no C_4AF) in an attempt to inhibit sulphate attack on cements [66]. The authors stated that the added 10 wt.% of $BaCO_3$

reacted with sulphates in the clinker, "favouring $BaSO_4$ and calcium monocarboaluminate over primary ettringite precipitation" [66]. The porosity of the mortars also increased. It is therefore reasonable to expect a rise in porosity and barite precipitation with increasing amounts of barium incorporation. The studies presented in the literature all examined the incorporation of barium or barium compounds directly into cement as a part of raw materials during mixing, and thus, there is a lack of data on the interaction of barium with hardened cement bodies, such as what will occur in nuclear wasteforms when caesium encapsulated inside cement decays into barium.

$$Ca_6Al_2(SO_4)_3(OH)_{12} \cdot 26H_2O + 3BaCO_3 \rightarrow 3BaSO_4 + (1-x)Ca_4Al_2(CO_3)(OH)_{12} \cdot 5H_2O + (2+x)CaCO_3 + 2xAl(OH)_3 + 21H_2O$$

Equation 0.4

2.6 Leaching of Cement and Accelerated leaching techniques

2.6.1 Leaching

For nuclear wasteforms, leaching is one of the most significant form of degradation [5]. Leaching is a joint diffusion-dissolution process driven by a chemical potential gradient among the hardened cement structure, the pore solution in the cement, and the properties of the external environment such as chemical composition and temperature [51]. Hardened cement has a porous network filled with an aqueous solution containing a mixture of different ions. In the case of a flowing groundwater environment, the aqueous solution in the pores of the cement diffuses into the surroundings. As the hardened cement seeks to remain in chemical equilibrium with the pore solution, and the pore solution is diffusing out of the matrix, the hardened cement dissolves into the pore solution over a period of time with a continuous effect [67]. As shown by Revertegat et al. [68], in pure PC cement pastes the degradation is mainly driven by portlandite dissolution and subsequently dissolution of a decalcified C-S-H phase, allowing the Ca/Si ratio of the C-S-H to be an adequate measure of the leaching

progression. The decalcification causes an increase in the overall porosity of the cement [67] and a decrease in both the flexural and compressive strength [69], [70]. The next phases to be leached are the AFm phases and the ettringite, as shown by Adenot et al. [71]. They proposed a numerical model, where the depth of the diffusion propagating into the sample correlated with the square root of time. This model was developed in order to take into account the three concentric leaching zones and the fact that the pore solution is assumed to be in chemical equilibrium with the surrounding solid cement at every point in the cement paste [71]. It is also common for Na and K to have high leaching rates because they are commonly observed in the pore solution [72], and Si tends to have low leaching rates due to the low solubility of quartz (SiO_2).

2.6.2 Static and Semi-Static Leaching

The standard leaching test to carry out is a static or semi-static leaching test, where a cement sample is submerged in water for a period of time. The ASTM C1220-10 standard is the most commonly used static test for the testing the leaching of general radioactive wasteforms [73], whilst the ANSI/ANS 16.1 standard is a more widely accepted semi-static leaching test for cementitious wasteforms [74]. The semi-static leaching test is a variation of the static leaching tests. Here, the entire leachate is replaced at regular intervals. Faucon et al. found that, by placing model cement pastes in demineralised water, the local chemical equilibrium drove leaching [75]. This model is illustrated in Figure 0.6. Because leaching begins at the surface exposed to the leachant, they showed a gradient in the leaching of calcium depending on the depth, which leads to an unaltered zone within the sample that gets smaller as the test progresses.

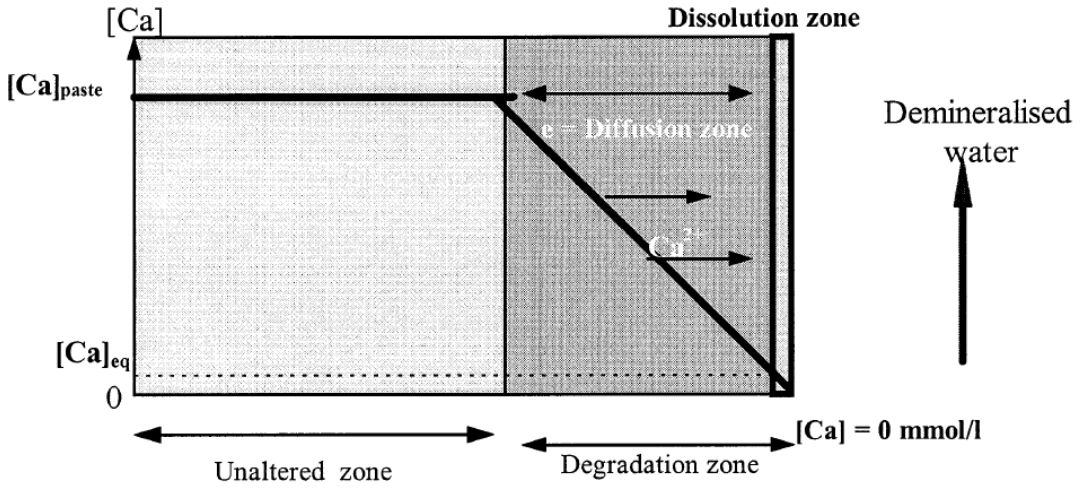

Figure 0.6 "Model of the progressive (but not necessarily linear) decrease in [Ca^{2+}] in interstitial solution" [75]

As past research has shown, there are abrupt edges in the dissolution when leaching takes place [76], and the point between the unaltered zone and the degradation zone is known as the dissolution front. The progress of the leaching can therefore be measured by the depth of these dissolution fronts and the amount of soluble species separated from insoluble species by percolation or filtering the leachate through the cement sample [77]. In 2005 Marion et al. published a paper [78] that among other things examined whether BFS:PC paving slabs could contaminate the soil they were placed upon by conducting static leaching tests and examining the heavy metal content of the leachate and the slabs. They found that the leaching of slag-portland cement composites shows a similar mechanism to the leaching of Portland cement and that after 64 days of leaching the heavy metals contained in the leachate was low enough to be fit for human consumption [78] according to European Directive 98/83/EC [79]. The heavy metal elements analysed in the bulk cement and the subsequent leachate included Ag, As, Ba, Cd, Cr, Cu, Hg, Mn, Ni, Pb, Sb, Zn, and Se [78].

Fick's laws of diffusion mathematically define the relationships governing the diffusion and transport of ions and can be applied to their movement through a porous medium like cement. They use mass balance equations and assume/require instantaneous

dissolution/precipitation to maintain chemical equilibrium locally within the cement matrix between the solid phases and the interstitial pore solution. For a phase such as portlandite in the cement body that is both in the solid phase and dissolved in the pore solution, the total mass can be defined by *m*:

$$m = m_{sm} + m_{sol} = m_{sm} + \varphi\rho_{sol}$$

Equation 0.5

Where m_{sm} is the mass of the solid mineral, m_{sol} is the mass in the pore solution, ϕ is the connected porosity of the material, and ρ_{sol} is the 'real mass density' (e.g. concentration) of the material in the pore solution [76]. The diffusion coefficient D is related to the change in internal mass over time as displayed in Equation 0.6 below where ∇· is the standard gradient operator and ∇ is the standard derivative [80].

$$\frac{\partial m}{\partial t} = \frac{\partial \varphi\rho_{sol}}{\partial t} + \frac{\partial m_{sm}}{\partial t} = \mathrm{D}\nabla \cdot (\varphi\nabla\rho_{sol})$$

Equation 0.6

Taking calcium as an example, it is clear that within the cement matrix, Ca is present in several different minerals which form during curing. Therefore, to examine the leaching of Ca in cements, the above equation needs to be altered and fitted to experimental data in order to account for each mineral's Ca content and individual dissolution rates. A full derivation of this equation was laid out by Mainguy and Coussy [76], based on the work done previously by others [29], [69], [71], [75]. The effective diffusion coefficient for calcium D_{Ca} is shown in Equation 0.7 with a = 9.95 and D_0 = 2.35 m^2s^{-1}. Natural leaching is dependent on the equilibrium condition of the concentration in the solid C_{Ca} and the interstitial pore solution S_{Ca} shown in Equation 0.8, and the non-linear diffusion equation shown in Equation 0.9 [76]. The function $f(S_{Ca})$ has to be fitted to experimental data, for example the data shown in Figure 0.7 [81].

$$D_{Ca}(\varphi) = D_0 e^{a\varphi}$$

Equation 0.7

$$C_{Ca} - f(S_{Ca}) = 0$$

Equation 0.8

$$\frac{\partial[\varphi(S_{Ca})C_{Ca}]}{\partial t} + \frac{\partial S_{Ca}}{\partial t} - \nabla \cdot \left[D_{Ca}\left(\varphi(S_{Ca})\right)\nabla C_{Ca}\right] = 0$$

Equation 0.9

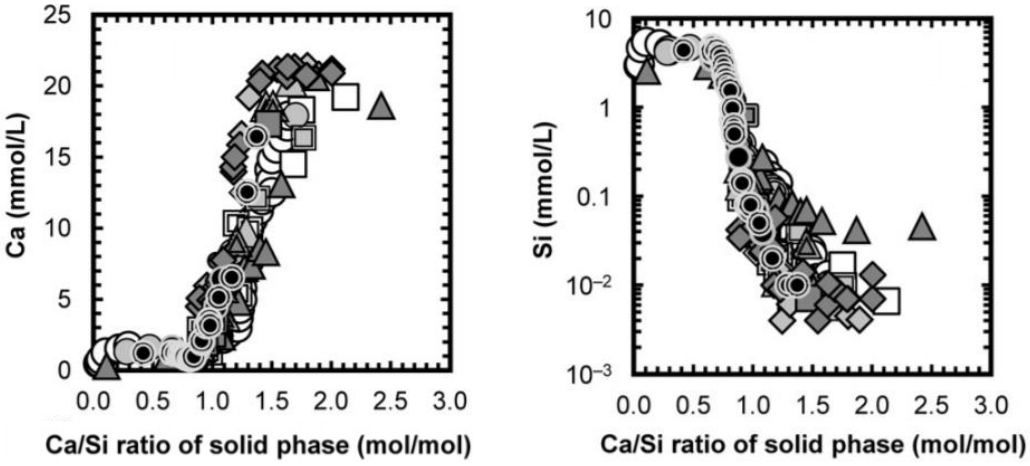

Figure 0.7 Normalised selected C-S-H gel solubility data, corresponding to a selection of 207 solutions at near-room temperature (17-30 °C) shown as the concentration in the pore solution of Ca (left) and Si (right) as a function of molar Ca/Si ratio of the solid phase (mol/mol) at equilibrium [81]

In the case of real concrete structures such as bridges, complete degradation of portlandite by natural leaching has been observed in the region of 4-9 mm from the surface after up to 100 years of exposure in various conditions, as found by Lagerblad [82]. They predicted that, when using slag composite cements, the degradation of portlandite would be less than 20 mm after a thousand years in the concrete water basins examined, as his research showed that the rate at which the leaching rate diminishes proportional to the square root of time.

2.6.3 Acidic Leaching

Leaching can further be driven by an enhanced chemical potential gradient through the cement paste [83], because a cement structure typically has a pH of 13 or higher and the groundwater can have a lower pH, causing a thermodynamic imbalance [82]. Acidic leaching is one method of conducting accelerated leaching tests on short timescales. It increases the dissolution of the cement, where an overall effect of up to 100 times leaching acceleration is

possible [84], i.e. a one-day acidic leaching test can remove a similar amount of material from a sample as a one-hundred day static test. Acidic leaching is similar to the static and semi-static leaching test in that a sample is placed in a leachant for a period of time, but it differs in that the leachant itself consists of a solution of NH_4NO_3 rather than demineralised water/simulated groundwater.

Conducting an acidic leaching experiment has the additional benefit of showing the behaviour of cement pastes under different pH conditions [68]. A common leachant used for this type of research is ammonium nitrate solution (NH_4NO_3), at various concentrations and resulting pH levels [54], [69], [84]–[86]. Carde et al. used ammonium nitrate at 50% concentration (pH 4.5) and showed that the leaching process was chemically similar to the static version, and that physically, material was removed also in a similar fashion, but on a shorter timescale due to the 'aggressive' environment [69], [84]. As in static leaching, deterioration is attributed to portlandite dissolution followed by a decalcification of the C-S-H phase [86]. Inside the cement, there is a basic (high pH) environment where the intruding (acidic) ammonium nitrate disassociates. The calcium present in portlandite reacts readily with nitrate as shown in Equation 0.10, producing calcium nitrate, a compound that has a high solubility and subsequently leaves the matrix. NH_3^+ is also released as a gas, and the calcium nitrate is able to react with hydrated aluminates present in the cement to form a nitrate AFm compound with the formula $3CaO{\cdot}Al_2O_3{\cdot}Ca(NO_3)_2{\cdot}10H_2O$ [85]. This can crystallise within the cement in dry conditions, so following acidic leaching, a high humidity or immersion in water is required until the sample is analysed to avoid the crystallisation, because the crystallisation is known to induce cracking in the cement, affecting the mechanical properties [84].

$$Ca(OH)_2 + 2NH_4NO_3 \rightleftharpoons Ca^{2+} + 2OH^- + 2H^+ + 2NH_3 + 2{NO_3}^- \rightleftharpoons Ca(NO_3)_2 + 2NH_{3g} + 2H_2O$$

Equation 0.10 [70]

The reaction to form calcium nitrate in the pore solution and its subsequent diffusion into the leachate reduces the Ca/Si ratio of C-S-H at an accelerated rate when compared with static and semi-static tests, and shows similar porosity alterations for the same degree of leaching [87], although the effects of the gaseous ammonia are controversial [83]. Some researchers believe the ammonia contributes to a reduction of the pH in the cement's pore solution [88] and thus prevents the reaction from reaching equilibrium, whereas others argue that its presence can be neglected entirely [89], as they suggest it has no effect on the dissolution of portlandite. A low pH level, however, has been found to increase the precipitation of silicon complexes, which may have an effect on the perceived dissolution of Si in the cement matrix in the presence of ammonium nitrate [90]. Whilst acidic leaching has been significant in studying the leaching behaviour of portlandite, it does not automatically favour diffusion [84] and may not be a suitable technique to investigate the diffusion of the pore solution in general, because it is "based on the application of chemicals which enhances the rate of [only the] calcium dissolution from the calcium containing phases" [91].

2.6.4 Electrical Leaching

Electrical acceleration methods "are based on the migration concept which enhances the transport of [all] charged species with an electrical field" [91]. When a potential gradient is applied to an electrolyte, either by planting electrodes internally to the testing materials or attaching them externally, anions present in the system will migrate towards the anode and cations move towards the cathode. This is known as electrophoresis [92]. As stated previously, cement has a porous network filled with an aqueous phase containing a mixture of different ions. When an electric field is applied to cement, it acts as an electrolyte allowing

an electric charge to be passed through it. The driving factor in the leaching of cement is the migration of calcium ions out of it [68]. An acceleration of this ion migration is therefore analogous to an acceleration of the leaching process. This is what occurs in electrical leaching [24], [93]. In addition to the accelerated ion migration, there are several differences in the chemical behaviour of ions in the pore solution during electrical leaching when compared to static leaching [94]: In electrical leaching test, the local chemical equilibrium is no longer valid because the movement of ions already present in the pore solution is accelerated [94]. In contrast, in static leaching, the rate of dissolution and precipitation in static leaching is assumed to be much faster than the transport of species, and locally chemical equilibrium is maintained throughout the cement body [82]. In electrical leaching with a potential gradient of 400 V/m, ions move through the cement body at a rate which is higher than the kinetics of chemical reaction [95], [96]. Agreeing with this, Yuan wrote that when an electric potential is applied (such as during electrical leaching) that "Most of the published results show that the influence of chemical activity gradient on the transport of ions is negligible" [97] but the chemical gradient is still significant in static leaching [82].

Utilising electricity to accelerate the leaching of cement was first presented by Saito et al. in 1992 [92], where they placed concrete disks (5 cm diameter, 1 cm height) produced with 1:1 PC to Toyoura sand (the JIS standard sand) and a 0.65 w/c ratio between two carbon electrodes held in distilled water as displayed in Figure 0.8. After initially using tap water as a leachant, they conducted their experiments later with distilled water. The tap water was found to contain so much initial Ca – roughly 25ppm – that the dissolving Ca^{2+} from the cement could not be detected after a certain point.

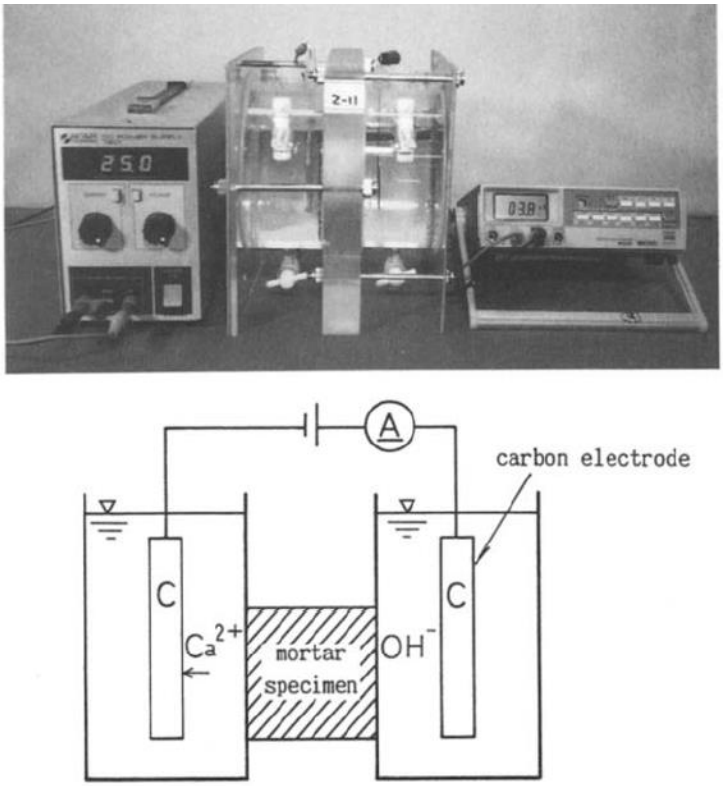

Figure 0.8 "Experimentation apparatus", photograph and diagram Saito et al, 1992 [92]

In their study, a constant voltage of 25 V was held between the two electrodes for 290 days, and the solution around the cathode was periodically collected. By using atomic absorption analysis, the concentration of Ca^{2+}, Na^+, and K^+ was measured. Saito et al. state that "applying a potential gradient to the specimen significantly accelerated the [leaching] of Ca^{2+}" [92] compared to a test with no applied current. The cumulative quantity of Ca measured in the leachate was 3590 mg in the electrical test compared with 318 mg in the static test. Na^+ and K^+ are also strongly leached and, in fact, leached faster than Ca with 90% of the Na and K content being leached in the first 12 days of the test [92]. The mechanism of these results, however, was not fully explained in their paper, and the movement of anions through the cement was not reported.

After 48, 92 and 290 days, the samples were analysed under XRD. After the 48-day test, the cathode and anode side of the cement specimen were separated and XRD revealed the

difference between the two samples. This data and the Ca concentration data are shown in Figure 0.9. Their XRD data illustrates that, after 48 days, portlandite (labelled as CH in Figure 0.9) was still present in the anode side of the sample. After 92 days this phase had been removed: the reduction of $Ca(OH)_2$ was seen to proceed gradually from the interface between the cement and the catholyte, and the control sample placed in the experimental apparatus with no applied electric potential still showed portlandite after 290 days. The XRD of the 290-day electrically leached sample displayed no crystalline C-S-H at all, with only broad lines attributed to SiO_2 gel. This is indicative of a completely deteriorated sample, which had "an extremely brittle condition" [92]. The reduction of portlandite and the subsequent decalcification of the C-S-H phase is similar to the alteration seen during the leaching of cement samples that occurs in the presence of a large quantity of water [68], but at a much faster rate, and progresses gradually from the side facing the cathode [92].

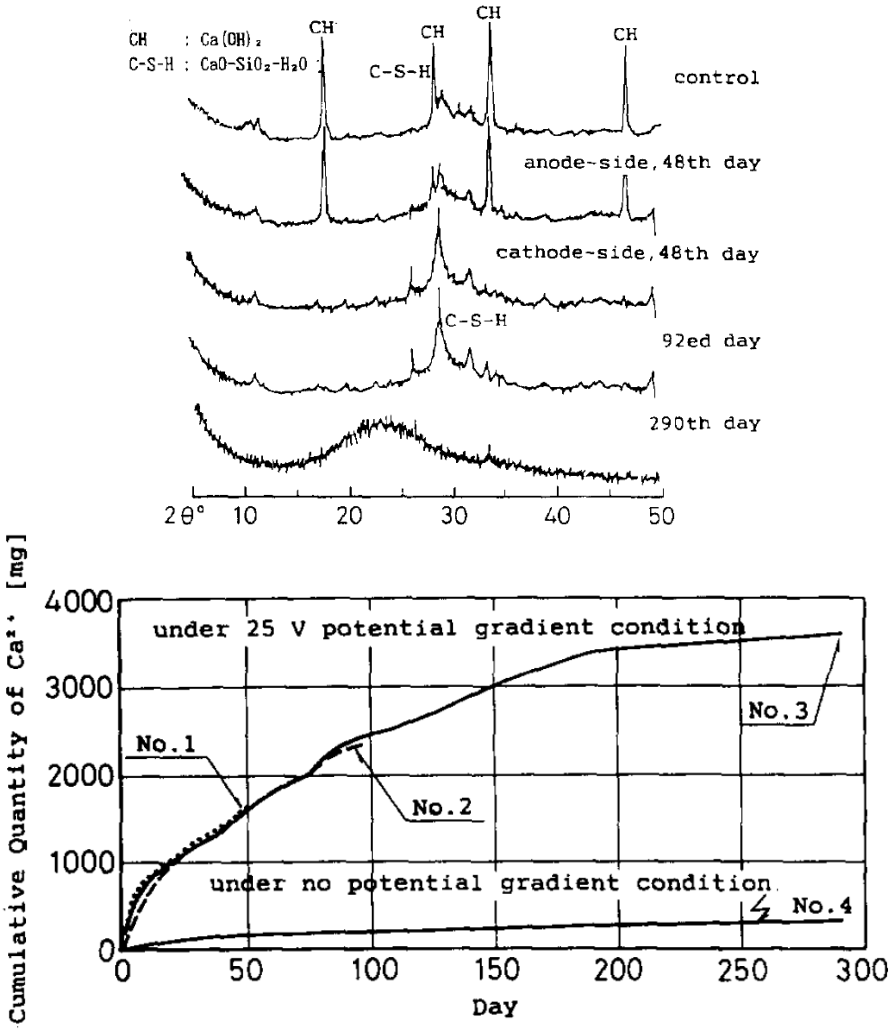

Figure 0.9 XRD of Saito's specimens (above), cumulative Ca^{2+} concentration after leaching under constant 25V and with no voltage applied (below) [92]

In 2000, Saito et al. published a second paper on electrical leaching [93], where they conducted electrical leaching tests using a similar setup to their previous work, this time however with a platinum anode and a stainless steel cathode, with a constant potential gradient of 10 V/cm applied. They tested different mortars with various sand/cement ratios, w/c ratios, and admixture compositions with either BFS or silica fume (SF), as listed in Table 0.5. Mortars 1-8 (group A) were cured in water for 4 weeks and 9-13 (group B) had 8 weeks of curing. Group A was then electrically leached for four months, and group B was electrically leached for six months.

Table 0.5 Mix proportions of the mortars used by Saito et al. [93]

Type of test		W/C	S/C	BF replacement ratio (%)	SF replacement ratio (%)
Test on different sand contents	No. 1	0.41	1.62	0	0
	No. 2	0.41	1.00	0	0
	No. 3	0.41	0.57	0	0
	No. 4	0.41	0.25	0	0
Test on different water/cement ratios	No. 5	0.32	0.67	0	0
	No. 6	0.41	0.77	0	0
	No. 7	0.50	0.89	0	0
	No. 8	0.60	0.97	0	0
Test on admixture replacement ratios	No. 9	0.41	1.00	30	0
	No. 10	0.41	1.00	50	0
	No. 11	0.41	1.00	70	0
	No. 12	0.41	1.00	0	10
	No. 13	0.41	1.00	0	20

The amount of Ca^{2+} ions entering the water varied with the mix proportions, and increased with increasing water/cement ratio. They concluded that their results reflect the differences in the quantity and quality of the cement hydrate phases present in the mortars. The pore volume after leaching is shown in Table 0.6. The compressive strength of their samples decreased as leaching occurred, which seemed to follow the increase in the pore volume in the cement as shown in Figure 0.10 and ties in with an increase in the water permeability. They stated that it is unclear whether the reduction in Ca^{2+} leaching in BFS:PC or SF:PC is simply due to a lower amount of Ca present in those samples: the data presented was not normalised and the chemical composition was not given. Ca was also the only element whose concentration in the leachant was discussed in the paper. In the unleached regions of the mortars the pore volume decreased by 5% to 18% after leaching, showing that, during the 4 and 6 months of the testing period, the cement hydrate structure "became tighter" [93] as the mortar continued to cure. The pore volume of the degraded region had also increased by about two times in group A and 40% to 50% in group B.

Table 0.6 Pore volume after leaching determined via MIP [93]

		Degraded region		Undegraded region		
		PV [cm^3/cm^3]	PV/V_p [cm^3/cm^3]	PV [cm^3/cm^3]	PV/Vp [cm^3/cm^3]	Remarks
Sand content	No. 1	0.274	0.505	0.142	0.261	S/C = 1.62
	No. 2	0.317	0.482	0.139	0.212	S/C = 1.0
	No. 3	0.357	0.463	0.166	0.215	S/C = 0.57
	No. 4	0.417	0.471	0.185	0.209	S/C = 0.25
Water/cement ratio	No. 5	0.311	0.435	0.123	0.173	W/C = 0.32
	No. 6	0.338	0.474	0.150	0.210	W/C = 0.41
	No. 7	0.384	0.537	0.210	0.295	W/C = 0.5
	No. 8	0.444	0.622	0.244	0.341	W/C = 0.6
Admixture replacement	No. 9	0.226	0.344	0.148	0.225	BF = 30
	No. 10	0.193	0.293	0.123	0.186	BF = 50
	No. 11	0.201	0.305	0.147	0.224	BF = 70
	No. 12	0.261	0.397	0.171	0.260	SF = 10
	No. 13	0.221	0.336	0.155	0.235	SF = 20

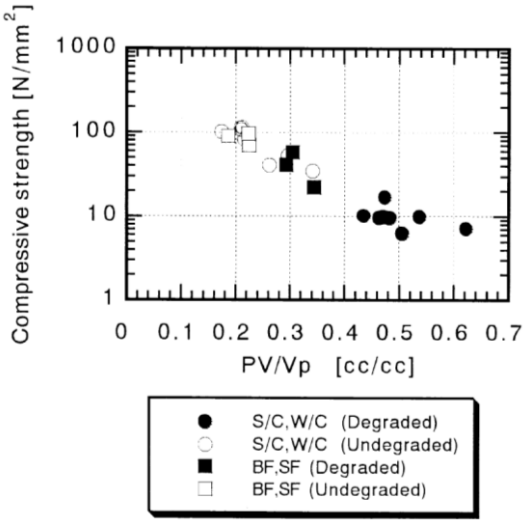

Figure 0.10 Relationship between PV (Pore Volume) and compressive strength [93]

Otsuki et al. compared 100 year old concrete with samples made using the same mix proportion that had undergone a combined diffusion and electrochemical test [98]. They applied the Vickers hardness test, the needle penetration test and a measurement of the Ca/Si molar ratio to analyse them. 10 x 10 x 40 cm concrete samples with a titanium mesh anode embedded inside were used for the electrochemical leaching test. This mesh was soldered to an electrical lead and placed 8.5cm above the base of the moulds before the cement paste was poured in. After 24 hours of curing the samples were cut into 10 x 15 x 3 cm pieces as shown in Figure 0.11 and sealed in epoxy resin, leaving one surface open to ensure that all leaching (material actually leaving the sample) occurred in one direction only.

The experimental setup was as shown in Figure 0.11, and a current density of 10 Am^{-2} was selected.

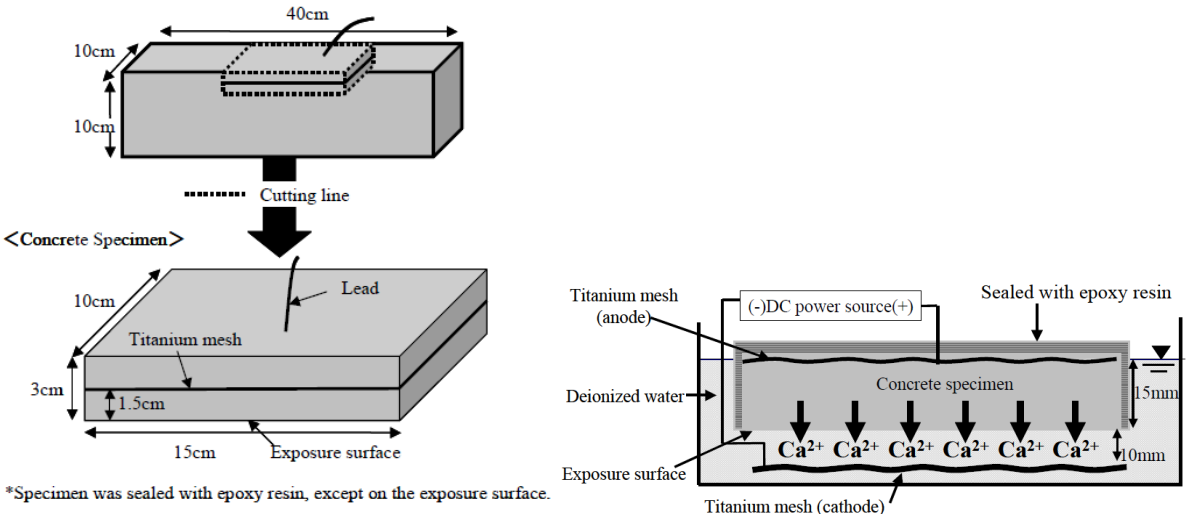

Figure 0.11 outline of Otsuki's concrete specimens and experimental setup [98]

This study stated that electrical leaching is a valid technique of accelerating the leaching and subsequent deterioration of concrete. A near linear relationship between the Ca/Si ratio and the Vickers hardness of the sample was discovered as shown in Figure 0.12, and, by comparing needle penetration test results with 100 year old concrete samples (as they did not have concentration data for the 100 year old samples), they stated that 100 years of leaching could be achieved in 1500 hours (62.5 days) using the above method. Comparing strength tests as well as the Ca/Si ratio between samples appears to be a valid technique of determining whether equal levels of degradation had occurred, however, Otsuki did not discuss the leaching and concentration of elements other than Ca present in the concrete samples. The effects of embedding the anode inside the cement sample were also not discussed. The leaching behaviour of cations other than Ca^{2+}, and of anions of a whole, needs to be investigated in order to test the validity of electrical leaching as a technique. The fact that leaching of other ions does not play a large role in natural leaching does not mean their role

can be discounted in electrical leaching. Without investigation, this cannot be assumed to be true – one of the purposes of this thesis is to examine whether this assumption is justified.

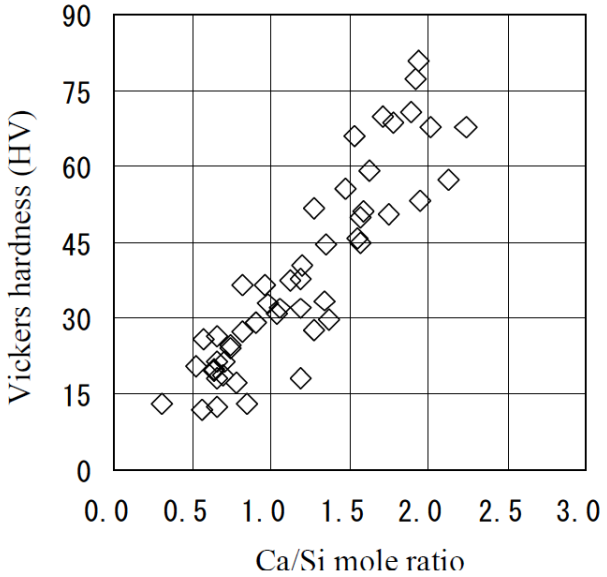

Figure 0.12 Relationship between Vickers hardness of the bulk concrete and the Ca/Si ratio

In a similar electrical leaching test discussed by Ryu et al. [99], a cement sample went through two periods of static testing for a short time with a period of electrical leaching in between displayed in Figure 0.13. After each test, they measured the Ca concentration in the leachate. This was done in order to convert the diffusion time, i.e. the time it would take for the equivalent amount of leaching to take place using a traditional static test;

$$V_{\mathrm{d}} = \frac{X_{\mathrm{d}}}{\Delta t A}$$

Equation 0.11 and Equation 0.12 below are used [99]. V_d = leaching rate of Ca per unit area (g/s m^2); X_d = amount of Ca that dissolved by the diffusion (g); Δt = diffusion test period; and A= exposure surface area of specimen (m^2). Equation 0.12 is used to convert the results, with $Td_{t\text{-}t'}$ = time for amount of Ca to leach out of the sample ($X_{t'}$ - X_t) during electrical leaching.

$$V_{\mathrm{d}} = \frac{X_{\mathrm{d}}}{\Delta t A}$$

Equation 0.11 [99]

$$T_{\mathrm{d}_{t-t'}} = \frac{X_{t'} - X_t}{\frac{V_{\mathrm{d}_t} + V_{\mathrm{d}_{t'}}}{2}}$$

Equation 0.12 [99]

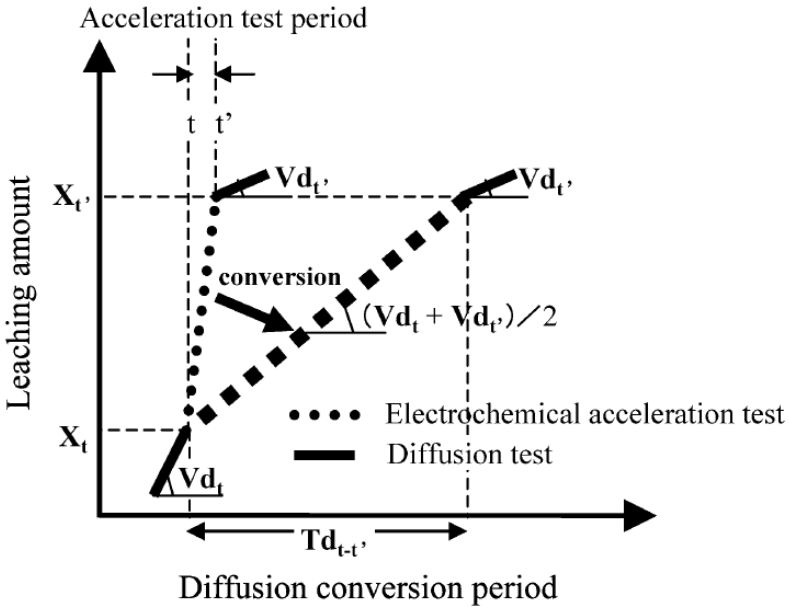

Figure 0.13 "Outline of the calculation for the conversion period" [99]

In a similar series of experiments to Saito et al., Hashimoto et al. [24] later conducted leaching tests, where a titanium mesh was embedded in cement mortar samples internally as an anode and was also used for the external cathode in order to examine the acceleration of Ca leaching. They applied a current density of 10 Am^{-2} across the sample, which was covered in epoxy resin apart from the exposure surface, as show in Figure 0.14. The mortar sample was cured in 50 ^{o}C water for 56 days before undergoing electrical treatment for 1000 and 2000 hours. The ratio of solution volume (distilled water) to exposure surface area was 100 cm^3/cm^2, and was kept constant during the test by replacing the leachant. It was observed

that the depth of degradation increased with increasing w/c ratio by measuring the $Ca(OH)_2$ weight concentration with thermogravimetric analysis (TG). XRD revealed that monosulphate and ettringite were also leached out. The Ca/Si ratio of C-S-H was decreased by the electrical treatment, and the cumulative pore volume was increased. They deduced that they had simulated over one decade of standard leaching after 1200 hours of electric leaching test, comparing their results with the work of Otsuki et al. [98].

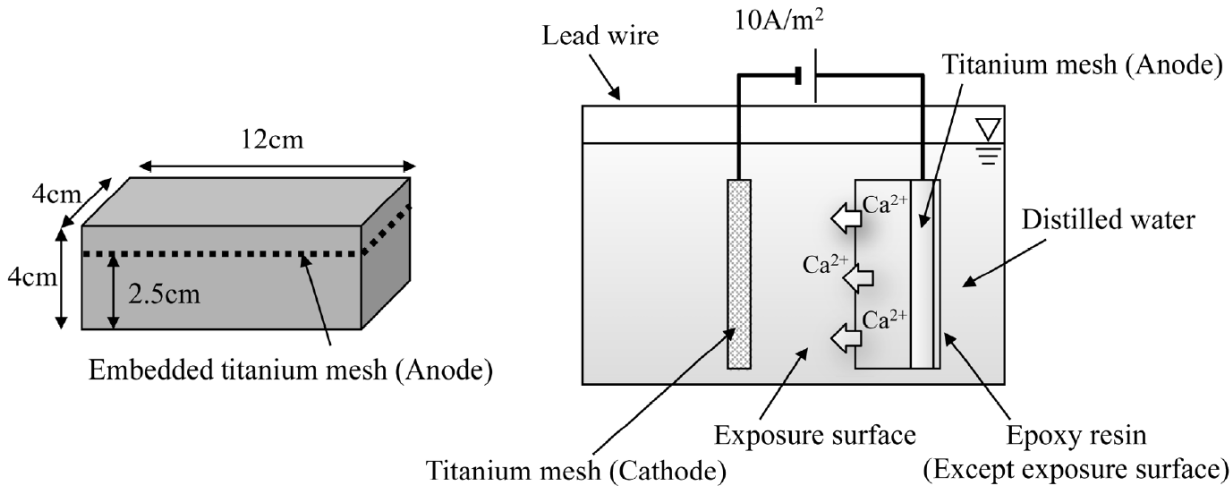

Figure 0.14 outline of mortar sample and electrical treatment setup

More recently Babaahmadi et al. published two papers [91], [100] expanding upon Saito's work on electrochemical leaching [93] with the aim of developing the technique to allow physical and mechanical testing of larger cement samples. The experimental setup discussed in the papers is shown in Figure 0.15 and was also "inspired by the rapid chloride migration test" [101] and the "Nordtest chloride migration method" [102]. The mix design of the cement samples was a Swedish structural Portland cement designated as CEM I 42.5N MH/SR/LA with a water to cement ratio of 0.5. The sample size used was cylinders of 50 mm diameter and 75 mm in length. In order to accelerate the dissolution of the portlandite (as well as the migration of ions out of the cement sample via the electric current), they used ammonium nitrate at a

concentration of 0.3M as the catholytic solution, thereby combining the acidic and electrical techniques in an attempt to further accelerate the leaching of calcium. The sample was held at an angle to prevent hydrogen gas produced at the cathode from accumulating underneath the sample.

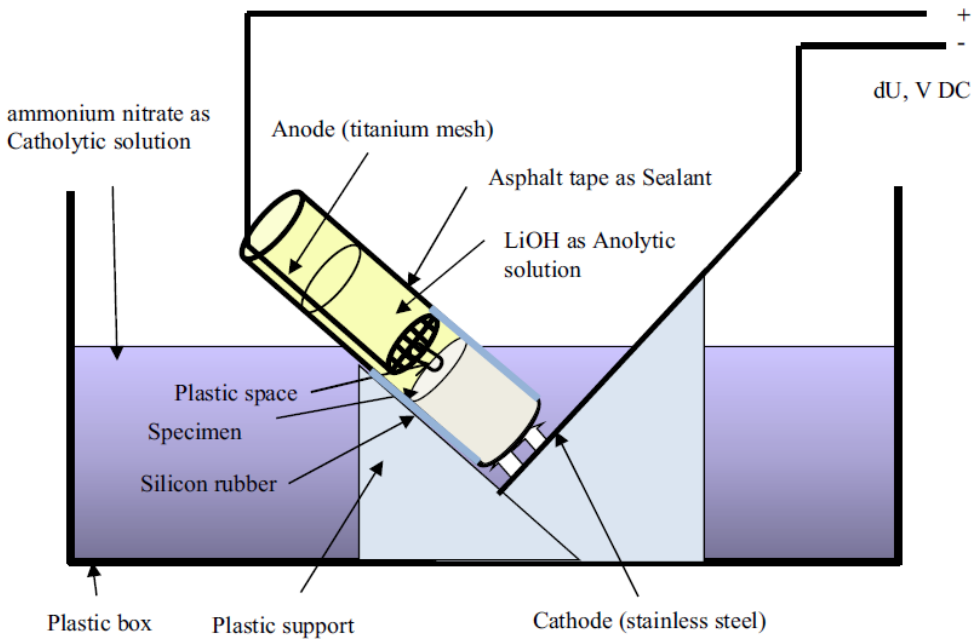

Figure 0.15 'Final setupdesign of electrochemical migration method', Babaahmadi et al, 2015 [91]

To make the anolyte solution, with an aim of maintaining the level of pH, a lithium hydroxide salt was chosen, as lithium is not present in the pore solution so that any lithium observed in the cement sample must have originated from the anolyte. The pH of the anolyte is usually reduced over time by the production of H^+ ions at the anode through electrolysis. This can induce some corrosion of the specimen in contact with it. To maintain a constant pH in the anolyte and catholyte, the contents were regularly "recharged" [91] to replenish the ions consumed over time by adapting Equation 0.13, Faraday's law of electrolysis, where I is the current (A), t is the time that has passed in seconds, F is the Faraday number (96,485 C/mol), z is the valence number of the ions, m is the weight of the substance (g) and M is the molecular weight (g/mol). They stated that for an applied current of 0.25A used in the test (current

density across the sample was 127 Am^{-2}), approximately 6 g of lithium hydroxide and 20g of ammonium nitrate was required to be added as a powder every 24 hours, and a "high acceleration rate is obtained as both dissolution and diffusion processes involved in leaching are enhanced" [91]. A diagram displaying the movement of ions in their test is shown in Figure 0.16. Due to the constant current, an initial voltage of 100 V was observed which dropped to 20V after 6 weeks at the end of the test. There were no clear explanations for the decrease, and whether the decrease was linear with respect to time, or followed another pattern was not stated. The charged species in the catholyte were characterised using Ion Chromatography, and calcium concentration was analysed using potentiometric titration. The solid sample was tested by XRD and the Ca/Si ratio within the cement by laser ablation-inductive coupled plasma-mass spectrometry (LA-ICP-MS). SEM-EDX, XRF, MIP and TGA were also conducted.

$$I \times t = F \times z \times \left(\frac{m}{M}\right)$$

Equation 0.13 [91]

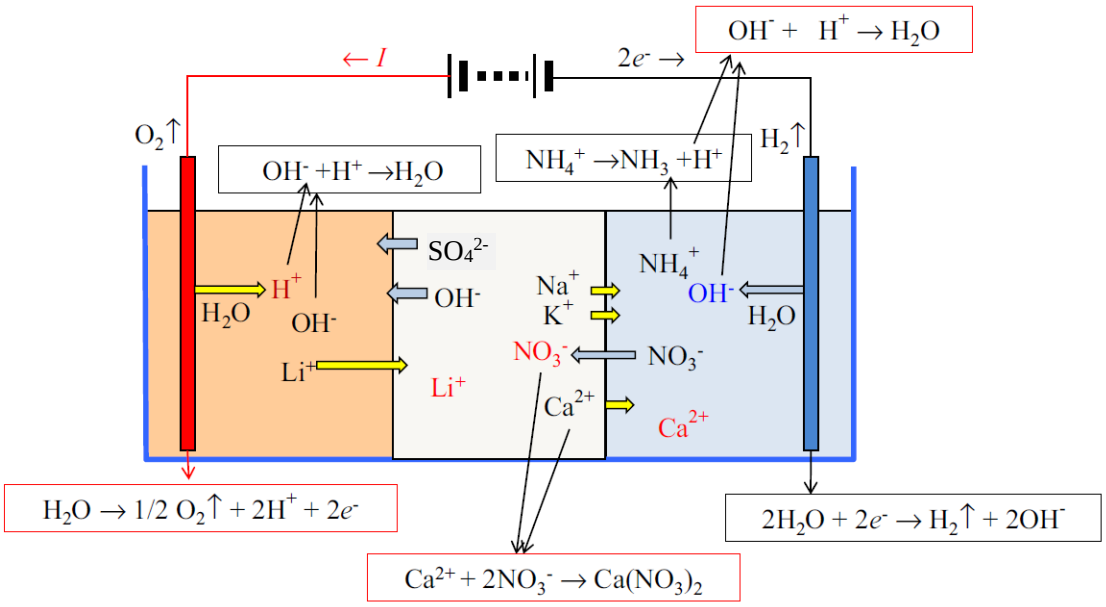

Figure 0.16 Movement of ions in Babaahmadi's electrochemical-migration method [91]

As expected, they found that portlandite was leached preferentially, as seen in their TG analysis as shown in Figure 0.17. The portlandite peak is not observed in the TG data after 53 days of electrical leaching. The paper concluded that this was a test comparable to natural leaching, as total dissolution of the portlandite and then followed by a progressive decalcification of the C-S-H gel from the cathode side to the anode side was observed. The change in porosity caused by the leaching was also seen to move from the cathode towards the anode side, and the increase in porosity after the portlandite had been leached (Figure 0.18) was in good agreement with research studying natural leaching reported by Haga et al.[77] but was achieved in a shorter time in the accelerated test.

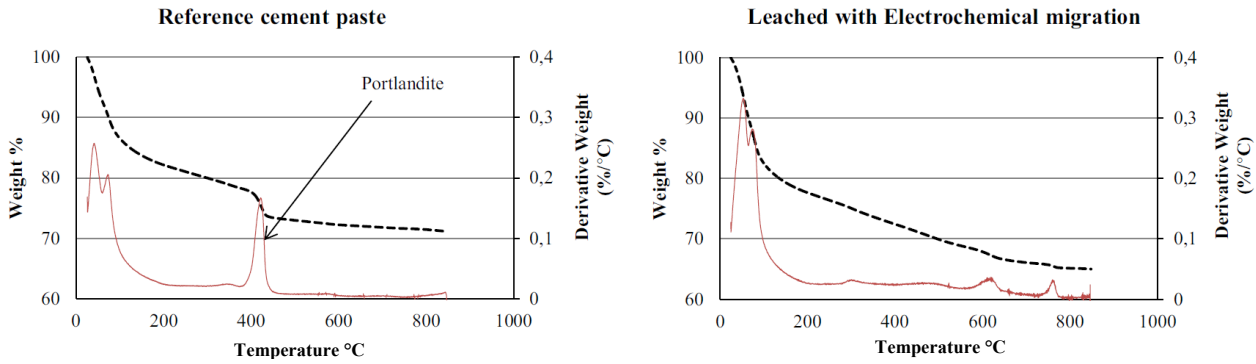

Figure 0.17 TG analysis by Babaahmadi et al. of a pristine sample and after 53 days of leaching. The red line is the first derivative of the weight % [91]

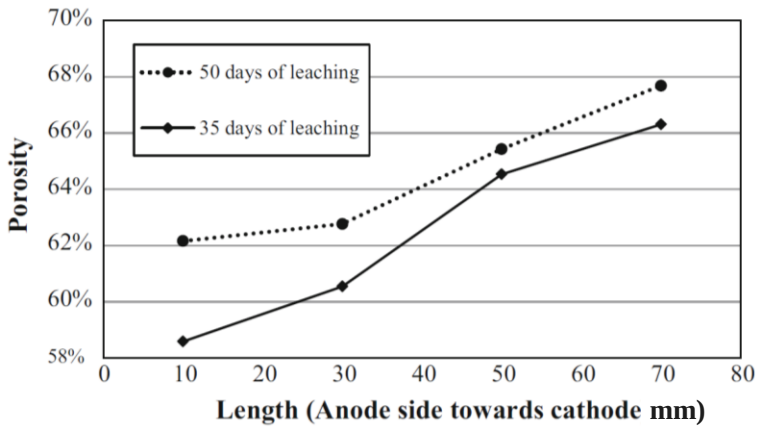

Figure 0.18 Porosity as a function of depth (Porosity of unleached sample was 40-45%) [91]

2.7 Migration of ions into and out of cement by applying a direct current

The most widely used ion-migration technique is the rapid chloride penetration test developed by AASHTO to investigate the corrosion of steel rebar through chloride intrusion, a key factor in the degradation of civil structures [103], [76]. During actual chloride attack, the chloride penetration is driven by the difference in the external and internal concentration of chloride in the cement, which has been modelled in the past as a coupled diffusion–sorption process [76]. A review by Andrade [104] shows that the sorption effects of chloride are mainly lost during this accelerated test, where an electrical current is applied to enhance the migration of chloride ions to increase the speed with which they move through the cement, which they stated calls into question the validity of the test.

In a similar set of experiments discussed by Castellote et al., a potential gradient was used to enhance ion transport through concrete samples with a w/c = 0.4 [105]. To characterise the transport of Cs, Sr, Co and Fe through concrete, and to examine whether using an applied potential could accelerate the experiments, a disk of concrete was placed between two 350 cm^3 chambers holding the corresponding solution as outlined in Table 0.7. During the electrical migration tests set up as shown in Figure 0.19, a constant voltage of 12V was held between the cathode and anode. For comparison, longer standard diffusion tests were conducted under the same conditions where no potential gradient was applied.

Table 0.7 Summary of tests carried out by Castellote et al. [105] with detailed experimental conditions (reproduction of table)

Driving Force	Species	Voltage V	Electrodes		Electrolyte		Test: days
			Anode	Cathode	Anolyte	Catholyte	
Migration	Cs^+		Steel	Steel	CsCl 0.1 M	Distilled Water	7
	Sr^{2+}		Steel	Steel	$SrCl_2$ 0.05 M	Distilled Water	15
	Co^{2+}	12	Steel	Steel	$CoCl_2$ 0.05 M	Distilled Water	13
	Fe^{3+}		Copper	Platinum	$FeCl_3$ 0.1 M	Distilled Water	13
	Fe^{3+}		Platinum	Steel	Distilled Water	$FeCl_3$ 0.1 M	16
	Cs^+				CsCl 0.05 M	NaCl 0.2 M	18

	Sr^{2+}	12	Steel	Steel	$SrCl_2$ 0.05 M	NaCl 0.2 M	18
	Co^{2+}				$CoCl_2$ 0.05 M	NaCl 0.2 M	18
Diffusion	Cs^{+}				Distilled Water	CsCl 0.05 M	300
	Sr^{2+}	–	–	–	Distilled Water	$SrCl_2$ 0.05 M	300
	Co^{2+}				Distilled Water	$CoCl_2$ 0.05 M	300
	Fe^{3+}				Distilled Water	$FeCl_3$ 0.05 M	300

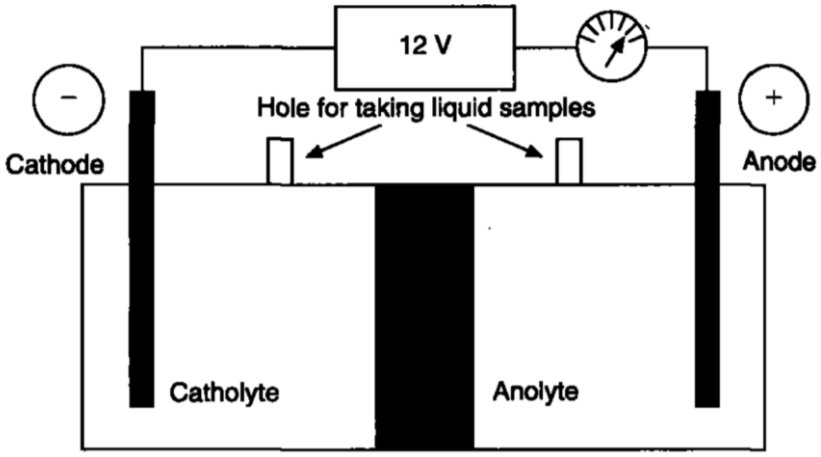

Figure 0.19 Experimental setup used for accelerated migration test in Castellote et al.'s 1999 paper [105]

The key conclusions of these experiments were that ions such as Sr^{2+} and Cs^{+}, which move as a single ionic species, had a similar diffusion coefficient after two weeks of the migration test as after ten months of the diffusion test. However, Fe^{3+} and Co^{2+} were seen to form complex compounds in the electric migration tests, but not in the standard diffusion tests –for example, in the electrical migration test some of the $CoCl_2$ reacted to form $(CoCl_4)^{2-}$ at the anode. This ionic species is negatively charged, which meant that not all of the Co initially present was attracted towards the cathode, and therefore, this acceleration technique was not entirely successful to study the migration of Co. They suggest that accelerated migration testing requires a similar experimental study for each ion of interest in order to ensure that the investigated ions do not form new complexes under a potential gradient.

To expand upon these findings, Castellote et al. [53] published another paper in 2002, outlining the use of electrophoresis as a non-destructive method of decontaminating

construction materials/cement of radionuclides. To investigate different levels of decontamination, they produced several sets of samples as outlined in Table 0.8, with samples where the contaminant solution was intermixed with the mortar before curing (Series A in Table 0.8) and also samples that were contaminated externally through contact with a contaminant solution for 3 days (Series B and C in Table 0.8). They found that the externally contaminated samples could be decontaminated to a greater extent through applying an electrical current, than when the same voltage was applied to the intermixed samples as shown in Figure 0.20. For the study of nuclear waste, their treatment of intermixed samples is of great importance, because "when the contaminants are added to the cementitious material to block and immobilize wastes, the treatment can [also] be used to characterize the confining ability of the matrix" [53].

Table 0.8 Mix proportions for decontamination testing [53]

series	matrix	cement (kg/m^3)	sand (kg/m^3)	coarse aggregate (kg/m^3)	ratio (water/cement) weight	ratio cement/ sand weight	casting solution
A	mortar				0.5	1:3	0.001 M Cs^{+}, Sr^{2+} Co^{2+} Fe^{3+}
B	concrete	380	771	1177	0.4		water
C	mortar				0.6	1:4	water

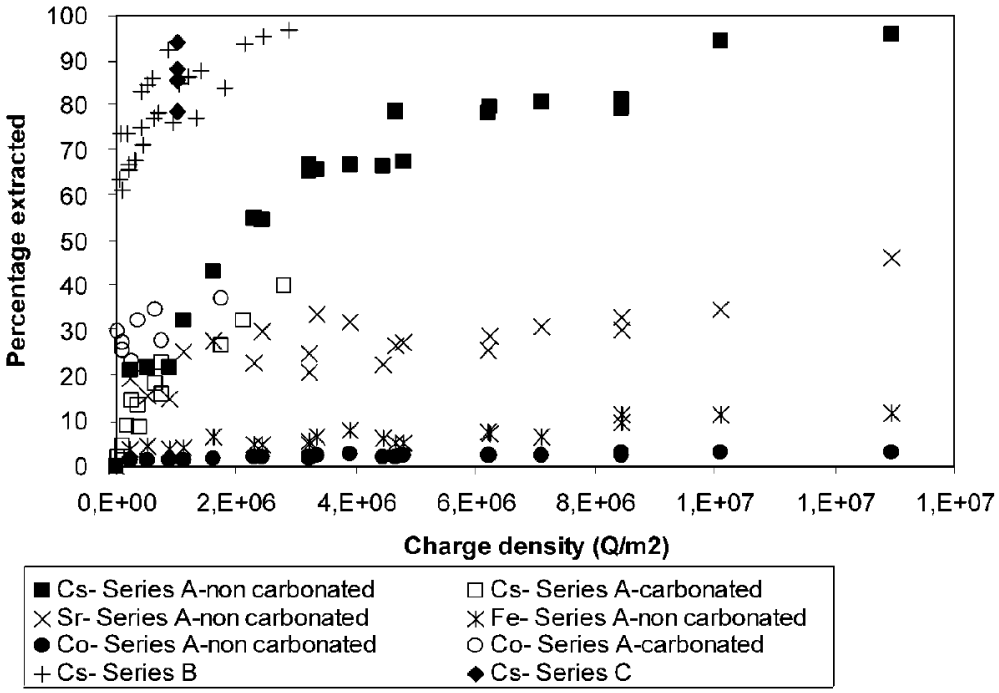

Figure 0.20 Percentage of extraction as a function of the charge density. Refer to Table 2.8 for series A, B and C [53]

Parker et al. presented a similar technique [106], [107] which they call electrokinetic remediation, where concrete is decontaminated by applying an electric field to extract radionuclides. In the first paper [106], they used $^{40}K^{+}$ as a simulant for ^{137}Cs to investigate the movement of radionuclides through concrete samples by applying a constant voltage of 60V and a current of 35 mA. The $^{40}K^{+}$ was migrated into the sample from a 3g/l KCl solution placed in the anode tank. The cathode tank initially contained deionised water. To calculate the diffusion coefficients D_k of the ionic species k, they used Equation 0.14 and Equation 0.15, where J_k is the steady state ionic flux of the kth ion (mol $m^{-2}s^{-1}$), V is the cathodic volume, Δc_k is the change in concentration in the cathode tank, A is the surface area of the concrete, Δt is the change in time, R is the ideal gas constant (8.314 J $mol^{-1}k$), T is the absolute temperature in kelvin, L is the thickness of the sample in m, z is the valence of the ionic species, F is the Faraday constant (96484.6 C mol^{-1}), c_{ka0} is the initial concentration in the anode tank, and E is the electric potential (V). Depending on whether a leaching test or a migration test is being

conducted, which could change the ion of interest, V and c_{ka0} can be replaced with the anodic volume and the initial concentration in the pore solution or cathode tank respectively depending on the experimental conditions.

$$J_k = \frac{V\Delta c_k}{A\Delta t}$$

Equation 0.14

$$D_k = \frac{J_k RTL}{zFc_{ka0}E}$$

Equation 0.15

Parker et al. then went on to further develop the indirect Cs detection technique and published a second paper using this technique in 2014 [107] with a K loaded ion exchange resin attached onto the cathode side of a cement sample and a solution of Cs initially placed in the anode tank, the idea being that when an electric potential is applied the incoming Cs would displace the K, and the K could then be detected in the cathode tank as displayed in Figure 0.21 (diagram from a later paper [108]).

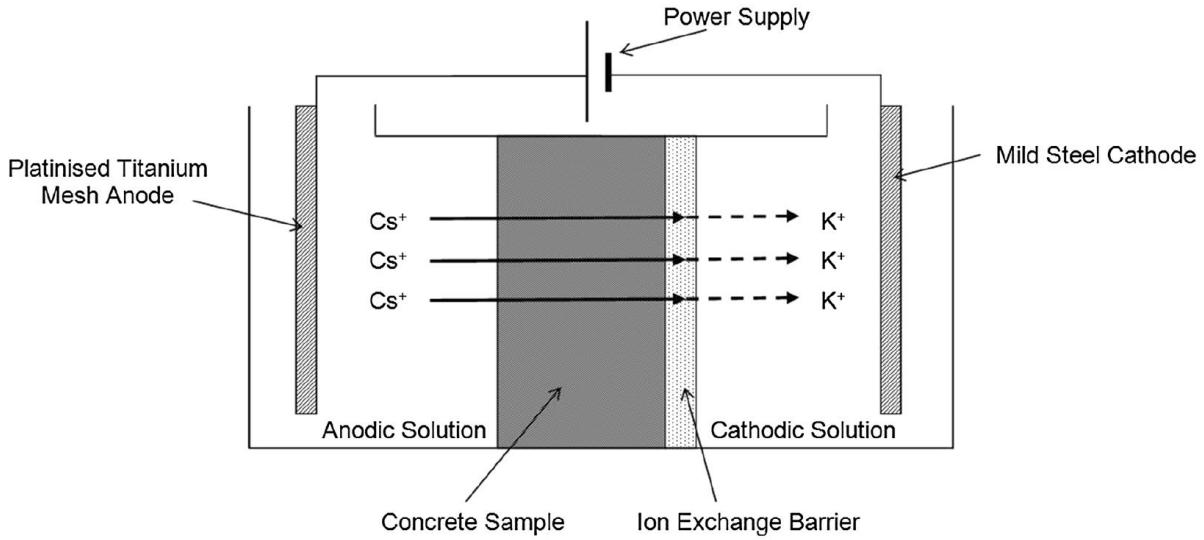

Figure 0.21 Sketch of the Cs migration test conducted by Parker et al. [108] with a K-loaded ion exchange barrier attached to the cathode side of the cement

300 hours after 60 mol m^3 of Cs^+ was placed in the anolyte, they expected to determine the amount of Cs ions migrated from anolyte based on the amount of K ions leached into

catholyte. ~85mol m^3 of K^+ was detected in the catholyte, higher than the added Cs, which they attributed partially to the K naturally present in the concrete, as well as originating from a displacement due to the intruding Cs. They suggested that more work to be done to validate this as a technique to indirectly detect Cs movement, such as conducting an initial test without added Cs to validate how the K^+ concentration is altered. As the goal of this work was remediation and not the aging of samples, analysing and reducing the degradation of the concrete by monitoring "any affects [sic!] that the electrochemical reactions have" [107] was a key aspect of the research. To understand the effects of changes in the pH level, Parker et al. performed two comparative experiments, one with the pH of the anolyte uncontrolled, and the other with a controlled value of ~13. As shown in Figure 0.22, an applied electric current lowers the pH level in the anode tank, leading to significantly more degradation. Although they stated that the generation of an acidic front at the anode is the greatest concern for remediation, identifying a technique to accelerate degradation could be useful for studying long-term behaviour of materials in leaching environments, such as nuclear wasteforms in a GDF.

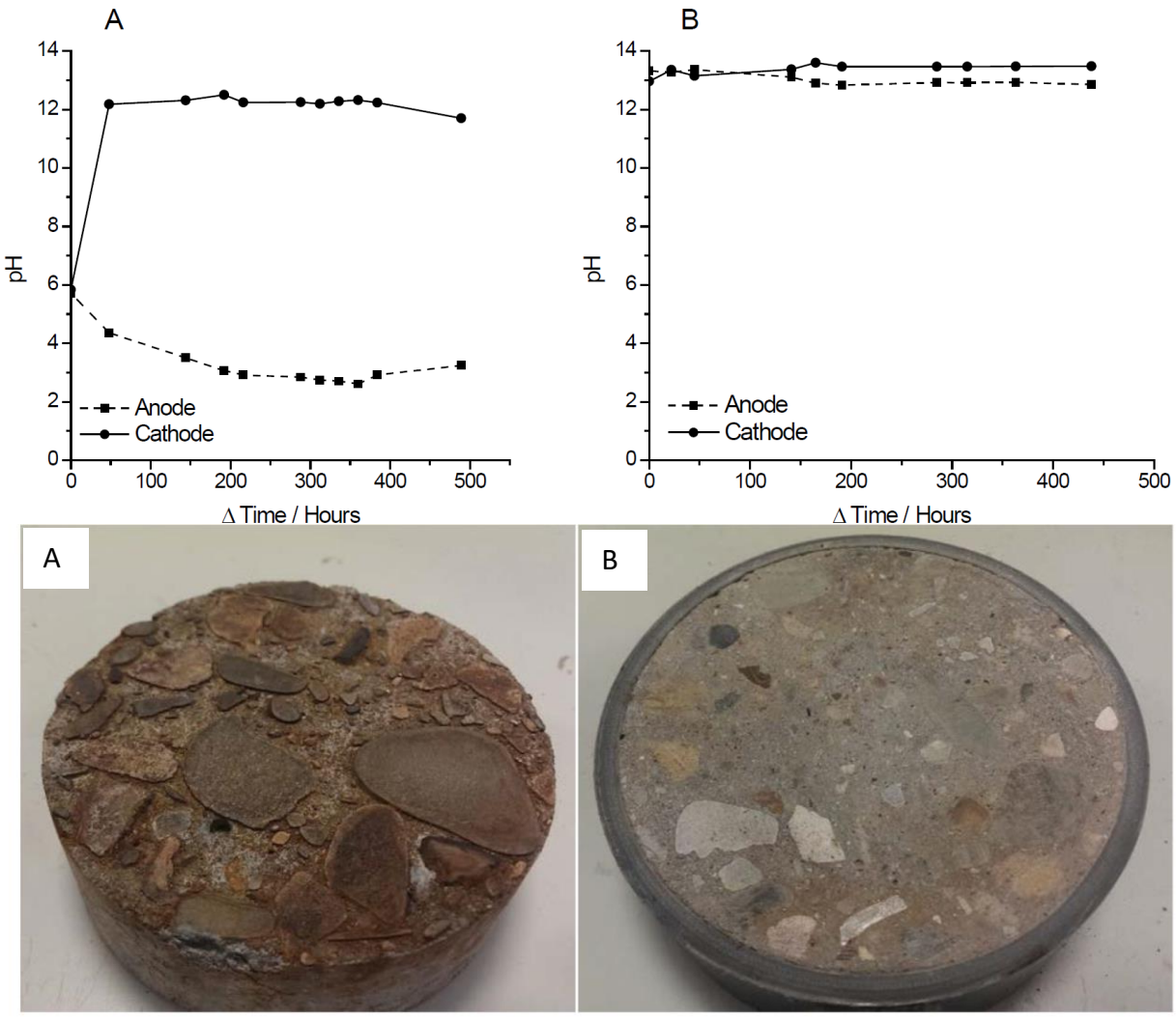

Figure 0.22 pH data and photographs of the anode side of uncontrolled (A) and pH controlled (B) concrete samples after 500 hours of applied voltage [107]

2.8 Summary

Cement is a suitable material for nuclear waste encapsulation, however, certain aspects such as the decay of problematic radionuclides such as caesium into barium and the chemical durability of the wasteform cannot be investigated directly within real-life timeframes. Therefore, accelerated methods have to be utilised. This review has shown that there is little data on the incorporation of Cs into BFS:PC systems, but it is reasonable to assume that it may mostly remain in the pore solution and sorb onto the C-S-H gel over time, competing with other alkali cations present, although the specifics vary with the BFS:PC and w/c ratios. It is not known what level of Cs can be incorporated in 3:1 BFS:PC cement without precipitation of soluble Cs compounds. Ettringite forms in BFS:PC systems, and ettringite has been seen to

decompose in the presence of intermixed barium carbonate to form barite. A similar reaction can be expected to occur in BFS:PC systems when barium is introduced later to the hardened system, but no research has been conducted investigating this aspect in 3:1 BFS:PC systems.

The use of an electric current to accelerate the migration of ions such as Cs into hardened cement bodies has been studied and successfully utilised previously, most notably with chloride ions to investigate rebar corrosion. Barium, the decay product of ^{137}Cs, however, has not been investigated in this manner. It is of particular interest to clarify whether it would interact with the hardened cement matrix, and if so, how it would impact the nature of the wasteforms for intermediate level nuclear waste. Electrical leaching is an accelerated leaching technique where the anions in the cement are enhanced to migrate towards the anode and the cations to the cathode through electrophoresis. The literature data on the degradation of cement samples through leaching, such as the calcium concentration and compressive strength, shows that the leaching results of static and electrical leaching tests are comparable, but static tests need to be conducted over much longer periods of time to obtain similar results. During electrical leaching, the phases appear to leach out of the cement matrix in the same fashion as in natural leaching but at an accelerated rate. The main focus of the literature has been the leaching of Ca, with a lack of information on Si, Al and other elements. Behaviour of these cations and anions are also important to gain further understanding of the materials behaviour in the long-term. Since there is no data reported in the open literature, it is currently not clear whether electric leaching tests are suitable to study these aspects.

2.9 References

[1] H. Young and R. Freedman, *University Physics*, 12th ed. Harlow, England: Sears & Zemansky, 2008.

[2] G. Choppin, L. Liljenzin, and J. Rydberg, *Radiochemistry and Nuclear Chemistry*, 3rd

Editio. Woburn: Butterworth-Heinemann, 2002.

[3] NDA, "Understanding activities that produce radioactive wastes in the UK," 2015. [Online]. Available: http://ukinventory.nda.gov.uk/wp-content/uploads/sites/2/2014/01/Understanding-activities-that-produce-radioactive-wastes-in-the-UK.pdf. [Accessed: 17-Jun-2017].

[4] National Nuclear Data Centre, "Chart of Nuclides," 2016. [Online]. Available: http://www.nndc.bnl.gov/chart/. [Accessed: 17-Jun-2017].

[5] M. I. Ojovan and W. E. Lee, *An Introduction to Nuclear Waste Immobilisation*, First Edit. Kidlington, Oxford, England: Elsevier, 2005.

[6] IAEA, "GSG-1, Classification of Radioactive Waste," 2009. [Online]. Available: http://www-pub.iaea.org/MTCD/publications/PDF/Pub1419_web.pdf.

[7] NDA, "2013 UK Radioactive Waste Inventory: waste quantities from all sources," 2014. .

[8] F. G. F. Gibb, N. A. McTaggart, K. P. Travis, D. Burley, and K. W. Hesketh, "High-density support matrices: Key to the deep borehole disposal of spent nuclear fuel," *J. Nucl. Mater.*, vol. 374, pp. 370–377, 2007.

[9] M. I. Ojovan, *Handbook of advanced radioactive waste conditioning technologies*. Philadelphia: Woodhead Publishing Limited, 2011.

[10] R. L. Murray, *Nuclear Energy*, Sixth Edit. Oxford, England: Butterworth-Heinemann, 2009.

[11] OECD and Nuclear Energy Agency, "Cementitious materials in safety cases for geological repositories for radioactive waste: Role evolution and interactions," 2009. [Online]. Available: https://www.oecd-nea.org/rwm/docs/2012/rwm-r2012-3.pdf. [Accessed: 17-Jun-2017].

[12] P. V. Brady, B. W. Arnold, G. A. Freeze, P. N. Swift, S. J. Bauer, J. L. Kanney, R. P. Rechard, and J. S. Stein, "Sandia Report SAND2009-4401, Deep borehole disposal of high-level radioactive waste," 2009. [Online]. Available: http://prod.sandia.gov/techlib/access-control.cgi/2009/094401.pdf. [Accessed: 17-Jun-2017].

[13] ONR, "Geological Disposal Fact Sheet." [Online]. Available: http://www.onr.org.uk/documents/fact-sheet-gdf.pdf. [Accessed: 17-Jun-2017].

[14] N. C. Collier, N. B. Milestone, K. P. Travis, and F. G. F. Gibb, "The effect of organic retarders on grout thickening and setting during deep borehole disposal of high-level radioactive waste," *Prog. Nucl. Energy*, vol. 90, pp. 19–26, 2016.

[15] Department of Energy & Climate Change, "Implementing Geological Disposal," *White Paper*, 2014. [Online]. Available: https://www.gov.uk/government/uploads/system/uploads/attachment_data/file/332890/GDF_White_Paper_FINAL.pdf. [Accessed: 17-Jun-2017].

[16] NDA, "NDA/ST/STY(11)0004, The 2010 UK radioactive waste inventory: main report," 2010. [Online]. Available: https://www.cumbria.gov.uk/elibrary/Content/Internet/538/755/1929/4211794318.pdf. [Accessed: 17-Jun-2017].

[17] W. Gashier, T. Miura, K. Hashimoto, R. J. Hand, and H. Kinoshita, "Leaching behaviour of cementitious nuclear wasteforms containing caesium and strontium," *Adv. Appl.*

Ceram., vol. 113, no. 8, pp. 447–452, 2014.

[18] I. G. Crossland, "Crossland Report CCL/2007/1, Cracking of the Nirex Reference Vault Backfill: A review of its likely occurrence and significance," *Crossland Consulting*, 2007. .

[19] G. Baston, T. Heath, F. Hunter, and S. Swanton, "Modelling of cementitious backfill interactions with vitrified intermediate-level waste," *Phys. Chem. Earth*, vol. x, no. x, pp. 1–10, 2017.

[20] J. Peterson, M. MacDowell, L. Haroun, and F. Monette, "Radiological and chemical fact sheets to support health risk analyses for contaminated areas," 2005. [Online]. Available: https://www.remm.nlm.gov/ANL_ContaminantFactSheets_All_070418.pdf. [Accessed: 17-Jun-2017].

[21] I. Odler, "Investigation of the hydration of portland blastfurnace slag cement: composition, structure and properties of the hydrated material," *Adv. Cem. Res.*, vol. 2, no. 5, pp. 15–20, 1989.

[22] N. J. Bowmer and S. Curwen, "WP1- Details of encapsulation processes at Sellafield." BNFL Commerical, Sellafield, UK, p. 46, 2007.

[23] J. Cronin and N. C. Collier, "NNL (11) 11524 Issue 3, Expansion of grouted magnox corrosion & expansion of grouted magnox," 2011. [Online]. Available: https://rwm.nda.gov.uk/publication/corrosion-and-expansion-of-grouted-magnox-november-2011/. [Accessed: 17-Jun-2017].

[24] K. Hashimoto, N. Otsuki, T. Saito, and Y. H, "Application of electrical treatment to alteration of cementitious material due to leaching," *J. Adv. Concr. Technol.*, vol. 11, no. 3, pp. 108–118, 2013.

[25] D. Rothstein, J. J. Thomas, B. J. Christensen, and H. M. Jennings, "Solubility behavior of Ca-, S-, Al-, and Si-bearing solid phases in Portland cement pore solutions as a function of hydration time," *Cem. Concr. Res.*, vol. 32, pp. 1663–1671, 2002.

[26] N. D. M. Evans, "Binding mechanisms of radionuclides to cement," *Cem. Concr. Res.*, vol. 38, pp. 543–553, 2008.

[27] M. Atkins and F. P. Glasser, "Application of portland cement based materials to radioactive waste immobilization," *Waste Manag.*, vol. 12, pp. 105–131, 1992.

[28] J. Aspdin, "Aspdin's improvements in the modes of producing artifical stone," *Br. Pat. no. 5022*, 1824.

[29] P. C. Hewlett, "Lea's Chemistry of Cement and Concrete." Elsevier, 1998.

[30] United States Geological Survey, "USGS Mineral Survey Cement Report," 2014. [Online]. Available: https://minerals.usgs.gov/minerals/pubs/commodity/cement/mcs-2014-cemen.pdf. [Accessed: 17-Jun-2017].

[31] P. C. Hewlett, *Lea's Chemistry of Cement and Concrete*, no. 4th edition. Amsterdam: Elsevier Ltd, 2004.

[32] R. Ylmén, U. Jäglid, B. M. Steenari, and I. Panas, "Early hydration and setting of portland cement monitored by IR, SEM and Vicat techniques," *Cem. Concr. Res.*, vol. 39, pp. 433–439, 2009.

[33] S. J. Way and A. Shayan, "Early hydration of a portland cement in water and sodium

hydroxide solutions: composition of solutions and nature of solid phases," *Cem. Concr. Res.*, vol. 19, no. 5, pp. 759–769, 1989.

[34] B. Lothenbach, G. Le, E. Gallucci, and K. Scrivener, "Influence of limestone on the hydration of Portland cements," *Cem. Concr. Res.*, vol. 38, pp. 848–860, 2008.

[35] K. L. Scrivener, P. Juilland, and P. J. M. Monteiro, "Advances in understanding hydration of portland cement," *Cem. Concr. Res.*, vol. 78, pp. 38–56, 2015.

[36] H. Minard, S. Garrault, L. Regnaud, and A. Nonat, "Mechanisms and parameters controlling the tricalcium aluminate reactivity in the presence of gypsum," *Cem. Concr. Res.*, vol. 37, pp. 1418–1426, 2007.

[37] ASTM International, "ASTM C150, Standard specification for portland cement," 2010.

[38] P. T. Durdzin, M. Ben Haha, S. A. Bernal, N. De Belie, E. Gruyaert, B. Lothenbach, E. M. Mendez, J. L. Provis, A. Scholer, C. Stabler, Z. Tan, Y. V. Zaccardi, A. Vollpracht, F. Winnefeld, M. Zajac, and K. L. Scrivener, "Outcomes of the RILEM round robin on degree of reaction of slag and fly ash in blended cements," *Mater. Struct.*, vol. 50, no. 135, pp. 1–15, 2017.

[39] C. A. Utton, "The encapsulation of BaCO3 waste in composite cements," University of Sheffield, Sheffield, 2006.

[40] F. P. Glasser, "Progress in the immobilization of radioactive waste in cement," *Cem. Concr. Res.*, vol. 22, pp. 201–216, 1992.

[41] K. R. Backe, O. B. Lile, and S. K. Lyomox, "Characterizing curing cement slurries by electrical conductivity," *SPE Drill. Complet.*, vol. 16, no. 4, pp. 201–207, 2001.

[42] Z. Li, X. Wei, and W. Li, "Preliminary interpretation of portland cement hydration process using resistivity measurements," *ACI Mater. J.*, vol. 100, no. 3, 2003.

[43] R. Taylor, "Composition and microstructure of 20-year-old ordinary Portland cement-ground granulated blast-furnace slag blends containing 0-100% slag," *Cem. Concr. Res.*, vol. 40, pp. 971–983, 2010.

[44] E. Gruyaert, N. Robeyst, and N. De Belie, "Study of the hydration of Portland cement blended with blast-furnace slag by calorimetry and thermogravimetry," *J. Therm. Anal. Calorim.*, vol. 102, pp. 941–951, 2010.

[45] I. G. Richardson, C. R. Wilding, and M. J. Dickson, "The hydration of blastfurnace slag cements," *Adv. Cem. Res.*, vol. 2, no. 8, pp. 147–157, 1989.

[46] V. S. Ramachandran, R. M. Paroli, J. J. Beaudoin, and A. H. Delgado, *Handbook of Thermal Analysis of Construction Materials*. Norwich, NY: Noyes Publications/William Andrew Publishing, 2002.

[47] Heidelberg Cement, "Production and use of GGBS," 2007.

[48] C. Fredericci, E. D. Zanotto, and E. C. Ziemath, "Crystallization mechanism and properties of blast furnace slag glass," *J. Non. Cryst. Solids*, vol. 273, pp. 64–75, 2000.

[49] J. R. Harbour, E. K. Hansen, T. B. Edwards, V. J. Williams, R. E. Eibling, D. R. Best, and D. M. Missimer, "Characterization of slag, fly ash and portland cement for saltstone," 2006. .

[50] S. Akbarnejad and L. J. M. Houben, "Chemical and mineralogical characterization of blast furnace slag as a road base material," in *9th International Sustainable Construction Materials in Asphalt, Pavement Engineering and Highway Maintenance*,

2010.

[51] O. Hussein, C. Utton, M. I. Ojovan, and H. Kinoshita, “The effects of BaSO4 loading on OPC cementing system for encapsulation of BaSO4 scale from oil and gas industry,” *J. Hazard. Mater.*, vol. 261, no. 1, pp. 11–20, 2013.

[52] I. Odler and W. Hinrichs, “Investigation of the hydration of Portland blastfurnace slag cement: hydration kinetics,” *Adv. Cem. Res.*, vol. 2, no. 5, pp. 9–13, 1989.

[53] M. Castellote, C. Andrade, and C. Alonso, “Nondestructive decontamination of mortar and concrete by electro-kinetic methods: application to the extraction of radioactive heavy metals,” *Environ. Sci. Technol.*, vol. 36, pp. 2256–2261, 2002.

[54] P. Côté, “Contaminant leaching from cement-based waste forms under acidic conditions,” McMaster University, hamilton, Ontario, canada, 1986.

[55] K. G. Papadokostaki and A. Savidou, “Study of leaching mechanisms of caesium ions incorporated in ordinary portland cement,” *J. Hazard. Mater.*, vol. 171, pp. 1024–1031, 2009.

[56] R. W. Crawford, C. Mcculloch, M. Angus, F. P. Glasser, A. A. Rahman, M. Walk, O. Aberdeen, and U. K. Scotland, “Intrinsic sorption potential of cement components for 134Cs,” *Cem. Concr. Res.*, vol. 14, no. 3, pp. 595–599, 1984.

[57] M. Ochs, I. Pointeau, and E. Giffaut, “Caesium sorption by hydtrated cement as a function of degradation state: Experiments and modelling,” *Waste Manag.*, vol. 26, pp. 725–732, 2006.

[58] J. V. Hanna, L. P. Aldridge, and E. R. Vance, “Cs speciation in cements,” in *Materials Research Society*, 2001, vol. 663, pp. 89–101.

[59] A. Vollpracht and W. Brameshuber, “Binding and leaching of trace elements in portland cement pastes,” *Cem. Concr. Res.*, vol. 79, no. 1, pp. 76–92, 2016.

[60] I. Akkurt, H. Akyıldırım, B. Mavi, S. Kilincarslan, and C. Basyigit, “Photon attenuation coefficients of concrete includes barite in different rate,” *Ann. Nucl. Energy*, vol. 37, no. 7, pp. 910–914, 2010.

[61] Y. Esen and B. Yilmazer, “An investigation of X-ray and radio isotope energy absorption of heavyweight concretes containing barite,” *Bull. Mater. Sci.*, vol. 34, no. 1, pp. 169–175, 2011.

[62] M. A. Sharaf and G. M. Hassan, “Radiation induced radical in barium sulphate for ESR dosimetry : a preliminary study,” *Nucl. Instruments Methods Phys. Res. B*, vol. 225, pp. 521–527, 2004.

[63] J. R. Clifton and J. M. Ponnersheim, “NISTIR 5390, Sulfate attack of cementitious materials: volumetric relations and expansions,” 1994. [Online]. Available: http://fire.nist.gov/bfrlpubs/build94/PDF/b94040.pdf.

[64] C. A. Utton, E. Gallucci, J. Hill, and N. B. Milestone, “Interaction between BaCO3 and OPC/BFS composite cements at 20°C and 60°C,” *Cem. Concr. Res.*, vol. 41, pp. 236–243, 2011.

[65] P. M. Carmona-Quiroga and M. T. Blanco-Varela, “Ettringite decomposition in the presence of barium carbonate,” *Cem. Concr. Res.*, vol. 52, pp. 140–148, 2013.

[66] P. M. Carmona-Quiroga and M. T. Blanco, “Use of barium carbonate to inhibit sulfate attack in cements,” *Cem. Concr. Res.*, vol. 69, pp. 96–104, 2015.

[67] T. Ekström, "TVBM-3090, Leaching of concrete," 2001. [Online]. Available: http://portal.research.lu.se/ws/files/4827018/1766469.pdf. [Accessed: 17-Jul-2017].

[68] E. Revertegat, C. Richet, and P. Gegout, "Effect of pH on the durability of cement pastes," *Cem. Concr. Res.*, vol. 22, no. 2–3, pp. 259–272, 1992.

[69] C. Carde and R. François, "Effect of the leaching of calcium hydroxide from cement paste on mechanical and physical properties," *Cem. Concr. Res.*, vol. 27, no. 4, pp. 539–550, 1997.

[70] F. H. Heukamp, F.-J. Ulm, and J. T. Germaine, "Mechanical properties of calcium leached cement paste: triaxial stress states and the influence of pore pressure," *Cem. Concr. Res.*, vol. 31, no. 5, pp. 767–774, 2001.

[71] F. Adenot and F. Buil, "Modelling of the corrosion of the cement paste by deionized water," *Cem. Concr. Res.*, vol. 22, pp. 489–496, 1992.

[72] T. Banba, J. Matsumoto, and S. Muraoka, "Leaching behaviour of carbon-14 contained in portland cement," *Cem. Concr. Res.*, vol. 22, pp. 381–386, 1992.

[73] ASTM, "C1220-10, Standard Test Method for Static Leaching of Monolithic Waste Forms for Disposal of Radioactive Waste." [Online]. Available: https://www.astm.org/Standards/C1220.htm. [Accessed: 17-Jun-2017].

[74] American Nuclear Society, "ANSI/ANS-16.1-2003; R2008; R2017: Measurement of the leachability of solidified low-level radioactive wastes by a short-term test procedure," 2003. [Online]. Available: http://www.ans.org/store/item-240249/. [Accessed: 17-Jun-2017].

[75] P. Faucon, F. Adenot, J. F. Jacquinot, J. C. Petit, R. Cabrillac, and M. Jorda, "Long-term behaviour of cement pastes used for nuclear waste disposal: review of physico-chemical mechanisms of water degradation," *Cem. Concr. Res.*, vol. 28, no. 6, pp. 847–857, 1998.

[76] M. Mainguy and O. Coussy, "Propogation fronts during calcium leaching and chloride penetration," *J. Eng. Mech.*, vol. 126, no. 3, pp. 250–257, 2000.

[77] K. Haga, M. Shibata, M. Hironaga, S. Tanaka, and S. Nagasaki, "Change in pore structure and composition of hardened cement paste during the process of dissolution," *Cem. Concr. Res.*, vol. 35, pp. 943–950, 2005.

[78] A. M. Marion, A. De Grauw, and M. De Lanéve, "Study of the leaching behaviour of paving concretes: quantification of heavy metal content in leachates issued from tank test using demineralized water," *Cem. Concr. Res.*, vol. 35, pp. 951–957, 2005.

[79] "Council Directive 98/83/EC On the quality of water intended for human consumption," The Council of the European Union, 1998.

[80] M. Stone and P. Goldbart, *Mathematics for Physics*. London: Pimander-Casaubon, 2008.

[81] C. S. Walker, S. Sutou, C. Oda, M. Mihara, and A. Honda, "Calcium silicate hydrate (C-S-H) gel solubility data and a discrete solid phase model at 25 ° C based on two binary non-ideal solid solutions," *Cem. Concr. Res.*, vol. 79, pp. 1–30, 2016.

[82] B. Lagerblad, "TR-01-27, Leaching performance of concrete based on studies of samples from old concrete constructions," *TR-01-27*, 2001. [Online]. Available: http://www.skb.com/publication/18731/TR-01-27.pdf. [Accessed: 17-Jun-2017].

[83] M. Alexander, N. Belie, and A. Bertron, *Performance of cement-based materials in aggressive aqueous environments*, Volume 10. Rilem, 2013.

[84] C. Carde, G. Escadeillas, and R. Francois, "Use of ammonium nitrate solution to simulate and accelerate the leaching of cement pastes due to deionized water," *Mag. Concr. Res.*, vol. 49, no. 181, pp. 295–301, 1997.

[85] F. M. Lea, "The action of ammonium salts on concrete," *Mag. Concr. Res.*, vol. 17, no. 52, pp. 115–116, 1965.

[86] F. Agostini, Z. Lafhaj, F. Skoczylas, and H. Loodsveldt, "Experimental study of accelerated leaching on hollow cylinders of mortar," *Cem. Concr. Res.*, vol. 37, pp. 71–78, 2006.

[87] Q. T. Phung, D. Jacques, G. De Schutter, G. Ye, and N. Maes, "Investigation of the changes in microstructure and transport properties of leached cement pastes accounting for mix composition," *Cem. Concr. Res.*, vol. 79, no. 1, pp. 217–234, 2016.

[88] G. Escadeillas and H. Hornain, *La durabilie des betons vis-a-vis des environnements chiquement*. .

[89] J. M. Torrenti, V. H. Nguyen, H. Colina, F. Le Maou, F. Benboudjema, and F. Deleruyelle, "Coupling between leaching and creep of concrete," *Cem. Concr. Res.*, vol. 38, no. 6, pp. 816–821, 2008.

[90] R. Pandya, "Precipitation and processing of solids from high pH, high Si groundwater," University of Washington, 2015.

[91] A. Babaahmadi and L. Tang, "Development of an electro-chemical accelerated ageing method for leaching of calcium from cementitious materials," *Int. J. Concr. Struct. Mater.*, vol. 9, no. 3, pp. 705–718, 2016.

[92] H. Saito, S. Nakane, S. Ikari, and A. Fujiwara, "Preliminary experimental study on the deterioration of cementitious materials by an acceleration method," *Nucl. Eng. Des.*, vol. 138, no. 2, pp. 151–155, 1992.

[93] H. Saito and A. Deguchi, "Leaching tests on different mortars using accelerated electrochemical method," *Cem. Concr. Res.*, vol. 30, pp. 1815–1825, 2000.

[94] R. Barbarulo, J. Marchand, K. A. Snyder, and S. Prené, "Dimensional analysis of ionic transport problems in hydrated cement systems Part 1. theoretical considerations," *Cem. Concr. Res.*, vol. 30, no. 12, pp. 1955–1960, 2000.

[95] E. Samson, J. Marchand, and K. A. Snyder, "Calculation of ionic diffusion coefficients on the basis of migration test results," *Mater. Struct.*, vol. 36, no. 257, pp. 156–165, 2003.

[96] E. Samson and J. Marchand, "Modeling the effect of temperature on ionic transport in cementitious materials," *Cem. Concr. Res.*, vol. 37, pp. 455–468, 2007.

[97] Q. Yuan, C. Shi, G. De Schutter, D. Deng, and F. He, "Numerical model for chloride penetration into saturated concrete," *J. Mater. Civ. Eng.*, vol. 23, no. 3, pp. 305–311, 2011.

[98] N. Otsuki, H. Minagawa, S. Miyazato, and T. Nishida, "Fundamental study on prediction of concrete deterioration caused by calcium leaching over 100 years," *Proc. JSCE*, vol. 51, no. 679, 2001.

[99] J. Ryu, N. Otsuki, and H. Minagawa, "Long-term forecast of ca Leaching from mortar and associated degeneration," *Cem. Concr. Res.*, vol. 32, pp. 1539–1544, 2002.

[100] A. Babaahmadi, L. Tang, Z. Abbas, and P. Ma, "Physical and mechanical properties of cementitious specimens exposed to an electrochemically derived accelerated leaching of calcium," *Mater. Struct.*, vol. 9, no. 3, pp. 295–306, 2015.

[101] L. Tang, "Electrically accelerated methods for determining chloride diffusivity in concrete-current development," *Mag. Concr. Res.*, vol. 48, no. 176, pp. 173–179, 1996.

[102] Nordtest, "NT Build 492, Concrete, mortar and cement-baed repair materials: Chloride migration coefficient from non-steady-state migration experiments," 1999. [Online]. Available: http://www.nordtest.info/images/documents/nt-methods/building/NT build 492_Concrete mortar and cement-based repair materials_Chloride migration coefficient from non-steady-state migration experiments_Nordtest Method.pdf. [Accessed: 17-Jun-2017].

[103] Z. Kamaitis, "Damage to concrete bridges due to reinforcement corrosion: Part II design considerations," *Transport*, vol. XVII, no. 5, pp. 163–170, 2002.

[104] C. Andrade, "Calculation of chloride diffusion coefficients in concrete from ionic migration measurements," *Cem. Concr. Res.*, vol. 23, pp. 724–742, 1993.

[105] M. Castellote, C. Andrade, and C. Alonso, "Characterisation of transport of caesium, strontium, cobalt and iron ions through concrete by steady state migration and natural diffusion tests," *Adv. Cem. Res.*, vol. 11, no. 4, pp. 161–168, 1999.

[106] A. J. Parker, M. J. Joyce, and C. Boxall, "A radioanalytical phantom for assessing the efficacy of electrokinetic decontamination of entrained radioactivity within concrete media," *J. Radioanal. Nucl. Chem.*, pp. 769–777, 2014.

[107] A. J. Parker, C. Boxall, and M. J. Joyce, "An evaluation of electrokinetic transport of radioactive species through concrete for application as a non-destructive in situ remediation technique - 14102," in *WM2014 Conference*, 2014, pp. 1–13.

[108] A. J. Parker, M. J. Joyce, C. Boxall, and A. J. Parker, "Radiometric detection of non-radioactive caesium flux using displaced naturally abundant potassium," *J. Radioanal. Nucl. Chem.*, pp. 769–776, 2016.

Chapter 3: Materials and Experimental Methods

3.1 Introduction

This PhD project has three main stages of research, which will be examined in the following results Chapters. The areas of research are:

1. The incorporation of caesium (Cs) and barium (Ba) in 3:1 Blast Furnace Slag:Portland Cement (BFS:PC)
2. Electrical leaching of 3:1 BFS:PC
3. The simultaneous electrical migration of Cs and Ba

This Chapter introduces the experimental methods conducted during this project, such as electrical leaching and electrical migration. It then discusses the analytical techniques used to examine both the solid cement samples and the liquid leachate solutions gathered during these experiments. Specific examples of some of the analytical techniques are then shown as the initial materials are characterised.

3.2 Experimental Methods

3.2.1 Production of Cement Samples

For all tests, 3:1 BFS:PC cement compositions were prepared with several experiments requiring additions dissolved in the water used to hydrate the dry powders. The method of producing the cement sample is outlined below, with the specific cement formulations produced during the project shown in the relevant Chapter. The method used largely follows the British standard for producing cement [1], although point 7 is only relevant to the samples used in leaching tests.

1. The dry powders were weighed to obtain the desired amount of each sample and mixed in a Kenwood mixer set to speed setting 1 to reach a consistent mix.

2. Water was added slowly to the dry mixture to achieve the desired water to binder ratio (w/b), typically 0.34. w/b ratio was used rather than water to cement ratio (w/c) to avoid confusion, as the BFS was included in the weight of the binder.
    a. Additions to the cement such as $CsNO_3$ as required were dissolved into the water used to hydrate the cement at this point
3. The speed of the mixer was then raised to speed setting 3 and kept at a steady speed until the cement had a consistent fluidity (typically 2-3 minutes, tested manually using a spatula).
4. It was then poured into the required moulds, either 40 x 40 x 40 mm steel moulds or centrifuge tubes, depending on the testing and analysis to be carried out. The cement placed in the steel moulds was left in a sealed plastic bag for up to 48 hours to be de-moulded after setting to prevent contamination from the moulds. The cement samples cured in centrifuge tubes did not require demoulding until the desired age was reached.
5. The cement cubes were stored and left in the sealed plastic bag to cure for 28 days in total at ambient temperature, after which they could be used for testing and analysis.
6. The samples were cut using a water-cooled Buehler Isomet 5000 into 5 mm thick tiles, and then placed in acetone for ½ hour to arrest hydration so they could be stored for future use in a desiccator. 40 x 40 x 5 mm is the size requirement for the migration cells used in this research.
7. 24 hours prior to a leaching test, several samples in which the reaction was halted at 28 days were placed in a beaker of deionised water, which was then placed in a desiccator under vacuum to forcibly rehydrate the sample. The rehydrated samples are referred to as ‘wet’ samples, otherwise the samples are referred to as ‘dry’. During

sample cutting, fines (e.g. powdered cement) can get caught in the exposed pores of the sample. These fines can easily dissolve due to their large surface area, affecting elemental concentration data in the early stages of leaching tests; the impact of these fines is reduced by the rinsing and rehydration process. The concentration of elements in the rehydration solution after 24 hours is displayed in Table 3.1.

Table 3.1 Concentration of key elements in the rehydration solution

Element	Concentration mg/l
Ca	6.02
K	0.655
Na	0.646
Si	0.0675

As the cement pastes studied continue to react and change over time [2]–[4], it is a standard practice in cement and concrete research to attempt to arrest the hydration of the cement phases in order to compare samples at different ages [5]. This can be done using various methods, including vacuum drying [6] or saturating the sample in an organic solvent such as acetone to flush out the water [7]. In this PhD project the hydration of the cement sample is arrested by placing them in acetone for a period of time, and then stored in a desiccator held in a vacuum. This is done to ensure that in each experiment, samples can be assumed to have a similar level of hydration before any experiment begins, though the effects of introducing acetone to a synthetic tricalcium silicate paste (e.g. hydrated alite) has been studied in the past by Taylor et al. [6]. In 1957, Hickenbottom et al.

published a paper [8] where slices of tricalcium silicate that had been aged in water for 25 years were soaked in acetone for periods of two to thirty days. Visually, all samples began to turn yellow immediately before gradually turning to a reddish yellow after a few days. Gas chromatography mass spectroscopy revealed that several components had formed, three of which are known to form from acetone under alkaline conditions [8]. Ultimately they suggest that the use of polar organic liquids such as acetone to arrest hydration should be done with caution (e.g. for periods of an hour or less), and that the effect of acetone on the results of TG increase with time submerged though it has little to no effect on XRD. In 1989, Thomas et al. [9] investigated the suitability of solvent exchange methods and found no evidence of detrimental effects when studying the pore structure of hardened cement pastes (unlike direct drying techniques [5]). If acetone is used to arrest the hydration of a cement sample, during TG any residual acetone can oxidise and react with portlandite to form calcium carbonate, artificially reducing the presence of portlandite in the data as shown by Srivener et al. [5]. They also stated that it had no effect on the presence of portlandite peaks in XRD data. As all of the samples produced and tested in the current project were placed in acetone for the same period and then compared with each other, there will not be a significant impact caused by this effect, as this project largely discusses the differences between experiments conducted using cement samples produced using the same method. If any reduction in portlandite occurs due to exposure to acetone, it should occur by the same amount in each sample.

3.2.2 Incorporation of Cs and Ba in 3:1 BFS:PC

In Chapter 4, 3:1 BFS:PC is prepared with different weight % (wt.%) of $CsNO_3$ incorporated. The blend of 3:1 BFS:PC was used as this is commonly used for waste encapsulation as discussed in Chapter 2 [11], although some previous studies have investigated 9:1 BFS:PC cements to examine the maximum permitted BFS:PC ratio used [7]. The cement powder was prepared as previously described with a 3:1 BFS:PC ratio, and placed into the mixer as discussed above. The $CsNO_3$ or was dissolved into the water, the amount depending on the formulation, and then poured into the mixer, after which the cement was prepared as previously described and poured into centrifuge tubes. 8 wt.% was chosen as the upper limit for the $CsNO_3$ based on the solubility limit of $CsNO_3$ in water. These samples were characterised using X-ray Diffraction (XRD), ThermoGravimetry (TG), Differential Thermal Analysis (DTA), Differential Scanning Calorimetry (DSC), Mercury Intrusion Porosimetry (MIP), and Scanning Electron Microscopy (SEM). The details of these analytical techniques are explained below in Section 3.3 and 3.5. The results of a second series of incorporation experiments are then shown, where Ba is the element of interest. To match the amount of Cs^+ and $(NO_3)^-$ ions as in the first series, a mixture of $Ba(NO_3)_2$ and $Ba(OH)_2{\cdot}8H_2O$ is dissolved into the water used to hydrate the cement. These samples are characterised in the same way, and the results discussed.

3.2.3 Electrically Accelerated Leaching

In Chapter 5, a previously used procedure for E-Leaching [7], [12], [13] is investigated, using 3:1 BFS:PC cement samples prepared as above (40 x 40 x 5 mm). The samples were set in the sample holder as shown in Figure 3.1: In the holder, the cement sample is encased in rubber packing, resulting in the actual exposure surface to be 32 x 32 mm rather than the entire area of the sample directed towards the electrodes. The current density applied to the cement

sample for the experiments in this project was therefore calculated using this area of exposure– see Equation 3.1

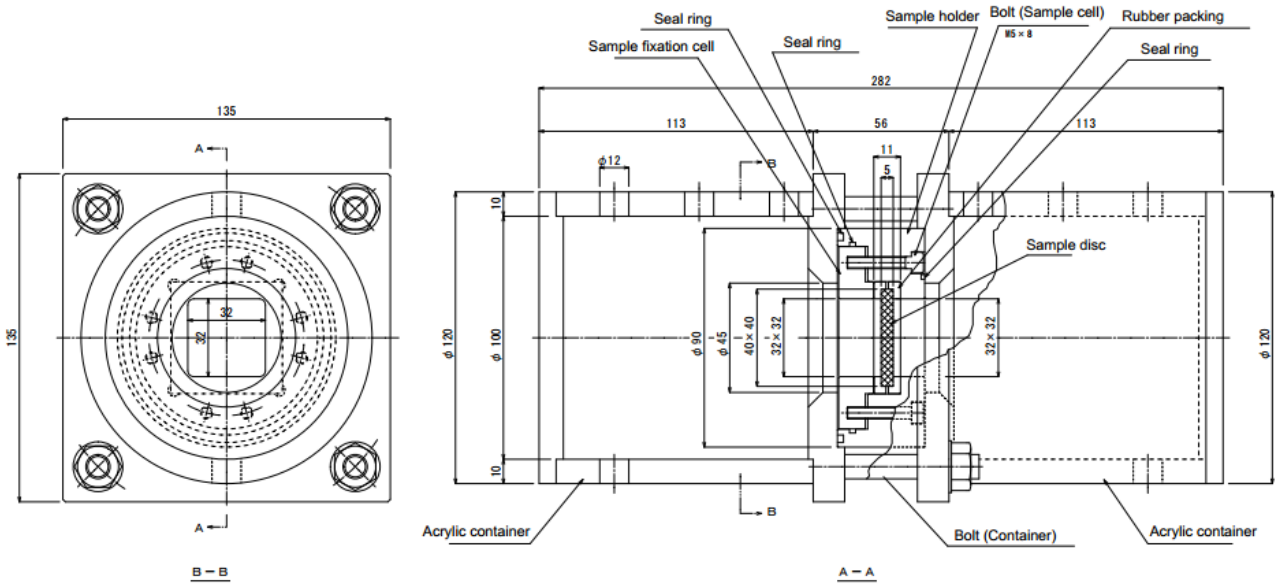

Figure 3.1 The design of the electrically accelerated leaching device. Image used with permission of Proffesor Katsufumi Hashimoto [12]

$$J = I/A$$

Equation 3.1

Where J is the current density (Am^{-2}), I is the direct current (DC) across the electrodes in the migration cell (Amps), and A is the sample's area of exposure (m^2). A photograph of the equipment is shown in Figure 3.2.

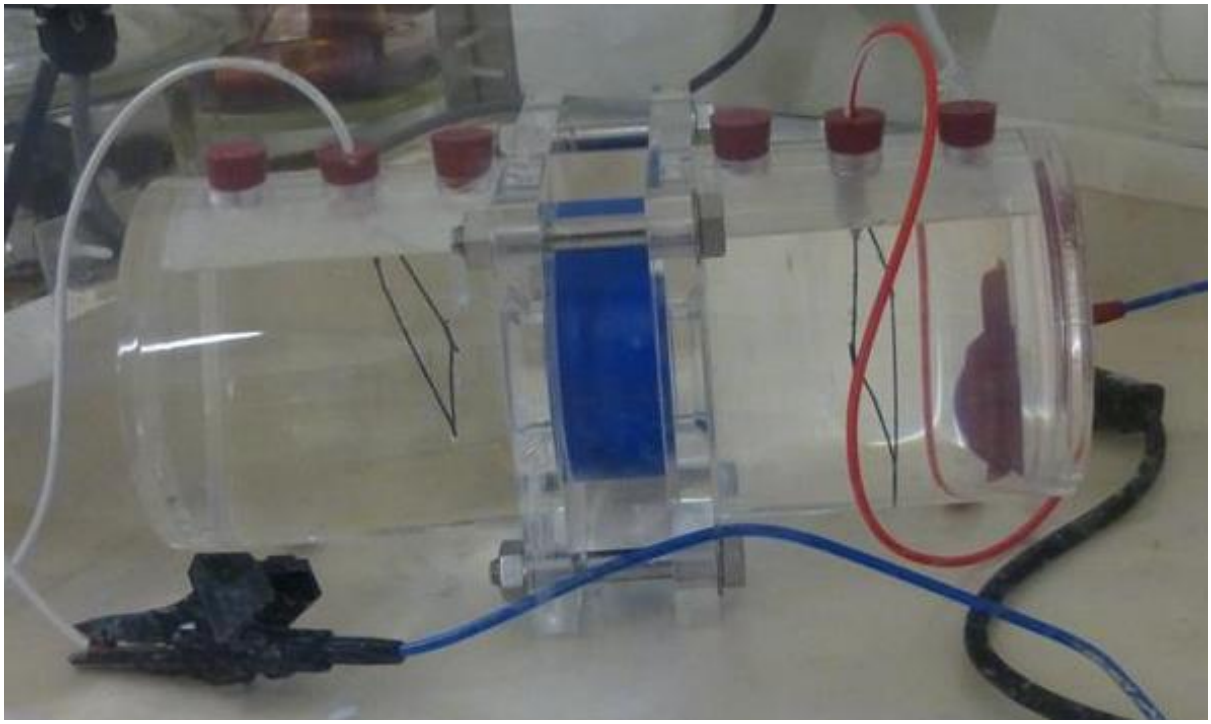

Figure 3.2 Photograph of the electrically accelerated leaching equipment; during use, it is held within a safety shutoff box that prevents the flow of current when the lid is removed.

The standard procedure to prepare a sample for electrical leaching is as follows:

1. The cement sample is placed into a container of water, which is then put into a desiccator under vacuum for 24 hours prior to leaching.
2. The sample is placed in the rubber packing, which is put into the first seal ring, the second seal ring is pushed into the first, and the seal rings are bolted together.
3. The electrodes to be used are placed in both of the acrylic containers. Electrodes and containers are marked either anode or cathode.
4. The acrylic containers are bolted together with the seal rings between them to create a water-tight seal, and a bung is inserted into the bottom of each container (used to drain the containers after the test) and the migration cell is placed into the safety shutoff box.
5. 750ml of the leachant to be used (typically distilled H_2O) is poured into each container.

6. Bungs are inserted into the holes on the top of the containers – the holes the electrodes come out of require a bung with a hole drilled through it. This is done so that during a test, little to no leachant escapes via steam etc.
7. The electrodes are attached to the power supply and the safety shutoff box is closed, and the desired maximum voltage and current (current calculated from the desired current density) are selected on the power supply.
8. The power supply is manually activated and the test begins. The temperature of the solutions in the tanks was not measured during the experiments.

3.2.4 Use of Electrical Leaching to experimentally simulate nuclear decay in a 3:1 BFS:PC cementitious wasteform

Electrical leaching as a technique is in many ways similar to the Rapid Chloride Permeability Test (RCPT), where a concrete sample is held between two cells, one containing a 3.0% NaCl solution and the other containing a 0.3 M NaOH solution, and a DC voltage of 60V is held between them over six hours [14]. This induces the accelerated migration of the NaCl into the concrete over this time, and the electric current between the two electrodes is measured over time. This well-established process of using a direct current to introduce material into a concrete sample, rather than electrical leaching where a DC is used to pull material out of the sample, naturally lead to applications in radioactive decay research, as in ILW radionuclides such as Cs-137 decay into Ba.

As shown in Table 3.2, various combinations of anode solution and cement sample were tested for different durations of time (3, 7 and 14 days). Three types of sample were studied: 'Blank cement' which is plain 3:1 BFS:PC, 'Cs cement', 3:1 BFS PC with $CsNO_3$, and 'Ba cement', which is 3:1 BFS PC with $Ba(OH)_2.8(H_2O)$ and $Ba(NO_3)_2$. The complete formulations are shown

in Table 3.2. The amount of $Ba(OH)_2.8(H_2O)$ and $Ba(NO_3)_2$ was chosen based on the solubility limit, and the amount of $CsNO_3$ was chosen to match with that of Ba in moles similar to work done in Chapter 4. The electrical leaching tests were conducted based on the same basic procedure described in Section 3.2.3. All leaching experiments were conducted at 25 Am^{-2}. To examine the effect of the current applied, one cement sample of each formulation was placed into a migration cell with distilled water and electrodes but with no applied electrical current.

40ml of the solution from each tank was collected for ICP-OES testing and replaced with the same amount of deionised water after 3, 7, 14, 21 and 28 days for the control tests. The cement samples were then crushed and analysed using XRD and XRF. Included in this report are those analyses carried out by the author. For the experiments where the anode solution was altered, the amount of $Ba(OH)_2{\cdot}8(H_2O)$ and $CsNO_3$ dissolved was 0.32g and 0.2g respectively, which was calculated using the average weight of the samples and the cement formulations, to match with the total moles of $CsNO_3$ and $Ba(OH)_2{\cdot}8(H_2O)$ in the cement sample, respectively: the amount of Cs (or Ba) dissolved into the anode solution is equal to the average amount of Ba (or Cs) in the equivalent cement sample.

Table 3.2 Table of experiments conducted for the work in Chapter 6

Cement sample	Control test Solutions gathered at:	No addition	$Ba(OH)_2.8(H_2O)$
Blank 3:1 BFS:PC	**A**	**B**	**B**
$CsNO_3$ 3:1 BFS:PC	**A**	**B**	**B**
$Ba(OH)_2.8(H_2O)$ and $Ba(NO_3)_2$ 3:1 BFS:PC	**A**	**B**	**–**

Key: A 1, 7, 14, 21, 28 days; **B** leaching experiments conducted for 3, 7, 14 days; **-** no such test conducted

3.3 Analytical Techniques – Phase Analysis

3.3.1 X-Ray Fluorescence

X-ray fluorescence (XRF) is a technique used to gather data on the specific oxide content of a powdered sample [15]. X-rays with a short wavelength and thus with a high energy as shown in Equation 3.2 are fired at the sample to induce the photoelectric effect [16], where h = Planck's Constant, c = the speed of light in a vacuum and λ = the wavelength of the x-ray. The incident x-ray can induce excitation of an atom and cause it to eject an electron from its inner orbital.

$$E = \frac{hc}{\lambda}$$

Equation 3.2 [16]

In return, an electron from the atom's outer orbitals falls down to fill this gap, and due to the difference in energy levels an x-ray is emitted, with an energy characteristic of the element in question. The energy of the emitted x-rays from the sample is detected, and the intensity of each wavelength (i.e. number of photons with that wavelength) is proportional to the amount of each element in the sample. This data is presented as a weight % of the sample that is due to each element detected. During the project two XRF machines where used to analyse different powdered samples: untreated BFS powder and PC powder were characterised using a PANalytical Zetium XRF machine. Otherwise the XRF was conducted by the author on secondment to Hokkaido University, Japan using a JEOL JSX-3100R II Elemental Analyser.

3.3.2 X-Ray Diffraction

X-Ray Diffraction (XRD) is used to identify the crystalline phases present in powdered cement samples with a particle size diameter ≤ 63µm. A source of X-rays is incident on a powdered cement sample, whose photons are then diffracted by the atoms in the crystalline phases

present [15]. The diffractions from different planes interfere constructively at certain angles based on Bragg's Law (Equation 3.3):

$$n\lambda = 2d\ sin\theta$$

Equation 3.3 [15]

Where n is an integer, λ is the wavelength of the x-rays, d is the distance between two lattice planes within the crystal and θ is the incident angle of the incoming x-rays as shown in Figure 3.3. The intensity of the diffraction can be plotted as a function of the diffraction angle, producing XRD pattern data. As XRD gathers the data of crystalline phases only, distinct peaks are difficult to obtain for more amorphous phases (sometimes colloquially referred to as "glassy phases" [17]) such as those present in BFS.

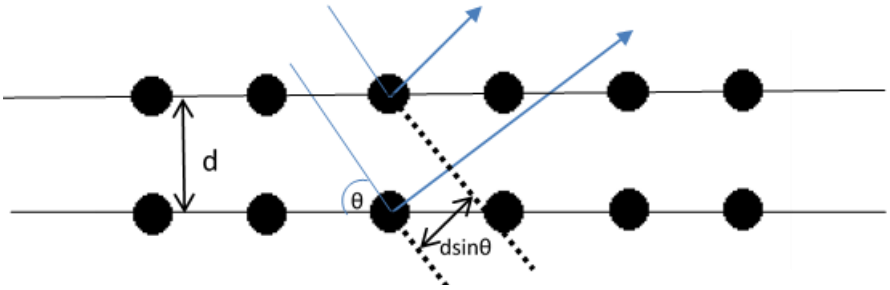

Figure 3.3 Bragg diffraction of a crystalline lattice

Cement samples were crushed into powder in acetone using a ceramic mortar and pestle, and then put through a sieve to ensure a particle diameter of ≤ 63µm to ensure random orientation of the crystal structure. A Siemens D5000 Diffractometer with a sample changer was used with a 2θ range of 5-65° with a step size of 0.02° and the detector rotated through one degree per minute (1 second per step). A scan was conducted with an empty sample

holder, and this dataset is referred to as the background, although the background test was not conducted in each case due to the high quality of the instrument. The prepared sample was then placed into a plastic sample holder and both the sample and the x-ray source were held static whilst the detector was rotated to detect the diffracted X-rays. The data was analysed using the PDF-4+ software to compare data with the ICDD database and identify phases; the relevant peak information is shown in Table 3.3. Two other XRD scanning procedures were used to gather data for the work in Chapter 5 and 6: One with a 2θ range of 5-65°, a step size of 0.02° and 7.2 second per step, and a second in the range of 5-15° with a step size of 0.02° and 30 seconds per step.

Table 3.3 XRD peak information and PDF card sources

Label	Name	Chemical formula	Peak position (2θ)	PDF Card Number
G	gehlenite	$Ca_2Al_2SiO_7$	23.89, 29.02, **31.29, 33.28, 36.81,** 43.8, 51.87	04-015-3030
5	gypsum	$CaSO_4 \cdot 1/2H_2O$	**11.62, 20.74, 32.13**	00-021-0816
P	portlandite	$Ca(OH)_2$	**18.1,** 28.7, **34.12, 47.18,** 50.9, 54.4	00-004-0733
H	hydrotalcite	$Mg_6Al_2(CO_3)(OH)_{16} \cdot (H_2O)_4$	**5.5, 11.2, 22.7**	00-041-1428
He	hemicarbonate	$(Ca_4Al_2(OH)_{12})(OH_{0.4}(CO_3)_{0.8}(H_2O)_4$	**11.45, 23.01, 31.09**	00-041-0725
E	ettringite, aFt	$Ca_6(Al(OH)_6)_2(SO_4)_3(H_2O)_{26}$	**9.12, 15.8, 22.9**	01-073-6239
M	monosulfate, aFm	$Ca_4Al_2(SO_4)(OH)_{12} \cdot (H_2O)_6$	**9.87, 19.85, 38.15**, 41.28	00-050-1607
C-S-H	C-S-H	$Ca_3Si_2O_7 \bullet (H_2O)_3$	7.07, **29.06, 31.94, 49.79**	00-034-0002
2	calcite	(Trigonal) $CaCO_3$	**29.41,** 35.97, **39.40, 43.15,** 47.49, 48.51	00-005-0586
1	aragonite	(Orthorhombic) $CaCO_3$	**26.21,** 27.22, **33.13, 45.85,** 48.32, 50.23	00-041-1475
$CsNO_3$	caesium nitrate	$CsNO_3$	**19.87, 28.30, 34.86,** 40.41, 45.37, 50.12	00-009-0403
–	barium nitrate	$Ba(NO_3)_2$	**18.94, 21.9, 31.17, 36.48, 38.42**	04-006-5677
*	barium hydroxide octahydrate	$Ba(OH)_2 \cdot 8H_2O$	**15.14, 25.26, 27.54, 33.54**	00-026-0155
Bc	barium carbonate	$BaCO_3$	**23.88, 34.6, 41.94, 44.9**	
B	barite	$BaSO_4$	**25.95, 26.95,** 28.8, **42.74,** 43.05	04-002-9537

XRD analysis is widely used in cement science as it allows users to quickly test a cement sample to see what phases have formed in the hydration process, and even though the sample is crushed in the process, the same cement formulation will give the same results under XRD and is highly repeatable, and is a qualitative test. PDF-4+ is a software package that allows users to compare their data with single-phase XRD patterns held in a large database to find the most likely phases that are present in the sample. The data is firstly imported as intensity against 2θ. Scans conducted over longer periods of time have less noise,

and any scans that do not follow the above procedure to reduce noise are shown. The main peaks in the data are then selected. Separately within PDF-4+ the user can create filters to sort through the ICDD database – the two main methods to create the filters used in this project were based on sorting what minerals were expected to be present, or more often what elements may have been present in the phases. The second method lists all combinations of those elements found in the database, and when applied to the data finds the most likely minerals and sorts them by the highest intensity. Each phase found by the software can then be peak-matched by the user to confirm phases, and each phase in the database lists information such as the date acquired and the experimental conditions used to aid in confirmation.

With simpler samples where all phases are known, it is possible to conduct Rietveld analysis, sometimes called Rietveld refinement. In this project Rietveld refinement is used to examine the percentage weight of phases present in the precipitate found in tanks after leaching has been conducted. This analysis gives a weight % of each phase present in a sample, for instance 23% calcite, 77% aragonite, and is a quantitative test that further refines the data from XRD. It should be noted that when using PDF-4+ and all phases in the data are selected – that is, each peak in the data is linked to a PDF card in the database – Rietveld analysis is an automatic function, but the relevant formula is also noted below (Equation 3.4).

$$W_p = 100 \cdot S_p(MVZ)_p / \sum_{i=1}^{n} S_i(MVZ)_i$$

Equation 3.4 Formula used in Rietveld phase analysis where in a mixture of n phases where p is the phase of interest, Wp is the weight% of the phase, S is the Rietveld scale factor, M is the atomic mass of the formula unit, V is the unit cell volume (in Angstroms^3), and Z is the number of formula units per cell

Due to cement's complexity in the number of phases present as well as the presence of amorphous and anhydrous material, Rietveld analysis is not widely used, but in the past it has been used to examine the rate of hydration. It is more commonly applied to the analysis of ceramics, where the production of single or dual phases is desired and the fraction of reacted material is of interest.

3.3.3 Thermal Analysis

3.3.3.1 Thermal Gravimetry

TG measures the percentage mass loss of a powdered sample over a programmed temperature range, known as a heating profile. It provides quantitative information related to the weight of phases present in a sample as they begin to decompose, melt or evaporate at different temperatures [18]. For the measurement, cured cement samples were crushed in acetone using a pestle and mortar, then put through a 63µm sieve. Typically, around 40 mg of the fine powder was then placed in an alumina sample pan, which was put in a PerkinElmer STA8000, a simultaneous thermal analyser capable of conducting both TG and DTA on the same sample concurrently. The temperature scheme was to start gathering data when 40°C was reached, and then raise the temperature to 1000°C at 10°C per minute with the sample held in either a flowing nitrogen or air environment. Pyris software was used as an interface to gather the data.

3.3.3.2 Differential Thermal Analysis

As stated in 3.2.3.1, DTA was run concurrently with TG. This is a different method of thermal analysis. An empty alumina pan was used as a reference in a separate part of the PerkinElmer STA8000 and underwent the same thermal cycle as the sample being analysed – the sample and the reference received the same heat energy over time. The difference in temperatures between the sample and the reference is recorded as a function of time or temperature (as

the increase in temperature over time is constant), although the first differential of the data is usually shown as it gives sharper peaks [18]. DTA is useful when used in conjunction with TG, as it shows peaks in the data when there are phase transitions and reactions as well as weight loss events, because these are exothermic or endothermic depending on the material [18].

3.3.3.3 Differential Scanning Calorimetry

DSC is a third thermal analysis method similar to DTA, however, in DSC the sample and the reference are held in thermal lockstep through the heating profile and the difference in the energy required to raise the temperature of both at 10°C per minute is recorded [18]. A PerkinElmer DSC7 was used with a heating profile from 25 to 600°C at 10°C per minute and the analysis was carried out in a flowing nitrogen environment.

3.4 Analytical Techniques – Solutions and Leachate Analysis

3.4.1 Inductively Coupled Plasma Optical Emission Spectrometry

Inductively Coupled Plasma Optical Emission Spectrometry (ICP-OES) is an analytical technique that allows users to quickly test the concentration of elements in a solution [19], [20]. It is also known as Inductively Coupled Plasma Atomic Emission Spectroscopy (ICP-AES). As suggested by the title, it uses an inductively-coupled-plasma to induce the emission of photons from the sample, which are characteristic of the atoms present. The ICP-OES machine first needs to be calibrated with a standard solution containing the elements required and where the concentration is known. These are commercially available. The technique works as follows:

1. The sample solution containing the leached ions is pumped using a peristaltic pump into an analytical nebuliser to produce a mist of the sample.

2. This mist is then introduced to a plasma torch, which is produced by an RF (Radio Frequency) generator discharging an arc into an Argon flow.

3. The collision of the mist with the plasma breaks down the sample into charged atoms which repeatedly gain and lose electrons.

4. This causes the emission of photons due to the photoelectric effect, similar to that seen in XRF.

5. The wavelengths of the photons are characteristic of the ions present [16], and the intensity of these photons is used to automatically calculate the concentration, with repeat measurements conducted to find an average.

There are other techniques for analysing a solution's content such as ion chromatography, which gives information about the oxidation state and concentration of different positive or negative ions. However, using these techniques, the user has to decide to test for either positively or negatively charged ions, whereas ICP-OES can test for the elemental concentration of atoms in a solution regardless of whether they are positive or negative in the same test without the need for recalibration.

3.4.2 pH Measurements

The acidity or basicity of a solution can be measured using a pH meter. According to the Arrhenius definition, when a material is dissolved in pure water, it is an acid if H^+ or H_3O^+ ions are released (making the solution acidic), and it is a base if OH^- ions are produced/released, making the solution basic or alkaline. The concentration is such that when the concentration of H^+ is multiplied with the concentration of OH^-, the result is always 1×10^{-14} mol^2/l^2 (at 25°C), and as a simplification, pH is mathematically defined in Equation 3.5 to be on a scale from 1 to 14. A pH of 7 indicates a neutral solution and an equal concentration of H^+ and OH^- ions

(10^{-7} mol/l each). pH<7 indicates the solution is acidic, and pH>7 means it is alkaline. It should be noted that within the cement body, the pH is usually high, in the range of 11-13 [21]–[23]. This is why acidic leaching is effective at dissolving the solid cement phases as submerging a sample in acid can drastically lower the internal pH.

$$pH = -log_{10}H^+$$

Equation 3.5 pH is the negative logarithm to the base ten of the hydrogen ion concentration

In this project the pH of leachates in the anode and cathode tanks is of interest as the different chemical content is expected to alter the pH in the tanks over time. A potentiometric pH meter is used, which utilises the Nernst equation (Equation 3.6) developed in 1889 [24] relating the concentration of H^+ ions to the voltage, E. E_0 is the potential at standard-state conditions. R is the molar gas constant 8.3144598 m^2 kg s^{-2} K^{-1} mol^{-1}, T is the temperature in Kelvin, n is the number of moles of electrons and F is the Faraday constant 96 485.3329 C Mol^{-1} The pH is measured by examining the voltage in the electrode between the two wires as shown in the diagram in Figure 3.4. If the concentration of hydrogen ions outside the bulb is equal to the concentration inside, the voltage will be 0; if it is greater outside (acidic) the voltage will be positive, and negative if it is greater inside (alkaline solution). The electrode is connected to a digital metre, which automatically displays the correct pH after the electrode has been calibrated in three buffer solutions of pH 4, 7 and 10.

$$E = E_0 + \frac{RT}{nF} \cdot ln(H^+)$$

Equation 3.6

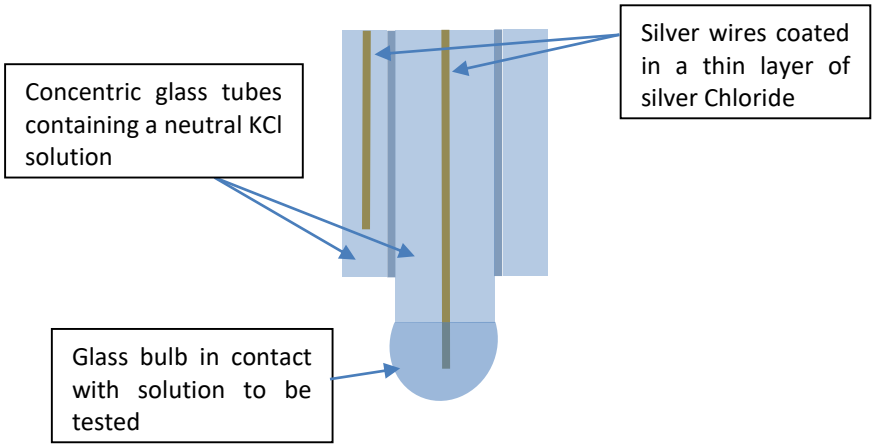

Figure 3.4 Silver chloride electrode for the pH meter used in this project

3.4.2.1 Expected pH effects of electrolysis

In static and semi-static leaching, any change in the leachate's pH is caused by the change in elemental concentration, however, the introduction of electrodes is expected to change the pH behaviour dramatically due to electrolysis, and both tanks will behave differently. In the cathode tank, H^+ ions are attracted to the cathode where two can combine to form H_2 gas, which then escape the solution leaving an abundance of OH^- in the tank, increasing the measured pH as shown in Equation 3.7 [25]. In the anode tank, however, OH^- ions are attracted to the electrode, where four can combine as shown in Equation 3.8 releasing O_2 gas, leaving an abundance of H^+ ions [25]. To remain charge balanced the electrons donated at the anode cause the reduction reaction at the cathode to occur twice. These reactions along with the change in elemental concentration are expected to change the measured pH in electrical leaching tests.

$$2H^+ + 2e^- \longrightarrow H_2$$
$$2H_2O + 2e^- \longrightarrow H_2 + 2OH^-$$

Equation 3.7 [25]

$$4\ OH^- \longrightarrow O_2 + 4H^+ + 4e^-$$
$$2H_2O \longrightarrow O_2 + 4H^+ 4e^-$$

Equation 3.8 [25]

3.5 Analytical Techniques – Microstructure Analysis

3.5.1 Scanning Electron Microscopy/Energy Dispersive X-ray spectroscopy

Scanning Electron Microscopy (SEM) is a technique that can be used to analyse solid cement samples, and gives information on the microstructure and morphology of the cement, with features such as pores, cracks, unhydrated cement particles, discernible in the Back-Scattered Electron (BSE) images this technique produces [5]. As the name suggests, this technique works by firing electrons at a sample using a Scanning-Electron Microscope. As these electrons approach the nucleus of an atom, they are deflected, and can be reflected (or back scattered) at high angles up to 180° towards a detector, producing a grey-scale image based on the number of electrons detected for that area of the sample. Cracks and pores in the cement are visible as dark or black areas as few electrons can be scattered, and as heavier atoms will scatter more electrons, these tend to be lighter or even white areas in the BSE image – lighter elements appear darker. In the samples analysed in this project, the bulk hydrated cement appear darker than any unhydrated cement particles observed.

Once a BSE image is obtained, elemental maps can be produced using energy-dispersive x-ray spectroscopy (EDX) – this can give information about the elemental makeup of the selected area of the sample [5]. EDX works by firing electrons at the sample that have a high enough energy to ionise the atoms at the surface (forcing an inner orbital electron to escape the atom), which in turn causes a transition of an outer shell electron to fill the lower orbital, and a characteristic X-ray is emitted to account for the energy difference of these orbits [5]. Some of the released X-rays interact with a detector, and since the software knows where on the sample the x-ray came from (based on where the electron beam was aiming at the time), the

Quantax software can make a map of elements on the sample, and the number of these x-rays is directly related to the amount.

The machine used in this project was a Hitachi TM3030 where the sample first needs to be mounted in resin. The resin is mixed with 4-parts epoxy resin to 1-part hardener. The cement sample is placed in a mould, and approximately 25 ml of the resin mixture is poured in, producing SEM 'stubs', which are left to harden for 24 hours. These can then be stored for later use as the resin on the surface of the sample prevents carbonation. To prepare for SEM analysis, the stubs were ground (to remove the resin on the surface) and polished using a Ketmet manual polisher, with isopropanol as a lubricant. Once a sample was ready to be analysed, the general operating procedure was setting the microscope to a low magnification, and then moving the sample in the machine to find an area of interest – the sample was held in a vacuum. A working distance of 8.5 mm and an accelerating voltage of 15 kV is used. Once the sample was being examined, the auto focus and contrast were used and adjusted to obtain a clear picture, and then a slow scan was activated to create a BSE image which was then saved. An EDX software called Quantax was then used with the Hitachi 3030 to produce EDX maps of the same area of the sample.

3.5.2 Mercury Intrusion Porosimetry

Mercury Intrusion Porosimetry (MIP), as the name suggests, is a technique that gives information about the *porosity* of a sample by forcibly *intruding mercury* into it by placing a cement sample in a container of mercury, and applying a steadily increasing pressure [26]. A Micrometrics Poresizer 9320 was used to analyse samples that had been dried in isopropanol and placed under vacuum in a desiccator. Mercury can be forced into the cement's pores as it is a non-wetting element, and the MIP machine has a low-pressure stage (up to 5000 psia)

that can fill the larger pores first, and then a high pressure stage (5000-30,000 psia) that fills smaller pores [26]. The volume of mercury entering the sample at these pressures gives various sets of data. The data shown in this project is the total porosity and the pore size distribution. The total porosity is calculated from the amount of mercury that could be pumped into the sample, and is given as a percentage of the sample's volume. The pore size distribution is shown as a function of the volume of mercury that has intruded into the sample against the pore diameter on the x-axis. The y-axis shows the function, the logarithmic differential intrusion, which is calculated using Equation 3.9, where V is the volume of mercury that has intruded the cement sample, and D is the pore diameter.

$$\text{Log (differential intrusion)} = dV/d\log(D) \qquad \textbf{Equation 3.9} \text{ [26]}$$

3.6 Characterisation of Initial Materials

3.6.1 Cementitious Materials

CEM I strength class 52.5n Portland cement and Ribblesdale Ground Granulated Blast Furnace Slag provided by Hanson Heidelberg Cement Group are used for this research project, as these are the types of cement currently in use for nuclear waste management in the UK [11], as discussed in Chapter 2. XRF data for both anhydrous PC and BFS, as well as the calculated oxide content for the 3:1 BFS:PC mixture, are shown in Table 3.4. The main components of BFS are CaO and SiO_2, which constitute over 2/3 of the total oxide content, consistent with previous analysis of BFS [27]. Typical BFS SiO_2 content is in the range of 10-12%; the high SiO_2 content in the BFS used here is due to the addition of Calumite, which produces a blended BFS with "high flow […] without the use of chemical admixtures" [28], [29].

Table 3.4 XRF data in Parts Per Million (PPM %) of the Sellafield encapsulation grade Regen BFS and Hanson Cement 52.5n PC used in this project (data gathered by the author)

	BFS	PC	3:1 BFS:PC (calculated)
Oxide Content	PPM (%)	PPM (%)	PPM (%)
CaO	39.68	65.37	46.103
Al_2O_3	11.81	4.55	9.997
BaO	0.068	0.03	0.0585
Cr_2O_3	0.049	0.01	0.0390
Fe_2O_3	0.418	3.12	1.0936
K_2O	0.632	0.67	0.6414
MgO	8.118	2.09	6.6112
Mn_3O_4	0.486	0.09	0.3871
Na_2O	0.379	0.31	0.3619
P_2O_5	0.049	0.17	0.0790
SiO_2	35.58	19.99	31.686
SO_3	1.673	3.23	2.060
SrO	0.087	0.11	0.09313
TiO_2	0.817	0.24	0.6725
Total	99.85	99.98	99.8825

Figure 3.5 shows the XRD pattern of the anhydrous PC with the background removed using the ICDD's (International Centre for Diffraction Data) embedded search indexing software in their PDF4+ software package [30] – the labels used in the graph for the mineral phases are identified in Table 3.3 with the relevant PDF card. This shows a typical spectrum for PC [31], [32] with the four main clinker phases identifiable, as well as some calcium carbonate originating from reaction of these clinker phases with atmospheric carbon dioxide. Figure 3.6 shows the XRD data of anhydrous BFS, and exhibits a large area caused by diffuse scattering of X-rays due to low or non-crystalline phases [33], [34]. Some Gehlenite peaks are observed. When the background of XRD data is removed, some of the diffraction due to amorphous content, present for example in BFS, used can be lost [5]. The rest of the XRD data shown in this thesis is shown unaltered (e.g. with no background removal applied) to allow for full interpretation of the results.

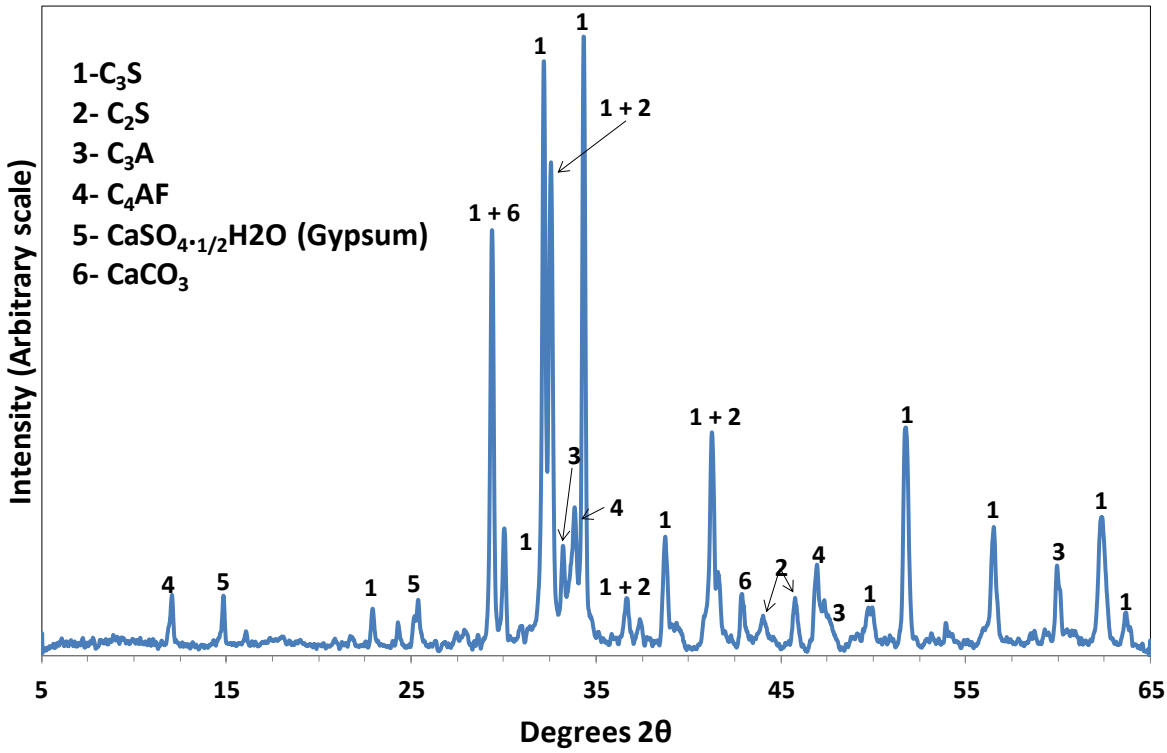

Figure 3.5 X-ray pattern of anhydrous PC

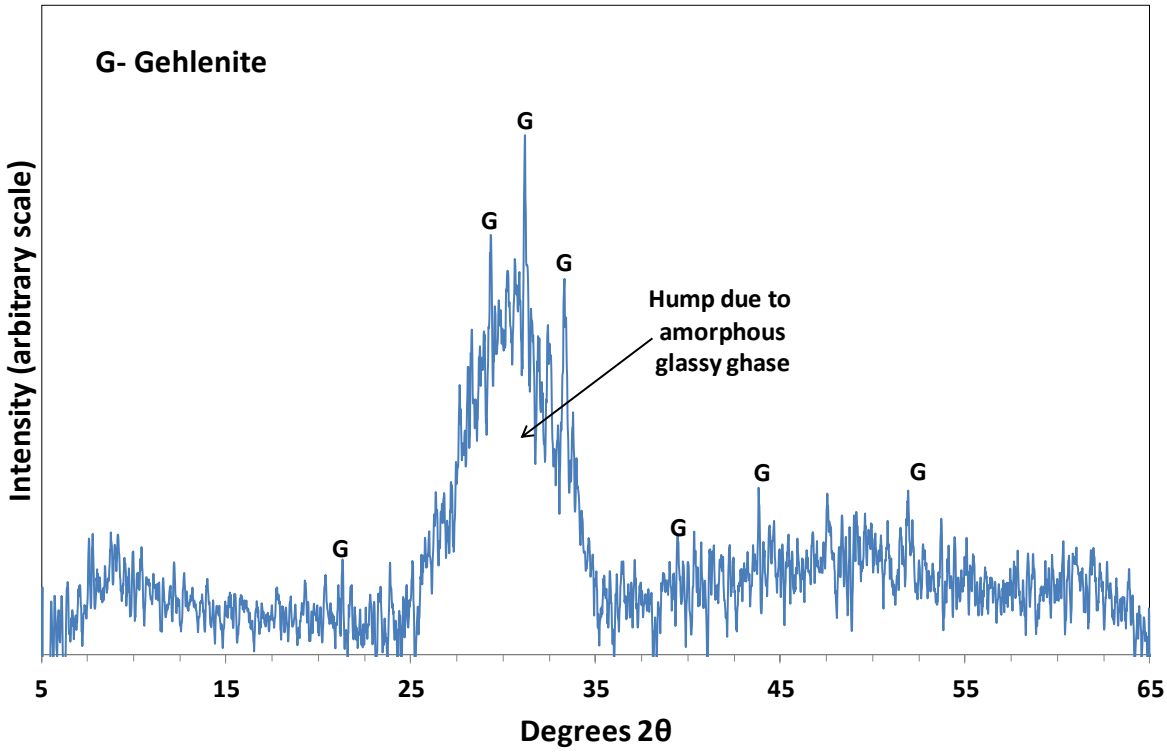

Figure 3.6 X-ray pattern of Hanson Cement BFS

Figure 3.7 and Figure 3.8 show the TG and DTA data, respectively, of BFS in both oxidising (air) and inert (N_2) atmospheres. TG data shows BFS experiences a slight mass loss during heating in both atmospheres up to around 600°C, and mass gain above this temperature, similar to previous observations [35]. In 2002, Ramachandran et al. suggested that this mass gain may be due to reaction of the sample with the oxygen present in the system, causing sulphide to become sulphate, changing the oxidation state of sulphur from S^{2-} to S^{4+} [18]. Even in the nitrogen atmosphere, there is still some oxygen present as an impurity, likely due to the machine not having a perfect environmental seal. The reason for the slightly greater weight loss (by 0.2 wt.%) at up to 600°C in air is not very clear, but it may be related to the behaviour of sulphur, as the weight difference became negligible when sulphide oxidised to sulphate. If this weight loss was not related to the behaviour of sulphur content, the weight difference would remain even after the oxidation of sulphide at higher temperature. A distinctive exothermic reaction is observed in the DTA data at 850°C, which others have attributed to the devitrification event taking place in BFS [36], [37]. There appears to be a peak at 90°C which is likely H_2O, and another event around 680°C, which is likely calcite originating from CaO on the surface of the glassy phase reacting with atmospheric CO_2 [18], [36], [38].

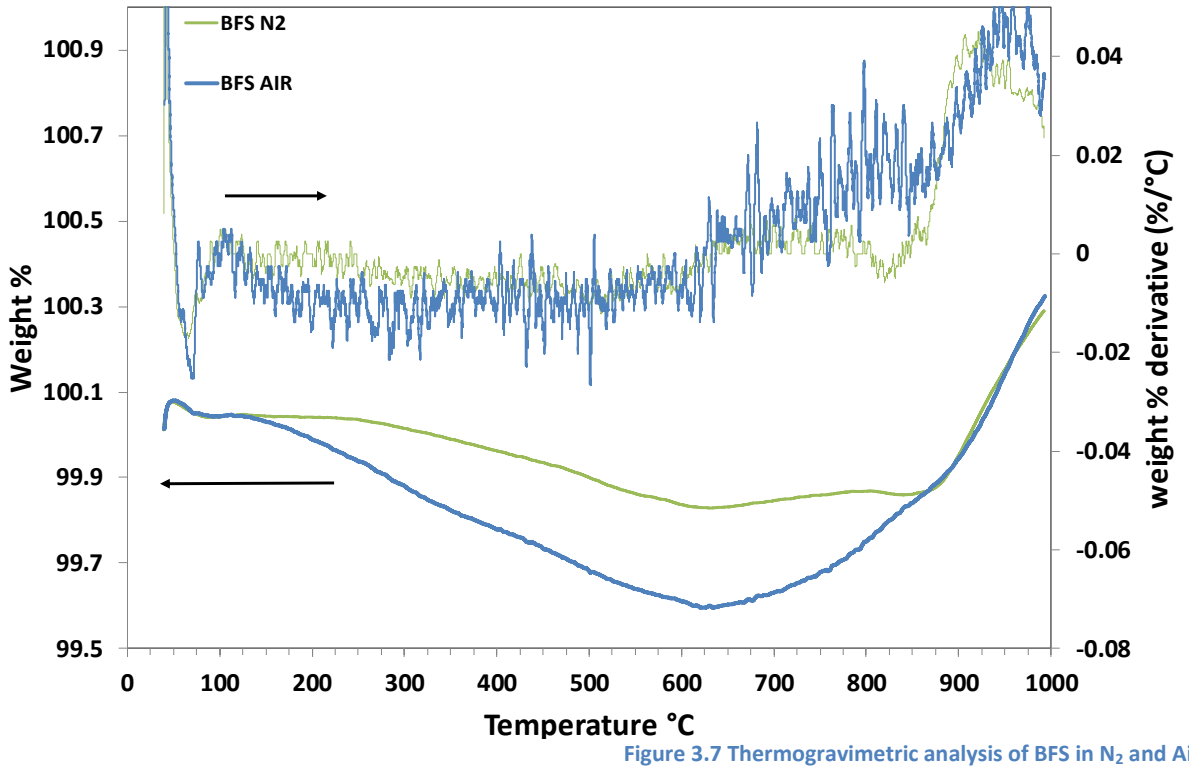

Figure 3.7 Thermogravimetric analysis of BFS in N_2 and Air

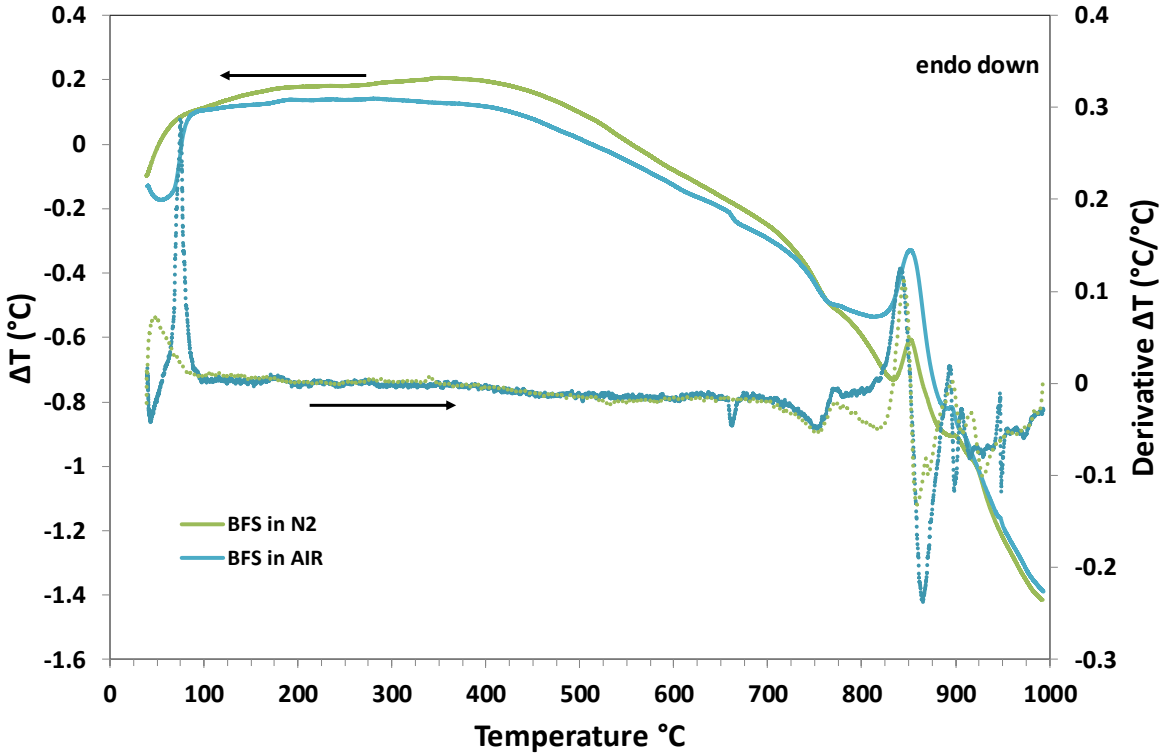

Figure 3.8 DTA of BFS in N_2 and Air

Figure 3.9 displays the TG analysis of anhydrous PC, and Figure 3.10 shows the DTA obtained simultaneously. The significant weight loss on the TG curve and corresponding to the trough on the DTG curve at 320 to 390°C is due to hydrogarnet [18]. The response at 500-650°C is likely due to the decomposition of calcium carbonate present in the powder [18]. DTA data also indicate the endothermic dehydroxylation of hydrogarnet up to 390°C. As PC experiences elevated temperatures over 1450°C during the production, these phases must have formed during storage, reacting with moisture and CO_2 in air, which caused a total weight loss of 0.88% as the temperature of 1000°C was reached.

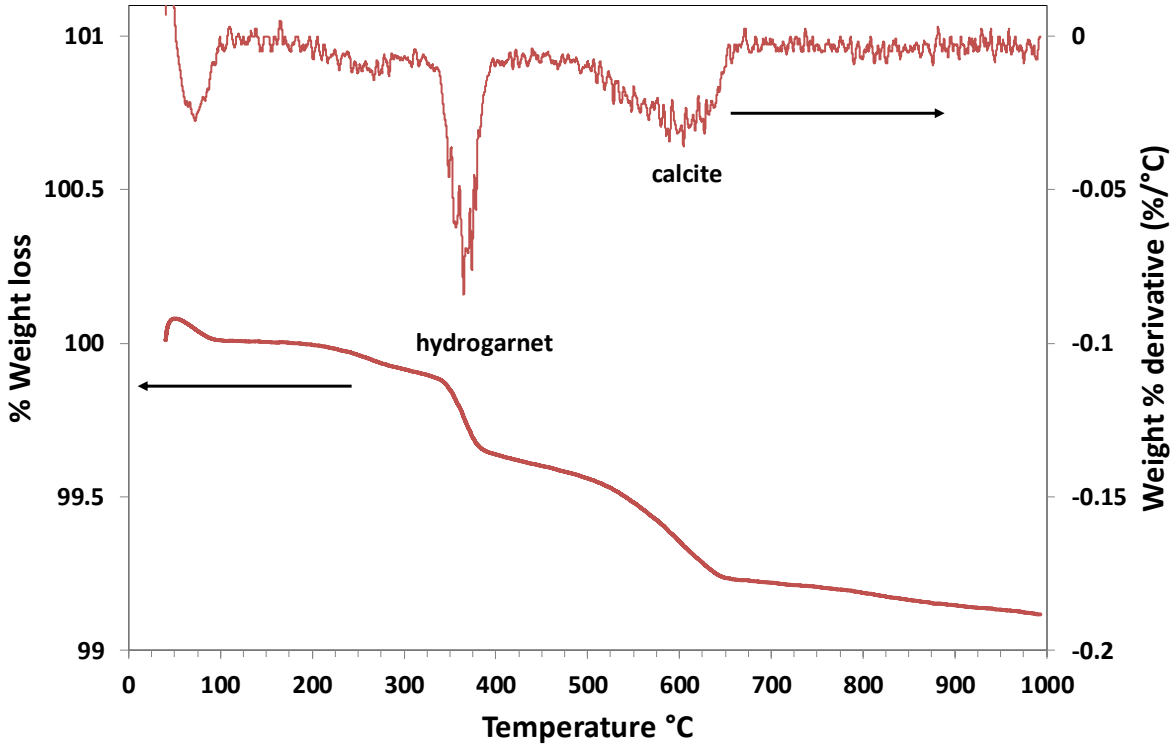

Figure 3.9 Thermogravimetric analysis of PC powder in N_2

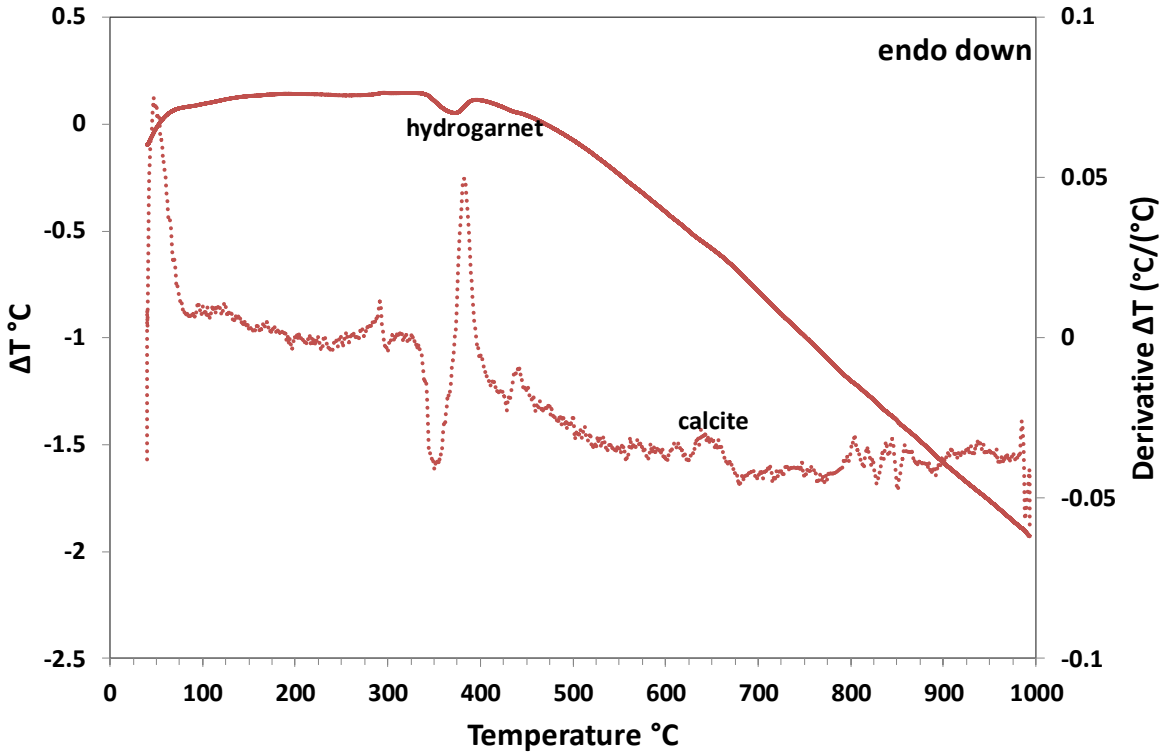

Figure 3.10 Differential Thermal Analysis of PC powder in N_2

3.6.2 Additional Materials used: Caesium Nitrate, Barium Hydroxide Octahydrate and Barium Nitrate

XRD of the caesium nitrate used in Chapter 4 and 6 is shown in Figure 3.11– all peaks observed are attributed to this molecule.

XRD of the barium hydroxide octahydrate used in both Chapter 4 and 6 is shown in Figure 3.12 – note that whilst barium carbonate was observed in the sample (resulting from a reaction with atmospheric CO_2) it is likely that some of this was produced when the powder was being crushed and prepared for XRD analysis.

XRD of the barium nitrate used in Chapter 4 is shown in Figure 3.13 – all peaks observed are attributed to this molecule.

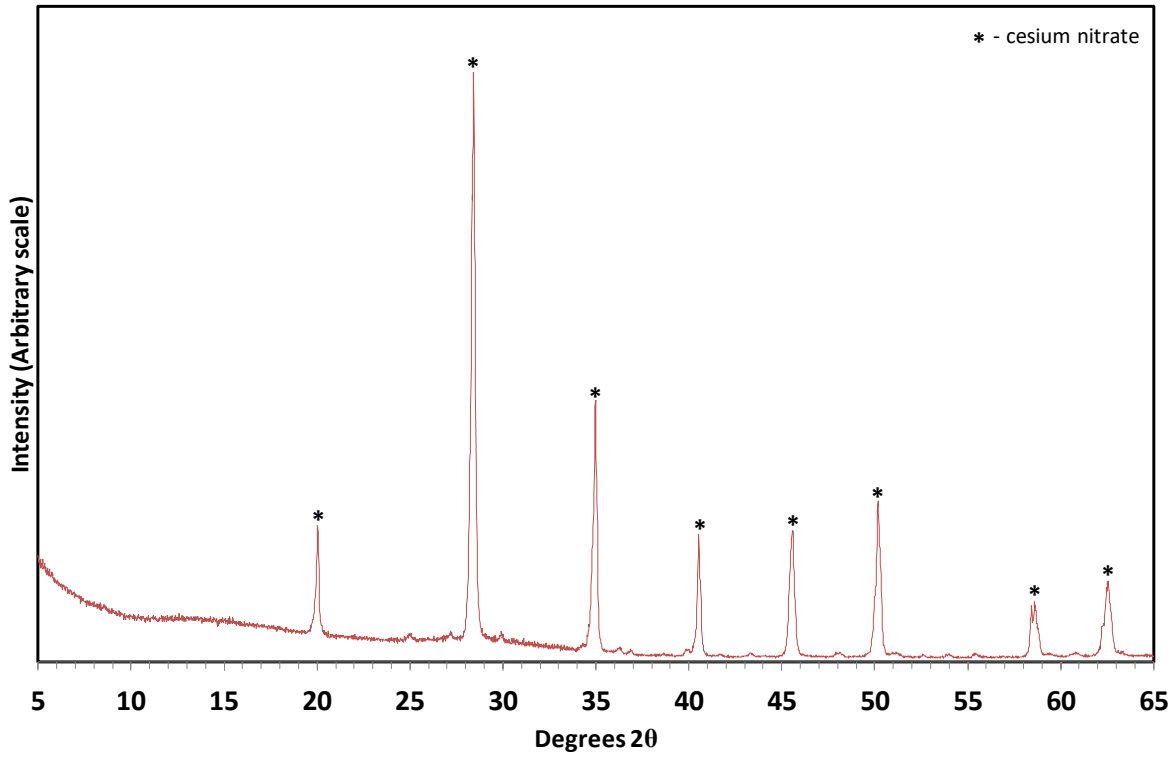

Figure 3.11 XRD Pattern of the caesium nitrate used in this project – all peaks identified as $CsNO_3$

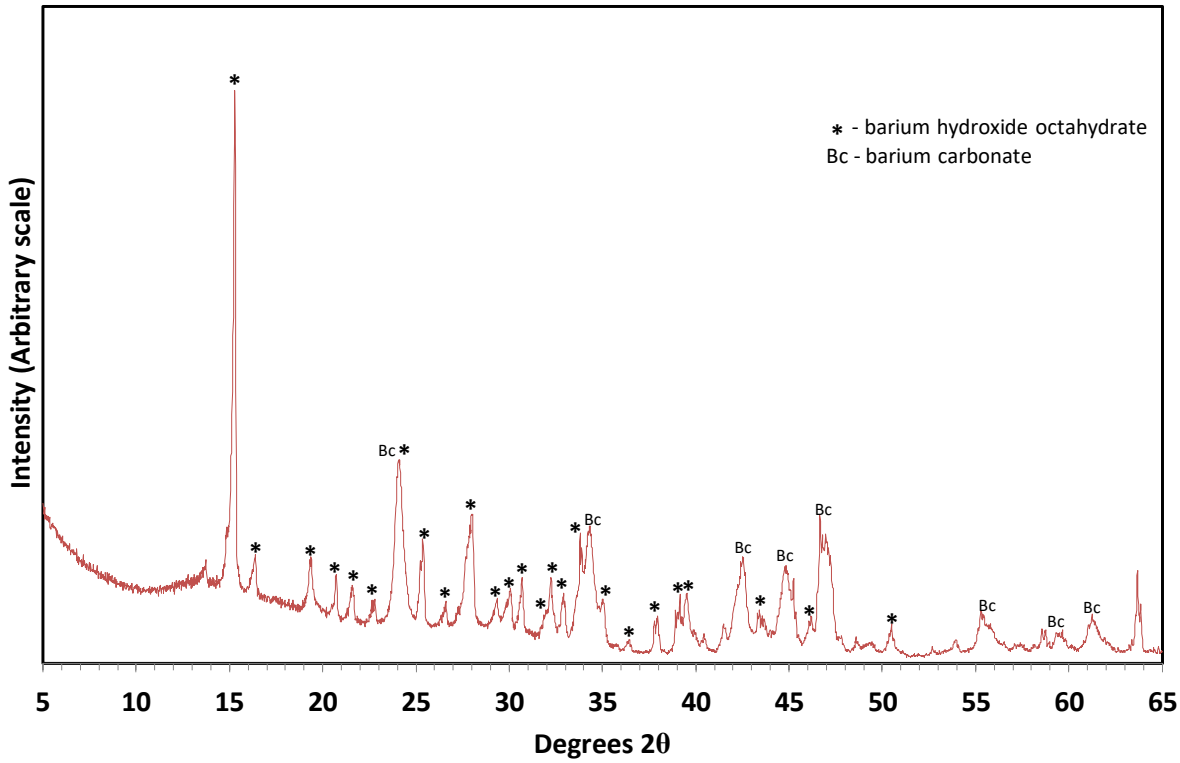

Figure 3.12 XRD pattern of the barium hydroxide octahydrate used to examine the incorporation of Cs and Ba in Chapter 4

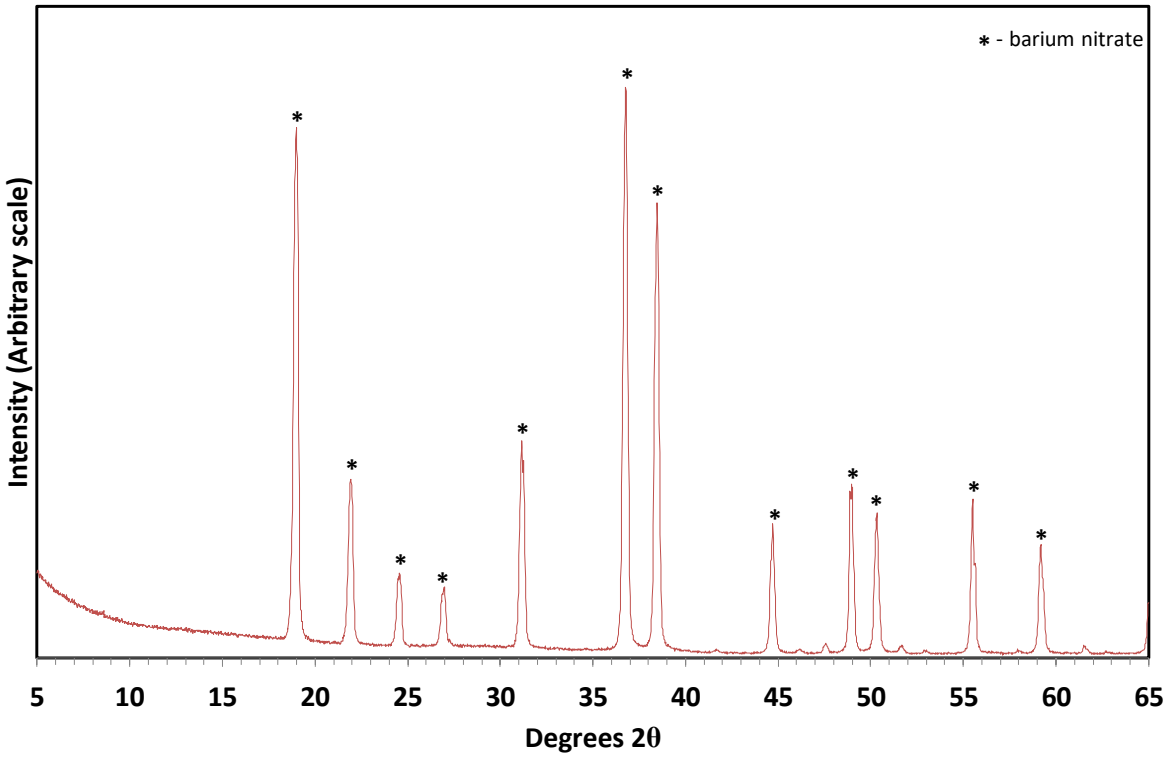

Figure 3.13 XRD Pattern of the barium nitrate used to examine the incorporation of Cs and Ba in Chapter 4 – all peaks identified as $Ba(NO_3)_2$

3.6.3 Preliminary Testing of Cement Matrices

In the beginning of this project, 3:1 BFS:PC samples produced in the 5 x 40 x 40 mm steel mould were analysed after 28 days of curing. Figure 3.14 shows the XRD data of a 2-hour scan, with a 2θ range of 5-65° with a step size of 0.02° and the detector moved through 0.5 degrees per minute. There is an area of diffuse scattering between 25° and 35° due to the low crystalline nature of the BFS. There is evidence of PC clinker phases that have not reacted, though the formation of C-S-H is evident as well as portlandite, hydrotalcite and monosulphate. There is a distinct C-S-H peak in the 3:1 sample at 49.79°.

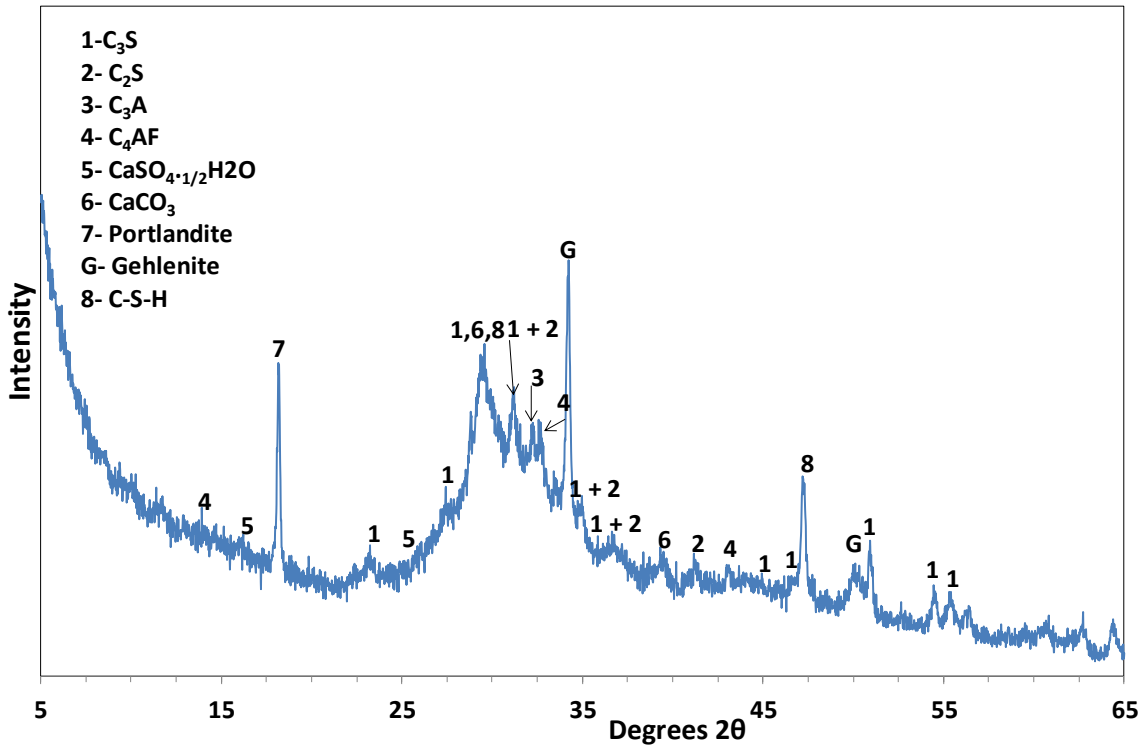

Figure 3.14 Two-hour XRD scan of 28D 3:1 BFS:PC

This cement sample was also analysed using TG and DTA, shown in Figure 3.15 and Figure 3.16 respectively. In the tested sample, the thermally induced mass changes are observed, which can be due to the evaporation of phases or water, or the oxidation of ions. The mass loss or gain at certain temperature ranges can be used to identify phases in the sample as these changes for each phase are temperature dependant. For example, phases such as C-S-H, monosulphate, hydrotalcite, portlandite and calcium carbonate are observed based on the response at around 100°C, 160°C, 190°C, 440°C and 600°C, respectively [18], [21], [39].

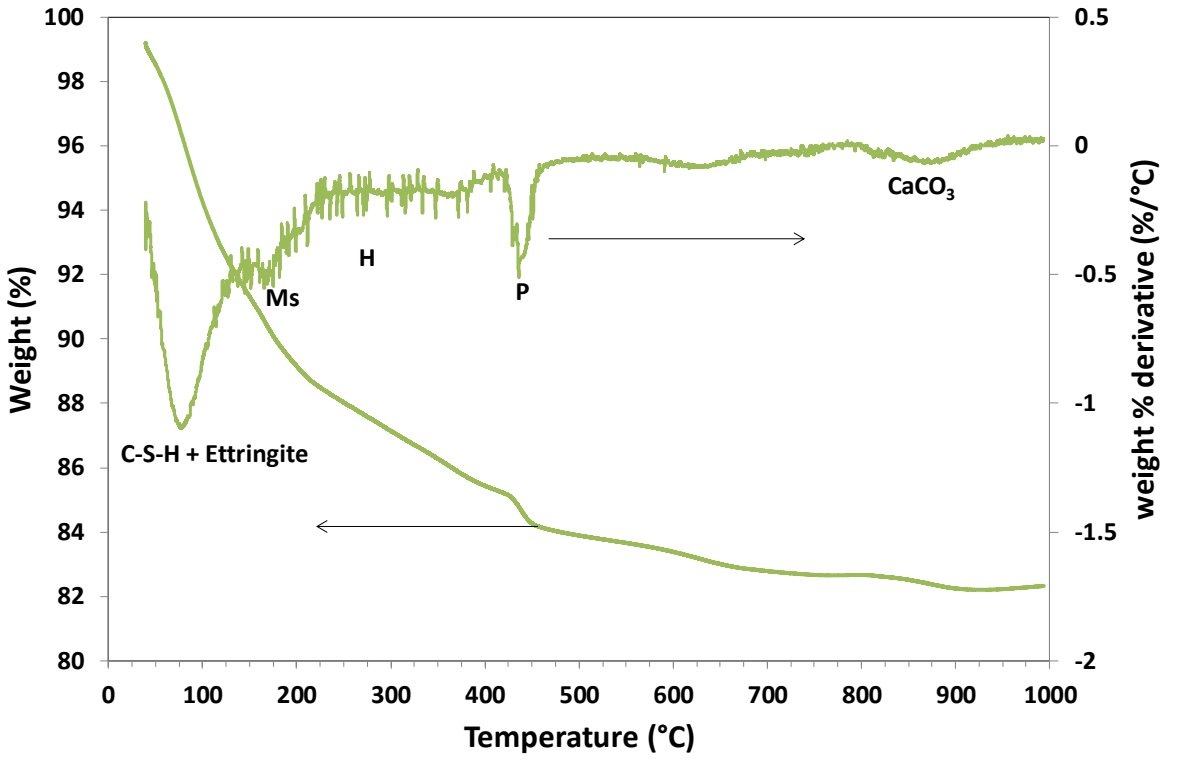

Figure 3.15 TG of 28 Day 3:1 BFS:PC

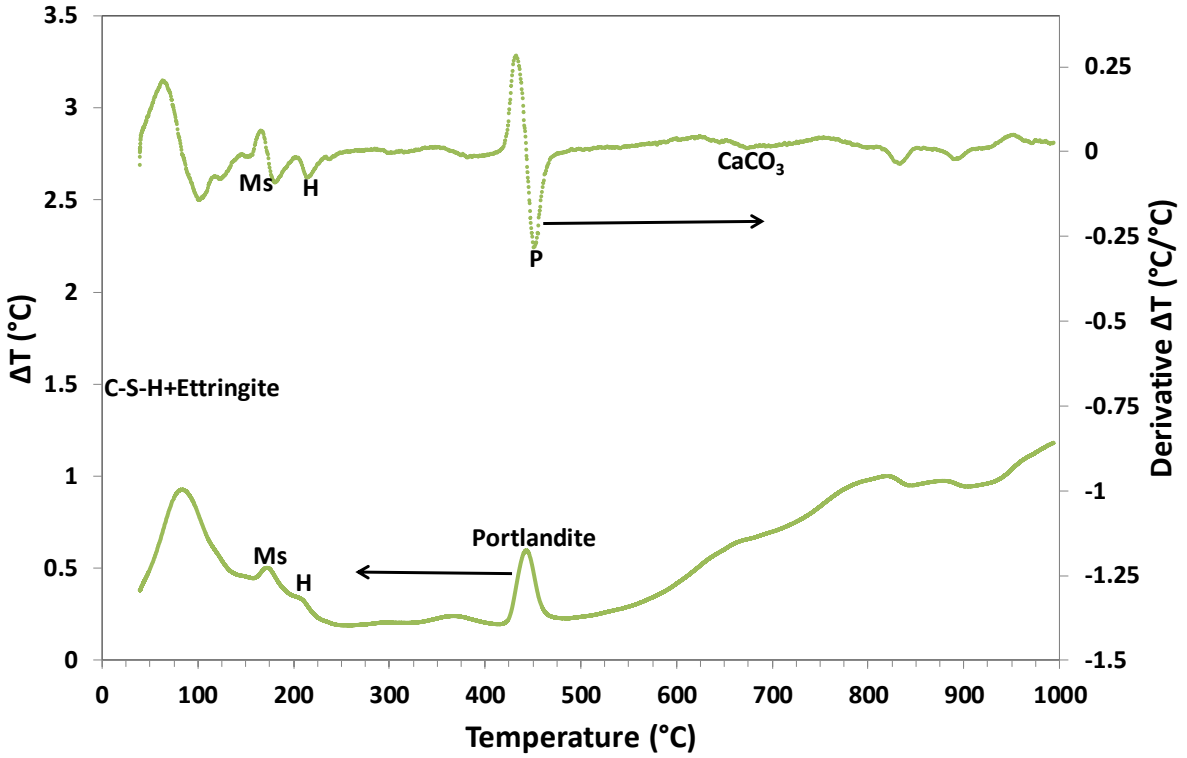

Figure 3.16 DTA of 28 Day 3:1 and 9:1 BFS:PC

3.7 References

[1] British Standards Institution, "BS EN 197-1:2011 Cement Part 1: Composition, specifications and conformity criteria for common cements," 2011. [Online]. Available: http://shop.bsigroup.com/ProductDetail/?pid=000000000030331489. [Accessed: 17-Jun-2017].

[2] R. Taylor, "Composition and microstructure of 20-year-old ordinary Portland cement-ground granulated blast-furnace slag blends containing 0-100% slag," *Cem. Concr. Res.*, vol. 40, pp. 971–983, 2010.

[3] K. Yokozeki, J. Nakasone, K. Kakizaki, and K. Watanabe, "Study on the durability of underground concrete structures used over 100 years," *Japan Concr. Inst. Proc.*, vol. 20, no. 1, pp. 251–256, 1998.

[4] N. Otsuki, H. Minagawa, S. Miyazato, and T. Nishida, "Fundamental study on prediction of concrete deterioration caused by calcium leaching over 100 years," *Proc. JSCE*, vol. 51, no. 679, 2001.

[5] K. L. Scrivener, R. Snellings, and B. Lothenbach, *A practical guide to microstructural analysis of cementitious materials*. Boca Raton: CRC Press, 2016.

[6] H. F. W. Taylor and A. B. Turner, "Reactions of tricalcium silicate paste with organic liquids," *Cem. Concr. Res.*, vol. 17, no. 4, pp. 613–623, 1987.

[7] K. Hashimoto, N. Otsuki, T. Saito, and Y. H, "Application of electrical treatment to alteration of cementitious material due to leaching," *J. Adv. Concr. Technol.*, vol. 11, no. 3, pp. 108–118, 2013.

[8] W. J. Hickinbottom, *Reactions of Organic Compounds*, 3rd ed. London: Longmans, Green and Co, 1957.

[9] M. D. A. Thomas, "The suitability of solvent exchange techniques for studying the pore structure of hardened cement paste," *Adv. Cem. Res.*, vol. 2, no. 5, pp. 29–34, 1989.

[10] T. Ekström, "TVBM-3090, Leaching of Concrete: Experiments and Modelling," 2001. [Online]. Available: http://portal.research.lu.se/ws/files/4827018/1766469.pdf. [Accessed: 17-Jul-2017].

[11] N. J. Bowmer and S. Curwen, "WP1- Details of encapsulation processes at Sellafield." BNFL Commerical, Sellafield, UK, p. 46, 2007.

[12] K. Hashimoto, H. Kinoshita, W. Gashier, A. J. MacArthur, and H. Yokota, "Development of an electrical leaching technique - evaluation of leaching from a hardened cement body," *34th Cement and Concrete Science Conference, Sheffield*. University of Sheffield, 2014.

[13] W. Gashier, T. Miura, K. Hashimoto, R. J. Hand, and H. Kinoshita, "Leaching behaviour of cementitious nuclear wasteforms containing caesium and strontium," *Adv. Appl. Ceram.*, vol. 113, no. 8, pp. 447–452, 2014.

[14] ASTM International, "C1202 Standard Test Method for Electrical Indication of

Concrete's Ability to Resist Chloride Ion Penetration," 2010. [Online]. Available: https://www.astm.org/Standards/C1202.htm. [Accessed: 17-Jun-2017].

[15] R. Snellings, "Chapter 4: X-ray powder diffraction applied to cement," in *A practical guide to microstructural analysis of cementitous materials*, 1st ed., K. L. Scrivener, R. Snellings, and B. Lothenbach, Eds. Boca Raton, Florida, USA: CRC Press, 2016, pp. 107–176.

[16] H. Young and R. Freedman, *University Physics*, 12th ed. Harlow, England: Sears & Zemansky, 2008.

[17] B. Lothenbach, K. Scrivener, and R. D. Hooton, "Supplementary cementitious materials," *Cem. Concr. Res.*, vol. 41, no. 12, pp. 1244–1256, 2011.

[18] V. S. Ramachandran, R. M. Paroli, J. J. Beaudoin, and A. H. Delgado, *Handbook of Thermal Analysis of Construction Materials*. Norwich, NY: Noyes Publications/William Andrew Publishing, 2002.

[19] P. Patnaik, *Handbook of Inorganic Chemicals*. New York: McGraw-Hill, 2002.

[20] P. C. Hewlett, "Lea's Chemistry of Cement and Concrete." Elsevier, 1998.

[21] E. Gruyaert, N. Robeyst, and N. De Belie, "Study of the hydration of Portland cement blended with blast-furnace slag by calorimetry and thermogravimetry," *J. Therm. Anal. Calorim.*, vol. 102, pp. 941–951, 2010.

[22] I. G. Richardson, C. R. Wilding, and M. J. Dickson, "The hydration of blastfurnace slag cements," *Adv. Cem. Res.*, vol. 2, no. 8, pp. 147–157, 1989.

[23] K. L. Scrivener, P. Juilland, and P. J. M. Monteiro, "Advances in understanding hydration of portland cement," *Cem. Concr. Res.*, vol. 78, pp. 38–56, 2015.

[24] W. Nernst, *Begründung der Theoretischen Chemie: Neun Abhandlungen, 1889-1921*. Frankfurt am Main: Verlag Harri Deutsch, 2003.

[25] C. W. Davies, *Principles of electrolysis*. London: Royal Institute of Chemistry, 1968.

[26] E. Berodier, J. Bizzozero, and A. C. A. Muller, "Chapter 9: Mercury intrusion porosimetry," in *A practical guide to microstructural analysis of cementitous materials*, 1st Editio., K. Scrivener and R. Snellings, Eds. Boca Raton, Florida, USA: CRC Press, 2016, pp. 419–444.

[27] S. Akbarnejad and L. J. M. Houben, "Chemical and mineralogical characterization of blast furnace slag as a road base material," in *9th International Sustainable Construction Materials in Asphalt, Pavement Engineering and Highway Maintenance*, 2010.

[28] Heidelberg Cement, "Production and use of GGBS," 2007.

[29] Heidelberg Cement, "GGBS and related products: Sellafield," 2014. [Online]. Available: http://www.heidelbergcement.com/uk/en/hanson/products/cements/ggbs_and_rela

ted_products/sellafield_.html. [Accessed: 17-Jun-2017].

[30] "ICDD, PDF-4 Technical Bulletin," 2013. [Online]. Available: http://www.icdd.com/products/technicalbulletins/PDF-4_Technical_Bulletin.pdf. [Accessed: 03-Jul-2017].

[31] C. A. Utton, "The encapsulation of BaCO3 waste in composite cements," University of Sheffield, Sheffield, 2006.

[32] L. Gordon, "The encapsulation of clinoptilolite in cementitious systems," University of Sheffield, Sheffield, 2008.

[33] N. Mobasher, S. A. Bernal, O. H. Hussain, D. C. Apperley, H. Kinoshita, and J. L. Provis, "Characterisation of Ba (OH)2 – Na2 SO4 – blast furnace slag cement-like composites for the immobilisation of sulfate bearing nuclear wastes," *Cem. Concr. Res.*, vol. 66, pp. 64–74, 2014.

[34] W. Mozgawa and J. Deja, "Spectroscopic studies of alkaline activated slag geopolymers," *J. Mol. Struct.*, vol. 924–926, no. C, pp. 434–441, 2009.

[35] J. R. Harbour, E. K. Hansen, T. B. Edwards, V. J. Williams, R. E. Eibling, D. R. Best, and D. M. Missimer, "Characterization of slag, fly ash and portland cement for saltstone," 2006. .

[36] C. Fredericci, E. D. Zanotto, and E. C. Ziemath, "Crystallization mechanism and properties of blast furnace slag glass," *J. Non. Cryst. Solids*, vol. 273, pp. 64–75, 2000.

[37] D. Furuya, N. Otsuki, T. Saito, and L. Yun sub, "A study of the effects of seawater as mixing water on the hydration characteristics of blast-furnace slag cement," *34th Conference on Our World in concrete & Structures*. Singapore, 2009.

[38] P. C. Hewlett, *Lea's Chemistry of Cement and Concrete*, no. 4th edition. Amsterdam: Elsevier Ltd, 2004.

[39] C. A. Utton, E. Gallucci, J. Hill, and N. B. Milestone, "Interaction between BaCO3 and OPC/BFS composite cements at 20°C and 60°C," *Cem. Concr. Res.*, vol. 41, pp. 236–243, 2011.

Chapter 4: The Incorporation of Cs and Ba in 3:1 BFS:PC

4.1 Introduction

In this Chapter, the incorporation of caesium (Cs) and barium (Ba) in 3:1 BFS:PC systems is discussed. In the experiments presented, Cs was incorporated in the form of $CsNO_3$ at various weight percentages (wt.%). The results of fundamental materials characterisation of the products are presented and the effects of composition are discussed. Whilst the hydration of BFS:PC cement systems has been widely studied in the past [1]–[5], and the interactions of cements such as geopolymers and Portland cements with Cs have been investigated [6]–[9], there is little data in the literature specifically examining the interactions of Cs with BFS:PC systems when added during hydration. Therefore, the experiments discussed in this Chapter were devised to investigate this gap in research. Gashier et al. published a paper in 2014 [10] where the leaching of Cs from 9:1 BFS:PC samples was discussed; this Chapter aims to expand upon this work using 3:1 BFS:PC and incorporating increasing amounts of $CsNO_3$ into 3:1 BFS:PC to investigate at which point $CsNO_3$ will begin to precipitate inside the cement sample. The cement samples were produced using the procedure described in the previous Chapter (Section 3.3.1 and 3.3.3). The incorporation of Ba was also of particular interest, as the radioactive ^{137}Cs commonly found in ILW [6] eventually becomes Ba as the result of its radioactive decay [11], [12].

Ba was incorporated as a mixture of $Ba(NO_3)_2$ and $Ba(OH)_2{\cdot}8H_2O$, to match the number of moles of barium (Ba^{2+}) and nitrate (NO_3^-) ions to the system with the corresponding $CsNO_3$ incorporation. When ^{137}Cs decays, 1 mole of $CsNO_3$ yields 1 mole of Ba and 1 mole of NO_3. However, caesium ions have a charge of 1+, whereas barium ions have a charge of 2+, so 1 mole of barium nitrate contains 2 moles of nitrate ($Ba(NO_3)_2$). So, to match the molar content of NO_3^-, only half of the Ba is introduced as $Ba(NO_3)_2$, with the remainder added as barium

hydroxide octahydrate ($Ba(OH)_2 \cdot 8H_2O$). Due to the water held in barium hydroxide octahydrate, the w/b is altered, although the actual distilled water used would result in a 0.34 w/b ratio as shown in Table 4.1, which displays the cement formulations produced for this Chapter. Produced in this way, the 1 wt.% Ba sample has the same number of nitrate ions as the 1 wt.% $CsNO_3$ sample, and the other Ba and Cs samples are likewise matching, as shown in Table 4.1. In this Chapter the caesium samples are named according to the weight percentage of $CsNO_3$ (and the molar equivalent of Ba) they contain. Using this notation, samples prepared by Gashier et al. [10] using a 9:1 BFS:PC ratio contained 6.8 and 6.2 wt.% $CsNO_3$. The samples were analysed using XRD and thermal analysis techniques, such as DTA and DSC as described in Chapter 3 Section 3.4.2 and 3.4.3. TG data also gathered is shown in the Appendix. Selected samples were also examined using SEM and EDX. The 1, 3, 6 and 8 wt.% Cs samples were examined after 7, 14 and 28 days of hydration. The 1, 3 and 6 wt.% Ba samples were tested at 28 days only. 6 wt.% was the highest Ba wt.% produced due to the low solubility. At 25°C, the solubility of $Ba(OH)_2 \cdot 8H_2O$ in water is 37.6 g/l [13], the solubility of $Ba(NO_3)_2$ in water is 105 g/l [13]. $CsNO_3$ is significantly more soluble [14]–[16] and so higher concentrations were expected to be required for precipitation. $CsNO_3$ has a solubility of 239.5 g/l [16]. As examples of the extreme case, 16 wt.% $CsNO_3$ samples were additionally produced, which is beyond the solubility limit given the amount of water used, and these were then analysed using DTA, DSC and SEM-EDX to gain further information.

Table 4.1 Weight composition of 3:1 BFS:PC samples produced.

Sample name wt.%	PC (g)	BFS (g)	H_2O (g)	w/b ratio	$CsNO_3$ (g)	$Ba(OH)_2 \cdot 8H_2O$ (g)	$Ba(NO_3)_2$ (g)	Hydration solution	
								pH	Conductivity (mS/cm)
1 wt.% $CsNO_3$	99.1	300.0	136	0.34	4.01	–	–	6.61	17.12
3 wt.% $CsNO_3$	99.4	299.8	136	0.34	12.0	–	–	7.16	44.50
6 wt.% $CsNO_3$	100	300.2	136	0.34	24.1	–	–	7.33	79.99
8 wt.% $CsNO_3$	100	299.9	136	0.34	32.0	–	–	8.42	101.85
16 wt.% $CsNO_3$	100	300.1	136	0.34	36.1	–	–	8.42*	101.85
–	–	–	–	–	–	–	–	–	–
1 wt.% Ba	50.0	150	68.74	0.344	–	1.62 g	1.35 g	12.71	36.43
3 wt.% Ba	50.0	150	69.84	0.349	–	4.86 g	4.02 g	13.02	86.44
6 wt.% Ba	50.0	150	71.68	0.358	–	9.71 g	8.05 g	13.28	135.17

wt.% refers to adding an amount of $CsNO_3$ equal to the binder weight to the cement sample and the molar equivalent of barium. For example, a 10wt.% $CsNO_3$ sample could consist of 40g $CsNO_3$ dissolved into 136g of water, which is then mixed with a blend of 100g PC and 300g BFS. w/b ratio for the barium-containing samples includes the calculated water within barium hydroxide octahydrate to 3 significant figures, and otherwise the binder refers to the combined weight of the PC and BFS only. Due to the solubility limit of $CsNO_3$ (239.5 g/l), in the 16 wt.% sample almost half of the $CsNO_3$ was added as a dry powder once the water had been saturated. *$CsNO_3$ added up to saturation limit

4.2 Incorporation of $CsNO_3$ in 3:1 BFS:PC

3:1 BFS:PC was prepared with different wt.% of $CsNO_3$ incorporation as shown in Table 4.1 Weight composition of 3:1 BFS:PC samples produced. . The blend of 3:1 BFS:PC was used, as this is a blend commonly used for acceptance tests for waste encapsulation in the UK [17], whilst 3.44:1 is a common formulation used in practice [18]. Some previous studies have instead focused on 9:1 ratios [19]. The cement powder was mixed as described in Chapter 3 with a 3:1 BFS:PC ratio, and placed into the mixer on a low speed. The desired amount of $CsNO_3$ powder was dissolved into the water, then poured into the mixer as no temperature change was observed, after which the cement paste was poured into centrifuge tubes, sealed and kept until required for testing.

4.2.1 Effect of $CsNO_3$ on Phases Present in 3:1 BFS:PC– X-Ray Diffraction and Thermal Analysis

Figure 4.1 to Figure 4.4 are XRD data of 3:1 BFS:PC grouped by the wt.% of $CsNO_3$ (1 to 8 wt.%), showing the data at different curing stages for each formulation. The XRD data in these figures and all of the XRD patterns in this thesis were not normalised. These samples were

analysed using the conditions as described in Chapter 3, and labelled using the notation shown in Table 4.2 based on PDF card numbers, with a range of 5° to 65° at one degree per minute. In the system with 1 wt.% $CsNO_3$, peaks are attributed to C-S-H (PDF# 00-034-0002) and portlandite (PDF# 00-004-0733) formed from the hydration and development of typical cement phases [1]. The formation of ettringite, monosulphate and hydrotalcite is also observed, (PDF#s 01-073-6239, 00-050-1607, and 00-041-1428 respectively) with a strong peak for gehlenite (PDF# 04-015-3030) also apparent at all stages measured. These reflection peaks attributed to the crystalline phases did not seem to change much between 7 and 28 days of curing. The area due to diffuse scattering of x-rays between 25-53° 2θ appears to increase slightly with time, which suggests an increase in the amount of the amorphous C-S-H gel phase. Each sample showed peaks attributed to the cement clinker phases alite, belite, tricalcium aluminate and a small amount of ferrite (C_4AF), all of which show a decrease with respect to the hydrated C-S-H phase as time progresses and the curing continues – this is normal behaviour that was expected to be seen as the alite, belite and the BFS react with water over time to form C-S-H [1], [4].

The XRD data for the system with 3 wt.% $CsNO_3$ shows very similar features as that of 1 wt.%. A clear difference is a larger peak attributed to ettringite observed at approximately 9° 2θ. On the other hand, in the data for the systems with 6 and 8 wt.% $CsNO_3$, clear peaks for $CsNO_3$ are observed. The change in the intensities of the $CsNO_3$ peaks with time appears to be rather random, for example in the 8 wt.% $CsNO_3$ data in Figure 4.4, the $CsNO_3$ peak at 20° 2θ is not visible at 14 days, although it can be seen in the 7-day and most strongly in the 28-day data. There is more than one possible reason for this behaviour: (i) the $CsNO_3$ crystals could have a tendency of strong orientation in the cement sample, or (ii) possibly $CsNO_3$ slowly dissolved

in the pore solution in the first 14 days, and precipitated again as the water was consumed to hydrate more cement. This would require further research to confirm, for example by analysing how the Cs concentration in the pore solution changes over time. Although the formation of phases which indicate the hydration of the cement do not seem to be hindered by an increase in the wt.% of $CsNO_3$ added, this increase seems to encourage the formation of ettringite. The formation of hemicarbonate and hydrotalcite is observed at 7 days in the systems with higher $CsNO_3$ content, whereas it seems slower in the systems with lower $CsNO_3$ content.

Table 4.2 XRD peak information and PDF card numbers shown

Label	Name	Chemical formula	Peak position (2θ)	PDF Card Number
G	gehlenite	$Ca_2Al_2SiO_7$	23.89, 29.02, **31.29, 33.28, 36.81,** 43.8, 51.87	04-015-3030
P	portlandite	$Ca(OH)_2$	**18.1,** 28.7, **34.12, 47.18,** 50.9, 54.4	00-004-0733
H	hydrotalcite	$Mg_6Al_2(CO_3)(OH)_{16}\cdot(H_2O)_4$	**5.5, 11.2, 22.7**	00-041-1428
He	hemicarbonate, an AFm phase	$(Ca_4Al_2(OH)_{12})(OH_{0.4}(CO_3)_{0.8}(H_2O)_4$	**11.4451, 23.01, 31.09**	00-041-0725
E	ettringite, an AFt phase	$Ca_6(Al(OH)_6)_2(SO_4)_3(H_2O)_{26}$	**9.12, 15.8, 22.9**	01-073-6239
M	monosulfate, an AFm phase	$Ca_4Al_2(SO_4)(OH)_{12}\cdot(H_2O)_6$	**9.87, 19.85, 38.15**, 41.28	00-050-1607
Hg	hydrogarnet	$CaO_3Al_2O_3(H_2O)_6$	**17.26, 39.22, 44.4**	00-024-0217
C-S-H	C-S-H	Many known formulae, for example $Ca_3Si_2O_7\cdot(H_2O)_3$	7.07, **29.06, 31.94, 49.79**	00-034-0002
1	aragonite	(Orthorhombic) $CaCO_3$	**26.21,** 27.22, **33.13, 45.85,** 48.32, 50.23	00-041-1475
2	calcite	(Trigonal) $CaCO_3$	**29.41,** 35.97, **39.40, 43.15**, 47.49, 48.51	00-005-0586
$CsNO_3$	caesium nitrate	$CsNO_3$	**19.87, 28.30, 34.86,** 40.41, **45.37**, 50.12	00-009-0403
B	barite	$BaSO_4$	**25.95, 26.95,** 28.8, **42.74,** 43.05	04-002-9537
a	alite (C_3S)	Ca_3SiO_5	**32.25, 32.66, 34.41**	01-070-8632
b	belite (C_2S)	Ca_2SiO_4	**29.66, 32.66, 47.83**	00-001-1029
c	tricalcium aluminate (C_3A)	Ca_3AlO_6	**33.16, 47.60, 59.22**	00-032-0149

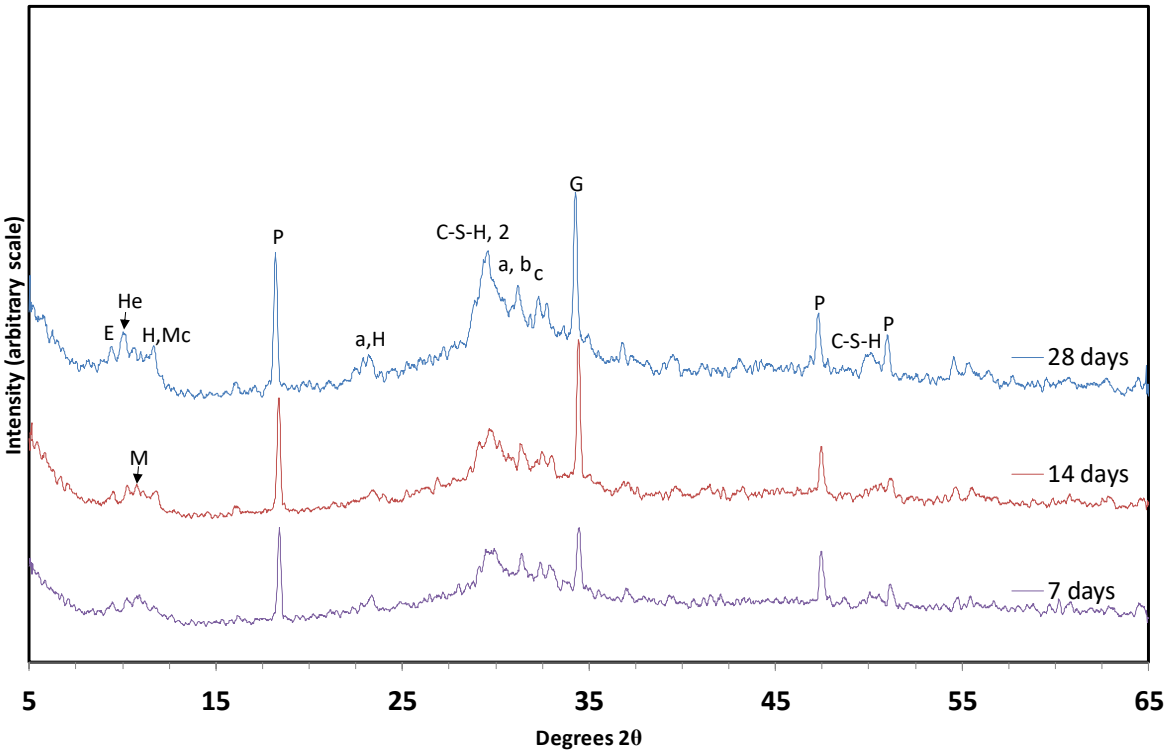

Figure 4.1 XRD patterns of 1 wt.% $CsNO_3$ 3:1 BFS:PC, various ages

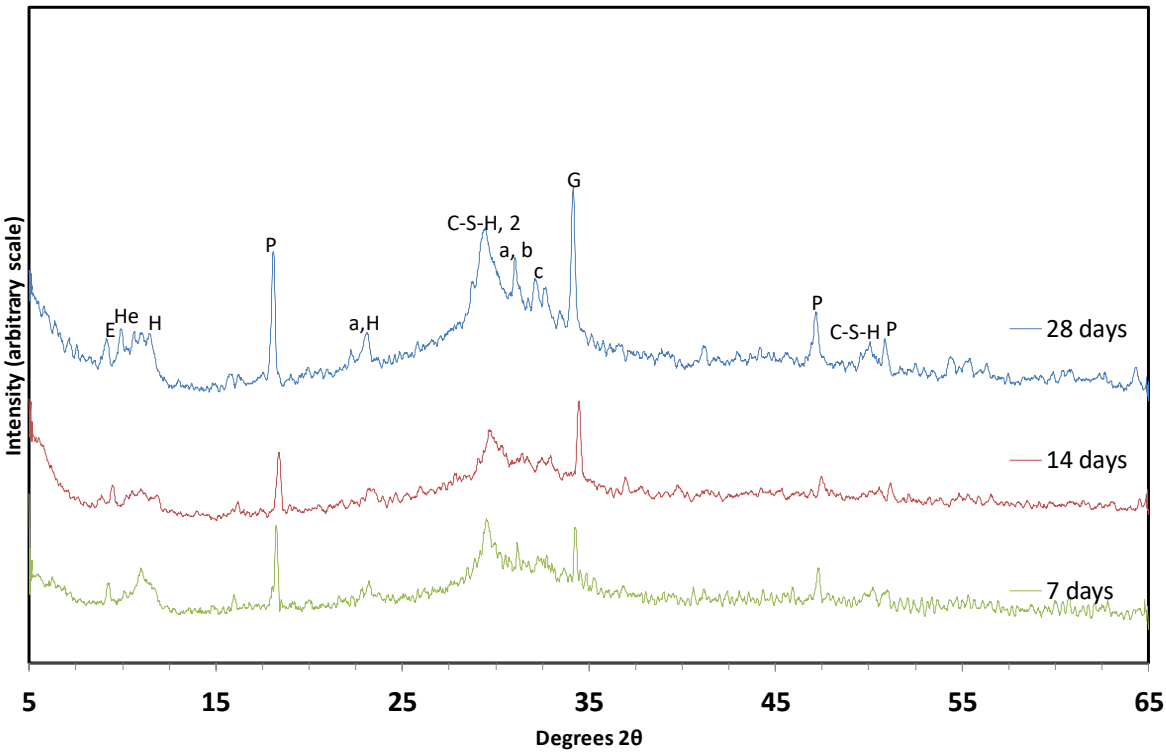

Figure 4.2 XRD patterns of 3 wt.% $CsNO_3$ 3:1 BFS:PC, various ages

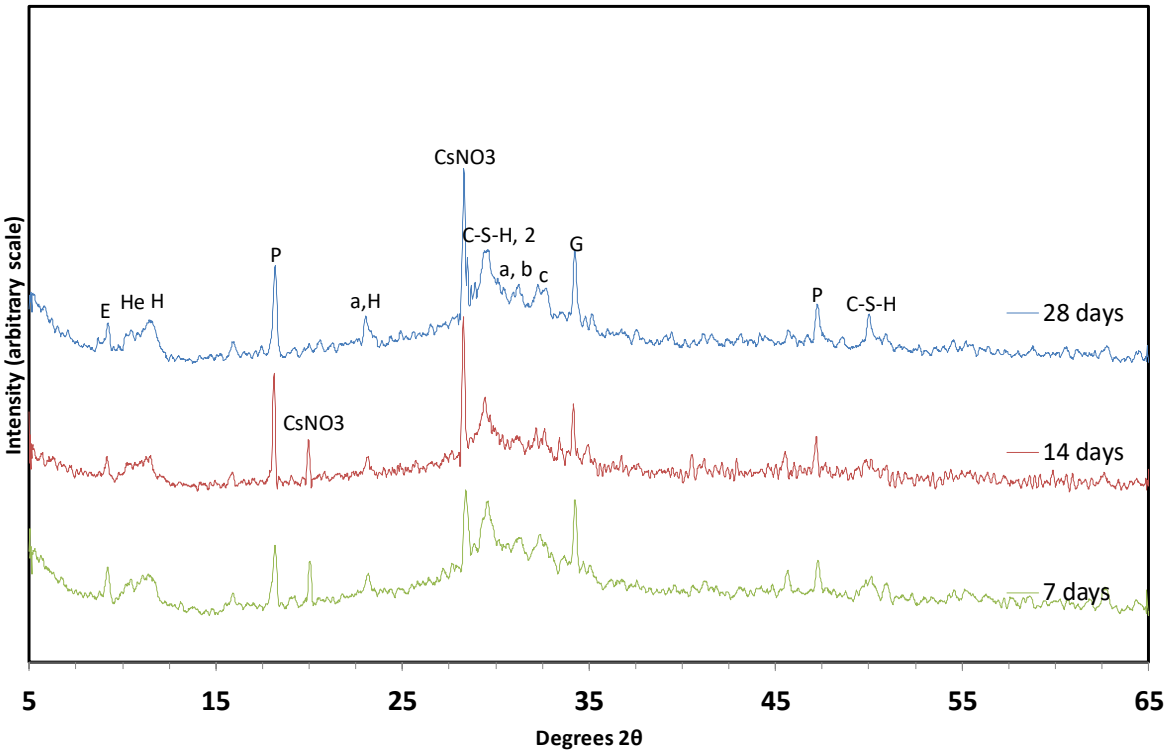

Figure 4.3 XRD patterns of 6 wt.% $CsNO_3$ 3:1 BFS:PC, various ages

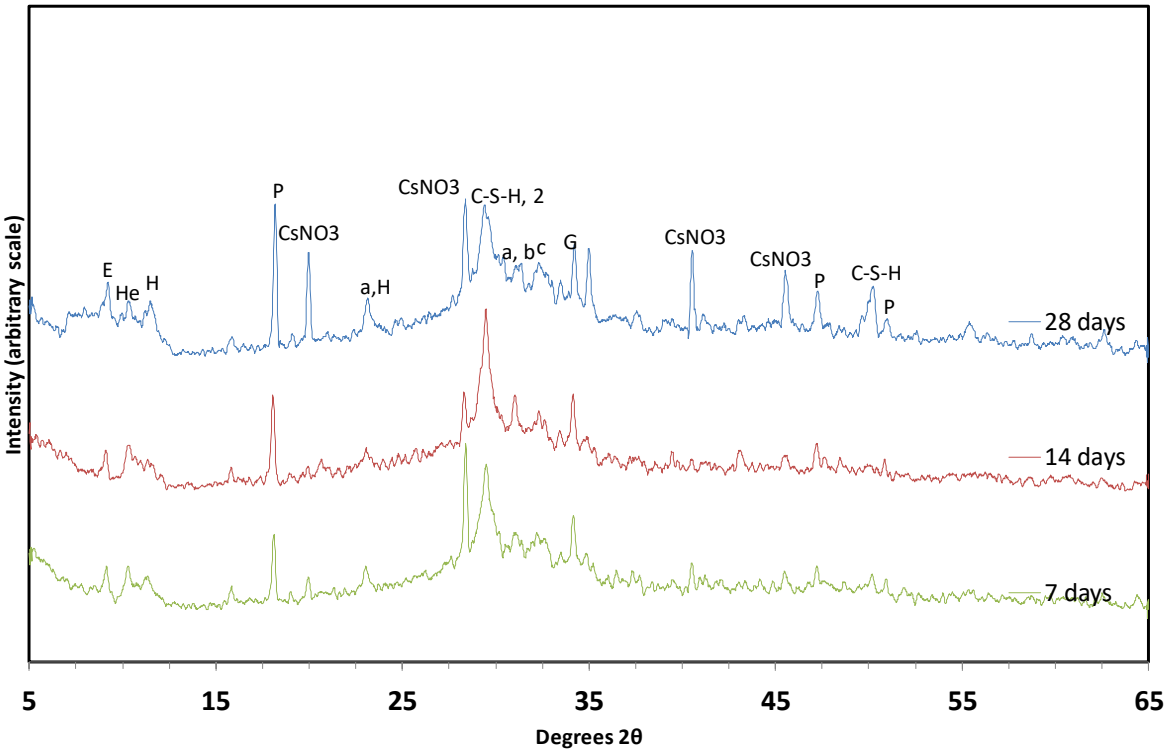

Figure 4.4 XRD patterns of 8 wt.% $CsNO_3$ 3:1 BFS:PC, various ages

Figure 4.5 compares the 28-day XRD patterns of each $CsNO_3$ cement formulation, including the 16 wt.% $CsNO_3$ sample shown as an extreme case. In the 16 wt.% sample the $CsNO_3$ peaks dominate and the main peak at 28.3° is significantly larger than both the portlandite and C-S-H peaks. The peaks for $CsNO_3$ are not visible in the samples below 6 wt.% $CsNO_3$ as discussed above, and the 6 wt.% sample does not display the secondary $CsNO_3$ peaks at 34.86° and 45.37° which are observable at 8 and 16 wt.%.

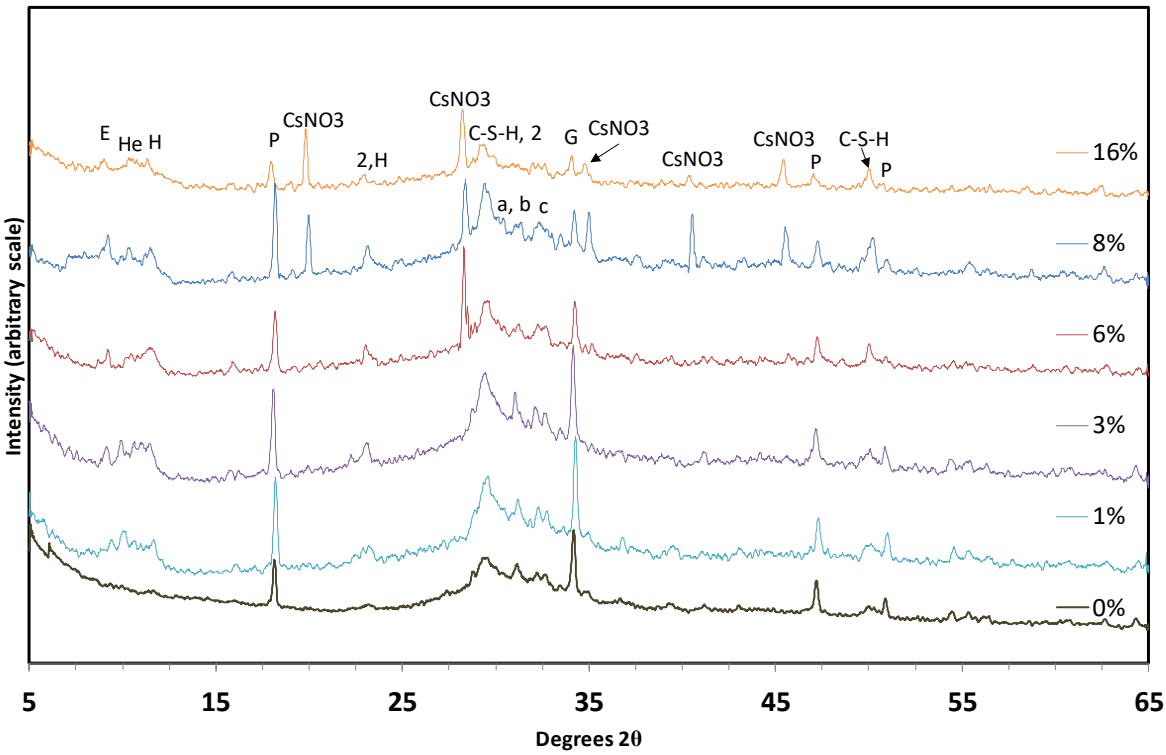

Figure 4.5 XRD patterns of 28 day old 3:1 BFS:PC containing various wt.% of $CsNO_3$

DTA data for the 7 day old 3:1 BFS:PC containing 1 to 8 wt.% $CsNO_3$ are shown in Figure 4.6 and are labelled using the information displayed in Table 4.3. The data are organised by age in order to compare the development of each formulation over time. TG and DTG data gathered concurrently is shown in the Appendix Section A.2 and confirms the results discussed here. The data show a larger endothermic peak up to 100°C in the 1 wt.% sample due to a larger amount of free water present, possibly due to insufficient drying. This sample

does not seem to have a connection to the amount of $CsNO_3$ present as suggested by the XRD patterns above, and the event at 180°C is attributed to AFm. There was an endothermic peak at 450°C due to the dehydroxylation of portlandite. These thermal events have been discussed previously in literature concerning BFS:PC systems [2], [4], [20], [21]. The 3 wt.% sample has a smaller initial peak below 100°C which is suggestive of less free water, and instead of a monosulphate peak the data displays a peak due to monocarbonate – this peak is indistinguishable from hemicarbonate as they decompose in the same temperature range [22]. Both hemicarbonate and monocarbonate can be present where portlandite reacts with carbon dioxide to form calcium carbonate, and this carbonate (or any that is already present in the cement powder before mixing) can react with any monosulphate present to form hemicarbonate; further reaction with carbon dioxide in this way can form monocarbonate [23]. There was some $CaCO_3$ present in the initial PC before mixing, however, as shown in the XRD pattern in Figure 3.1 so this is the likely source. The 6 wt.% and 8 wt.% also showed a peak in this range. The 1 wt.% and 8 wt.% samples both showed a larger endothermic peak below 100°C, whereas the 3 wt.% and 6 wt.% samples had smaller peaks, both with a similar size – this is thus unlikely to be related to the amount of $CsNO_3$, as the samples with the lowest and greatest amounts of $CsNO_3$ displayed the largest peaks in this temperature range, so this is likely attributable to insufficient drying. In the data shown the temperature region of particular interest for $CsNO_3$ is between 400°C and 500°C, as $CsNO_3$ decomposes and melts at 414°C [12] and portlandite dehydroxylates at 450°C as shown in Equation 4.1 and Equation 4.2 below.

$$CsNO_3 \rightarrow CsNO_2 + 1/2\ O_2$$

Equation 4.1

$$Ca(OH)_2 \rightarrow CaO + H_2O$$

Equation 4.2

Although it is difficult to clearly observe the former in the DTA data, this event can be easily observed using the first derivative with respect to time of the DTA curves shown in Figure 4.8, magnified in the region 402-405°C where the 1 and 3 wt.% samples show a peak here for the dehydroxylation of portlandite only. When the sample contains larger amounts of $CsNO_3$, the portlandite peak starts at a lower temperature, by approximately 30°C, corresponding to the decomposition of $CsNO_3$ and there is a sharp feature attributed to $CsNO_3$ at 402.5±1 °C.

Table 4.3 Cement components and their corresponding thermal events

Label	Component	Formula	Temperature range °C	Source
Free water	H_2O	H_2O	100	-
C-S-H	C-S-H	C-S-H	110-120 decomposition	[21]
Ettringite	ettringite	$Ca_6(Al(OH)_6)_2(SO_4)_3(H_2O)_{26}$	100-120 decomposition	[15]
monocarbonate	monocarbonate	$C_4A\bar{C}H_{11}$	150	[22]
$CsNO_3$	Caesium nitrate	$CsNO_3$	162 crystalline transition 414 melting	[24], [25] [26],[12]
AFm	monosulphate	$Ca_4Al_2(SO_4)(OH)_{12}\cdot(H_2O)_6$	180-200	[21]
P	portlandite	$Ca(OH)_2$	450	[21]
$Ba(NO_3)_2$	barium nitrate	$Ba(NO_3)_2$	592	[27]
B	barium sulphate	$BaSO_4$	1580 (beyond apparatus capabilities)	[28]
bh8	barium hydroxide octahydrate	$Ba(OH)_2\cdot 8H_2O$	78	[14]

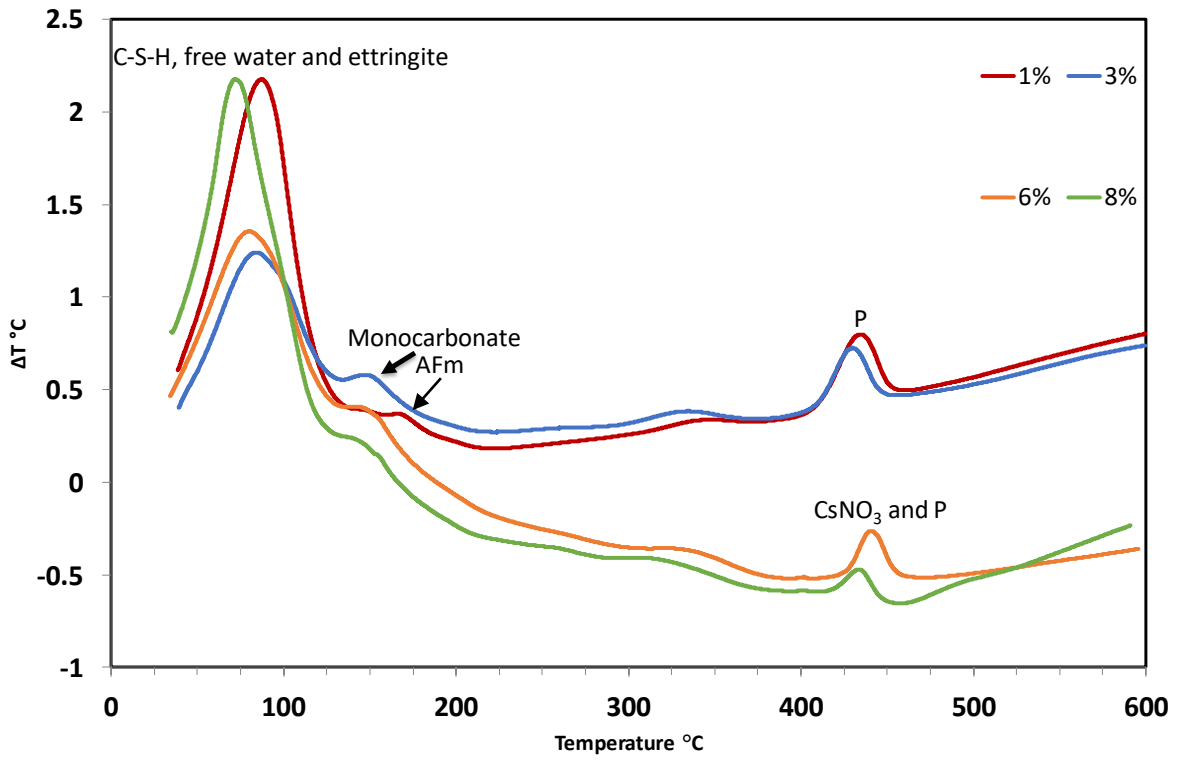

Figure 4.6 DTA of 7 Day 1 to 8 wt.% $CsNO_3$ 3:1 BFS:PC

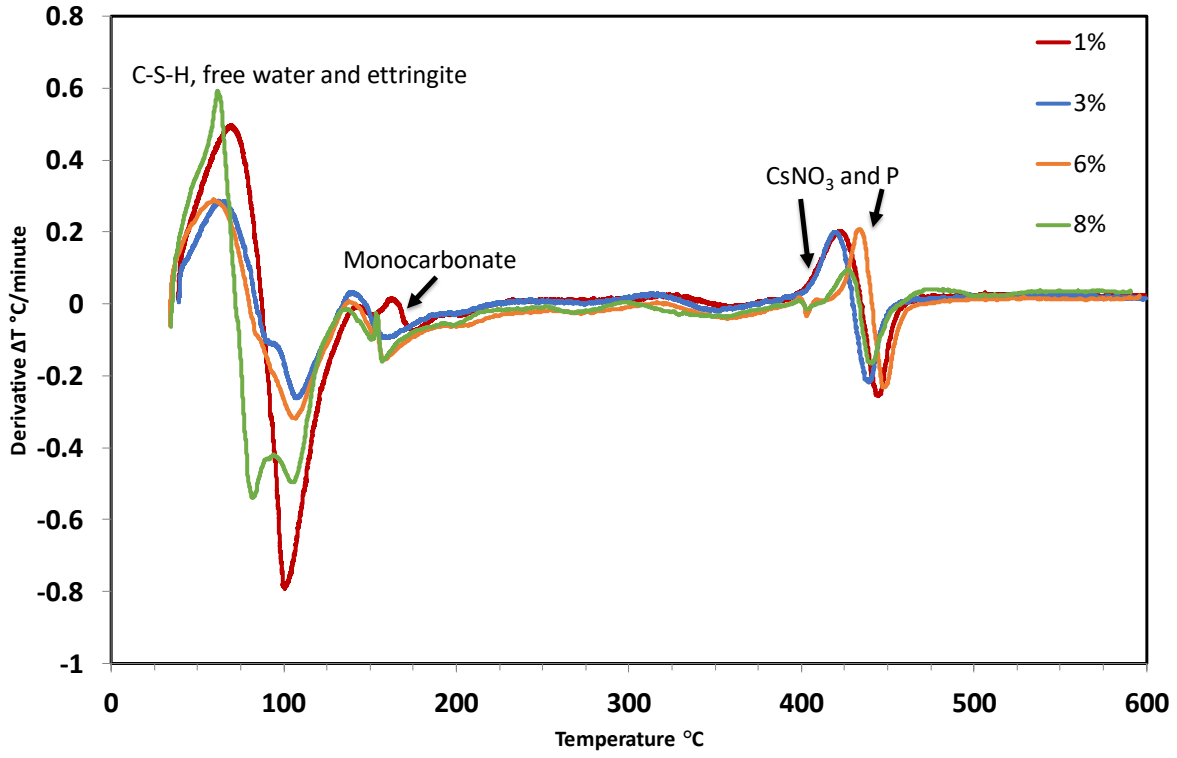

Figure 4.7 The first derivative of the 7 day DTA data

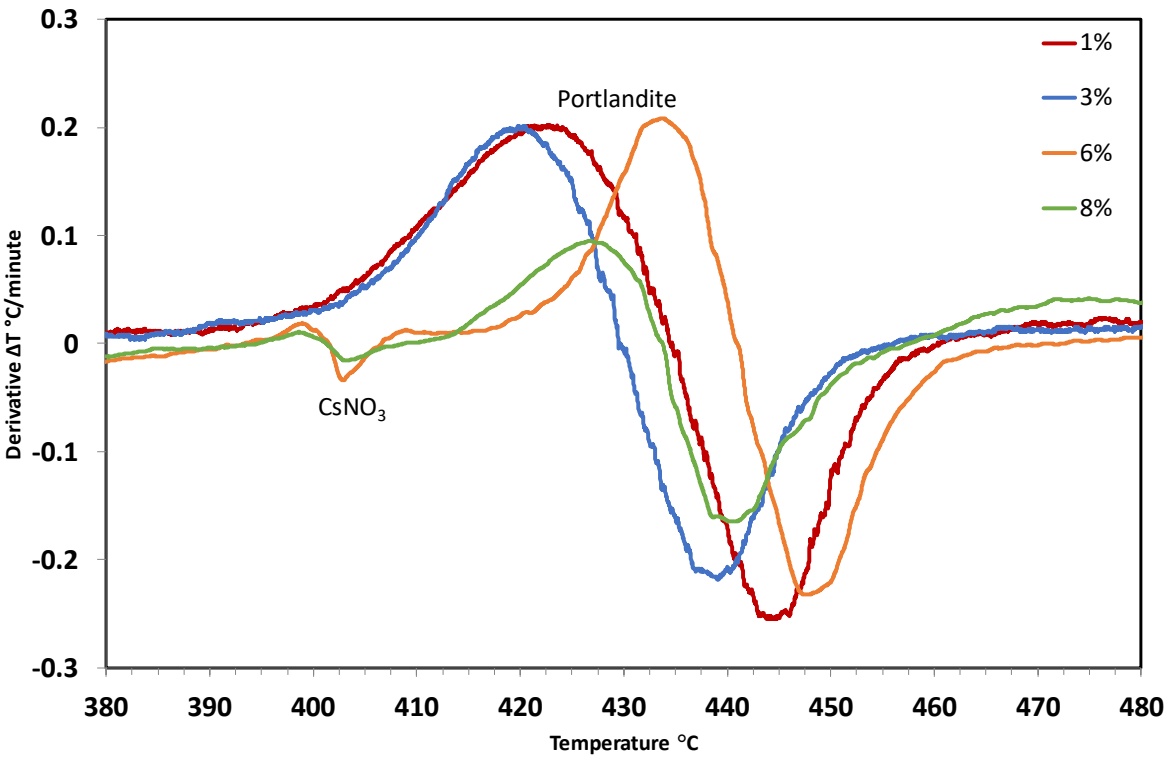

Figure 4.8 Magnification of Figure 4.7 in range 380°C to 480°C

The thermal analysis data for the 1-8 wt.% samples after 14 days of curing are shown in Figure 4.9 to Figure 4.11. As in the 7-day samples, the decomposition of $CsNO_3$ is visible in the system containing 6 wt.% $CsNO_3$ and above. Whilst it is not observed in the 1 wt.% DTA data, in the 3 wt.% data a feature due to monocarbonate is seen between 130-160°C in the DTA (Figure 4.9) and first derivative DTA (Figure 4.10) data. This is more distinct in the 6 wt.% and 8 wt.% data. As shown in Figure 4.11, at 14 days, the decomposition of caesium nitrate can be observed by looking at the derivative DTA data, and is only seen in the 6 and 8 wt.% data – the area of this peak is smaller than in the 7-day old samples, which agrees with the XRD data. The thermal analysis data for the 1-8 wt.% samples after 28 days of curing are shown in Figure 4.12- Figure 4.14 as well as the 16 wt.% DTA data. Between 14 and 28 days there is not a large change in the 1 to 8 wt.% range with the peak below 100 °C increasing in size in the DTA data as the wt.% $CsNO_3$ increases.

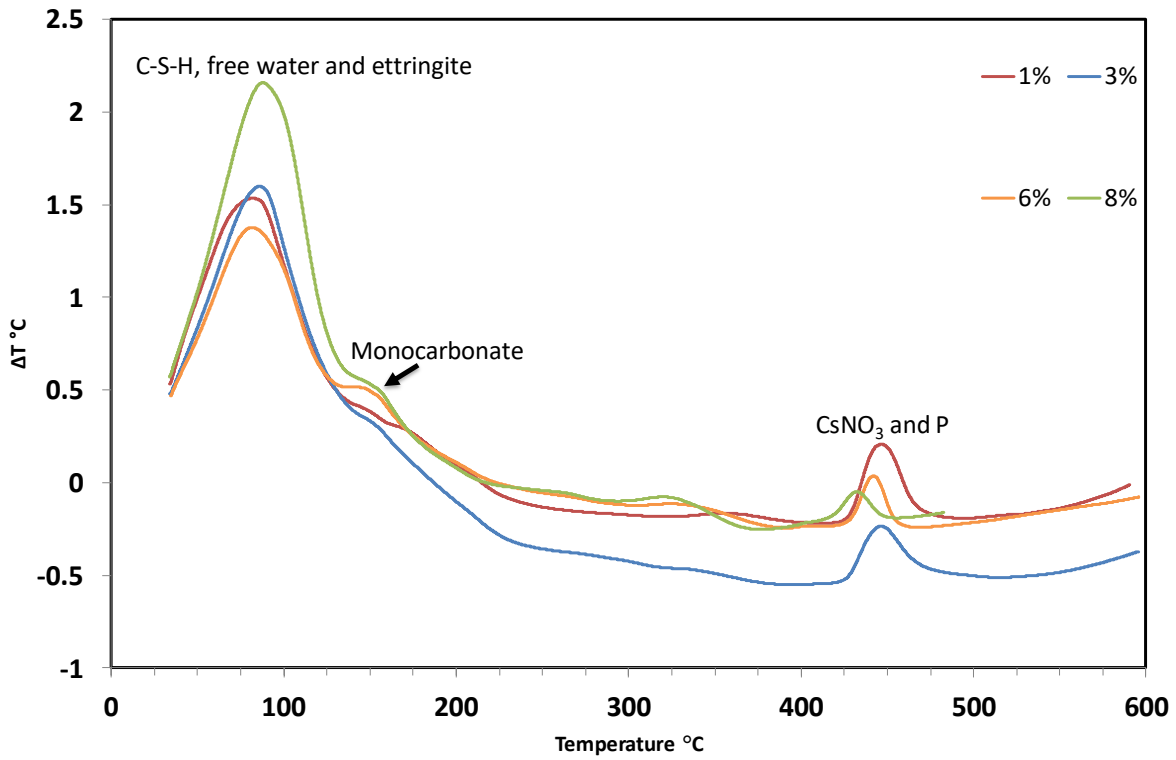

Figure 4.9 DTA of 14 Day 1 to 8 wt.% CsNO3 3:1 BFS:PC

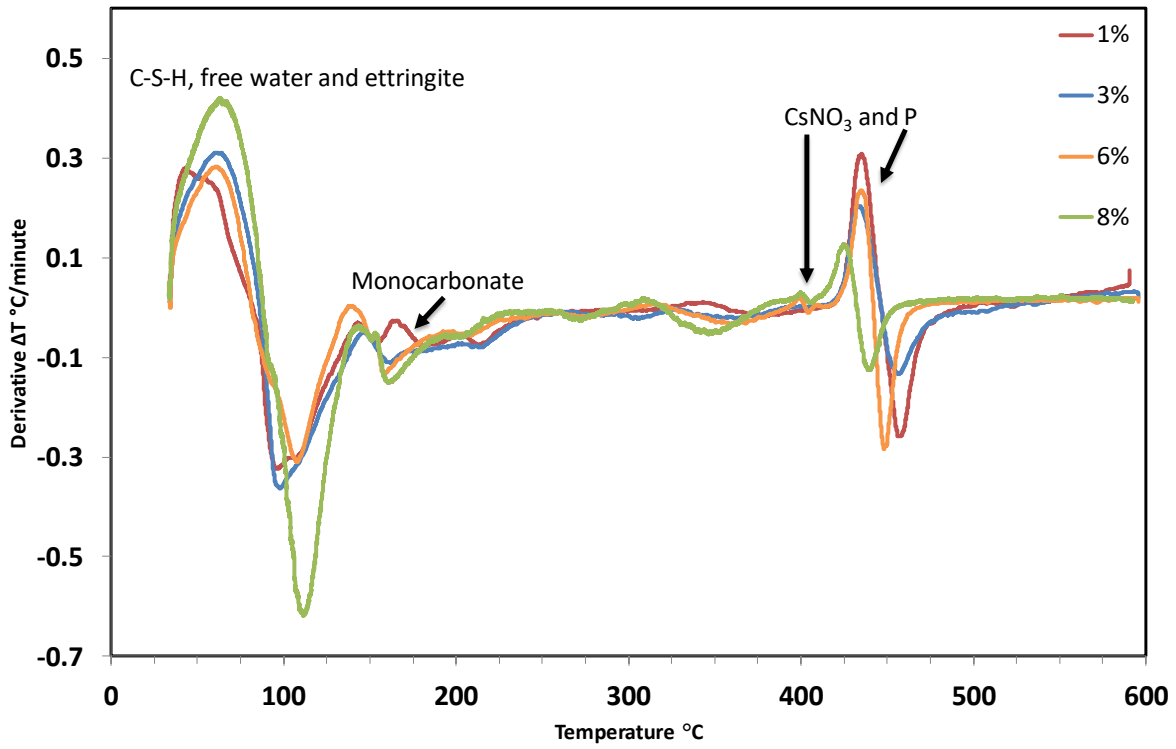

Figure 4.10 The first derivative of the 14 day DTA data

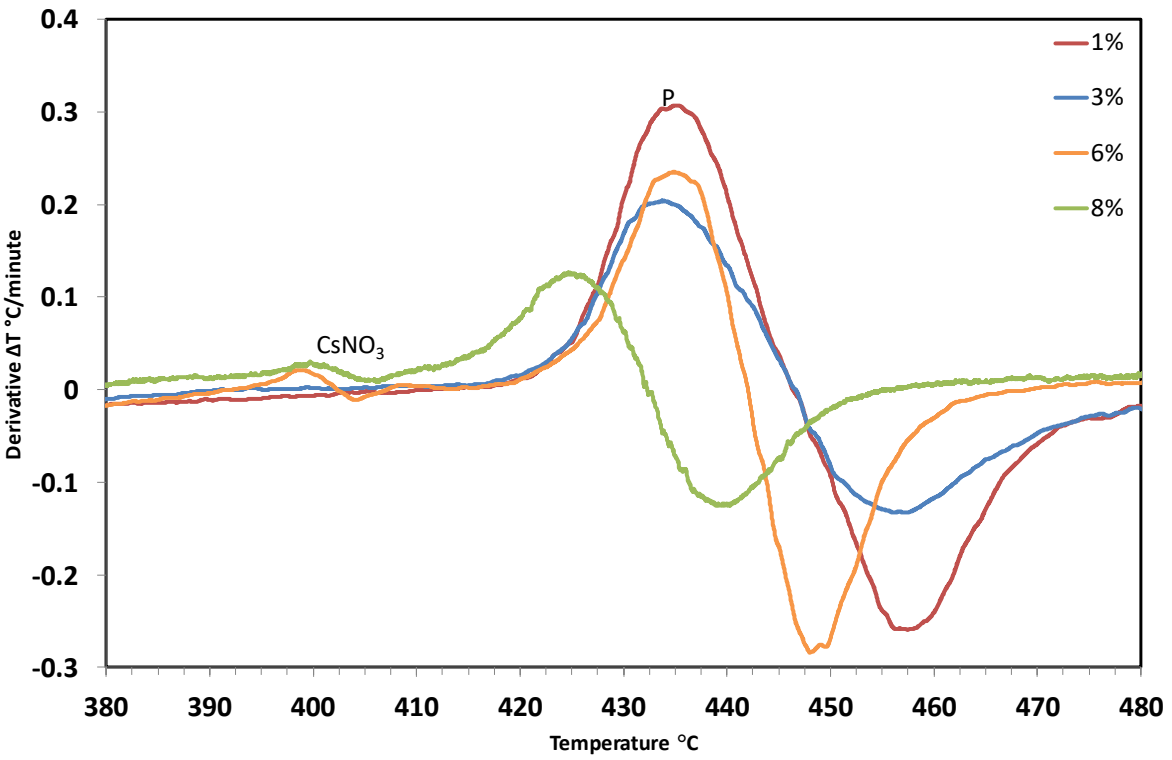

Figure 4.11 Magnification of Figure 4.10 in range 380°C to 480°C

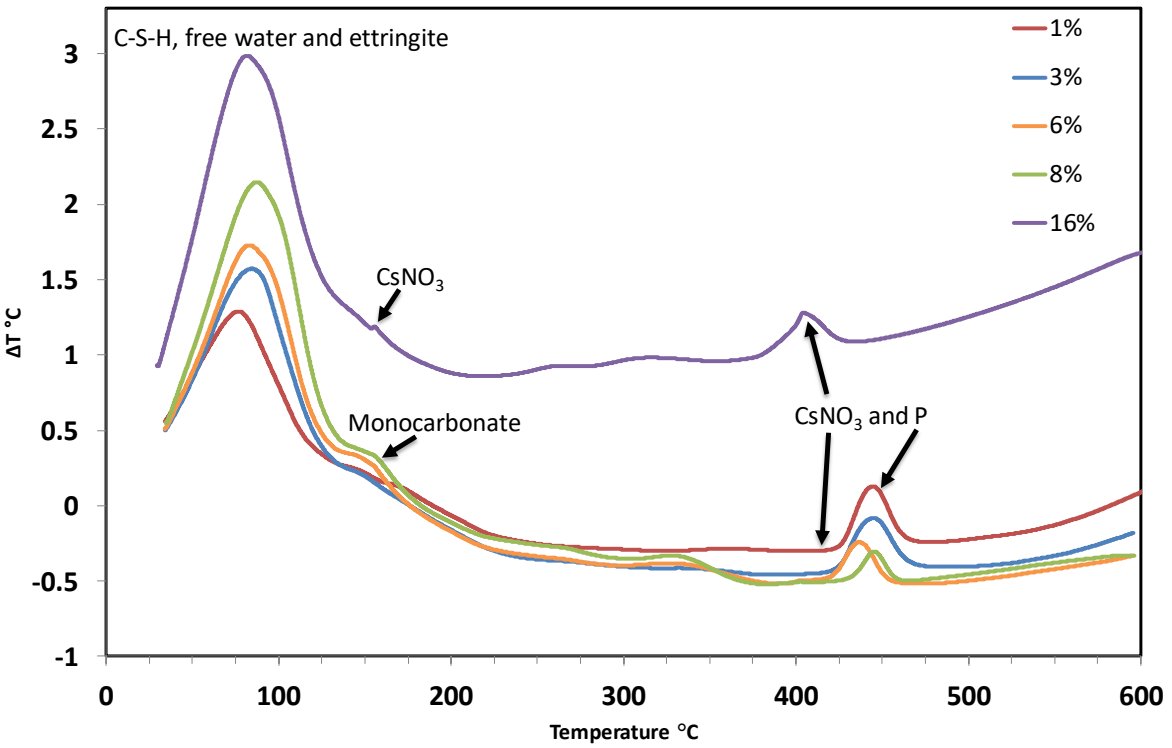

Figure 4.12 DTA of 28 Day 1% to 16% CsNO3 3:1 BFS:PC

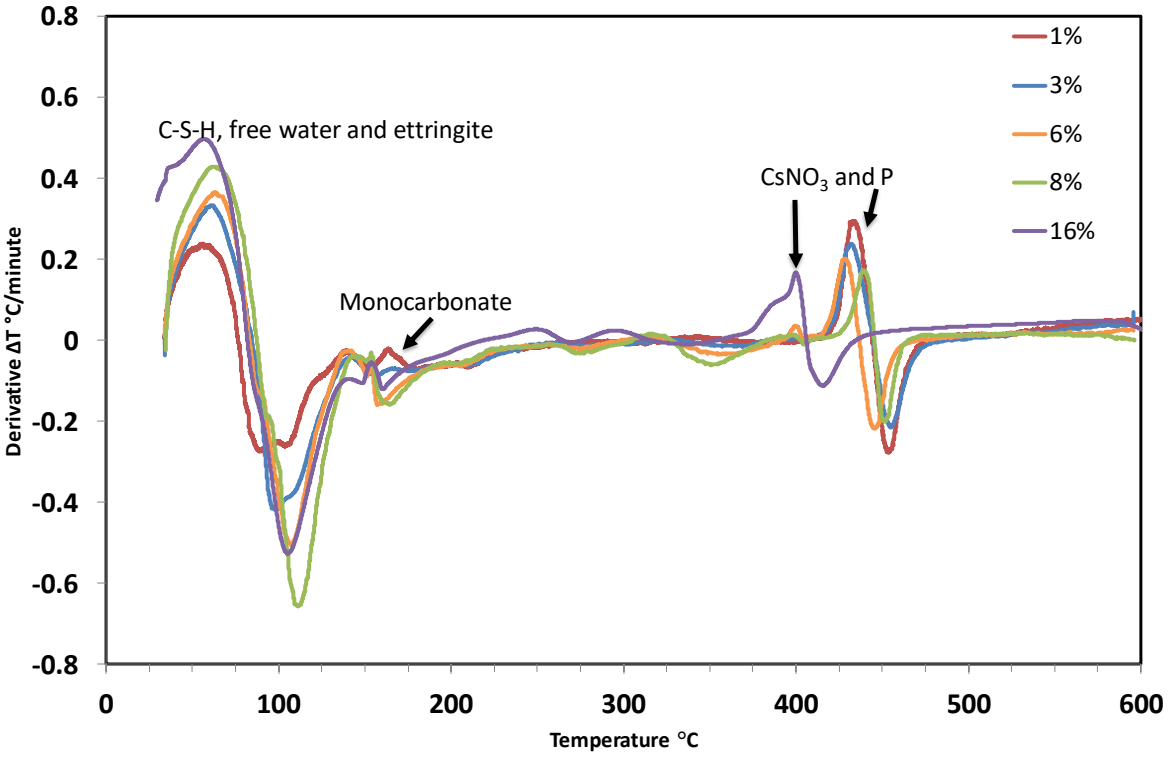

Figure 4.13 The first derivative of the 28 day DTA data

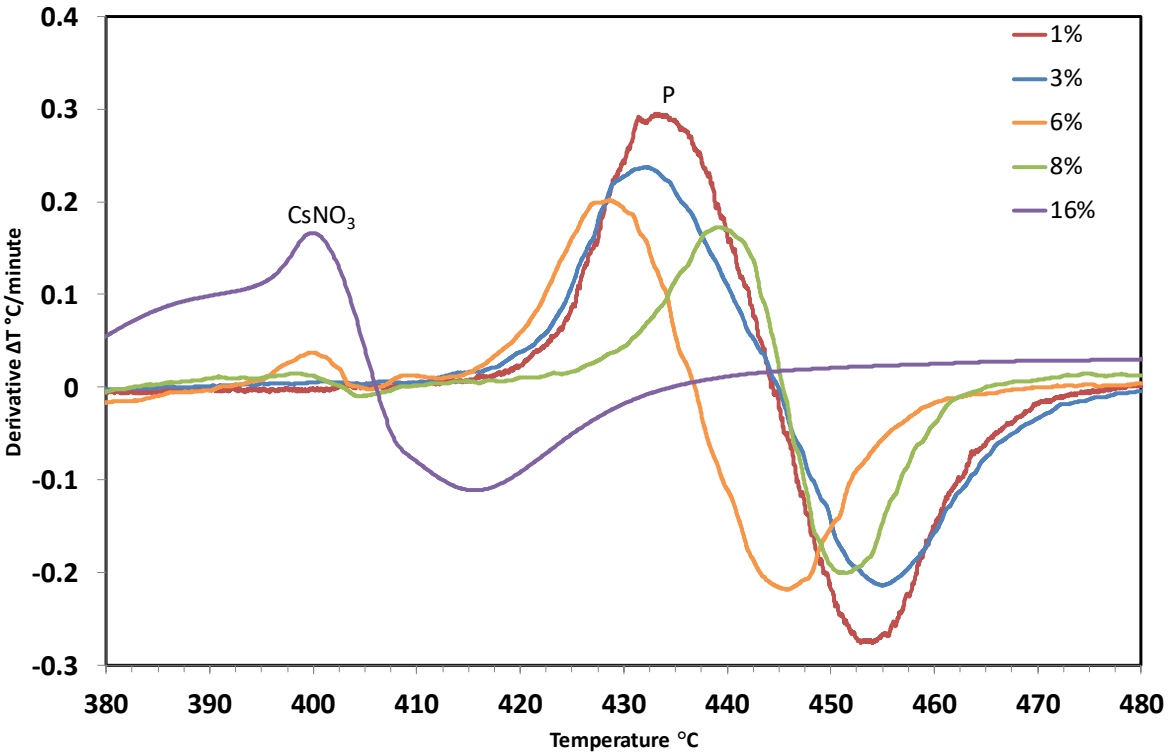

Figure 4.14 Magnification of Figure 4.13 in range 380°C to 480°C

Analysing the DTA data of the 28 day samples further, the peak areas of the regions attributed to portlandite were calculated using the Pyris Manager software. A plot of the peak area of portlandite as a function of wt.% $CsNO_3$ is shown in Figure 4.15 and shows a clear trend that increasing amounts of $CsNO_3$ decrease the amount of portlandite present. The peak area for portlandite of the 16 wt.% sample is also shown, however this peak was indistinguishable from the $CsNO_3$ peak (it also dominated in the XRD data), and in fact the local peak maximum in this sample was at 403 °C. Up to 8 wt.% the trend shows that there is a reduction in the portlandite present, but between 8 wt.% and 16 wt.% the rate of decrease slows down. The XRD patterns (Figure 4.5) show that there is still portlandite present in the 16 wt.% sample so the feature at 403 °C must be due to the small amount of portlandite as well as $CsNO_3$ even though only one feature was observed. The pH of the solution used to hydrate the 3:1 BFS:PC increased with increased $CsNO_3$ added (see Table 4.1). It is possible that the increased alkalinity increases the hydration reaction of the cement, reducing the amount of portlandite present [29], [30].

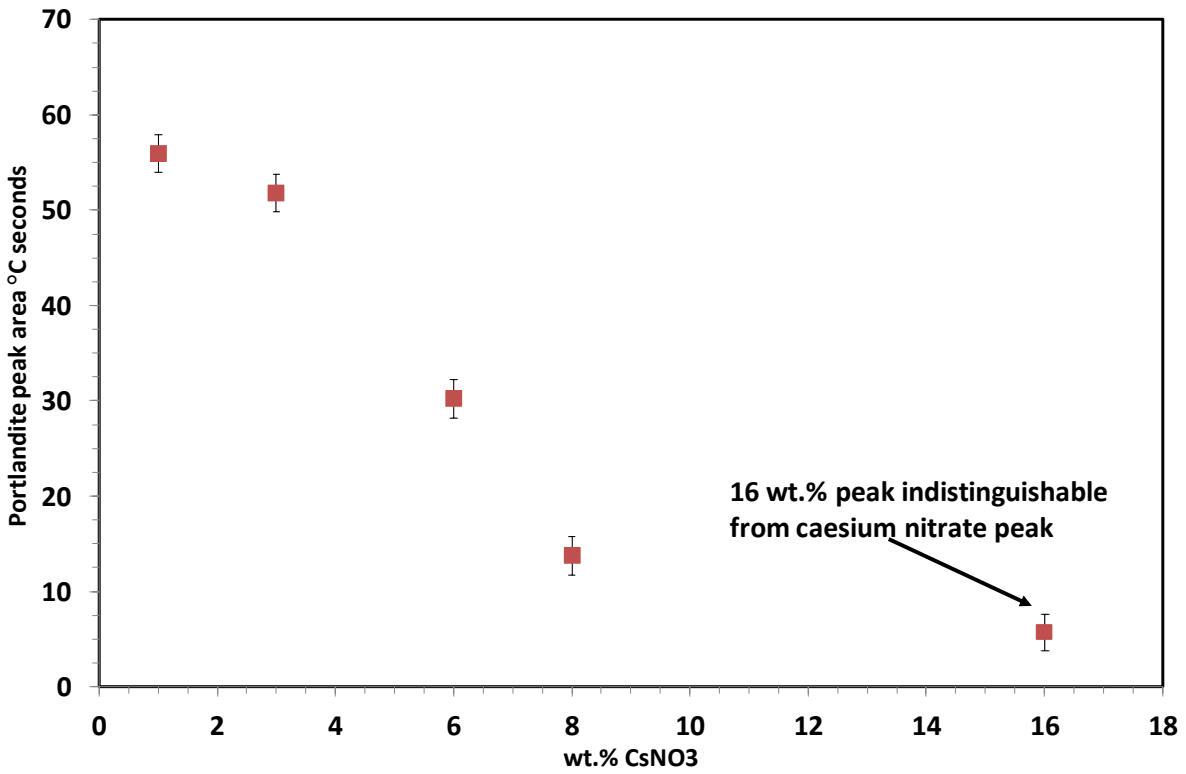

Figure 4.15 Portlandite peak area as a function of wt.% $CsNO_3$

The 28-day old samples were also examined under Differential Scanning Calorimetry (DSC) from room temperature to 600°C, and 16 wt.% samples were produced as an extreme case to verify the data further as well as a sample of some of the powdered $CsNO_3$ used to make the cements. $CsNO_3$ undergoes an endothermic transition in the crystalline structure from a hexagonal to a cubic form at 162°C [24]–[26], and so the data is shown in Figure 4.16 in the region 140-180°C, as this was the area of interest – other regions revealed no new features not observed in the DTA data and thus are not shown. The high precision of DSC compared with DTA allowed for the resolution of this peak. As the amount of $CsNO_3$ is increased in the cement samples, this peak is observed from 6 wt.% onwards and increases in intensity – the 8 wt.% peak is wider than the 6 wt.% peak indicating a higher consumption of energy. The peak temperature varies in different samples, but this variation was verified with three repeated measurements for each sample type. The areas of the peaks correspond to the energy required for the total $CsNO_3$ present in each system to change its crystal structure.

When the peak area of this transition is plotted as in Figure 4.17, the trend line reveals that $CsNO_3$ begins to precipitate in the 3:1 BFS:PC system from 2.8 wt.% of incorporation although no $CsNO_3$ peak was observed in the XRD pattern of the 3 wt.% sample or in its DSC data. Possibly the amount of precipitated $CsNO_3$ was too small to be detected. The data presented do not provide the mechanism of this incorporation below 2.8 wt.%, but it does demonstrate that excess incorporation of over 2.8 wt.% would result in the precipitation of $CsNO_3$.

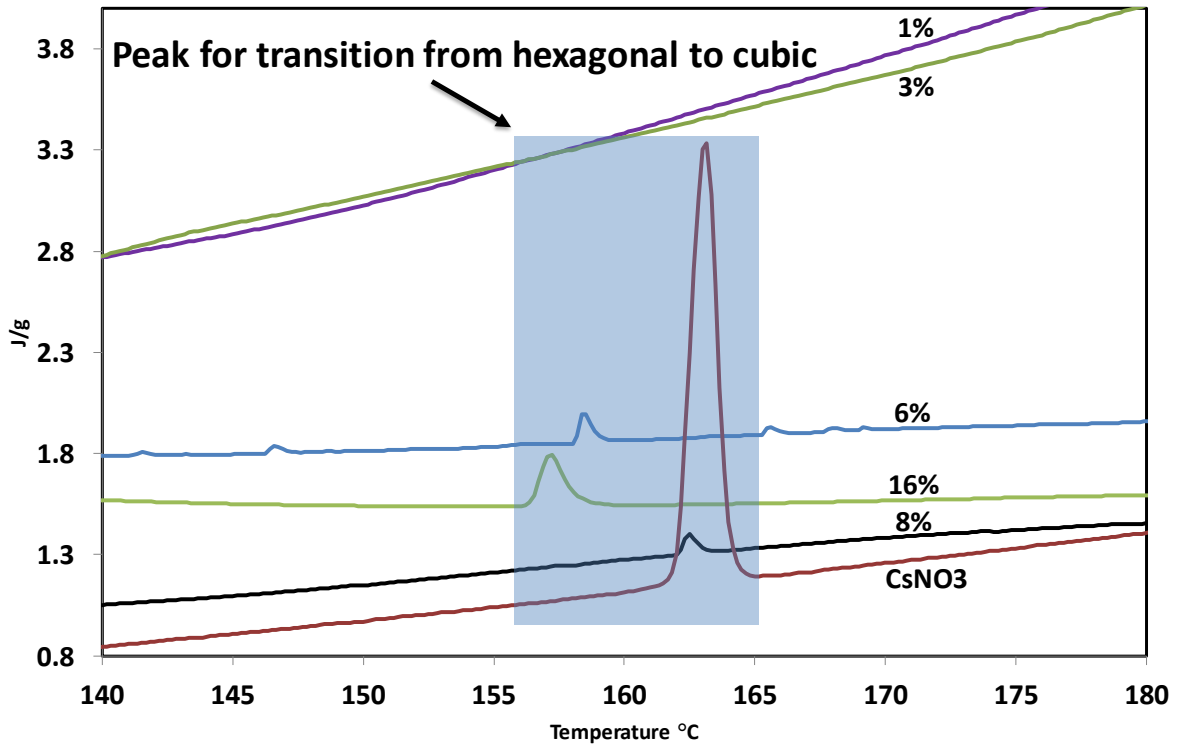

Figure 4.16 DSC of 3:1 BFS:PC containing increasing amounts of $CsNO_3$. The highlighted area shows a crystalline transition of $CsNO_3$, and does not begin at the same temperature in each sample.

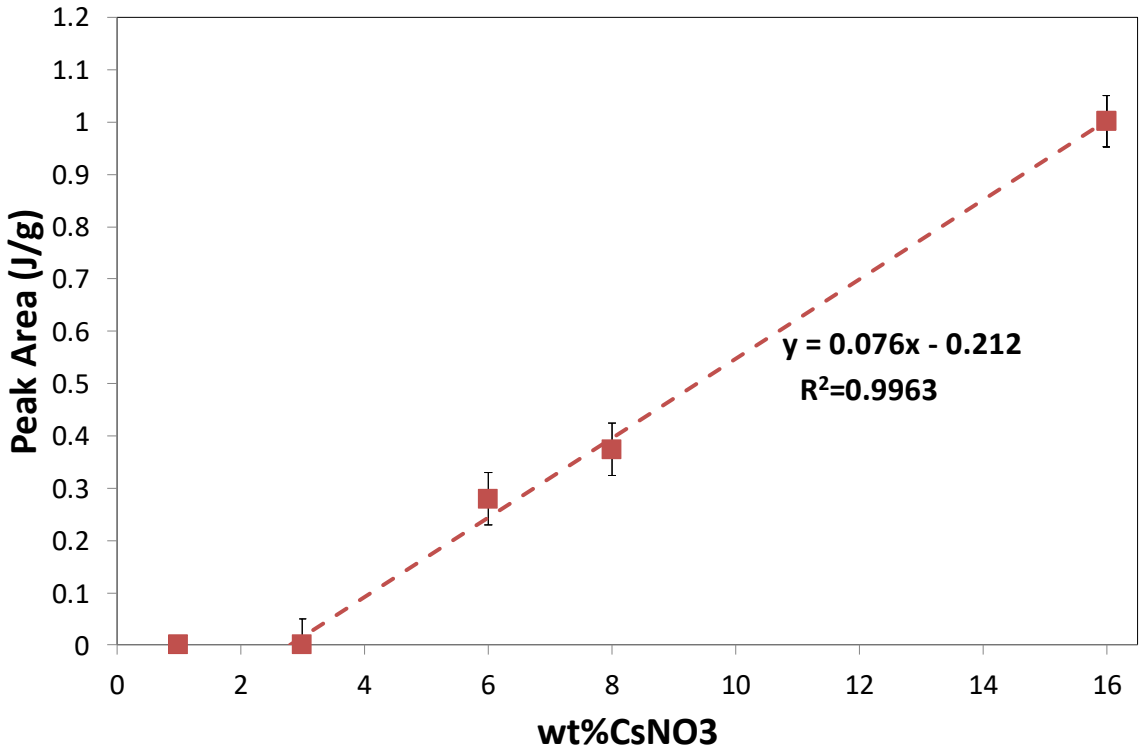

Figure 4.17 Peak area of the phase transition of $CsNO_3$ at approximately 160°C as the weight % increases. This data suggests $CsNO_3$ would begin to precipitate in the cement matrix at a 2.8 wt.% incorporation.

4.2.2 Effect of $CsNO_3$ on the Microstructure of 3:1 BFS:PC– Scanning Electron Microscopy

Back-Scattered Electron (BSE) images of 3:1 BFS:PC with 1 wt.% $CsNO_3$ are shown in Figure 4.18 and Figure 4.19 with EDX elemental mapping at a low and high magnification respectively. The EDX maps are shown, as they reveal more information of where the Cs and N are concentrated in the cement samples and potentially which minerals they will precipitate onto. Ca, Si, Al and Mg are shown as they are elements with a high concentration in the cement (see Table 3.2) and these maps together with the BSE images give information of the elemental makeup of the cement and the composition of different areas. Bright spots correspond to particles of Fe and are expected to originate from residual C_4AF in unreacted PC. Generally speaking, cracks are not visible in the samples analysed. The lower-resolution images are shown to give an overview of the sample at a low magnification, whilst the higher-

resolution images give more detail but in a smaller area. In the 1 wt.% sample, Cs and N are spread throughout the sample with no areas of high concentration. Unhydrated cement particles are visible in the BSE images, these can be seen to correspond with higher concentrations of the elements shown depending on their composition, with S and Fe having a high association in the map shown. The images suggest that the 1 wt.% sample showed the highest amount of porosity compared with the 3 and 6 wt.% samples described below, and this is confirmed in MIP data shown later in the Chapter.

Figure 4.20 and Figure 4.21 show representative BSE images and elemental mapping of the 3 wt.% sample. Similar to the 1 wt.% sample, the image also shows a porous microstructure and several unhydrated cement particles ~0.1-0.2 mm in diameter although the 3 wt.% sample appears less porous than the 1 wt.% sample. Also like the 1 wt.% sample, there are no areas with a high concentration Cs and N in either magnification. This agrees with the DSC data that suggests $CsNO_3$ does not precipitate in 3:1 BFS:PC below 3 wt.% when initially dissolved in the hydration water. At 6 wt.% $CsNO_3$, the behaviour of Cs and N changes, as shown in Figure 4.22 and Figure 4.23 which show BSE images at a low and high magnification respectively. Higher concentrations of both Cs and N are visible in some regions in the sample, implying precipitation of $CsNO_3$ – remember all of the $CsNO_3$ had been initially dissolved in the water used to hydrate the binding cement powder. However, individual particles of $CsNO_3$ are not observed as they are likely too small to be seen – further scans at a higher resolution did not reveal any $CsNO_3$ particles or additional information. As in the transition from 1 wt.% to 3 wt.%, the 6 wt.% sample seems to show a decrease in the porosity. Larger pores are visible within unhydrated cement particles and appear unaltered i.e. these pores were present before the cement was mixed.

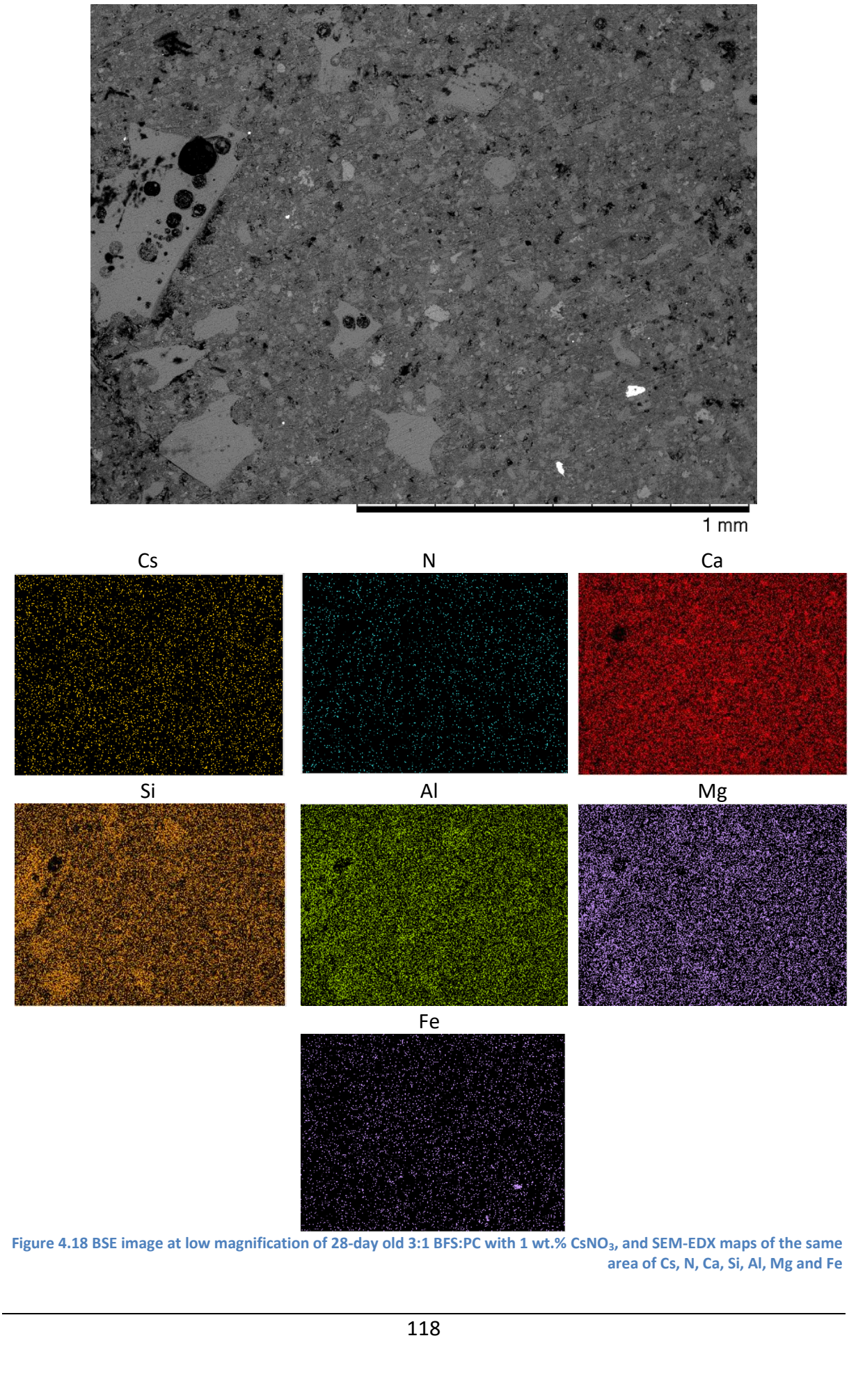

Figure 4.18 BSE image at low magnification of 28-day old 3:1 BFS:PC with 1 wt.% $CsNO_3$, and SEM-EDX maps of the same area of Cs, N, Ca, Si, Al, Mg and Fe

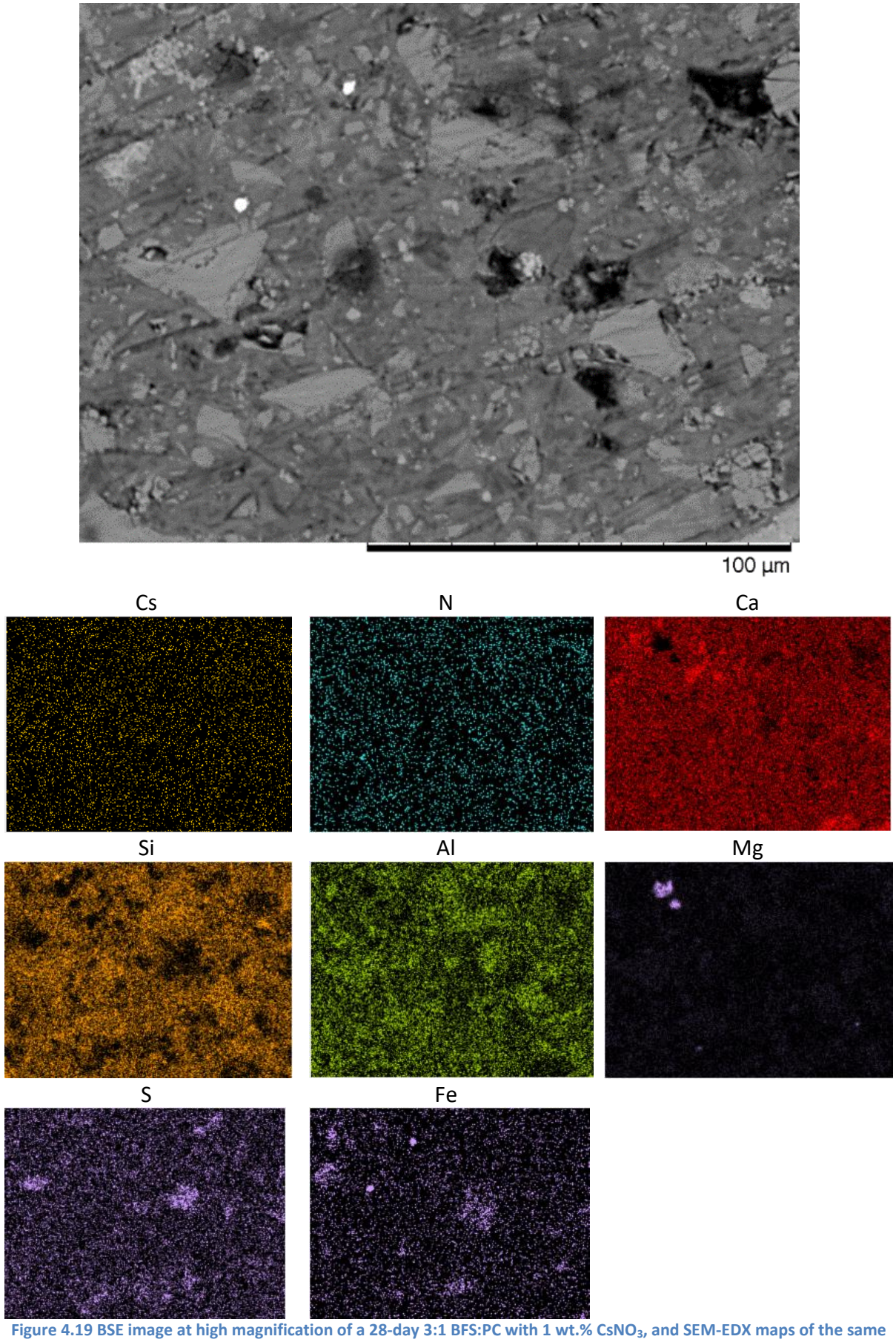

Figure 4.19 BSE image at high magnification of a 28-day 3:1 BFS:PC with 1 wt.% $CsNO_3$, and SEM-EDX maps of the same area of Cs, N, Ca, Si, Al, Mg, S and Fe

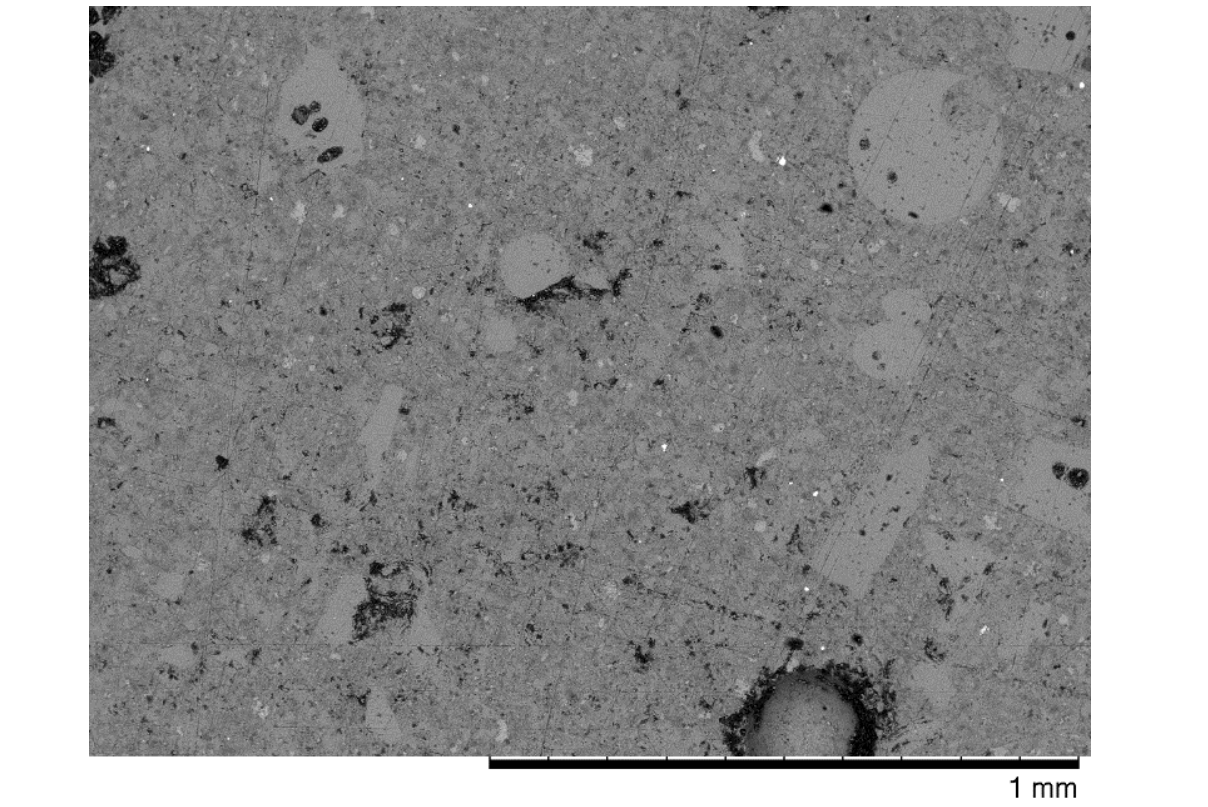

Figure 4.20 BSE image at low magnification of a 28-day 3:1 BFS:PC with 3 wt.% $CsNO_3$, and SEM-EDX maps of the same area of Cs, N, Ca, Si, Al and Mg

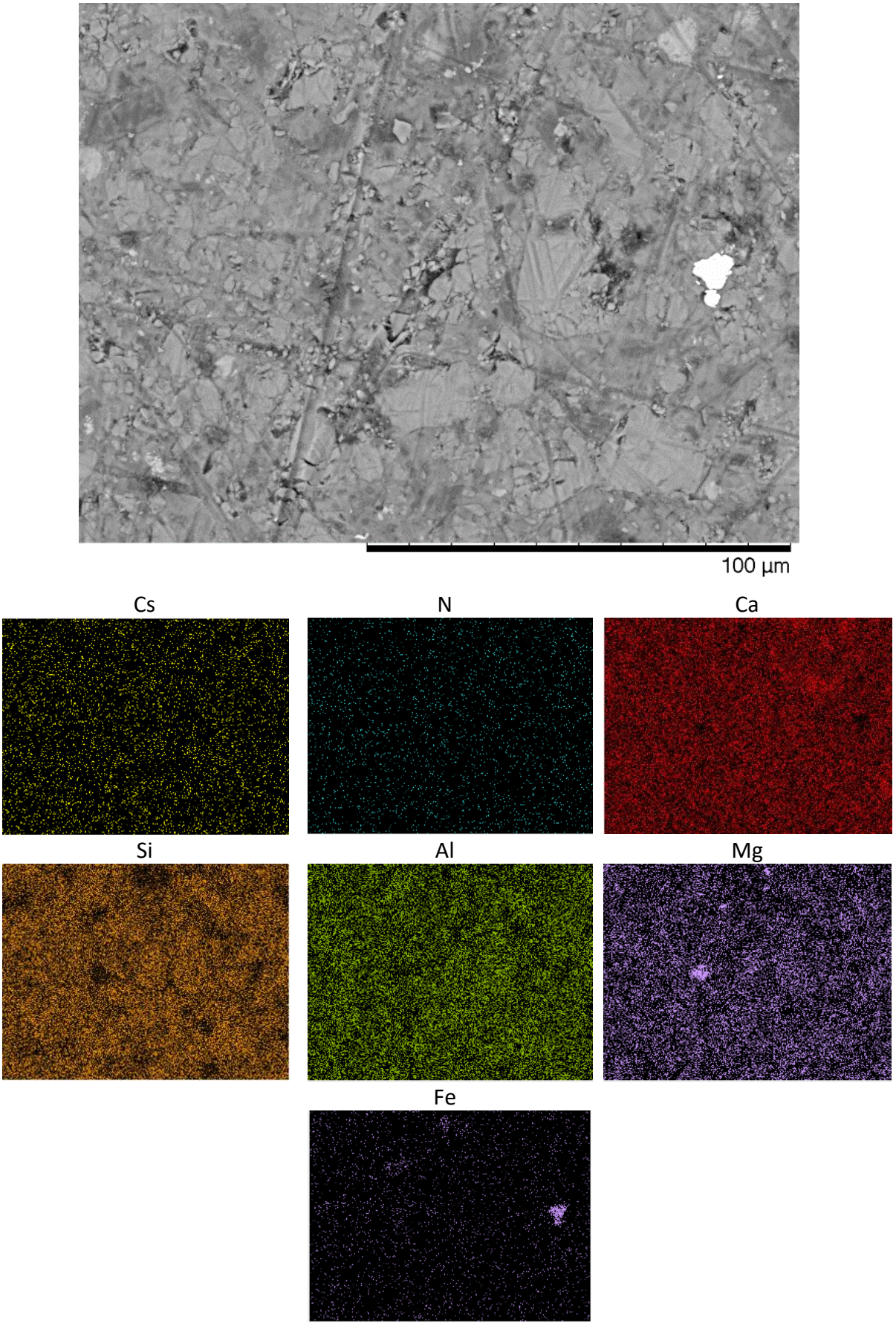

Figure 4.21 BSE image at high magnification of a 28-day old 3:1 BFS:PC with 3 wt.% $CsNO_3$, and SEM-EDX maps of the same area of Cs, N, Ca, Si, Al, Mg and Fe

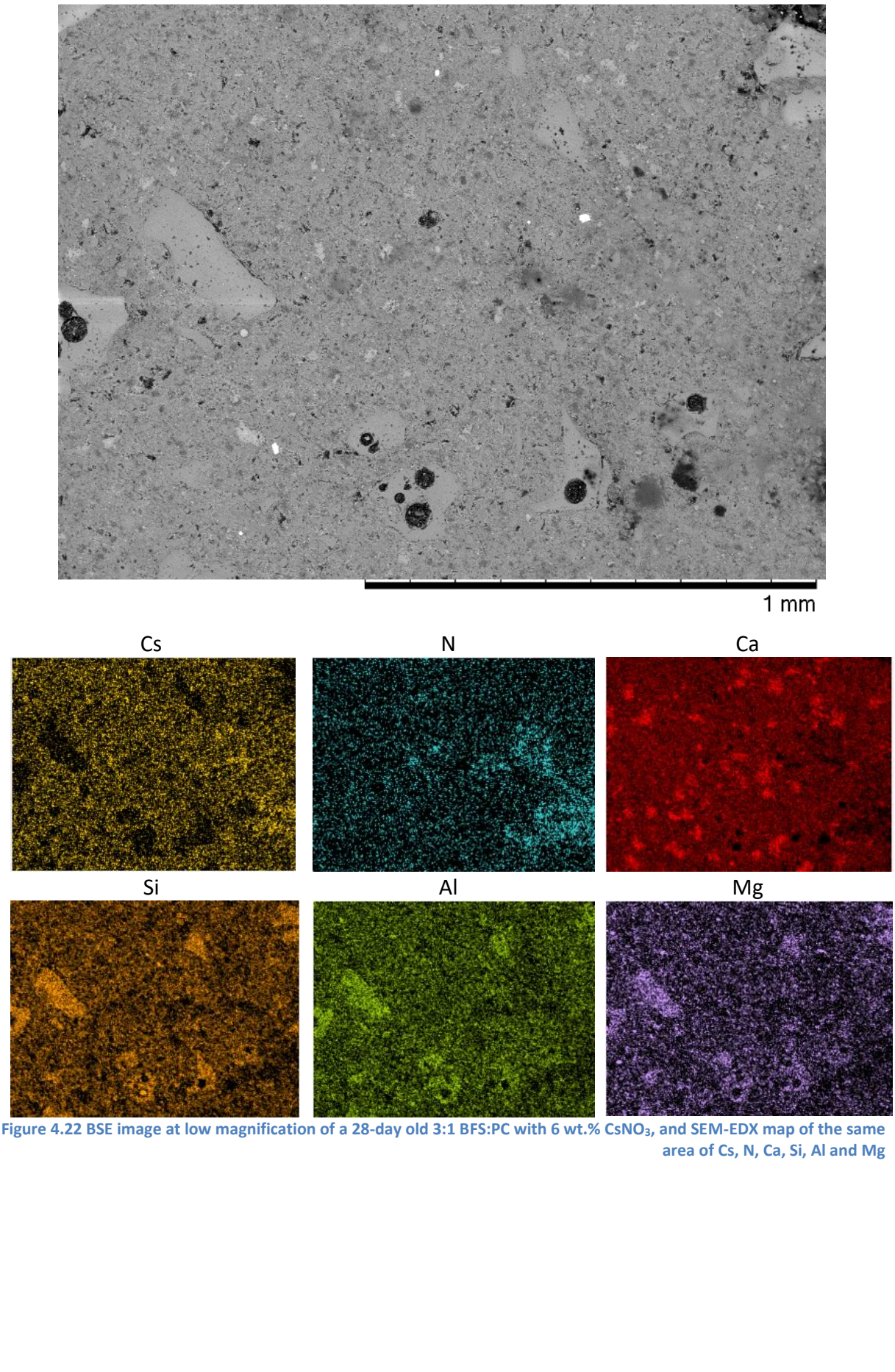

Figure 4.22 BSE image at low magnification of a 28-day old 3:1 BFS:PC with 6 wt.% $CsNO_3$, and SEM-EDX map of the same area of Cs, N, Ca, Si, Al and Mg

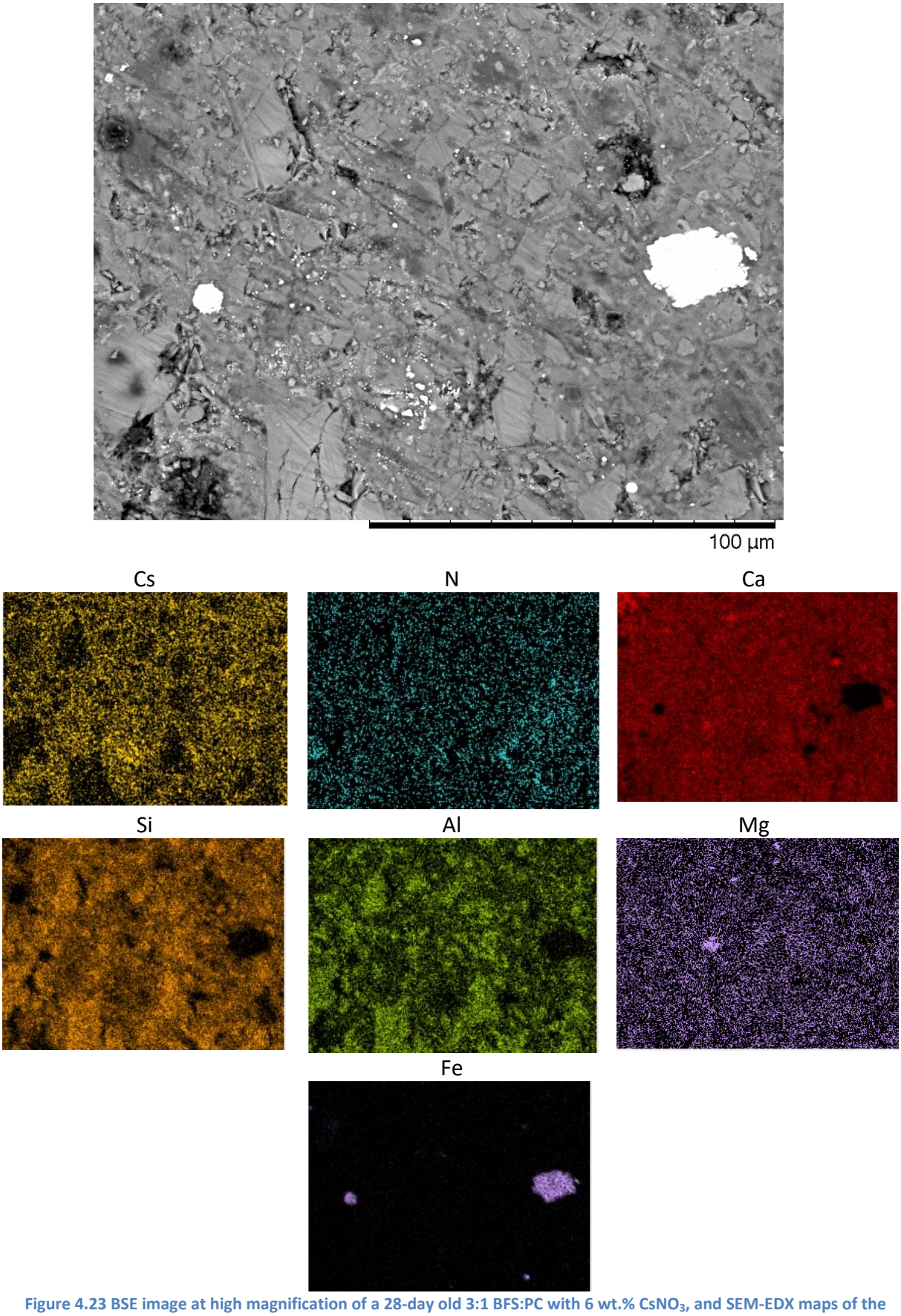

Figure 4.23 BSE image at high magnification of a 28-day old 3:1 BFS:PC with 6 wt.% $CsNO_3$, and SEM-EDX maps of the same area of Cs, N, Ca, Si, Al, Mg and Fe

A low magnification BSE image of 3:1 BFS:PC with 16 wt.% $CsNO_3$ is shown as Figure 4.24 with EDX maps of several elements. Pores (black areas), unhydrated cement particles (dark grey areas) and caesium nitrate particles (white areas) can be seen at low magnification, with caesium also being spread throughout the hydrated cement, which constitutes the majority of the sample (the light grey areas). In this sample, unhydrated cement particles (originating from PC or BFS) are identifiable due to a decrease of caesium and an increase of calcium in those areas. The large particles of $CsNO_3$ present are likely just particles of $CsNO_3$ that had not dissolved when the cement was being made.

A BSE image of a 16 wt.% $CsNO_3$ sample with high magnification is shown in Figure 4.25 with EDX mapping of N, Cs, Ca, Si, Al and Mg. Cracks are visible in this sample at higher magnifications. Caesium is seen throughout the sample. There are areas where caesium nitrate is present and may have precipitated, but most likely had just not been dissolved – half of the $CsNO_3$ in the 16 wt.% sample had to be added to the dry 3:1 BFS:PC powder mix rather than the water used to hydrate the mix – the limit of how much $CsNO_3$ can be integrated into the cement matrix has been reached. Pores can be observed as dark spots in the BSE images as well as around the large caesium nitrate area, where they naturally form in the Interfacial Transition Zone (ITZ) between large particles and the bulk cement, as smaller cement particles are less able to fill this space [31], [32]. This is further evidence which suggests that the larger $CsNO_3$ particles had already formed when the cement began hydrating (e.g. this $CsNO_3$ did not dissolve in the water/cement mix).

The two strong Mg areas in the high resolution maps are attributed to hydrotalcite which agrees with the XRD patterns as Al is distributed there as well. Ca, Si and Al are seen through

the whole sample, which is expected for slag-portland cements and agrees with the XRF data in Table 3.2. In Figure 4.26 there is a broken particle of $CsNO_3$, some of which surrounds a particle with a high silica concentration, which was likely already in the cement powder prior to mixing and is unaltered during curing – this possibly originates from the BFS as PC does not generally contain silica that is not bonded with calcium. Due to the presence of aluminium and magnesium through the whole image (though there is less present in the caesium nitrate area), it is believed that the caesium nitrate particle precipitated during the cement hydration process, as 99.9% pure $CsNO_3$ was used in the experiments so any undissolved particles would not originally contain Al and Mg.

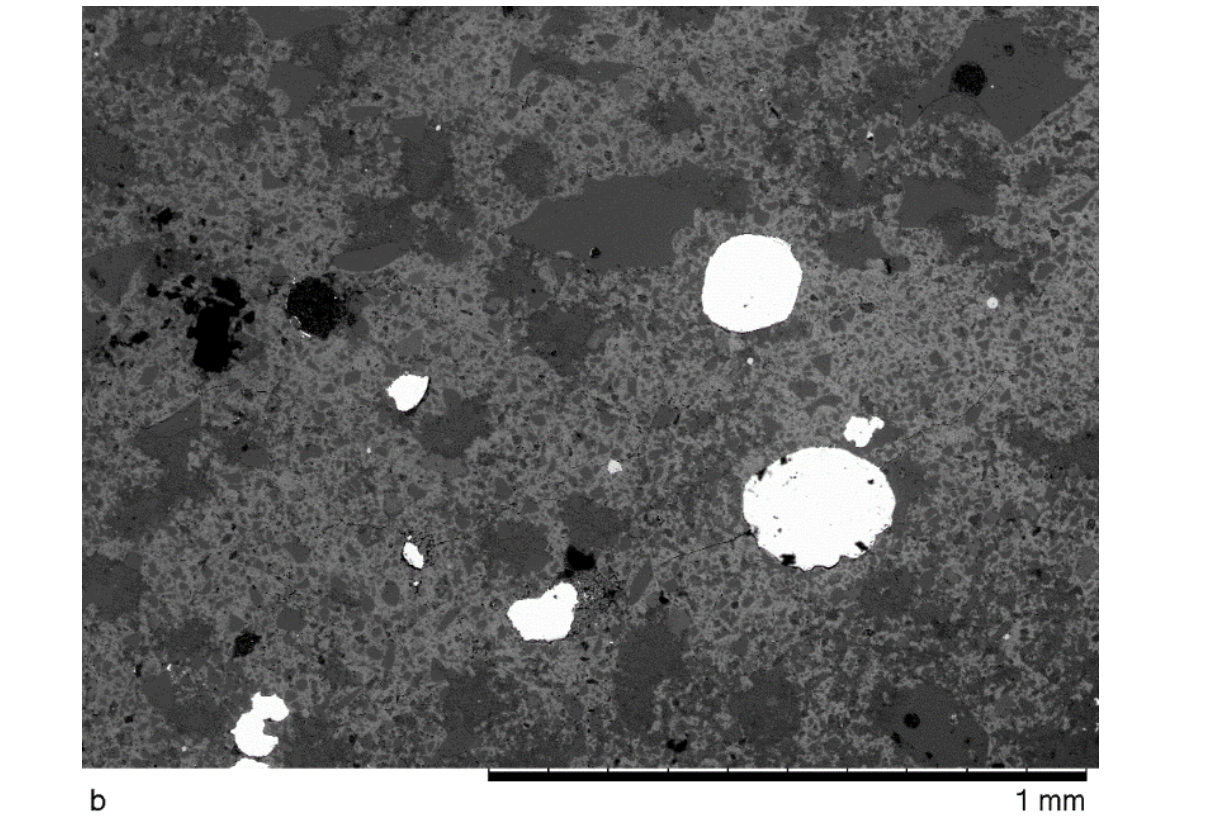

Figure 4.24 BSE image at low magnification of a 28-day old 3:1 BFS:PC with 16 wt.% $CsNO_3$, and SEM-EDX maps of the same area of Cs, N, Ca, Si, Al and Mg

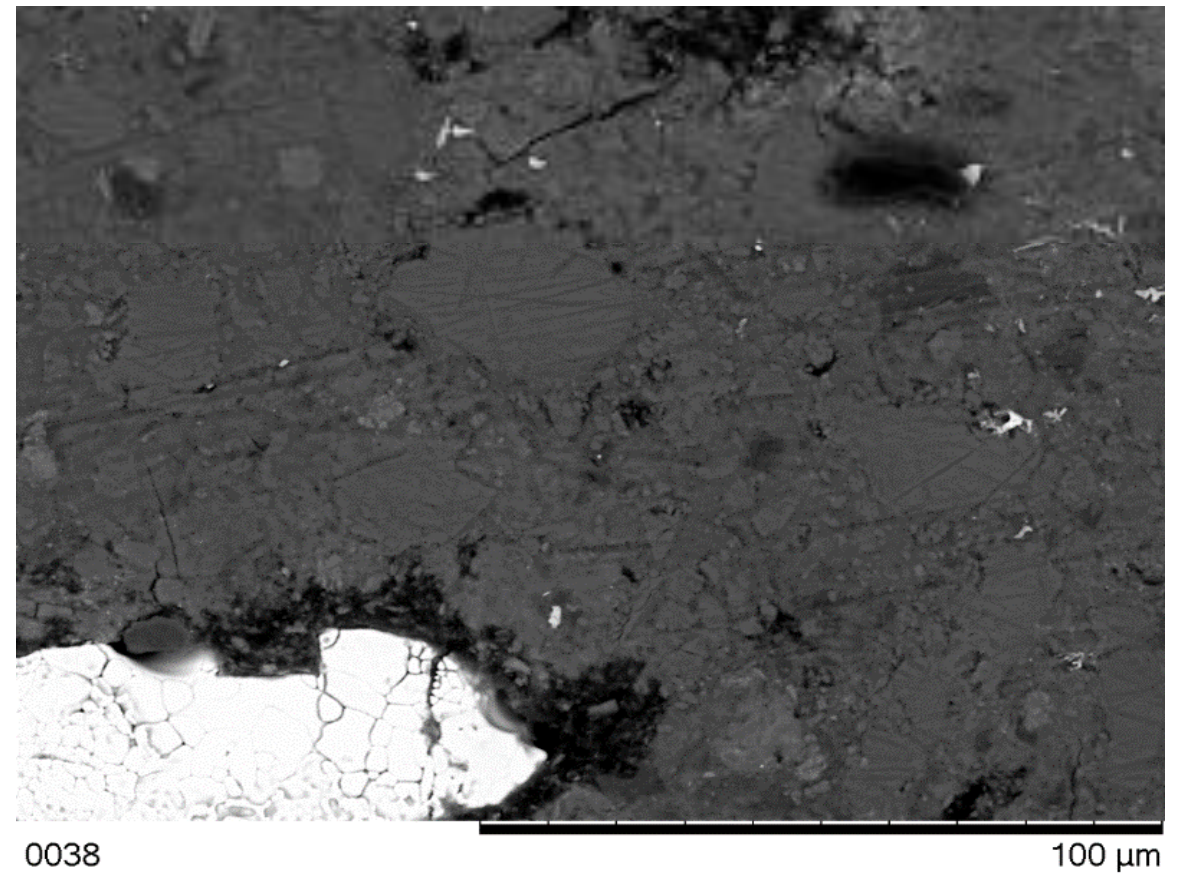

Figure 4.25 Composite BSE image at high magnification of a 28-day old 3:1 BFS:PC with 16 wt.% $CsNO_3$, with SEM-EDX maps of the same area of N, Cs, Ca, Si, Al and Mg

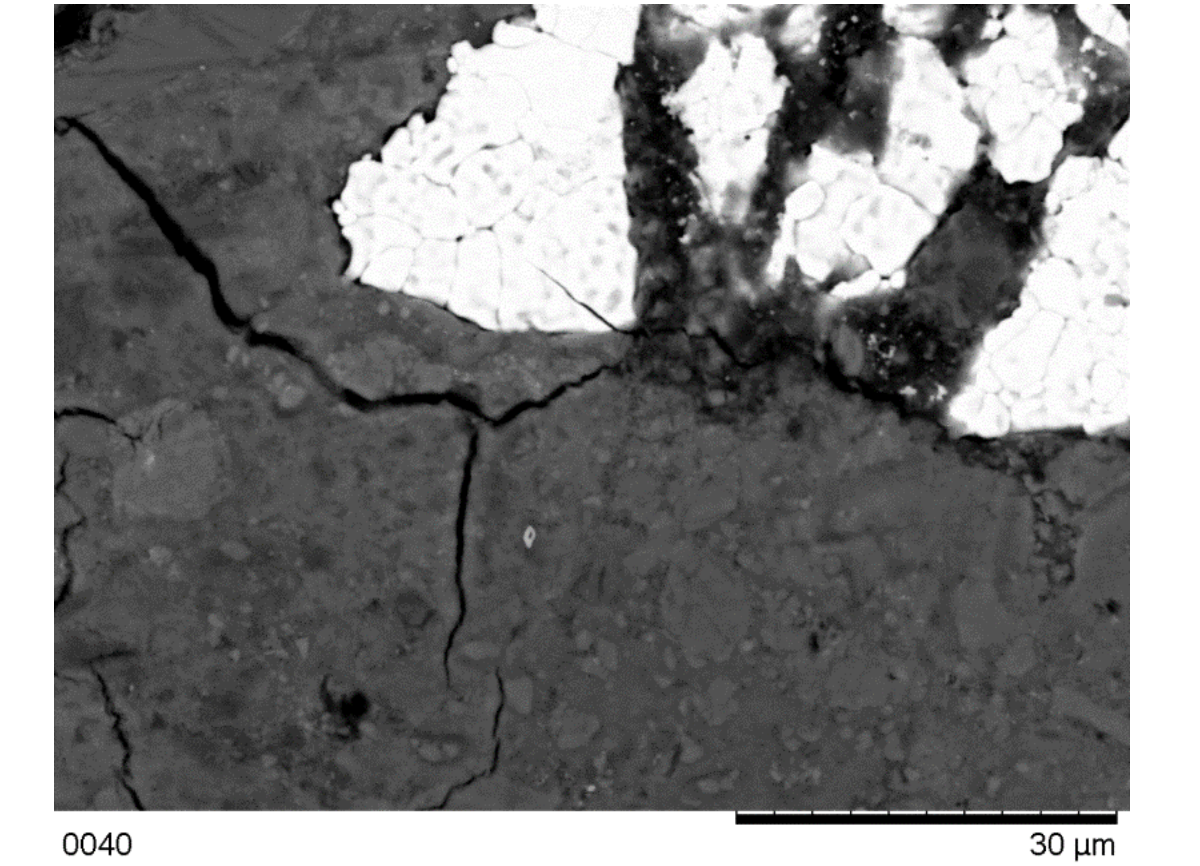

Figure 4.26 BSE image at high magnification of a 28-day old 3:1 BFS:PC with 16 wt.% $CsNO_3$,and SEM-EDX maps of the same area of Cs, N, Ca, Si, Al and Mg

4.2.3 Effect of $CsNO_3$ on the Microstructure of 3:1 BFS:PC– Mercury Intrusion Porosimetry

The total porosity data of both the samples containing $CsNO_3$ obtained from MIP is shown in Figure 4.27. The effect of increased $CsNO_3$ incorporation appears to be rather mild on the total porosity. With 1 wt.% $CsNO_3$, there is a small increase in porosity by 3.21 ± 1% compared with the 0 wt.% $CsNO_3$ system. The porosity then decreases as the amount of $CsNO_3$ increases up to 6 wt.%. The pore size distribution is shown in Figure 4.28, with the 5-50 nm and 50-5000 nm ranges presented in Figure 4.29 and Figure 4.30 respectively. The x-axis shows the pore diameter, and the y-axis shows the logarithmic differential intrusion, calculated using Equation 4.3;

$$\text{Log (differential intrusion)} = dV/d\log(D) \qquad \text{Equation 4.3}$$

Where V is the volume of mercury that has intruded the cement sample, and D is the pore entry diameter. In the 5-50 nm range, there is an increase in average diameter and a decrease in the intrusion with the increase in the $CsNO_3$ content from 0-6 wt.%. This pore diameter range contains the small gel pores of the hydrated material, and an increase in these pores is suggestive of a decrease in the cement's level of hydration [33]. At the same time, the porosity in the 50-5000 nm (capillary pores) significantly increases in the 1 wt.% sample compared with the 0 wt.% sample, which decreases when $CsNO_3$ is further increased. This trend is the same as in the total porosity. It appears that the porosity in this range is dominating the general trend of porosity. These larger pores are named capillary pores whose volume typically increases with increasing water/binder ratios [30] – however in these samples the w/b ratio is constant. Valori et al. state that during hydration "the inter-hydrate pore size [of C-S-H] is distinct in so much as it rapidly evolves down to the characteristic size of 10 nm, after which the size remains constant" [34]. This region corresponds to a peak in the 0 wt.% sample,

and in other samples the pore entry diameter corresponding to this peak increases as the wt.% of $CsNO_3$ increases. This suggests that increasing amounts of $CsNO_3$ are linked to an increase in the inter-hydrate pores of C-S-H, meaning that $CsNO_3$ could potentially be held within these C-S-H interlayers, but this has not been confirmed in these experiments. The pore size distribution in the 6 wt.% sample in this range is different from the 1 and 3 wt.% samples. This may be related to the fact that 6 wt.% sample had $CsNO_3$ particles in the system.

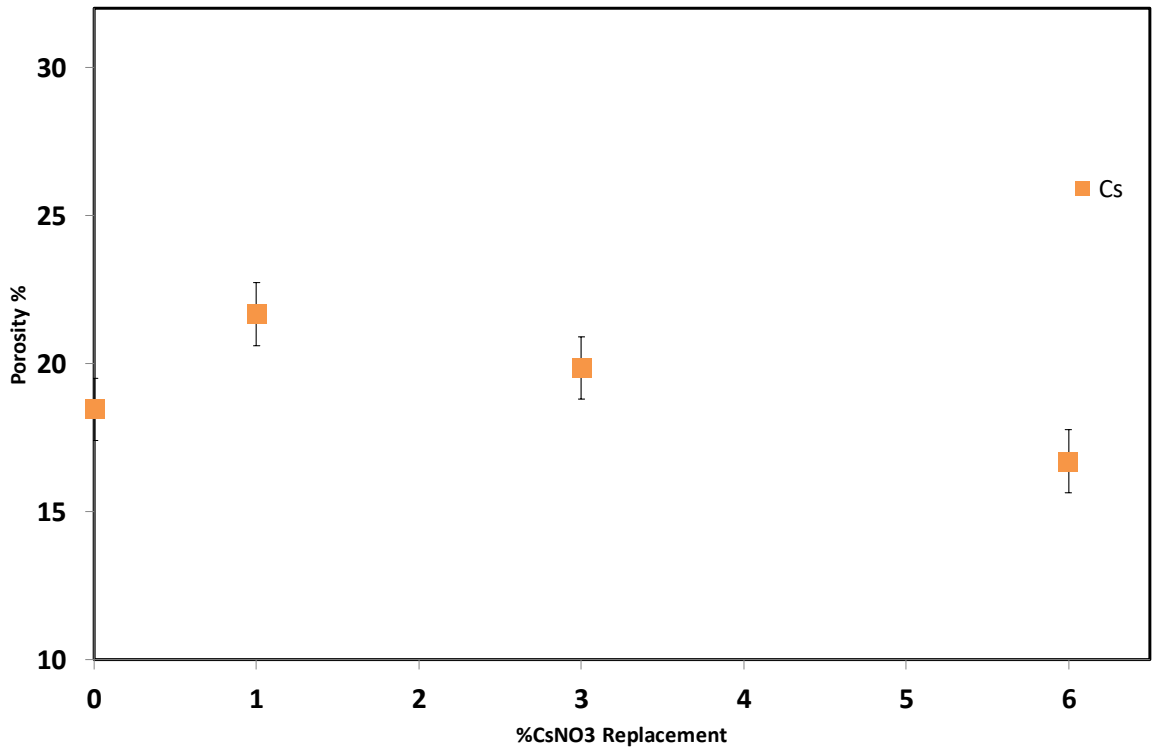

Figure 4.27 Porosity of 3:1 BFS:PC containing different amounts of $CsNO_3$

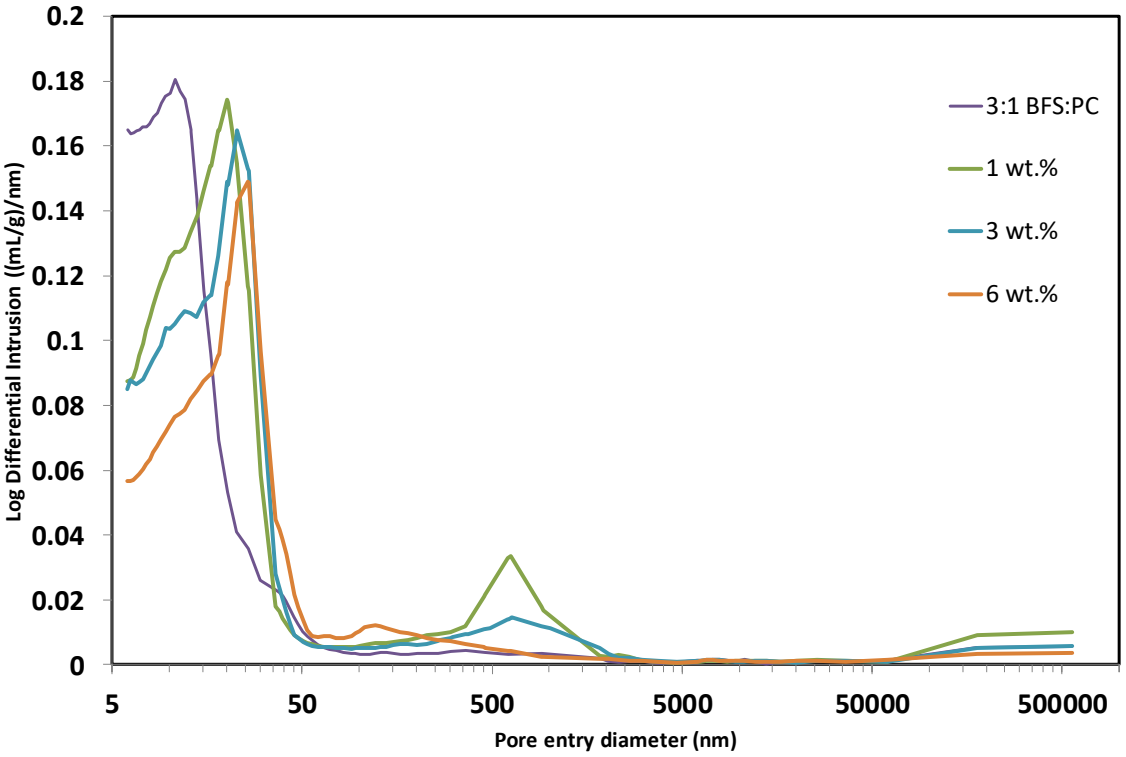

Figure 4.28 Pore Size distribution of 3:1 BFS:PC containing increasing amounts of $CsNO_3$

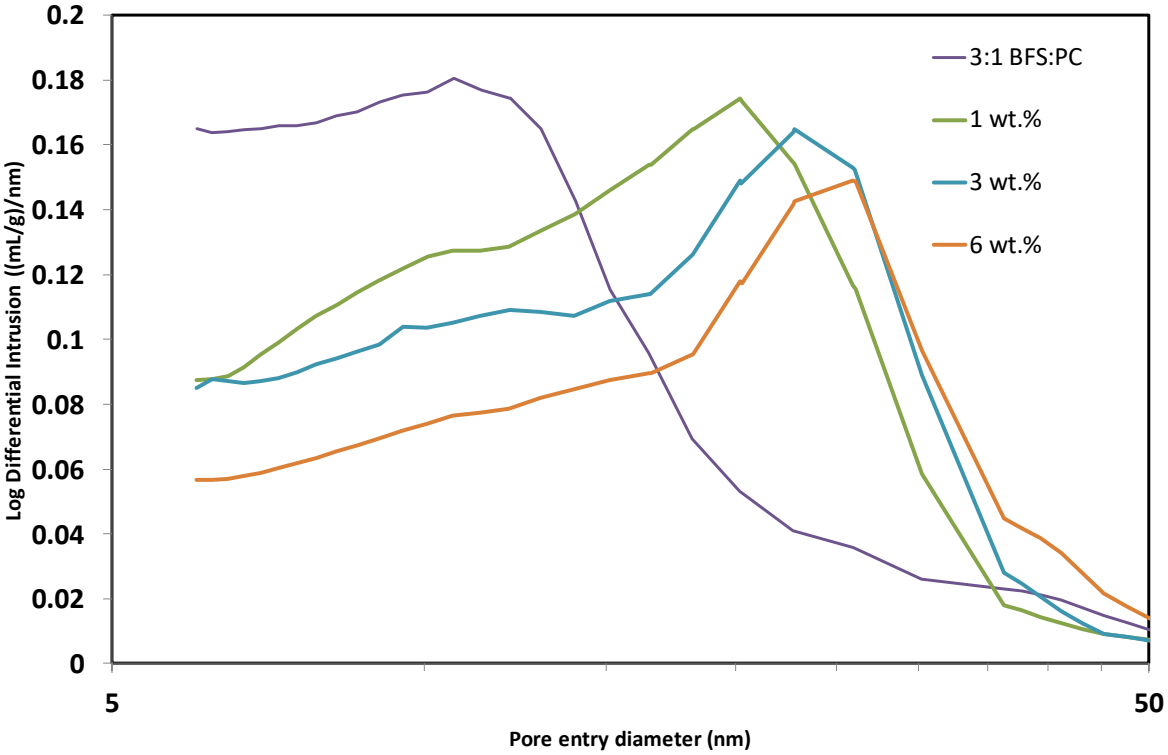

Figure 4.29 Pore Size distribution of 3:1 BFS:PC containing increasing amounts of $CsNO_3$ in the 50-5 nm range

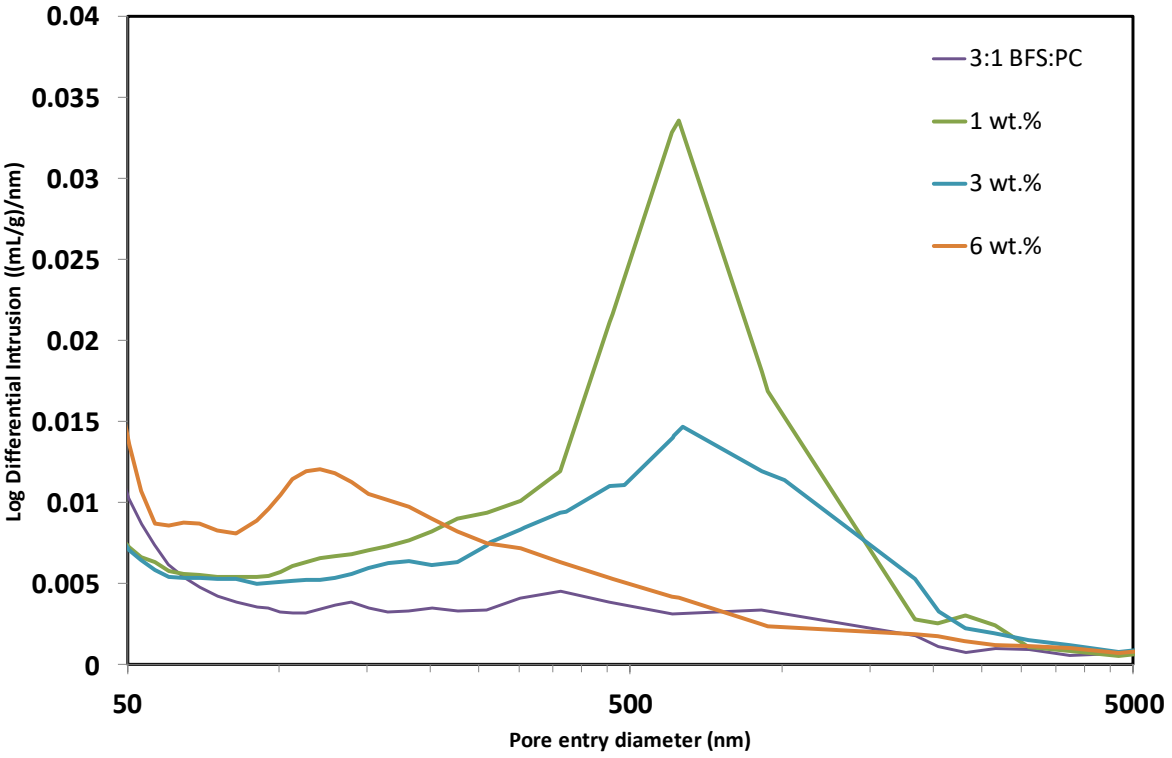

Figure 4.30 Pore Size distribution of 3:1 BFS:PC containing increasing amounts of $CsNO_3$ in the 500-50 nm range

4.3 Incorporation of Ba in 3:1 BFS:PC

3:1 BFS:PC samples were prepared with different wt.% of $Ba(OH)_2 \cdot 8H_2O$ and $Ba(NO_3)_2$ incorporation as shown in Table 4.1 Weight composition of 3:1 BFS:PC samples produced. , and were otherwise prepared using the same methods as in Section 4.2.

4.3.1 Effect of barium on Phases Present in 3:1 BFS:PC– X-Ray Diffraction and Thermal Analysis

The XRD data of the 3:1 BFS:PC samples containing Ba after 28 days of curing are shown in Figure 4.31. As the wt.% Ba is increased, the sharpness of the C-S-H peak decreases, which signifies a decrease in the crystallinity, however portlandite does not show a similar trend. Mobasher et al. showed that barium hydroxide can act as an alkali activator for BFS:PC [35], which agrees with these results as the cement mixture has extra hydroxide to react with. It is possible that hydration at high alkalinity due to the added barium hydroxide reduced the

degree of hydration of the cement, or precipitated more portlandite and less C-S-H [36]. This behaviour is the opposite of the C-S-H in the caesium incorporation series. As Ba is increased, the barite peaks ($BaSO_4$, labelled B in the Figure) seem to become clearer and the ettringite peaks are not observed. Peaks due to barium hydroxide and barium nitrate were not observed in the XRD patterns. A similar phenomenon has been reported [15], where ettringite was observed to decompose in the presence of barium carbonate (witherite), and barite was formed. The results obtained in the present study show that a similar reaction also takes place when barium is present in the form of nitrate and/or hydroxide.

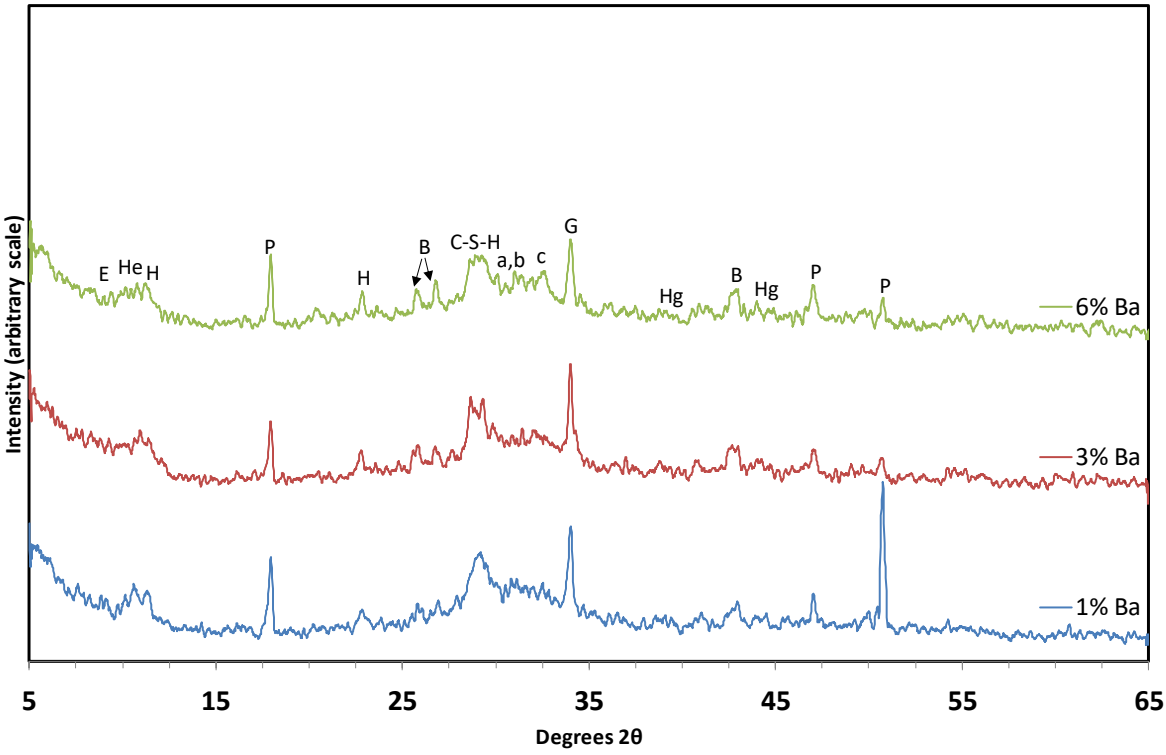

Figure 4.31 XRD of 3:1 BFS:PC with increasing amounts of Ba

The thermal analysis consisting of TG and DTA and their first derivative for the barium-containing samples are shown in Figure 4.32 to Figure 4.35, which are labelled according to the description in Table 4.3. In the TG data, the 1 wt.% sample displayed the greatest weight loss in the 40-110 °C region with the 3 wt.% and 6 wt.% samples displaying a similar but smaller weight loss behaviour. Barium can cause the reduction of ettringite in the system as mentioned previously, and this was observed in the XRD data. The decreased weight loss in the 40-110°C region as wt.% Ba is increased may reflect this effect, and this is also likely in agreement with the XRD patterns, which showed a reduction in the sharpness of the C-S-H peaks. Even though the XRD analysis did not detect any ettringite in the samples, small traces of ettringite could still be present even after 28 days as this mineral phase was observed in the samples with no Ba added. The 3 wt.% and the 6 wt.% samples would most likely contain less ettringite than the 1 wt.% sample, explaining the increased weight loss for this sample in the 40-110°C temperature region (compared with the 3 wt.% and 6 wt.% samples). The increased weight loss of the 1 wt.% sample can be seen clearly in the DTG shown in Figure 4.33 and seems to agree with the XRD patterns. As the data for the 3 wt.% and 6 wt.% samples show, less weight is lost as the amount of barium increases. The next obvious feature in the TG data is the dehydroxylation of portlandite around 450 °C. Again, the DTG data shows that the weight loss associated with the dehydroxylation of portlandite decreases as the wt.% Ba increases. The 3 and 6 wt.% Ba samples show similar behaviour in the TG data up to around 500°C, where they begin to diverge. All of the 1, 3 and 6 wt.% Ba systems indicate a small peak in the DTG data in the range of 500-700°C, attributed to the presence of calcium carbonate [21]. However, the DTG data also reveals a unique feature in the 6 wt.% data, which is likely to be the decomposition of $Ba(NO_3)_2$ [27]. To confirm this thermal event a repeat measurement of a separate 6 wt.% Ba sample showed the same feature, therefore confirming

that between 3 and 6 wt.% Ba some of the added $Ba(NO_3)_2$ is not able to dissolve in the cement matrix. The DTG data reveal that there is weight loss due to hemicarbonate and monocarbonate around 150°C, again being a stronger feature in the 1 wt.% sample due to a larger amount of hemicarbonate present in this composition. A similar analysis was conducted to find the peak area of the portlandite peaks in the DTA data as in Figure 4.15, but no trend was observed, and otherwise the DTA data confirmed the results and features observed in the TG data.

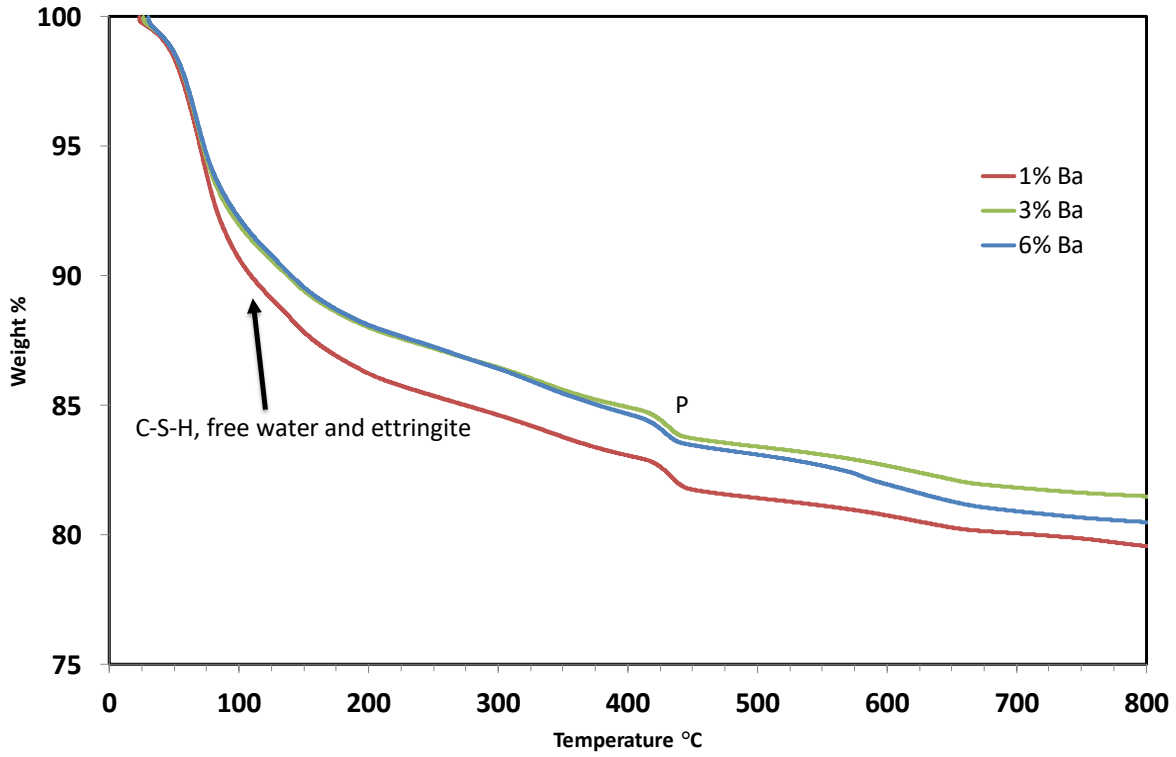

Figure 4.32 TG of 28 Day old 3:1 BFS:PC with addition of 1 to 6 wt.% Ba

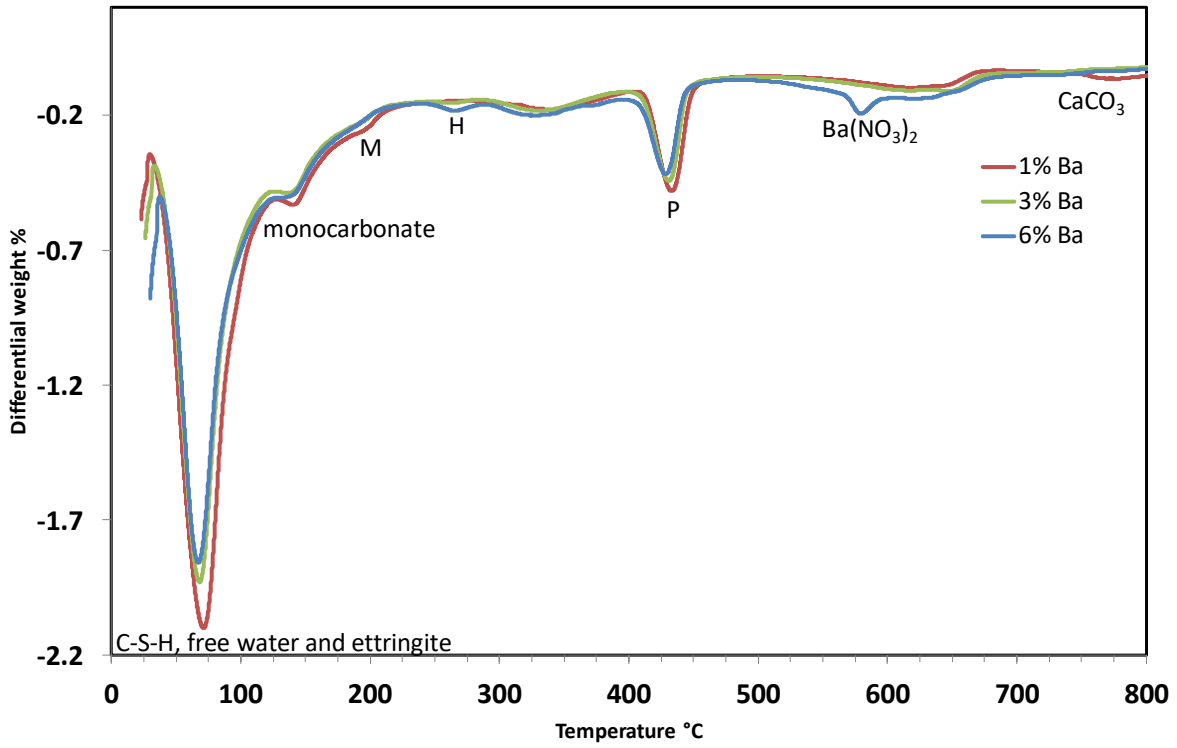

Figure 4.33 The DTG data of 28 Day old 3:1 BFS:PC with addition of 1 to 6 wt.% Ba

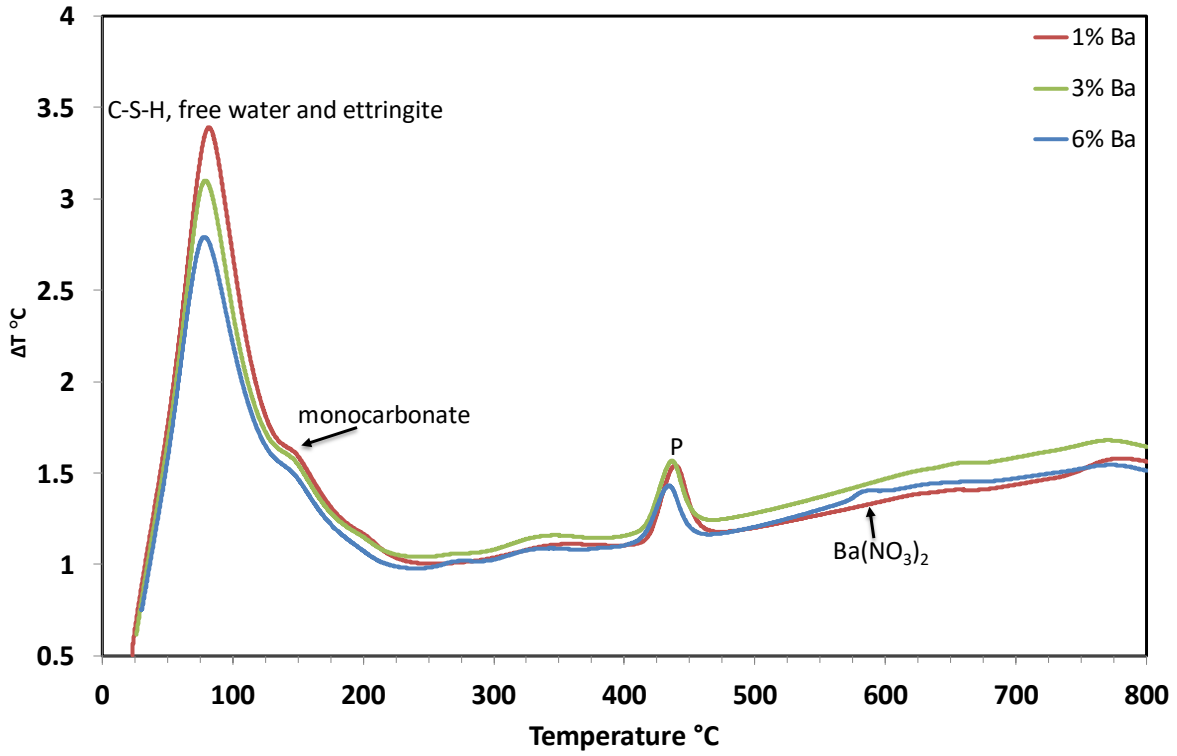

Figure 4.34 DTA of 28 Day old 3:1 BFS:PC with addition of 1 to 6 wt.% Ba

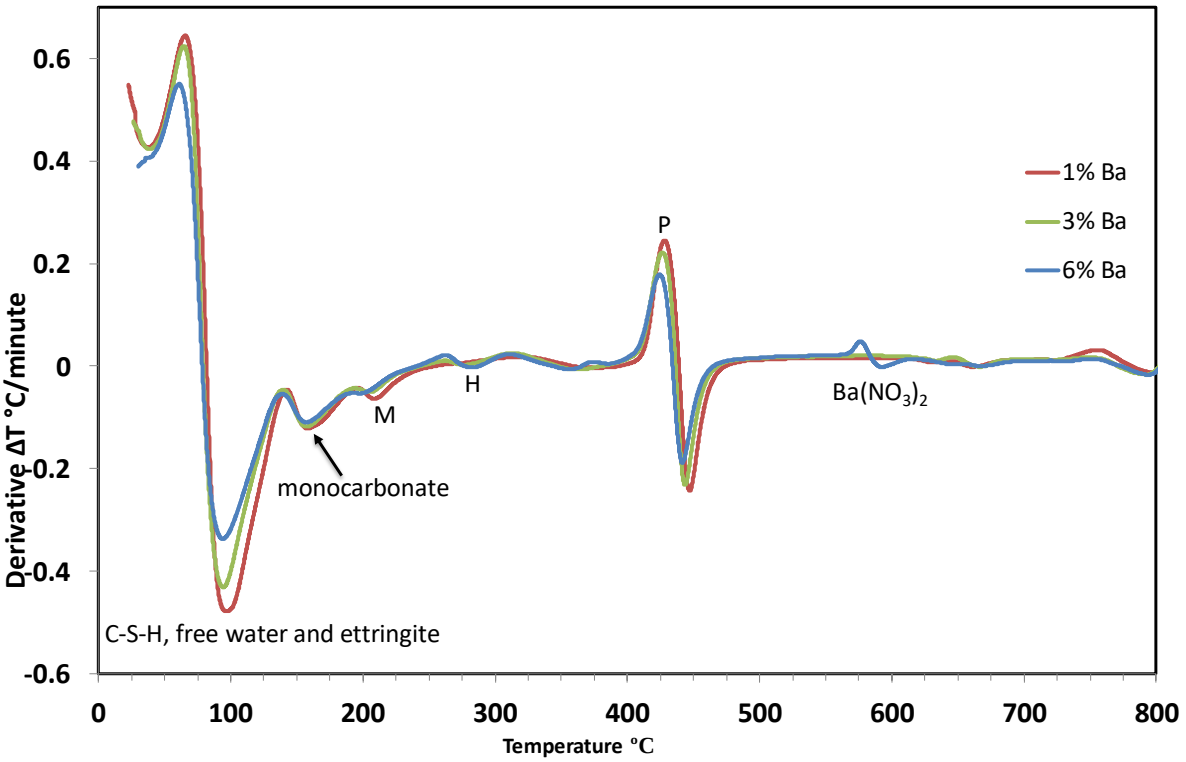

Figure 4.35 The first derivative of the DTA of 28 Day old 3:1 BFS:PC with addition of 1 to 6 wt.% Ba

4.3.2 Effect of barium on Microstructure in 3:1 BFS:PC– Scanning Electron Microscopy and Mercury Intrusion Porosimetry

BSE images and elemental mapping of the 1 wt.% Ba composition at low and high magnifications are shown in Figure 4.36 and Figure 4.37 respectively. The porosity of the sample (corresponding to darker areas in the image as described above), however, is visibly higher than in the cement samples with no additions. In the previously shown maps the brighter areas corresponded to area of higher Fe concentration, but in the following BSE images bright areas correspond to Ba as it is a heavy atom. Note that none of the barium-containing samples had distinct/interesting features when maps of nitrogen were examined, and so these are not shown below. The lack of particles with a high concentration of nitrogen suggests that $Ba(NO_3)_2$ had fully dissolved in the 1 wt.% Ba sample. Ba and S are spread through the sample and don't have many observable areas of higher concentration, except for a few small areas as shown in a 5000x magnification map displayed in Figure 4.38. This suggests that barite forms in the cement, as there is a strong overlap of these elements.

Figure 4.36 BSE image at low magnification of 3:1 BFS:PC with 1 wt.% Ba, and SEM-EDX maps of the same area of Ba, S, Ca, Si, Al and Mg

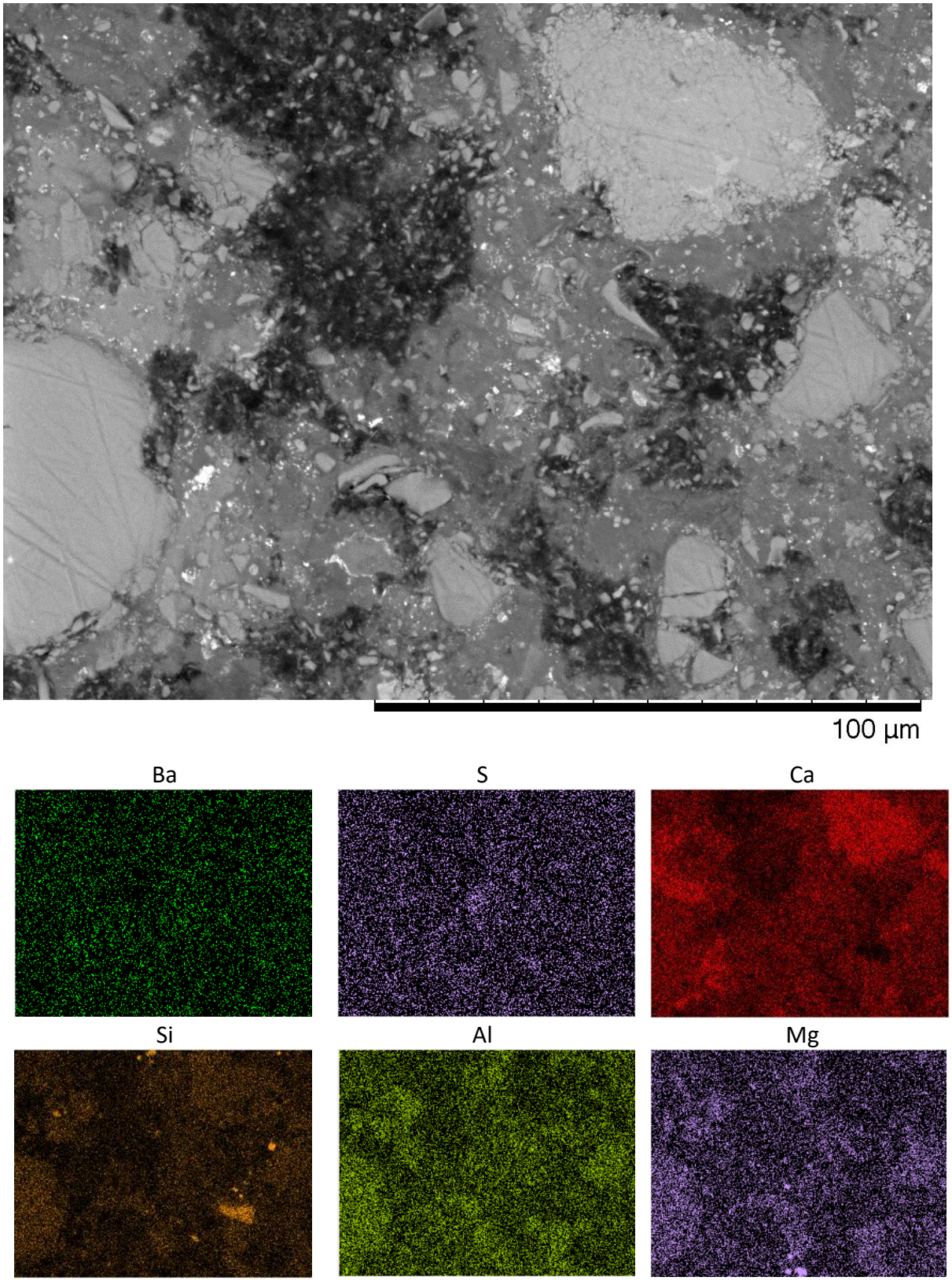

Figure 4.37 BSE image at high magnification of 3:1 BFS:PC with 1 wt.% Ba, and SEM-EDX maps of the same area of Ba, S, Ca, Si, Al and Mg

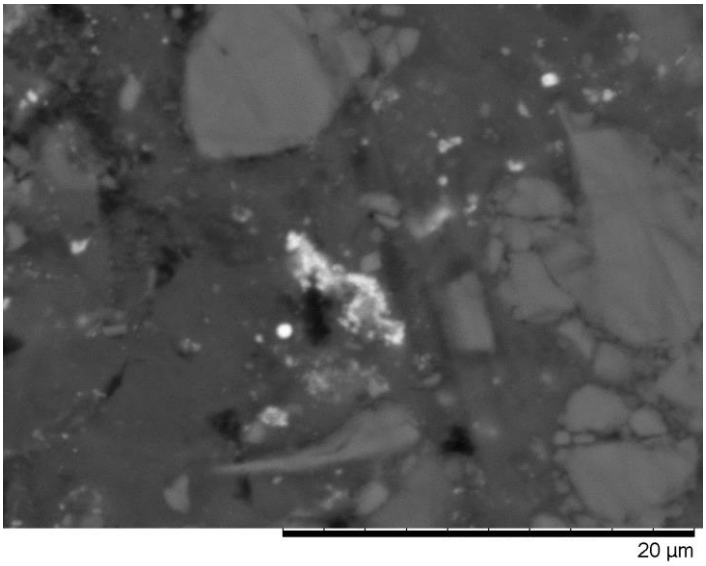

Barium

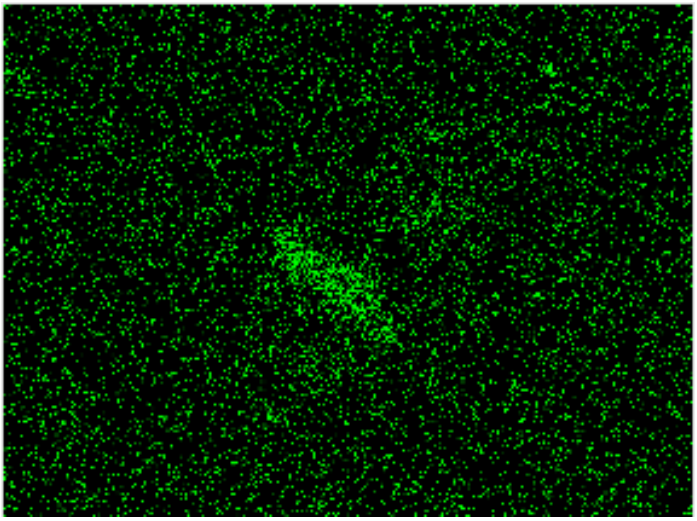

Sulphur

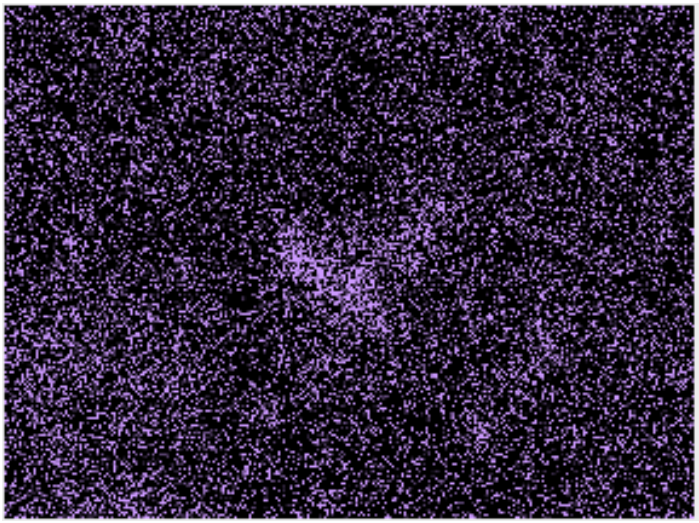

Figure 4.38 BSE image at high magnification of 3:1 BFS:PC with 1 wt.% Ba focusing on an area of barium sulphate, and SEM-EDX maps of the same area of Ba and S

A BSE image of the 3 wt.% Ba sample is shown in Figure 4.39 at a low magnification with EDX mapping. Again there are large pores held within unhydrated particles, and many pores within the bulk cement, seemingly more than in the data for the 1 wt.% Ba sample. No cracks were observed. There are small areas of Ba visible throughout the image; one of these areas is shown at a high magnification in Figure 4.40. There is an area of high S concentration surrounded by Ba. It is possible that the Ba reacted with the surface of a particle with a high amount of S to form barite. This particle was also high in Ca, and thus is likely a form of calcium sulphate, possibly in a hydrated form as gypsum ($CaSO_4 \cdot 2H_2O$), due to the low concentrations of Al and Si in that area compared with the rest of the sample. This image indicates that the presence of barium in the cement during the initial hydration may prevent the formation of ettringite ($Ca_6(Al(OH)_6)_2(SO_4)_3(H_2O)_{26}$). Ettringite would normally form from a reaction of the added gypsum particles with calcium aluminate [37]. In a 9:1 BFS:PC sample containing witherite, as studied and explained by Utton et al. in 2011 [38], ettringite and barite precipitation occurred simultaneously which compete for sulphate ions in solution. In their test ettringite was observed in XRD patterns after 24 hours of curing, but they found that after just 7 days the ettringite peak was significantly weaker. It is thus likely that at an early age the samples in the current project did contain ettringite, which then decomposed as time progressed and is no longer present after 28 days.

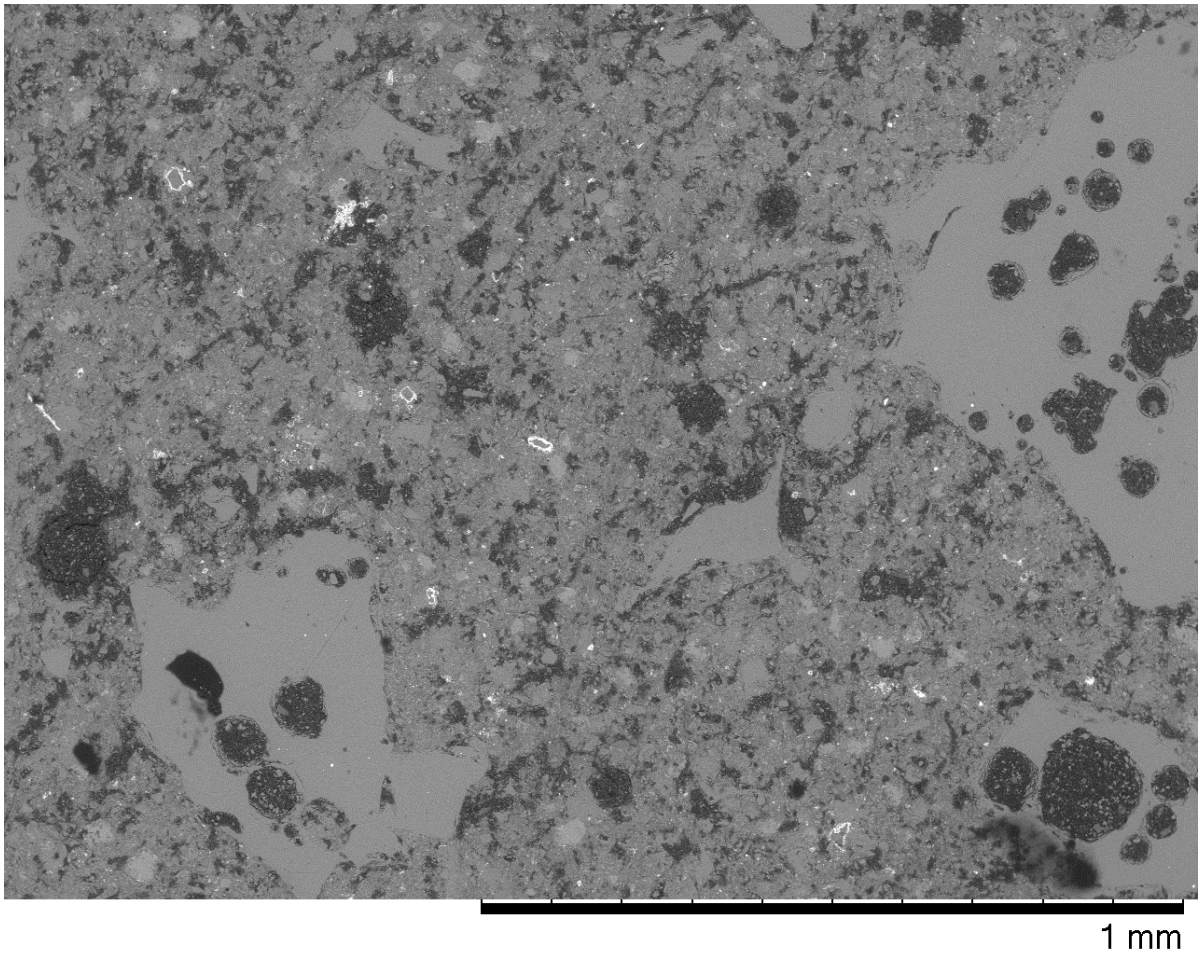

Figure 4.39 BSE image at low magnification of 3:1 BFS:PC with 3 wt.% Ba, and SEM-EDX maps of the same area of Ba, S, Ca, Si, Al and Mg

Figure 4.40 BSE image at high magnification of 3:1 BFS:PC with 3 wt.% Ba, and SEM-EDX maps of the same area of Ba, S, Ca, Si, Al and Mg

At a low magnification, the 6 wt.% sample (Figure 4.41) is similar in appearance to the 3 wt.% Ba sample with many pores seen throughout the sample and some unreacted particles. There are also a lot of areas with a higher Ba concentration corresponding to barite. In Figure 4.42,

at a high magnification, however, the 6 wt.% Ba sample shows that precipitations of barite are more common compared with the 3 wt.% Ba sample and here they are spread throughout the sample, seemingly in the cracks between unhydrated cement particles (e.g. the ITZ).

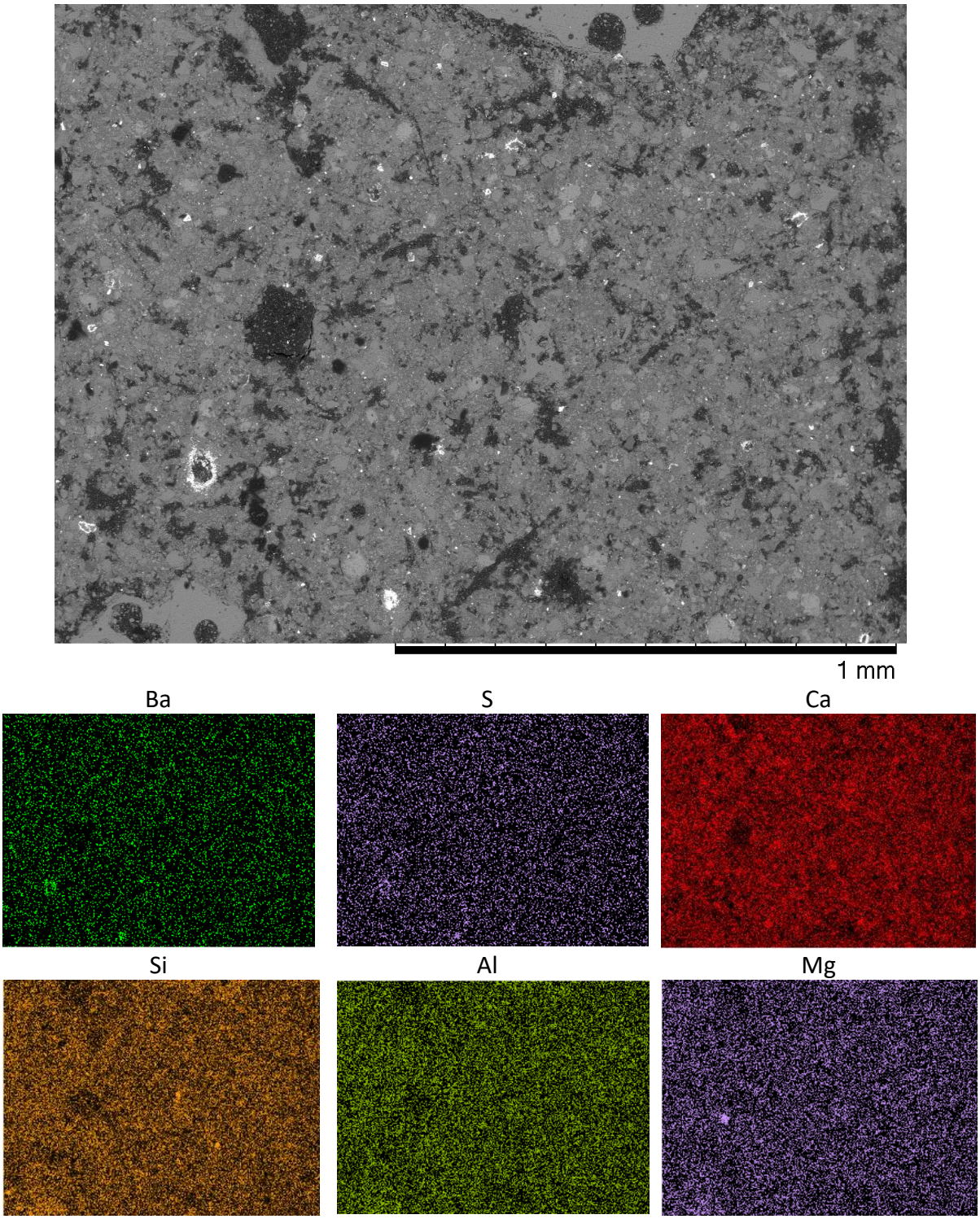

Figure 4.41 BSE image at low magnification of 3:1 BFS:PC with 6 wt.% Ba, and SEM-EDX maps of the same area of Ba, S, Ca, Si, Al and Mg

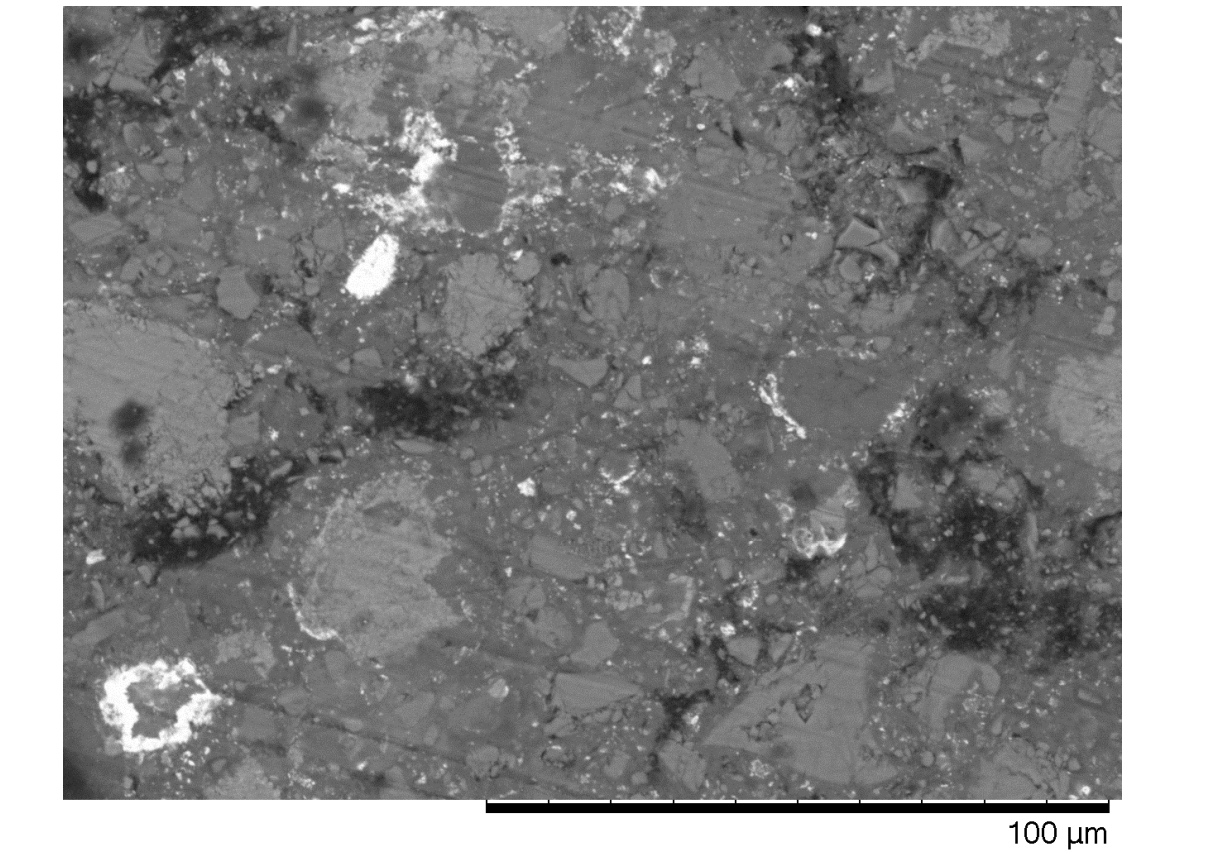

Figure 4.42 BSE image at high magnification of 3:1 BFS:PC with 6 wt.% Ba, and SEM-EDX maps of the same area of Ba, S, Ca, Si, Al and Mg

The porosity data gathered using MIP for the three formulations containing Ba are shown below in Figure 4.43 to Figure 4.27. The data for the system with Cs inclusion (the same data as in Figure 4.27) are also shown for comparison. The Ba containing samples display a higher porosity than the Cs containing samples. The porosity of the Ba containing systems increases as the addition of Ba increases, unlike the $CsNO_3$ samples, where the porosity decreased as addition increased (possibly due to enhanced pozzolanic reaction in the Cs containing samples). From comparing these results with the literature by Garcia-Lodeiro et al. which examined alkali effect on the hydration of PC [36], [39], it is also possible that the hydration in the Ba samples at a high alkalinity reduced the degree of hydration of the cement, or alternatively precipitated more portlandite and less C-S-H. These observations agree with data in the literature, where witherite ($BaCO_3$) incorporation increased the porosity of white cement mortars [40] – in that study witherite was included in the mix instead of gypsum in a successful attempt to reduce and control sulphate attack. The authors attributed the increase in porosity to the lowered proportional amount of clinker, specific surface and reduction in plasticity. The proportional reduction of the clinker most likely also impacts the porosity in this research. The pore size distributions of the Ba containing samples are shown in Figure 4.44 together with the system with no Ba inclusion. In the 1 wt.% sample, the average pore size in the 5 to 50 nm range is increased in comparison to the unaltered 3:1 BFS:PC sample. The 3 wt.% and 6 wt.% samples had a distinct distribution of pores in the 200-2000 nm range that was not seen in the 0wt.% and 1 wt.% samples. The change in the porosity distribution is likely caused by the increased barite formation that occurred in these samples. In this range the 3 wt.% and 6 wt.% samples are similar. Where the 3 wt.% and 6 wt.% differ, however, is clearly in the 5 to 100nm range, where, although the two samples display the same behaviour, the 6 wt.% is approximately 1.5 times larger than the 3 wt.%.

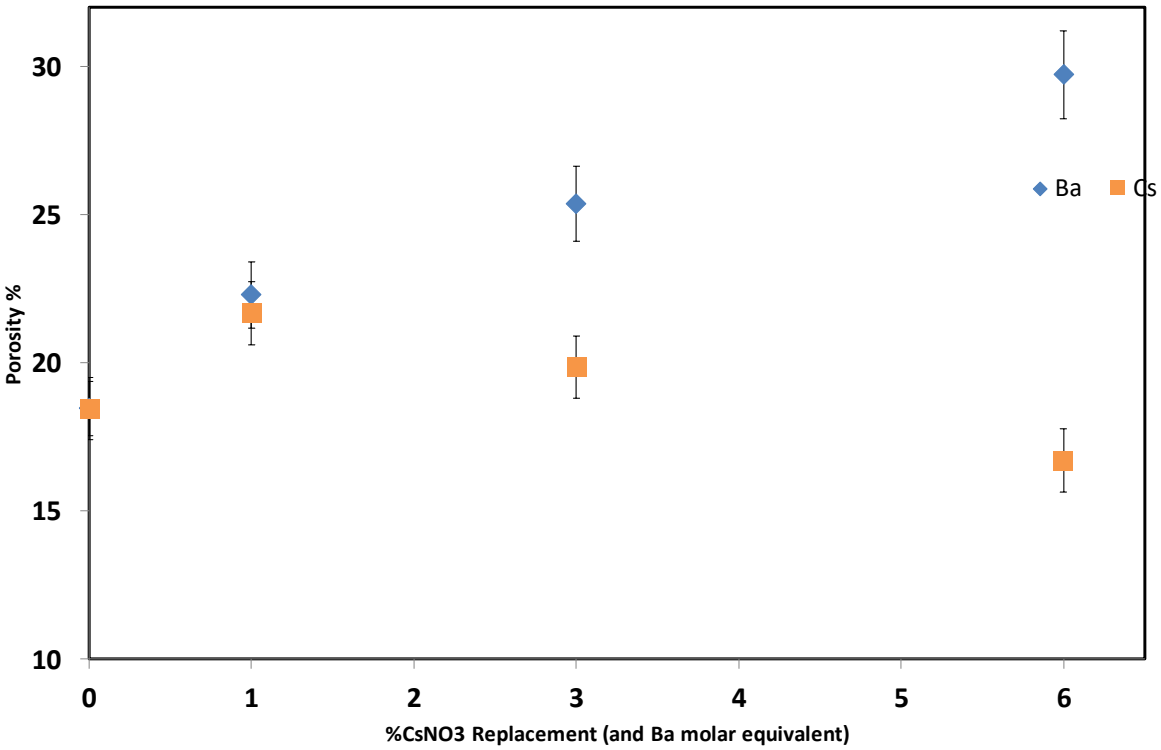

Figure 4.43 Porosity of 3:1 BFS:PC containing different amounts of $CsNO_3$ and $Ba(NO_3)_2$ + $Ba(OH)_2{\cdot}8H_2O$. In the Ba containing system, the quantity of Ba and NO_3^- were matched with the number of Cs and NO_3^- in the Cs containing system

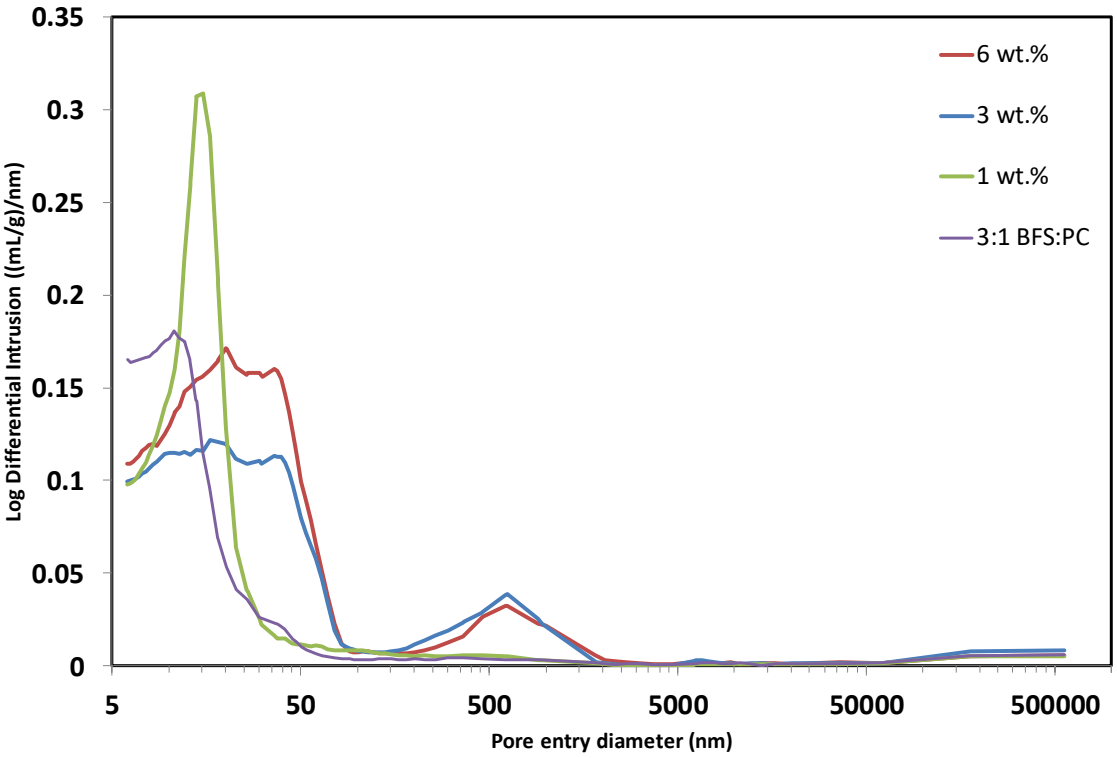

Figure 4.44 Pore size distribution displayed via cumulative differential intrusion as a function of pore diameter for samples containing barium. For comparison a sample with no addition is also shown.

4.4 Summary

The results of this Chapter imply that when caesium decays into barium in nuclear waste that is encapsulated in BFS:PC, the barium will react with the sulphur present and form barium sulphate. When $CsNO_3$ is in the system, ettringite is observed in the XRD patterns at every wt.% including 0 wt.%, and $CsNO_3$ is observed from 6 wt.%. Otherwise the introduction of $CsNO_3$ does not seem to have a large effect on the phases present. DSC analysis reveals that the introduction of $CsNO_3$ above approximately 2.8 wt.% will result in the precipitation of $CsNO_3$ in the system. Caesium nitrate particles are seen during SEM analysis in the 16 wt.% sample that had not dissolved.

From the XRD patterns, when barium is introduced no ettringite is observed and barium sulphate is seen in the data at 1 wt.% and above, apparently forming from sulphur-containing phases such as calcium sulphate. Because of the lack of ettringite observable in the data, it seems likely that the incorporation of barium into the cement samples prevents the formation of ettringite. With increasing barium content in the samples, a porosity increase was also detected. Due to this, the sample is exposed to greater amounts of atmospheric CO_2, and therefore more hemicarbonate and monocarbonate is observable in both the XRD and thermal analysis.

From the two Sections of this Chapter, the results suggest then that Cs encapsulated in 3:1 BFS:PC as ILW will not form any new phases and will be spread throughout the sample. It will precipitate at a level above ~2.8 wt.%. When it decays into Ba, it will likely react with ettringite to form barium sulphate. The data shown in this Chapter, however, is based on experiments where Ba is incorporated into the cement during hydration. During actual nuclear decay, the stark difference in porosity is unlikely to occur. To simulate more accurately Cs decaying into

Ba as it occurs in ILW, a different technique for barium incorporation is needed that allows for the investigation of the reaction between barium and cement that has already been cured: Electrical Migration.

4.5 References

[1] E. Gruyaert, N. Robeyst, and N. De Belie, "Study of the hydration of Portland cement blended with blast-furnace slag by calorimetry and thermogravimetry," *J. Therm. Anal. Calorim.*, vol. 102, pp. 941–951, 2010.

[2] I. Odler, "Investigation of the hydration of portland blastfurnace slag cement: composition, structure and properties of the hydrated material," *Adv. Cem. Res.*, vol. 2, no. 5, pp. 15–20, 1989.

[3] I. Odler and W. Hinrichs, "Investigation of the hydration of Portland blastfurnace slag cement: hydration kinetics," *Adv. Cem. Res.*, vol. 2, no. 5, pp. 9–13, 1989.

[4] I. G. Richardson, C. R. Wilding, and M. J. Dickson, "The hydration of blastfurnace slag cements," *Adv. Cem. Res.*, vol. 2, no. 8, pp. 147–157, 1989.

[5] S. J. Way and A. Shayan, "Early hydration of a portland cement in water and sodium hydroxide solutions: composition of solutions and nature of solid phases," *Cem. Concr. Res.*, vol. 19, no. 5, pp. 759–769, 1989.

[6] J. V. Hanna, L. P. Aldridge, and E. R. Vance, "Cs speciation in cements," in *Materials Research Society*, 2001, vol. 663, pp. 89–101.

[7] J. L. Provis, P. A. Walls, and J. S. J. van Deventer, "Geopolymerisation kinetics. 3. Effects of Cs and Sr salts," *Chem. Eng. Sci.*, vol. 63, pp. 4480–4489, 2008.

[8] E. Revertegat, C. Richet, and P. Gegout, "Effect of pH on the durability of cement pastes," *Cem. Concr. Res.*, vol. 22, no. 2–3, pp. 259–272, 1992.

[9] M. Castellote, C. Andrade, and C. Alonso, "Characterisation of transport of caesium, strontium, cobalt and iron ions through concrete by steady state migration and natural diffusion tests," *Adv. Cem. Res.*, vol. 11, no. 4, pp. 161–168, 1999.

[10] W. Gashier, T. Miura, K. Hashimoto, R. J. Hand, and H. Kinoshita, "Leaching behaviour of cementitious nuclear wasteforms containing caesium and strontium," *Adv. Appl. Ceram.*, vol. 113, no. 8, pp. 447–452, 2014.

[11] M. P. Unterweger, D. D. Hoppes, and F. J. Schima, "New and revised half-life measurements results," *Nucl. Instruments Methods Phys. Res. A*, vol. 312, no. 1–2, pp. 349–352, 1992.

[12] M. P. Unterweger, "Half-life measurements at the National Institute of Standards and Technology," *Appl. Radiat. Isot.*, vol. 56, pp. 125–130, 2002.

[13] P. Patnaik, *Handbook of Inorganic Chemicals*. New York: McGraw-Hill, 2002.

[14] AlfaAesar, "Barium hydroxide octahydrate Safety Data Sheet," 2013. [Online]. Available: https://www.alfa.com/content/msds/british/14499.pdf. [Accessed: 17-Jun-2017].

[15] P. M. Carmona-Quiroga and M. T. Blanco-Varela, "Ettringite decomposition in the presence of barium carbonate," *Cem. Concr. Res.*, vol. 52, pp. 140–148, 2013.

[16] Alfa Aesar, "Safety data sheet, Cesium nitrate," 2012. [Online]. Available: https://www.alfa.com/content/msds/british/12884.pdf. [Accessed: 17-Jun-2017].

[17] N. J. Bowmer and S. Curwen, "WP1- Details of encapsulation processes at Sellafield." BNFL Commerical, Sellafield, UK, p. 46, 2007.

[18] J. Cronin and N. C. Collier, "NNL (11) 11524 Issue 3, Expansion of grouted magnox corrosion & expansion of grouted magnox," 2011. [Online]. Available: https://rwm.nda.gov.uk/publication/corrosion-and-expansion-of-grouted-magnox-november-2011/. [Accessed: 17-Jun-2017].

[19] K. Hashimoto, N. Otsuki, T. Saito, and Y. H, "Application of electrical treatment to alteration of cementitious material due to leaching," *J. Adv. Concr. Technol.*, vol. 11, no. 3, pp. 108–118, 2013.

[20] J. R. Harbour, E. K. Hansen, T. B. Edwards, V. J. Williams, R. E. Eibling, D. R. Best, and D. M. Missimer, "Characterization of slag, fly ash and portland cement for saltstone," 2006. .

[21] V. S. Ramachandran, R. M. Paroli, J. J. Beaudoin, and A. H. Delgado, *Handbook of Thermal Analysis of Construction Materials*. Norwich, NY: Noyes Publications/William Andrew Publishing, 2002.

[22] B. Lothenbach, G. Le, E. Gallucci, and K. Scrivener, "Influence of limestone on the hydration of Portland cements," *Cem. Concr. Res.*, vol. 38, pp. 848–860, 2008.

[23] H. F. W. Taylor, *Cement Chemistry*, 2nd Ed. London: Thomas Telford, 1997.

[24] K. H. Stern, "High temperature properties and decomposition of inorganic salts part 3: Nitrates and nitrites," *J. Phys. Chem. Ref. Data*, vol. 1, no. 3, pp. 747–772, 1972.

[25] I. Yanase, J. Konakawa, and H. Kobayashi, "Influence of cesium nitrate and heating rate on densification and microstructure of Cs-deficient pollucite sintered body," *J. Am. Ceram. Soc.*, vol. 188, no. 20365, pp. 184–188, 2006.

[26] R. C. Weast, "CRC Handbook of Chemistry and Physics, 61st Edition." CRC, Boca Raton, Florida, USA, 1980.

[27] AlfaAesar, "Barium nitrate Safety Data Sheet," 2016. [Online]. Available: https://www.alfa.com/content/msds/british/A11305.pdf. [Accessed: 17-Jun-2017].

[28] "Acros Organics, Barium Sulfate BaSO4 MSDS," 2012. [Online]. Available: https://www.fishersci.com/shop/msdsproxy?productName=AC222515000&productDescription=BARIUM+SULFATE++EXTRA+PU+500GR&catNo=AC222515000&vendorId=VN00032119&storeId=10652. [Accessed: 17-Jun-2017].

[29] C. Carde and R. François, "Effect of the leaching of calcium hydroxide from cement paste on mechanical and physical properties," *Cem. Concr. Res.*, vol. 27, no. 4, pp. 539–550, 1997.

[30] P. C. Hewlett, *Lea's Chemistry of Cement and Concrete*, no. 4th edition. Amsterdam: Elsevier Ltd, 2004.

[31] K. L. Scrivener and K. M. Nemati, "The percolation of pore space in the cement paste/aggregate interfacial zone of concrete," *Cem. Concr. Res.*, vol. 26, no. 1, pp. 35–40, 1996.

[32] J. P. Ollivier, J. C. Maso, and B. Bourdette, "Interfacial transition zone in concrete," *Adv. Cem. Based Mater.*, vol. 2, no. 1, pp. 30–38, 1995.

[33] E. Berodier, J. Bizzozero, and A. C. A. Muller, "Chapter 9: Mercury intrusion porosimetry," in *A practical guide to microstructural analysis of cementitous materials*,

1st Editio., K. Scrivener and R. Snellings, Eds. Boca Raton, Florida, USA: CRC Press, 2016, pp. 419–444.

[34] A. Valori, P. J. Mcdonald, and K. L. Scrivener, "The morphology of C–S–H: Lessons from 1H nuclear magnetic resonance relaxometry," *Cem. Concr. Res.*, vol. 49, pp. 65–81, 2013.

[35] N. Mobasher, S. A. Bernal, O. H. Hussain, D. C. Apperley, H. Kinoshita, and J. L. Provis, "Characterisation of Ba (OH)2 – Na2 SO4 – blast furnace slag cement-like composites for the immobilisation of sulfate bearing nuclear wastes," *Cem. Concr. Res.*, vol. 66, pp. 64–74, 2014.

[36] A. Lodeiro, I García-Fernández-jimenez, A. Palomo, and D. E. Macphee, "Effect on fresh C-S-H gels of the simultaneous addition of alkali and aluminium," *Cem. Concr. Res.*, vol. 40, no. 1, pp. 27–32, 2010.

[37] Portland Cement Association, *PCA R&D Serial No. 2166, Ettringite formation and the performance of concrete*. Skokie, Illinois, 2001.

[38] C. A. Utton, E. Gallucci, J. Hill, and N. B. Milestone, "Interaction between BaCO3 and OPC/BFS composite cements at 20°C and 60°C," *Cem. Concr. Res.*, vol. 41, pp. 236–243, 2011.

[39] I. Garcia-Lodeiro, A. Fernandez-Jimenez, M. T. Blanco, and A. Palomo, "FTIR study of the sol–gel synthesis of cementitious gels: C–S–H and N–A–S–H," *J. Sol-Gel Sci. Technol.*, vol. 45, pp. 63–72, 2008.

[40] P. M. Carmona-Quiroga and M. T. Blanco, "Use of barium carbonate to inhibit sulfate attack in cements," *Cem. Concr. Res.*, vol. 69, pp. 96–104, 2015.

Chapter 5: Electrical Leaching of 3:1 BFS:PC

5.1 Introduction

In this Chapter, the results of electrically leaching 3:1 BFS:PC samples are presented and discussed. This was to understand the key aspects of testing conditions, and their influence on the behaviour of the base 3:1 BFS:PC matrix that had cured for 28 days. The method of cement production and the electrical leaching technique described in Chapter 3 was used for all experiments unless stated otherwise to examine the effects of specific variables.

As described in detail in Chapter 2 Section 2.6, leaching of cement is an important degradation factor and is not a new field of study [1]–[3]. Leaching of nuclear wasteforms is especially important, as radionuclides initially held in a GDF must not reach the biosphere [4]. There is therefore a need to study degradation of nuclear wasteforms using accelerated leaching methods due the long lifetime of hazardous waste. Electrically accelerated leaching has been studied in the past, and it has been shown that alterations to a hydrated cement matrix during static or semi-static leaching, e.g. the reduction of portlandite and the subsequent decalcification of the C-S-H phase [3], are reflected in the application of electrical leaching, and progresses gradually from the cathode side [5]. In electrical leaching studies it is often stated that the application of an electric current accelerates the leaching by electrophoresis, also called electro-osmosis, enhancing the migration of all charged species in the cement matrix. Unfortunately, in the open literature the leaching of Ca, K and Na are often the only ions whose accelerated leaching is discussed in any detail [5]–[10] which all leach preferentially into the cathode tank. The effects of electrical leaching on other cationic as well as anionic species is not known, and the impact of other variables, such as the effect of water saturation prior to leaching and the magnitude of the applied current density has not been shown. Moving towards solving these issues is the aim of this Chapter, and focusing on

electrical leaching of the base 3:1 BFS:PC matrix was required in order to investigate the leaching behaviour and electrical migration study of Cs and Ba, which will be discussed in Chapter 6.

Firstly, the effect of water saturation prior to electrically leaching a sample was investigated. This was done by comparing the leaching of a sample that had been immersed in acetone to stop the hydration ('dry') and a sample that had subsequently been rehydrated prior to the electrical leaching test ('wet'). This series of experiments was conducted because a resaturation procedure had been used in previous electrical leaching tests but its effects were not investigated [7]. Next, the effect of different current densities was investigated with samples leached at 5, 25 and 50 Am^{-2} for 6 hours with a maximum voltage of 450 volts. These current densities were selected because they represented a range of current densities that have been used in the past as discussed in Chapter 2 [5]–[7], [10], [11]. Then, to investigate the basic leaching behaviour of key elements over time, a 3:1 BFS:PC sample was electrically leached over 22 hours with a desired current density of 25 Am^{-2}. At each of 1, 2, 4, 10, 16 and 22 hours, 6 mL of solution were collected both each of the anode and cathode tanks for analysis by ICP-OES. Finally, the results of the electrical leaching of a 3:1 BFS:PC sample for 14 days at 25 Am^{-2} are presented in comparison with a 28 day static leaching test in the migration cell with no applied current. The leachate was analysed by pH measurements and ICP-OES at 3, 7, and 14 days in both cases, and the leachates in the static test were also analysed at 21 and 28 days. Following the tests, the phases in the cement samples were compared through XRD and thermal analysis. The microstructure is then examined through MIP and SEM-EDX.

5.2 Effect of water saturation prior to leaching

The effects of water saturation on the testing specimen were initially investigated: one with the immersion in acetone to arrest hydration and drying (referred to as “dry”); the other with additional immersion in distilled water for 24 hours prior to the leaching test (referred to as “wet”). This type of resaturation procedure has been implemented in the past in the study of electrical leaching [7], however its effects on the leaching behaviour of the testing specimen have not been studied. Figure 5.1 shows photographs of both a wet and dry 3:1 BFS:PC sample that have been leached at 5 Am^{-2} for 6 hours. Due to the leaching out of material from the samples, the cathode side of both the wet and dry sample display a clear alteration of colour in the exposure surface. Unsurprisingly it is unclear which sample is more affected by the electrical test from comparing photographs alone.

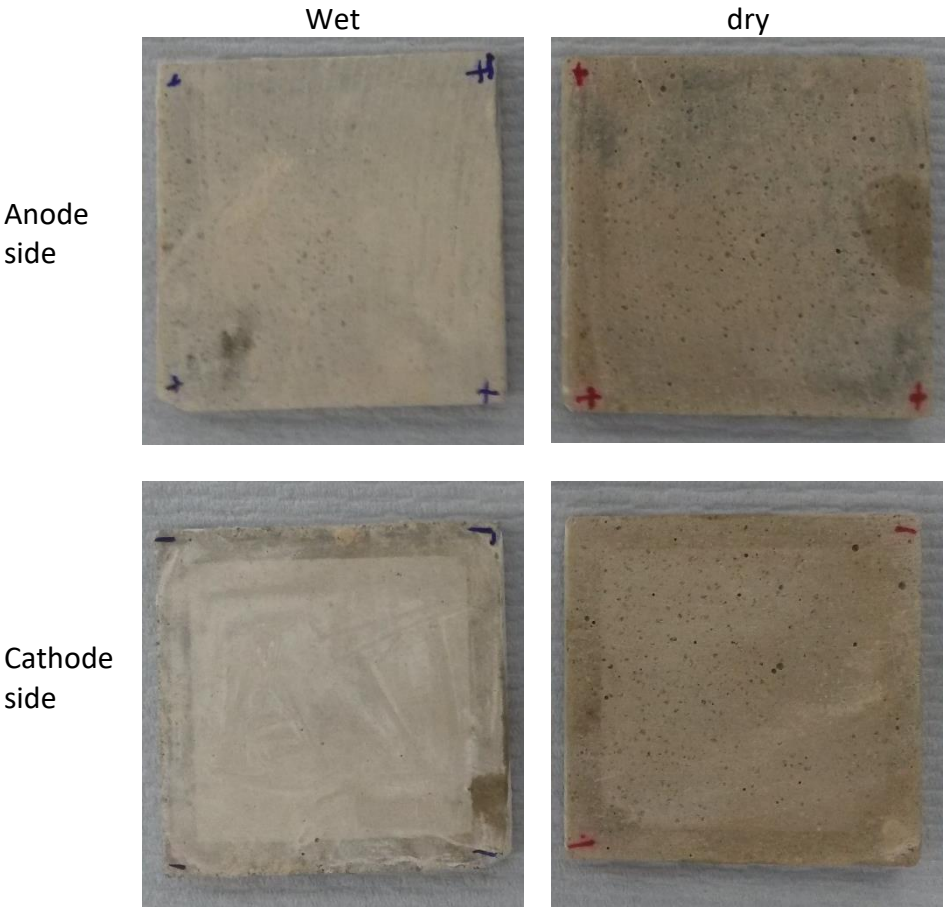

Figure 5.1 3:1 BFS PC samples after 6 hours of leaching at 5 Am 'wet' preparation on the left, dry preparation on the right. anode side top, cathode side below.

Figure 5.2 shows change in the current and voltage for the 6 hours of electric leaching tests on these samples. The solid lines are the current data (left-most y-axis) whilst the dashed lines are the voltage data which use the right-most y-axis. These tests were conducted aiming at a constant current density of 5, 25 or 50 Am^{-2}. The current density across the sample surface can be calculated using Equation 5.1, dividing the current value by the exposure surface area of 10.24 cm^2 (= 3.2 cm x 3.2 cm). The power supply could be set with a precision of 0.001 A.

$$J = I/A$$

Equation 5.1

The data show that, in all cases, the system required some time to gain sufficient conductivity to reach the desired current density. From a feature of the AC-DC converter used in the experiments, the power supply maintained the maximum voltage until the desired current was reached, and then the voltage decreases automatically to maintain that current. The 5 Am^{-2} test reached the target current within the first hour, both with the dried sample and that immersed in water for 24 hours prior to testing. In the 25 Am^{-2} experiments, the target current was reached within 6 hours in the dry sample, with the wet sample reaching only 10 ±1 Am^{-2} at the end of the test. In the 50 Am^{-2} experiments, the desired current density was not reached in the time frame for either sample, and thus was not analysed further. From a practical view point, it is therefore important to understand that the desired current density will not be achieved from the start of the tests. This becomes especially significant when the test is for a shorter period as the average current over time will be lower. When a leaching experiment lasts for 24 hours with a 25 Am^{-2} desired current density, the average current is 0.02379 A, which results in an average current density of 23.23 Am^{-2}. A 7-day test set to 25 Am^{-2} would have an average current density of 24.75 Am^{-2}.

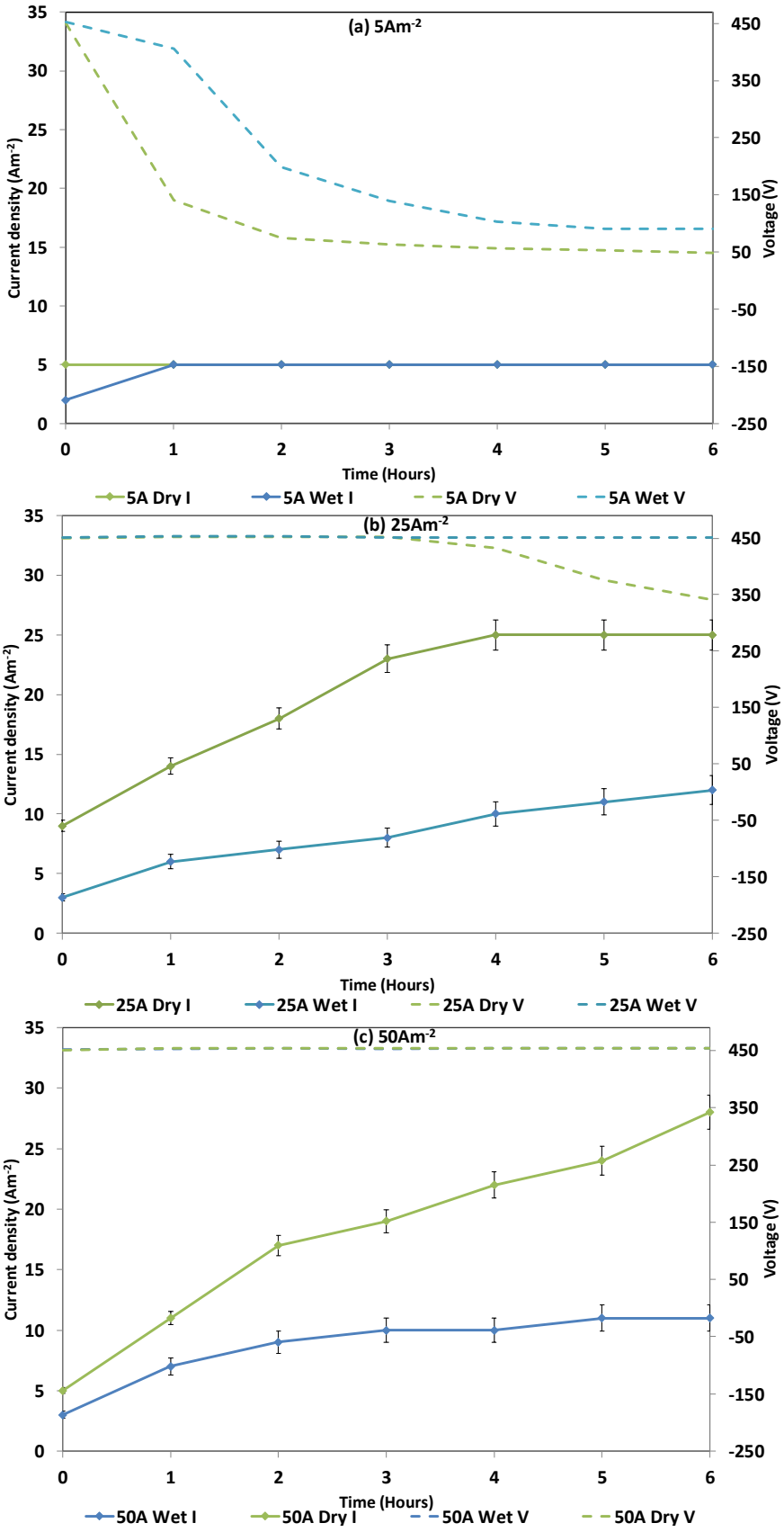

Figure 5.2 Current (left y axis) and voltage (right y axis) for 6 hour 3:1 BFS:PC electric leaching experiments with different desired current densities: (a) 5 Am^{-2}, (b) 25 Am^{-2} and (c) 50 Am^{-2}. The label 5A Dry I refers to the current in the 5 Am^{-2} leaching experiment of a dry sample, and 25A Wet V the voltage in the 25 Am^{-2} leaching experiment of a sample submerged in water 24 hours prior to leaching.

During the 25 Am^{-2} wet and dry tests, aliquots were taken from the anode and cathode tanks every hour for pH analysis, the results of which are displayed in Figure 5.3. It can be clearly seen that the pH of the cathode tank increases to 10-12 both in wet and dry tests. In part this must be due to the migration of alkaline components such as Ca, K and Na, as well as electrolysis effects which were described in Chapter 3. The increase in pH is slower in the wet test, similar to the trend found in the current density (i.e. taking a longer time to reach the target current). This suggests that the increase in the current density at the initial stage of testing is strongly related to the presence and migration of these elements. The cement samples must experience some degree of dissolution and leaching under exposure to the water during the 24 hours of resaturation procedure, and thus, a part of the ions readily available to leach into the water has been lost from the system during this time. A significant concentration of Ca^{2+}, K^{+} and Na^{+} in the 100 mL of distilled water used for the resaturation procedure has been recorded: 6.02 mg/L, 0.655mg/L and 0.646mg/L, respectively. Si had a concentration of 0.0675 mg/L.

The trend of pH level in the anode tank, on the other hand, is not very clear after 6 hours (shown in Figure 5.3 and Figure 5.4). For the dry test, a general increase in pH is observed while the pH in the wet test seems to be rather stably neutral. The increase in pH suggests a small amount of alkaline components existing in the anode tank. A small amount of natural dissolution (dissolution without influence of electrical potential) might have taken place under the test conditions. The pH data of the wet sample under 5 Am^{-2} is shown in Figure 5.4, and shows similar behaviour to the 25 Am^{-2} wet sample, although the pH the cathode tank reaches after 6 hours is lower at 5 Am^{-2}. This is likely due to the lower concentration of alkaline components in the tanks.

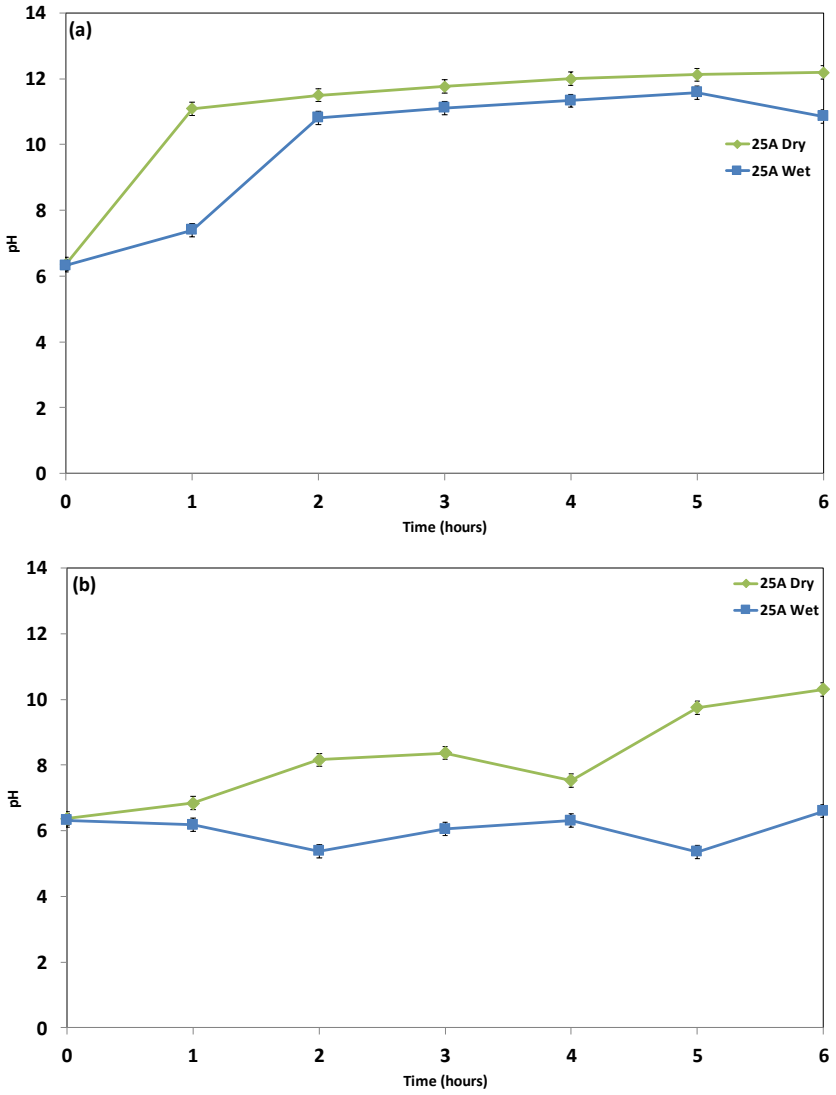

Figure 5.3 pH data of (a) cathode tank and (b) anode tank over the first 6 hours of leaching tests set to 25 Am^{-2}, with wet and dry sample preparation

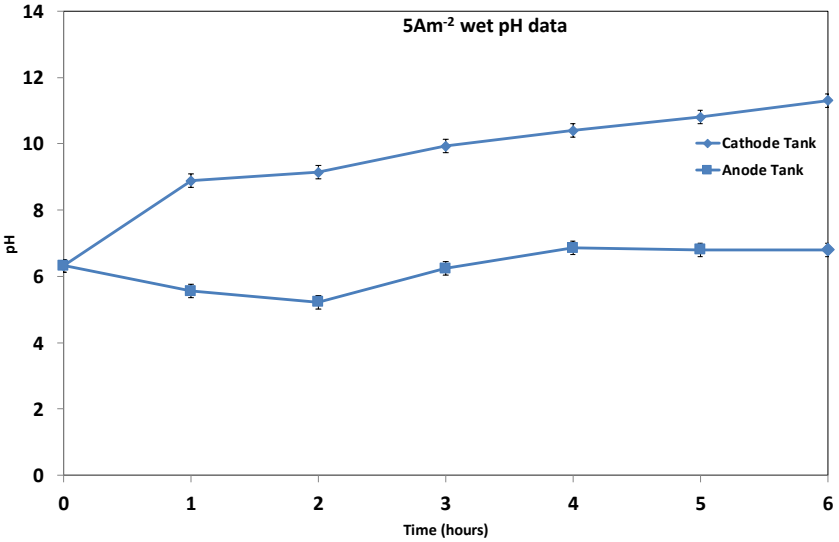

Figure 5.4 pH data of the cathode tank and anode tank over the first 6 hours of leaching tests set to 5 Am^{-2}, with wet sample preparation

The behaviour of the key ions can be further studied in the ICP-OES data in cathode and anode tanks shown in Figure 5.5. The amounts of alkaline components such as Ca, K and Na in leachate are larger in the cathode (negative electrode) tank than in the anode (positive electrode) tank. It is also observed that, compared to the wet test, the dry test generally resulted in a higher concentration of all elements detected other than the concentration of Ca in the 5 Am^{-2} test where the concentration was slightly higher in the wet test. This is generally in agreement with the pH data previously discussed.

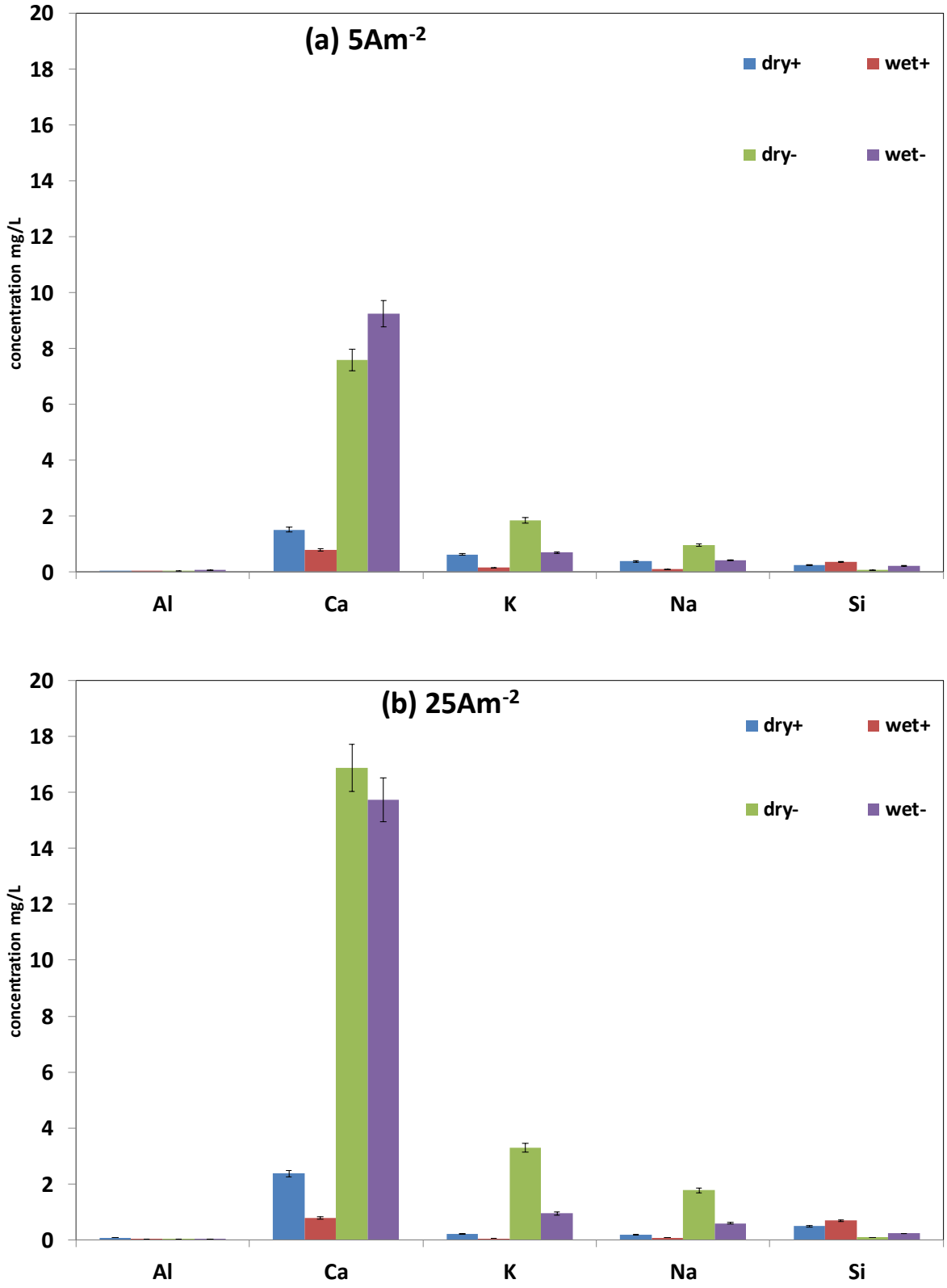

Figure 5.5 ICP-OES of 6 hour leaching experiments: (a) 5 Am^{-2} and (b) 25 Am^{-2} showing effect of wet vs dry preparation. + and – denote anode and cathode tanks, respectively.

These results support the suggestion that more material is available to leach out from the dry cement sample compared to the wet sample, which was immersed in distilled water for 24 hours prior to leaching. The ICP-OES data also show that a small amount of alkaline components are still present in the anode tank; this must be the cause of an increased pH level in the dry test as previously mentioned. Water within the interconnected cement pores, e.g. the pore solution, will contain ions that will be attracted to the electrodes from the beginning of the test. Due to the drying process, there will initially be a lower amount of pore water available containing these ions than in the wet test. However, this decrease is not enough to decrease the concentration of elements detected in the dry test. The conclusion is that there must be a dry 'barrier region' of cement in the dry test between the anode and cathode side where the leachant has not yet penetrated, and so cations in the anode region of the cement that has become saturated with leachate during the test, cannot migrate towards the cathode tank. The cations in the anodic region of the sample which are in contact with the anolyte leach out into the anode tank, most likely contributed from the natural dissolution of the material, while the anions in this region leached at an accelerated rate. The migration of cations from the anode tank to the cathode tank, through the cement sample, appears to have some limitation under the tested conditions which is further discussed in Section 5.6.

The tests also show that there is a significantly higher concentration of Ca compared with other elements in each leachate produced, reflecting the higher availability and solubility of this element. It appears that Ca is playing an important role influencing the pH of the leachates and the current density during the electrical leaching. It is interesting that, in the 5 Am^{-2} test, the level of Ca concentration is slightly higher in the wet tests, while at 25 Am^{-2} the

dry test shows a higher concentration compared with the wet test. The reasons for this is not very clear, but it may be worth mentioning that, according to the trend in the electrical current during the tests (Figure 5.2), the system provided sufficient migration of ions to achieve 5 Am^{-2} of current density both in the dry and wet test, whereas it only achieved sufficient migration of ions for the dry test to reach 25 Am^{-2} of current density. As previously discussed, the wet test did not reach 25 Am^{-2} of current density within the testing time of 6 hours.

5.2.1 Normalised mass loss of key components

Figure 5.6 shows the normalised elemental mass loss (mg/cm^{-2}) for K, Na, Ca and Si both in the cathode and anode tanks after leaching. Normalised elemental mass loss for element 'i' (NL_i) is calculated using the following equation [12]:

$$NL_i = M_i/(F_i SA) \quad \text{Equation 5.2}$$

Where M_i is the mass of the element 'i' in the leachate in mg, F_i is the fraction of the element in the 'pristine' or unleached sample and SA is the exposed surface area in cm^2, in the case of the present study 10.24 cm^2. [12] F_i is obtained using the XRF data of the PC and BFS shown in Chapter 3 (Table 3.3). Errors are calculated to be +/- 10.5% due to the standard reliability of the ICP-OES data, and the likelihood of a variable surface area (the equation assumes a perfectly flat surface, which is never the case in reality due to exposed porosity and the roughness of the surface). Normalised mass loss is useful to compare the behaviour of different elements as they are typically contained in the sample at different concentrations.

For Ca (Figure 5.6 c), a clear preference of migration into the cathode tank is observable. The in the cathode tank clearly indicates the influence of the applied electrical potential, while

the data in the anode tank shows a smaller concentration – this is due to the attraction of cations such as Ca to the cathode, and may be leaching into the anode tank by a natural leaching mechanism.

As observed for calcium, Na and K (Figure 5.6 a and b) showed a preference to leach into the cathode tank, but with a much larger normalised mass loss, by approximately 10 times. This clearly indicates that the dissolution observed in the test conditions are not congruent, and the leaching of K and Na are much easier than that of Ca. For both wet and dry tests, it is easy to see the effects of the applied electrical potential on the leaching of the ions: increasing the current density resulted in an increased amount of these ions in the cathode tank and a decrease in the anode tank. These results imply that Na and K are easily mobile. K and Na showed similar leaching behaviour in electrical leaching tests. Although the charge density of Na (10.813×10^{10} C m^{-2}) more than double that of K (4.877×10^{10} C m^{-2}) (calculated using data from [13]), this difference does not seem to have a significant effect on the leaching of these elements. The concentration of K and Na in the anode tank decreases as the applied current density increases, whilst Ca shows the opposite behaviour.

It is interesting to see that Si (Figure 5.6 d) shows a completely different normalised mass loss behaviour from Ca, K and N, with a clear preference to leach into the anode tank. Silicon can form silicic acid $Si(OH)_4$ in high pH environments [14] such as those found in cement, and silicic acid can be present in different anionic species depending on the level of pH. At pH less than 8, $Si(OH)_4$ is dominant. As the pH increases – between pH 10 and 13.2, $SiO(OH)_3^-$ is dominant and at pH > 13.2, $SiO_2(OH)_2^{2-}$ is dominant [14].

$$Si(OH)_4 \leftrightarrow [SiO(OH)_3]^- + H^+ \qquad \text{Equation 5.3}$$

$$[SiO(OH)_3]^- \leftrightarrow [SiO_2(OH)_2]^{2-} + 2H^+ \qquad \text{Equation 5.4}$$

The increased normalised mass loss value corresponded to an increase of current density in the anode tank, which supports that silicon ions are forming anionic species in the tested system using 3:1 BFS:PC samples. The amount of Si in the cathode tank showed little variation with the different applied current density, both in wet and dry conditions. This observation suggests that the Si content found in the cathode tank is not due to the electrical potential applied to the sample but due to the effect of natural dissolution and/or leaching.

Another observation from the Si leaching test is that, in both tanks, the wet test generally resulted in a higher normalised mass loss value compared to the corresponding dry test – this is different from the behaviour of Ca, K and Na which had higher concentrations in the dry tests. As previously discussed, Ca, K and Na are considered to have leached into the water during the 24 hours of resaturation conducted prior to the testing, leaving less ions readily available to migrate and leach out the system, but this was not the case for the Si. It appears that some level of interaction with water and/or less amount of Ca, K or Na ions readily available in the system enhances the dissolution and/or migration of Si. It might be that during the rehydration procedure, Si dissolves into the pore solution of the cement matrix but does not leave the system, and then when the electric current is applied Si migrates out at an increased rate – but it is easier for Ca, K and Na to leave the matrix during the resaturation procedure.

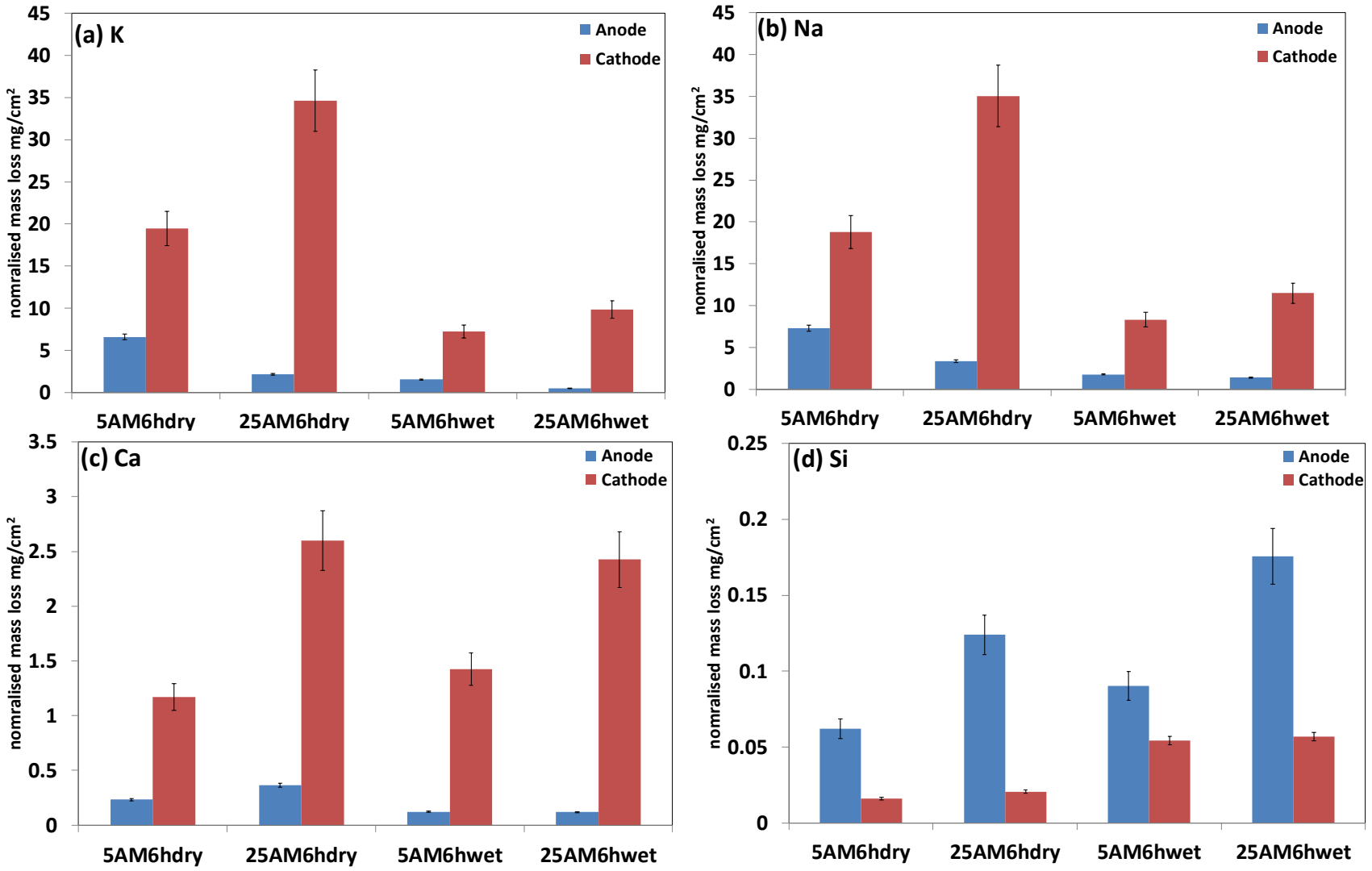

Figure 5.6 Normalised mass loss for 6 hour leaching tests at different current densities (5 and 25 Am^{-2}) and cement preparation methods (wet and dry) with (a) K (b) Na, (c) Ca, and (d) Si. The data for the anode tank are in blue, and for the cathode tank in red.

The normalised mass loss data shown in Figure 5.6 are further analysed in Figure 5.7. Each element displayed an increase of mass loss into the attracted tank as the current density was raised. For K, Na and Ca, more leaching was observed in the dry test than in the wet, whilst the opposite was true for Si, as previously discussed. This may suggest that Si present in the material needs to dissolve into the pore solution before leaching out; i.e. in the wet test during resaturation, the C-S-H and other Si-containing phases had had more time to dissolve than in the dry test, resulting in more Si present in the pore solution before the electric current was applied. K, Na and Ca, on the other hand, were already able to diffuse out during the resaturation as already discussed. These results suggest that though the rate of leaching is increased by the electric potential for charged species, the leaching is still significantly influenced by the dissolution of the cement phases. The current density does have an effect on the elemental concentrations in the anode tank. When the current is increased from 5 to 25 Am^{-2}, the normalised mass loss of these elements in the attracted tank (cathode for K, Na, Ca, and anode for Si) becomes approximately 2 times higher.

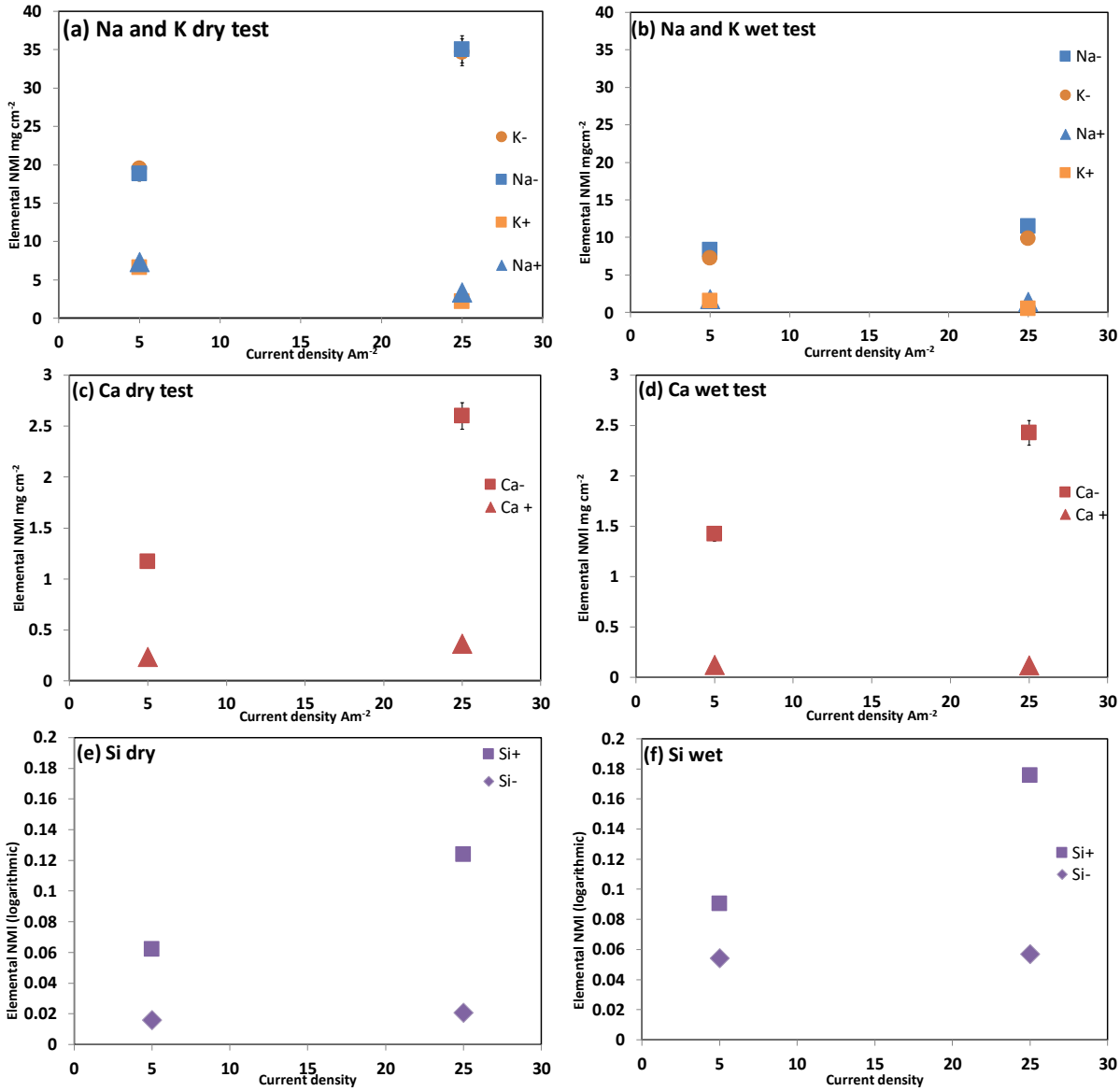

Figure 5.7 Normalised mass loss for 6 hour leaching tests at different current densities: (a) K and Na in the dry test, (b) Na and K in the wet test, (c) Ca in the dry test, (d) Ca in the wet test, (e) Si in the dry test, and (f) Si in the wet test. + and – in the legend denote anode and cathode tank content, respectively.

5.3 Effect of water saturation on microstructure - SEM-EDX mapping

BSE images gathered using an SEM and corresponding elemental mapping of the dry sample after 6 hours of leaching at 5 Am^{-2} are shown below, with the anode side in Figure 5.8 and the cathode side shown in Figure 5.9. These are cross sections, with the exposure surface to the anode or cathode tanks shown as the edge of the specimen as indicated on the BSE images. Maps of Ca, Si, Al, Mg, Na and K are displayed. Whilst S also had a strong presence in the sample, it was difficult to distinguish from the background detector noise. Ultimately the wet and dry tests showed similar results in the SEM analysis, and because of this only the dry test is shown and discussed here. Similar BSE images and SEM-EDX results of the wet test are available in the appendix Section A.2.

Both sides of the sample had a high concentration of Na and K at the surface even though due to being cations they are attracted into the cathode tank as shown by Figure 5.6. This concentration band was wider on the cathode side, and they indicated similar features in general, but the cathode side appears to have a Ca rich layer of approximately 10 µm at the exposure front. This may be due to the formation of calcium carbonate. The formation of calcium carbonate on the exposure surface during static leaching tests have been reported [15]. Na and K may also be precipitating as carbonate salts (Na_2CO_3 and K_2CO_3) in the pores close to the surface, but this was not confirmed.

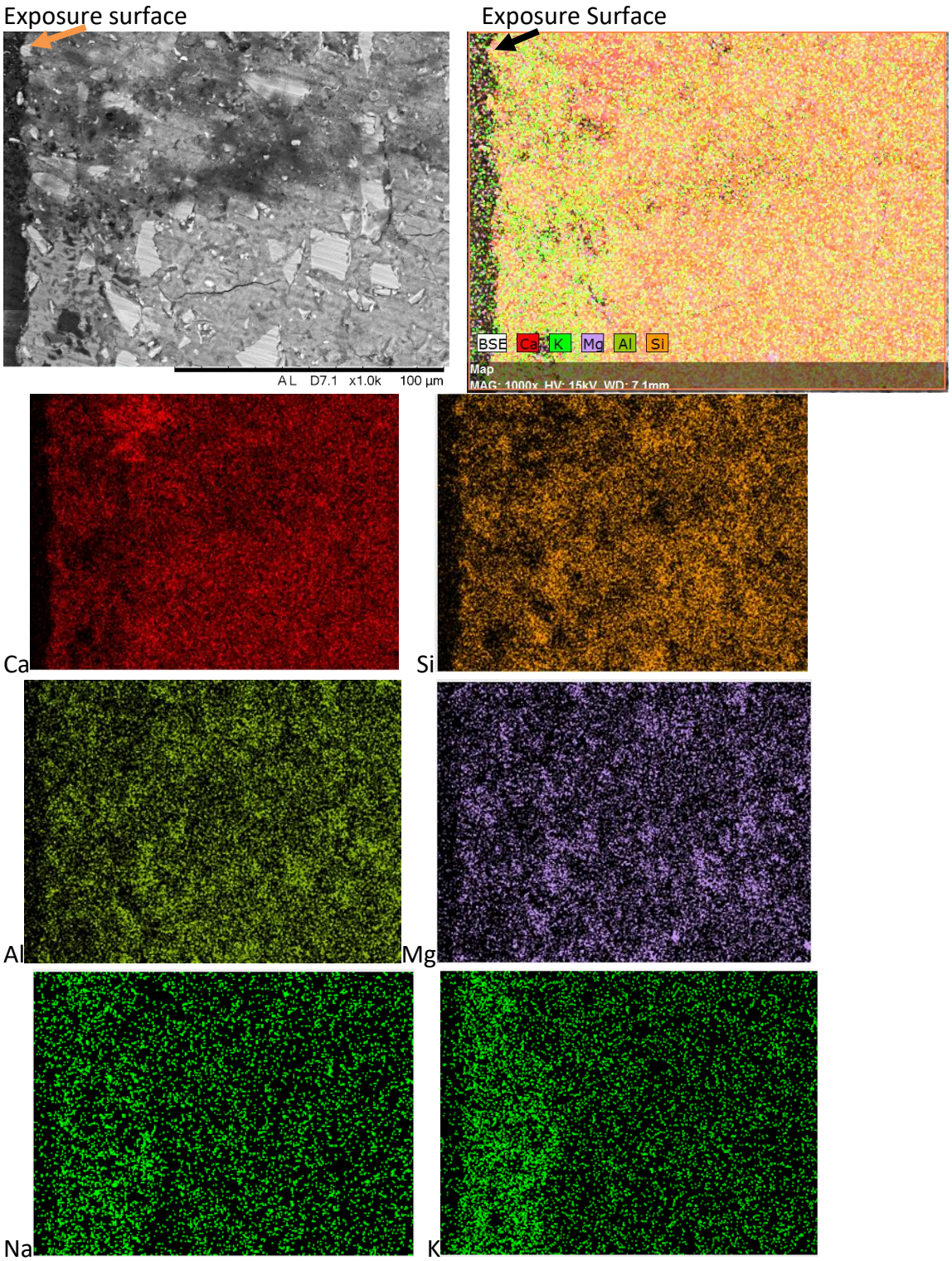

Figure 5.8 BSE image with high magnification and SEM-EDX elemental maps of a dry 3:1 BFS:PC sample on the anode side after 6 hours of electrical leaching at 5 Am^{-2}

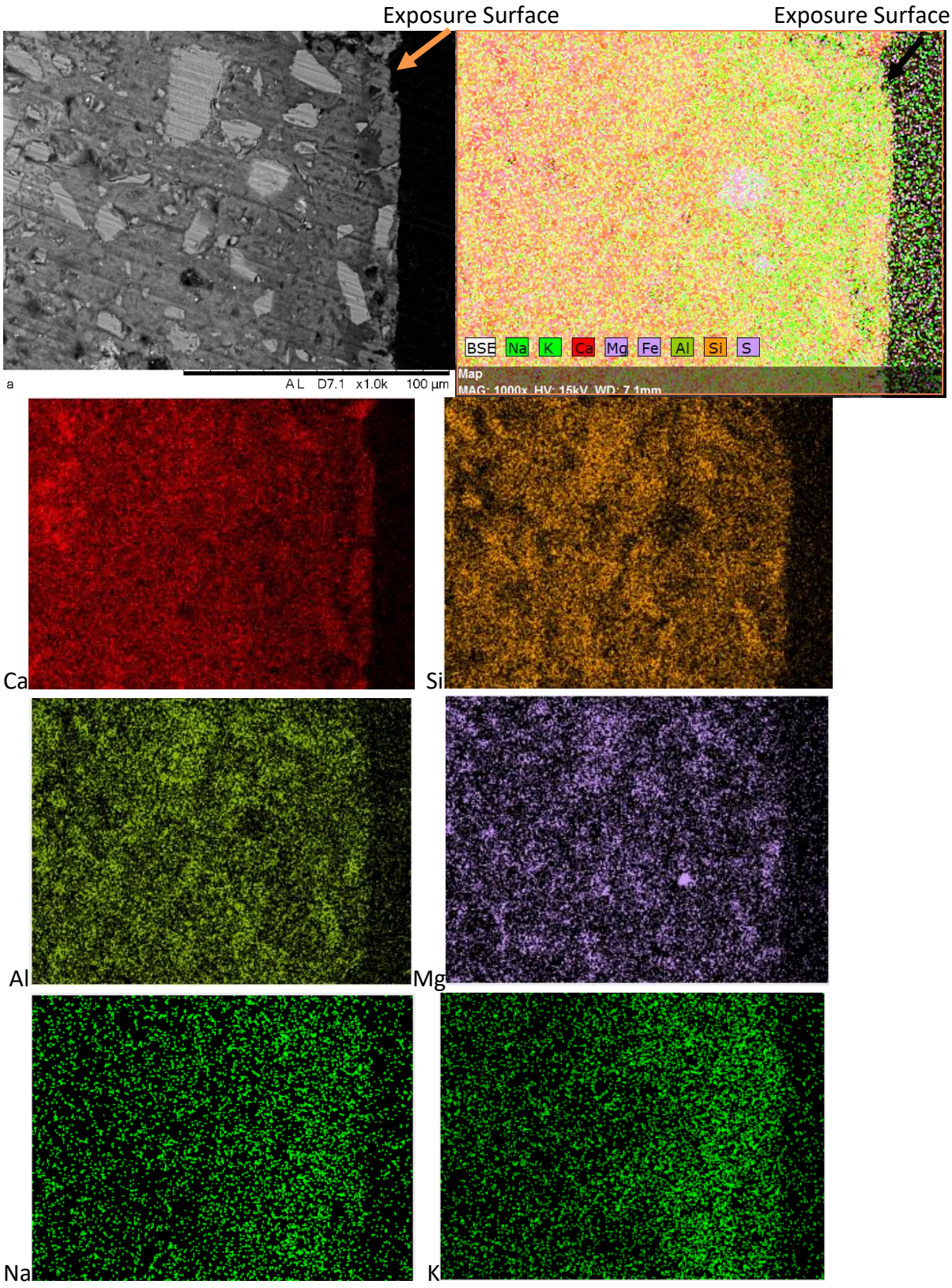

Figure 5.9 BSE image with a high magnification and SEM-EDX elemental maps of a dry 3:1 BFS:PC sample on the cathode side after 6 hours of electrical leaching at 5 Am^{-2}

5.4 Effect of current density on cement matrix: 5 and 25 Am^{-2}

Figure 5.10 shows examples of the cement specimens after 6-hour electric leaching dry tests at 5 and 25 Am^{-2}. The 25 Am^{-2} sample clearly shows an increased level of degradation over the 5 Am^{-2} sample.

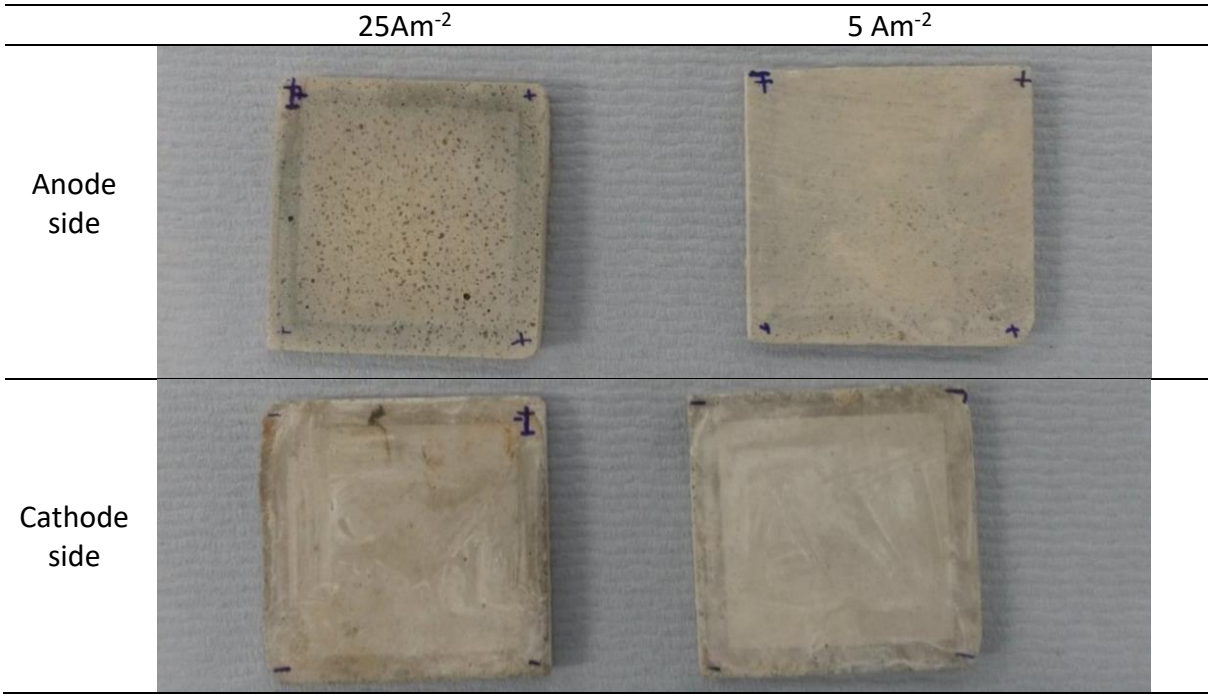

Figure 5.10 Photograph of 'dry' 3:1 BFS:PC samples after 6 hours of leaching: 25 Am^{-2} left, 5 Am^{-2} right, anode side above, cathode side below

Figure 5.11 shows the XRD data for the tested samples. It also shows the data for the sample before the leaching test. Table 4.2 shows the labelling used in the XRD graphs and lists the PDF reference numbers. As is typical for 3:1 BFS:PC samples, and observed in previous XRD patterns (Figure 3.13 and Figure 4.5 for example), the main observable phases are C-S-H, gehlenite, portlandite, hydrotalcite, ettringite and some monosulfate. After leaching, a decrease in the intensity of portlandite peaks (as is typically observed in e-leaching tests [16]) was not seen, suggesting that 6 hours is insufficient for a major effect on the phases present in the cement matrix to be observed – the most distinct results in this experimental series are in the leachate analysis shown above. Although the applied current density is varied (5 and

25 Am^{-2}), there is no obvious variation in the crystalline phases observed, neither in wet nor dry samples. This indicates that the wet/dry preparation does not significantly affect the general behaviour of the phases present under the tested conditions.

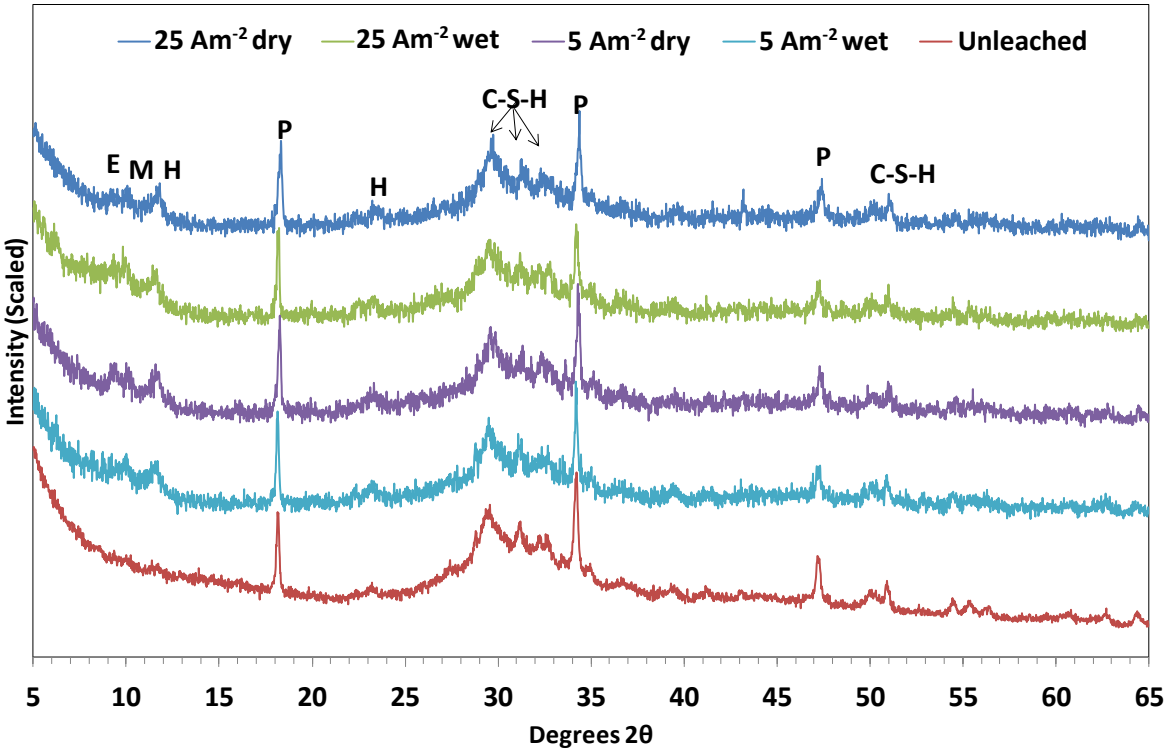

Figure 5.11 XRD of dry 3:1 BFS:PC samples leached for 6 hours at different current densities and preparation methods (Wet- resaturation in water prior to leaching, Dry-without resaturation)

When a dry sample is leached, there are some benefits: less preparation is required, and the desired current density is reached in a shorter time. There is also more leachable material present in the system. When the sample is resaturated before the test, the leachate does not need to penetrate the sample at the beginning of the test, and the overall pH behaviour is similar to the dry test. The additional time taken to reach the current density would not be an issue in longer experiments. In the ideal case, a test sample would be leached immediately after curing without arresting hydration. In situations where identical age of samples is desirable across different tests, such as in the present investigation, arresting hydration is often a necessary evil. From the results shown in this Section it was decided that for the rest

of the project, rehydrating the samples is the simplest course of action to test samples consistently, and is a better approximation of leaching samples where hydration has not been arrested.

5.5 Effect of time on electrical leaching – the first 22 hours

The following figures (Figure 5.12 to Figure 5.18) display data taken from a single electrical leaching experiment at 25 Am^{-2} for up to 22 hours. This was originally intended to be an extended leaching test until the cement sample suffered complete deterioration. As the end point of this test was not known at the beginning of the test, the extracted leachant was replaced with distilled water each time aliquots of the solutions were collected from both tanks for testing. This affects the concentration data with a minor dilution effect – 6 mL was extracted from 750 mL and replaced each time. Unfortunately, after seven weeks of the test a significant loss of leachant had occurred due to evaporation, rendering the solution data gathered in the later stage to be questionable. Therefore, only the reliable data from the first 22 hours are discussed here. XRD analysis of a white precipitate collected from the cathode tank following the test is shown in the Appendix Section A.3.1. The current and voltage data during this experiment are shown in Figure 5.12, and it took between 11 and 12 hours to reach 25 Am^{-2}. Figure 5.13 shows the pH data measured over this experiment. The pH in the anode tank slightly fluctuated at first, but remained around an average of 6.31, whereas the cathode tank increased continuously and approached 11.7 ± 0.4.

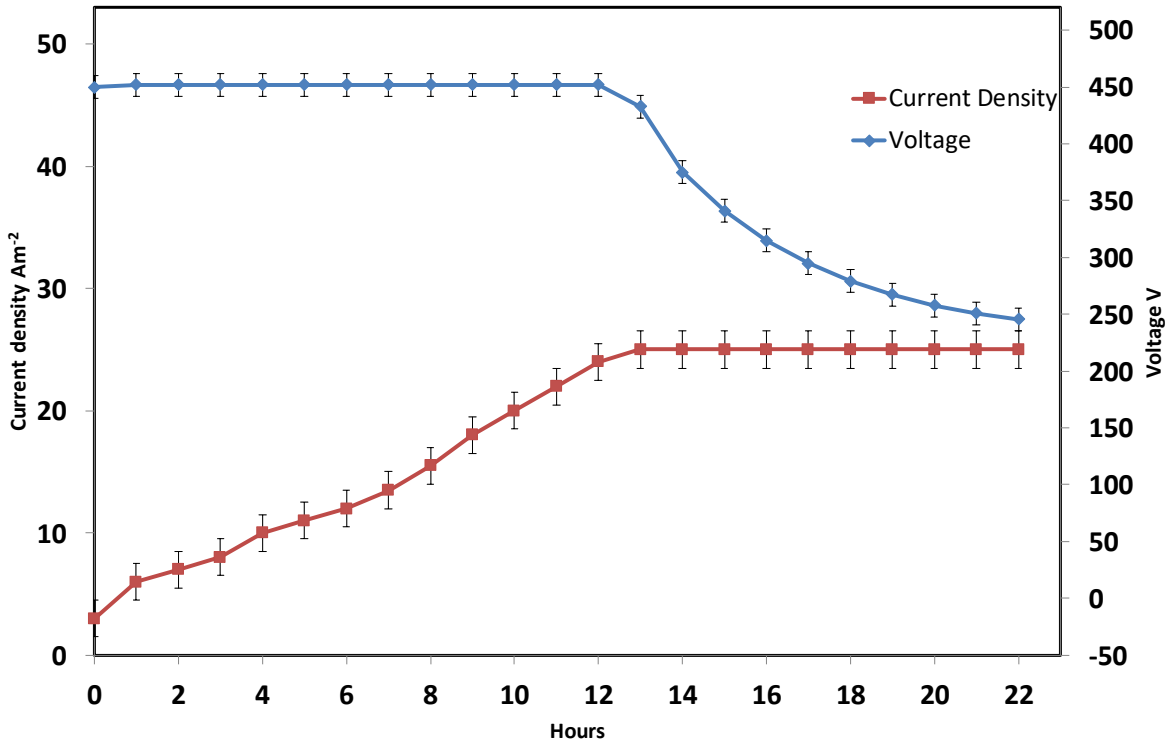

Figure 5.12 Recorded current density and voltage over the 22 hours leaching test

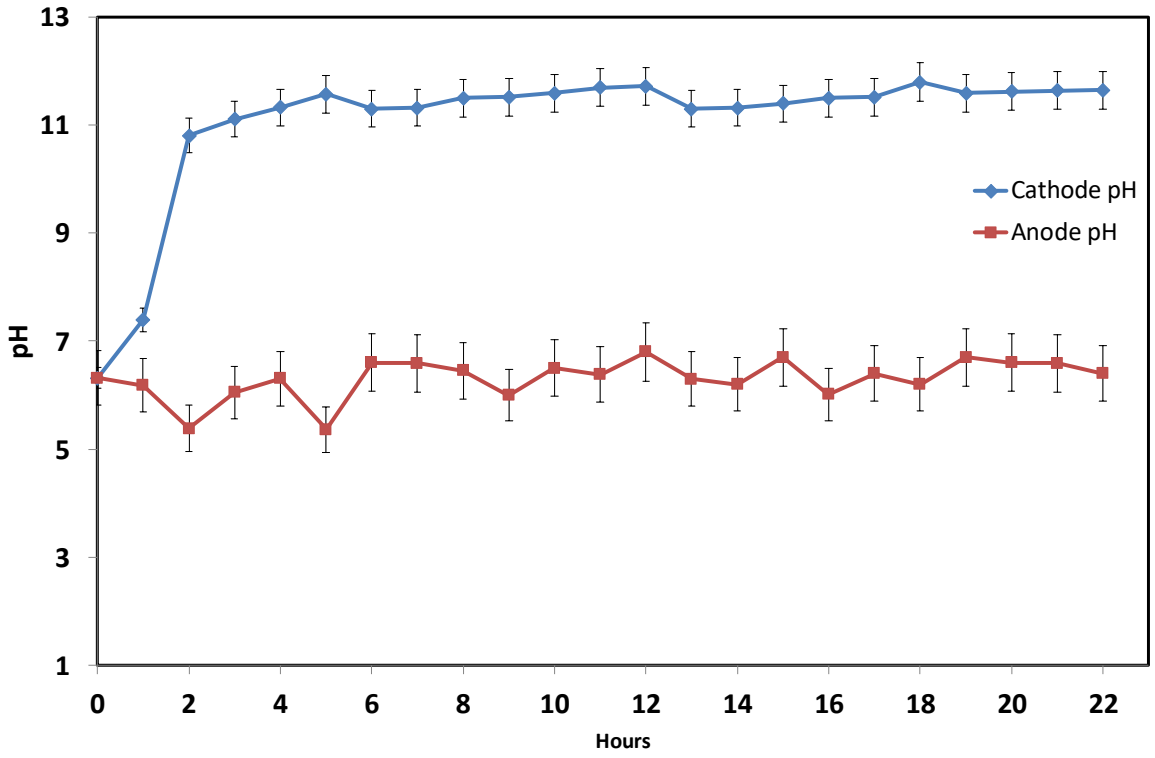

Figure 5.13 Measured pH data over the 22 hours leaching test

Figure 5.14 to Figure 5.16 show the ICP-OES data for elements which showed a higher concentration in the cathode solution (Ca, K, Na, Sr, Mg and Ba) in order of descending abundance). Figure 5.17 and Figure 5.18 show the data for elements with a higher concentration in the anode solution (Si, Al and Zn in order of descending abundance). Sr, Ba and Zn were detected in small amounts in the XRF of the PC and BFS as shown in Table 3.3. Figure 5.18 also shows the data for sulphur, which displayed no clear preference for which tank it leached into. Errors of ±0.0025 mg/L apply to all points in these graphs due to the detection limit of the equipment used, and as such cannot be seen in the graphs with a larger scale.

Alkali and alkali earth elements were clearly accumulated in the cathode solution (Figure 5.14 to Figure 5.16), indicating their presence as positive ions in the pore solution whereas Al, Si and Zn are accumulating in the anode solution (Figure 5.17 and Figure 5.18), showing that they are forming and leaching out as anionic species. It is well known that they can form anionic species such as $Al(OH)_4^-$, $SiO_2(OH)_2^{2-}$ and $Zn(OH)_4^{2-}$ in alkaline cements such as BFS:PC blends [17], [18] so this is not unexpected – although the leaching behaviour of these elements during electrical leaching tests has not been widely discussed previously. Pourbaix diagrams of Al, Si and Zn are displayed in Figure 5.19. The obtained results confirm that these species are also forming in the 3:1 BFS:PC cement pore solution tested in the present study. This is interesting with respect to the leaching behaviour of Si from the cement. Leaching of C-S-H, the main hydrate phase [18]–[21], will only occur when the pore solution or leachate are undersaturated with respect to C-S-H, and in leaching conditions the dissolved C-S-H will not reprecipitate. Therefore, the leaching behaviour of Si from cement systems is usually influenced by the Ca ions in the system in the conventional leaching technique. However, with

electrical leaching, it is possible to separate Si and Ca ions into different solutions, and thus, it may be possible to study the leaching behaviour of Si with a reduced influence of Ca ions, as they are forming (separate) soluble complex ions in solution which move in opposite directions due to the applied electric current.

It is difficult to say whether electric leaching has any effects on sulphur in a 3:1 BFS:PC matrix under the tested condition. Sulphur is expected to be present as sulphate (SO_4^{2-}) in PC [17] with the oxidation state of sulphur being 6+, while in BFS, it is present as sulphide (S^{2-}) [22] with an oxidation state of 2-. Therefore, in either case, sulphur should be migrating towards the anode. It is not clear why sulphur is equally observed in the cathode solution in the present investigation. This aspect will be further discussed in Section 5.6.

As expected the negatively charged ions are attracted to the anode tank, and the positively charged ions are attracted to the cathode tank. However, we also see an increase in the concentration of elements in the other tank over time, which must be attributable to the standard diffusion and dissolution mechanism as seen in static leaching tests. In the previous studies by other researchers [5]–[7], only the presence of calcium ions in the cathode tank is discussed, ignoring its presence in the anode tank (as little was expected to be present there) as well as the presence of other elements in either tank.

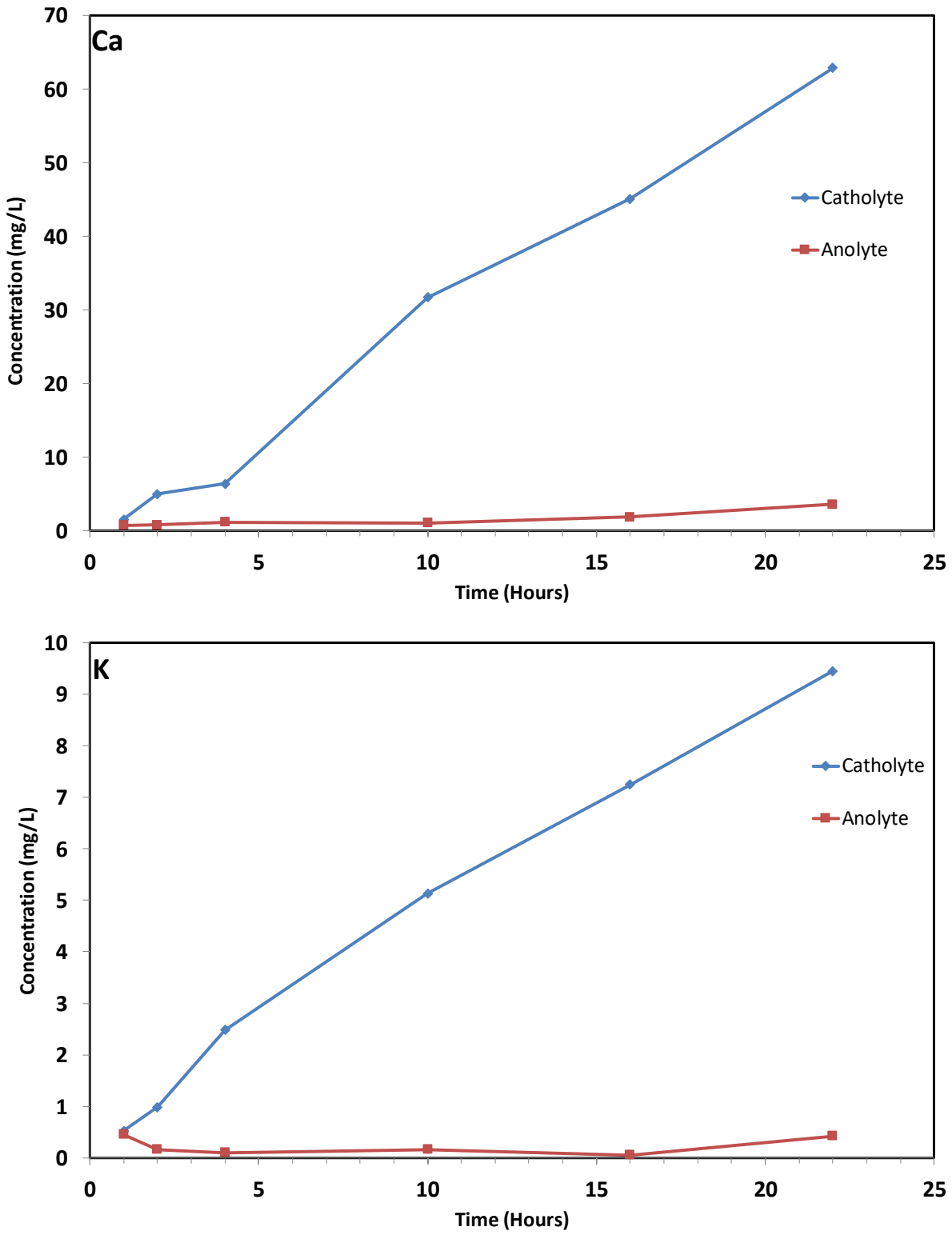

Figure 5.14 Elemental concentrations of Ca and K in the cathode and anode tanks over the first 22 hours of leaching

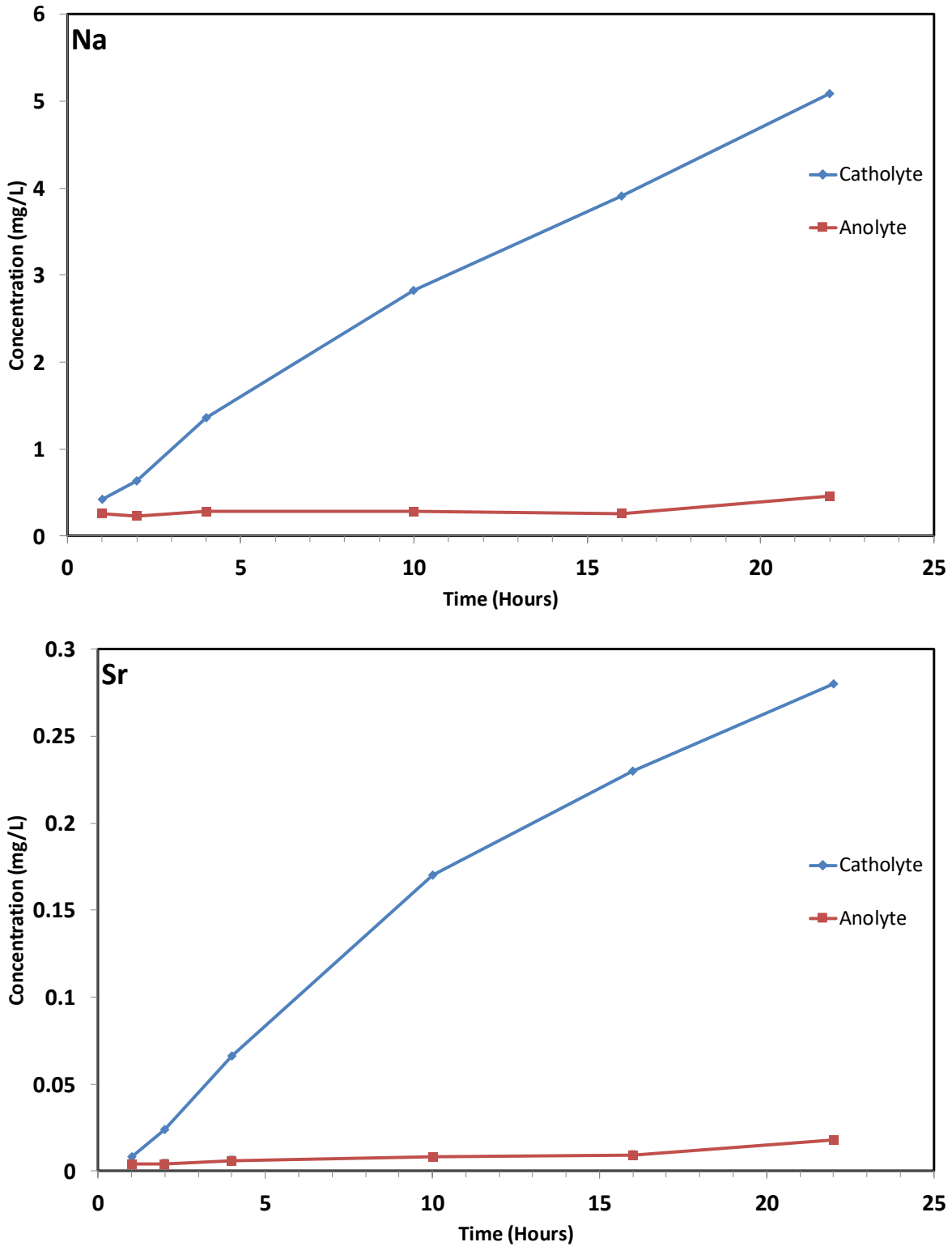

Figure 5.15 Elemental concentrations of Na and Sr in the cathode and anode tanks over the first 22 hours of leaching

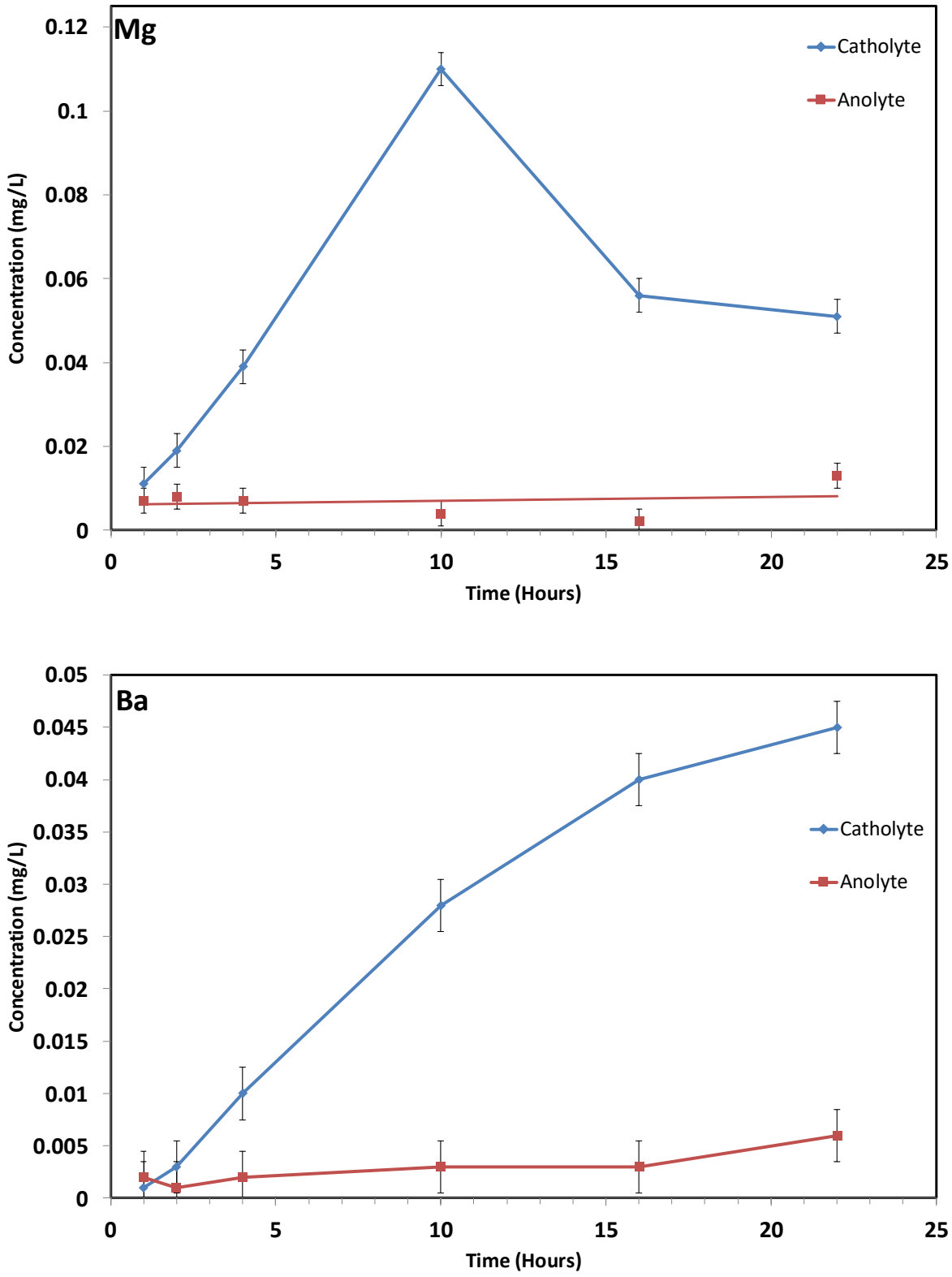

Figure 5.16 Elemental concentrations of Mg and Ba in the cathode and anode tanks over the first 22 hours of leaching

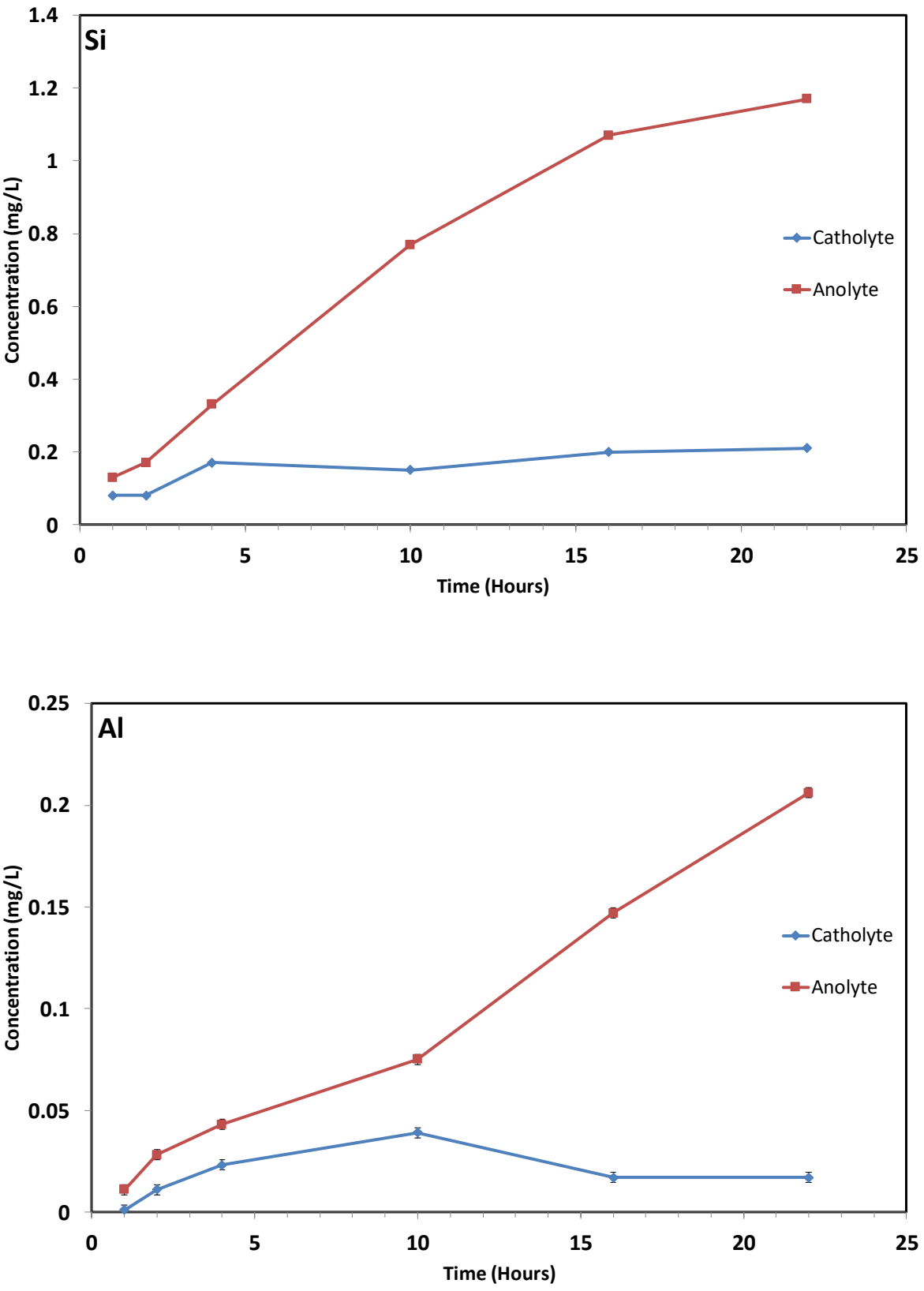

Figure 5.17 Elemental concentration of Si and Al in the cathode and anode tanks over the first 22 hours of leaching

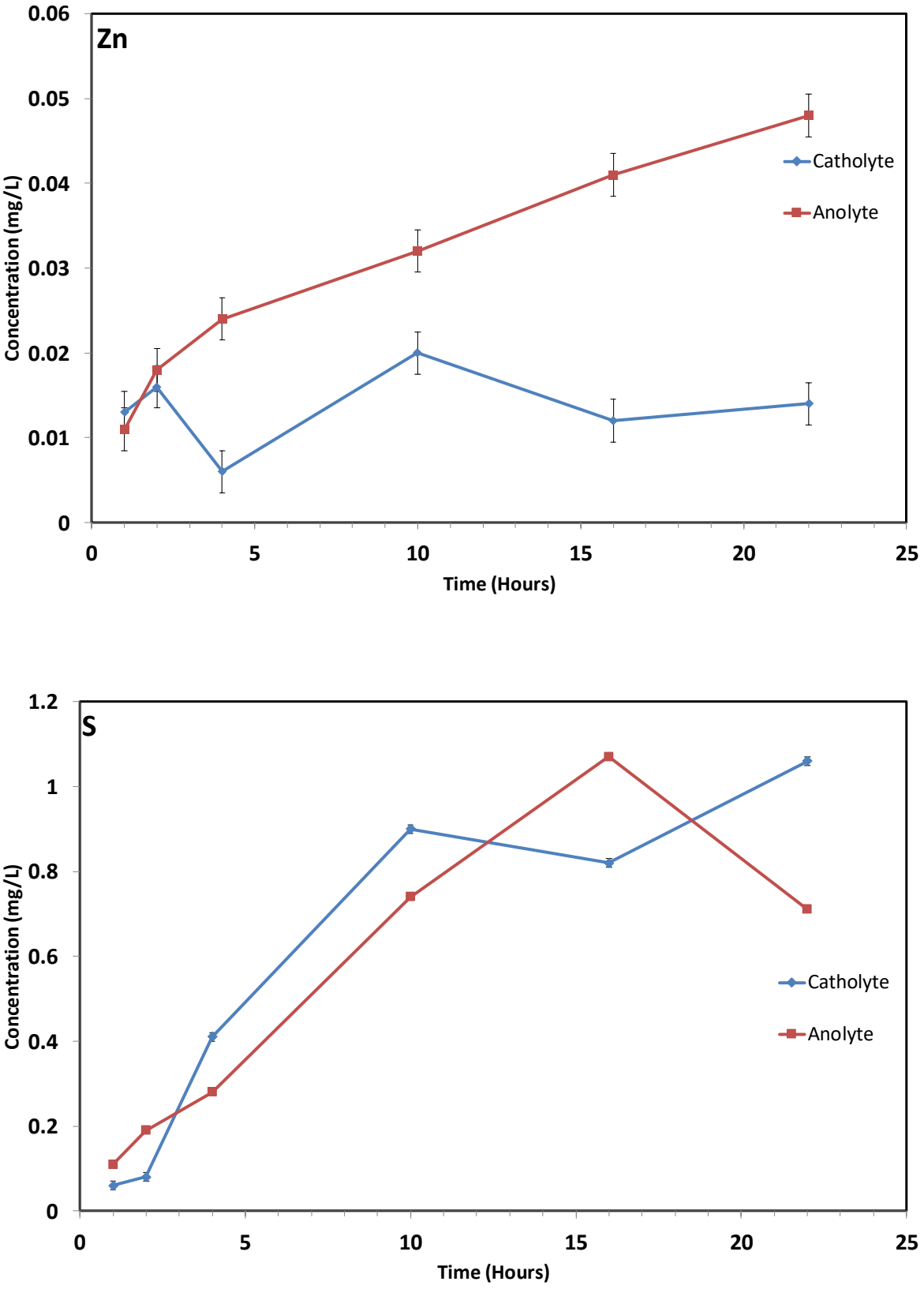

Figure 5.18 Elemental concentration of Zn and S in the cathode and anode tanks over the first 22 hours of leaching

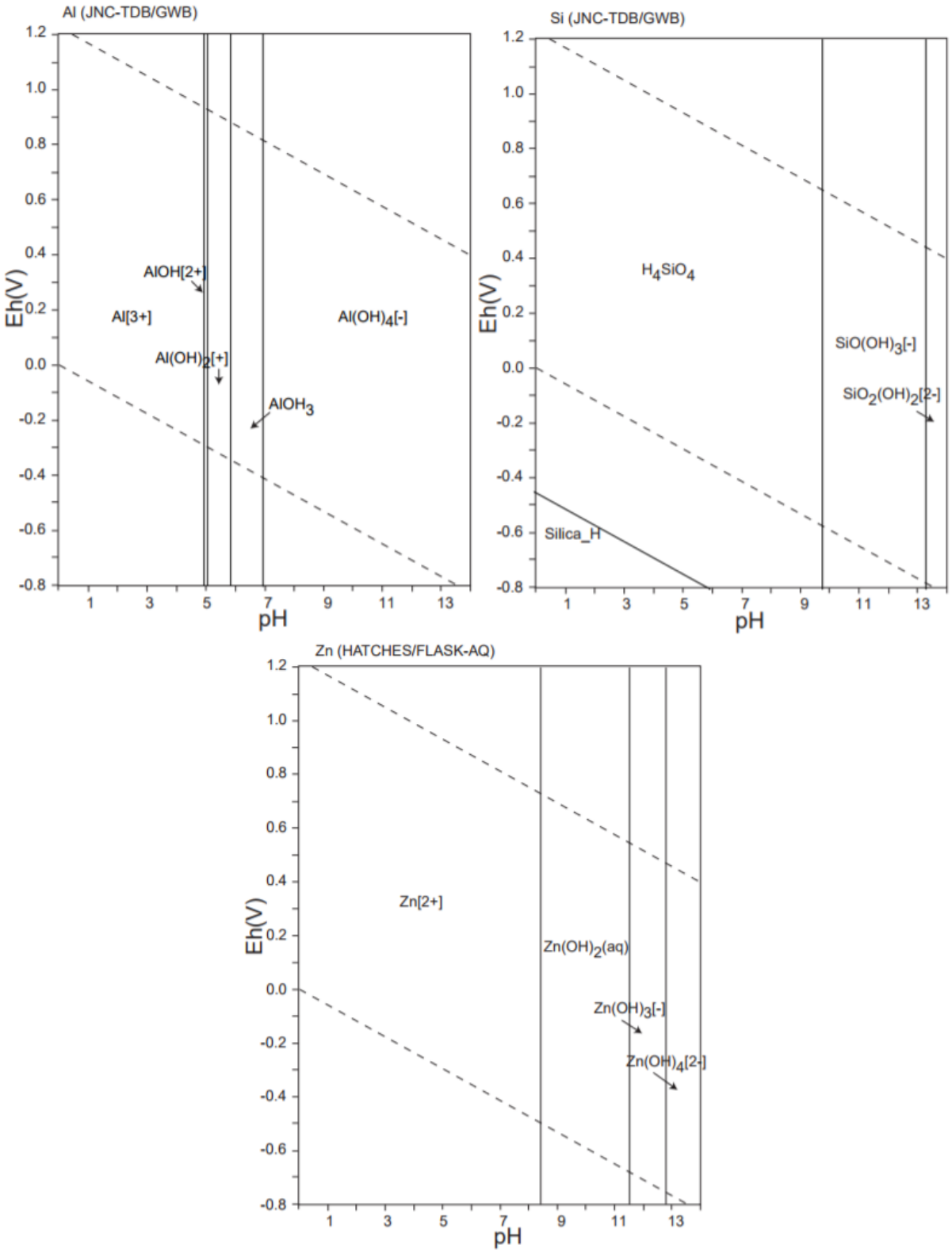

Figure 5.19 Pourbaix diagrams of Al, Si and Zn produced using databases distributed by the Japan Nuclear Cycle Organization (JNC-TDB) and the Nuclear Energy Agency (HATCHES) [23]

Based on the XRF data for the cement samples (Table 3.3), concentration data (Figure 5.14 to Figure 5.18) and Equation 5.2, the normalised leaching rate for each element detected was

calculated. The results of the calculations are shown in Figure 5.20. The leaching rates of the different elements obtained are shown in two graphs, (a) for the cathode tank and (b) for the anode tank. In Figure 5.20 (a) there are three distinct groups of elements in the leaching rate. The first group contains Na and K, the two most mobile species typically found in the BFS:PC cement matrix, which are attracted to the cathode due to their oxidation state (+1). The next group contains the alkaline earth elements that usually form divalent cation (+2) and leach more into the cathode tank than the anode tank. Sulphur, which did not indicate a clear preference in the leaching direction, also appears in this group. The third region contains Zn, Si and Al, which form protonated oxyanions. Interestingly, the general trend of these three groups are similar for the anode tank (b), although the leaching rate of zinc appears much higher than the other elements forming anionic species and overlaps with other groups. The leaching of Mg is discussed further in section 5.6.1.

These results show that, with an applied current density of 25 Am^{-2}, elements that display high leaching rates in static leaching tests (shown below in Section 5.6) still display the highest leaching rates in an electrical leaching test, even into the tanks that they should not be attracted into due to their oxidation state, e.g. Na and K still show a higher leaching rate in the anode tank than Si and Al. The mechanisms behind standard leaching are still a main driver in electrical leaching, but introducing a current increases the leaching rate of ions based on their charge, and the applied current.

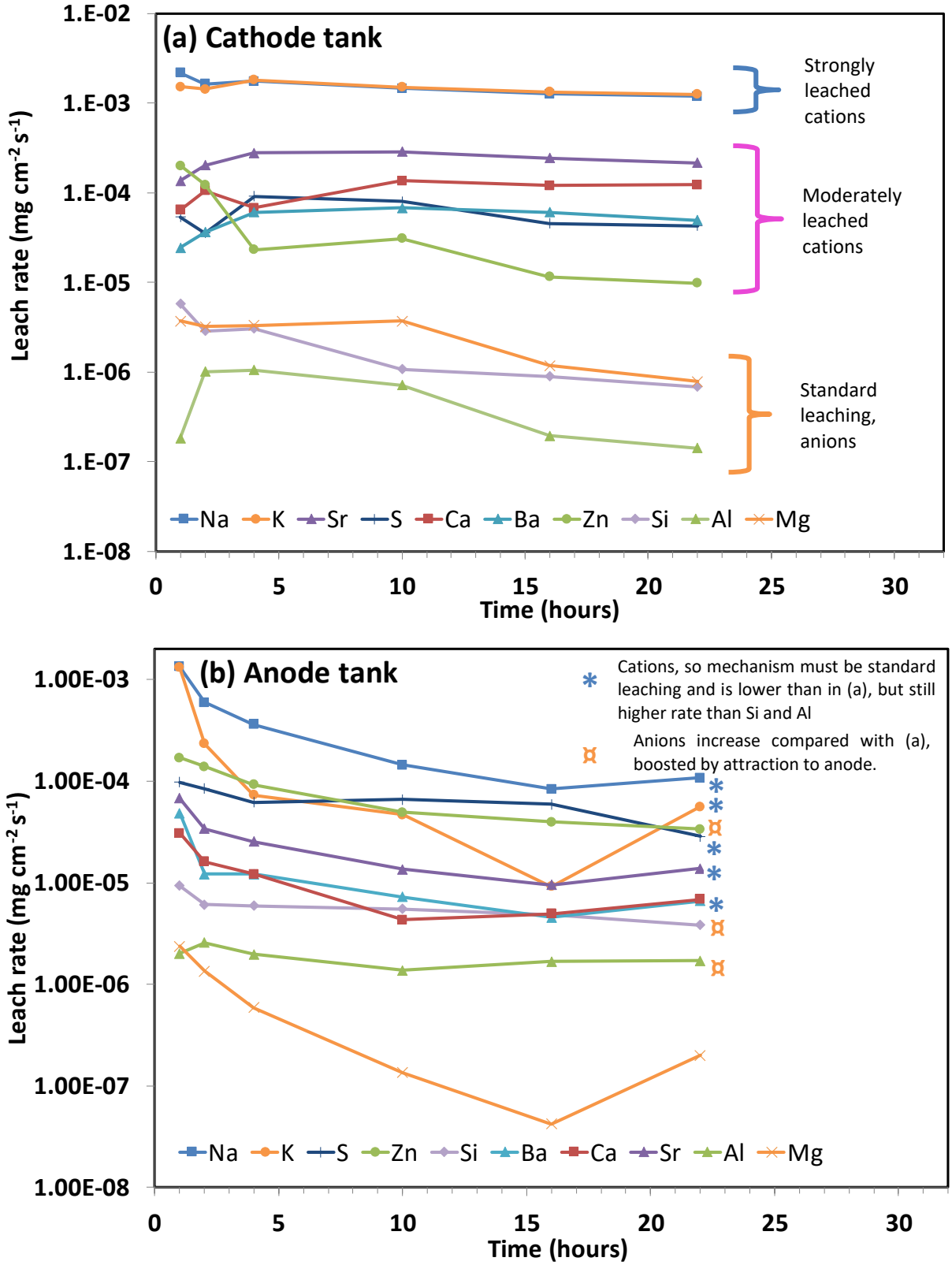

Figure 5.20 Leaching rate against time in (a) the cathode tank and (b) the anode tank for a 25 Am^{-2} test over 22 hours for all elements detected

5.6 Comparison of an electric leaching test with a static leaching test

In order to gain further understanding of electrical leaching, an electric leaching test was compared with a static leaching test carried out under a similar condition. The electric leaching test used a 3:1 BFS:PC sample in a migration cell with 750 mL of distilled water in each tank at 25 Am^{-2} applied current over 14 days, whereas the static test used the same setup but without the applied current for a 28 day period. The applied current and difference in leaching time were the only parameters directly altered. Samples of 6 mL from each tank (< 1% of the total solution each time) were collected periodically to test the pH, and the elemental concentrations by ICP-OES, at 3, 7 and 14 days for the electrically accelerated test, and 3, 7, 14, 21 and 28 days for the static test. The static test was conducted over a longer time period than the electric test as slower leaching was expected. The extracted solution was not replaced. After the test the cement samples were collected and analysed by TG, XRD, DTA, MIP and SEM-EDX.

The desired current density was achieved within the first day. Once it is achieved, the system no longer requires the maximum voltage, and the device automatically reduces the voltage between the electrodes as shown in Figure 5.21, with a significant reduction occurring in the first 3 days. As there is a constant current in the rest of the test, the small reduction of voltage during this period indicates that the conductivity of the system increases over time.

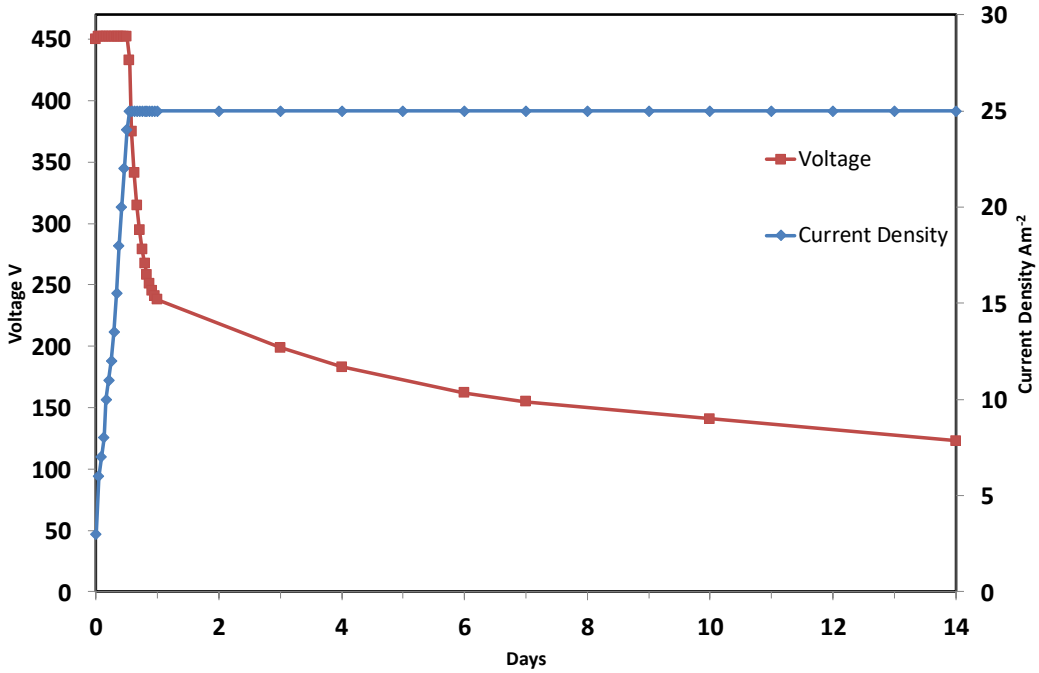

Figure 5.21 Measured voltage over the electrical leaching test

Photographs of the samples after the tests are shown in Figure 5.22. In the electrically leached sample there are clear alterations in the material, whereas the static test showed only a surface alteration upon visual inspection. Following later carbonation of the electrically leached sample, the colouring approached the grey colour observed in the statically leached sample, however the alteration later was still visible.

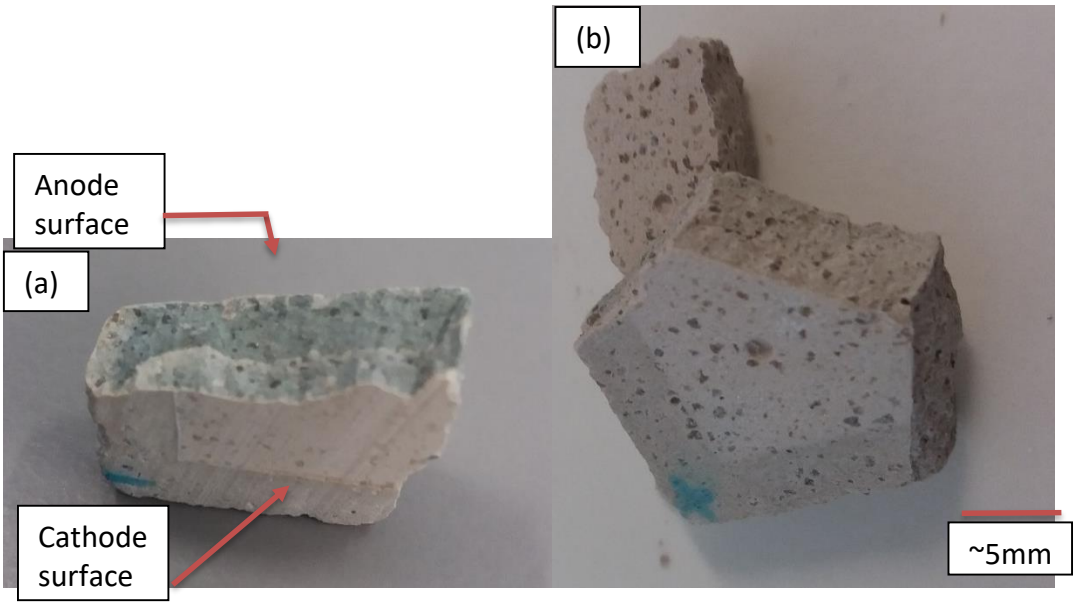

Figure 5.22 Photograph of a 3:1 BFS:PC sample dried under vacuum in a desiccator: (a) after 14 days of applied current with the cathode surface facing the viewer, and (b) after a 28-day static leaching test, both of which show a clear alteration layer.

5.6.1 Leachate analysis of statically and electrically leached 3:1 BFS:PC

The pH data for the anode and cathode tanks are displayed in Figure 5.23 for both the static and electric tests. The dotted line represents the anode tank and the solid line the cathode tank, although for the static test the distinction is only nominal. All datasets can be assumed to have a starting pH of 6.9. As was expected, there was little difference between the pH levels of the two tanks in the static test, with the pH level becoming 10.95 after 3 days and increasing to 11.35 over the course of the test. This increase in pH of the leachate is due to the natural leaching of elements from the cement, which has a high internal pH [24]. In the electrical leaching test, however, a significant difference between pH levels in the cathode and anode tanks can be observed, with the cathode tank having significantly higher pH values than the static test, approaching 13 over the 14 days, while the level in the anode tank decreases to 3.5. The change in the pH of both tanks is due to the combined effects of the change in the elemental concentration in the tanks as well as the electrolysis of water as mentioned in Chapter 3 (equation 3.6 and 3.7).

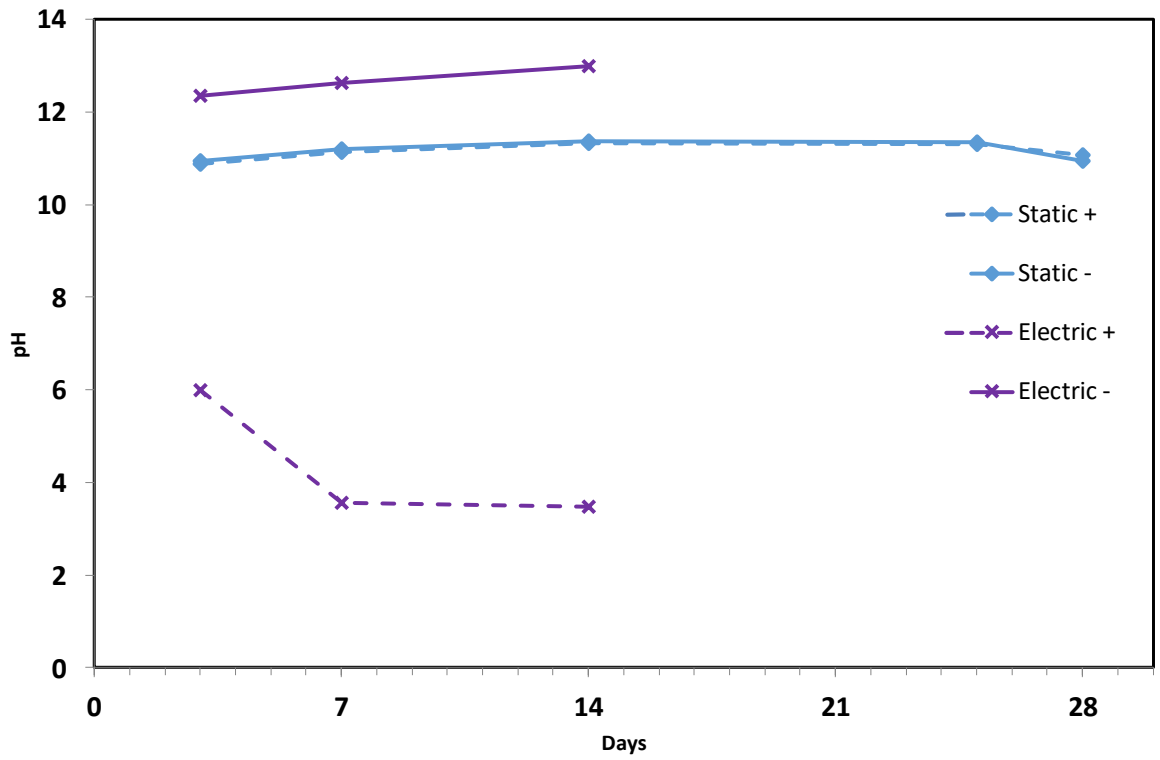

Figure 5.23 pH data of the anode (+) and cathode (-) tanks in the static and electrical leaching tests. The solid line represents the cathode tank, and the dotted line the anode tank

The concentration data are shown in Figure 5.24 to Figure 5.32. Ca, Ba, K, and Na leached more into the cathode tank in the electric test, and Si, Al, S and Mg leached more into the anode tank. The data for the 28-day static leaching test are also shown in these figures. Each dataset is labelled in the same way as the pH data. In the electric test, the amount of each element leached into the attractive tank was greater in the electric test than in the static test, whilst the other tank showed a lower concentration than in the static test. Thus, the leaching of elements into the other tank is not simply same as the static leaching behaviour as previously reported [6], but is also affected by the electric potential. The data shows that the electric field can suppress or redirect the natural leaching of elements, which has not been discussed previously in the literature. This may affect the analysis such as elemental mapping and Ca/Si ratios previously used to estimate the deterioration of the sample [11].

Calcium is the most abundant element leached out of the cement samples and is attracted to the cathode tank (Figure 5.24). In the electric test, the amount of Ca in the cathode tank after 14 days is 17-20 times the total Ca leached in the static test after 28 days. In the anode tank, the leaching of Ca is suppressed compared with the static test, showing the effect of the electrical field on the positive ions in the anode side of the cement sample. The reduction of Ca concentration in the anode tank also indicates that the acidification of the anolyte does not increase the leaching of Ca, unlike what is observed in acidic leaching tests [25].

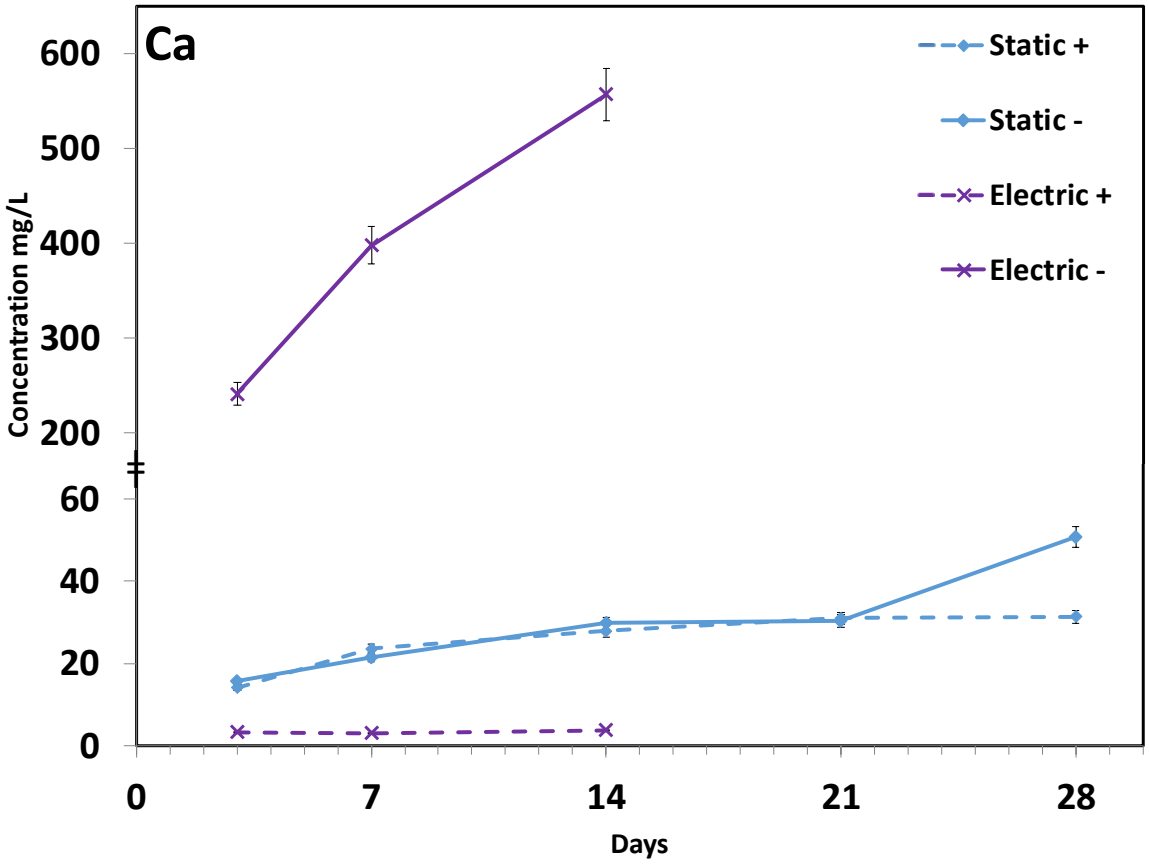

Figure 5.24 Elemental concentration of calcium in anode and cathode tanks in the static and electrical leaching test. The solid line represents the cathode tank, and the dotted line the anode tank. The y-axis is split to better see the data.

Barium appears to leach in a similar way to Ca but with a less amount in the static test, likely as there is Ba initially present in the cement sample (see Table 3.3). In the electrical test Ba is attracted into the cathode tank with a concentration 2.5 times higher than in the static tanks

after 14 days. The leaching of barium into the anode tank is suppressed when compared to the static experiment. One might expect that the leaching of each element with the same charge would be increased by the same factor when a current is applied. However, this is not the case. Even though Ba and Ca have the same charge (2+), the leaching of Ba in the electric test is approximately 2.5 times the amount in the static test, whereas that of Ca is approximately 19.3 times higher.

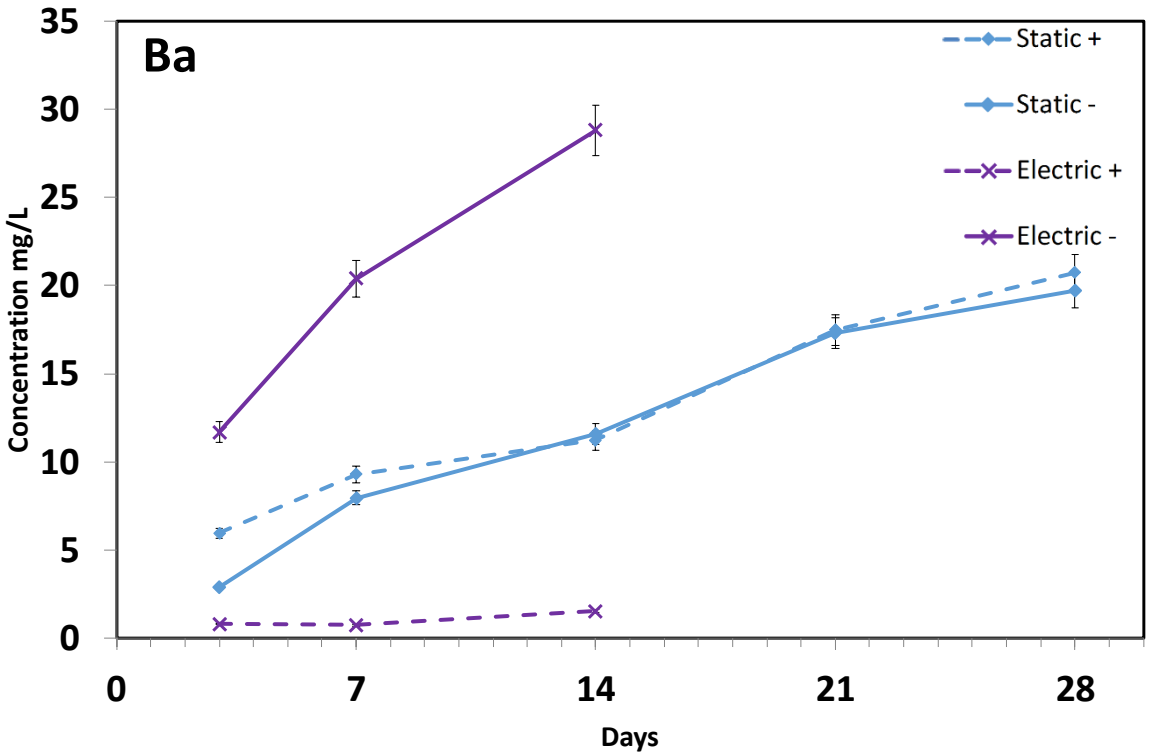

Figure 5.25 Elemental concentration of barium in anode and cathode tanks in the static and electrical leaching test. The solid line represents the cathode tank, and the dotted line the anode tank

Potassium showed a divergent leaching behaviour from Ca and Ba in the electrical leaching test: although K clearly leached into the cathode tank preferentially, the leaching into the anode tank was larger than in the static test. The acidic conditions of the anode tank should not be the reason for the increased leaching of K into the anolyte, because if this were the case, other elements would also show higher concentrations in the anode tank than in the

static test data. A suppression of leaching seems not to be occurring for K in the electric leaching, and K was the only ion indicating this behaviour. The reason for this behaviour is unknown.

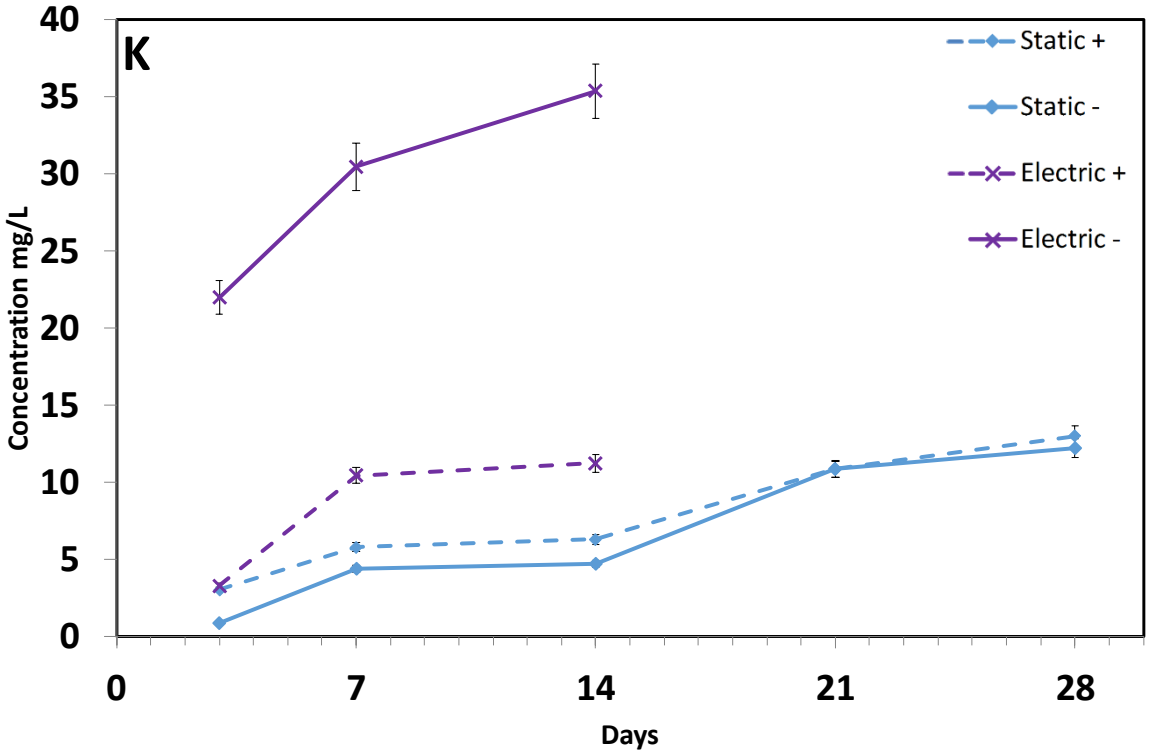

Figure 5.26 Elemental concentration of potassium in anode and cathode tanks in the static and electrical leaching test. The solid line represents the cathode tank, and the dotted line the anode tank

Sodium behaved in a similar way to Ca and Ba, leaching strongly into the cathode tank, and the leaching is suppressed in the anode tank. The level of suppression, however, seems small compared with that of Ca or Ba.

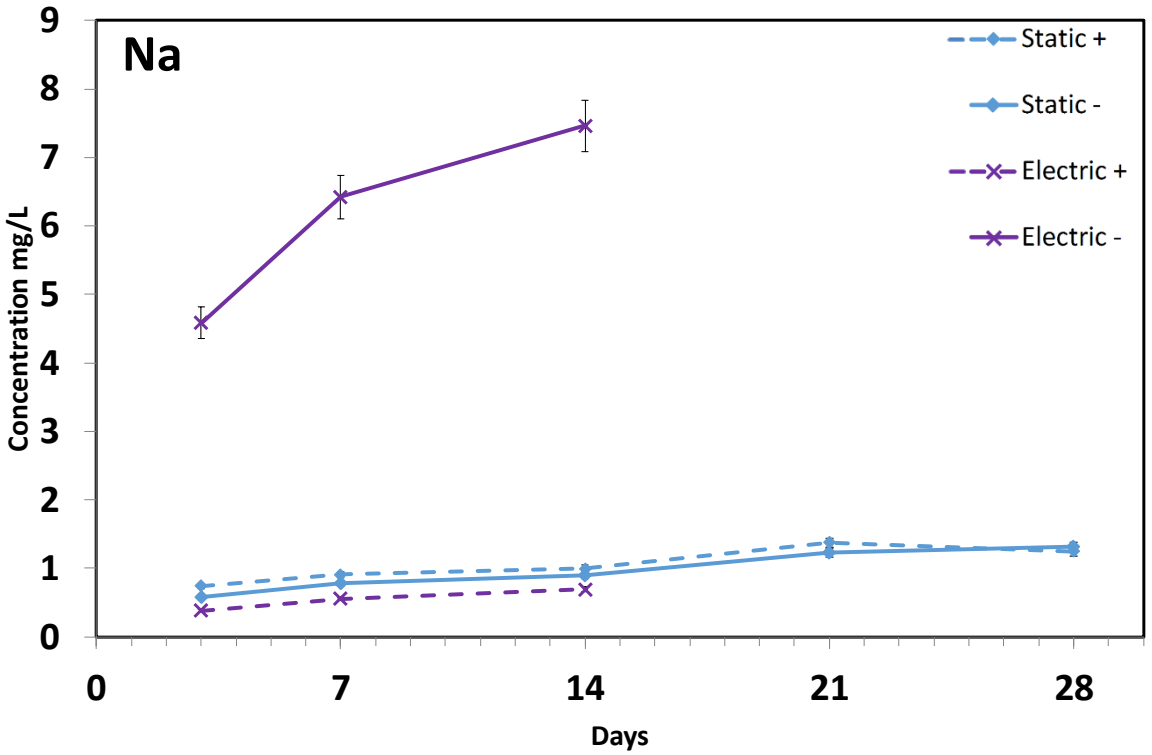

Figure 5.27 Elemental concentration of sodium in anode and cathode tanks in the static and electrical leaching test. The solid line represents the cathode tank, and the dotted line the anode

Si is attracted into the anode tank during the electric test due to its formation of anionic species (Equation 5.3 and Equation 5.4) [14], and its leaching into the cathode tank is suppressed – the opposite of Ca, Ba, K and Na. The behaviour of Si also supports the previously discussed theory that in electrical leaching the dissolution of a material is still a key factor in limiting the leaching rate like it is in static and semi-static leaching. Electrical leaching accelerates the migration of the dissolved cement out of the cement matrix, but it does not accelerate the dissolution.

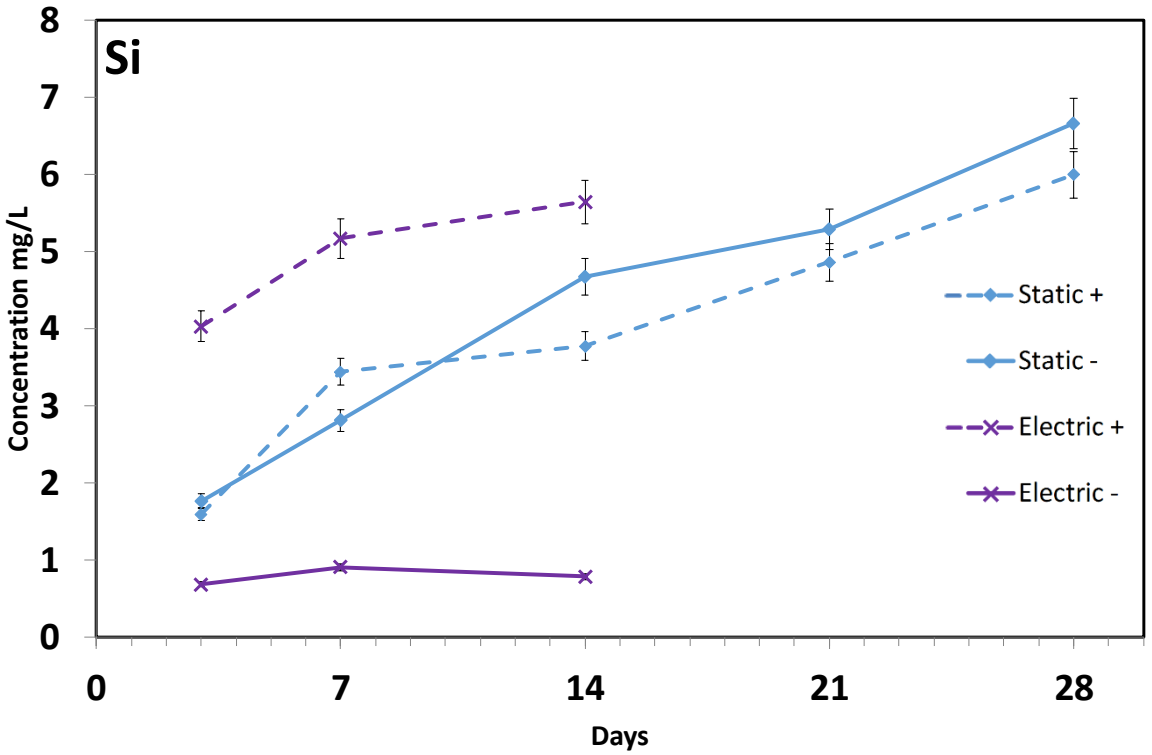

Figure 5.28 Elemental concentration of silicon in anode and cathode tanks in the static and electrical leaching test. The solid line represents the cathode tank, and the dotted line the anode

The aluminium concentration data displayed in Figure 5.29 show the unique behaviour of Al. Although Al indicated its preferred leaching into the anode tank, as expected due to formation of anionic species at high pH, the Al concentration in the anode tank kept decreasing over time whilst the cathodic concentration continued to increase. This behaviour of Al is distinct from Si which also form anionic species in cement [14]. The concentration of aluminium in the static test is greater than in the electric test at 14 days and further increases up to 21 days where it possibly stabilises.

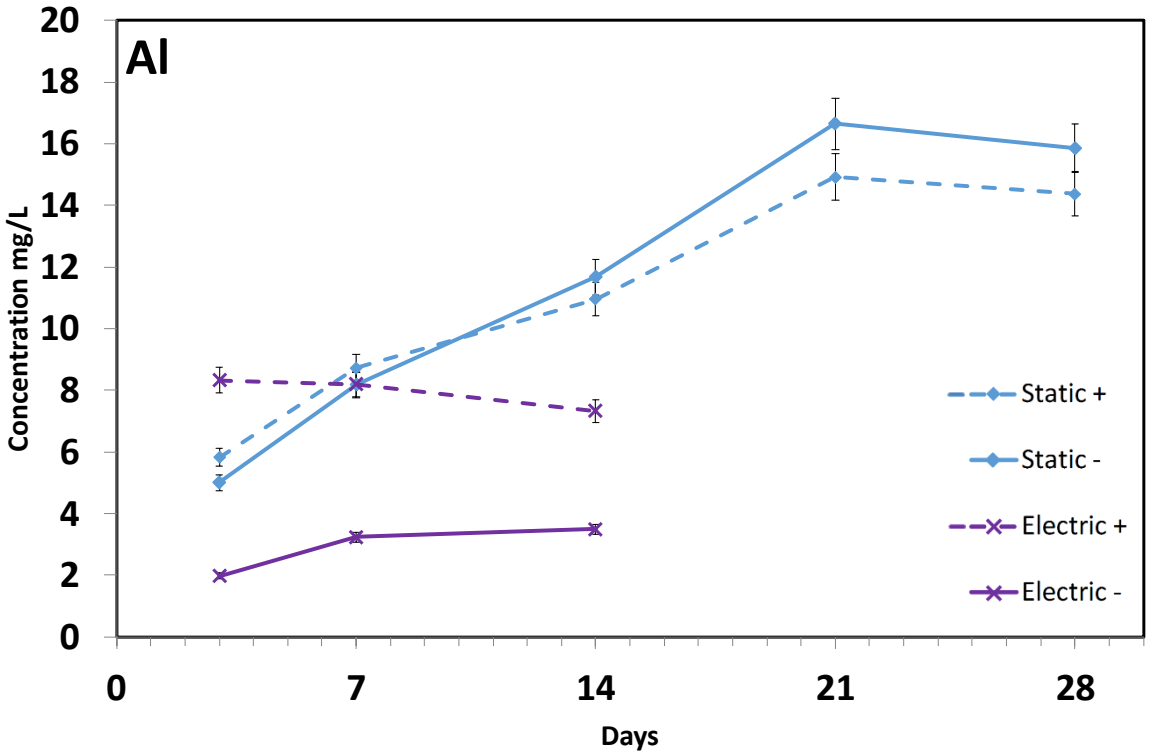

Figure 5.29 Elemental concentration of aluminium in anode and cathode tanks in the static and electrical leaching test. The solid line represents the cathode tank, and the dotted line the anode tank

The unique behaviour of Al in anode tank can be explained in relation to the pH of the system. The internal pH of the 3:1 BFS:PC cement is high (approximately 13 [15],[4], [26], [27]), and Al would form an anionic species $Al(OH)_4^-$ [28]. Because the pH of the leachant is high in the cathode tank (pH=12-13) as well as in the static leaching (pH=~11), Al is likely to remain forming anionic species in these tanks and indicates the expected behaviour, similar to Si. However, as Al leaches into the anode tank during electric leaching, anionic species become no longer stable due to the low pH environment in the anode tank (pH=6-3.5), and cationic species can be formed as suggested by Figure 5.30 which shows the pH dependence of the aluminium speciation. The formed cations can be either repelled by the anode or attracted towards the cathode tank due to their positive charge.

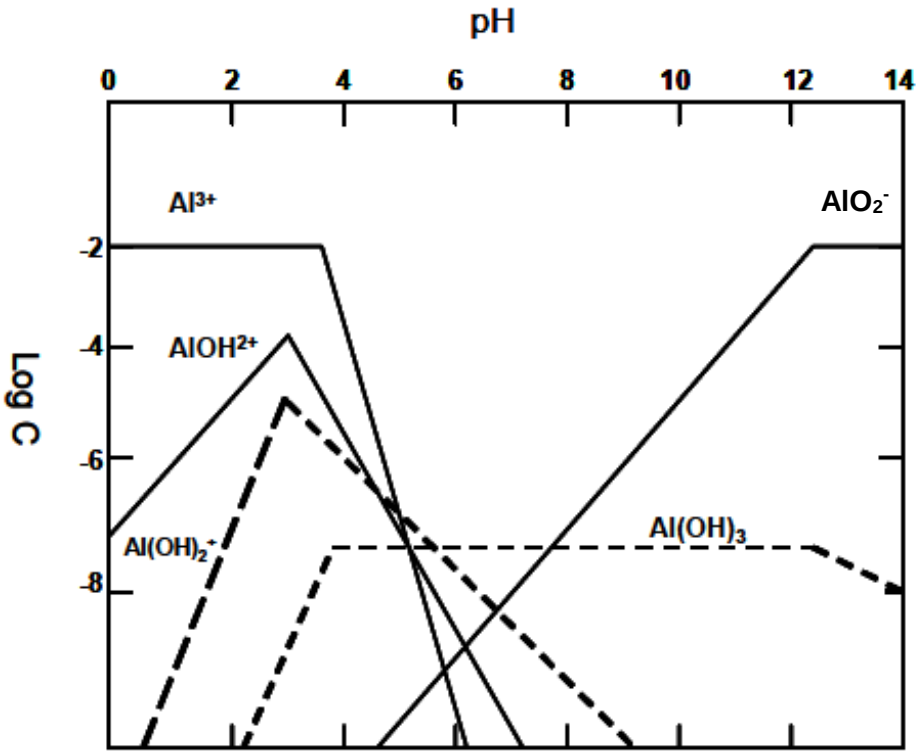

Figure 5.30 Log concentration-pH diagram for Al(III) [28]

Sulphur is relatively abundant in the 3:1 BFS:PC samples and reaches an average concentration of 2.35 ± 0.2 mg/l in the tanks of the static leaching test after 3 days. The concentration slowly increases to an average of 2.73 ± 0.2 mg/l after 28 days. The decrease between 3 and 7 days may not be significant due to the errors inherent in ICP-OES. In the electric test the sulphur leaches into the cathode tank with similar amounts to the static test although it is supposed to be forming anions [29] (data reproduced in Lea's Chemistry of Cement page 662 [30]), meaning that the leaching of sulphur is not necessarily suppressed by the presence of an electric field. The small influence from the electric field on the leaching of S was also observed in the 22-hour electric leaching previously presented in Section 5.5 above. The concentration in the anode tank, however, shows a clear influence of the electric field, increasing from 2.80 ± 0.2 after 3 days to 14.2 ± 0.7 mg/l after 14 days of leaching. This is different from the 22 hour electric leaching and confirms the presence of S as anionic species, S^{2-} and/or SO_4^{2-} [29] (data reproduced in [30]).

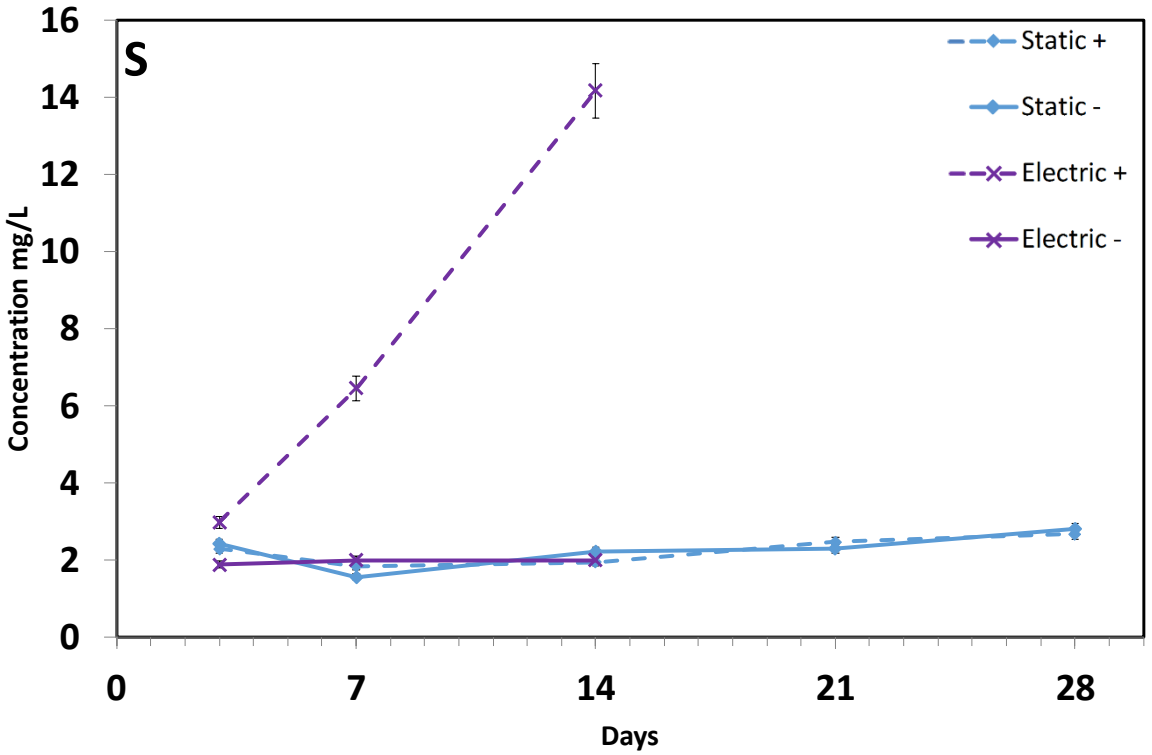

Figure 5.31 Elemental concentration of sulphur in anode and cathode tanks in the static and electrical leaching test. The solid line represents the cathode tank, and the dotted line the anode

Of the elements examined, magnesium is a unique case, as the concentration in the electric test is much lower than those in the static test for both tanks. The static test data shows some variability in magnesium concentration, but the concentration of Mg does appear to increase over time and potentially stabilises at the later stage of the test. During the electric test the concentration of Mg in the cathode tank decreases over time and ends up close to zero after 14 days, whereas in the anode tank there is a steady increase, although still resulting in a much lower concentration than in the static case. Similar behaviour was observed in the 22 hour electric leaching previously presented: Mg was initially attracted into the cathode tank and the concentration started to decrease (Figure 5.16).

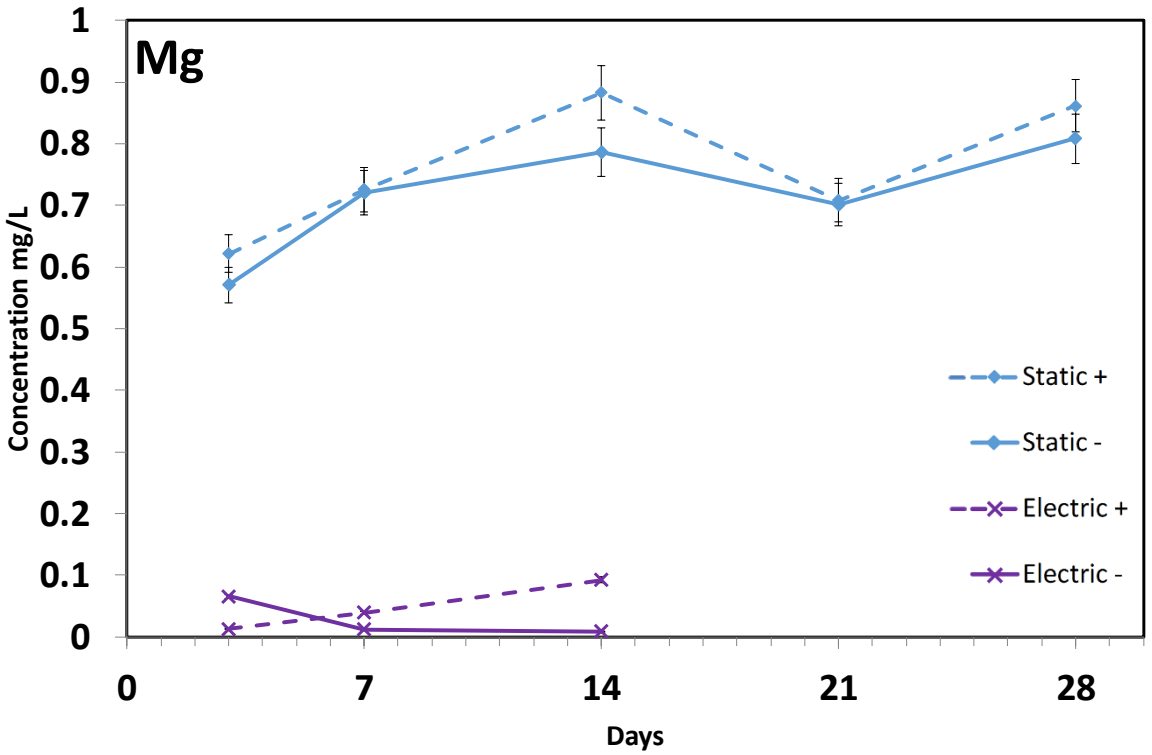

Figure 5.32 Elemental concentration of magnesium in anode and cathode tanks in the static and electrical leaching test. The solid line represents the cathode tank, and the dotted line the anode

The reduction of Mg in cathode tank must be related to the pH of the leachant. It is well known that Mg forms brucite $Mg(OH)_2$ in high pH aqueous solutions [31] which then precipitates out of the solution. As already presented in Figure 5.23, the pH of the cathode tank was approximately 12 to 13, whereas that of the anode tank was 3.5-6. According to the literature data shown in Figure 5.33, the solubility of brucite is highly limited at pH = 12-13, resulting in its precipitation. In the static test, the pH of the tanks was approximately 11, in which brucite can still form, but it has a higher solubility that in the cathode tank of electric leaching because of the lower pH.

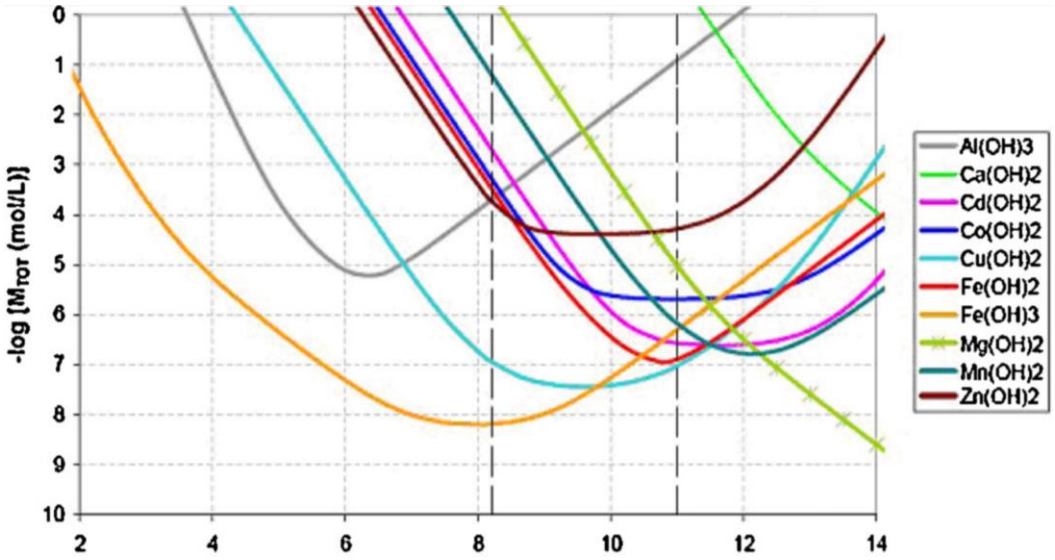

Figure 5.33 Solubility of metal hydroxides as a function of pH [32].

5.6.2 Leaching acceleration factor for comparing static and electric tests

The Leaching Acceleration Factor (LAF) for the elements studied are shown in Figure 5.34. The LAF was estimated using data at a certain leaching period based on the following equation:

$$LAF = \frac{(Concentation\ of\ element\ i\ in\ the\ attracted\ tank)}{(Average\ concentration\ of\ element\ i\ in\ the\ static\ leaching)}$$

Equation 5.5

For instance, the LAF for Ca at 3-days was estimated using the Ca concentration in the cathode tank after 3 days of the electric leaching, divided by the average Ca concentration after 3 days of the static test. If the acceleration factor is 1, then there is no increase in the leaching. For Al and Mg the LAF was below 1 depending on the period, as there was a lower concentration in the attracted tank in the electric test than in the static test.

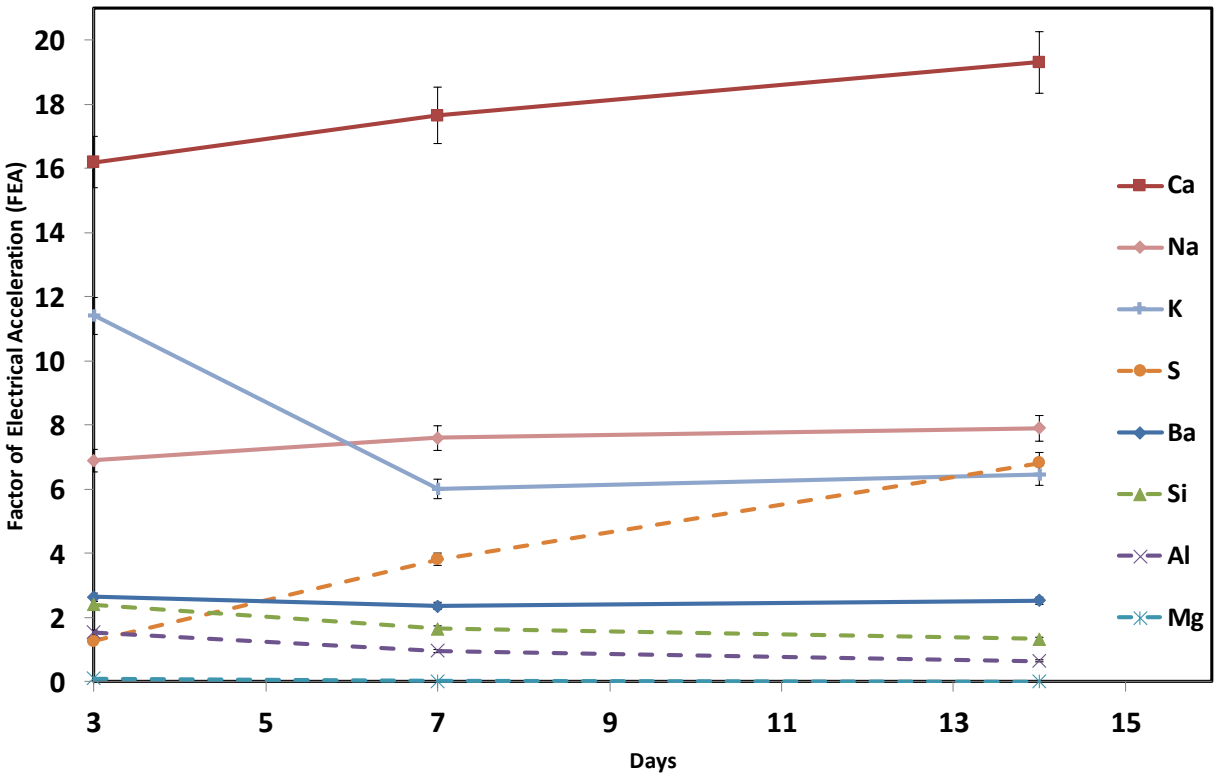

Figure 5.34 Leaching Acceleration Factor (concentration in the attractive tank divided by the average static concentration). The elements attracted into the cathode tank are represented by a solid line, and for the anode tank a dashed line.

A constant LAF means that the factor undergoes little change as time progresses, such as Ba that has a factor of 2.37 – 2.65 ± 0.3 throughout the test. A decrease over time such as the potassium data between 3 and 7 days means that the static test is 'catching up' with the electric test, though after this point LAF for K is fairly steady. Silicon has a slight decrease, but it is still above 1 after 14 days (1.34 ± 0.1). An increase of LAF over time as displayed by Ca and S indicates the impact of the electric leaching test is increasing further. After 14 days there are three main bands of elements, as observable in Figure 5.34. The group with the lowest LAFs consists of Ba, Si, Al and Mg – their ions appear to be less influenced by the electric potential. This may be related to the size and/or mass of the ions. Ba^{2+} is much larger than the ions studied here [33] with an ionic radius of 1.42×10^{-10} m [13]. Both Si and Al form various large anionic species with hydroxyl groups [14], [28]. Mg forms $Mg(OH)_2$ and likely

precipitates, as discussed above. The middle band consists of Na, K and S, receiving a moderate influence from the electric potential. Na and K have previously been reported as strongly leaching towards the cathode [11] so their behaviour is not surprising. S is initially in the lower band with a factor of 1.54 ± 0.1 after 3 days of leaching, and then increases to 6.82 ± 0.7, ending up between Na and K after 14 days. The unique behaviour of S may not be solely because of the electric potential as previously assumed. If it were the case, then S should already have had a higher LAF after 3 days of an applied current. A possible explanation is the effect of two different anionic species. It is known that S can be present both as sulphate SO_4^{2-} and sulphide S^{2-} in cements [17], [22]. Since sulphate can be provided by PC whereas sulphide has to rely on the dissolution of BFS, it is expected that S is available mainly as sulphate at the early stage of leaching. Sulphate is a larger anionic species with a mass of 96.062 $gmol^{-1}$, and is expected to behave similar to the anionic species of Al and Si.

At the test progresses and more BFS starts dissolving, the amount of sulphide available in the system would increase. Sulphide is a smaller anion and expected to behave similarly to the other smaller ions. The final band is for Ca only which has the greatest LAF of 19.3 ± 1.9 after 14 days. Ca does not form larger ionic species in cement and is present as Ca^{2+}. Ca receives the largest influence from the electric potential, probably because of its mobile nature in static leaching tests. Because K and Na are very mobile even without the electric potential [1], the impact of the electric potential appear moderate, whereas the impact of the electric potential appears more significant for Ca. The increase in the LAF over the testing period implies the increased dissolution of material as implied in the LAF of S.

5.6.3 Phase analysis of statically and electrically leached 3:1 BFS:PC

A 6 hour XRD scans of the samples from the static test and electric test are shown in Figure 5.35, together with an unleached cement sample. It should be noted that samples were prepared by crushing 1/4 of each tested specimen, including both anode and cathode sides. The three samples show very similar data, but there is a slightly larger C-S-H peak in the electric test. The peaks in the 5 to 15° 2θ range also look slightly different, and a further 4 hour scan displayed in Figure 5.36 clarifies the presence of ettringite, monosulphate, hemicarbonate, monocarbonate and hydrotalcite. Formation of these phases have been reported in cement systems produced with increased limestone and other carbonate materials [34]. These minerals can also be seen where portlandite reacts with carbon dioxide to form calcium carbonate, and this carbonate can then react with monosulphate present in the system to form hemicarbonate; further reaction with carbon dioxide or carbonate can form monocarbonate [18]. A similar reaction appears to be occurring in the cement samples examined. The static test resulted in the very similar peaks to the unleached sample for hemicarbonate and monocarbonate/hydrotalcite the hemicarbonate peak looks more pronounced than the monocarbonate/hydrotalcite peak. However, the 14-day electric test resulted in a different trend – the hydrotalcite/monocarbonate peak is larger and the hemicarbonate peak is significantly reduced, which suggests that the sample has reacted with carbon dioxide to a greater extent.

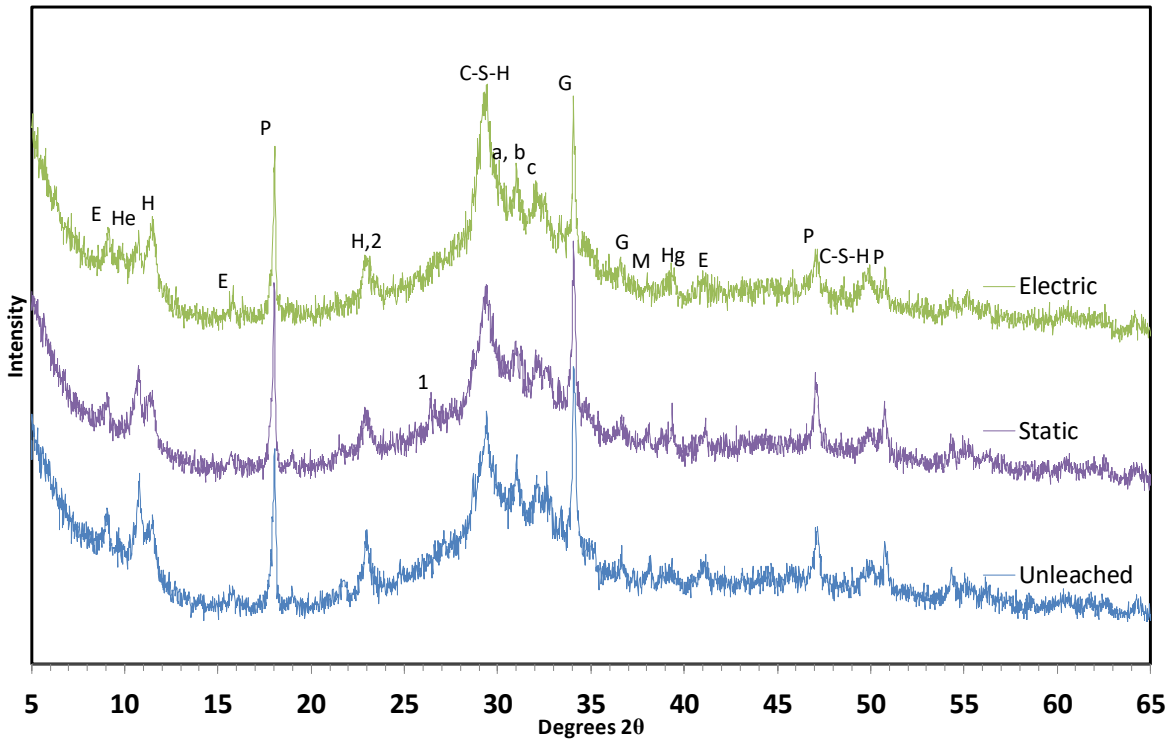

Figure 5.35 long (6 hour) XRD scan of cement samples that are unleached, after a static test and after an electric leaching test see Table 4.2 for corresponding peak abbreviations

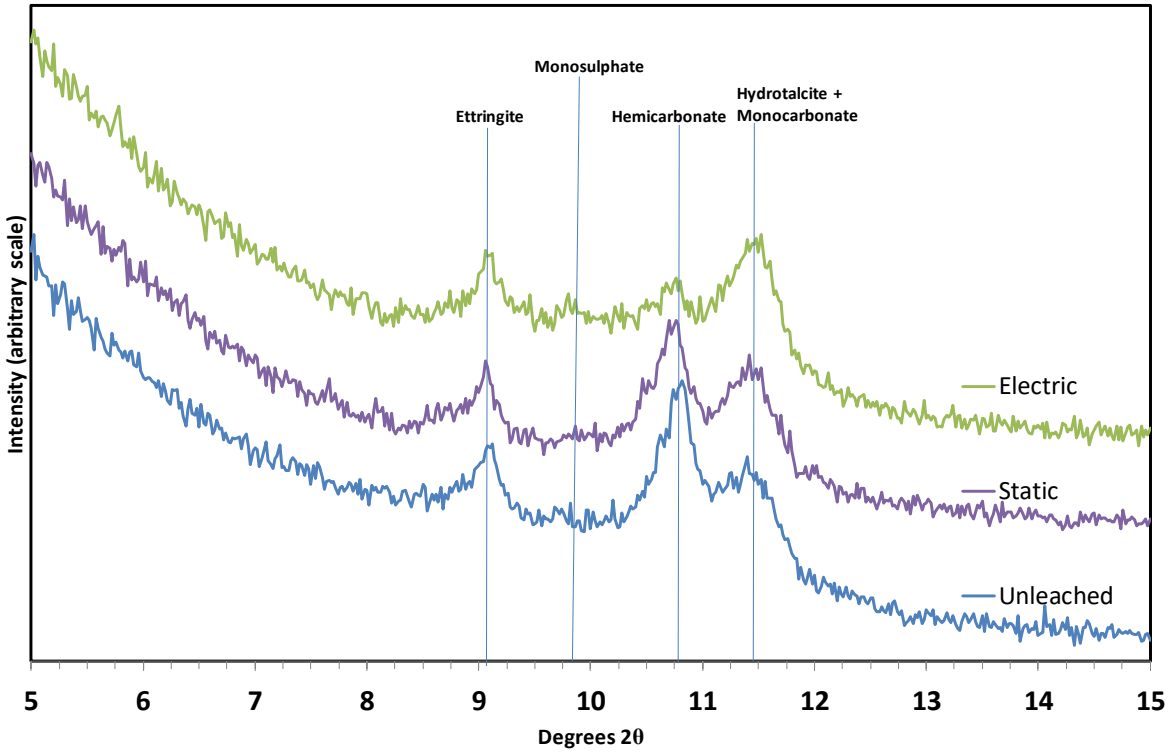

Figure 5.36 4 hour XRD scan of cement samples that are unleached, after a 28 day static test and after a 14 day 25 Am^{-2} electric leaching test

The samples from the static and electric leaching tests, as well as the unleached sample, were further studied using thermal analysis. Table 4.3 in Chapter 4 summarises the key thermal

events to be expected in these analysis. The thermogravimetric analysis of the three cement samples are shown in Figure 5.37. The Differential ThermoGravimetry (DTG) data are shown in Figure 5.38 which can show the thermal events more distinctly, for example the peak at 150°C due to the dehydroxylation of hemicarbonate (Hc) and monocarbonate (Mc). The sample from the electric test had the smaller monocarbonate/gypsum peak compared with the unleached sample, whereas the cement after the static test had the larger monocarbonate/gypsum peak compared with the unleached sample. This trend coincides with the XRD data.

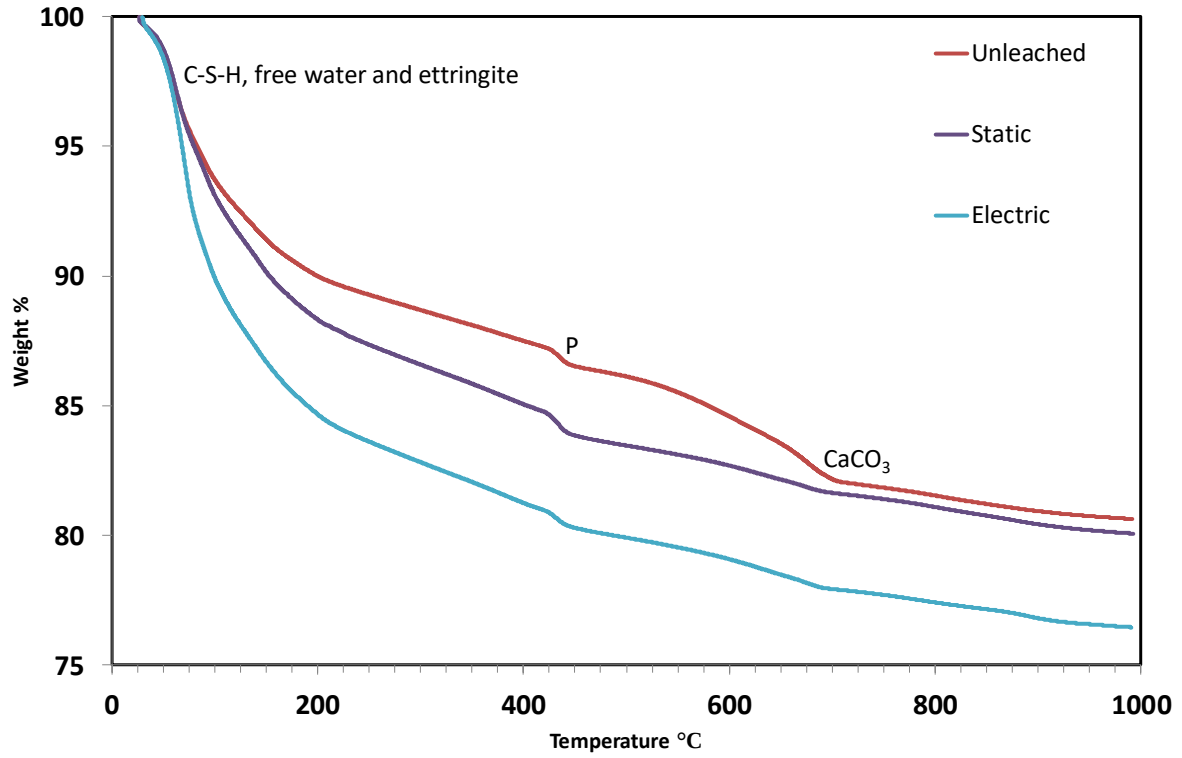

Figure 5.37 Thermogravimetric analysis cement samples that are unleached, after a 28 day static test and after a 14 day 25 Am^{-2} electric leaching test

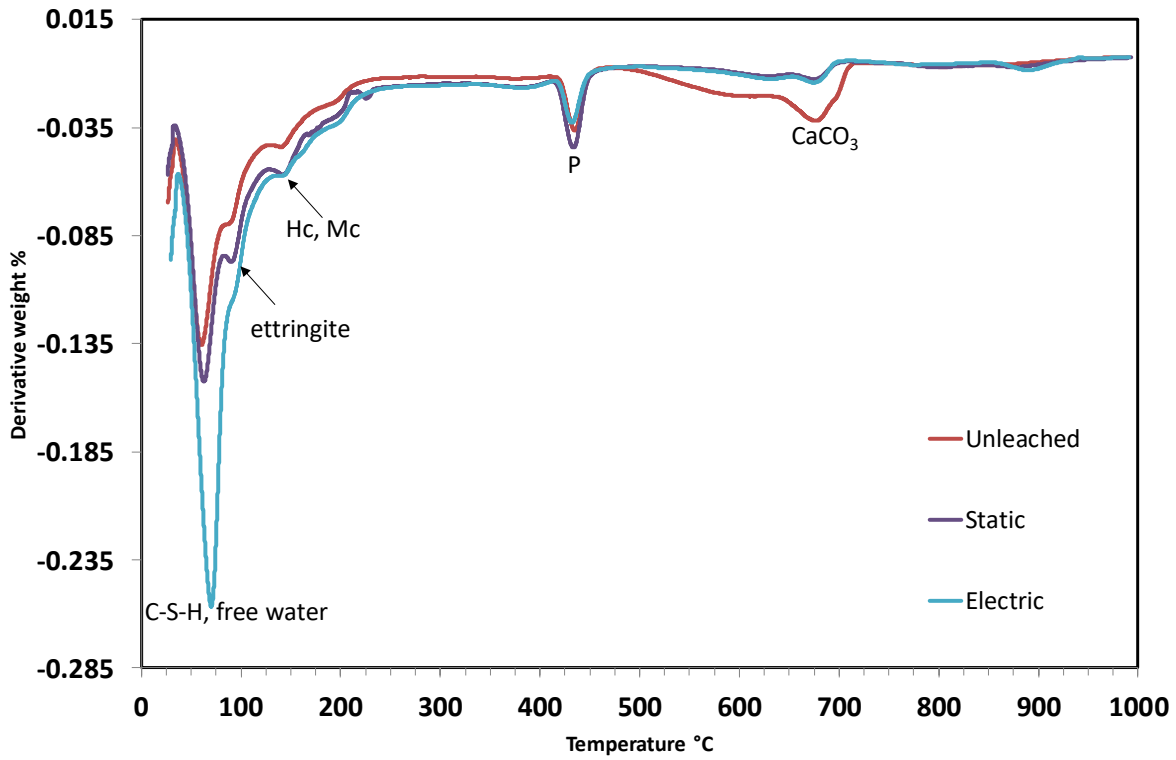

Figure 5.38 Differential Thermogravimetry (DTG) of the 3:1 BFS:PC cement samples

The sample from the electric test displayed the greatest amount of weight loss in the 50-120°C range which indicates a larger amount of free water present and the C-S-H phase which was also observed in the XRD data in Figure 5.35. The electric test also resulted in a smaller portlandite peak at 450°C in the sample, compared with the static test, which could suggest enhanced dissolution of portlandite in the electric leaching, and potentially an enhancement of the hydraulic reaction, leading to the increased formation of C-S-H. The direct comparison of these samples with the unleached sample is difficult, since the unreacted sample appears to have been significantly carbonated, shown as the large peak at 500-700 °C in the first derivative associated with $CaCO_3$ decomposition. Since enhanced carbonation was not observed in the XRD data of the unleached sample, this carbonation which usually involves the consumption of portlandite and C-S-H [18] appears to have occurred during the preparation of TG sample. The DTA data gathered concurrently with the TG data is presented in Figure 5.39. This data confirms the observations made in the TG data.

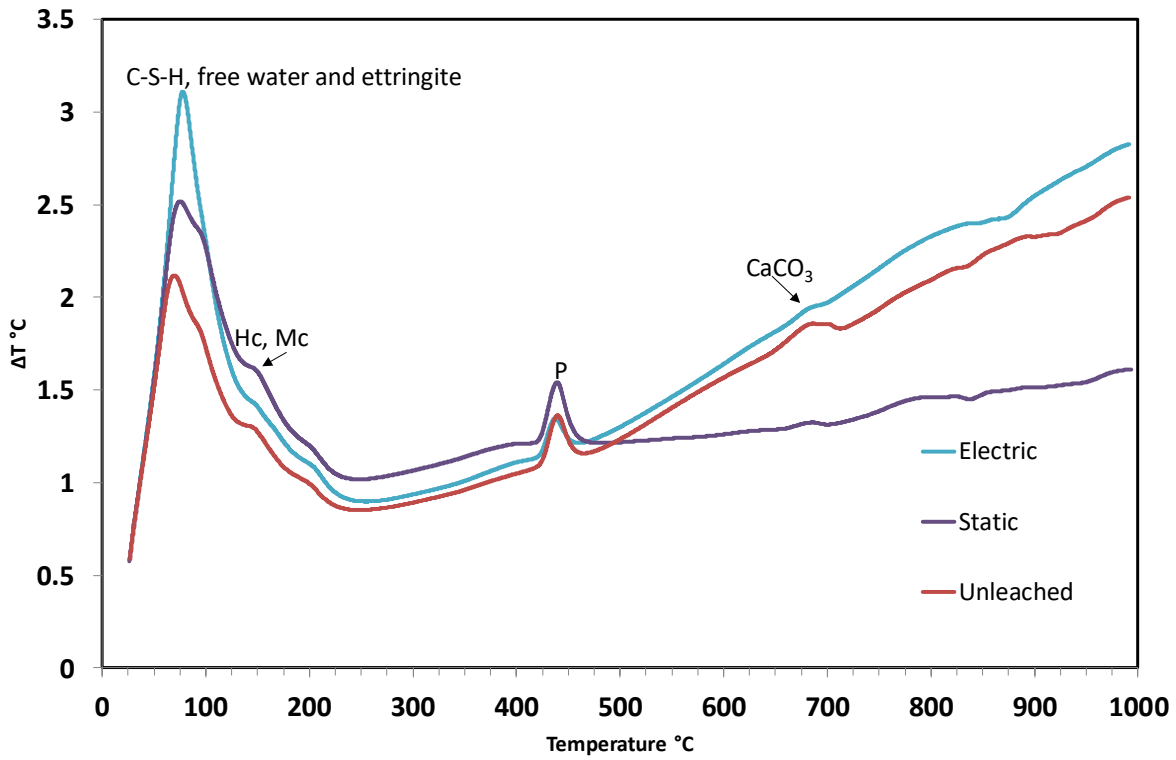

Figure 5.39 Differential Thermal Analysis of the 3:1 BFS:PC cement samples (endothermic up)

5.6.4 Microstructure of statically and electrically leached 3:1 BFS:PC

The total porosity and pore size distribution gathered by MIP for these samples are shown in Figure 5.40 and Figure 5.41, respectively. Whilst the 14-day electric leached sample shows a similar porosity to the unleached sample, the pore size distribution in the sample from the electric test is more concentrated in the 10-20 nm range (gel pores [17]) with a small but significant distribution in 200-1000 nm (capillary pores [17]) diameter range, whereas the unleached sample indicated less pores in this range. The static test resulted in a distribution concentrated in around 10 nm, with a reduced porosity in the other ranges, leading to the smaller total porosity compared with other systems. Both the static and electric leaching resulted in an increase in the porosity of the sample in the 10-20 nm range and a reduction in the porosity in the 20-50 nm ranges. The reduction of the pores in the 20-50 nm range is possibly suggesting that further hydration of the cement is occurring due to the exposure to the water during the leaching tests and could account for the decrease in porosity.

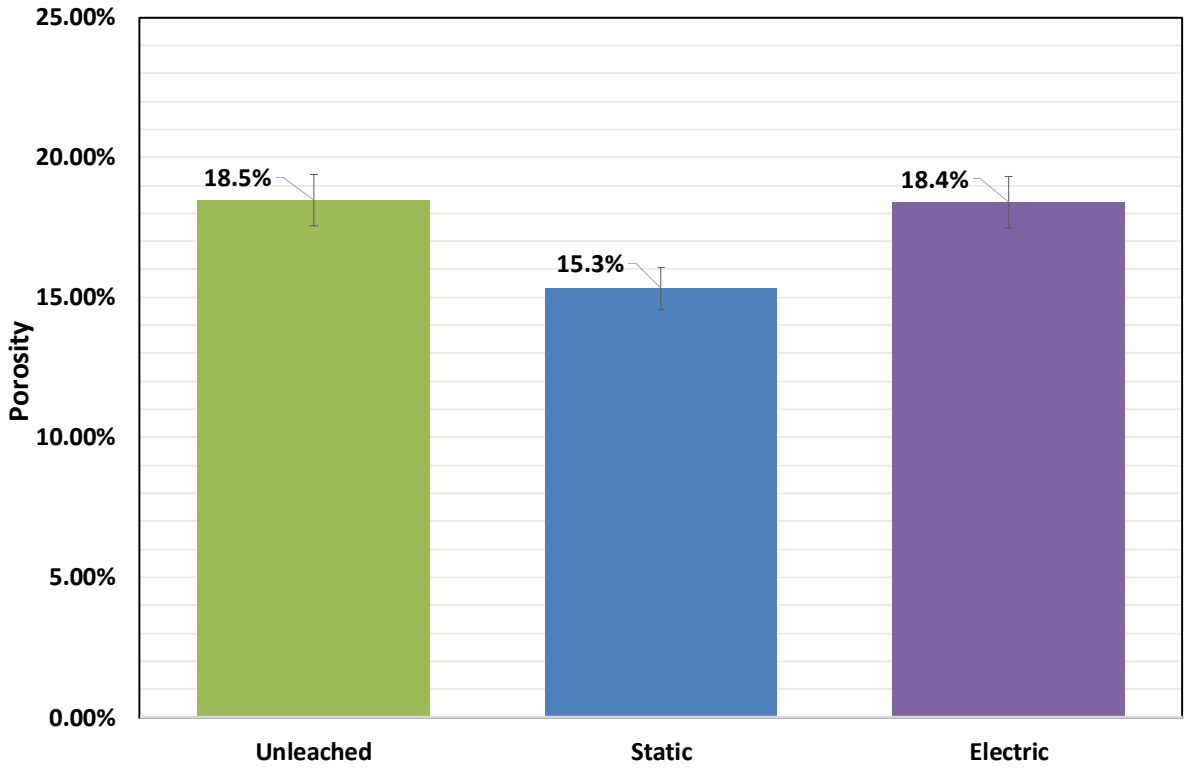

Figure 5.40 Porosity of 3:1 BFS:PC before and after leaching

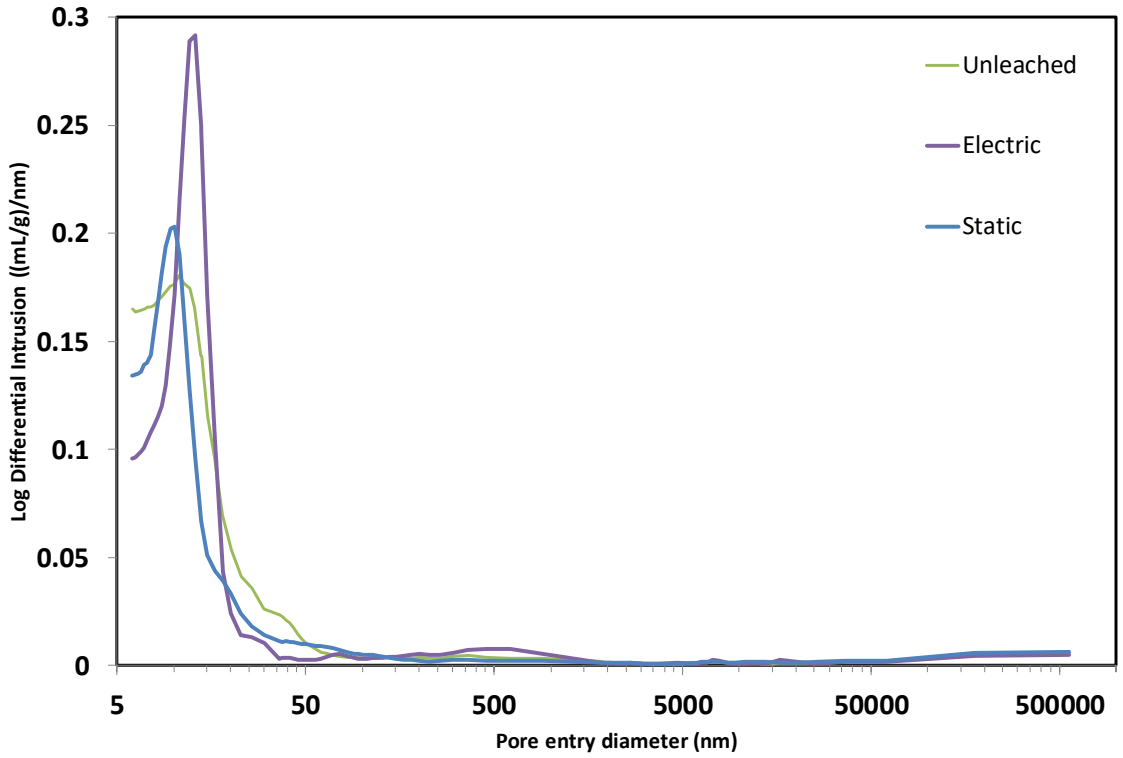

Figure 5.41 Pore Size distribution of 3:1 BFS:PC before and after leaching

A BSE image of the cement sample after the static leaching test is shown in Figure 5.42 along with elemental maps via SEM-EDX of calcium, silicon, aluminium and magnesium. This magnification was chosen as the degradation layer and the exposure surface were the areas of interest. There is a clear region of degradation in the image leading up to a layer at the surface, depicted by a significant decrease in the calcium and silicon in that area, and other elements to a less extent. There is a precipitation of what is mainly Ca at the exposure surface, likely as calcite based on the literature [15]. The degradation layer is approximately 20-25 µm. Beyond this point there are unreacted particles further into the cement sample where no obvious alteration.

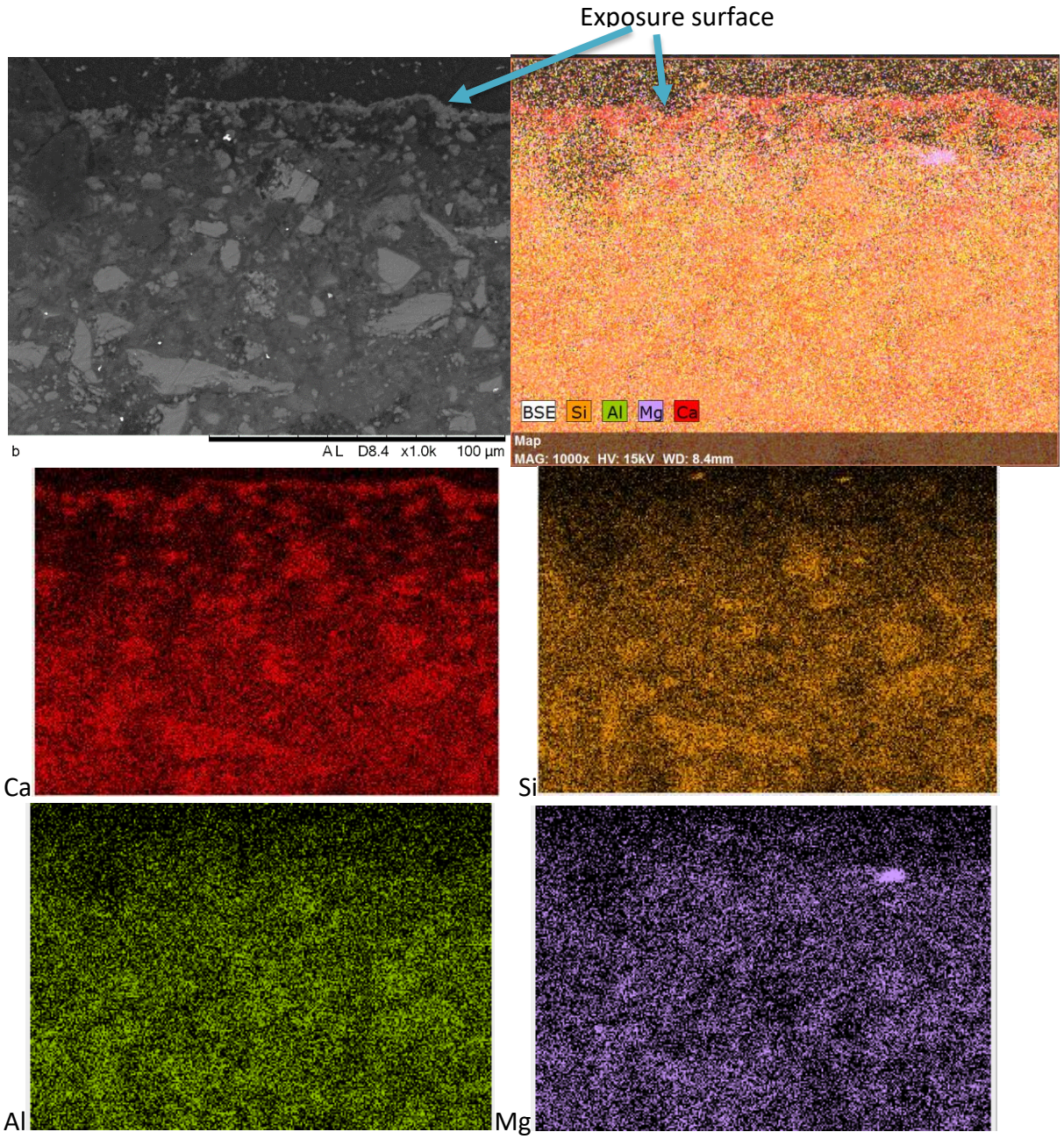

Figure 5.42 BSE image of 3:1 BFS:PC after a 28 day static leaching test, and SEM-EDX maps of Ca, Si, Al and Mg

The BSE and SEM-EDX images of the cement sample after the electrical leaching test are shown in Figure 5.43 and Figure 5.44, displaying cross sections on the anode and cathode sides respectively. For silicon, there is a gradual decrease in the distribution as the surface is approached both on the anode and cathode sides. The region of degradation layer for silicon

is deeper on the anode side as expected from the enhanced leaching of silicon on anode side (Figure 5.28). On the cathode side, there is a relatively strong signal throughout the sample.

The calcium indicated a similar behaviour to the silicon on the anode side, but overall concentration appears to be higher than silicon, which also agrees with the less leaching of Ca on the anode side. The cathode side indicated a calcium deficient region near the surface, and calcium concentration increases at a depth of ~20µm, similar to the static test.

Examining the aluminium maps, the cathode side has many areas of higher concentration corresponding to the unhydrated particles compared with the anode side which is more uniform. This is indicative of the enhanced leaching of aluminium in the anode tank. The unhydrated particle likely originates from the BFS due to the higher concentration of Al and Mg in these areas based on the XRF data, see Table 3.1. The magnesium map on the anode side is similar to the aluminium map, but more localised. On the cathode side there are several particles with a strong Mg and high Al concentration close to the exposure surface. These may be remnant slag grains, or possibly hydrotalcite resulting from the hydration of the Mg in slag.

Comparing the static and electric leaching tests, there is less clear Ca precipitate on either exposure surface in the electric test, and on the cathode side there is a larger dissolution front of ~35-40 µm (it varies across the image which is representative of the sample) after just 14 days compared with the 20-25 µm after the 28-day static test in Figure 5.42.

Expoure Surface

Exposure Surface

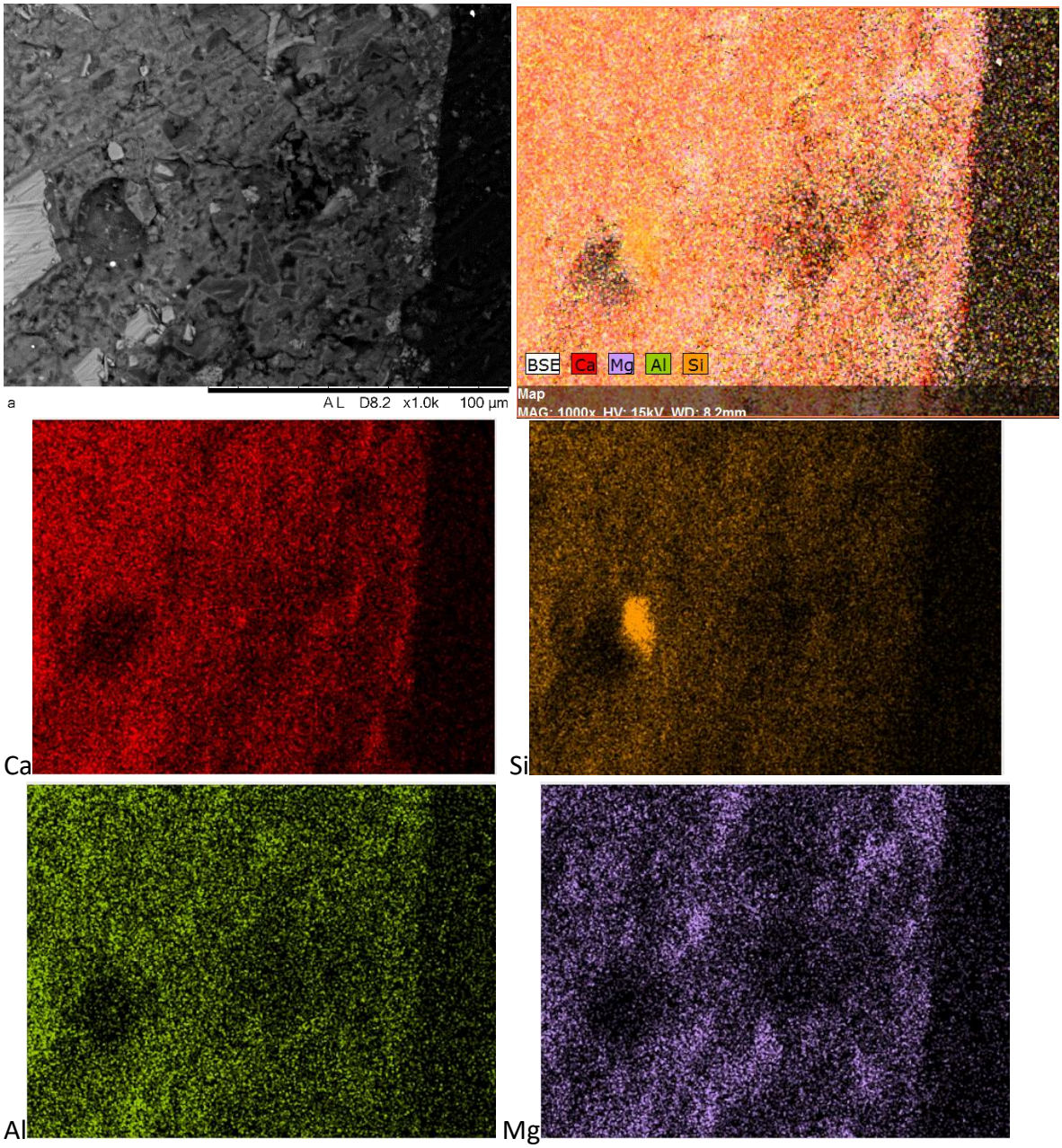

Figure 5.43 BSE image of the anode side of the 3:1 BFS:PC sample after 14 days of electrical leaching, and SEM-EDX elemental maps

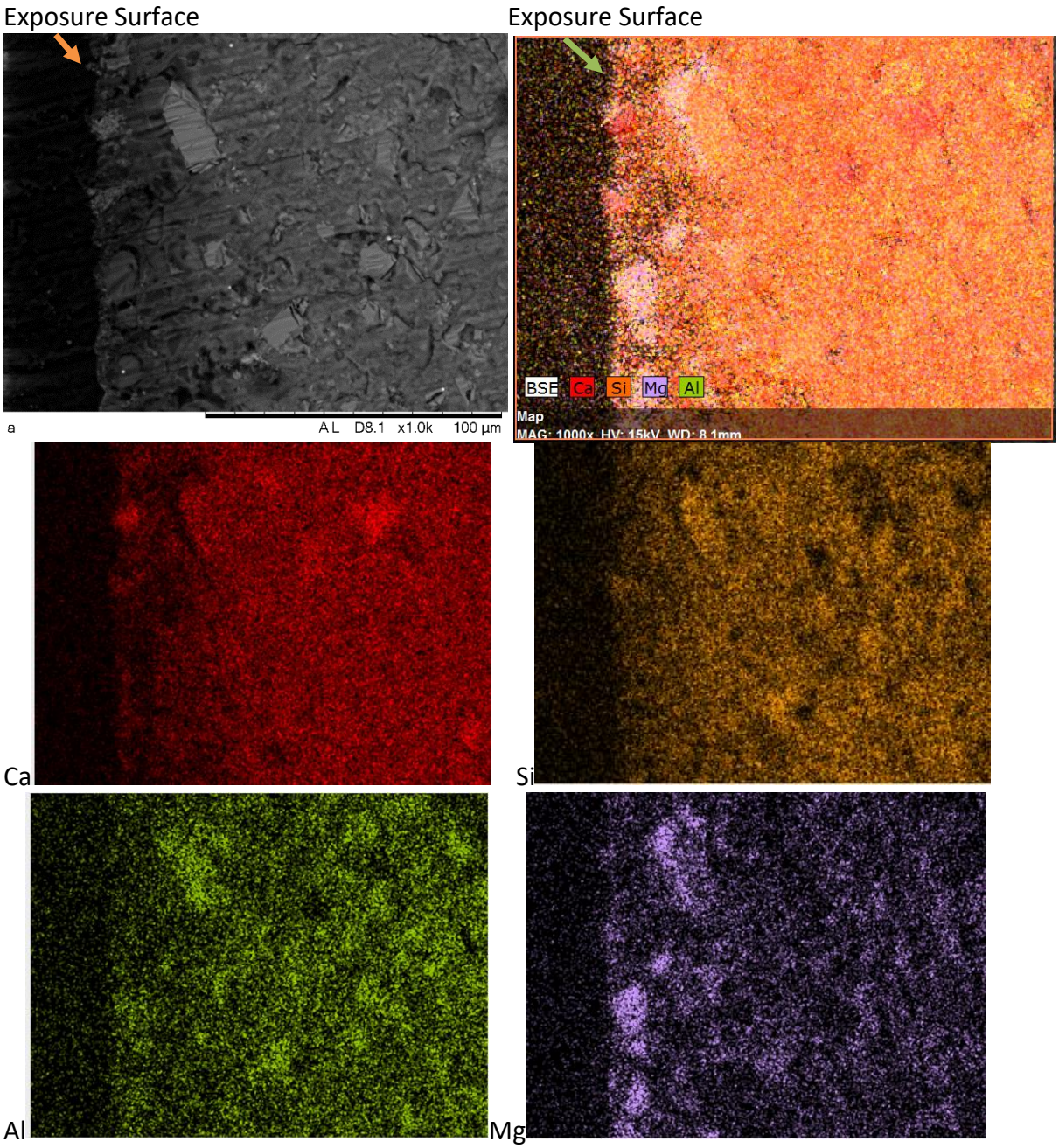

Figure 5.44 BSE image of the cathode side of the 3:1 BFS:PC sample after 14 days of electrical leaching, and SEM-EDX elemental maps

5.7 Discussion

One of the main aims of the project was to investigate and explain the mechanisms behind electrical leaching. As stated previously and found by others in this area [5]–[7], [11], [35], electrical leaching works as an accelerated leaching technique when charged ions are exposed to an electric field, as is the case in cement samples which is a porous medium containing pore water with a mixture of dissolved ions. However, the charge of the ions is not the only factor in determining normalised leaching rate. As the data in this Chapter shows there is little to no congruent leaching between elements with the same charge other than between sodium and potassium, even when charge density and normalised mass loss are used as normalisation measures. Secondary to this, there is the fact that rehydrating a cement sample prior to leaching will have an effect on results when the leaching out of a cement sample is the point of interest in an experiment.

Although calcium leaching has been the focus of previously reported studies on electric leaching [5]–[7], [16], due to the highest abundance in the cement samples, the data shown in the present study show that other elements are also affected dramatically by electric potential and show a clear preference for which tank they will leach into, depending on their charge in solution. The work also shows that all elements will leach into the tank with the 'wrong' electrode, for example Na which has an oxidation state of +1 still leaches in the anode tank (which has not been reported). Its concentration displays an increase in the anode tank over time – however, this concentration is much less than in a static test and so the static leaching must be suppressed by the electric field. The increase in concentration over time is probably due to the standard diffusion/dissolution process that cement undergoes in a static leaching test, and this process does still occur in electrical leaching tests.

One measure of degradation typically applied in static leaching is the calcium to silicon ratio of the cement matrix, and how this is altered as leaching occurs [36]. It is not clear if this technique can be directly applied to electrical leaching in the same way as in static leaching, because as the data in this Chapter shows, the leaching behaviour of Si and Ca are quite different in these leaching methods – in static leaching elements they do not have a preferred direction of migration but in electrical leaching a preferred direction of migration is clearly observed and leaching is suppressed on the other side. This may mean that inside the cement the Ca/Si ratio would not match up with an equivalent map of the ratio in a static test. It would require further investigation to quantify these effects, however, and in the BSE images of the electrically leached cement sample, both the anode and cathode sides showed that dissolution of hardened cement at the exposure surface is dominated by the leaching of calcium, and leaching of silicon has little impact on the exposure surface so this may not be a large effect.

5.8 Summary

The results shown in this Chapter show that most elements leach out of cement at an accelerated rate when a current is applied. The direction of leaching is dependent on the charge, but the extent of the acceleration did not show a correlation with the magnitude of the charge. The leaching was found to also occur into the tank with the unattractive electrode, but was found to be suppressed by the presence of the electric field when compared with a static leaching test. Applying a current causes electrically accelerated leaching of positively charged species towards the cathode tank, and towards the anode tank there are electrically accelerated effects on negatively charged species.

Arresting hydration after a certain curing time is a standard practice in cement science to ensure consistent testing. In the leaching test, this study found that if a sample is not rehydrated prior to testing there is more soluble material present at the beginning of the test, and the desired current density is reached in a shorter time. If a cement sample cannot simply be tested without being dried to arrest its hydration, rehydration appears to be better than testing it dry as whilst it does decrease the initial leaching of Na and K, the leaching of Si is increased compared with a dry sample (whose leaching has more of an impact on the cement matrix than Na and K). Increasing the current density increases the amount of material leached as predicted but this was not a one to one increase.

In the first 22 hours of electrical leaching, the concentration of each element increased in all tanks. When tested for a longer time, however, as seen in the 14-day leaching test, the concentration of Al was seen to decrease in the anode tank. The decrease in the concentration of Al appears to be a pH effect as the speciation of Al is pH dependent. If the dramatic increase in sulphur concentration in the anode tank was caused by the electric current one would expect the concentration after 3 days to be significantly higher than the static test was at that point in time. Since it had a similar concentration to the static test after 3 days and at 14 days was 6.8 times the amount, this increase is most likely to be an acidic effect. In the first 22 hours of the electrical leaching test Mg preferentially leached into the cathode tank. After 3 days of electrical leaching, however, Mg had a lower concentration than in the static leaching test. The cause of this is likely that the solubility of Mg is suppressed at a high pH, such as the high pH that develops in the cathode tank of the electrical leaching test. There is more monocarbonate and less hemicarbonate observed in the electric test than the static test, which suggests an increased reaction with carbon dioxide due to increased porosity.

Based on the results of this Chapter, there are several findings which affect the interpretation of previous literature written on electrical leaching. When reporting the acceleration of leaching in the past, as for example in Otsuki et al.'s calculation of the diffusion conversion time [37], authors have studied or stated the acceleration of Ca only, and have either assumed other elements to have the same acceleration, or not reported that data [7], [36]. In the past, it has been assumed that if the leaching of Ca is increased by a certain amount, the degradation of the entire cement sample, i.e. the leaching of all other elements, is increased by the same amount [36], [37]. This project has proven that this is not the case. Even though the key element of interest when examining the degradation of cement through leaching is the leaching of Ca [1], one element alone should not be used to calculate the total acceleration of leaching, as each element shows a different LAF (see Figure 5.34). However, the full impact of this finding is not known at this time, and requires further study to verify.

Another potentially problematic historical technique has been to embed the anode within the cement sample during the sample's production [7], [36], [37]. The impact of this technique on the cement surrounding the anode is not known, although the current project has shown the impact of an external anode on the leaching of cement, and shows an increase in the leaching of anions such as Si towards the anode tank. Testing the effects of an internal anode on the surrounding cement needs to be studied, in order to compare whether an internal or external anode is preferable.

My results show that, in the electrical leaching tests presented here, Ca leached 19.3 ± 1.9 times more than in the static leaching tests performed for the same time. From these results, it can be concluded that electrical leaching is a good test to accelerate the degradation of

cement samples which contain high amounts of Ca. This is due to both the large increase in the amount of Ca that is leached into the cathode tank compared with static leaching, and the fact that the samples originally contain a large amount of Ca (see Table 3.4). Other elements showed a significantly lower LAF (Figure 5.34). It can be argued that if the experiments had been conducted using cements containing low amounts of Ca, the conclusion might have been that electrically accelerated leaching does not accelerate the leaching to a large extent. Therefore, electrically accelerated leaching may not be a suitable technique to use for cement samples containing low amounts of Ca, such as metakaolin-based geopolymers or alkali-activated cements, depending on their chemical compositions [38], [39]. Research would need to be conducted to see whether electrically accelerated leaching is an effective technique to use for these different cement types.

5.9 References

[1] B. Lagerblad, "TR-01-27, Leaching performance of concrete based on studies of samples from old concrete constructions," *TR-01-27*, 2001. [Online]. Available: http://www.skb.com/publication/18731/TR-01-27.pdf. [Accessed: 17-Jun-2017].

[2] M. I. Ojovan and W. E. Lee, *An Introduction to Nuclear Waste Immobilisation*, First Edit. Kidlington, Oxford, England: Elsevier, 2005.

[3] E. Revertegat, C. Richet, and P. Gegout, "Effect of pH on the durability of cement pastes," *Cem. Concr. Res.*, vol. 22, no. 2–3, pp. 259–272, 1992.

[4] M. I. Ojovan, *Handbook of advanced radioactive waste conditioning technologies*. Philadelphia: Woodhead Publishing Limited, 2011.

[5] H. Saito, S. Nakane, S. Ikari, and A. Fujiwara, "Preliminary experimental study on the deterioration of cementitious materials by an acceleration method," *Nucl. Eng. Des.*, vol. 138, no. 2, pp. 151–155, 1992.

[6] H. Saito and A. Deguchi, "Leaching tests on different mortars using accelerated electrochemical method," *Cem. Concr. Res.*, vol. 30, pp. 1815–1825, 2000.

[7] K. Hashimoto, N. Otsuki, T. Saito, and Y. H, "Application of electrical treatment to alteration of cementitious material due to leaching," *J. Adv. Concr. Technol.*, vol. 11, no. 3, pp. 108–118, 2013.

[8] A. J. Parker, C. Boxall, and M. J. Joyce, "An evaluation of electrokinetic transport of radioactive species through concrete for application as a non-destructive in situ remediation technique - 14102," in *WM2014 Conference*, 2014, pp. 1–13.

[9] A. J. Parker, M. J. Joyce, C. Boxall, and A. J. Parker, "Radiometric detection of non-radioactive caesium flux using displaced naturally abundant potassium," *J. Radioanal. Nucl. Chem.*, pp. 769–776, 2016.

[10] A. J. Parker, M. J. Joyce, and C. Boxall, "A radioanalytical phantom for assessing the efficacy of electrokinetic decontamination of entrained radioactivity within concrete media," *J. Radioanal. Nucl. Chem.*, pp. 769–777, 2014.

[11] M. Castellote, C. Andrade, and C. Alonso, "Nondestructive decontamination of mortar and concrete by electro-kinetic methods: application to the extraction of radioactive heavy metals," *Environ. Sci. Technol.*, vol. 36, pp. 2256–2261, 2002.

[12] T. Banba, J. Matsumoto, and S. Muraoka, "Leaching behaviour of carbon-14 contained in portland cement," *Cem. Concr. Res.*, vol. 22, pp. 381–386, 1992.

[13] P. Patnaik, *Handbook of Inorganic Chemicals*. New York: McGraw-Hill, 2002.

[14] R. Pandya, "Precipitation and processing of solids from high pH, high Si groundwater," University of Washington, 2015.

[15] M. Atkins and F. P. Glasser, "Application of portland cement based materials to radioactive waste immobilization," *Waste Manag.*, vol. 12, pp. 105–131, 1992.

[16] W. Gashier, T. Miura, K. Hashimoto, R. J. Hand, and H. Kinoshita, "Leaching behaviour of cementitious nuclear wasteforms containing caesium and strontium," *Adv. Appl. Ceram.*, vol. 113, no. 8, pp. 447–452, 2014.

[17] P. C. Hewlett, "Lea's Chemistry of Cement and Concrete." Elsevier, 1998.

[18] H. F. W. Taylor, *Cement Chemistry*, 2nd Ed. London: Thomas Telford, 1997.

[19] I. Odler and W. Hinrichs, "Investigation of the hydration of Portland blastfurnace slag cement: hydration kinetics," *Adv. Cem. Res.*, vol. 2, no. 5, pp. 9–13, 1989.

[20] I. Odler, "Investigation of the hydration of portland blastfurnace slag cement: composition, structure and properties of the hydrated material," *Adv. Cem. Res.*, vol. 2, no. 5, pp. 15–20, 1989.

[21] I. G. Richardson, C. R. Wilding, and M. J. Dickson, "The hydration of blastfurnace slag cements," *Adv. Cem. Res.*, vol. 2, no. 8, pp. 147–157, 1989.

[22] C. M. Sangha, "Sulphide content variability in cement pastes containing ground granulated blastfurnace slag," *Cem. Concr. Res.*, vol. 22, pp. 181–185, 1992.

[23] "Atlas of Eh-pH diagrams Intercomparison of thermodynamic databases," Research Center for Deep Geological Environments Naoto TAKENO, 2005.

[24] E. Gruyaert, N. Robeyst, and N. De Belie, "Study of the hydration of Portland cement blended with blast-furnace slag by calorimetry and thermogravimetry," *J. Therm. Anal. Calorim.*, vol. 102, pp. 941–951, 2010.

[25] C. Carde, G. Escadeillas, and R. Francois, "Use of ammonium nitrate solution to simulate and accelerate the leaching of cement pastes due to deionized water," *Mag. Concr. Res.*, vol. 49, no. 181, pp. 295–301, 1997.

[26] D. Rothstein, J. J. Thomas, B. J. Christensen, and H. M. Jennings, "Solubility behavior of Ca-, S-, Al-, and Si-bearing solid phases in Portland cement pore solutions as a function of hydration time," *Cem. Concr. Res.*, vol. 32, pp. 1663–1671, 2002.

[27] N. D. M. Evans, "Binding mechanisms of radionuclides to cement," *Cem. Concr. Res.*, vol. 38, pp. 543–553, 2008.

[28] F. Burriel, F. Lucena, S. Arribas, and J. Hernández, *Química Analítica Cualitativa*. Madrid, 1998.

[29] P. Longuet, "La protection des armatures dans le beton arme elabore avec des ciments de laitier.," *Silic. Ind.*, vol. 41, no. 7/8, pp. 321–328, 1976.

[30] P. C. Hewlett, *Lea's Chemistry of Cement and Concrete*, no. 4th edition. Amsterdam: Elsevier Ltd, 2004.

[31] O. S. Pokrovsky and J. Schott, "Experimental study of brucite dissolution and precipitation in aqueous solutions: Surface speciation and chemical affinity control," *Geochim. Cosmochim. Acta*, vol. 68, no. 1, pp. 31–45, 2004.

[32] M. S. Öncel, A. Muhcu, E. Demirbas, and M. Kobya, "A comparative study of chemical precipitation and electrocoagulation for treatment of coal acid drainage wastewater," *J. Environ. Chem. Eng.*, vol. 1, pp. 989–995, 2013.

[33] R. C. Weast, "CRC Handbook of Chemistry and Physics, 61st Edition." CRC, Boca Raton, Florida, USA, 1980.

[34] B. Lothenbach, G. Le, E. Gallucci, and K. Scrivener, "Influence of limestone on the hydration of Portland cements," *Cem. Concr. Res.*, vol. 38, pp. 848–860, 2008.

[35] W. Gashier, "Accelerated leaching methods for cementitious niuclear waste forms," 2012.

[36] J. Ryu, N. Otsuki, and H. Minagawa, “Long-term forecast of ca Leaching from mortar and associated degeneration,” *Cem. Concr. Res.*, vol. 32, pp. 1539–1544, 2002.

[37] N. Otsuki, H. Minagawa, S. Miyazato, and T. Nishida, “Fundamental study on prediction of concrete deterioration caused by calcium leaching over 100 years,” *Proc. JSCE*, vol. 51, no. 679, 2001.

[38] P. T. Durdzin, M. Ben Haha, S. A. Bernal, N. De Belie, E. Gruyaert, B. Lothenbach, E. M. Mendez, J. L. Provis, A. Scholer, C. Stabler, Z. Tan, Y. V. Zaccardi, A. Vollpracht, F. Winnefeld, M. Zajac, and K. L. Scrivener, “Outcomes of the RILEM round robin on degree of reaction of slag and fly ash in blended cements,” *Mater. Struct.*, vol. 50, no. 135, pp. 1–15, 2017.

[39] W. Mozgawa and J. Deja, “Spectroscopic studies of alkaline activated slag geopolymers,” *J. Mol. Struct.*, vol. 924–926, no. C, pp. 434–441, 2009.

Chapter 6: Simultaneous Electrical Migration of Cs and Ba

6.1 Introduction

The study presented in this Chapter was partly conducted during a research placement at Hokkaido University in Japan. The common method used to investigate the effect of an element on the properties of hardened cement products, such as the phases present in cement and its microstructure, has been to intermix the element with the cement at production, either before mixing the powder with water, or by dissolving the element into the water used to hydrate the cement [1]–[3]. In some cases, however, such an element can be introduced to the cement and interacts with its phases after the cement has hardened, for example in pollution events and during the decay of radioactive waste. The effects of chloride intrusion into cement, for example, and the subsequent corrosion of steel rebar have been widely studied [4]–[7]. As described previously, ^{137}Cs is a problematic radionuclide in ILW with a half-life of 30.08 years [8], [9]. This nuclide ultimately decays into barium (^{137}Ba). This means that, after 150.4 years (5 times its half-life), the amount of Cs in the system decreases to 1/32 ($1/2^5$), transforming 96.875% of the ^{137}Cs present in the wasteform into Ba. The newly formed Ba coupled with the loss of Cs may have a significant impact on the properties of the hardened cement by interacting with the existing phases. This Chapter investigates the behaviour of barium and caesium in 3:1 BFS:PC during electrical leaching, and examines electrical migration of Ba into pre-cured cement as an analogy for the radioactive decay of Cs into Ba that will occur in ILW encapsulated in cementitious grouts. The effects of irradiation on samples is not the focus of this work, so for safety reasons non-radioactive Cs is used in the following experiments. All tests were conducted using 'wet' samples (see Section 5.3).

Initial materials analysis is shown, followed by the analysis of three series of migration experiments. In the first experimental series, the leaching behaviour of Ba out of the cement

matrix is examined. 3:1 BFS:PC samples were produced with barium hydroxide octahydrate ($Ba(OH)_2.8(H_2O)$) and barium nitrate ($Ba(NO_3)_2$) intermixed by dissolving them into the water used to hydrate the cement, with the amount based on the solubility limit of $Ba(OH)_2{\cdot}8(H_2O)$ [10]. As shown in Table 6.1, the sample was formulated to keep the number of Ba^{2+} ions in the sample the same as the number of Cs^+ ions used in the third series (see below), as well as that of NO_3^- in both series (similar to the methodology used in Chapter 4). These samples are referred to as 'Ba-cement' samples, and were then tested using static leaching for 28 days and electric leaching for 14 days at 25 Am^{-2}, the optimal current density used previously in Chapter 5, and solutions analysed via pH measurements and ICP-OES. Samples were analysed using XRD, DTA, TG, DTG, SEM-EDX and MIP, both prior to and after leaching tests.

The second experimental series discusses the introduction of Ba into a hardened cement matrix, and is shown in Figure 5.1. A standard 3:1 BFS:PC sample (see Table 6.1) with dimensions 40x40x5 mm was placed in a migration cell, and Ba was introduced from the anode tank, by dissolving $Ba(OH)_2{\cdot}8(H_2O)$, and applying a current with a density of 25 Am^{-2} for 14 days. Barium ions have a charge of 2+, so when a current is applied, the barium in the anode tank should be attracted towards the cathode tank and enter the cement matrix, potentially interacting with it. 0.32g of $Ba(OH)_2{\cdot}8(H_2O)$ was dissolved into the anode tank, based on the maximum solubility in the water used [10] to hydrate a cement sample of that volume (8 cm^3) as in the above Section. The results are discussed in comparison to the standard electric leaching of 3:1 BFS:PC without Ba introduction, which were described in the previous Chapter. This test is referred to as 'Blank-cement wBa' as a shortened name for Blank-cement sample with Ba (wBa) initially dissolved in the anode tank and exposed to an electric current.

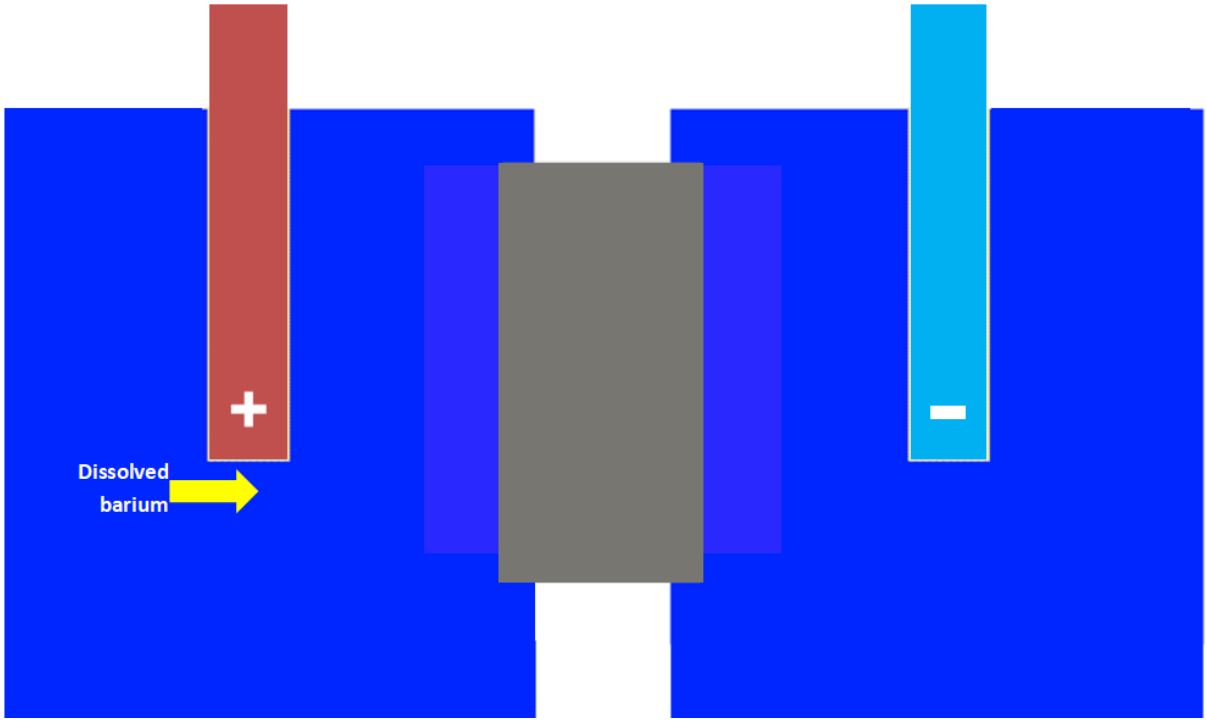

Figure 5.1 In the second experimental series, barium is dissolved into the water poured in the anode tank.

In the last experimental series, the interaction of $CsNO_3$ intermixed with 3:1 BFS:PC samples is investigated, and the simultaneous migration of Cs and Ba are examined. A diagram of this experiment is shown in Figure 6.2. The amount of Cs^+ was chosen based on the amount of Ba^{2+} used in the samples of the previous series. The number of NO_3^- in the samples was also kept constant in both series as listed in Table 6.1. After adding the $CsNO_3$ to the water to be used to hydrate the cement, the pH of the water was not altered to a large extent (from 6.28 to 6.78 ± 0.1 shown in Table 6.1), although the conductivity was raised by a large amount. The amount of $CsNO_3$ used is below the precipitation limit identified in Chapter 4.

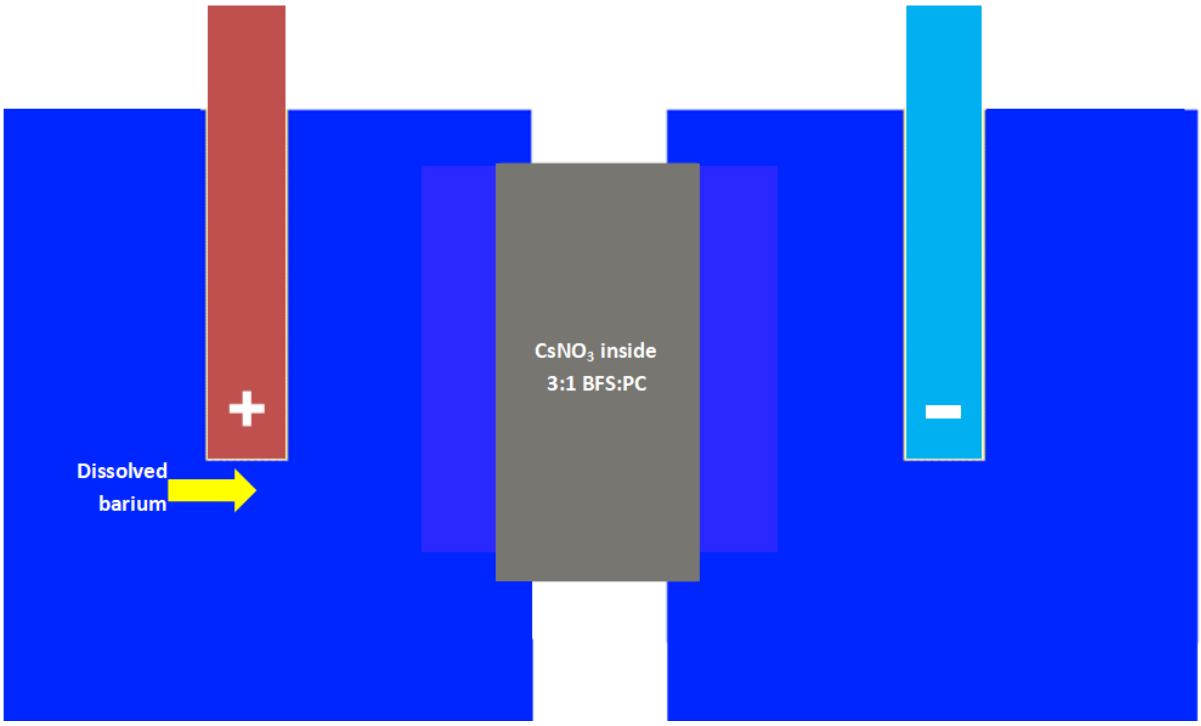

Figure 6.2 In the final experimental series, barium is dissolved into the water poured in the anode tank and 3:1 BFS:PC containing $CsNO_3$ is used.

Samples with this cement composition were produced for three comparative leaching experiments: One sample was tested using static leaching for 28 days, and a second sample was tested using electrical leaching (with no addition to the leachate in the anode tank) for 14 days with a current density of 25 Am^{-2}. A third sample was tested in a 14-day electrical leaching test with $Ba(OH)_2{\cdot}8(H_2O)$ dissolved into the anode tank, in a similar way to Section 6.4 of this Chapter. The cement samples were tested both prior and after the tests as described previously, and the solutions were also analysed via pH measurements and ICP-OES. The simultaneous migration of Cs and Ba was then investigated under electric potential, where the concentration of Cs in the cement system was decreased while that of Ba increased at the same time.

Table 6.1 Cement formulations produced for this Chapter

Formulation name	PC (g)	BFS (g)	H_2O (g)	w/b ratio	$CsNO_3$ (g)	$Ba(OH)_2 \cdot 8H_2O$ (g)	$Ba(NO_3)_2$ (g)	Hydration solution	
								pH	Conductivity (mS/cm)
Blank-cement	200	600	136	0.34	–	–	–	6.28	2.1
Ba-cement	200	600	136	0.34	–	7.60	6.34	13.54	6.00×10^4
Cs-cement	200	600	136	0.34	9.41	–	–	6.78	1.93×10^4

6.2 Preliminary Testing - Cement Formulations and Unleached Samples

The three different cement systems utilised in this Chapter are: 3:1 BFS:PC, 3:1 BFS:PC with $Ba(OH)_2 \cdot 8(H_2O)$ and $Ba(NO_3)_2$, and 3:1 BFS:PC with $CsNO_3$, each with a w/b ratio of 0.34 and with 28 days of curing. The XRD patterns of these cement samples before the leaching tests are displayed in Figure 6.3. The labelling of the XRD data is explained in Table 4.2 with PDF number as references. The XRD pattern of the 3:1 BFS:PC sample with no additional waste components, referred to as 'Blank-cement', which was discussed in Chapter 5, is shown here for comparison purposes. The Ba-cement system displayed barite (labelled B in the figure) after 28 days of curing (as expected from the data presented in Chapter 4) and had little ettringite, unlike the Blank sample. It also seems to have a larger hydrogarnet peak at 39.2° 2θ than the Blank cement sample, which is in agreement with the Ba-cement samples discussed in Chapter 4. The peak attributable to hemicarbonate at 11.45° 2θ was less distinct than for the Blank sample. For the 3:1 BFS:PC system with $CsNO_3$ (Cs-cement), the crystalline phases observed are the same as in the Blank cement system as the amount of $CsNO_3$ added was below the precipitation limit of 2.8 wt.% identified in Chapter 4. In this sample there is 0.995 wt.% $CsNO_3$.

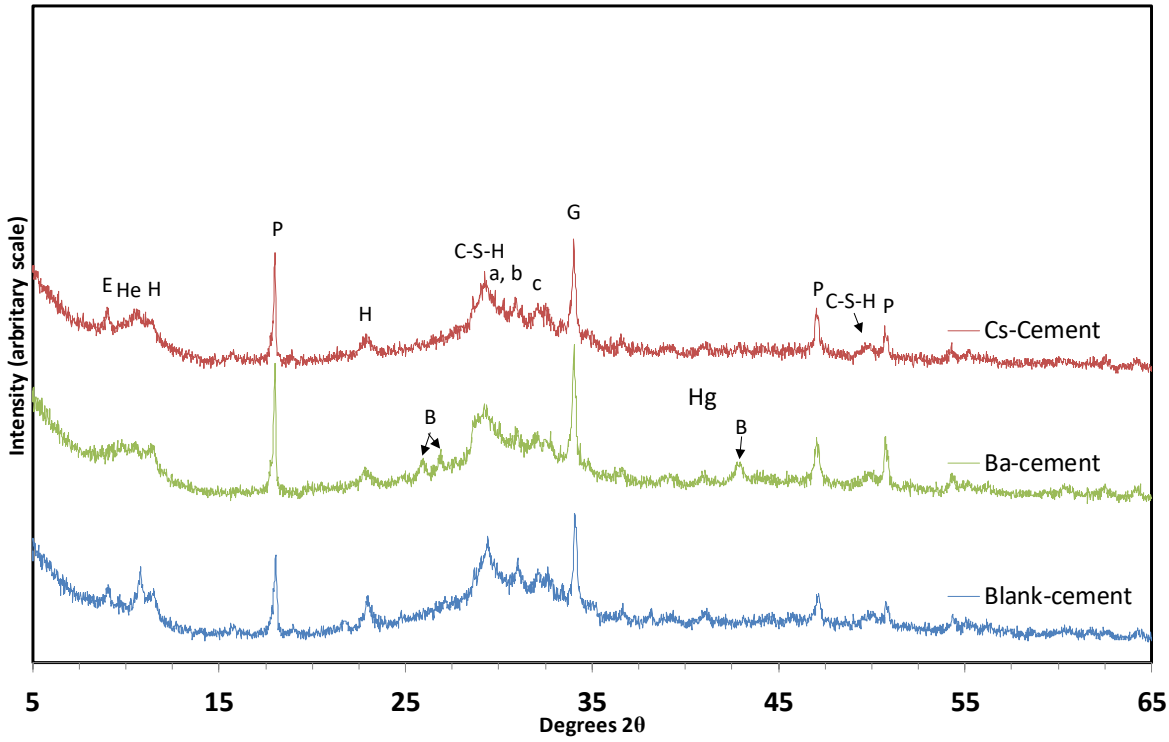

Figure 6.3 XRD patterns of the different cement formulations used in this Chapter

6.3 Electrical and Static leaching of 3:1 BFS:PC Ba-cement samples

As the results of Chapter 5 show, electrical leaching is a valid technique to accelerate the leaching of cement. The following set of experiments was conducted to investigate how the leaching behaviour of cement is altered when barium, a nuclear decay product, is intermixed during cement production, as an increased content of barium would be present in an actual ILW wasteform. Static and electrical leaching experiments were conducted using samples of 3:1 BFS:PC containing barium (Ba-cement samples): a 14-day electrical leaching test at 25 Am^{-2} and a 28-day static leaching test, with the data from an unleached Ba-cement sample also shown where appropriate. As shown in Table 6.1, the pH of the hydration solution was 13.54 ±0.3, which likely accelerated the hydration reaction due to the possibility for alkali-activation in slag-based cements [11]. The voltage data for the electrical leaching of the barium containing cement formulation are shown in Figure 6.4. This behaviour is similar to the

voltage of the Blank cement also shown, and shows a decrease over time – in this experiment the voltage drops to 141 volts after 14 days.

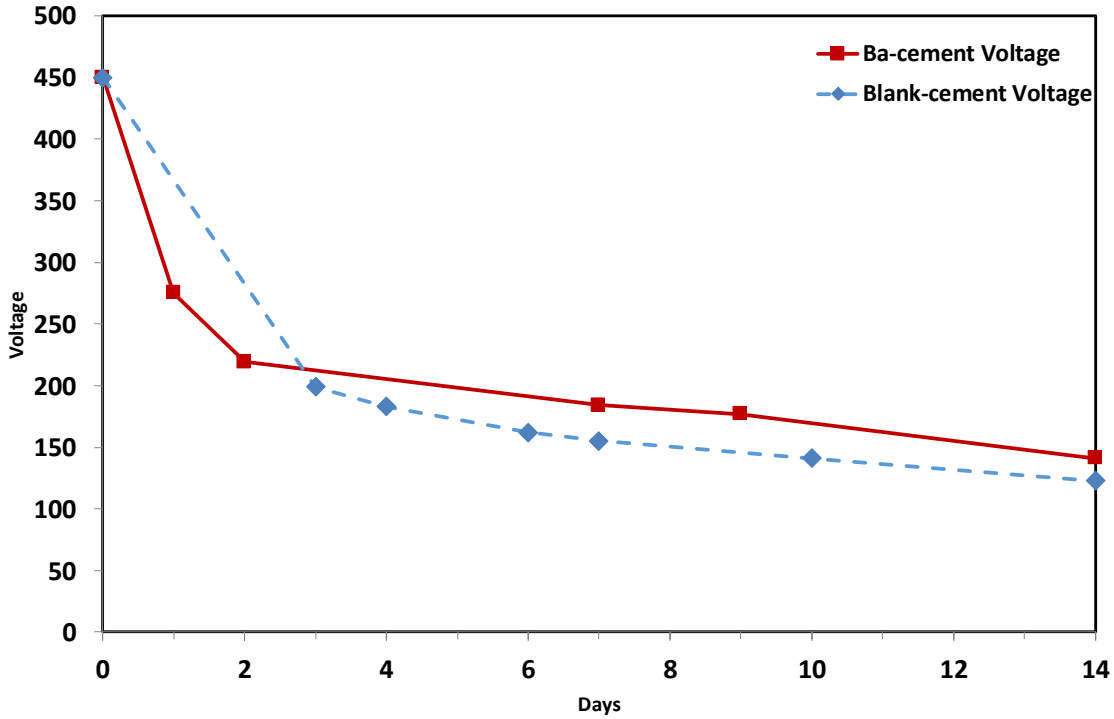

Figure 6.4 Voltage between the electrodes over the Ba-cement electrical leaching tests. Data from the electrical leaching test of the Blank-cement without inclusion of Ba (originally shown in Figure 5.22) are also shown for comparison.

6.3.1 Microstructural Analysis of the Ba-cement samples

The BSE images and SEM-EDX maps of an unleached Ba-cement sample are shown in Figure 6.5. Some cracks are visible, with areas of higher Ba concentration matching with some of the areas of higher sulphur concentration. The areas with a lighter appearance in the higher resolution BSE image have distinctly more Ca and Al than the surrounding cement matrix and thus are likely unhydrated BFS particles. The BSE images at different resolutions of a Ba-cement sample after the static leaching test are shown in Figure 6.6, with SEM-EDX maps of the higher resolution image. The barium and sulphur are difficult to distinguish from the background, unlike the other elements which show a clear surface boundary. In the static test, there is no obvious boundary in the sample as the exposure surface is approached where the elemental concentration decreases (i.e. a visible dissolution front is not seen), other than a possible slight reduction in Ca concentration. No obvious change was observed in these images compared with the data of the unleached sample shown in Figure 6.5, except for the already mentioned possible reduction in Ca concentration near exposure surface.

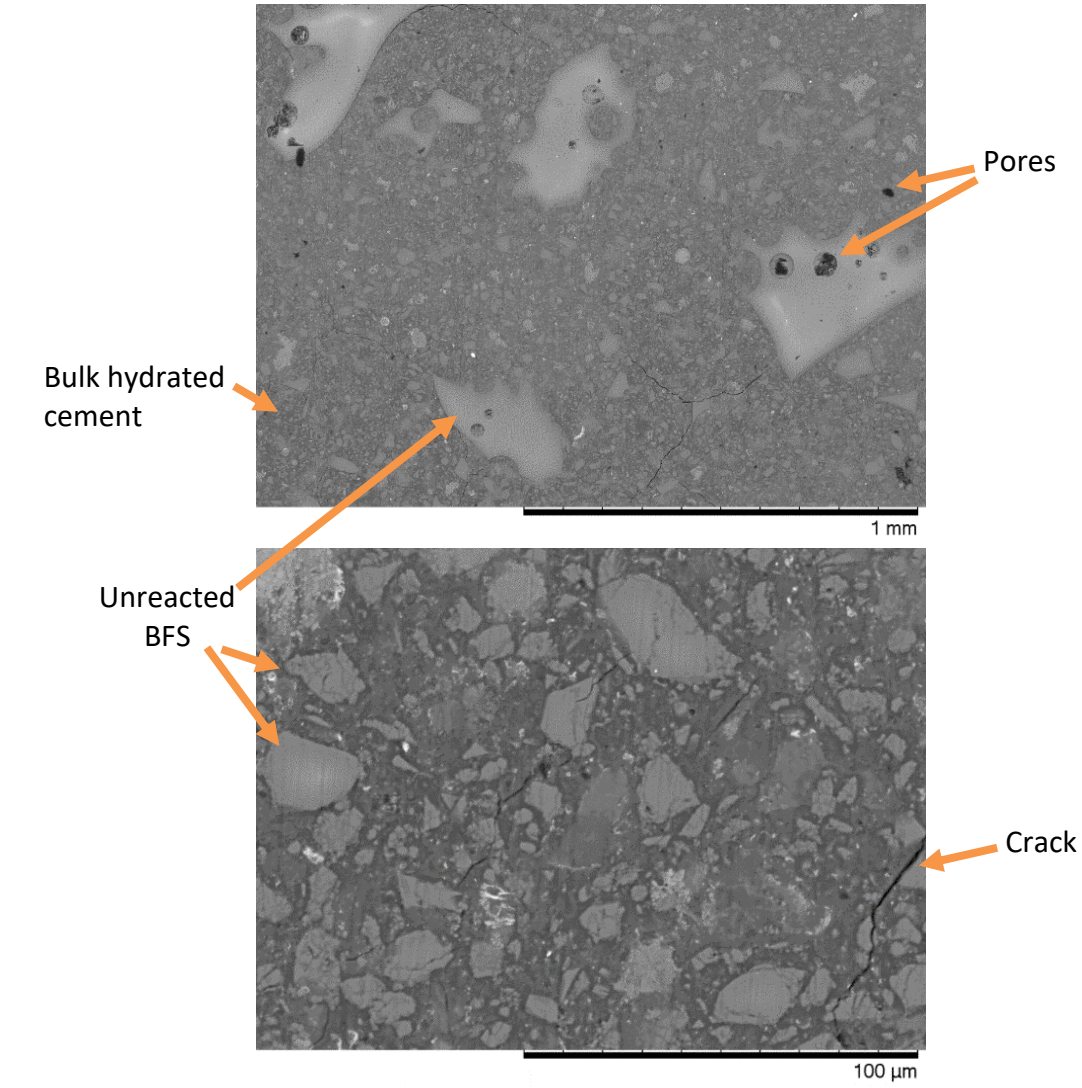

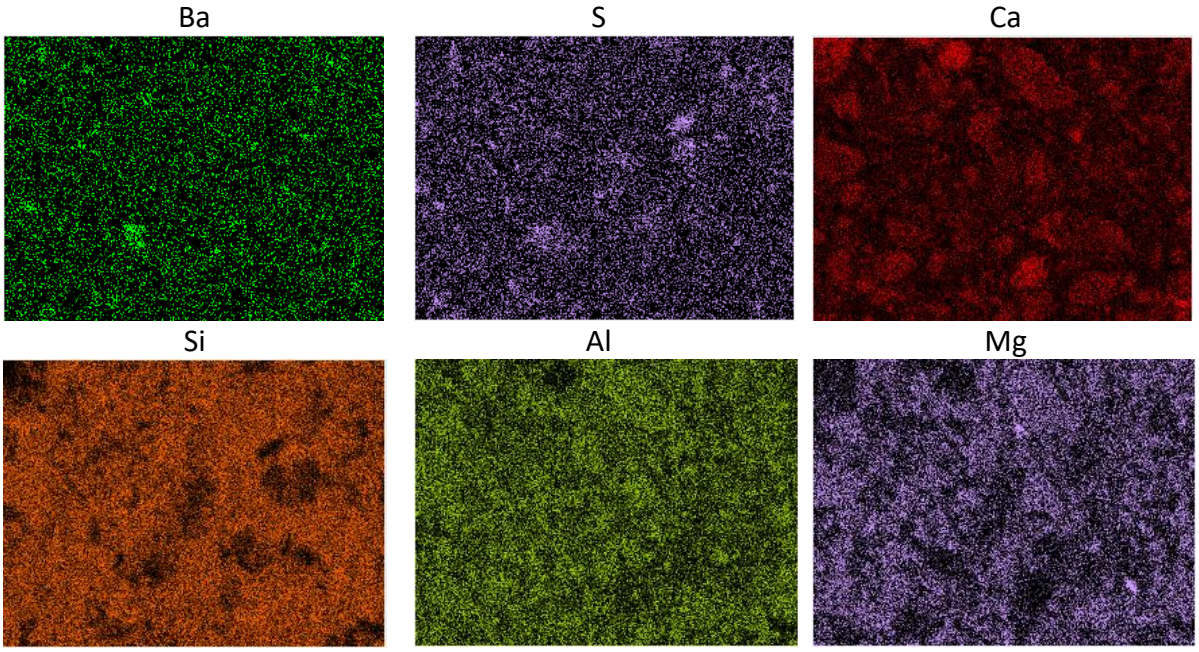

Figure 6.5 BSE images at low and high magnification and SEM-EDX elemental maps of the latter, for unleached 3:1 BFS:PC Ba-cement

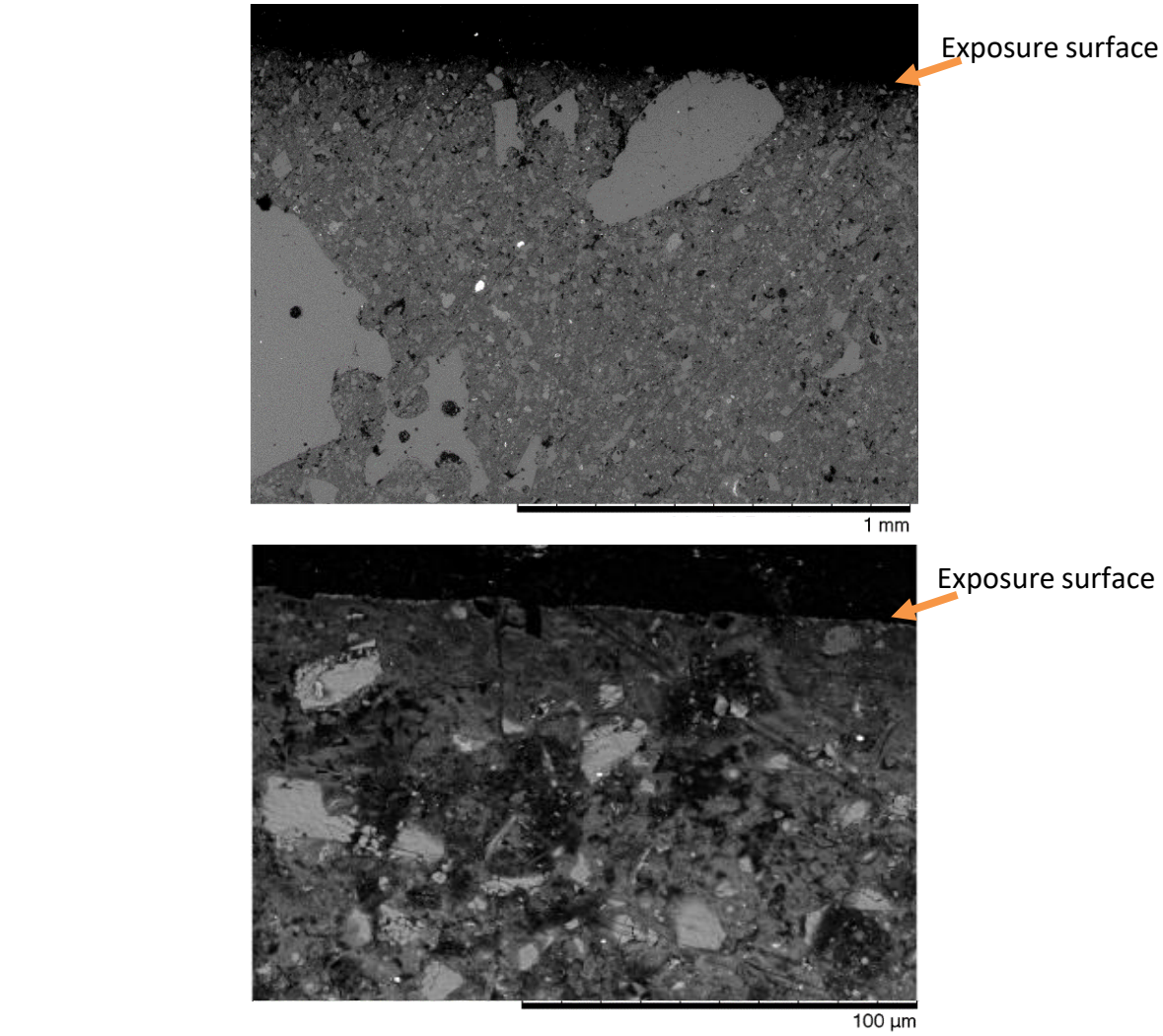

Figure 6.6 BSE images at low and high magnification, and SEM-EDX elemental maps of the latter, for 3:1 BFS:PC Ba-cement after a static leaching test

The BSE images and SEM-EDX maps of the side of the cement exposed to the cathode (i.e. the cathode side) of a Ba-cement sample after the electrical leaching test are shown in Figure 6.7. The cathode side shows a clear region of degradation, which has a similar depth to the cathode side of the other electrical leaching tests as shown in Figure 5.46, with a reduction of Ca concentration in the near-surface region. Ba in the cement sample is difficult to distinguish from the background, although the regions corresponding to the white dots in the BSE image have a higher concentration of Ba. Mg, likely in the form of crystallised brucite [12], [13], seems to show a higher concentration closer to the surface.

The BSE image of the anode side depicted in Figure 6.8 shows a clear crack in the low magnification image – it is unclear whether this crack was created during the leaching process or during sample preparation before the test, but since such sizeable cracks were not observed in the other leached samples, it was most likely the latter. The SEM-EDX mapping also shown in Figure 6.8 shows a clear region of degradation in the Al map, and in the Si map to a lesser extent. As shown in the previous Chapter, in electrical leaching tests Al and Si leach more strongly into the anode tank than into the cathode tank, so this is not unexpected.

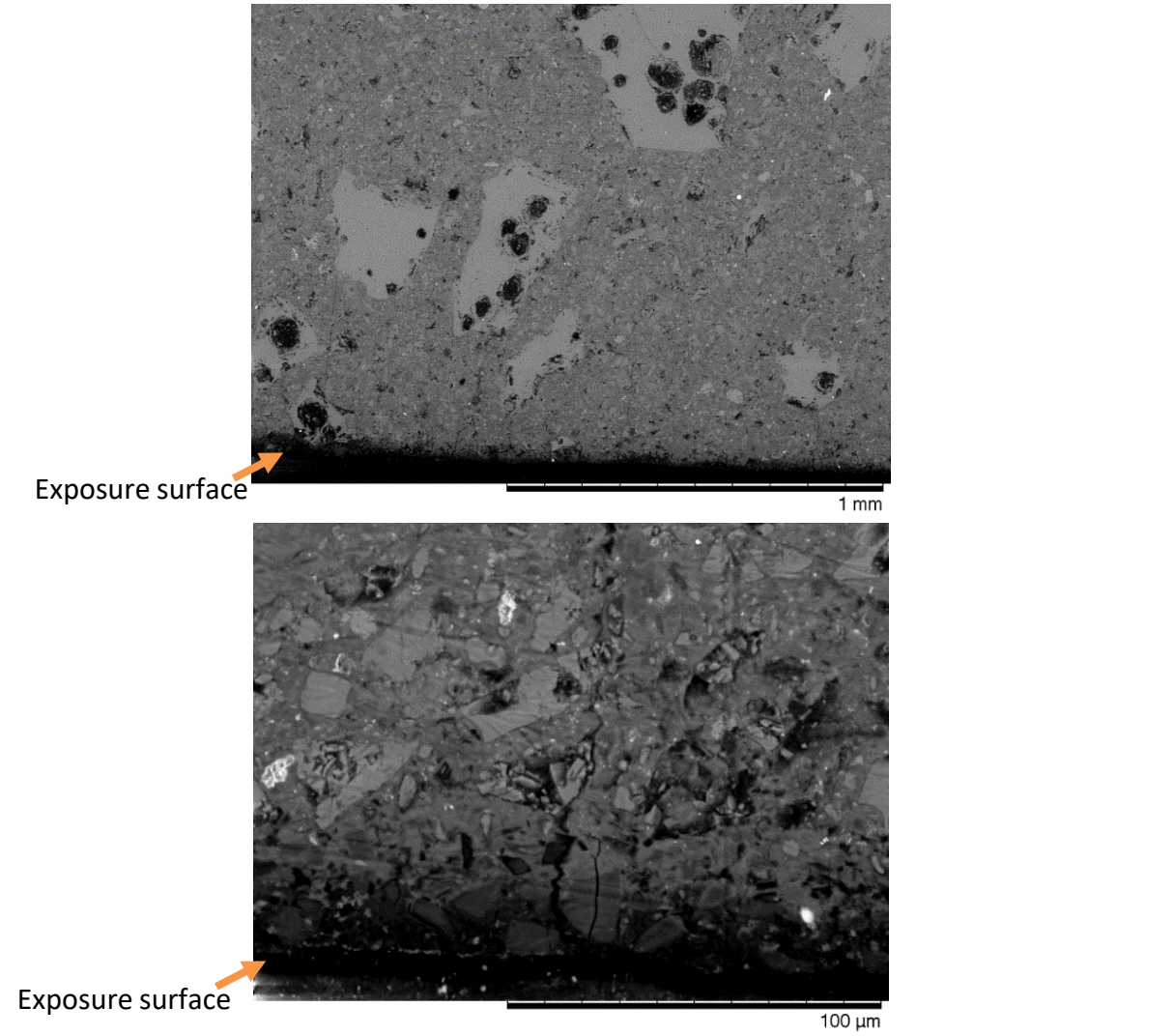

Figure 6.7 BSE images at low and high magnification and SEM-EDX elemental maps of the latter, for the cathode side of 3:1 BFS:PC Ba-cement sample after an electric leaching test

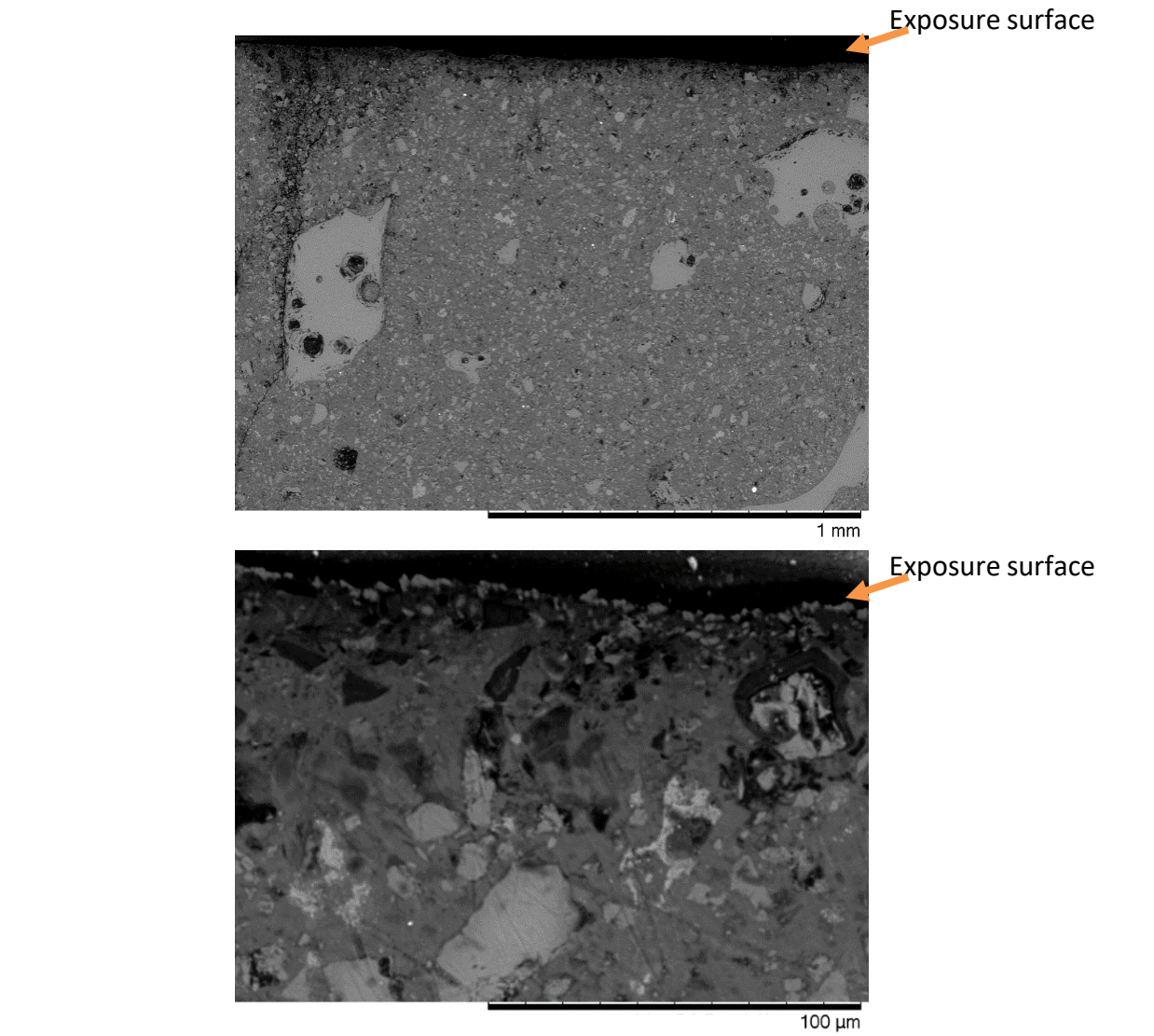

Figure 6.8 BSE images at low and high magnification, and SEM-EDX elemental maps of the latter, for the anode side of 3:1 BFS:PC Ba-cement sample after an electric leaching test

The porosity data and pore size distribution of the Ba-cement samples are shown in Figure 6.9 and Figure 6.10 respectively. There is an increase in porosity observed in the Ba-cement samples compared with the Blank-cement samples shown previously (Section 5.6.4). The unleached Ba-cement sample had a porosity of 23.7%, the largest porosity out of all cement samples tested in this thesis and larger than the unleached Blank-cement sample (18.5%). The increase in porosity is likely due to a decreased volume of the solid phases within the cement matrix. The intermixed barium reacts with ettringite, which most likely produces barite, hydrogarnet, portlandite and excess water [14] (see Equation 6.1). The resulting solid product phases take up only 35.7% of the volume of the initial ettringite. As the $Ba(OH)_2{\cdot}8(H_2O)$ is dissolved, ettringite is the only solid reactant and therefore the loss of volume due to this reaction leaves an empty space which might account for the increase in porosity. The volume change was calculated using data shown in Table 6.2. The statically and electrically leached samples had the same porosities of 18.5%. For each sample the majority of the pores were in the 5-50nm range, although the unleached sample displayed more porosity in the 6-2mm range accounting for its larger overall porosity.

$$Ca_6Al_2(SO_4)_3(OH)_{12} \cdot 26H_2O + 3\big(BaOH \cdot 8(H_2O)\big) = 3(BaO(SO_3)) + (\mathrm{CaO})_3(Al_2O_3)6H_2O + 3((\mathrm{CaO})(H_2O)) + 48H_2O$$

Equation 6.1

Table 6.2 Densities and molar volumes of various molecules

Compound	name	Formula	Molar volume (cm^3/mol)	Density (Kg/m^3)
H	Water	H_2O	55.5 [15]	1000
$C_3A{\cdot}3C\bar{S}{\cdot}32H$	ettringite	$Ca_6Al_2(SO_4)_3(OH)_{12}{\cdot}26H_2O$	710.3 [16]	1778 [17]
Barium sulphate	Barite	$BaSO_4$	51.98 [18]	4500 [19]
C_3AH_6	hydrogarnet	$Ca_3O_3Al_2O_3(H_2O)_6$	6.66 [15]	2530 [17]
CH	portlandite	$Ca(OH)_2$	30.2 [15]	2251 [17]

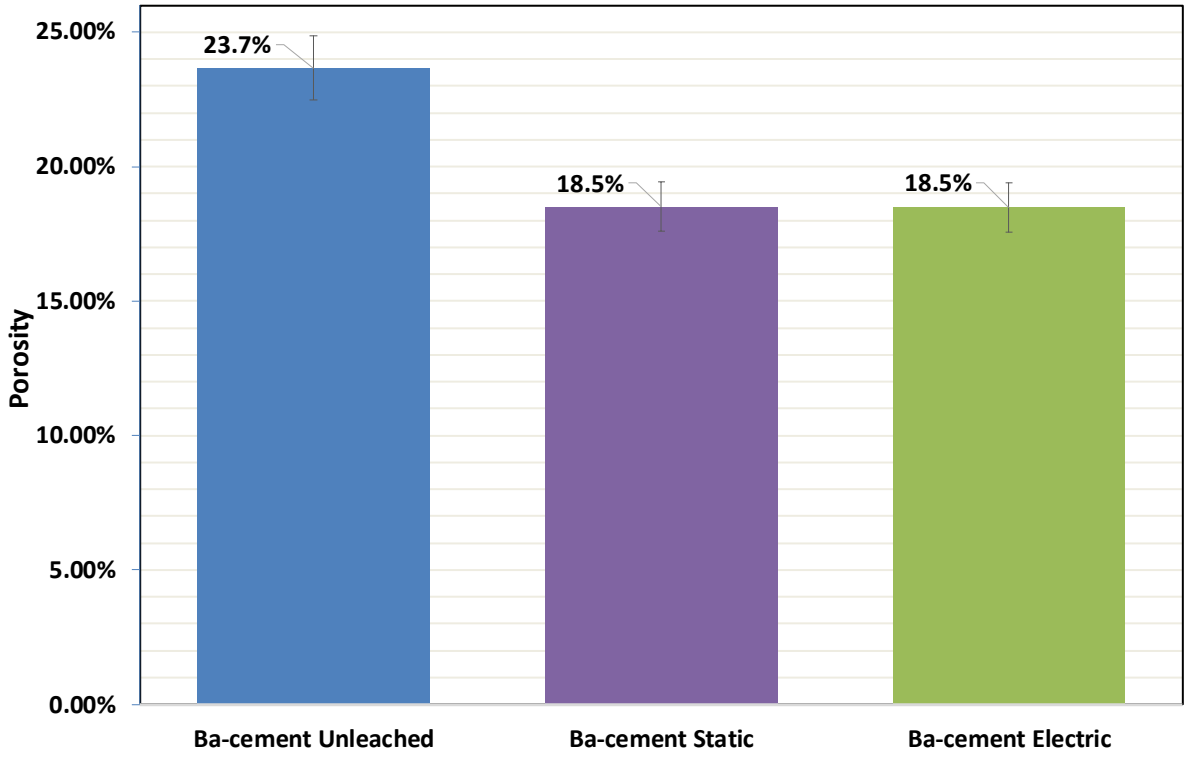

Figure 6.9 Porosity of 3:1 BFS:PC Ba-cement samples

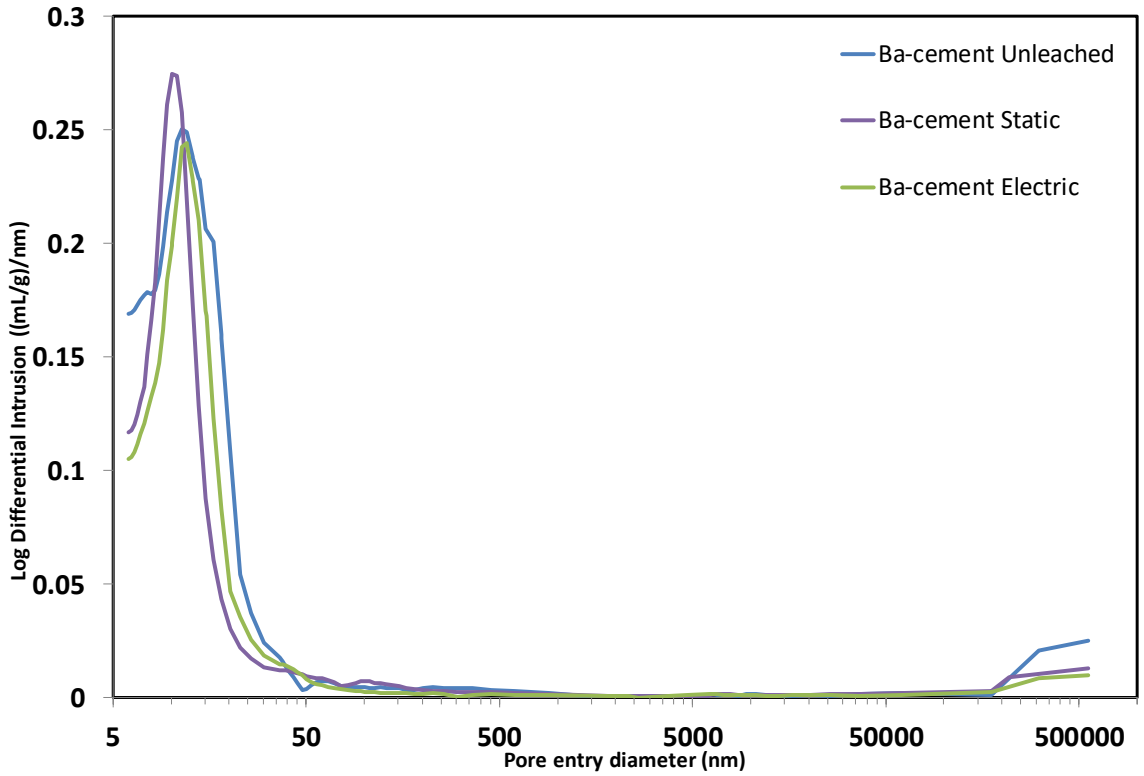

Figure 6.10 Pore size distribution of 3:1 BFS:PC Ba-cement samples before and after leaching

6.3.2 Leachate Analysis from Leaching Tests with Ba-cement samples

The pH data of the static test over 28 days and the electric test are shown in Figure 6.11. The electric leaching test has data at 7 and 14 days only. There is almost no difference between the two tanks in the static test, and the pH level remains stable at 11.5 within error bars. The pH behaviour during the electrical test is similar to the Blank sample shown in Figure 5.24 – the pH of the cathode tank is higher than the static test, and the anode tank is much lower and has a decrease over time.

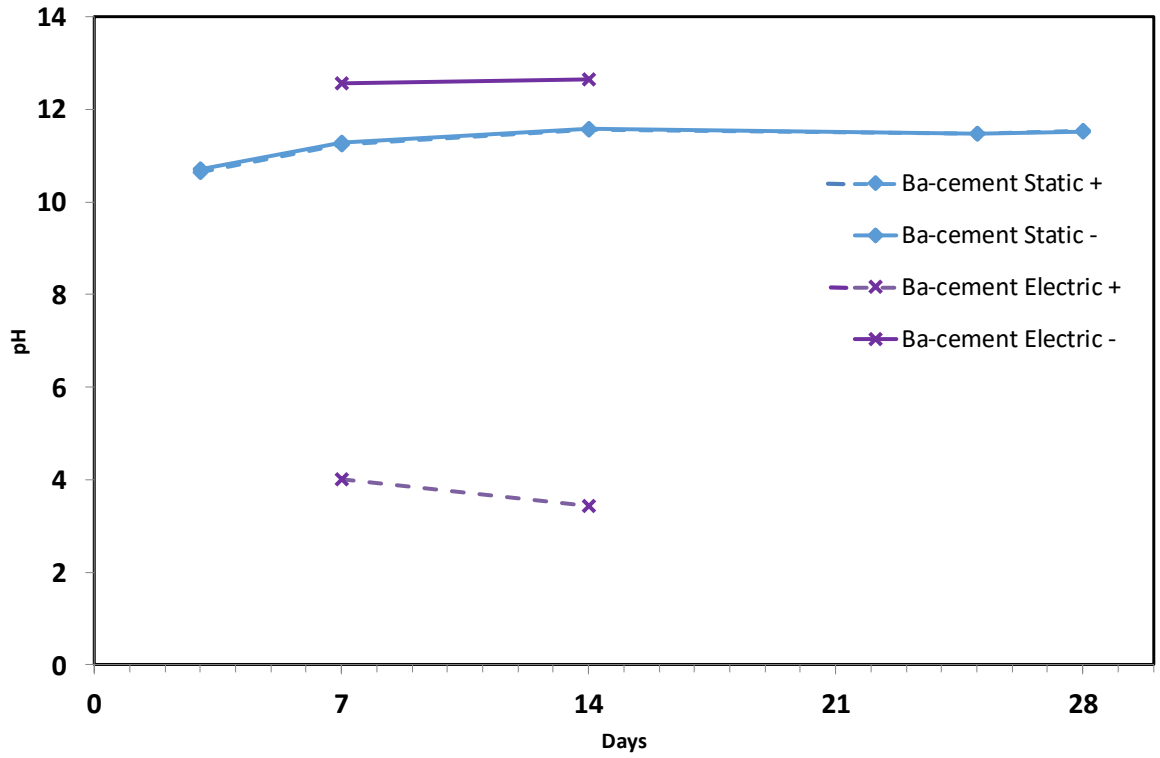

Figure 6.11 pH data of the leachates during static and electrical leaching tests with Ba-cement. The dashed line is the pH of the anolyte and the solid line the catholyte, though in the static test this is for labelling purposes only.

The elemental concentration data of the leachates from the Ba-cement leaching tests are shown in Figure 6.12 to Figure 6.14. The data were gathered by ICP-OES. Other than barium and sulphur, the concentration of elements observed in the tanks are much the same as the static and electrical leaching of the Blank-cement samples shown in Figure 5.25 to 5.34. As barium was intermixed with the cement, more barium is detected in the leachates of both the static and electrical leaching tests of Ba-cement than when Blank-cement was investigated. The leaching of sulphur, however, is significantly reduced compared to the Blank-cement tests. This is likely due to the formation of barium sulphate, as discussed in Chapter 4, which is largely insoluble in water (3.11 mg/L at 20 °C at pH 7) [20]–[22] and thus retains sulphur as a solid in the cement.

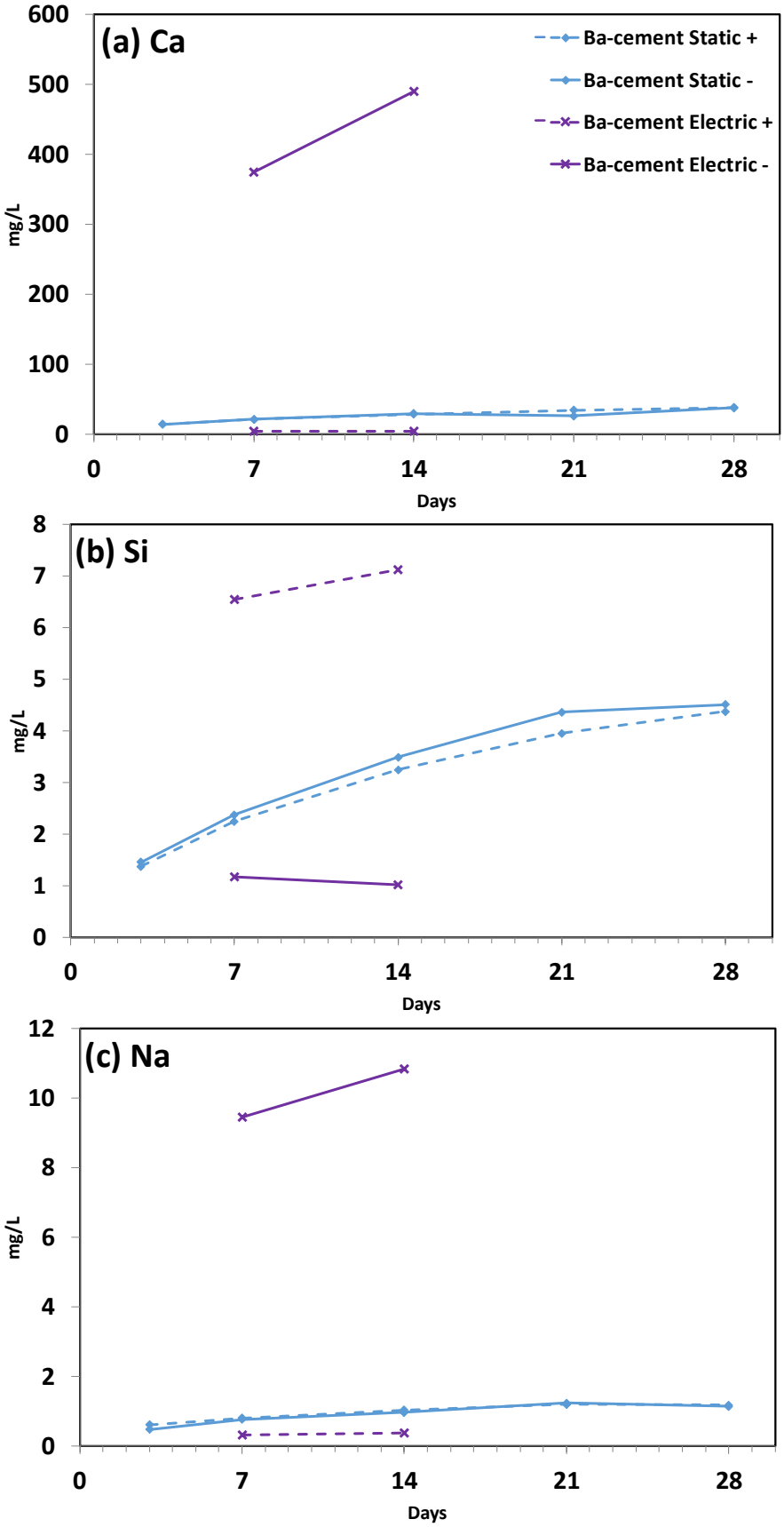

Figure 6.12 Elemental concentrations of (a) Ca, (b) Si and (c) Na in the anode and cathode tanks in the static and electrical leaching tests using Ba-cement. The solid line represents the concentration in the cathode tank, and the dotted line the anode.

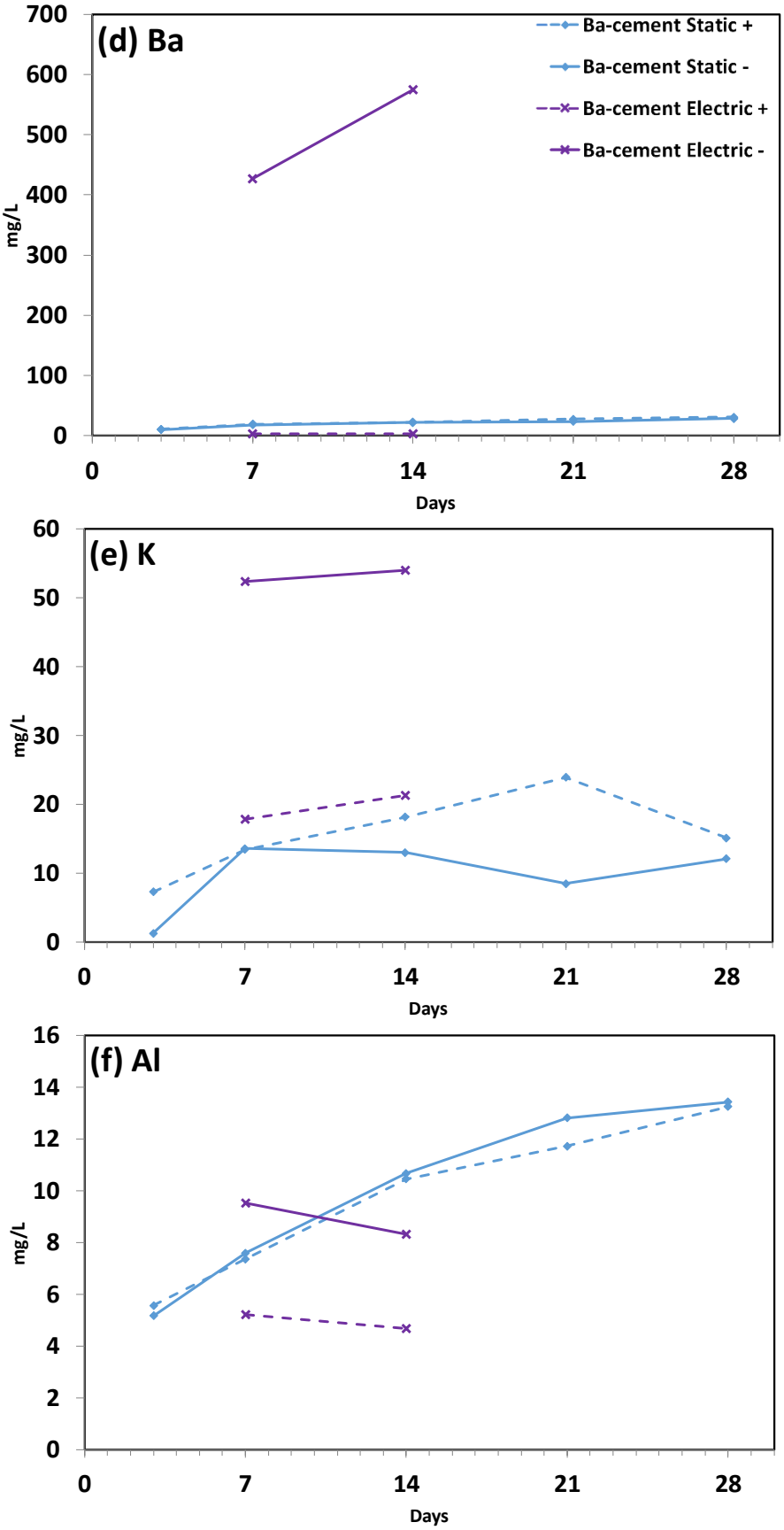

Figure 6.13 Elemental concentrations (d) Ba, (e) K and (f) Al in the anode and cathode tanks in the static and electrical leaching tests using Ba-cement. The solid line represents the concentration in the cathode tank, and the dotted line the anode.

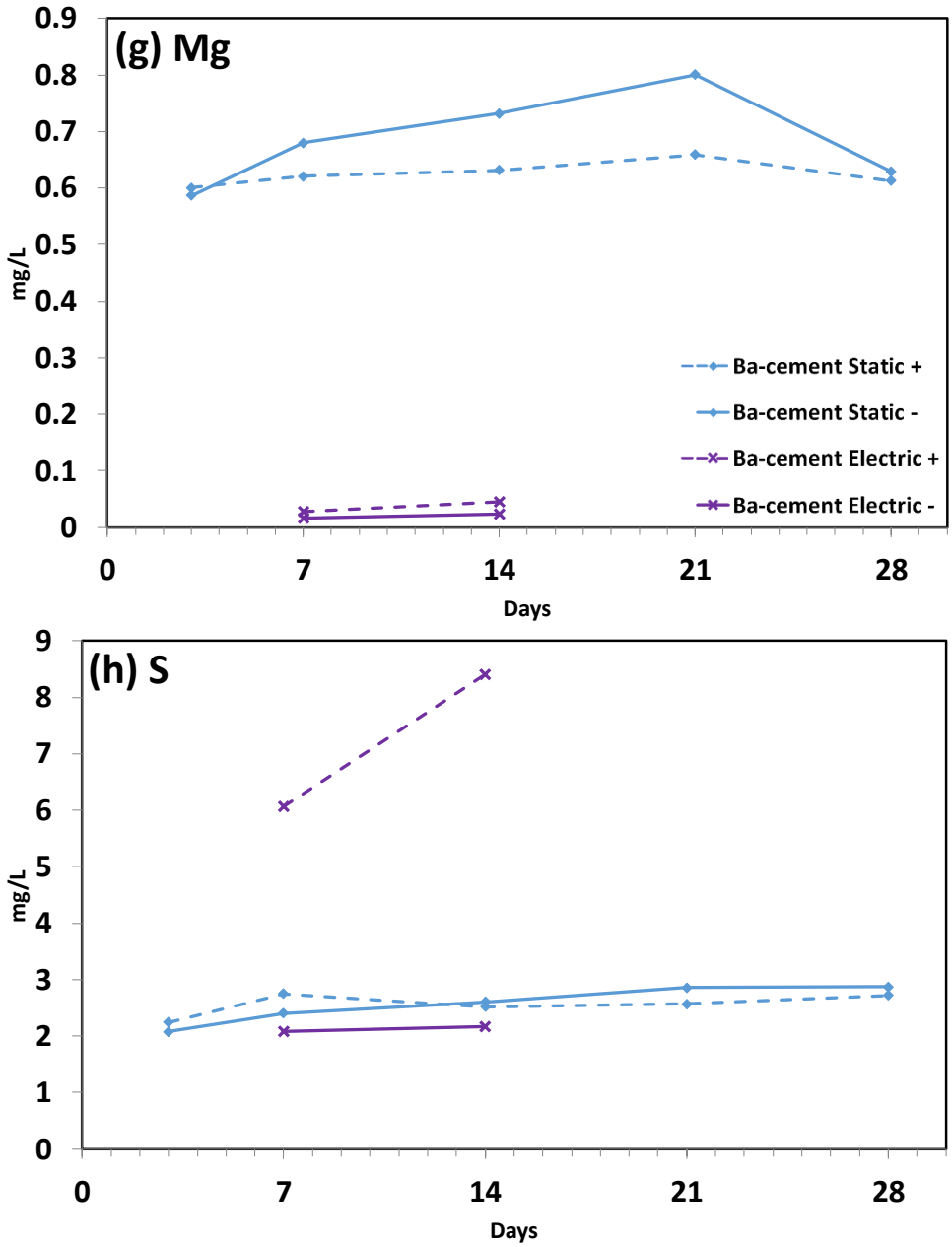

Figure 6.14 Elemental concentrations of (g) Mg and (h) S in the anode and cathode tanks in the static and electrical leaching tests using Ba-cement. The solid line represents the concentration in the cathode tank, and the dotted line the anode.

6.3.3 Phase Analysis of the Ba-cement samples

The XRD data of the Ba-cement samples before and after leaching are shown in Figure 6.15, and another set of XRD scans in the 5 to 15° 2θ range, taken with longer counting time per step, in Figure 6.16. All of the samples displayed clear peaks of barite, and these do not seem to be affected by either static or electrical leaching, likely due to the low solubility of barite [21], [23]. No samples showed peaks for ettringite as shown in Figure 6.16. Ettringite must either have reacted or not formed due to the presence of barium in the cement, as previously discussed [24], [25] and in the analysis in Chapter 4 of this thesis. The gehlenite peak appears to have decreased in the electrical leaching test, but as this is usually an inert phase in the slag, this change may be due to variability between slag grains.

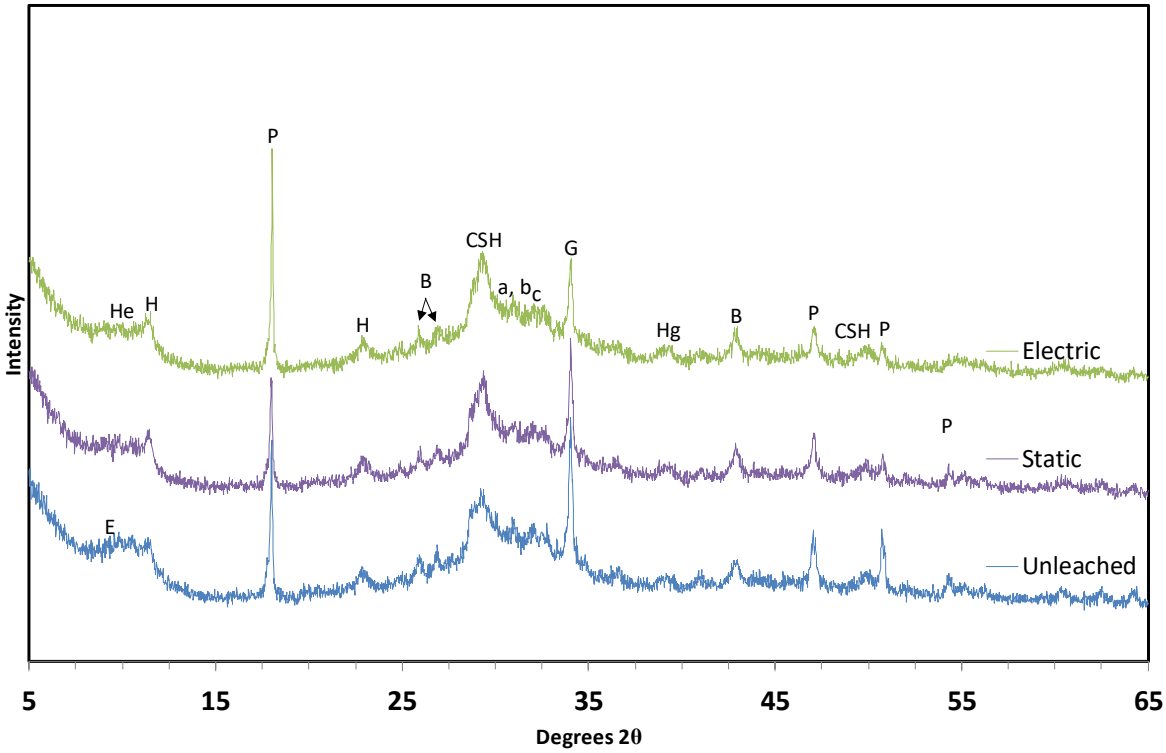

Figure 6.15 XRD of the Ba-cement samples in the range 5 to 65 degrees

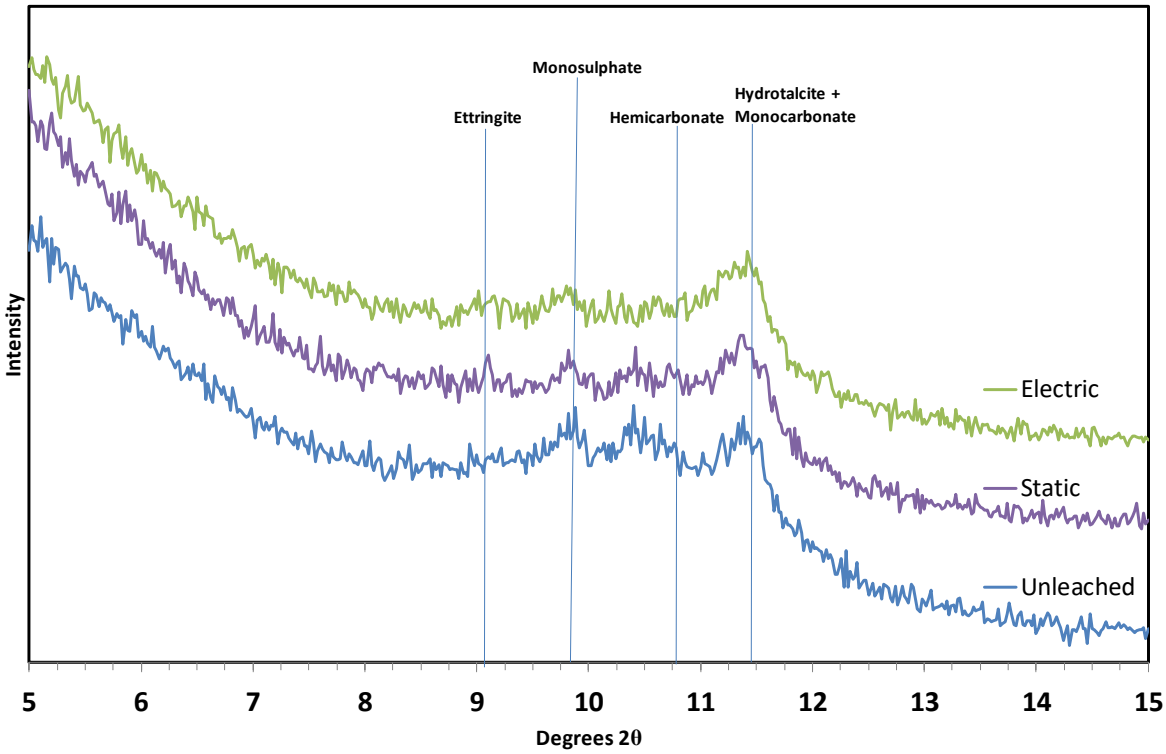

Figure 6.16 XRD of the Ba-cement samples in the range 5 to 15 degrees at a longer counting time per step than the data shown in Figure 6.15

The thermal analysis data for the Ba-cement samples are shown in Figure 6.17 to Figure 6.19, starting with the thermogravimetric analysis and its first derivative and ending with the DTA data. The statically and electrically leached samples showed a similar weight loss in the TG data (Figure 6.17), with the statically leached sample losing slightly more weight, and the majority of the loss occurred below 110°C. The unleached sample showed the least weight loss. The labelled thermal events are shown in Table 6.3.

The statically leached sample was leached for 28 days, and thus, this sample was in contact with water for 14 days longer than the sample from the electrical test. Both the statically leached and electrically leached Ba-cement samples had similarly increased weight loss at temperatures up to 110°C when compared with the unleached Ba-cement sample. The additional weight loss in this temperature range is suggestive of a larger amount of C-S-H

present [26], i.e. additional hydration had occurred in the leached samples. The unleached and statically leached Ba-cement samples contained similar amounts of portlandite, whose dehydroxylation occurs at 450°C. Both of these samples contained more portlandite than the electrically leached sample. Each Ba-cement sample showed evidence of calcite, and the unleached sample had the most. This suggests that the unleached sample had more exposure to atmospheric carbon, most likely during preparation. The DTA data shown in Figure 6.19 support the observations from the TG data.

Table 6.3 Cement components and their corresponding thermal events

Label	Component	Formula	Temperature range °C	Source
Free water	H_2O	H_2O	100	-
C-S-H	C-S-H	C-S-H	110-120 decomposition	[26]
ettringite	ettringite	$Ca_6Al_2(SO_4)_3(OH)_{12}\cdot 26H_2O$	100-120 decomposition	[14]
monocarbonate		$Ca_3Al_2O_6\cdot CaCO_3\cdot 11(H_2O)$	150	[27]
monosulphate	AFm	$Ca_4Al_2(SO_4)(OH)_{12}\cdot(H_2O)_6$	180-200	[26]
P	portlandite	$Ca(OH)_2$	450	[26]
B	Barium sulphate	$BaSO_4$	1580 (beyond apparatus capabilities)	[23]
bh8	barium hydroxide octahydrate	$Ba(OH)_2\cdot 8H_2O$	78	[10]

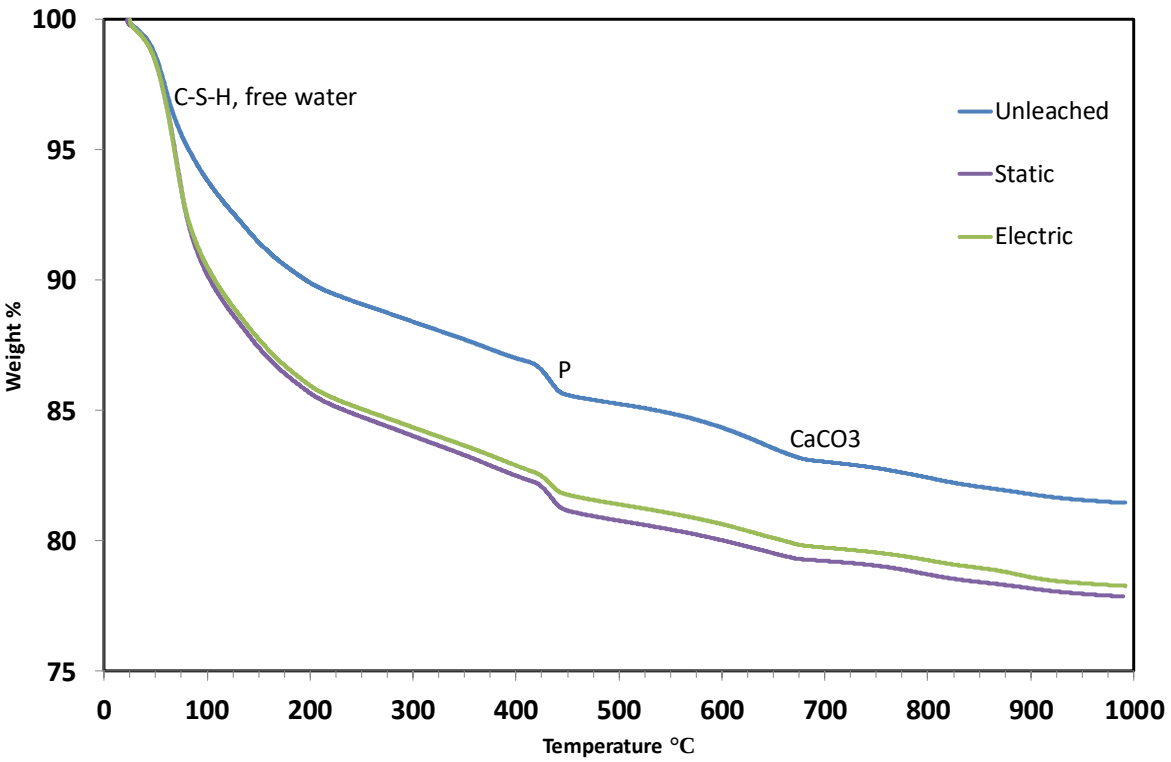

Figure 6.17 Thermogravimetric Analysis of the 3:1 BFS:PC Ba-cement samples

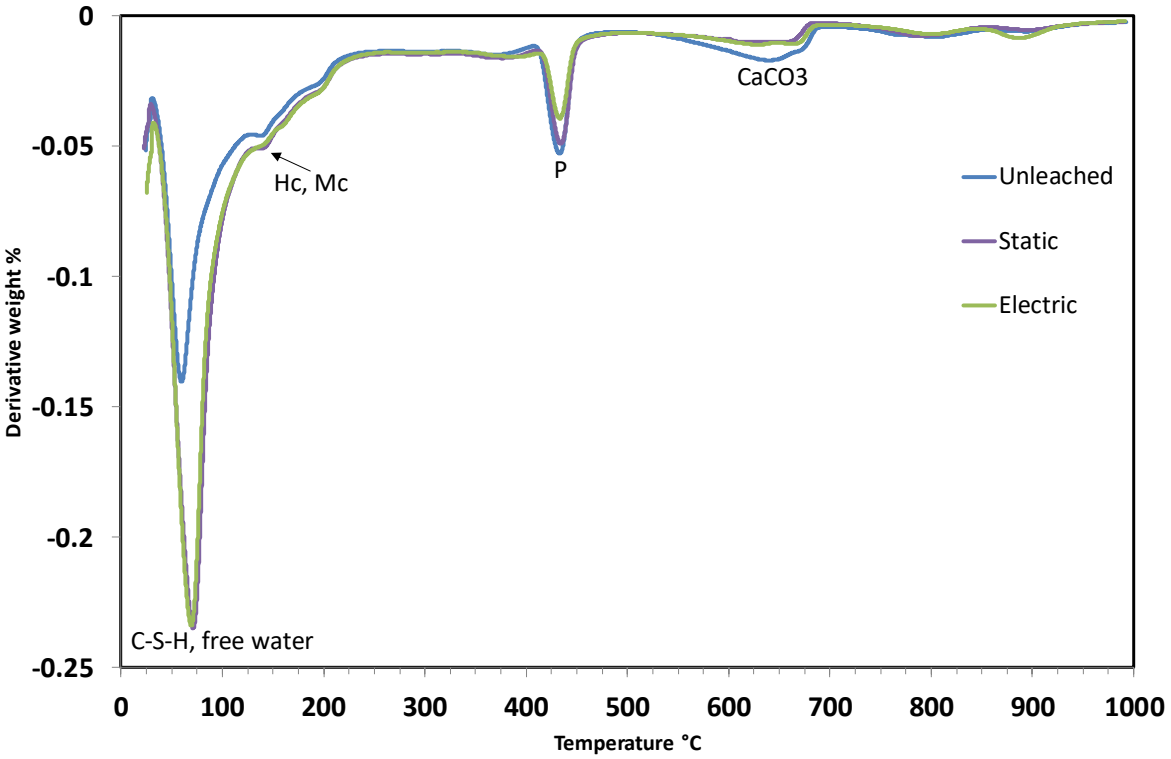

Figure 6.18 First derivative of the Thermogravimetric Analysis of the 3:1 BFS:PC Ba-cement samples

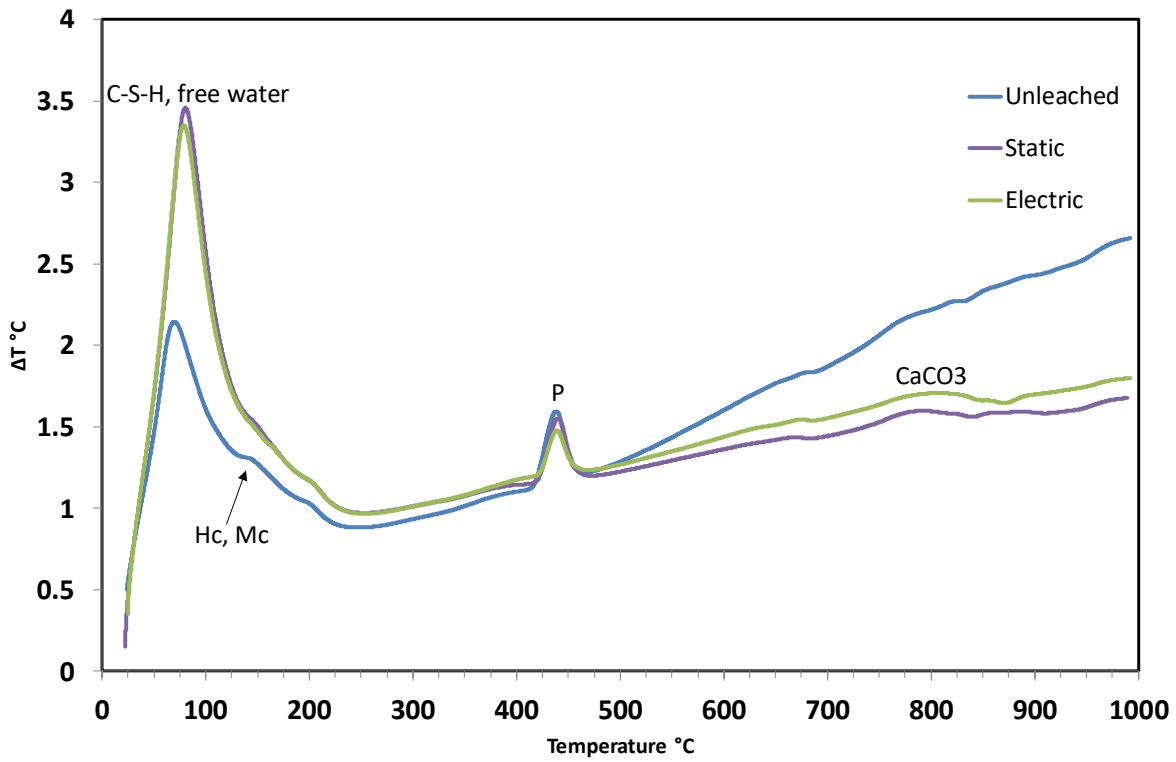

Figure 6.19 The Differential Thermal Analysis data of the 3:1 BFS:PC Ba-cement samples

6.4 Electrical Migration of Barium into pre-cured 3:1 BFS:PC

The results of Chapter 4 show that when Ba is intermixed with 3:1 BFS:PC in the form of $Ba(OH)_2 \cdot 8(H_2O)$ and $Ba(NO_3)_2$, barite forms from a reaction with the sulphur contained in the cement and ettringite is not observed. The previous Section 6.3 shows the release of a higher concentration of barium and a lower concentration of sulphur when cement of this type is statically and electrically leached, with the applied current density in the electrical leaching test enhancing the leaching of species as expected. However, in the real case of ILW, Cs that is encapsulated in BFS:PC will decay into barium over time. This means that the wasteform will have an increased barium content as time progresses, which is not truly reflected by the results shown thus far. Electrical migration is a technique which potentially provides the means to force barium into a pre-cured cement sample via electrophoresis to experimentally examine the interaction of barium with 3:1 BFS:PC that will occur in ILW. Due to the electrical attraction of barium towards the cathode (held in the cathode tank) the barium ions with a 2+ electric charge are expected to migrate into the cement. This is an alteration of a technique used by Castellote et al. [28] to examine the migration of ions through mortar samples. The samples in this test will be referred to as the Blank-cement wBa samples, as a shortened name for 'Blank-cement sample with Ba (wBa) initially dissolved in the anode tank and exposed to an electric current'.

As in the electrical leaching test in Chapter 5, a 3:1 BFS:PC sample was placed in the migration cell with 750 mL of distilled water each in the anode and cathode tanks. Since 0.32g of $Ba(OH)_2 \cdot 8(H_2O)$ was dissolved into the water in the anode tank (equivalent to the amount of Ba in the Ba-cement sample), the starting pH of the anode solution was 11.5, and the conductivity was 607.1 µS/cm at the start of the test. This test was conducted for 14 days at

a current density of 25 Am^{-2}, with leachate from both tanks being sampled at 3, 7 and 14 days for pH and ICP-OES measurements. After the test the cement sample was taken and analysed via XRD, TG, DTG and DTA, as well as MIP and SEM-EDX. The voltage data over the course of this test are shown in Figure 6.20 below, in comparison to the voltage of the electrical leaching test presented in Chapter 5 and the voltage of the electrical leaching test of Ba-cement. The voltage is lower in the test with barium than in the test with no addition, and steadily increases over time. This means that to maintain the required 25 Am^{-2} across the sample, less power is required when there is barium in the anode tank due to the comparatively high conductivity of the solution compared to distilled water, as shown in Table 6.1. As the leaching continues the power required increases at a steady rate, suggesting a decrease in conductivity, likely due to the decrease in the amount of ions in the anode solution.

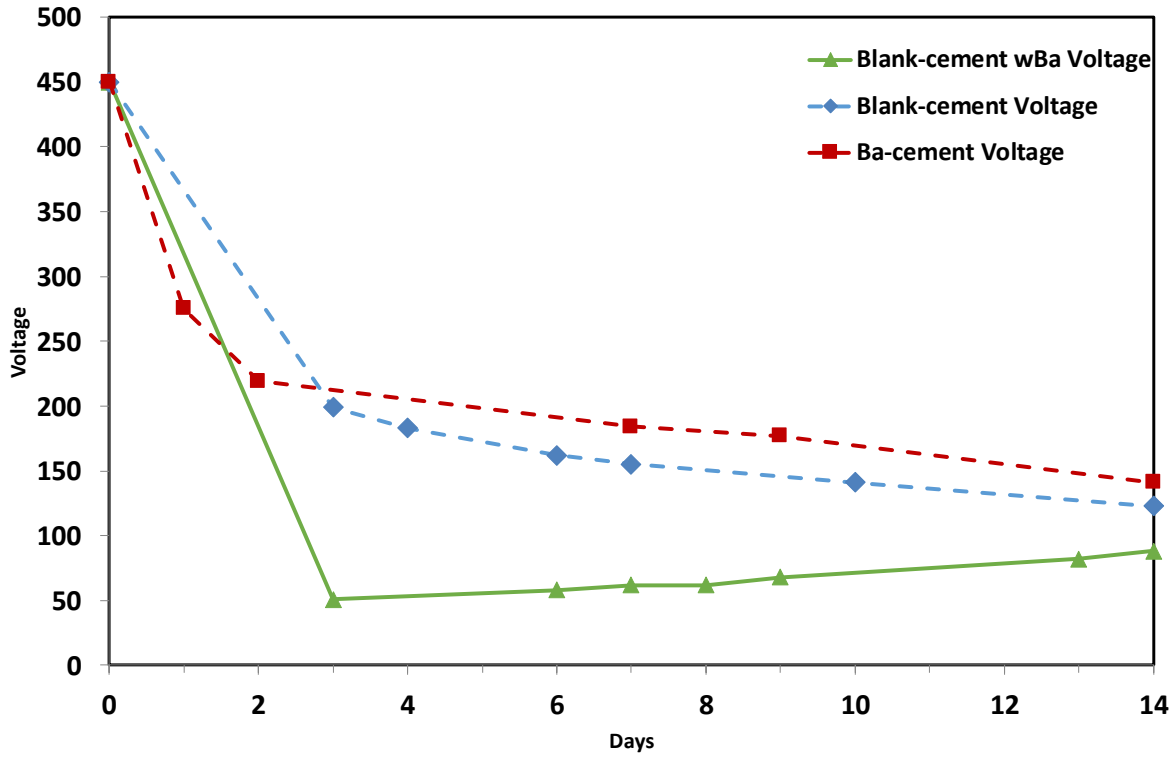

Figure 6.20 Voltage between the electrodes over the electrical leaching tests of Ba-cement, Blank-cement and Blank-cement wBa

6.4.1 Microstructural Analysis of the Blank-cement wBa sample

A BSE image of the side of the cement exposed to the anode (i.e. the anode side) is shown in Figure 6.21 at low magnification, with elemental mapping of barium, sulphur, calcium, silicon, aluminium and magnesium. Most of these elements appear to be uniformly spread though the sample. The surface edge of the sample is distinct. Most importantly Ba concentration in the near-surface area is observed, suggesting that the migration technique successfully introduced Ba ions into the cement, with some evidence of further ingress into areas of higher porosity. It is more likely that Ba migrated into existing porous regions, rather than that these areas became more porous as a result of the Ba ingress. Porous areas, some cracks and unhydrated BFS particles can be seen. Fine particles with bright white tone are observed in the Ba rich region. The bright tone implies the involvement of heavy atoms, suggesting precipitation of a Ba related compound.

Figure 6.22 shows the data for the same anode side at high magnification. A particle of barium compound, most likely hydroxide based on the lack of other cations, is visible on the exposure surface of the cement. Further inside the cement, there are areas of barium strongly associated with sulphur. These are most likely areas of barium sulphate. These areas of barium are visible as bright white spots and are visible at depths of ~60 µm into the cement. This is direct evidence that during the test barium is moving into the cement and reacting with sulphur present in the system.

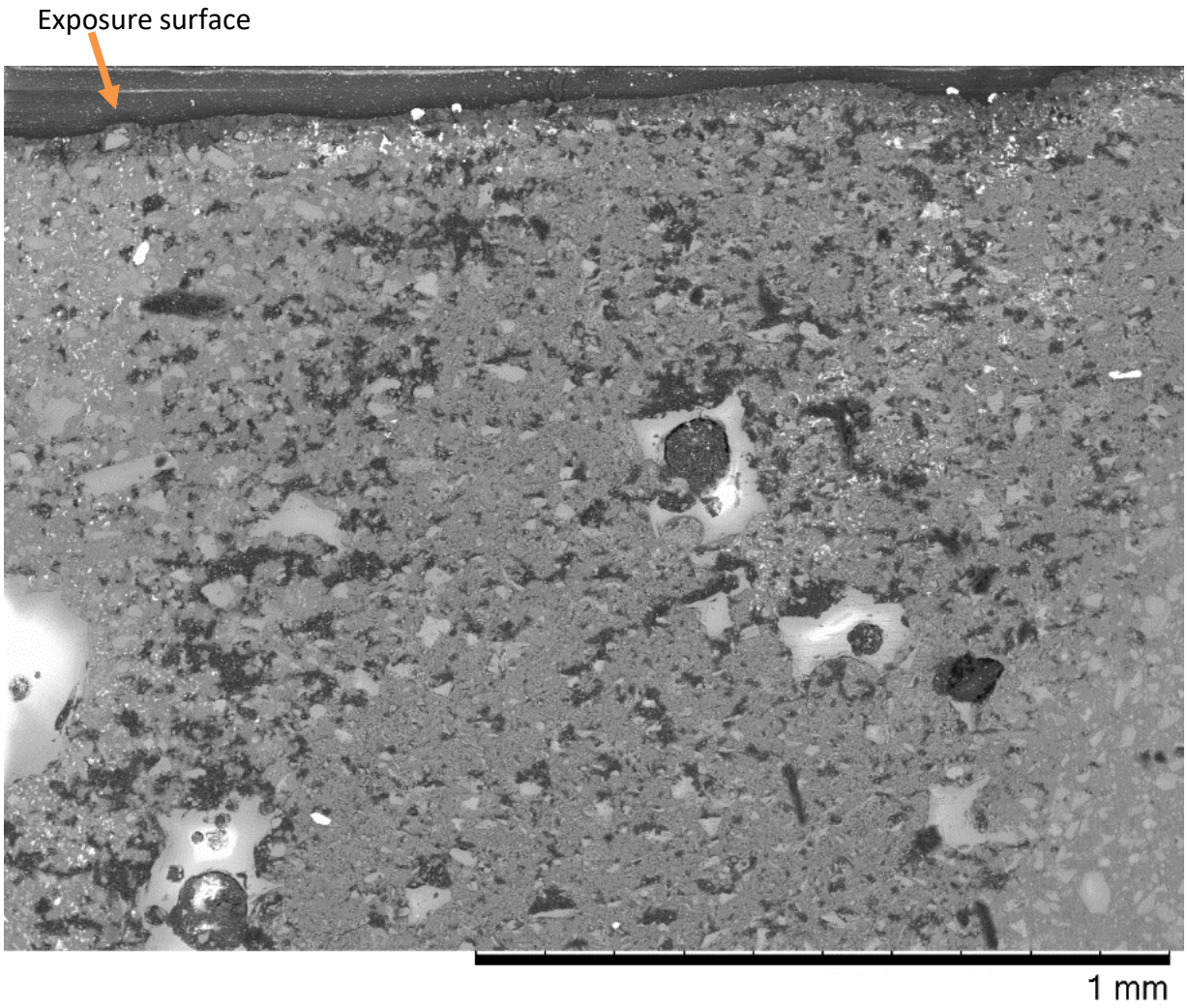

Figure 6.21 BSE image and SEM-EDX elemental maps at a low magnification of the anode surface of the Blank-cement wBa sample

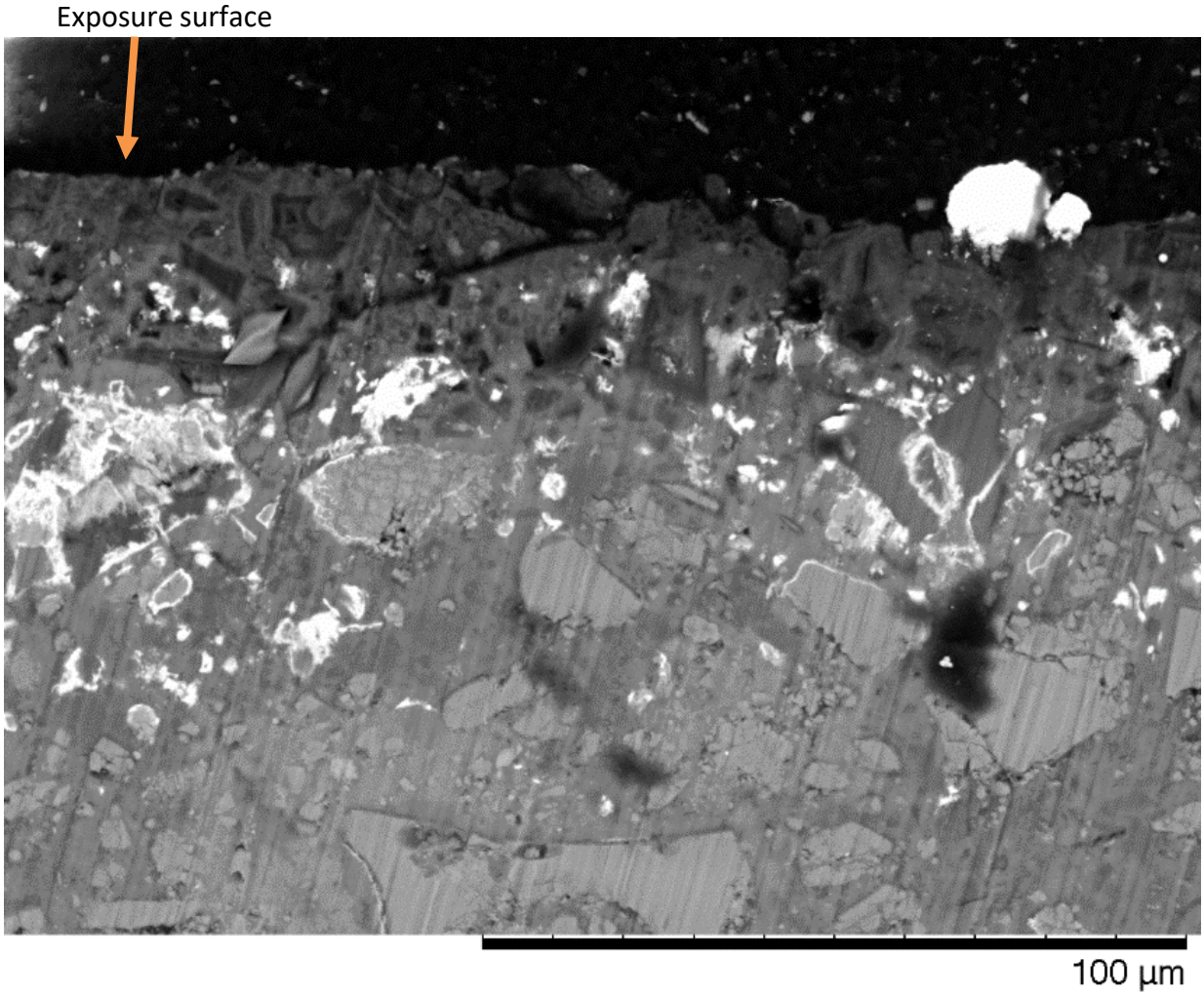

Figure 6.22 BSE image and SEM-EDX elemental maps at a high magnification of the anode surface of electrically leached 3:1 BFS:PC where $Ba(OH)_2 \cdot 8(H_2O)$ was dissolved into the anode tank

BSE images at low and higher magnification are shown alongside the elemental mapping of the cathode side in higher magnification in Figure 6.23. The low magnification image shows hydrated cement, unaltered clinker phases and areas of porosity. At higher magnification, the barium and sulphur maps of the cathode side do not have any obvious features neither inside nor on the surface of the cement sample. Since it is difficult to distinguish them from the background, the concentration of these elements must be very limited. This confirms that the barium seen on the anode side originates from the anode tank. The cathode map is similar to the unaltered electrical leaching test.

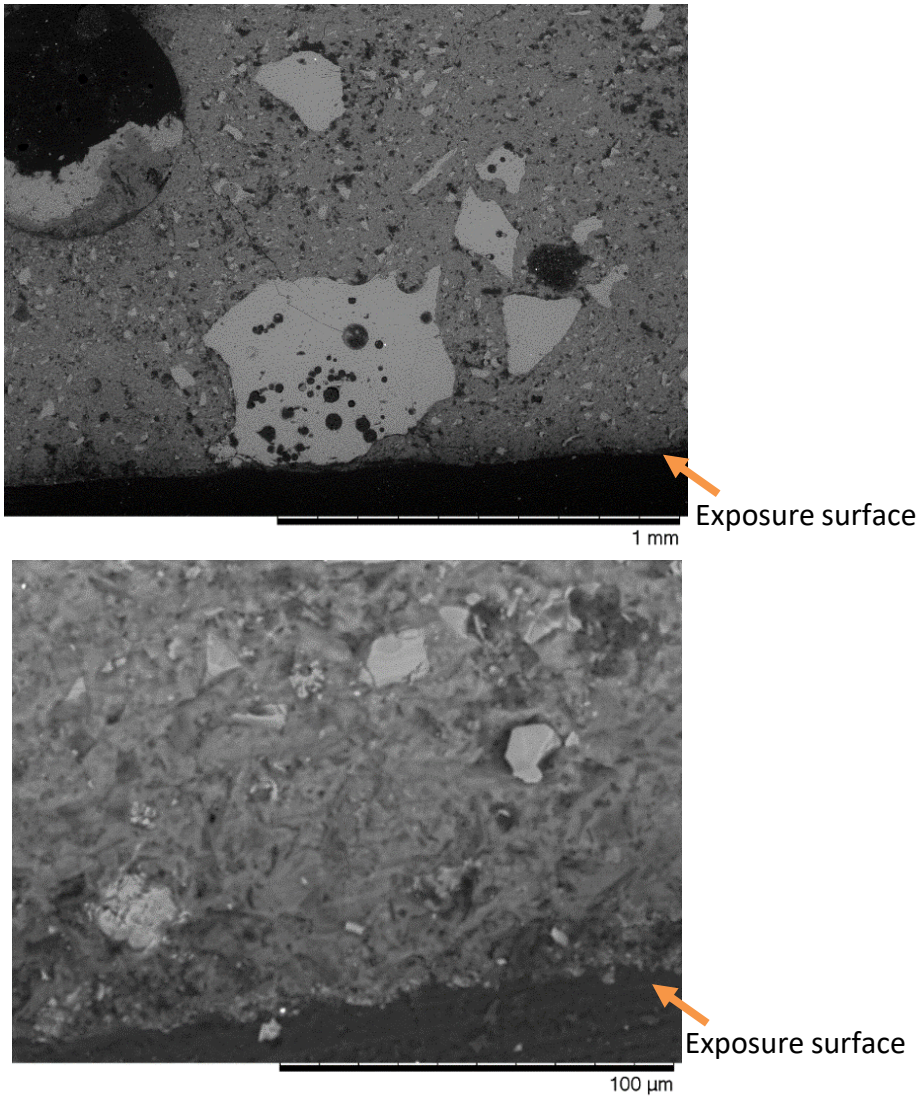

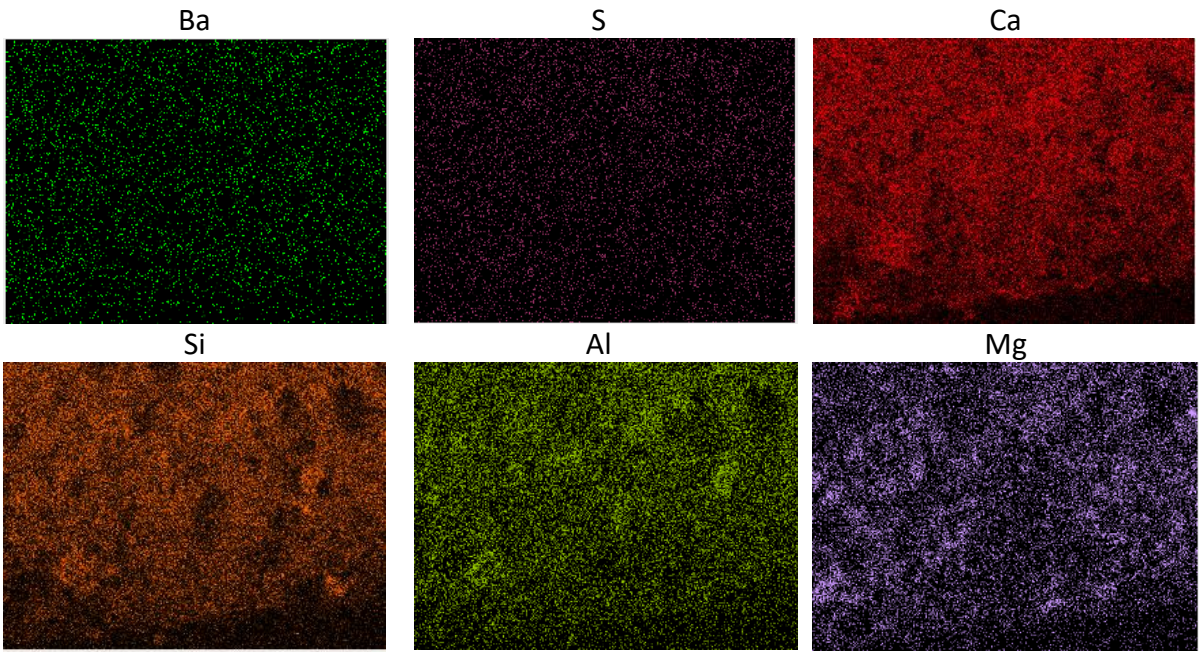

Figure 6.23 BSE images at low and high magnification of the cathode surface of the electrically leached Blank-cement wBa cement sample and SEM-EDX elemental maps of the high magnification image

The total porosity data of the samples gathered by MIP is shown in Figure 6.24, with the pore size distribution in Figure 6.25. The total porosity of the sample electrically leached with barium ions dissolved in the anolyte becomes higher than that of the other samples. This may be because of a large increase in the porosity at the 25-200 nm range compared with the other samples (Figure 6.24). This region corresponds with capillary pores [29], [30], which suggests that the reaction of ettringite with Ba leaves behind pores as barite forms. There was no 'bump' in the porosity in the 25-200 nm range in Figure 6.10, which suggests that in the Ba-cement samples the initial presence of Ba actually prevented ettringite formation in the first place, so there was no reduction in volume as barite formed. In Chapter 4, it was shown that the inclusion of barium supresses ettringite formation, as sulphate in the system would preferably react with barium to form barite. Particles rich in calcium and sulphur, likely gypsum, were seen to be surrounded by rings of Ba. This implies that the formation of barite is thermodynamically more favourable than that of ettringite. It is thus quite likely that the ettringite already formed in the hardened cement can also react with barium ions introduced externally. The reaction of ettringite in hardened cement in the presence of barium has been reported to form barite [14]. There is an increase in the porosity around 5 nm (gel pore region [29]) compared with the statically leached and the unleached samples, which is indicative of the increased leaching observed due to the applied electric current also seen in the electrically leached Blank-cement.

A second porosity increase is observed in the 25-200 nm range when Ba from the anode tank enters the Blank-cement sample, which is likely due to a similar reaction between barium and ettringite as in the Ba-cement sample, [14] which was discussed above (see Equation 6.1). The resulting solid product phases of this reaction (barite, hydrogarnet and portlandite) take up

only 35.7% of the volume of ettringite, the only solid reactant as the $Ba(OH)_2 \cdot 8(H_2O)$ is dissolved initially (calculated using data shown in Table 6.2), so there must be a reduction in the solid volume of the total cement matrix when this reaction takes place.

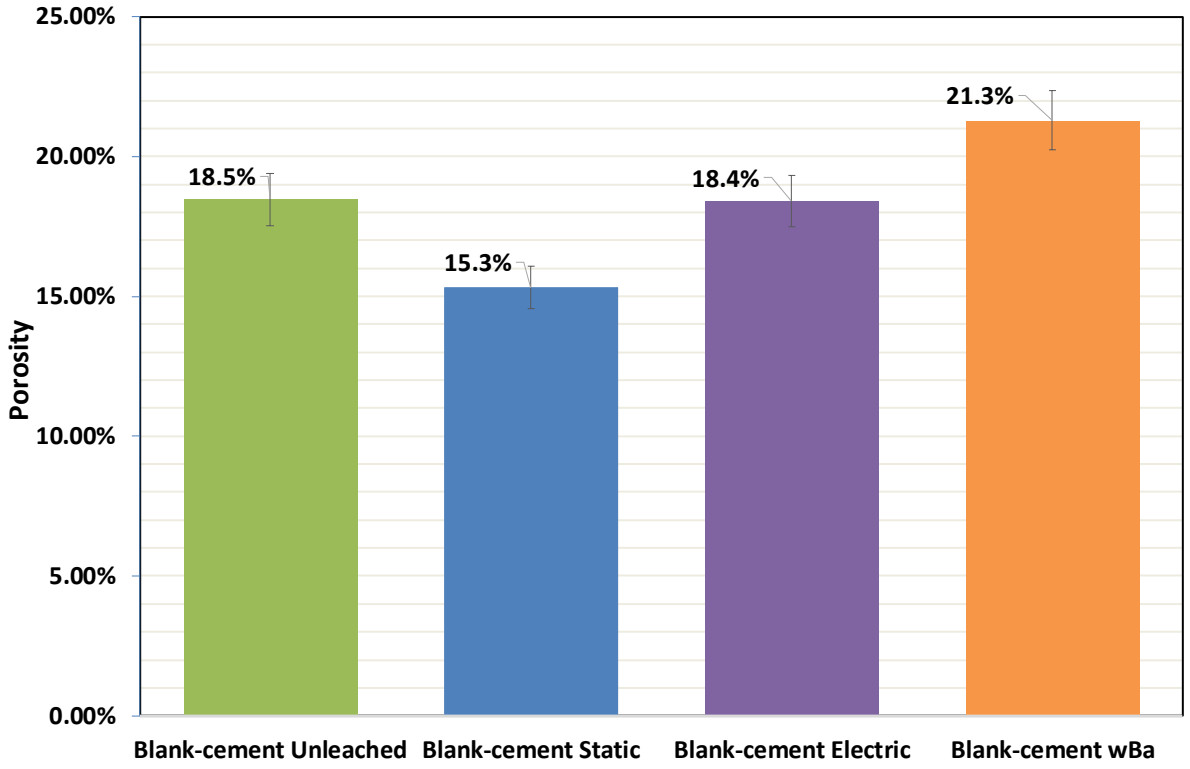

Figure 6.24 Total porosity of Blank-cement samples before and after leaching tests in different conditions

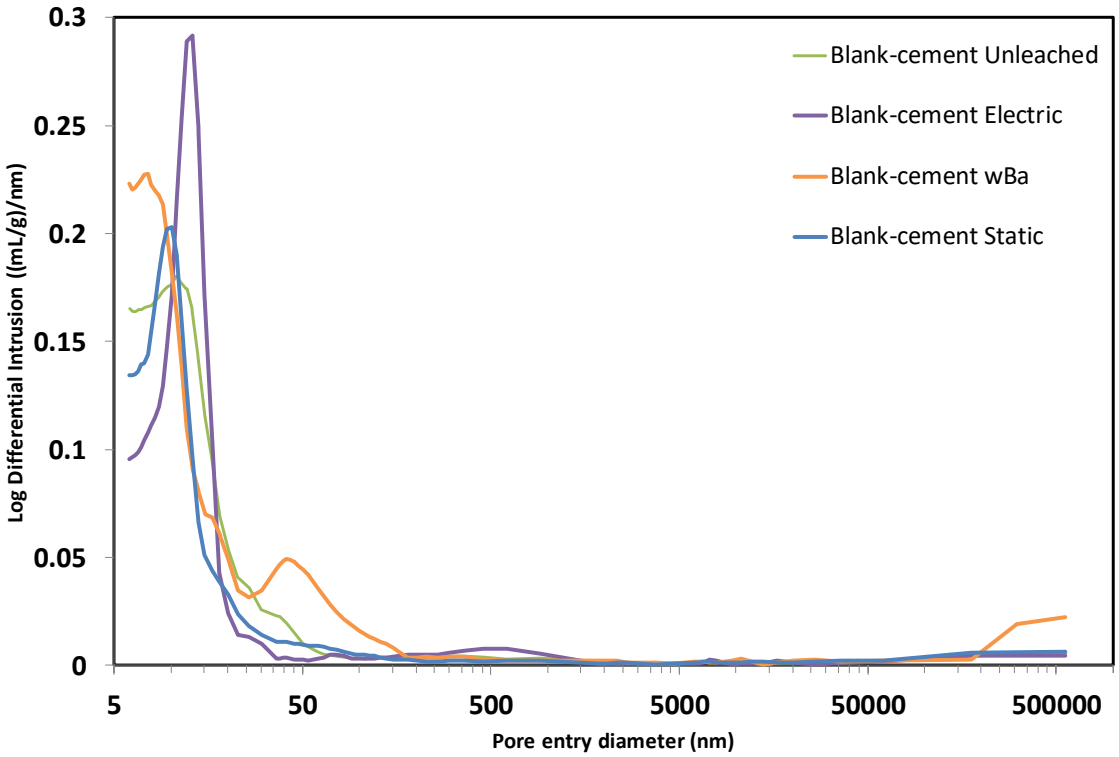

Figure 6.25 Pore size distribution of Blank-cement samples before and after leaching tests in different conditions

6.4.2 Leachate Analysis for the Blank-cement wBa sample

The pH data from the static and electrical leaching tests of the Blank-cement and the Blank-cement wBa sample are shown in Figure 6.26. The pH of the cathode tank displays the same behaviour in both electrical leaching tests, which suggests that the leaching behaviour into the cathode tank does not change significantly. However, the pH of the anolyte is very different because of the dissolution of $Ba(OH)_2 \cdot 8(H_2O)$. The pH of the anolyte does not display a clear change over time in the electrical leaching test with dissolution of $Ba(OH)_2 \cdot 8(H_2O)$ and remains in the range 11.21-11.35 ± 0.6.

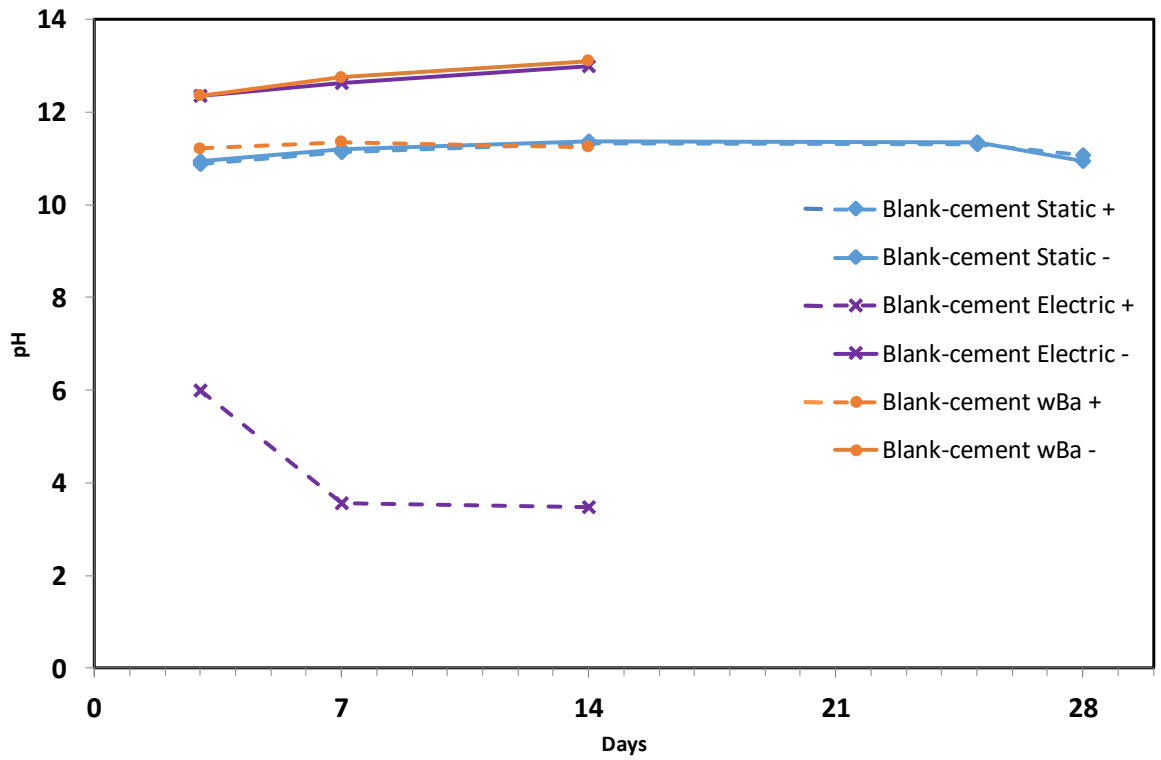

Figure 6.26 pH data of the leachates during a static leaching test of Blank-cement and electrical leaching test of Blank-cement with/out $Ba(OH)_2.8(H_2O)$ dissolved in anolyte. The dashed line is the pH of the anolyte and the solid line the catholyte, though in the static test this is for labelling purposes only.

The elemental concentration data gathered by ICP-OES are shown in Figure 6.28 to Figure 6.30 below. The leaching of Ca, Na and Mg into the cathode tank and the leaching of Si into the anode tank is higher than their leaching in the electrical leaching test without $Ba(OH)_2 \cdot 8(H_2O)$ dissolved in the anolyte, but the elements show a similar behaviour over time.

When barium is dissolved into the anode tank at the start of the test, the concentration in that tank is obviously higher than in the other leaching tests. Due to the attraction of the barium ions towards the cathode tank (and/or the repulsive force from the anode), the concentration in the anode tank steadily decreases over time. The concentration of Ba in the cathode tank increases between days 3 and 14, and is higher than in the electrical leaching test without dissolved $Ba(OH)_2 \cdot 8(H_2O)$ in the anode tank. This shows that some Ba ions are passing through or around the cement and reaching the cathode tank.

With regards to potassium, both the anode and cathode tank have a higher concentration of this element than in the static leaching test of the Blank-cement. The concentration in the anode tank of the leaching test of the Blank-cement wBa sample is similar to the concentration in the cathode tank of the electrically leached Blank-cement sample. It appears that the presence of Ba in the anode tank increases the leaching of potassium into it.

Al has a higher concentration in the anode tank than in the cathode tank in both electrical leaching tests. The decrease in the standard electric leaching test without $Ba(OH)_2{\cdot}8(H_2O)$ dissolved in the anolyte can be explained by the low pH in the anode tank, as previously discussed in Chapter 5, but in the test with $Ba(OH)_2{\cdot}8(H_2O)$ the pH of the anolyte remains high. A possible explanation for this is that $Al(OH)_3$ can precipitate at a high pH [31] so it may be precipitating in the tank or on the surface of the cement sample as discussed in the previous chapter.

The concentration of Mg in the anode tank changes in a similar way to the Mg concentration in the standard electrical leaching test without $Ba(OH)_2{\cdot}8H_2O$ dissolved in the anolyte, with an increase at 7 days but a decrease after 14 days. There was less magnesium present than in the static test with Blank-cement, but the concentration was higher than in the electrical leaching test with Blank-cement. The introduction of $Ba(OH)_2{\cdot}8H_2O$ increases the pH of the entire system. This will enhance the dissolution of slag, and result in higher concentrations for most of the elements in the anolyte, such as potassium and aluminium, as discussed above [32], [33]. The pH of the anode tank in this test is similar to the pH of the anode and cathode in the static test of the Blank-cement, meaning that the same amount of Mg can be in solution without precipitating, but because of the electric potential which attracts Mg ions to the

cathode tank the actual concentration of Mg in the anode is lower than in the static test. The high pH of the cathode tank, however, likely causes some of the Mg to precipitate out of the solution, decreasing the concentration detectable by ICP-OES [12], [13].

Unlike the rest of the elements detected, sulphur leached less in this test than in the electrical leaching test of the Blank-cement, because (as shown above in Figure 6.22) sulphur present in the cement matrix reacts with the intruding barium. The reduction in the leaching of sulphur could also support the idea discussed in Chapter 5 that the leaching of sulphur is strongly affected by the pH of the leachate (in the electrical leaching of Blank-cement the leaching of sulphur into the anode tank increased significantly as the pH of the anode tank decreased). A Pourbaix diagram of the Ba-O-H-C-S system is shown in Figure 6.277; between pH 1.2 and 11.6, $BaSO_4$ is dominant, and above pH 11.6, $BaSO_4$ is replaced by $BaCO_3$ [34]. The lack of $BaCO_3$ in the samples is indicative of a low amount of carbonation present in the system, as the internal pH of the cement is likely over 11.6 [35].

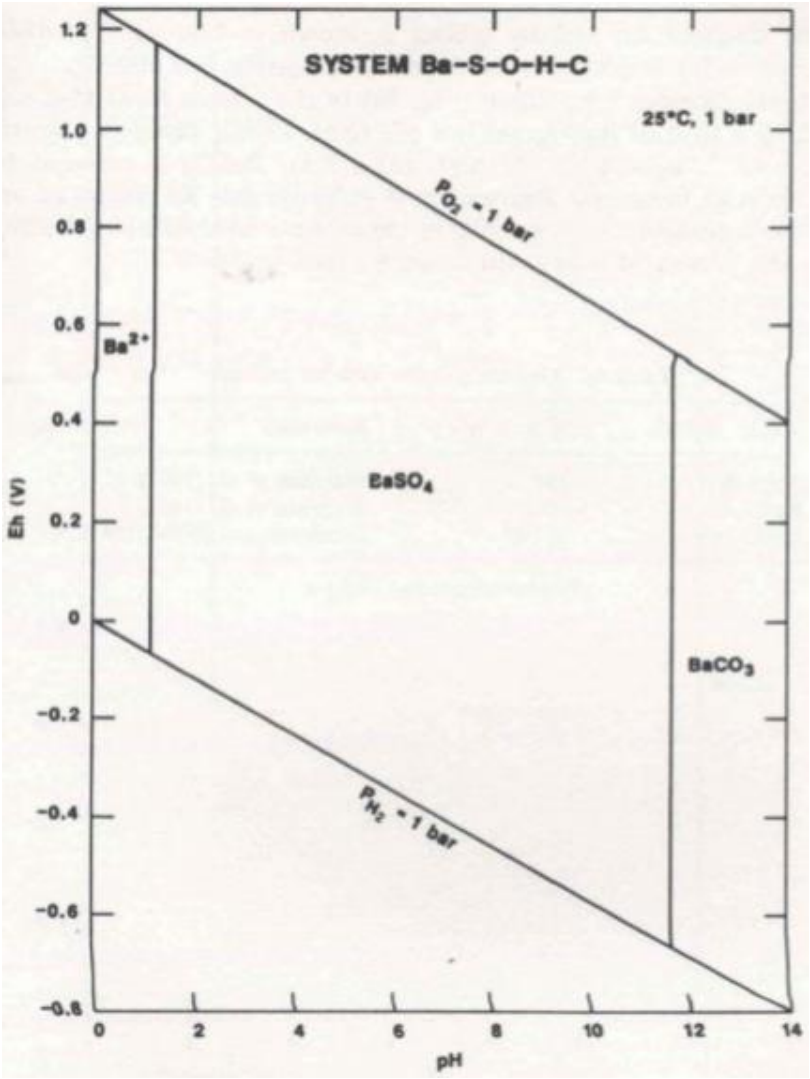

Figure 6.27 Pourbaix diagram of the Ba-S-O-H-C system [34]**.**

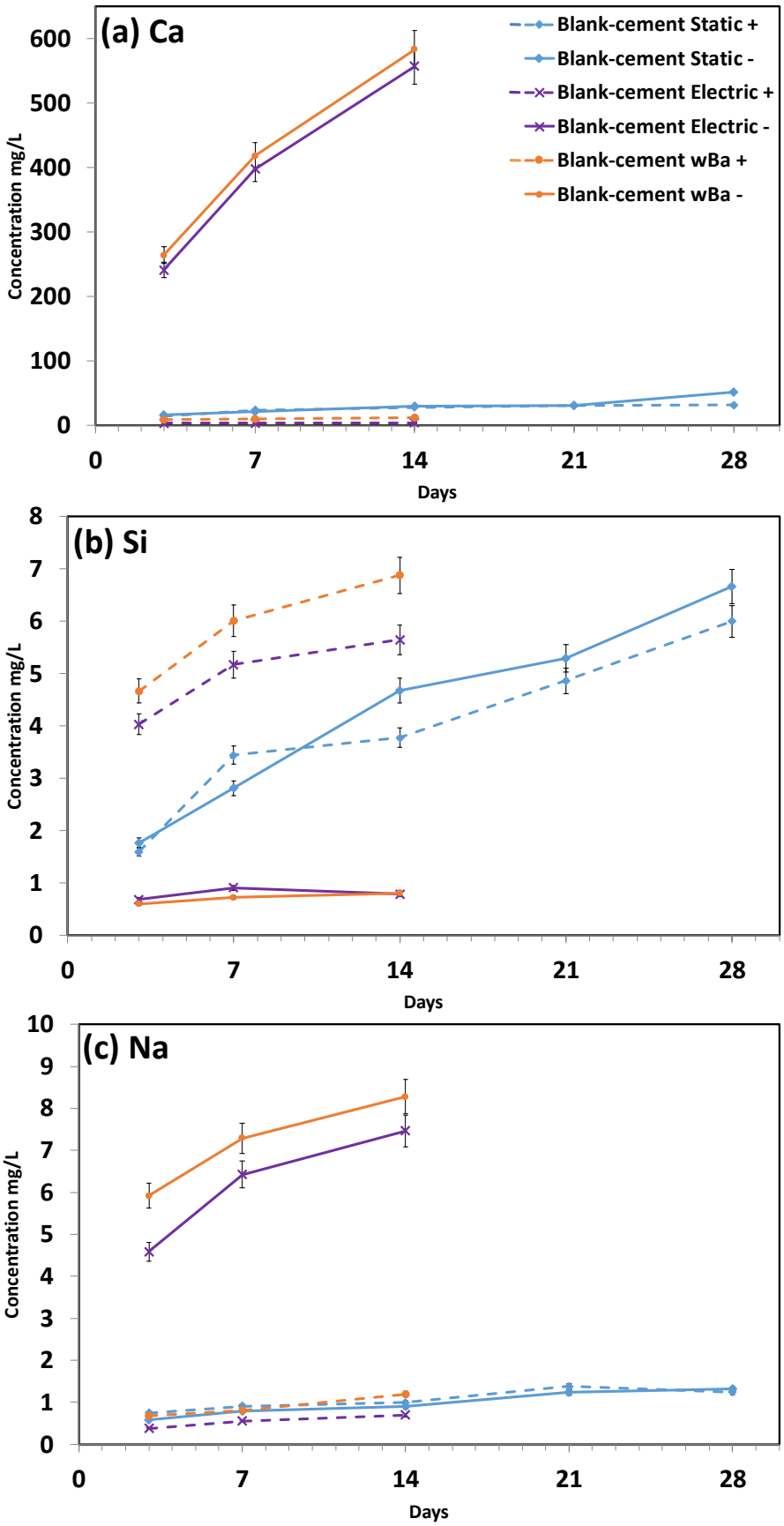

Figure 6.28 Elemental concentrations of (a) Ca, (b) Si and (c) Na in the anode and cathode tanks in the static and electrical leaching tests with/out $Ba(OH)_2.8(H_2O)$ dissolved in anolyte. The solid line represents the cathode tank, and the dotted line the anode tank

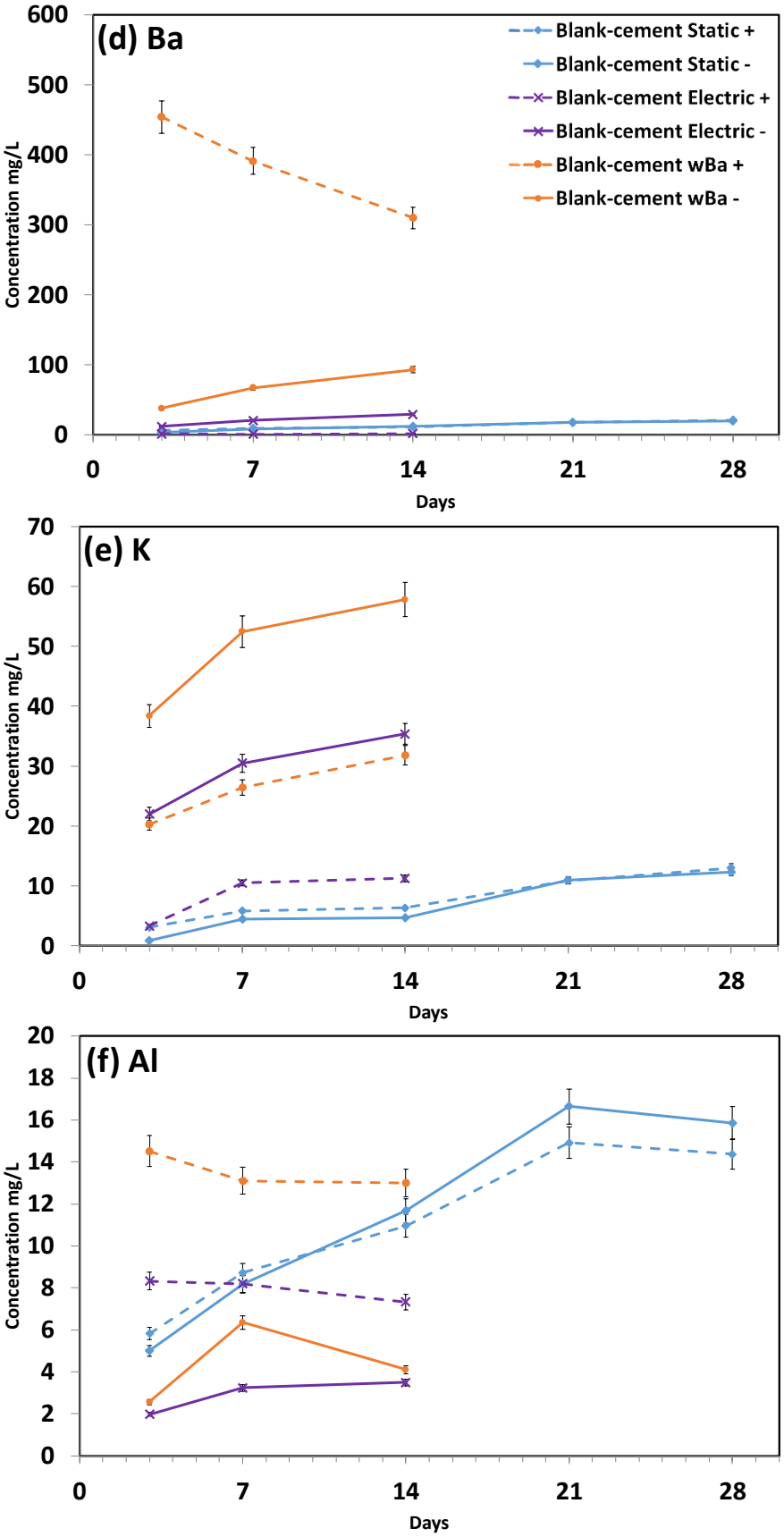

Figure 6.29 Elemental concentrations of (d) Ba, (e) K and (f) Al in the anode and cathode tanks in the static and electrical leaching tests with/out $Ba(OH)_2.8(H_2O)$ dissolved in anolyte. The solid line represents the cathode tank, and the dotted line the anode tank

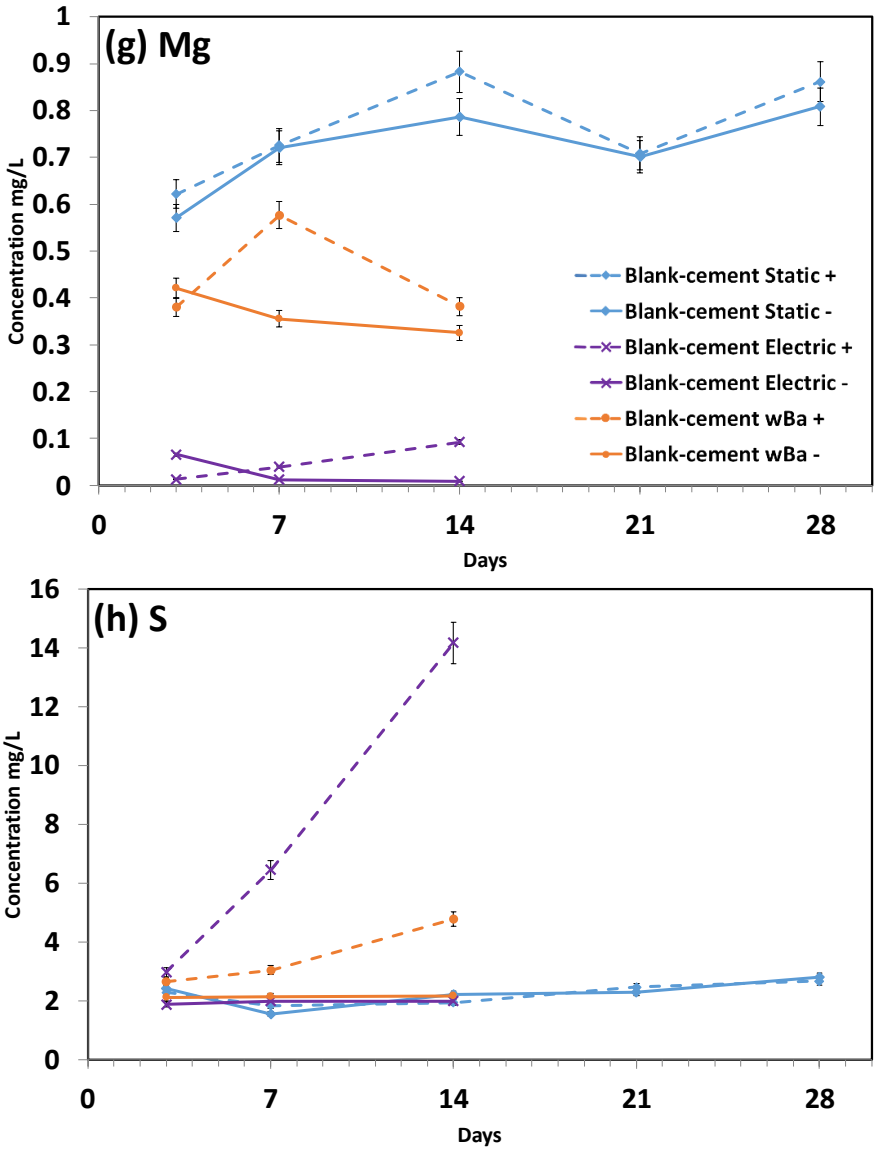

Figure 6.30 Elemental concentrations of (g) Mg and (h) S in the anode and cathode tanks in the static and electrical leaching tests with/out $Ba(OH)_2.8(H_2O)$ dissolved in anolyte. The solid line represents the cathode tank, and the dotted line the anode tank.

6.4.3 Phase Analysis of the Blank-cement wBa sample

The XRD data for the Blank-cement wBa sample after 14 days of electrical leaching are shown in Figure 6.31 to compare it with the unleached sample, statically leached and electrically leached Blank without $Ba(OH)_2 \cdot 8H_2O$ dissolution in the anolyte. There is a sign of small barite reflection peaks in the sample when the anolyte contains $Ba(OH)_2 \cdot 8H_2O$, but this appears to be smaller than when $Ba(OH)_2 \cdot 8H_2O$ is intermixed with the cement (Figure 6.3). Otherwise the XRD data are similar to the 14-day electrical leaching test without $Ba(OH)_2 \cdot 8H_2O$ in the anolyte. In the XRD scan taken at a longer counting time per step in the 5 to 15 degree range presented in Figure 6.32, there is what appears to be a shift to higher angle of both the ettringite peak and the hydrotalcite/monocarbonate peak in this particular sample. There is also a slight decrease of the hemicarbonate peak. The scanning procedures are described in Section 3.3.2.

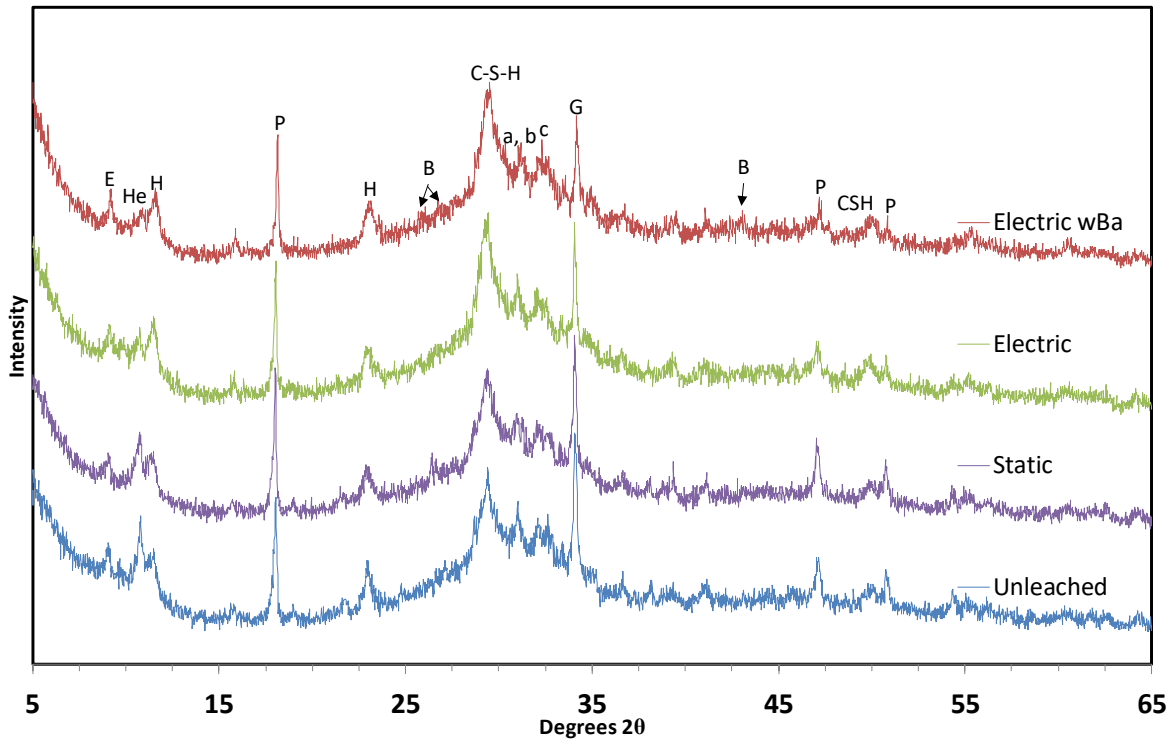

Figure 6.31 XRD of the Blank cement samples

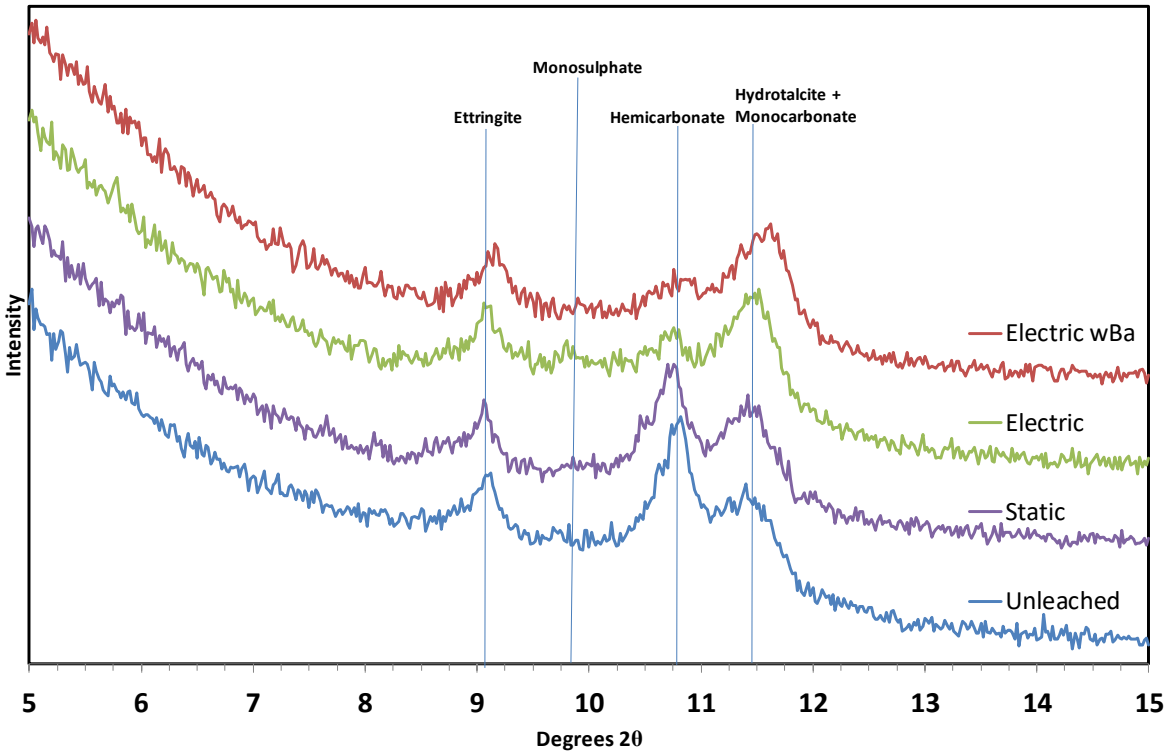

Figure 6.32 XRD in the range 5 to 15 degrees taken at a longer counting time per step

The thermal analysis data of the samples consisting of the TG, DTG and DTA data with respect to temperature are shown in Figure 6.33 to Figure 6.35 below. Whilst barium sulphate was observed during XRD, it melts at 1580°C [23] and so was not identified in the thermal analysis data. The addition of barium however did induce a greater weight loss in the 40-110°C region, which is suggestive of the presence of a greater amount of C-S-H. Unlike in the phase analysis of the Blank-cement samples tested without barium, ettringite was not observed in the phase analysis of the Blank-cement wBa sample.

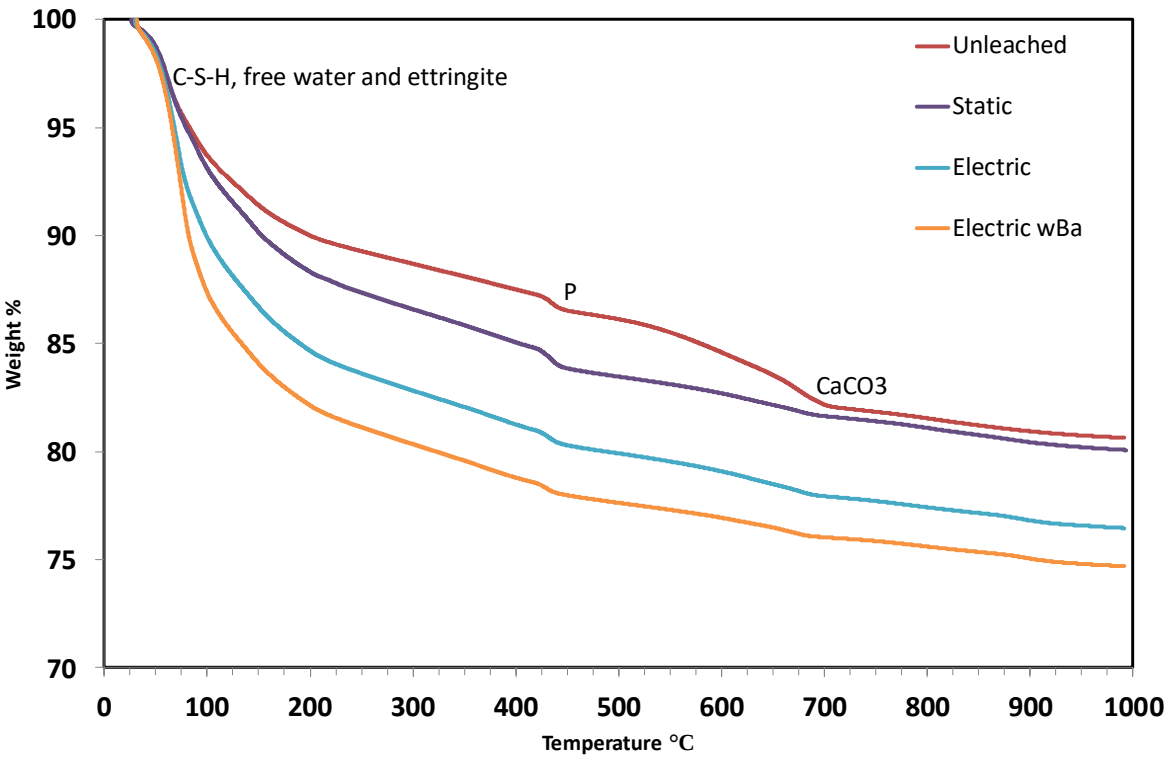

Figure 6.33 Thermogravimetric Analysis of the 3:1 BFS:PC cement samples

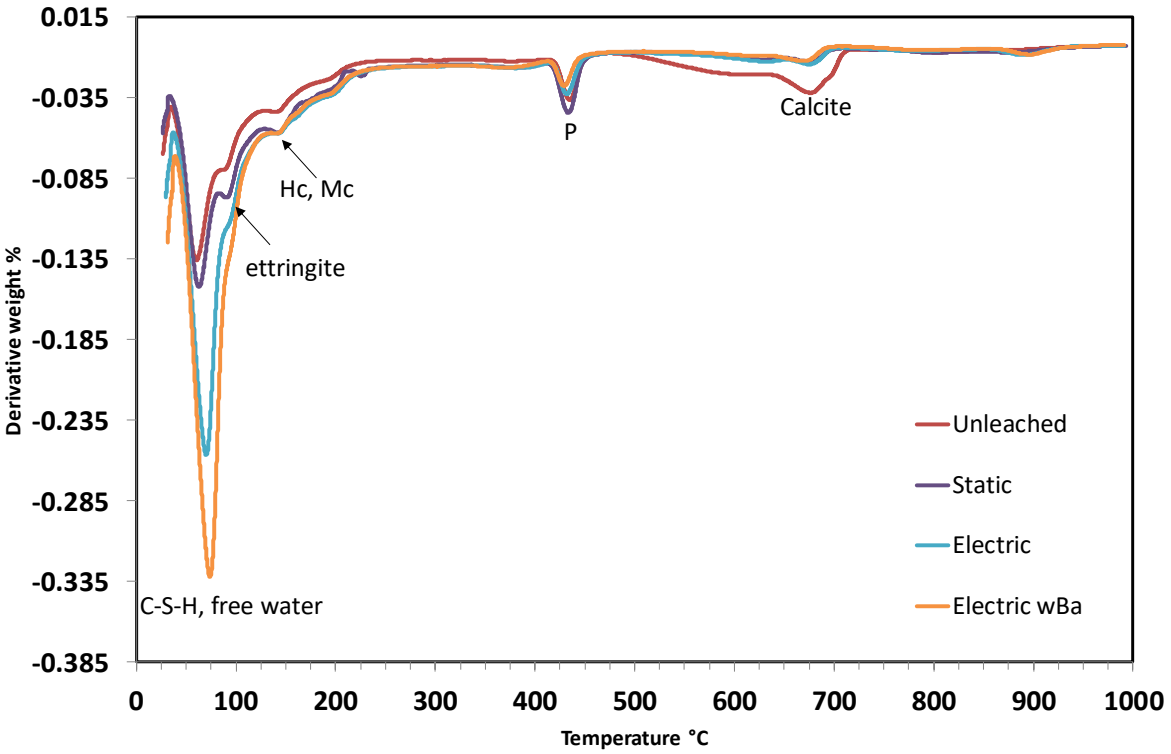

Figure 6.34 The first derivative of the Thermogravimetric Analysis of the 3:1 BFS:PC cement samples

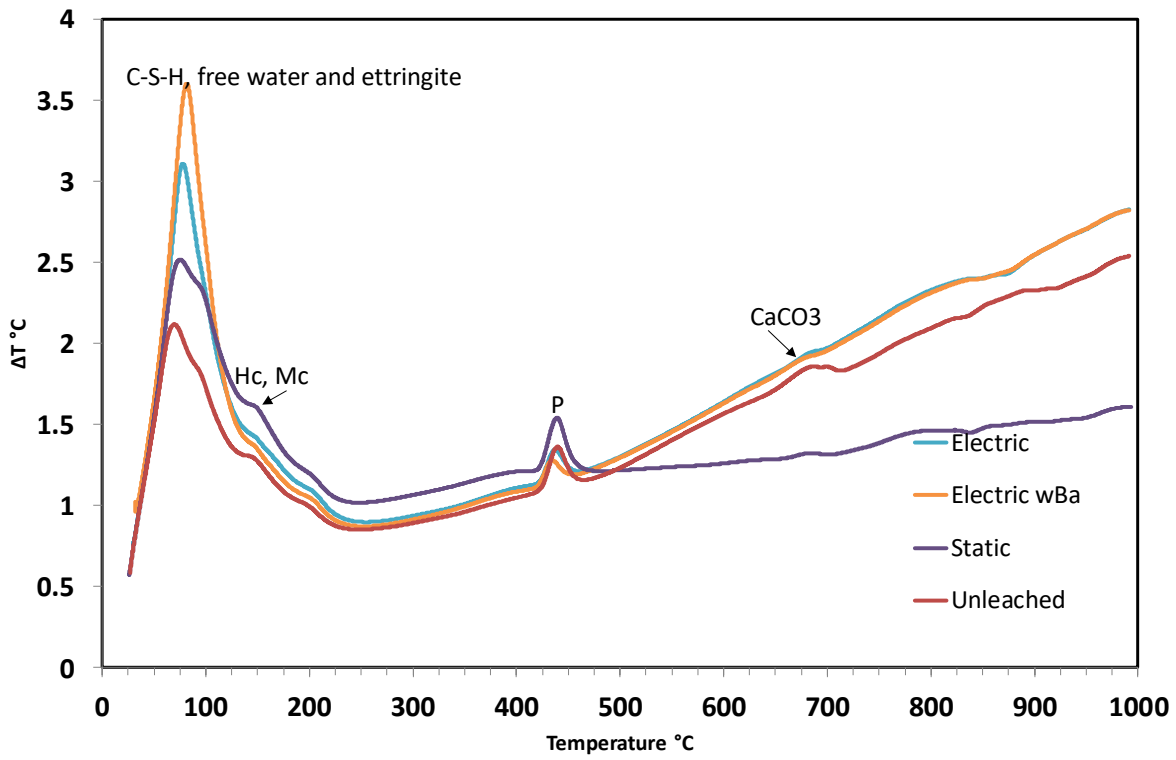

Figure 6.35 Differential Thermal Analysis of the 3:1 BFS:PC cement samples

6.5 Electrical & Static leaching of 3:1 BFS:PC containing $CsNO_3$ and Electrical Migration of Barium into pre-cured 3:1 BFS:PC containing $CsNO_3$

The main aim of this Section is the study of simultaneous migration events – the leaching of Cs out of and the migration of Ba into a cement sample –as an experimental model for the nuclear decay of Cs into Ba in ILW. Therefore, 3:1 BFS:PC samples are produced with caesium nitrate intermixed in the cement by dissolving it into the water used to hydrate the cement (Cs-cement), and the leaching behaviour observed both in a static and electrical leaching test is discussed. The results of these tests are compared with the findings from an electrical leaching experiment using Cs-cement with barium dissolved into the anode tank and pulled in by an electric current (Cs-cement wBa). This migration technique has several inherent limitations. Firstly, since Ba ions and Cs ions are both positively charged, Ba ions enter the cement sample from the anode tank, and Cs ions leave the sample on the cathode side. Therefore, the Ba-rich region is in a different location to the Cs-poor region of the sample. This test also does not simulate the damage on the cement caused by the radioactive decay itself. The removal of material from the sample is not selective for Cs, as leaching of other elements still occurs. This test is simply a model of the chemical change of Cs to Ba within ILW.

6.5.1 Microstructural Analysis of the Cs-cement and Cs-cement wBa samples

A BSE image of an unleached sample of 3:1 BFS:PC containing $CsNO_3$ at a low magnification is shown in Figure 6.36, along with a higher magnification image and its elemental mapping via SEM-EDX. Some cracks, pores and areas of unhydrated binder are visible in the lower magnification image. Cs is spread through the sample and does not seem to have precipitated – these samples are below the precipitation limit of 2.8 wt.% determined in Chapter 4. Some areas with a higher concentration of Si and Al can be seen in the elemental maps. As expected, no degradation was seen at the edges of the unleached sample.

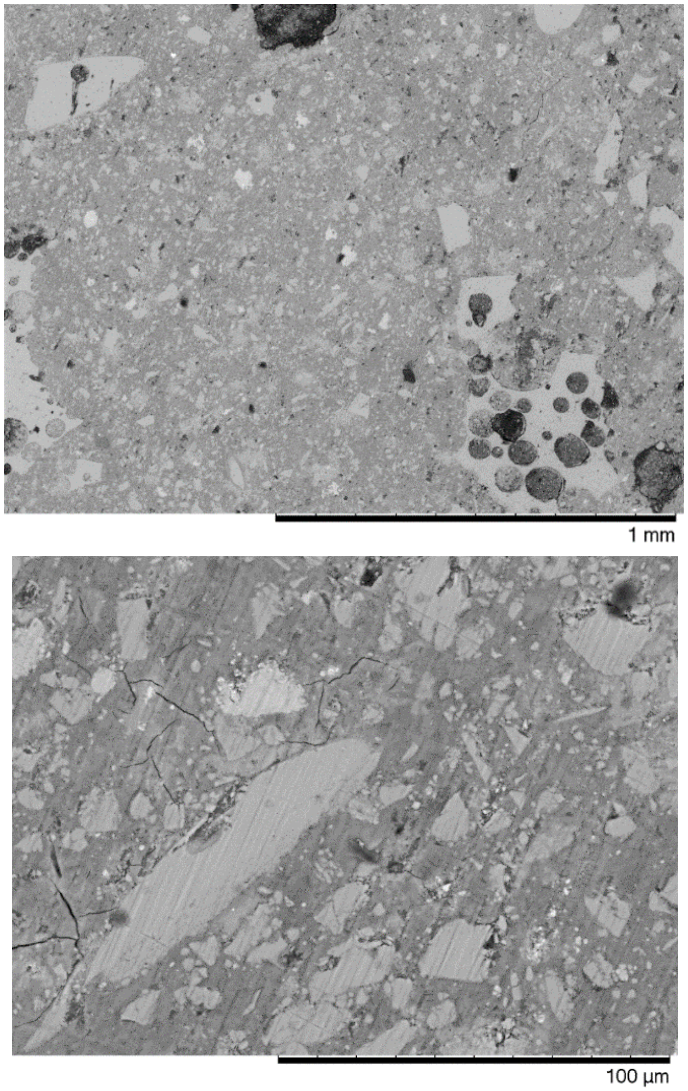

Figure 6.36 BSE images at low and high magnification, and SEM-EDX elemental maps of the latter, for an unleached 3:1 BFS:PC Cs-cement sample

BSE images and SEM-EDX maps of the exposure surface of the cement sample containing $CsNO_3$ after the static leaching test are shown in Figure 6.37. The lower magnification image shows a degraded region – both of the exposure surfaces of the sample showed similar degradation. The caesium and nitrogen are difficult to distinguish from the background, unlike the other elements displayed which show a clear boundary at the surface of the cement.

Exposure surfaces were also studied for the Cs-cement sample after the electrical leaching test. The BSE images and SEM-EDX maps of the cathode side are shown in Figure 6.38. The cathode side shows a region of degradation as previously observed in the other electrical leaching tests (Figure 5.46, Figure 6.7, Figure 6.23), and otherwise showed little effect caused by the inclusion of $CsNO_3$. The concentrations of caesium and nitrogen were difficult to distinguish from the background. Mg, likely in the form of crystallised brucite, seems to show a higher concentration closer to the surface. Brucite is not easy to observe in the XRD data however, shown below in Figure 6.49, because only a small part of the sample shows the high concentration of Mg. The anode side as shown in Figure 6.39 also does not show many features in the Cs and N maps, and interestingly, there seems to be only a small region of degradation, approximately 5 μm.

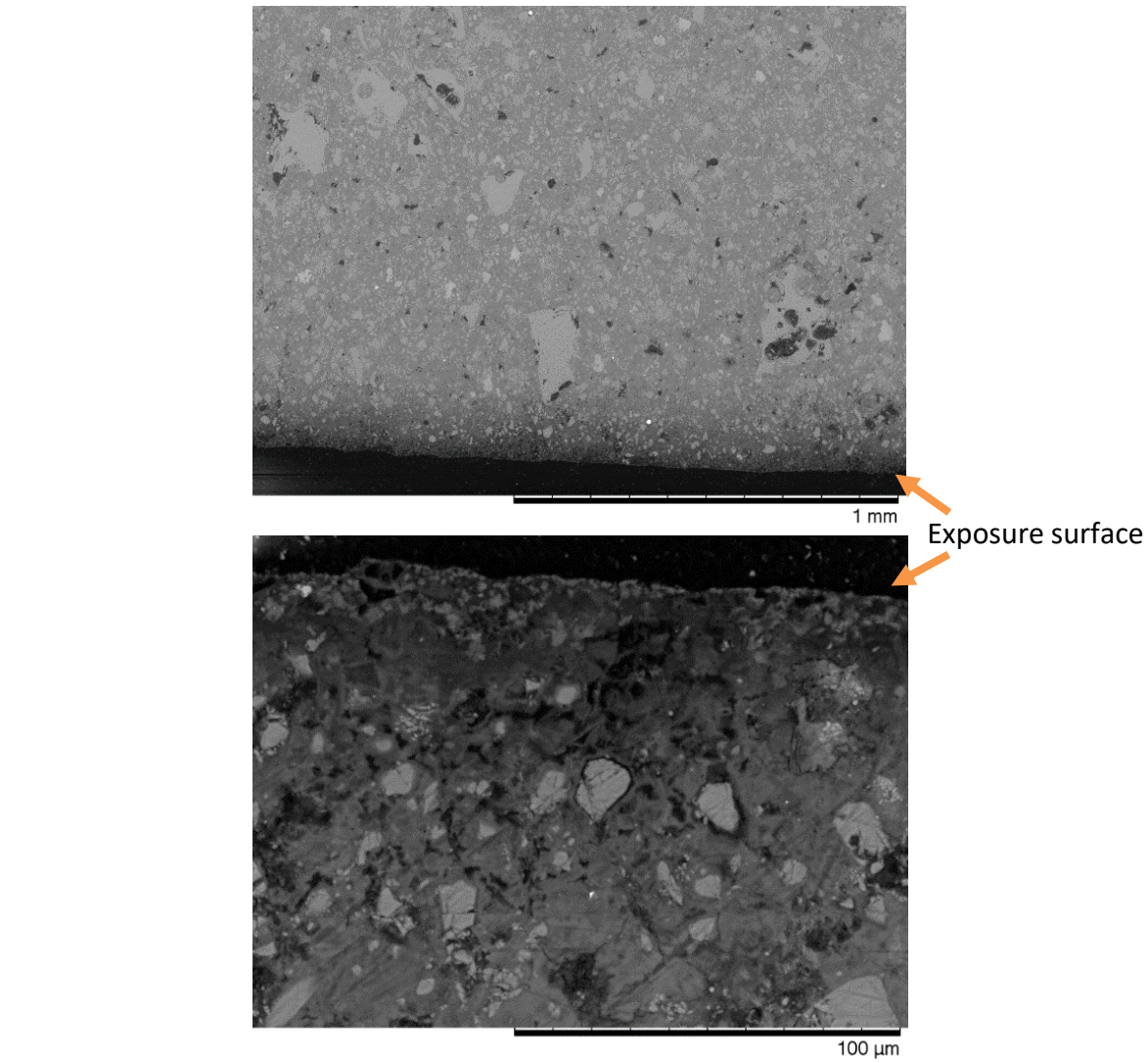

Figure 6.37 BSE images at low and high magnification, and SEM-EDX elemental maps of the latter, for a 3:1 BFS:PC Cs-cement sample after 28 days of static leaching

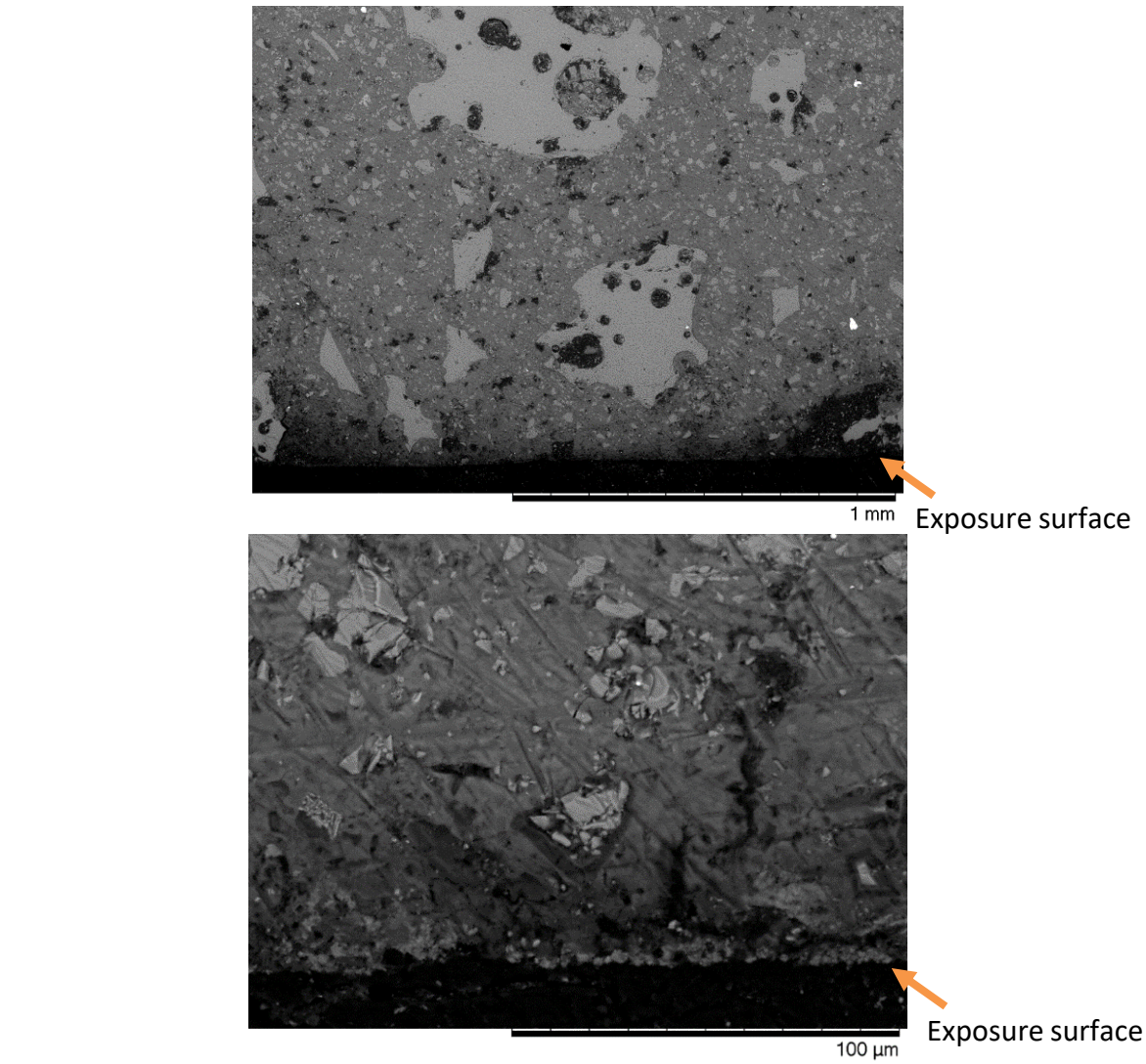

Figure 6.38 BSE images at low and high magnification and SEM-EDX elemental maps of the latter, for the cathode side of 3:1 BFS:PC Cs-cement sample after an electric leaching test

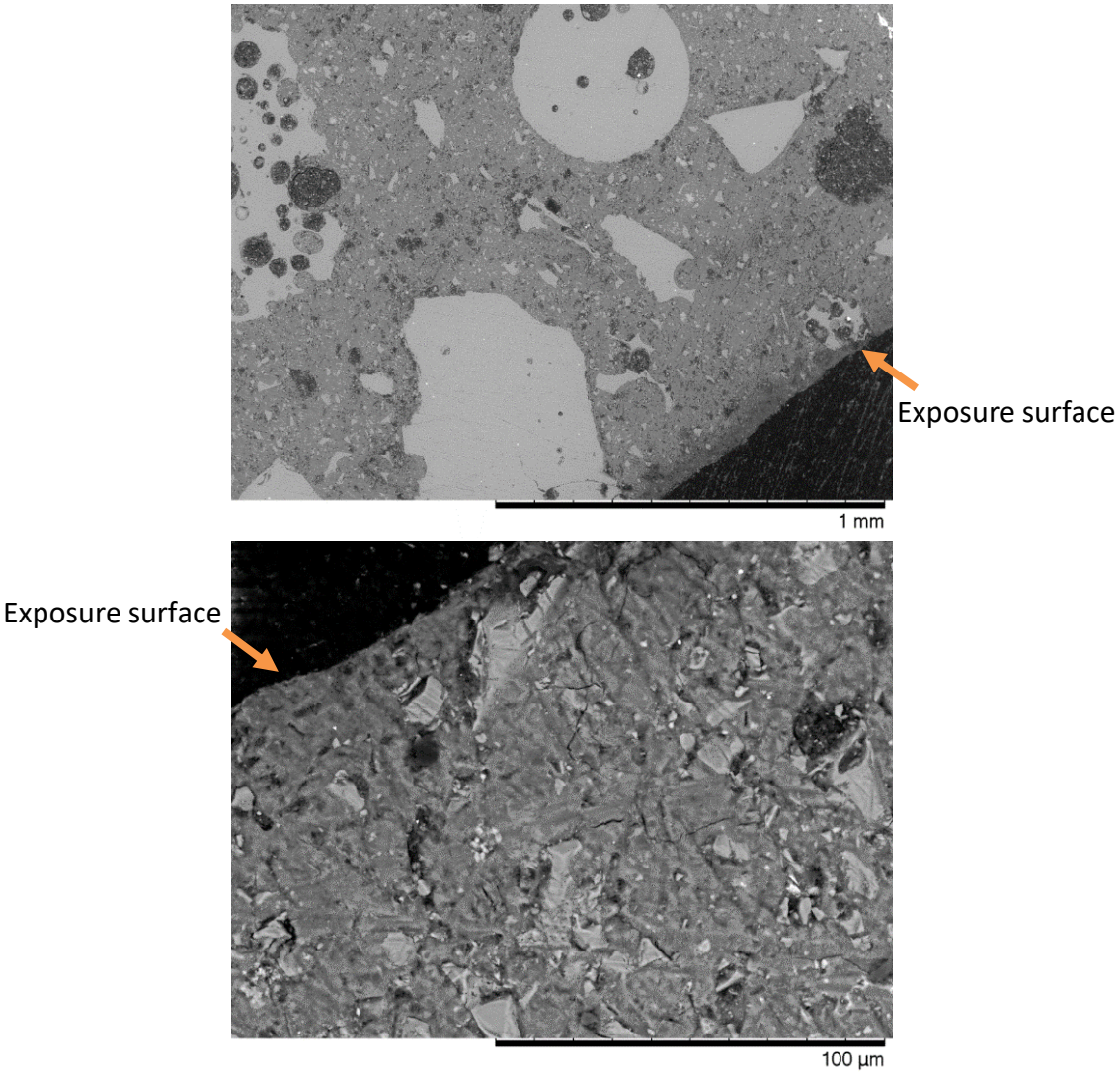

Figure 6.39 BSE images at low and high magnification and SEM-EDX elemental maps of the latter, for the anode side of 3:1 BFS:PC Cs-cement sample after an electric leaching test

A BSE image of the cathode side from the Cs-cement wBa sample is shown in Figure 6.40, and includes the SEM-EDX maps of barium and sulphur – these are similar to the electrical leaching test of the Cs-cement and are naturally present in small amounts in the cement. The maps of the elements were similar to the cathode side of the electrical leaching test of Cs-cement.

The anode side from the Cs-cement wBa test is shown in Figure 6.41 with elemental mapping of barium, sulphur, caesium and nitrogen, calcium, silicon, aluminium and magnesium shown. There are areas of barium sulphate visible as bright white spots in the BSE image and they are present at depths of ~60 µm in the cement. This is direct evidence that during the test barium is moving into the cement and reacting with sulphur present in the same way as in the Blank-cement wBa electrical leaching test. Otherwise the elemental mapping is similar to the anode side of the electrical leaching test of Cs cement, with a visible degradation layer rich in Si.

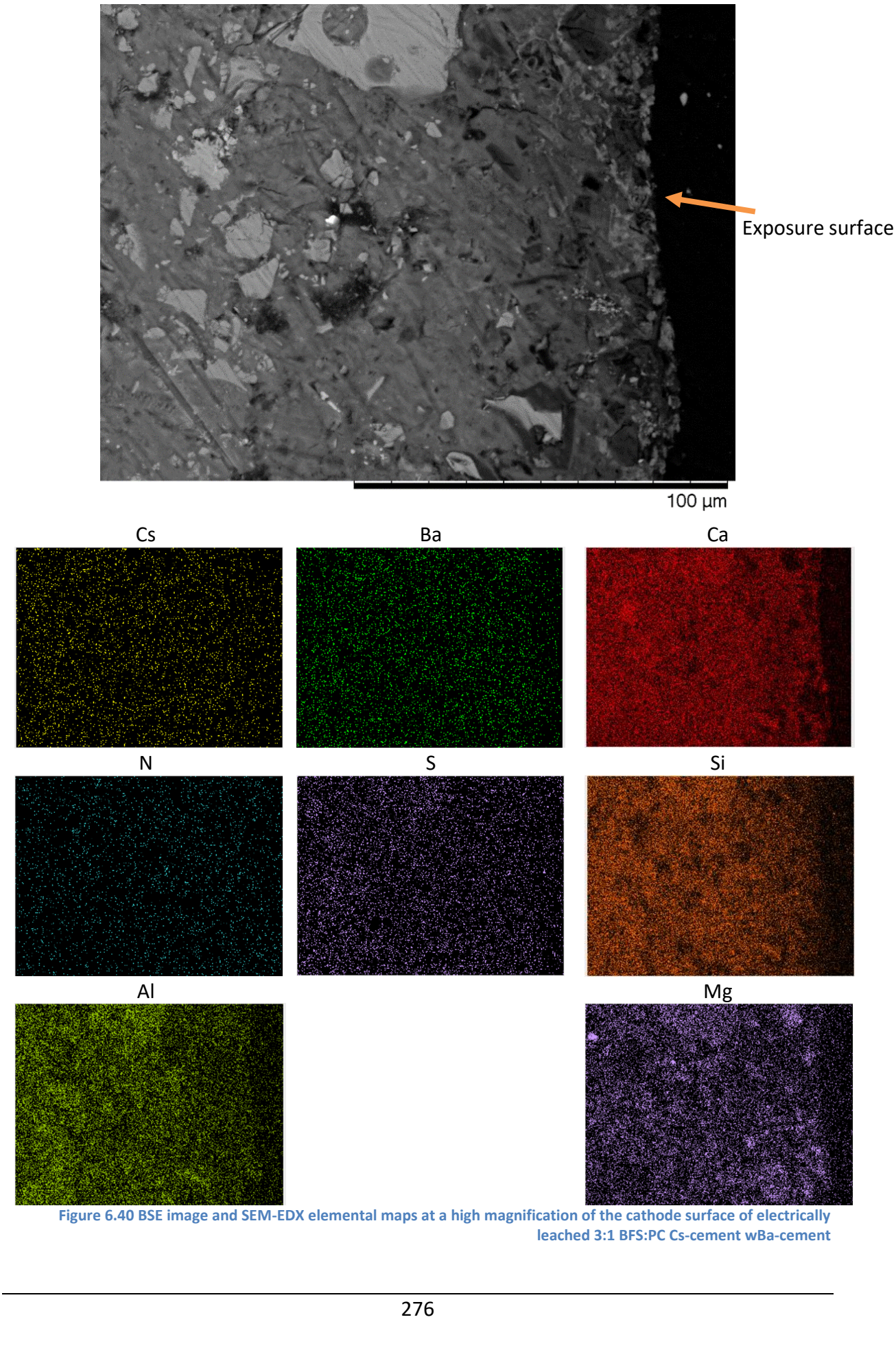

Figure 6.40 BSE image and SEM-EDX elemental maps at a high magnification of the cathode surface of electrically leached 3:1 BFS:PC Cs-cement wBa-cement

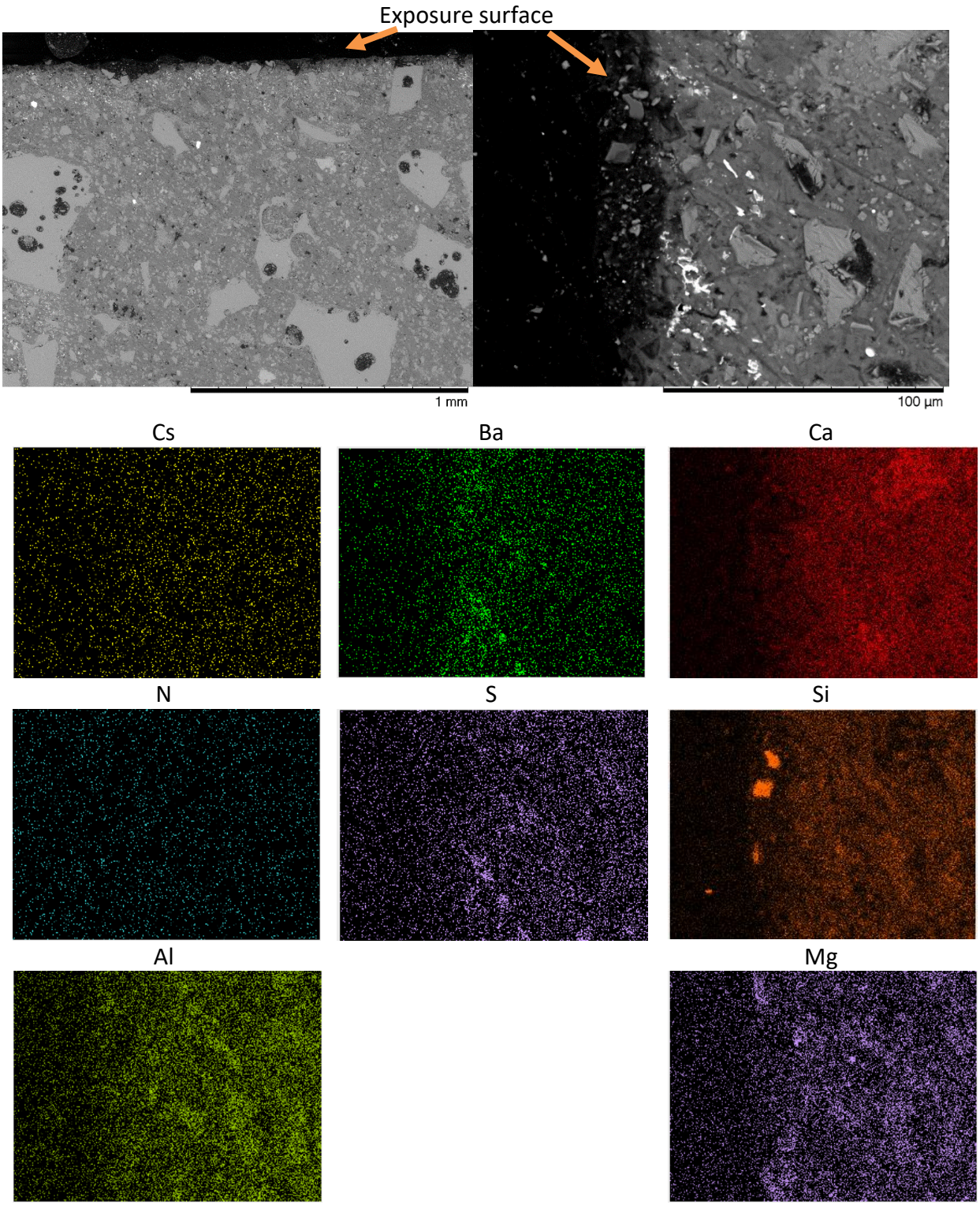

Figure 6.41 BSE image and SEM-EDX elemental maps at a high magnification of the anode surface of electrically leached 3:1 BFS:PC Cs-cement wBa-cement

The porosity data and pore size distribution of the Cs-cement samples are shown in Figure 6.42 and Figure 6.43 respectively. The Cs-cement wBa sample had the largest porosity of 19.5% whilst the statically and electrically leached samples were less porous than the unleached sample. For each sample the majority of the pores were in the 5-50 nm range, although the unleached sample displayed more porosity in the 6-20 nm range accounting for its larger overall porosity. In the Cs-cement wBa sample, there is a significant increase in the porosity at the 10-100 nm range compared with the other samples – the increase of these gel pores accounts for the sample's increased porosity, and is similar to the increase of porosity seen in the same test on the Blank-cement wBa sample shown in Figure 6.25. This is likely the result of the reaction of barium ions with ettringite (Equation 6.1).

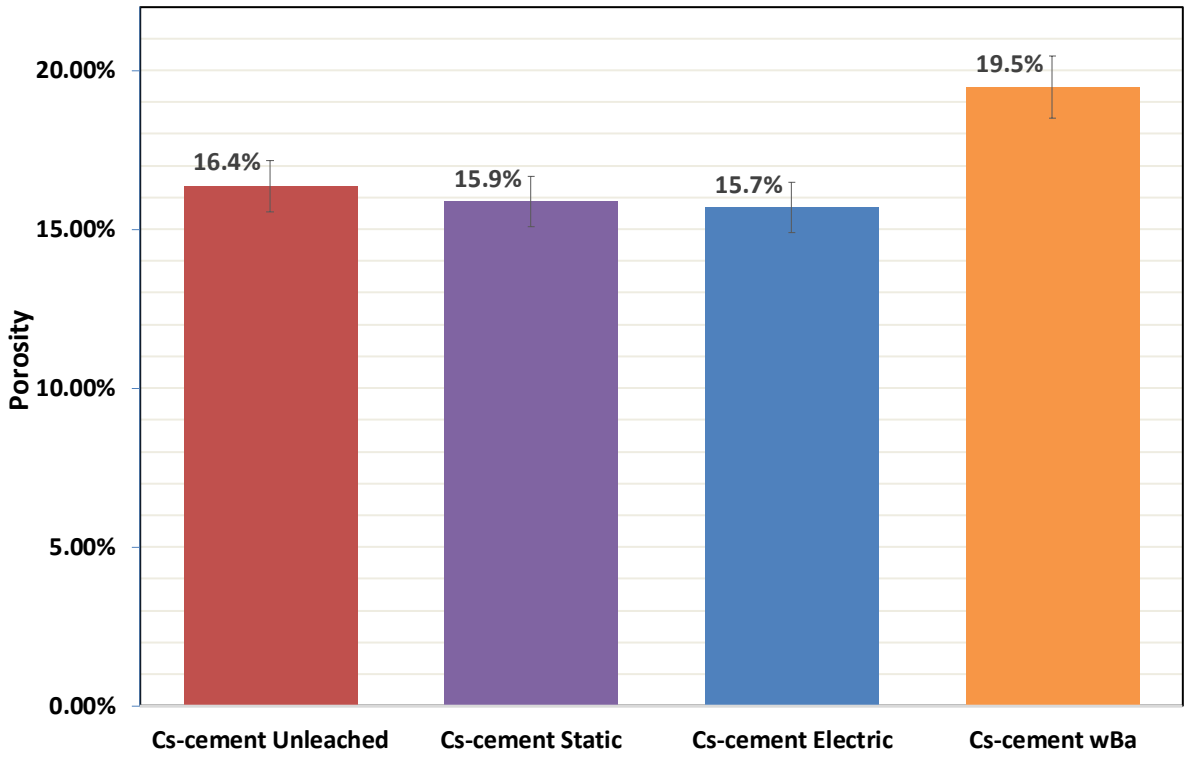

Figure 6.42 Porosity of 3:1 BFS:PC samples containing $CsNO_3$ with and without leaching tests

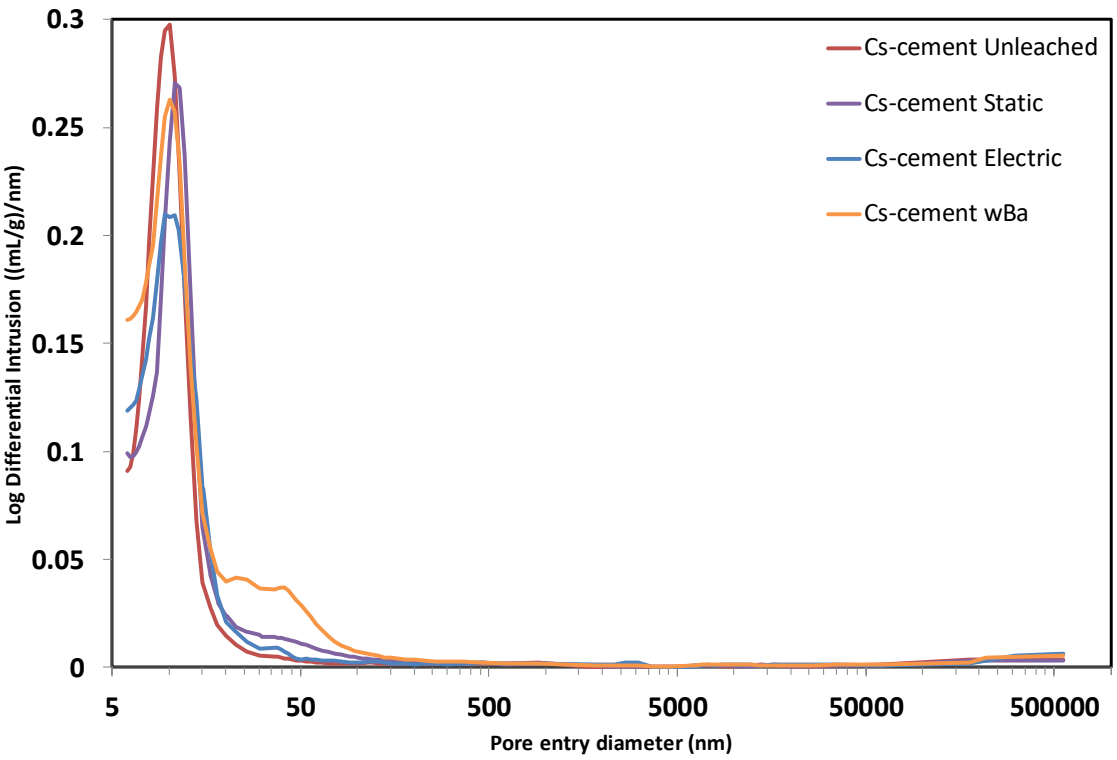

Figure 6.43 Pore size distribution of 3:1 BFS:PC samples containing $CsNO_3$ with and without exposure to leaching tests

6.5.2 Leachate Analysis from Leaching tests with Cs-cement and Cs-cement wBa samples

The pH data of the static test and the electrical tests are shown in Figure 6.44. There is almost no difference between the two tanks in the static test: although it is not constant, within error bars, the pH level remains stable at around 11.5. In the electrical leaching test of the Cs-cement sample, the pH of the cathode tank is higher than in the static leaching test of the sample, and the pH of the anode tank is much lower. This behaviour is similar to the pH differences of the static and electrically leached Blank-cement and Ba-cement samples. The pH level of the electrically leached Cs-cement wBa sample and the Blank-cement wBa sample also show similarities: the pH of anode and cathode tank are initially high. While the data for the Cs-cement wBa sample show a decrease of pH in the anode tank over time, the data for the Blank-cement wBa sample did not show this decrease. It is expected, however, that such a decrease would occur if the experiment was prolonged due to electrolysis occurring at the

electrodes in a test with an applied current [36], as discussed in Chapter 3[36][36][36][36][36][36][36][35][35][35][35].

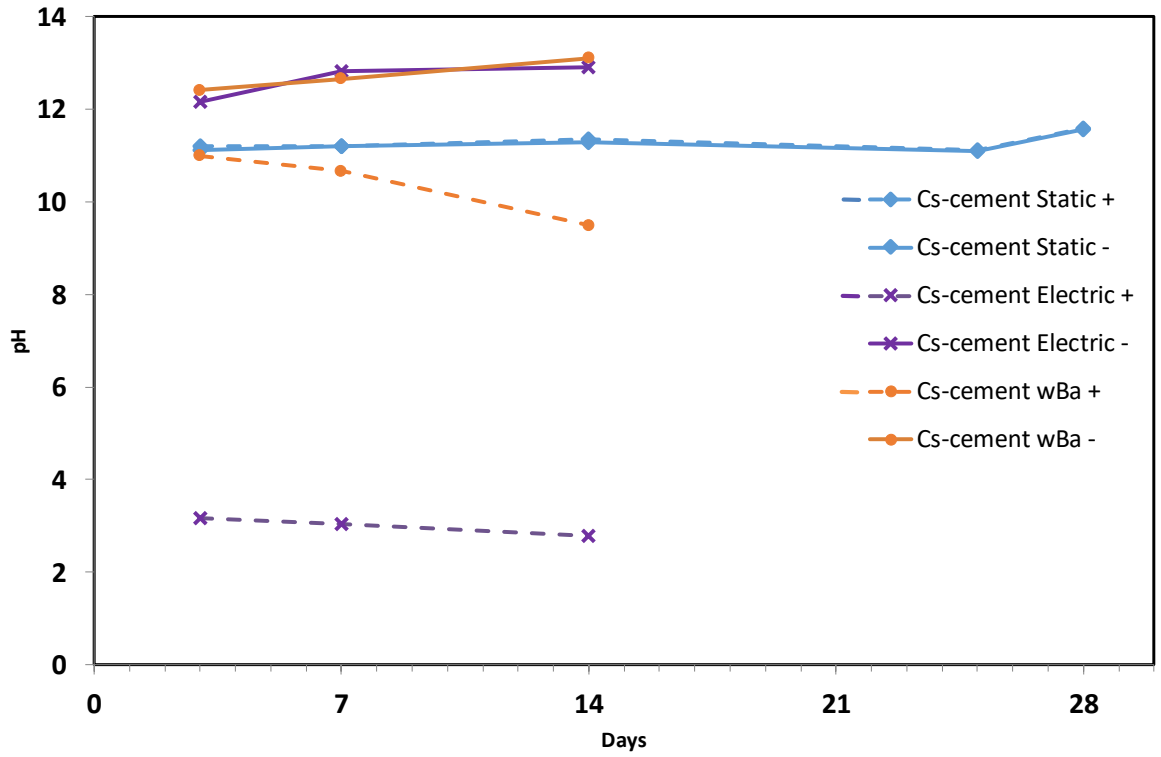

Figure 6.44 pH data of the leachates during static and electrical leaching tests of Cs-cement with no addition to the leachates, and an electrical leaching test of Cs-cement wBa. The dashed line is the pH of the anolyte and the solid line the catholyte, although in the static test this is for labelling purposes only.

The elemental concentration data of Cs in the leachates gathered by ICP-OES are shown below in Figure 6.45. In the static leaching test, the concentration of Cs in the tanks is low and does not increase over time. This is likely due to the low initial concentration of Cs in the sample – the leaching would potentially increase if the incorporation was above 2.8 wt.% as discussed in Chapter 4. During the electrical leaching test of the Cs-cement without added Ba in the anolyte, the leaching of Cs towards the cathode is enhanced, as expected from the behaviour of other cations shown above. Notably, the leaching towards the anode tank is also enhanced, however, which may be due to the low pH level and acidic environment in the anode, which is a similar pH effects as discussed during the leaching of sulphur observed in Chapter 5. In

the electrical leaching test with the Cs-cement wBa sample, leaching towards the cathode is similarly enhanced as in the previous electrical leaching test. The leaching into the anode tank, however, which in this case had a high pH due to the added Ba, is at the same level as in the static leaching test. This is further evidence for the effect of the lowered pH on the leaching of Cs observed in the electrical leaching test of the Cs-cement sample.

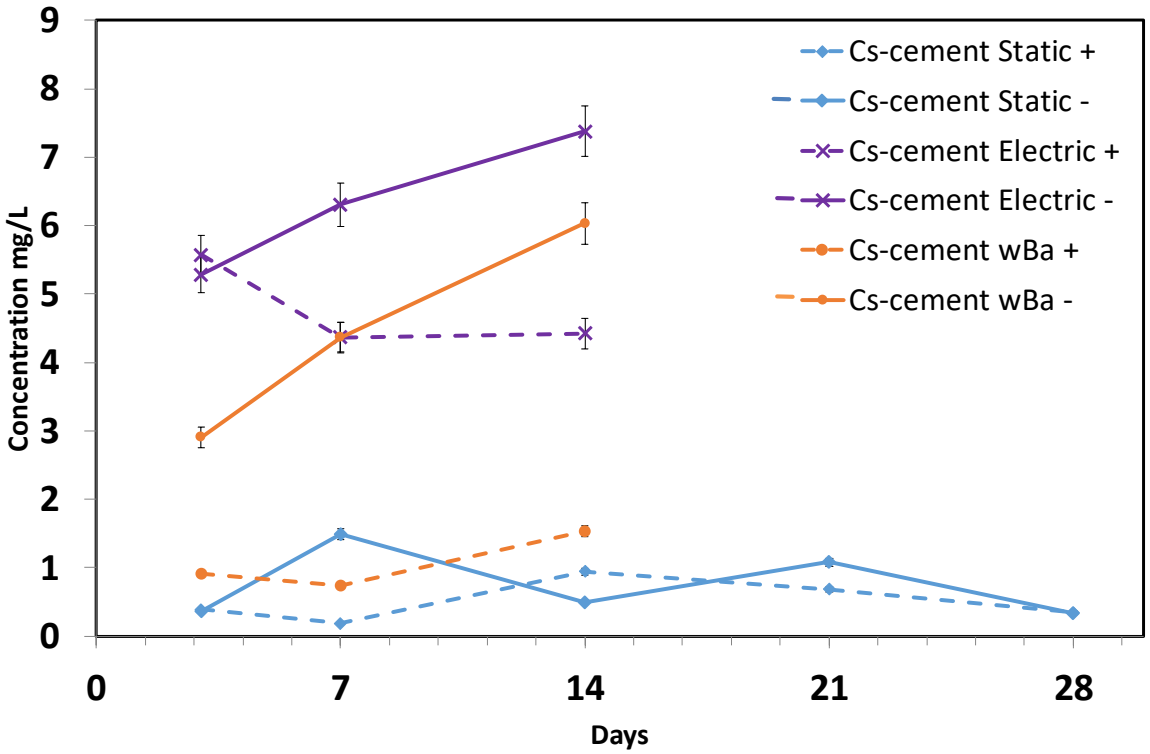

Figure 6.45 Elemental concentrations of caesium detected in the anode and cathode tanks in the static and electrical leaching test, and in an electrical leaching test of Cs-cement wBa. The solid line represents the cathode tank, and the dotted line the anode

The concentrations of the rest of the elements studied are shown in Figure 6.46 to Figure 6.48. Several elements, such as Ca, Si, Ba, Al and S leached less in the static leaching test with Cs-cement than in the static test with Blank-cement and Ba-cement. The same is true for the electrical leaching test with Cs-cement and Cs-cement wBa when compared to the other electrical leaching tests discussed in this chapter. The MIP results shown above suggest that the inclusion of $CsNO_3$ reduces the porosity of the sample, which is likely the cause of the reduction in the leaching of these elements. As less total porosity was measured (Figure 6.42),

it would be more difficult for elements to leave the sample than in the Blank-cement and Ba-cement samples. Especially significant was the decrease in the leaching of Al, which was significantly suppressed when compared with the behaviour in the electrical leaching tests with the Ba—cement and Blank-cement sample: a reduction of almost 90% was detected.

K and Na, on the other hand, leached more in the electrical leaching tests with the Cs-cement samples than in the electrical test with Blank-cement and Ba-cement samples – this could be caused by an increased dissolution and subsequent hydration of BFS and PC in the Cs-cement samples. Additional hydration would also account for the decrease in porosity observed, as well as the decrease in the leaching of Ca, Si, Ba, Al and S. As the slag dissolves, Ca, Si etc. become bound up in phases such as C-S-H, reducing the total porosity, and elements such as Na and K are dissolved in the pore solution, ready to be leached out when an electric current is applied. K and Na ions have shown a strong leaching behaviour when under an electrical current [37], and in the Cs-cement samples it is possible that these ions have to compete with Cs for the limited number of alkali metal binding sites in the hydrate phase assemblage.

It should be noted that, for S, the observed leaching into the anode tank was less for the electrically leached Cs-cement sample where Ba was pulled in, than for the electrically leached Cs-cement sample without barium. This decrease must be due to the reaction of S in the sample with barium to form barium sulphate and is similar to the leaching behaviour of S observed in the electrically leached Blank-cement wBa sample shown above.

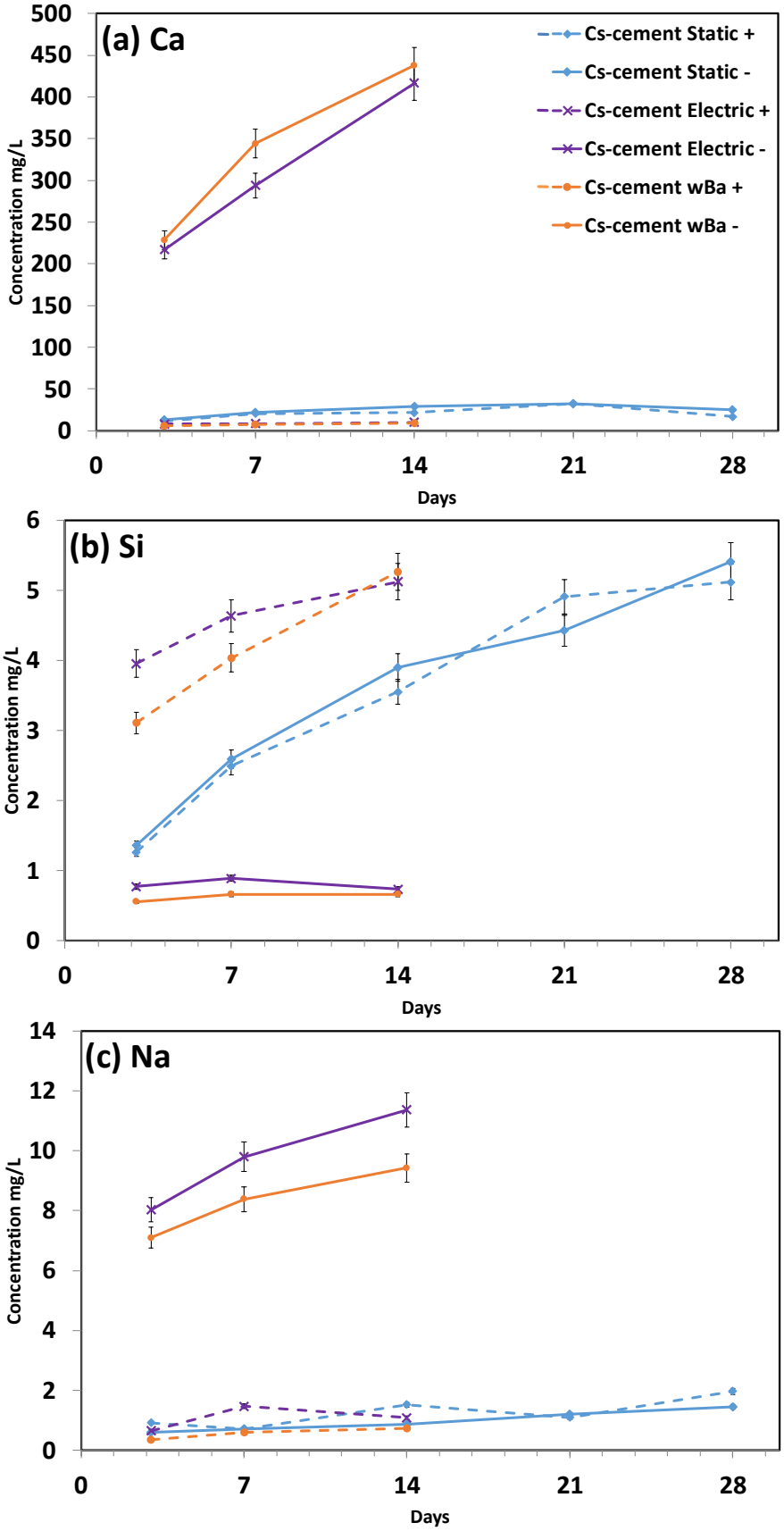

Figure 6.46 Elemental concentrations of (a) Ca, (b) Si and (c) Na in the anode and cathode tanks in the static and electrical leaching tests, and in an electrical leaching test of Cs-cement wBa. The solid line represents the cathode tank, and the dotted line the anode

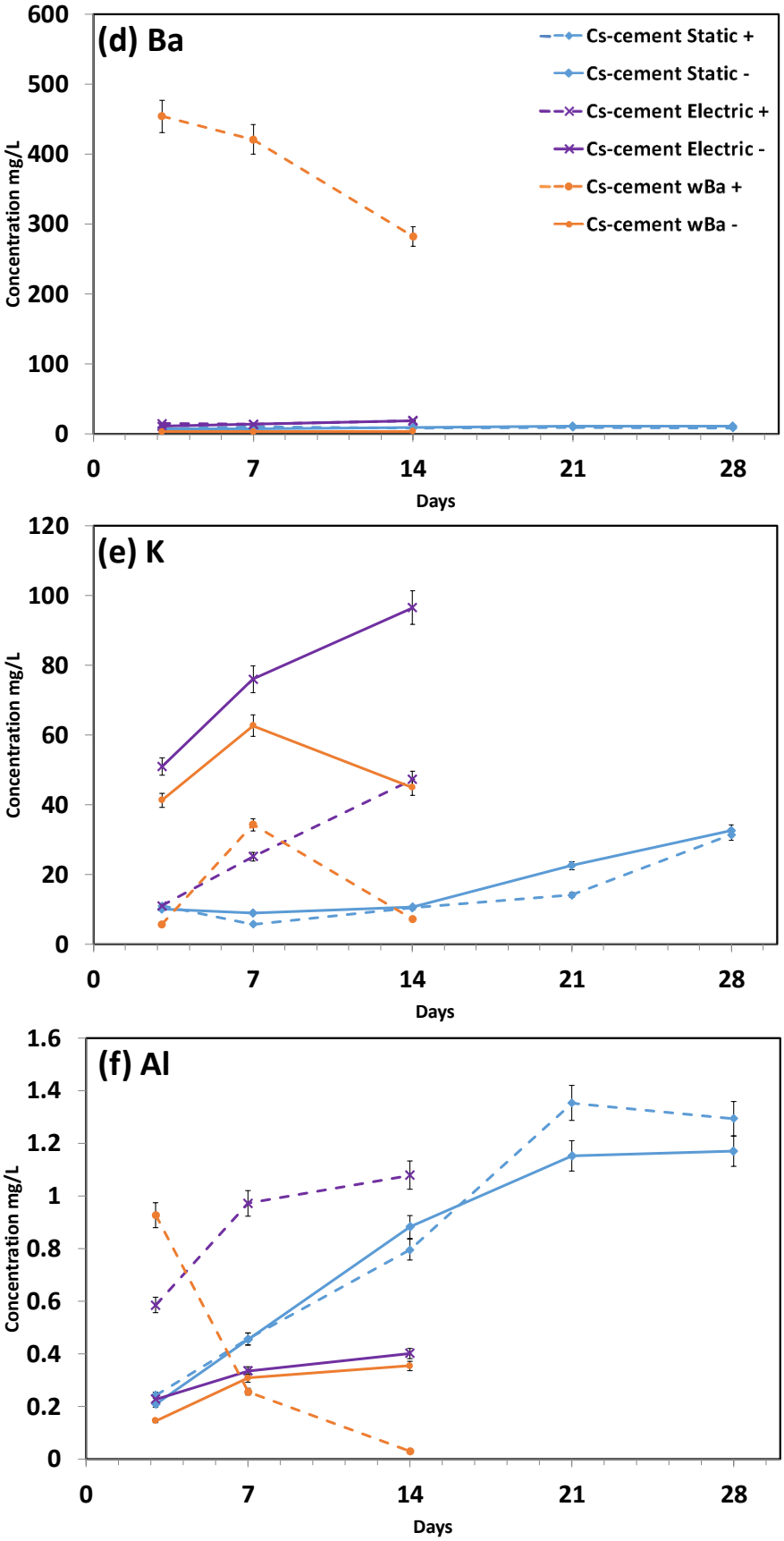

Figure 6.47 Elemental concentrations of (d) Ba, (e) K and (f) Al in the anode and cathode tanks in the static and electrical leaching tests, and in an electrical leaching test of Cs-cement wBa. The solid line represents the cathode tank, and the dotted line the anode

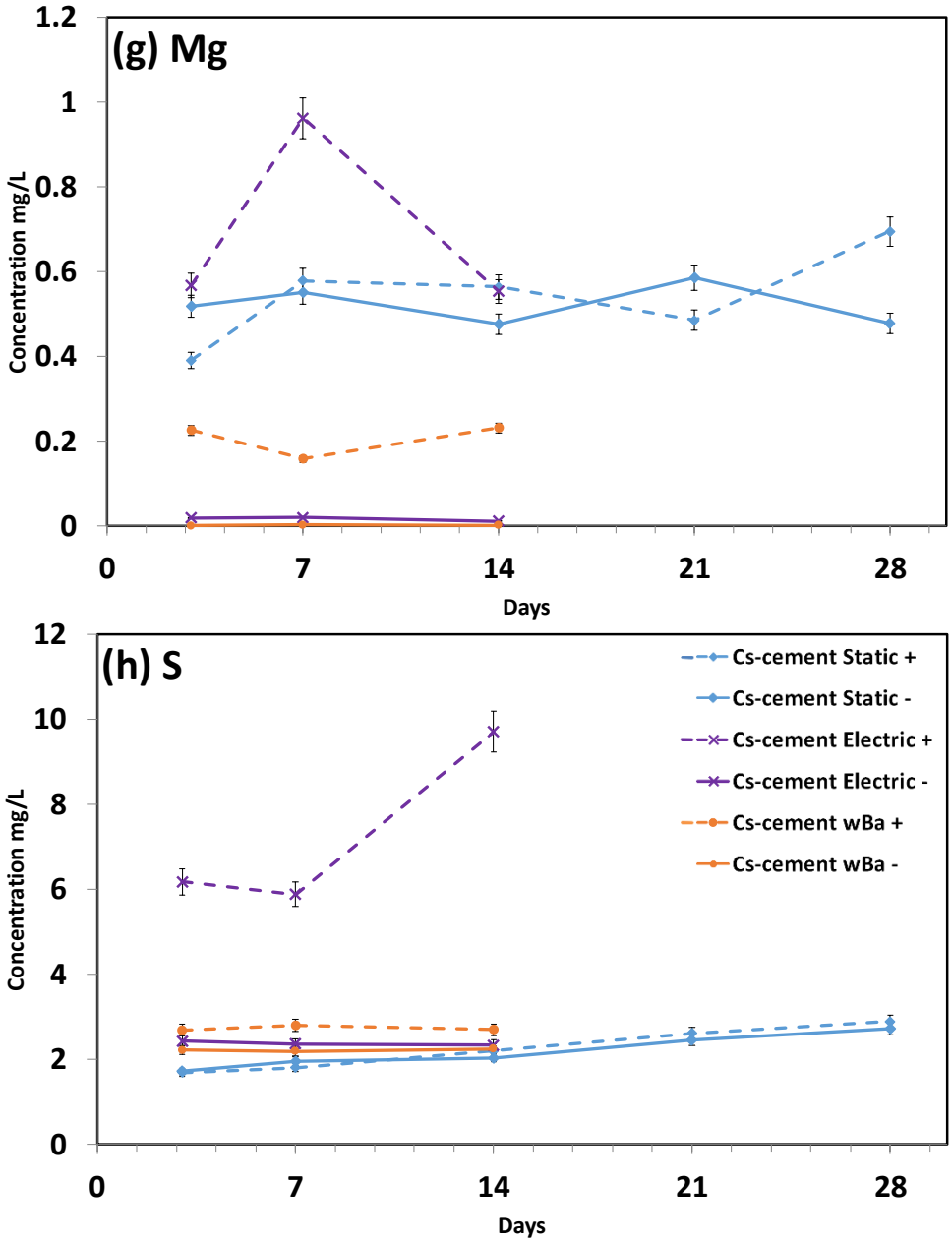

Figure 6.48 Elemental concentrations of (g) Mg and (h) S in the anode and cathode tanks in the static and electrical leaching tests, and in an electrical leaching test of Cs-cement wBa. The solid line represents the cathode tank, and the dotted line the anode

6.5.3 Phase Analysis of the Cs-cement and Cs-cement wBa-cement samples

The XRD data of the Cs-containing samples with/without leaching are shown in Figure 6.49, and an additional XRD scan in the 5 to 15 degree range with long counting time per step is shown in Figure 6.50. Small diffraction peaks due to barite are observable in the Cs-cement wBa test. The gehlenite peak has decreased in the Cs-cement wBa electrical leaching test. The peaks distinctive of ettringite seem to be slightly reduced in the Cs-cement wBa test as shown in Figure 6.50 – ettringite can react due to the introduction of barium into the cement as shown in Chapter 4 and in Section 6.4. There is also a slight increase in the monosulphate peak in this sample.

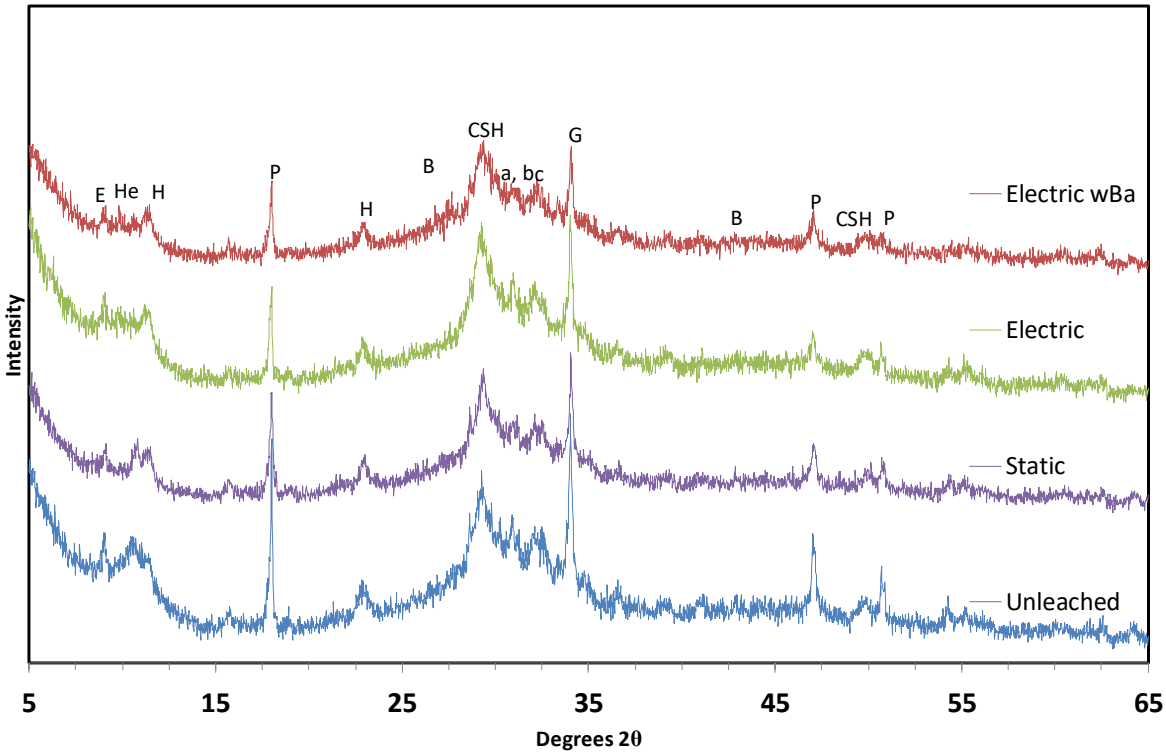

Figure 6.49 XRD of the Cs-cement samples in the range 5 to 65 degrees taken over 6 hours

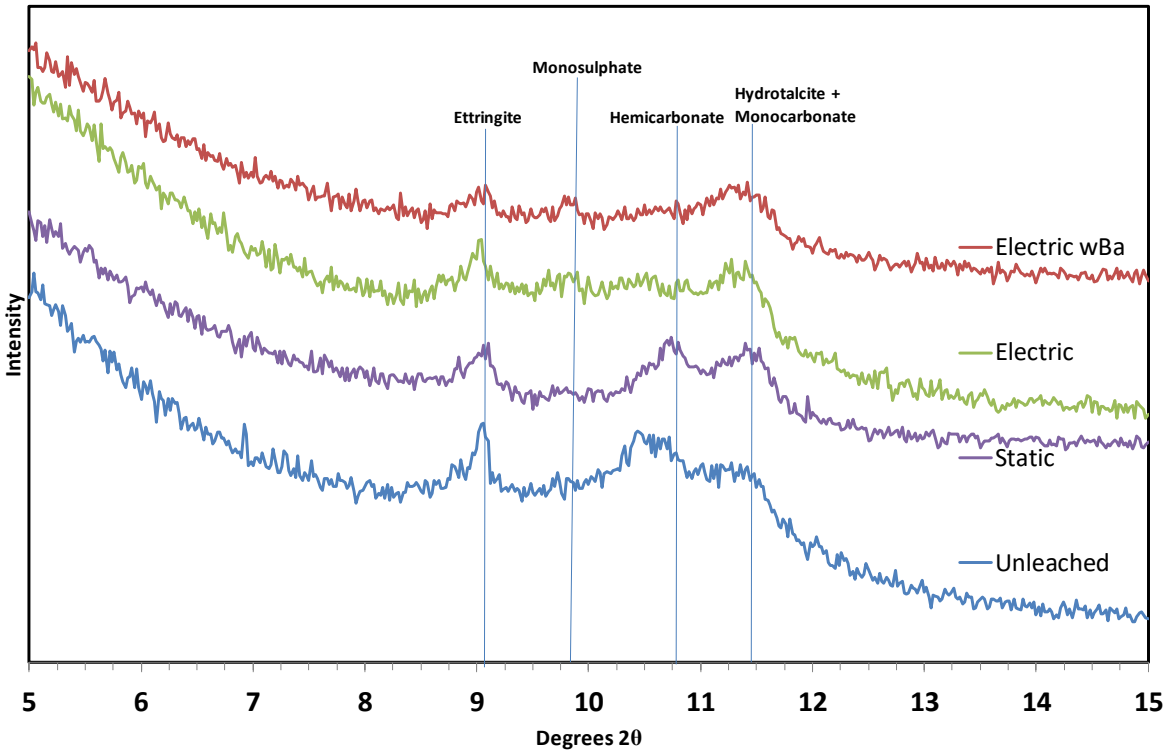

Figure 6.50 XRD of the Cs-cement samples in the range 5 to 15 degrees taken at a longer counting time per step

The thermal analysis data of the Cs-cement samples are shown in Figure 6.51 to Figure 6.53, starting with the thermogravimetric analysis and its first derivative and ending with the DTA data. All three samples contained the same phases as shown by the DTA data. The response of $CsNO_3$ usually observed at 162°C [22], [38], [39] was not identifiable because of the concentration of less than 2.8 wt.% as shown in Chapter 4.

In the TG data, the unleached sample showed the lowest weight loss as the temperature increased, but had anomalous data in the range 87-117°C. The Cs-cement wBa electrically leached and the Cs-cement statically leached samples showed a similar weight loss, with the statically leached sample losing slightly more mass. The majority of the weight loss occurs below 110°C. Around 450°C the unleached Cs-cement sample had a similar amount of weight loss to the statically leached sample due to the dehydroxylation of portlandite. Both the

unleached and statically leached Cs-cement sampled lost more weight at around 450°C than the electrically leached Cs-cement and the Cs-cement wBa samples, although the first derivative of the TG shows that the unleached sample had slightly more portlandite. The reduction in the amount of portlandite observed in the electrically leached samples is due to the increased leaching of calcium observed. The unleached sample had a considerable amount of calcite; leaching appears to reduce the calcite present. There was a slight increase in the amount of C-S-H detected in the Cs-cement samples compared with the Ba-cement and Blank-cement samples. These data seem to agree with the above leachate analysis, which suggested an increased dissolution and subsequent hydration of the Cs-cement samples.

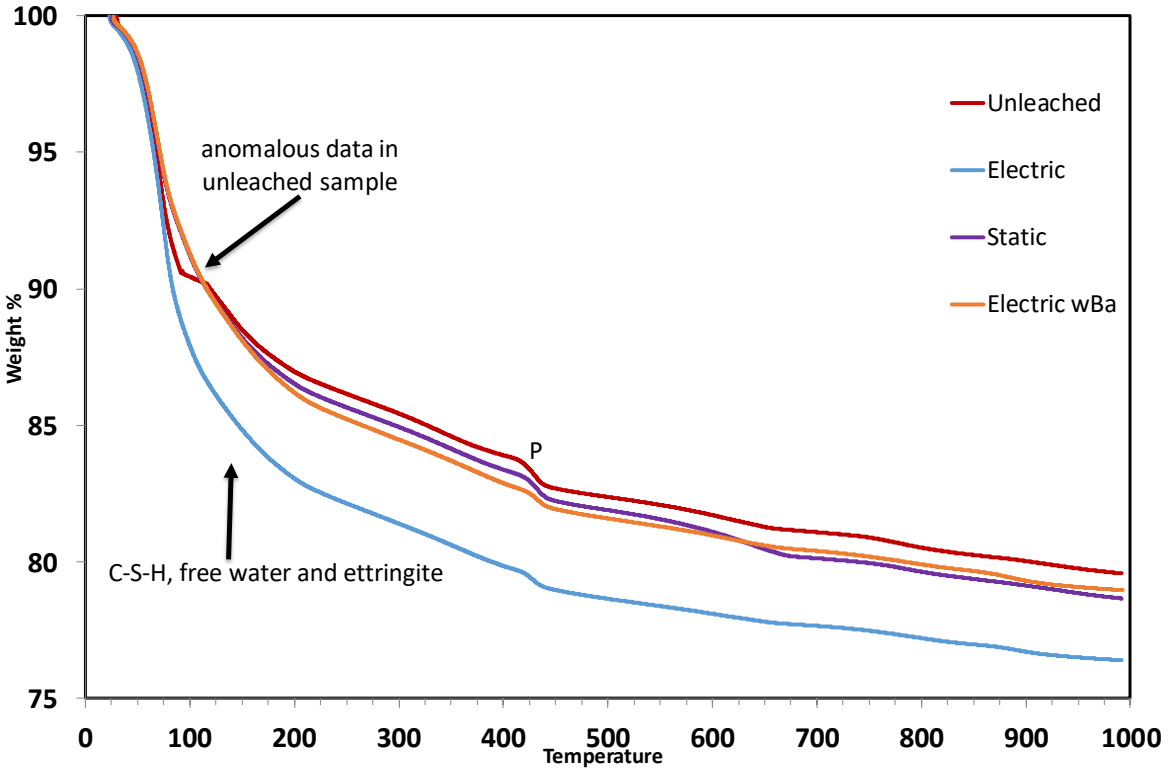

Figure 6.51 TGA of the 3:1 BFS:PC Cs-cement samples before and after leaching

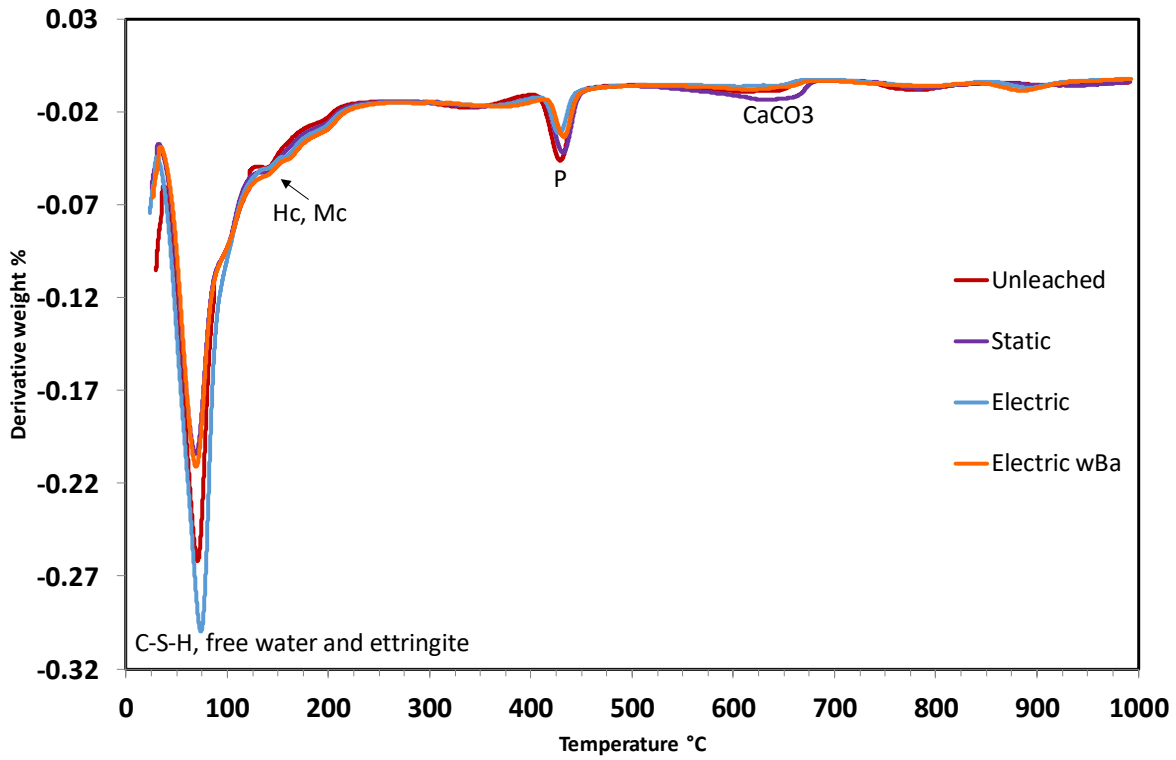

Figure 6.52 DTG data of the 3:1 BFS:PC Cs-cement samples before and after leaching

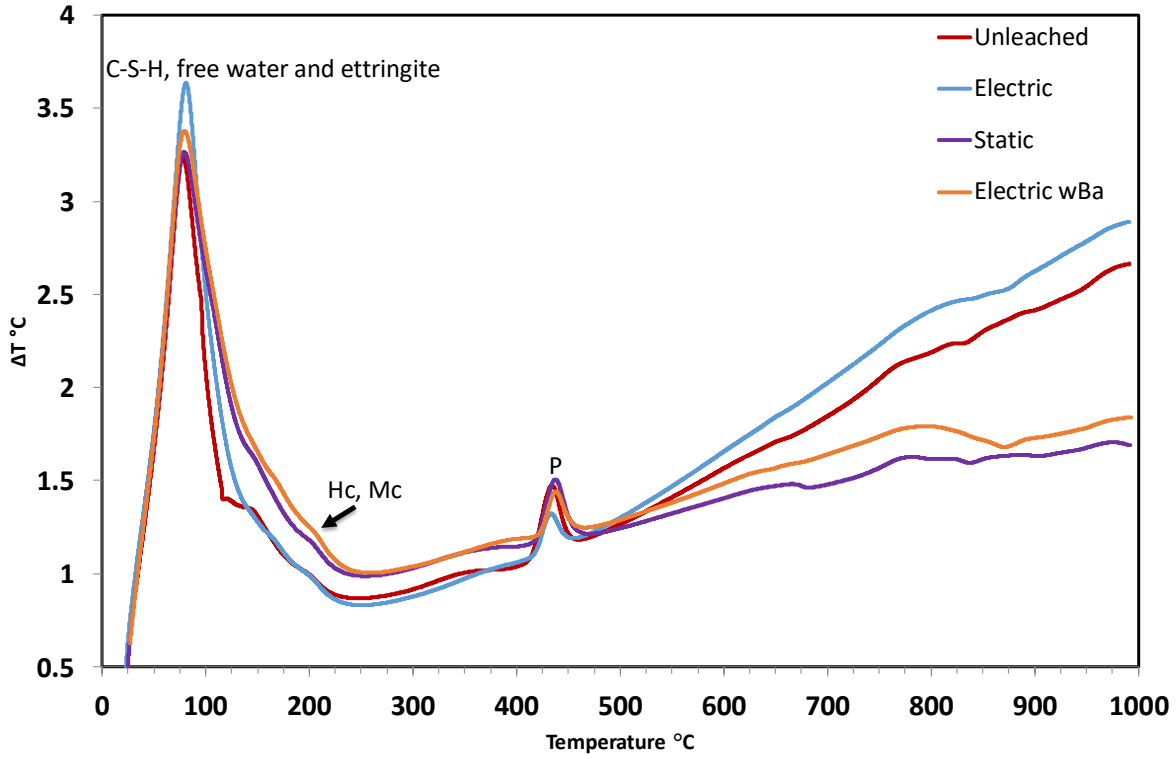

Figure 6.53 The DTA data of the 3:1 BFS:PC Cs-cement samples before and after leaching

6.6 Discussion and Conclusions

When barium is mixed in with the cement during curing (Ba-cement), the unleached sample is similar to the unleached sample of the Blank-cement – with the addition of barium sulphate among the phases present (observable in the XRD and SEM data) and the reduction in ettringite formation. Barium is otherwise spread throughout the cement sample at a higher concentration than in the Blank-cement sample. When this cement formulation with barium intermixed undergoes static and electrical leaching, and shows much the same leaching behaviour as the Blank-cement sample discussed in Chapter 5 in all analyses, apart from the obvious increase in the concentration of barium and a decrease of sulphur in the leachates. Also, when Ba is intermixed, the porosity of the Ba-cement sample increases when compared with the Blank-cement sample, which is likely due to a reduction in volume following the reaction of ettringite with barium resulting in barite, hydrogarnet, portlandite and water – the volume of the solid phases is only 35.7% the size of the solid reactants.

The introduction of barium into a pre-cured cement via dissolving barium into the anolyte (Blank-cement wBa) and pulling it in with an electric current is a valid method to examine the interaction of ions with pre-cured cement that works consistently – barium was seen to intrude into the cement sample. Barium was observed to interact with the sulphur content in the cement matrix and form barium sulphate (barite), a form that is highly insoluble and stable. Sulphur also leaches less into the anode tank in the electrical leaching test with Ba-cement than in the electrical leaching test with Blank-cement discussed in Chapter 5, which supports this theory. An increase in the porosity is observed in the electrically leached Blank-cement wBa samples in comparison to the electrically leached Blank and Cs-cement samples, which may be a result of this reaction.

When $CsNO_3$ is intermixed with the cement during curing, there are no alterations to the phases present – the amount added was below the precipitation concentration of 2.8 wt.% as identified in Chapter 4. Cs was detected in the leachates and appears to leach into the cathode tank more readily than the anode tank, as expected, given its ionic charge of +1. The leaching behaviour of Cs-cement in all experiments conducted with it is generally very similar to the behaviour observed in the experiments with Blank-cement samples. When cement samples initially containing $CsNO_3$ are used in a barium-migration test, the leaching behaviour of the Cs-cement wBa sample differs from the electrically leached Cs-cement sample, mirroring the differences between electrically leached Blank-cement wBa and Blank-cement samples – barite is seen to form, and an increase in porosity is observed in the electrically leached Cs-cement wBa sample when compared with the electrically leached Cs-cement sample. An increase in porosity will likely induce a reduction in the compressive strength of the wasteform [40]; further testing is required to verify the severity of this reduction. The increase of free pore space in the wasteform over time may be beneficial, as hydrogen gas produced by the radiolysis of water (caused by the radiation within the wasteform) could move into the extra pore space, reducing the pressure and strain felt by the steel canisters containing the waste. The reaction of S with Ba in ILW over time may have another beneficial trait, as the formation of ettringite in cement by sulphate influx can cause volume expansion and cracking inside the cement, depending on the sulphate content of the intruding groundwater [41].

The electrical migration technique does not appear to be a valid model for testing the *transmutation* of an element into another, as the removal aspect is not ion selective. It is however a valid and repeatable technique to analyse the *appearance* of elements in cement

samples, e.g. the appearance of Ba within ILW following nuclear decay. This technique could also be adapted to test the effects of pollution events on different cement types. In the tests shown here the Ba enters from the anode tank, and the exiting Cs enters into the cathode tank. The removal of the 'mother' element from and the introduction of the 'daughter' element to the cement sample will not always occur in the same area and is charge dependent. The formation of barite following barium ingress is a desirable result, as barite is a highly insoluble substance. This observation strongly suggests that when barium is introduced into the hardened cement, for example following the nuclear decay of ^{137}Cs into barium, it will subsequently react with sulphur, becoming highly immobile in the cementitious wasteform.

6.7 References

[1] J. L. Provis, P. A. Walls, and J. S. J. van Deventer, "Geopolymerisation kinetics. 3. Effects of Cs and Sr salts," *Chem. Eng. Sci.*, vol. 63, pp. 4480–4489, 2008.

[2] N. D. M. Evans, "Binding mechanisms of radionuclides to cement," *Cem. Concr. Res.*, vol. 38, pp. 543–553, 2008.

[3] A. Vollpracht and W. Brameshuber, "Binding and leaching of trace elements in portland cement pastes," *Cem. Concr. Res.*, vol. 79, no. 1, pp. 76–92, 2016.

[4] M. Mainguy and O. Coussy, "Propogation fronts during calcium leaching and chloride penetration," *J. Eng. Mech.*, vol. 126, no. 3, pp. 250–257, 2000.

[5] Q. Yuan, C. Shi, G. De Schutter, D. Deng, and F. He, "Numerical model for chloride penetration into saturated concrete," *J. Mater. Civ. Eng.*, vol. 23, no. 3, pp. 305–311, 2011.

[6] C. Andrade, "Calculation of chloride diffusion coefficients in concrete from ionic migration measurements," *Cem. Concr. Res.*, vol. 23, pp. 724–742, 1993.

[7] ASTM International, "C1202 Standard Test Method for Electrical Indication of Concrete's Ability to Resist Chloride Ion Penetration," 2010. [Online]. Available: https://www.astm.org/Standards/C1202.htm. [Accessed: 17-Jun-2017].

[8] M. P. Unterweger, D. D. Hoppes, and F. J. Schima, "New and revised half-life measurements results," *Nucl. Instruments Methods Phys. Res. A*, vol. 312, no. 1–2, pp. 349–352, 1992.

[9] M. P. Unterweger, "Half-life measurements at the National Institute of Standards and Technology," *Appl. Radiat. Isot.*, vol. 56, pp. 125–130, 2002.

[10] AlfaAesar, "Barium hydroxide octahydrate Safety Data Sheet," 2013. [Online].

Available: https://www.alfa.com/content/msds/british/14499.pdf. [Accessed: 17-Jun-2017].

[11] I. Odler, "Investigation of the hydration of portland blastfurnace slag cement: composition, structure and properties of the hydrated material," *Adv. Cem. Res.*, vol. 2, no. 5, pp. 15–20, 1989.

[12] O. S. Pokrovsky and J. Schott, "Experimental study of brucite dissolution and precipitation in aqueous solutions: Surface speciation and chemical affinity control," *Geochim. Cosmochim. Acta*, vol. 68, no. 1, pp. 31–45, 2004.

[13] D. Rothstein, J. J. Thomas, B. J. Christensen, and H. M. Jennings, "Solubility behavior of Ca-, S-, Al-, and Si-bearing solid phases in Portland cement pore solutions as a function of hydration time," *Cem. Concr. Res.*, vol. 32, pp. 1663–1671, 2002.

[14] P. M. Carmona-Quiroga and M. T. Blanco-Varela, "Ettringite decomposition in the presence of barium carbonate," *Cem. Concr. Res.*, vol. 52, pp. 140–148, 2013.

[15] J. R. Clifton and J. M. Ponnersheim, "NISTIR 5390, Sulfate attack of cementitious materials: volumetric relations and expansions," 1994. [Online]. Available: http://fire.nist.gov/bfrlpubs/build94/PDF/b94040.pdf.

[16] "Institute of Experimental Mineralogy, Russian Academy of Sciences, Crystallographic and crystallochemical database for minerals and their structural analogues: ettringite," 2009. [Online]. Available: http://database.iem.ac.ru/mincryst/s_carta.php?ETTRINGITE. [Accessed: 28-Jun-2017].

[17] M. Balonis and F. P. Glasser, "The density of cement phases," *Cem. Concr. Res.*, vol. 39, pp. 733–739, 2009.

[18] "Institute of Experimental Mineralogy, Russian Academy of Sciences, Crystallographic and crystallochemical database for minerals and their structural analogues: barite," 2009. [Online]. Available: http://database.iem.ac.ru/mincryst/s_carta.php?BARITE+395. [Accessed: 28-Jun-2017].

[19] P. Patnaik, *Handbook of Inorganic Chemicals*. New York: McGraw-Hill, 2002.

[20] C. W. Blount, "Barite solubilities and thermodynamic quantities up to 300 degrees C and 1400 bars," *Am. Mineral.*, vol. 62, pp. 942–957, 1977.

[21] O. Hussein, C. Utton, M. I. Ojovan, and H. Kinoshita, "The effects of BaSO4 loading on OPC cementing system for encapsulation of BaSO4 scale from oil and gas industry," *J. Hazard. Mater.*, vol. 261, no. 1, pp. 11–20, 2013.

[22] R. C. Weast, "CRC Handbook of Chemistry and Physics, 61st Edition." CRC, Boca Raton, Florida, USA, 1980.

[23] "Acros Organics, Barium Sulfate BaSO4 MSDS," 2012. [Online]. Available: https://www.fishersci.com/shop/msdsproxy?productName=AC222515000&productDescription=BARIUM+SULFATE++EXTRA+PU+500GR&catNo=AC222515000&vendorId=VN00032119&storeId=10652. [Accessed: 17-Jun-2017].

[24] C. A. Utton, E. Gallucci, J. Hill, and N. B. Milestone, "Interaction between BaCO3 and OPC/BFS composite cements at 20°C and 60°C," *Cem. Concr. Res.*, vol. 41, pp. 236–243, 2011.

[25] P. M. Carmona-Quiroga and M. T. Blanco, "Use of barium carbonate to inhibit sulfate attack in cements," *Cem. Concr. Res.*, vol. 69, pp. 96–104, 2015.

[26] V. S. Ramachandran, R. M. Paroli, J. J. Beaudoin, and A. H. Delgado, *Handbook of Thermal Analysis of Construction Materials*. Norwich, NY: Noyes Publications/William Andrew Publishing, 2002.

[27] B. Lothenbach, G. Le, E. Gallucci, and K. Scrivener, "Influence of limestone on the hydration of Portland cements," *Cem. Concr. Res.*, vol. 38, pp. 848–860, 2008.

[28] M. Castellote, C. Andrade, and C. Alonso, "Characterisation of transport of caesium, strontium, cobalt and iron ions through concrete by steady state migration and natural diffusion tests," *Adv. Cem. Res.*, vol. 11, no. 4, pp. 161–168, 1999.

[29] A. M. Gajewicz, E. Gartner, K. Kang, P. J. Mcdonald, and V. Yermakou, "A 1H NMR relaxometry investigation of gel-pore drying shrinkage in cement pastes," *Cem. Concr. Res.*, vol. 86, pp. 12–19, 2016.

[30] A. Valori, P. J. Mcdonald, and K. L. Scrivener, "The morphology of C–S–H: Lessons from 1H nuclear magnetic resonance relaxometry," *Cem. Concr. Res.*, vol. 49, pp. 65–81, 2013.

[31] F. Burriel, F. Lucena, S. Arribas, and J. Hernández, *Química Analítica Cualitativa*. Madrid, 1998.

[32] I. G. Richardson, C. R. Wilding, and M. J. Dickson, "The hydration of blastfurnace slag cements," *Adv. Cem. Res.*, vol. 2, no. 8, pp. 147–157, 1989.

[33] I. Odler and W. Hinrichs, "Investigation of the hydration of Portland blastfurnace slag cement: hydration kinetics," *Adv. Cem. Res.*, vol. 2, no. 5, pp. 9–13, 1989.

[34] D. G. Brookins, *Eh-pH Diagrams for Geochemistry*. Albuquerque, New Mexico: Springer-Verlag, 1988.

[35] P. C. Hewlett, "Lea's Chemistry of Cement and Concrete." Elsevier, 1998.

[36] C. W. Davies, *Principles of electrolysis*. London: Royal Institute of Chemistry, 1968.

[37] H. Saito and A. Deguchi, "Leaching tests on different mortars using accelerated electrochemical method," *Cem. Concr. Res.*, vol. 30, pp. 1815–1825, 2000.

[38] K. H. Stern, "High temperature properties and decomposition of inorganic salts part 3: Nitrates and nitrites," *J. Phys. Chem. Ref. Data*, vol. 1, no. 3, pp. 747–772, 1972.

[39] I. Yanase, J. Konakawa, and H. Kobayashi, "Influence of cesium nitrate and heating rate on densification and microstructure of Cs-deficient pollucite sintered body," *J. Am. Ceram. Soc.*, vol. 188, no. 20365, pp. 184–188, 2006.

[40] X. Chen, S. Wu, and J. Zhou, "Influence of porosity on compressive and tensile strength of cement mortar," *Constr. Build. Mater.*, vol. 40, pp. 869–874, 2013.

[41] P. Barret and Glasser, F.P, *Chemistry of Cements for Nuclear Applications*. Strasbourg, France: Pergamon Press, North Holland, 1992.

Chapter 7: Conclusions and Suggestions for Future Work

7.1 Incorporation of Cs and Ba into 3:1 BFS:PC

Increasing amounts of caesium nitrate were mixed with 3:1 BFS:PC cement samples by dissolving it into the water used to hydrate the cement powder mix. The presence of $CsNO_3$ did not result in an obvious alteration to the cement hydrate phases, however $CsNO_3$ was seen in the XRD data from 6 wt.% and above, whilst DSC analysis revealed that $CsNO_3$ begins to precipitate in the cement matrix from 2.8 wt.%. The incorporation of $CsNO_3$ in the 3:1 BFS:PC blend beyond this level will result in precipitation of $CsNO_3$ particles, which may not be ideal for the integrity of wasteforms, especially because $CsNO_3$ is readily soluble in water.

In a similar way, 3:1 BFS:PC samples with increasing amounts of barium content were studied. Even at the equivalent of 1 wt.%, no ettringite was observed in the samples – instead, barium sulphate had formed. When 3:1 BFS:PC is prepared with intermixed Ba, it changes the phases that form in the system, AFt phases in particular, resulting in enhanced carbonation and increase in porosity.

7.2 Electrical leaching and its effects on 3:1 BFS:PC

The leaching of the charged species studied is accelerated into the tank containing the corresponding electrode as shown in Chapter 5 – cations leach more into the cathode tank, and anions more into the anode tank. The 'Leaching Acceleration Factor' (LAF) was different for every element detected, and the valence of the ion in solution was not the main factor in determining the LAF. Elements such as Ca, K and Na which leach readily in static leaching tests were also the elements most affected by the applied electrical current, which is further evidence that electrical leaching accelerates the migration of species out of the pore solution, and does not directly affect the dissolution of the cement matrix (unlike acidic leaching).

The results obtained also show that the leaching of charged species into the alternate tank, e.g. the leaching of anions into the cathode tank, and of cations into the anode tank, is actually suppressed compared with a static leaching test, which has not been reported in the past. This can have a significant influence on the interpretation of the data up to 14 days of electrical leaching. For instance, in the cathode tank the leaching of calcium is increased, and the leaching of silicon in the same direction is actually decreased compared with a traditional static leaching test, which may affect perceived results such as the measured Ca/Si ratio, which has been used in the past to determine the degradation of cement samples. This may not be the case for longer leaching tests, but it is difficult to know as the suppression of leaching has not been reported so the full impact of this phenomenon is unknown. The pH of the anode tank is strongly affected by the electrolysis that occurs at the anode, and reduces over time – this means that on the anode side of the cement matrix the leaching is affected by both acidic and electrical leaching effects.

For the most realistic test, static leaching is still the truest to life technique to use when leaching samples. However, as the results of experiments in this thesis show, electrical leaching does accelerate the leaching of cement in a consistent and repeatable manner. There is still work to be done before standardisation of this method can be accomplished. In the tests shown in this project, a high level of leaching acceleration can be assumed only because of both the abundance of Ca in the cement, and the fact that Ca's LAF was so high. Other elements showed much lower levels of leaching acceleration. Essentially, it is not known how effective the acceleration would be in systems with low amounts of Ca as the LAF for other elements was not as high. This suggests that different cement compositions would have different overall LAFs depending on their elemental content when they undergo the same

electrical treatment. More work is also needed to be able to relate the LAFs of the different elements in a cement sample to the total degradation experienced by the sample.

7.3 Simultaneous Electrical Migration of Cs and Ba

The electrical migration of barium into a pre-cured cement matrix both with and without initial $CsNO_3$ incorporation was successfully performed. Other than a higher concentration of Cs, the obtained results showed no difference in leaching behaviour when Cs was incorporated. Barium sulphate was observed in the near-surface of the cement sample exposed to the anode during the migration tests, forming from a reaction with the intruding Ba ions and the sulphate ions present in the cement. The concentration of sulphur in the anode tank was less in the migration tests compared with electrical leaching of 3:1 BFS:PC using deionised water, which supports that this reaction is taking place. A slight increase in porosity was also observed as a result of this reaction. A similar reduction in the leaching of sulphur was observed during static and electrical leaching tests when Ba was initially intermixed in the system. The results strongly suggest that when barium is introduced to the hardened cement by the nuclear decay of ^{137}Cs, the barium will subsequently react with sulphur compounds present, and form barite ($BaSO_4$) in the cementitious wasteform. This is a desirable result, as barite is a highly insoluble substance, and therefore when Cs decays into Ba, the toxic Ba will be immobilised in the cement matrix.

7.4 Suggestions for future work

1. One of the aims of this series of experiments was to examine the interaction of barium with cement samples that had already been cured. An alternate method could have been to crush the cement samples and place the powder in a solution containing barium, for example, which obviously increase the available surface area for reaction

sites. However, this would also mean destruction of the cement sample, and could only test for chemical changes. The electrical migration method used in this project allows the experimenter to also test for physical changes to the cement sample, such as the observed changes in the porosity, which would not be possible in a powdered test. Another alternative technique would be to submerge a cement sample in a solution containing barium, however this would be more time consuming than using an applied electric current to drive Ba ions into the cement.

2. As the leaching into the opposite tank is suppressed during electrical leaching, it would be interesting to examine the effect of increasing the thickness of the sample, or of electrically leaching a sample exposed to either an anode or cathode in isolation, and the other electrode exposed to a separate electrolyte solution. Would the leaching be similarly suppressed when the effect of the attractive electrode cannot be felt? If the suppression is reduced (which is likely) or if no suppression is observed, then the suppression phenomenon which was observed in the current study could be controlled in future electrical leaching experiments.
3. In this work, when the leaching equipment was initially activated it took 11 to 12 hours to reach the target current density of 25 Am^{-2}, the pH of the anode tank lowered over time and the leachant was not replaced over the course of the tests. If leachant replacement was conducted, then the pH effects observed in the anode tank, such as decrease in Al concentration and eventual acceleration in the leaching of S, would likely be reduced. Also, each time the leachant was replaced it would likely take a similar amount of time to reach the target current density. To test this, the leachant should be replaced every three days as the pH decrease was not significant up to this point, and the target current density was reached.

4. Moving on from point 2, the identification of a suitable electrolyte solution for the leachant to increase the conductivity and thereby reduce the time taken to reach the target current density. This could be a potentially sizeable project itself, examining the impact of each test electrolyte used. Lithium hydroxide has been used as an electrolyte in the past to control the pH of the anode tank [1], [2], but the impact of this control has not been fully investigated. This would be an important piece of information to have, as it could be used to confirm or disprove the suggested pH-dependent leaching behaviour of Al and S observed in the current project.
5. A comparison between static leaching tests and electrical leaching test was presented in this thesis to estimate the acceleration in the leaching of elements. It would be beneficial to produce a similar comparison between electrical and acidic leaching to understand the differences they make to the leaching of cement samples.
6. As shown in this project, electrical migration can be used to introduce Ba into a pre-cured cement system and information about how they interact can be studied. Electrical migration therefore potentially provides a suitable method of examining the interaction of cementitious wasteforms with other decay products, such as ^{90}zirconium (decaying from ^{90}yttrium, itself a short-lived decay product of ^{90}Sr), and ^{99}ruthenium (decaying from ^{99}technetium) [3], [4].
7. It would be interesting to examine the effects of using different forms of Cs and Ba on leaching tests in the cement, for example CsCl rather than $CsNO_3$, as the molecules have different properties. CsCl has a solubility of 191 g/100 g H_2O, whereas $CsNO_3$ has a reported solubility of 27.9 g/100 g H_2O [5], so an increase in the leaching of Cs would be expected.

8. This project showed the acceleration of anionic species in to the anode tank due to the presence of the anode. Therefore, the anode has a degrading effect on the cement when placed externally. The effect of having an internal anode on the surrounding cement during an electrical leaching test has not been studied in the past, and studying these effects needs to be done if researchers decide to embed the anode in their cement.
9. As this PhD project was designed to gain further insight into the mechanisms driving electrically accelerated leaching, the methods used e.g. in Chapter 5, were similar to previous studies. Moving forward, measuring variables such as the temperature in the tanks, as well as stirring and replacing the leachates during the experiments, would improve the validity of the technique and help to prevent precipitation of material.
10. To gain further understanding of the degradation of cement caused by electrical leaching, future work is required to relate the key electrical leaching variables such as magnitude of applied current and leaching time, to the decrease in compressive and flexural strength of cement samples.

In summary, this study has successfully investigated the incorporation of Cs and Ba into 3:1 BFS:PC, and helped to close significant knowledge gaps in the mechanisms and limitations of electrically accelerated leaching. Electrically accelerated leaching is a valid technique to accelerate the degradation of cement, but likely only when the cement contains significant amounts of highly affected species such as Ca. From the results of the migration and incorporation experiments, the conclusion is that when Cs decays into Ba inside cementitious nuclear wasteforms, when S is available in the cement matrix, Ba will react to form $BaSO_4$ and become largely immobilised due to $BaSO_4$'s solubility, which is a desired result for the

purposes of nuclear waste containment. There are several possible avenues for future research, and the results of this work have hopefully inspired increased interest in the techniques used as there is a great potential to gain further understanding in the fields of nuclear waste and cement science.

7.5 References

[1] A. Babaahmadi, L. Tang, Z. Abbas, and P. Ma, "Physical and mechanical properties of cementitious specimens exposed to an electrochemically derived accelerated leaching of calcium," *Mater. Struct.*, vol. 9, no. 3, pp. 295–306, 2015.

[2] A. Babaahmadi and L. Tang, "Development of an electro-chemical accelerated ageing method for leaching of calcium from cementitious materials," *Int. J. Concr. Struct. Mater.*, vol. 9, no. 3, pp. 705–718, 2016.

[3] National Nuclear Data Centre, "Chart of Nuclides," 2016. [Online]. Available: http://www.nndc.bnl.gov/chart/. [Accessed: 17-Jun-2017].

[4] J. Peterson, M. MacDowell, L. Haroun, and F. Monette, "Radiological and chemical fact sheets to support health risk analyses for contaminated areas," 2005. [Online]. Available: https://www.remm.nlm.gov/ANL_ContaminantFactSheets_All_070418.pdf. [Accessed: 17-Jun-2017].

[5] W. M. Haynes, *CRC Handbook of Chemistry and Physics, 95th Edition*, 95th Editi. Boca Raton, Florida, USA: CRC Press, 2014.

A. Appendix- Additional figures

A.1 Chapter 4 Thermogravimetric Analysis

The below figures (Figure A.1 to Figure A.3) are additional analyses of the 3:1 BFS:PC samples containing increasing amounts of $CsNO_3$. They were not included in the main Chapter as they revealed less information than the DTA data.

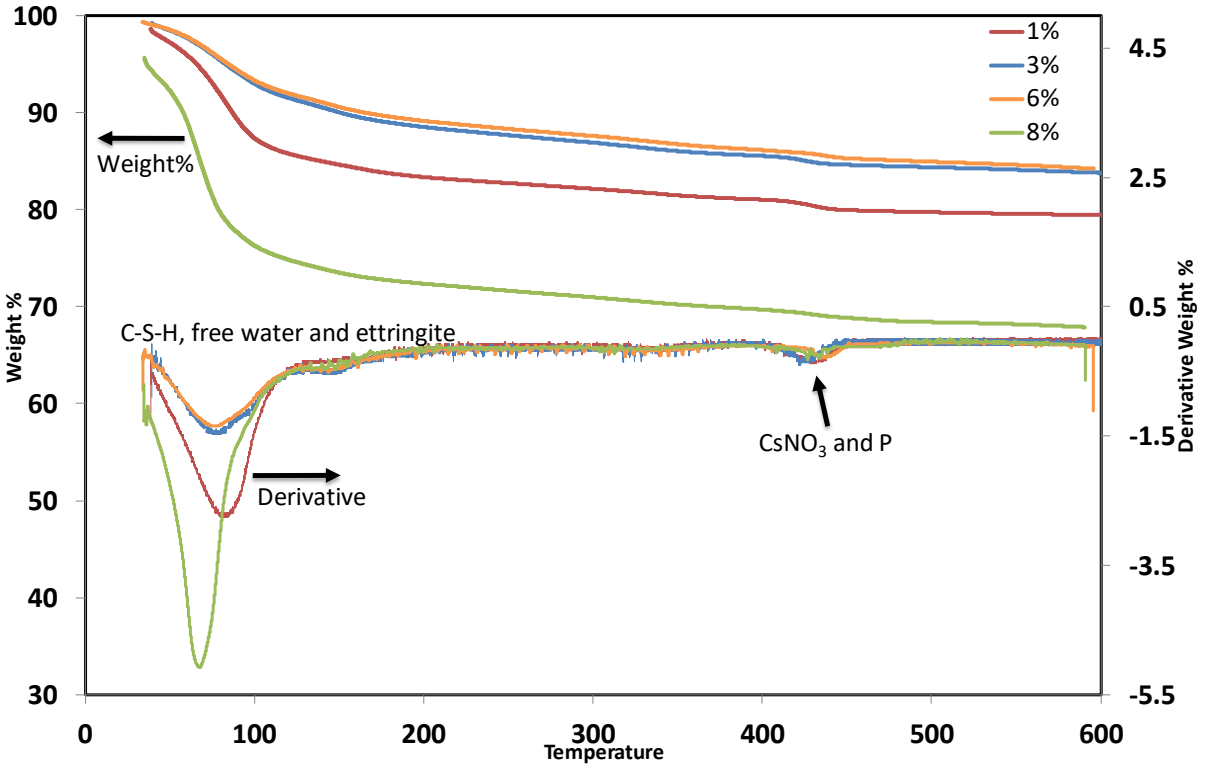

Figure A.1 TG of 7 Day old 1% to 8% $CsNO_3$ 3:1 BFS:PC from room temperature to 600 °C

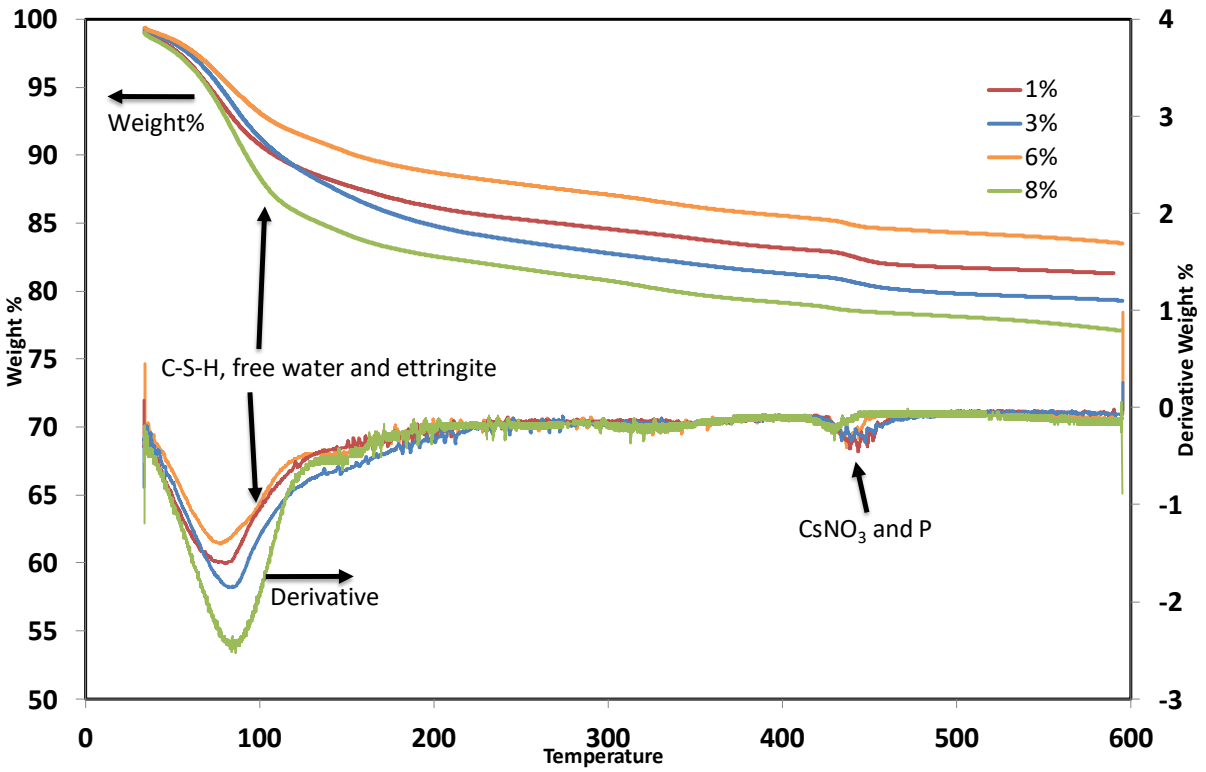

Figure A.2 TG of 14 Day old 1% to 8% $CsNO_3$ 3:1 BFS:PC from room temperature to 600 °C

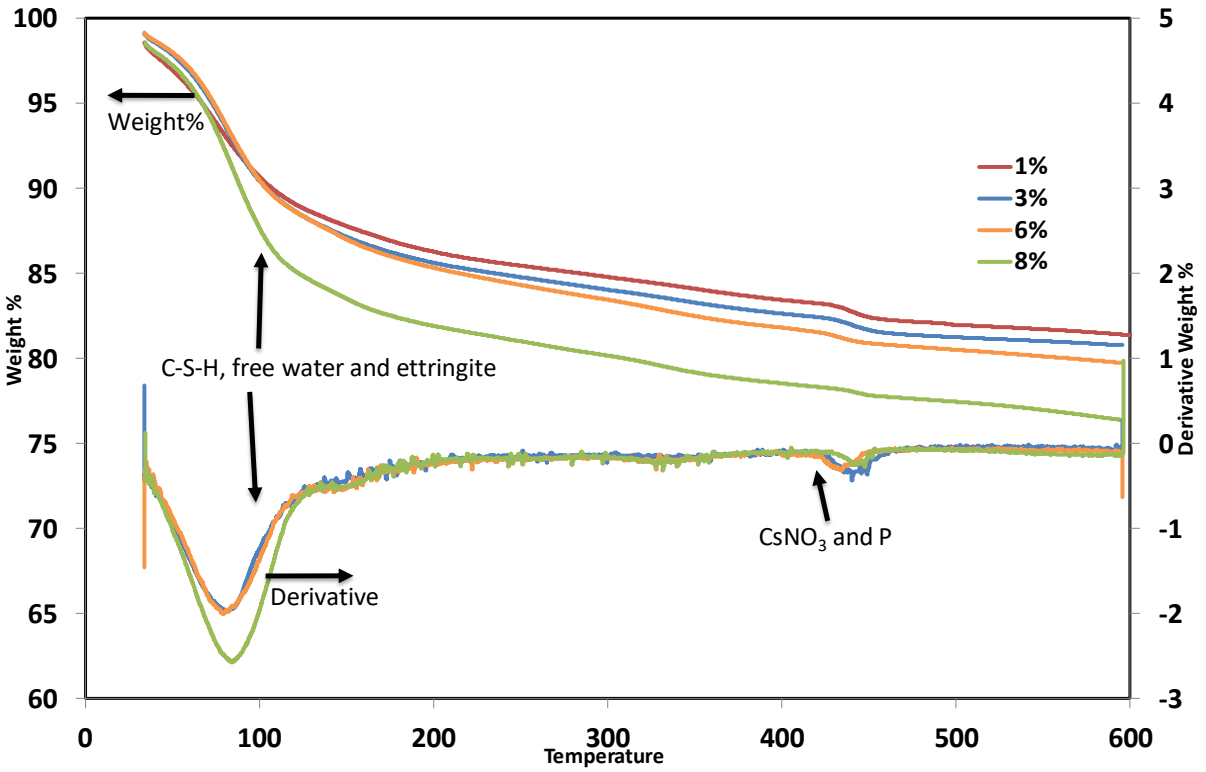

Figure A.3 TG of 28 Day old 1% to 16% $CsNO_3$ 3:1 BFS:PC from room temperature to 600 °C

A.2 Chapter 5 – BSE images and SEM-EDX mapping of 'wet' samples leached for 6 hours at 5 Am^{-2}

Figure A.4 and Figure A.5 similarly show the BSE images and elemental maps for the 5 Am^{-2} wet test conducted over 6 hours. Figure A.5 (the cathode side) is showing a large region of high iron concentration. Based on the brightness in the BSE image, it appears to be metallic iron (rather than oxides). Whilst iron was not spread throughout the sample, these iron particles were not uncommon (based on maps of similar 3:1 BFS:PC samples produced and analysed for this project) and assumed to have originated from the BFS. Similar to the dry sample, the wet sample also had a layer at the surface with a higher concentration of Na and more obviously K on both anode (Figure A.5) and cathode sides, together with the dense calcium rich layer at the exposure front on the cathode side. This calcium rich layer on the wet sample appears to be slightly thinner than that on the dry sample. Although the cause of this is not clear, this may be a reason for the higher Ca concentration in the leachate (Figure 5.5 a) and the larger normalised mass loss in wet sample (Figure 5.6 c) for the wet test compared with the dry test.

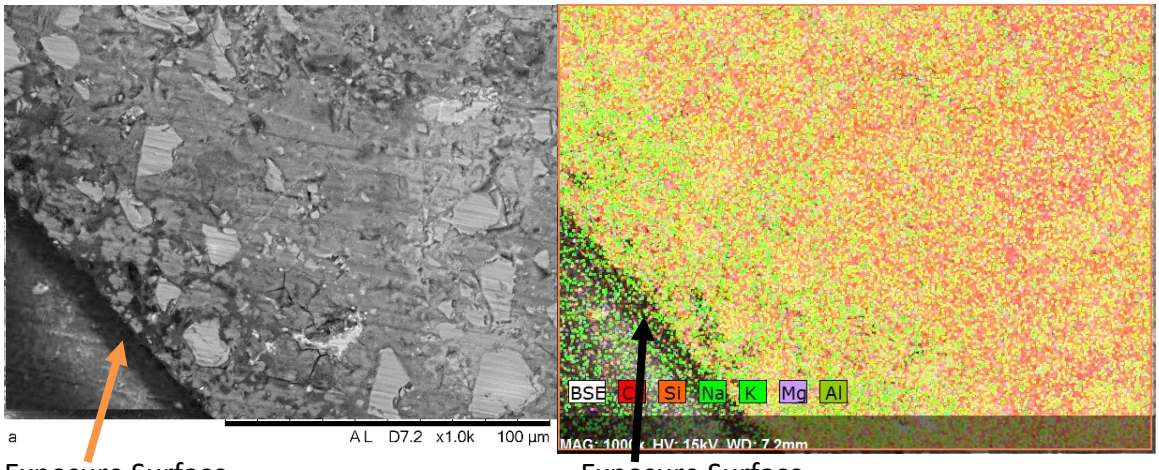

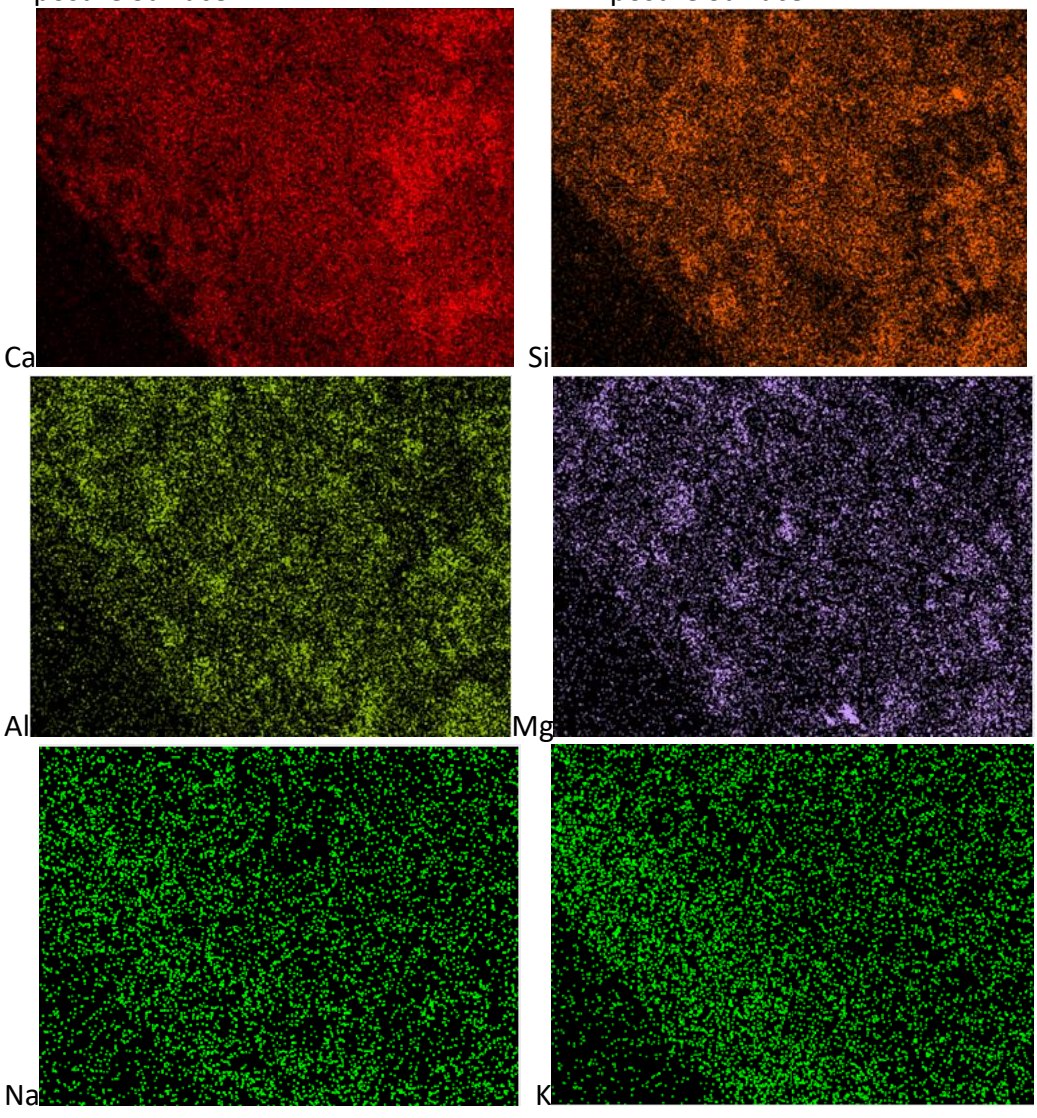

Figure A.4 BSE image with high magnification and SEM-EDX elemental maps of a wet 3:1 BFS:PC sample on the anode side after 6 hours of electrical leaching at 5 Am^{-2}

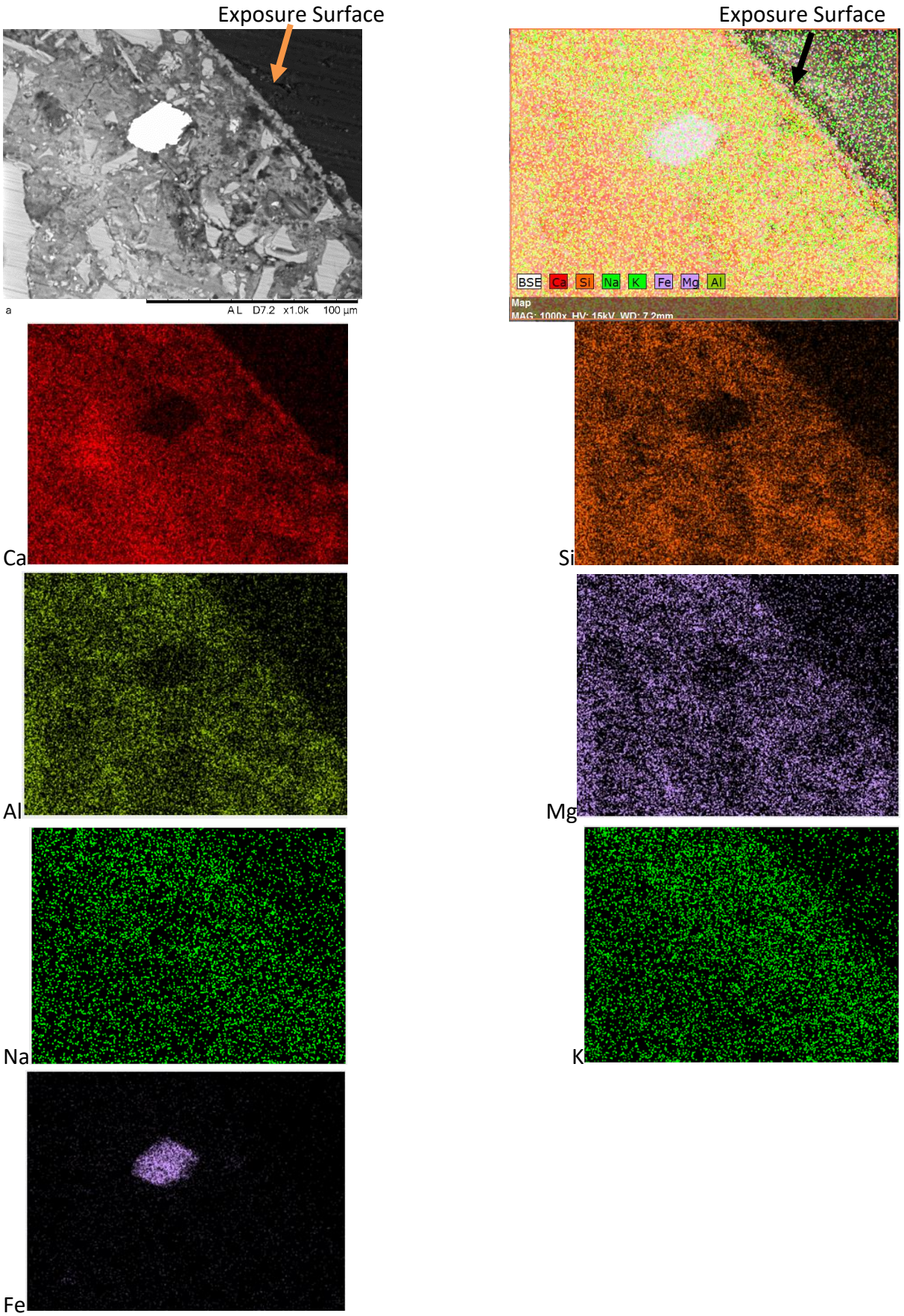

Figure A.5 BSE image with high magnification and SEM-EDX elemental maps of a wet 3:1 BFS:PC sample on the cathode side after 6 hours of electrical leaching at 5 Am^{-2}

A.3 Chapter 5 Additional issues to consider in electrical leaching

A.3.1 Precipitate observed in cathode tank after extended electrical leaching

Following on from Section 5.5, where a 3:1 BFS:PC sample was electrically leached for 22 hours at 25 Am^{-2}, the sample was left with the applied electric current for two months. A white precipitate was observed in the cathode tank and subsequently collected. A 6 hour XRD scan was conducted and the data is shown below in Figure A.6, which indicates two different forms of $CaCO_3$. Owing to the good quality of the data, it was possible to conduct Rietveld analysis. The result indicated that 23% of the sample was calcite with a trigonal symmetry, and 77% aragonite an orthorhombic structure, a form found in nature and is known to naturally transform into calcite over an extended period in the range of 10^7 to 10^8 years [1]. The precipitation of elements in a leaching test can affect the concentration data, as any precipitation will not be detected using techniques such as ICP-OES. These results indicate that for extended electrical leaching tests in the future the leachate should be replaced before the concentration of Ca reaches this point, even though it would take time (up to 12 hours, see Figure 5.14) to reach the desired current density after replacement.

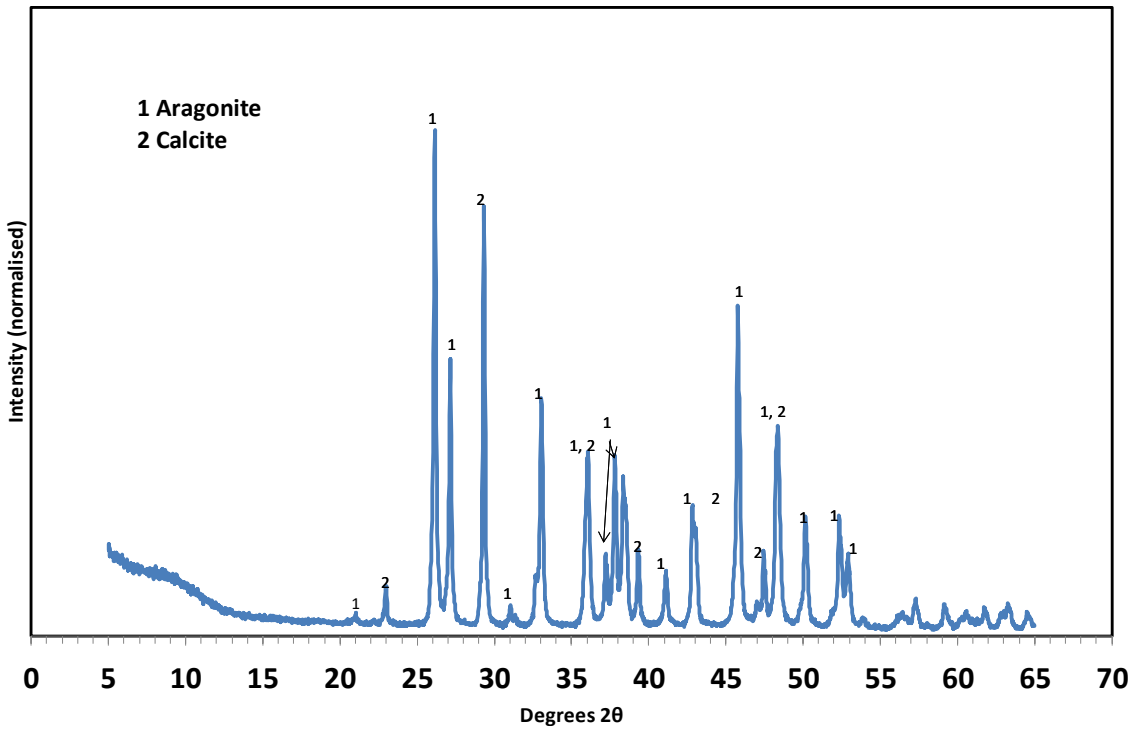

Figure A.6 XRD data (a 6 hour scan) of white precipitate taken from an extended e-leaching test showing different polymorphs of $CaCO_3$, calcite and aragonite [2]

A.3.2 Blue-green precipitate observed in the anode tank

In some of the electric leaching tests conducted at the start of the project, a blue-green precipitate was seen on the surface of the cement sample on the anode side. This was most clearly seen in an experiment presented for the work in Chapter 6, where a 3:1 BFS:PC sample electrically leached for 14 Days with Ba dissolved into the anode solution: a photograph of this is shown in Figure A.7. The photograph shows the anode side of the sample still in the casing with a blue/green precipitate. The precipitate was fragile and required delicate collection. This precipitate was gathered and analysed under XRF, and the data is displayed in Figure A.8. Whilst barium was dissolved into the anode solution, it was not seen in the precipitate. The precipitate is mainly lead (55.7wt.%) and copper (26.9wt.%), with silicon being the third most prevalent at 13.8wt.%. In electrical leaching experiments the titanium electrodes used are attached to copper wires via lead solder, and this connection is usually isolated from the leachate by epoxy resin. The cause of the precipitate on the cement surface

is likely cracks in and/or degradation of the epoxy resin used to separate the wire from the leachant. The anodic solution must have penetrated the epoxy resin, leading to the enhanced leaching of wire and the solder materials and precipitating on the surface of the cement. Fortunately, this was observed early in the experiments schedule, and the anode wire was replaced by a titanium wire without soldering. The blue green precipitates were not observed thereafter, and experiments were repeated. As shown in Figure A.9, copper and lead were not seen in the XRF data of a specimen tested under the improved system.

Figure A.7 Photograph of 3:1 BFS:PC leached for 14 Days with Ba dissolved in the anode solution. Image shows the sample still in the casing with a blue/green precipitate and shows the anode side.

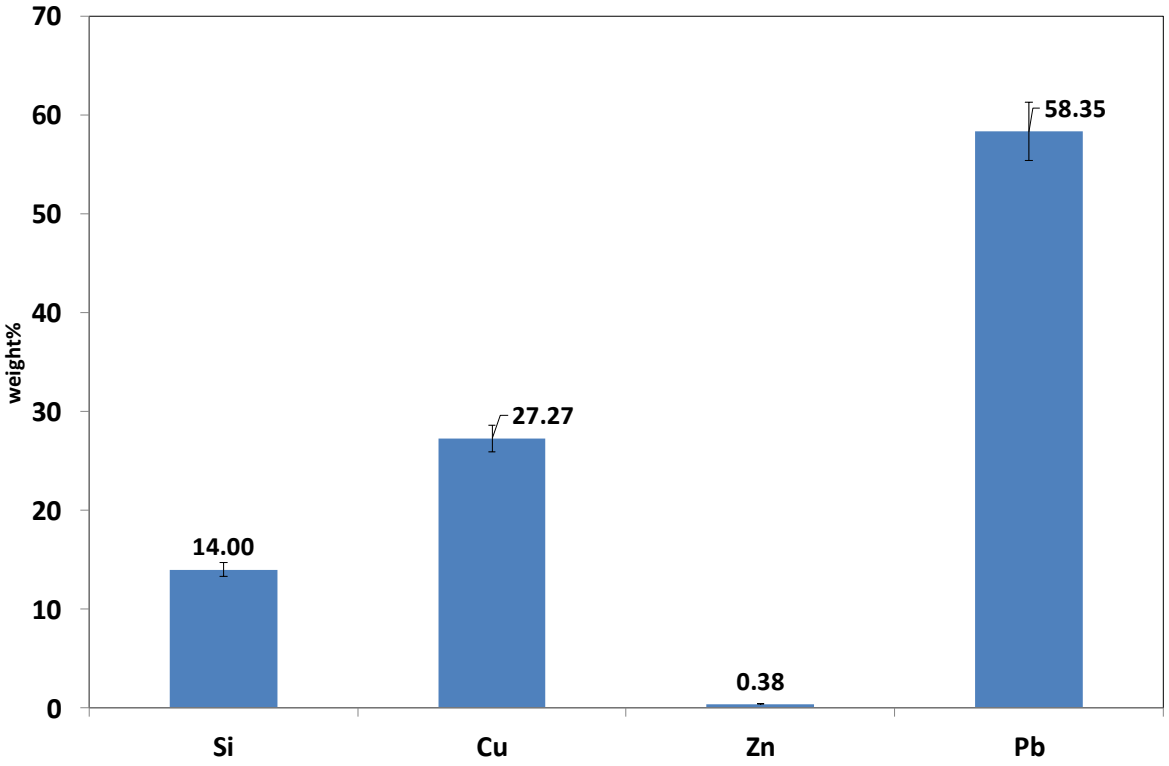

Figure A.8 XRF of the precipitate from Figure A.7. Note that whilst Cs is present, no Ba was observed

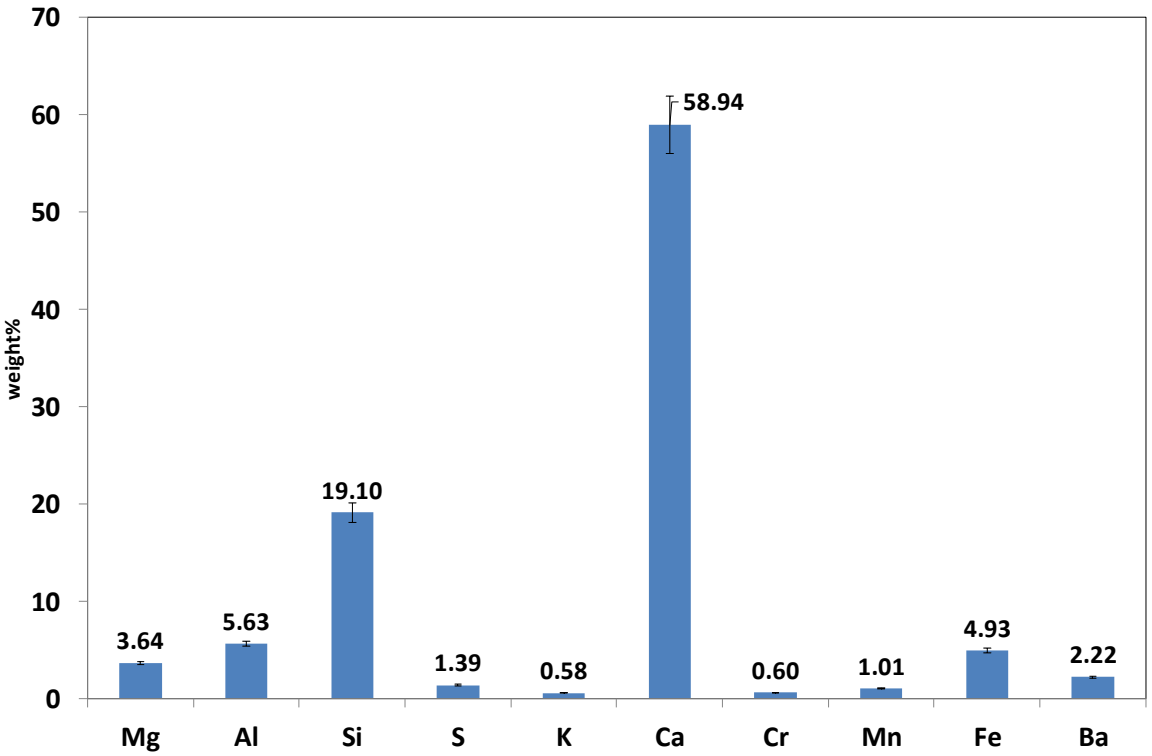

Figure A.9 XRF of a 3:1 BFS:PC sample leached for 14 Days with Ba dissolved in the anode solution with an improved setup.

These results show that when the epoxy resin becomes deteriorated, the leachate can interact with the copper electrical wire and lead solder used to connect it to the electrode, a blue-green precipitate can be seen on the surface of the cement, and also alter the colour of the leachate which consists largely of copper. The copper wire had begun to corrode in the anode tank due to the reduction in pH and the anolyte must have reached saturation for the precipitate to be observed. The quality of the electrode is thus important and should be checked before leaching tests are conducted.

A.4 References

[1] J. W. Anthony, R. A. Bideaux, K. W. Bladh, and M. C. Nichols, *Handbook of Mineralogy*. Chantilly, VA 20151-1110, USA, 2005.

[2] B. Xu and K. M. Poduska, "Linking crystal structure with temperature- sensitive vibrational modes in calcium carbonate minerals," *Phys. Chem. Chem. Phys.*, vol. 16, no. 4, pp. 17634–17639, 2014.